

Synthesis, Biophysical and Cellular Uptake Studies of Fluorinated Peptide Nucleic Acid Analogs

A thesis

**Submitted in partial fulfilment of the requirements for
the degree of
Doctor of Philosophy**

By

Satheesh Ellipilli

ID: 20103058

Research Supervisor

Prof. Krishna N. Ganesh



INDIAN INSTITUTE OF SCIENCE EDUCATION AND RESEARCH PUNE

April 2015

This Thesis is dedicated to...

My parents

and

Teachers.





Prof. Krishna N. Ganesh

Professor and Coordinator, Chemistry

Director, IISER Pune

J. C. Bose Fellow (DST), NCL Pune

CERTIFICATE

Certified that the work incorporated in the thesis entitled “*Synthesis, Biophysical and Cellular Uptake Studies of Fluorinated Peptide Nucleic Acid Analogs*” submitted by **Mr. Satheesh Ellipilli** was carried out by the candidate, under my supervision. The work presented here or any part of it has not been included in any other thesis submitted previously for the award of any degree or diploma from any other university or institution.

Date: 21st April 2015, Pune

Prof. Krishna N. Ganesh
(Research Supervisor)

DECLARATION

I declare that, this written submission represents my ideas in my own words and where other's ideas have been included, I have adequately cited and referenced the original sources. I also declare that I have adhered to all principles of academic honesty and integrity and have not misrepresented or fabricated or falsified any idea / data / fact / source in my submission. I understand that violation of the above will be cause for disciplinary action by the Institute and can also evoke penal action from the sources which have thus not been properly cited or from whom proper permission has not been taken when needed.

Date: 21st April 2015, Pune

Mr. Satheesh Ellipilli

ID: 20103058

Acknowledgements

It gives me an immense pleasure to express my deep sense of gratitude towards my research supervisor Prof. Krishna N. Ganesh for his constant encouragement and inspiration throughout my doctoral research. It would not be possible to pursue research in an unknown area like chemical biology in particular nucleic acid chemistry without his well-directed teaching, guidance and support. He has always taken efforts to inculcate independent thinking, presentation skills and writing skills many more and finally mould me into a perfect researcher.

I am very grateful to my research advisory committee members Prof. Dilip. D. Dhavale and Dr. Srinivas Hotha for their fruitful suggestions, comments and encouragement during various RAC meetings.

I would like to thank Dr. Raghvendra Kikeri and Dr. Raghavandra Murthi who helped me to carry the cell permeation studies in their lab.

I thank my seniors Dr. Ashwani, Dr. Roopa, Dr. Shridhar, Dr. Gitali, Dr. Mahesh, Dr. Manaswini, Dr. Tanpreet and Pradnya for their help in the initial years of my research at NCL. I would like to thank my colleagues Dr. Deepak, Nitin, Vijay, Madhan Dr. Dhruvajyoti Datta and juniors Shahaji, Prabhakar, Pramod B, Pramod (Topi) and Manoj for their kind help and creating a cheerful atmosphere around. My special thanks goes to Vijay kadam and Madhana Gopal who helped during my ups and downs in research and scientific discussions.

It really requires some serious relaxation outside the laboratory to kick back the power to move forward afresh. My days at IISER were made colorful with friendship of Gopal, Prakash, Sachin, Dharma, Kiran Reddy, Maroti, Sandip, Arun, Ananth raj, Ganesh, Susheel, Biplab, Pramod PS, Willbe, Indu, Ramya, Libi, Rini, Anurag, Sanjog, Ganesh Murhade, Rahul, Harshal Chaudhari, Ram, Deepak Nagarale, Subrahmanyam (subbarao), Gurivi reddy (Yettapu), Venky (boddu), Sivakoti, Harikrishna(kikeri bros), Ashok, Kishor, Chenna,

Narashimha, Bapu, Kiran chinnagulla, Kishore, Rajesh, Rajkumar(Raj), Krishna (Kittu), Satish(Dhasari), Sundeep (Palu), Jaggu (potti), Mahesh(gudem), Shiva shankar (mastar), Rajender(rangu), Rajender(choudhiri), Veeresh (dhonic, 99), Raviraja, Rahul roy, Priyatam, Satish,also they filled the gaps of my loneliness with numerous joyous moments and happiness. My special thanks to Gopala krishna (Tullimulli) who is always beside me in all difficulties and happy moments.

I am grateful to thank the technical staff, Pooja (NMR), Archana (SXRD), Swati (chotu) and Mayura (MALDI), Nayana (HRMS), Vijay Vittal (Confocal), Roopali (FACS), Megha (AFM), Yathesh and Anil (SEM) for their help. I am also grateful to the purchase section especially Vrushali, Zunjarrao, Nitin and Mahesh for their immediate response for purchase indents. Finally, I would like to thank the whole IISER family for their help either directly or indirectly.

I sincerely thank Director of IISER Pune for providing world class facilities to carry out my doctoral research and CSIR India, for the financial support. I would also like to thank Directors of NCL, Dr. Sivaram and Dr. Sourav Pal for allowing me to work in NCL lab in early research period.

Last but not the least; I shall always remain indebted to my parents and teachers, for their unconditional love, blessings, patience, support and encouragement.

Satheesh

Table of Contents

Chapter 1: Introduction to Peptide Nucleic Acids

1.1	Introduction to Nucleic Acids	1
1.2	Base Pairing via Hydrogen Bonding	2
1.3	Antisense Technology	4
1.4	Design of Antisense Oligonucleotides	5
1.5	Antisense Mechanism of Action	6
1.6	Chemical Modifications of Nucleic Acids	9
1.7	Peptide Nucleic Acids (PNAs)	15
1.8	Scope of Present Work	30
1.9	References	32

Chapter 2: Design, Synthesis and Characterization of Fluorinated PNA Monomers and Their Oligomerization

2.1	Introduction	43
-----	--------------	----

Section 2A: Synthesis and Characterization of Fluorinated and Control PNA Monomers

2A.1	Aim of the present work	51
2A.2	Synthesis of fluorinated PNA monomers	52
2A.2.2	Synthesis of nucleobase modified (<i>5FU-αeg</i> , <i>5CF₃U-αeg</i>) PNA monomers 1 & 2	54
2A.2.3	Synthesis of nucleobase and side chain fluorinated (<i>δ-F, αeg-T</i>), (<i>δ-F, 5FU-αeg</i>), and (<i>δ-F, 5CF₃U-αeg</i>) PNA monomers 3, 4 & 5	54
2A.2.4	Synthesis of backbone modified (<i>γ-CF₂-αpg</i>) PNA monomer 6	56
2A.2.6	Synthesis of backbone modified (<i>γ-5FBn-αeg</i> , <i>γ-Bn-αeg</i>) PNA monomers 8 & 9	58
2A.3	Crystal details of racemic compounds 20a, 20b and 20c	60
2A.4	Summary	64

Section 2B: Solid phase Synthesis, Purification and Characterization of Fluorinated and Control PNA oligomers

2B.1	Solid phase peptide synthesis	67
------	-------------------------------	----

2B.2	Aim of the present work	69
2B.3	Solid phase synthesis of PNA oligomers	69
2B.3.1	Synthesis of homo oligomers (octamers)	69
2B.3.2	Synthesis of mixed purine-pyrimidine PNA oligomers	70
2B.3.3	Fluorinated PNAs for the inhibition of telomerase activity	72
2B.4	Cleavage of the PNA oligomers from the solid support	72
2B.5	Purification and characterization of PNA oligomers	72
2B.6	¹⁹ F-NMR shifts of various fluorinated compounds	73
2B.7	¹⁹ F-NMR of PNA 14 & 17	76
2B.8	Summary	77
2.2	Experimental section	79
2.3	References	116
2.4	Appendix-I	117

Chapter 3: Biophysical Evaluation of Fluorinated PNA Oligomers

3.1	Introduction	201
3.1.1	Hydrophobicity (lipophilicity) studies of fluorinated homooligomers	201
3.1.2	Biophysical techniques used to study the hybridization properties	202
3.2	Results and Discussion	204
3.2.1	Hydrophobicity studies of fluorinated PNA homooligomers (octamers)	204
3.3	Biophysical studies of fluorinated PNAs with complementary DNA	207
3.4	UV- T_m studies of the fluorinated PNAs with complementary RNA	211
3.5	UV- T_m mismatch studies of PNA:DNA and PNA:RNA hybrids	217
3.6	CD-Studies of PNA:DNA and PNA:RNA Duplexes	218
3.7	Discussion	221
3.8	Experimental procedures	222
3.9	References	223
3.10	Appendix-II	224

Chapter 4: Cell Permeation Studies of Fluorinated PNAs and Nanoparticles Formation of PNA:DNA/RNA Duplexes

4.1	Introduction	227
4.2	Aim of the present work	228

4.3	Results and discussion	229
4.4	Cellular Uptake Studies	231
4.5	Quantitative estimation of cell permeation in HeLa and NIH 3T3 cells	238
4.6	Discussion	243
4.7	PNA based Nanoparticles Formation and their Cellular Uptake Studies	244
4.8	Objective of the present work	245
4.9	Results and Discussion	246
4.10	Summary	253
4.11	Experimental procedures	253
4.12	References	256
4.13	Appendix-III	257

Abbreviations

A	Adenine
Abs.	Absolute
Ac ₂ O	Acetic anhydride
ACN	Acetonitrile
<i>aeg</i>	Aminoethylglycine
<i>apg</i>	N-(3-aminnopropyl)glycine
<i>aep</i>	Aminoethylprolyl
ap	Antiparallel
<i>aq.</i>	Aqueous
(Boc) ₂ O	Boc anhydride
Bn	Benzyl
5FBn	Pentafluorophenylmethylene
BIAB	(Diacetoxiodo)benzene
Bt	Benzotriazole
C	Cytosine
Calcd	Calculated
Obsvd	Observed
Cbz	Benzyloxycarbonyl
CD	Circular Dichroism
CF/5(6)-CF	5(6)-Carboxyfluorescein
ch	Cyclohexyl
CHCA	α -cyano-4-hydroxycinnamic acid
cp	Cyclopentyl
DCC	Dicyclohexylcarbodiimide
DCM	Dichloromethane
DHB	2,5-dihydroxybenzoic acid
DIC	N,N'-diisopropylcarbodiimide
DIPEA	N,N-Diisopropylethylamine
DMAP	N,N-Dimethyl-4-aminopyridine
DMEM	Dulbecco's Modified Eagle Medium
DMF	N,N-dimethylformamide
DMSO	N,N-Dimethyl sulfoxide
DNA	2'-deoxyribonucleic acid
ds	Double stranded
EBA	Ethylbromo acetate
EDTA	Ethylene diamine tetraacetic acid
Et	Ethyl
EtOAc	Ethyl acetate
FACS	Fluorescence Activated Cell Sorter
FBS	Fetal bovine serum
Fmoc	9-Fluorenylmethoxycarbonyl
g	gram
G	Guanine
gly	Glycine
h	Hours
his	Histidine

HBTU	2-(1H-Benzotriazole-1-yl)- 1,1,3,3 tetramethyl-uronum-hexafluoro- phosphate
HOBt	N-Hydroxybenzotriazole
HPLC	High Performance Liquid Chromatography
HRMS	High resolution mass spectrometry
in situ	In the reaction mixture
in vivo	Within the living
IR	Infra-red
LC-MS	Liquid Chromatography-Mass Spectrometry
Lys	Lysine
mL	milliliter
mM	millimolar
mmol	millimoles
mp	melting point
MS	Mass spectrometry
MsCl	Mesyl Chloride
MW	Molecular weight
N	Normal
nm	Nanometer
NMR	Nuclear Magnetic Resonance
ONs	Oligonucleotides
p	Parallel
PCR	Polymerase chain reaction
Pd	Palladium
ppm	Parts per million
PPh ₃	Triphenylphosphine
PNA	Peptide Nucleic Acid
PS-oligo	Phosphorothioate-oligo
Rt	Retention time
RNA	Ribonucleic Acid
RP	Reverse Phase (-HPLC)
rt	Room temperature
RT	Retention time
S	Sinister
SAR	Structure Activity Relationship
SPPS	Solid Phase Peptide Synthesis
ss	Single strand/single stranded
T	Thymine
TEA/Et ₃ N	Et ₃ N/ Triethylamine
TEMPO	Tetramethylpiperidine 1-oxyl
TFA	Trifluoroacetic acid
Tf ₂ O	Triflicanhydride
TFMSA	Trifluoromethane sulfonic acid
THF	Tetrahydrofuran
TLC	Thin layer chromatography
TMSCl	Trimethylsilyl chloride
TBDMSCl	<i>tert</i> -butyldimethylsilyl chloride
<i>T_m</i>	Melting temperature
UV-Vis	Ultraviolet-Visible

Abstract of thesis

The thesis entitled “**Synthesis, Biophysical and Cellular Uptake Studies of Fluorinated Peptide Nucleic Acid Analogs**” comprises of studies on peptide nucleic acids which are fluorinated at different chemical sites. Nucleic acid therapeutics has emerged as effective technology for gene inhibition, but limited by susceptibility to cellular enzymes and poor cell uptake. Hence chemically modified nucleic acids have been used to resist degradation by the cellular enzymes. Peptide nucleic acids are a class of DNA analogs that are stable to cellular enzymes, but suffer from poor aqueous solubility and insufficient cell uptake. During the past two decades several PNA analogs have been reported to address their drawbacks. In the present work PNAs have been modified by substituting hydrogen with bioisosteric fluorine which is well known to increase lipophilicity and bioavailability. The different fluorinated PNA units were incorporated into PNA sequences site specifically using solid phase peptide synthesis protocol. The effect of fluorine on hydrophobicity was studied using HPLC, and their binding affinity to complementary DNA and RNA investigated by various biophysical techniques. This is followed by examining their cell permeation properties in different cell lines.

The thesis is divided into four chapters:

Chapter 1 gives an introduction to Peptide Nucleic Acids, encompassing the diversity of chemical modifications and their effect on biophysical and biological properties.

Chapter 2 describes the design, synthesis and characterization of various fluorinated PNA monomers and their site-specific incorporation into PNA sequences.

Chapter 3 reports on hydrophobicity studies and biophysical evaluation of fluorinated PNA oligomers.

Chapter 4 deals with cell permeation studies of fluorinated PNAs and their ability to form nanoparticles.

A.1 Chapter 1: Introduction to peptide nucleic acids

This chapter gives an overview on the background literature for the undertaking research work, emphasizing the recent advancements in the field of peptide nucleic acids. Watson and Crick unveiled the molecular architecture of DNA in 1953, where the two DNA strands are held together by specific hydrogen bonding pattern (A:T and G:C) to form antiparallel double helical structure. The base recognition is the central feature for the DNA hybridization and utilized in their various biological applications. The short oligonucleotide analogues can hybridize with the complementary mRNA in a sequence-specific manner via Watson-Crick

base pairing resulting in down-regulation of expression of target proteins through antisense mechanism. But for effective biological response, antisense oligonucleotides must be resistant to chemical or enzymatic degradation in cells and should be sufficiently absorbed from the site of administration, distributed to various tissues, should possess sufficient residence time and concentration at the site of action.

In order to meet the above requirements of a successful medicinal agent, it is necessary to chemically modify the natural structure of DNA in a suitable manner. This chapter presents a survey of the literature in the area of nucleic acid therapeutics. It focuses on the attempts done in the last few years to optimize the properties of oligonucleotides through chemical modifications. One such DNA mimic is the Peptide Nucleic Acid (PNA), first introduced by Nielsen *et al* in 1991, which has high binding affinity and specificity towards their complementary DNA/RNA and are resistant to hydrolytic enzymes like proteases and nucleases. These exceptional properties of PNAs are a favourable attribute for their applications as gene therapeutic agents with important advantages for genetic diagnostics and molecular biology. In spite of having many advantages, peptide nucleic acids suffer from a few drawbacks like low water solubility, poor cell permeability and ambiguity in orientational binding. In this regard, PNA has been chemically modified to improve their properties to some extent. The effect of the different structural modifications on biophysical and biological properties of PNA is overviewed in this chapter to rationalise the aims of the present work, on fluorinated PNAs.

A.2 Chapter 2: Design, Synthesis and Characterization of Fluorinated PNA Monomers and Their Oligomerization

The objective is to address the major limitation of inefficient cell permeability with rationally designed fluorinated PNA analogs. This chapter deals with the introduction of fluorine in peptide nucleic acid at various positions. It is well known in literature that introduction of fluorine in a molecule modulates its physicochemical properties like lipophilicity, acidity, basicity, hydrogen bonding etc. More than 20% of drugs in market have at least one fluorine atom suggesting the importance of fluorine in medicinal chemistry. The special properties of fluorine collectively may lead to increase the cell permeability and bioavailability of the fluorinated PNA analogs compared to corresponding non-fluorinated PNAs. In this context, the work in this chapter demonstrates different ways to incorporate fluorine in PNA at various sites. They include, modifications on nucleobase, in the side chain and on backbone to generate fluorinated PNA analogs (Figure 1).

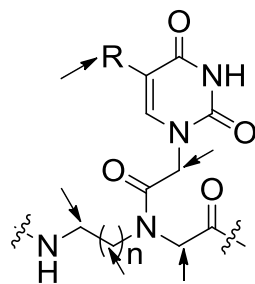


Figure 1 Possible sites for fluorination.

A.2A Section 2A: Synthesis and Characterization of Fluorinated and Control PNA Monomers

This section describes the synthesis of designed fluorinated PNA monomers and their characterisation using appropriate spectroscopic techniques.

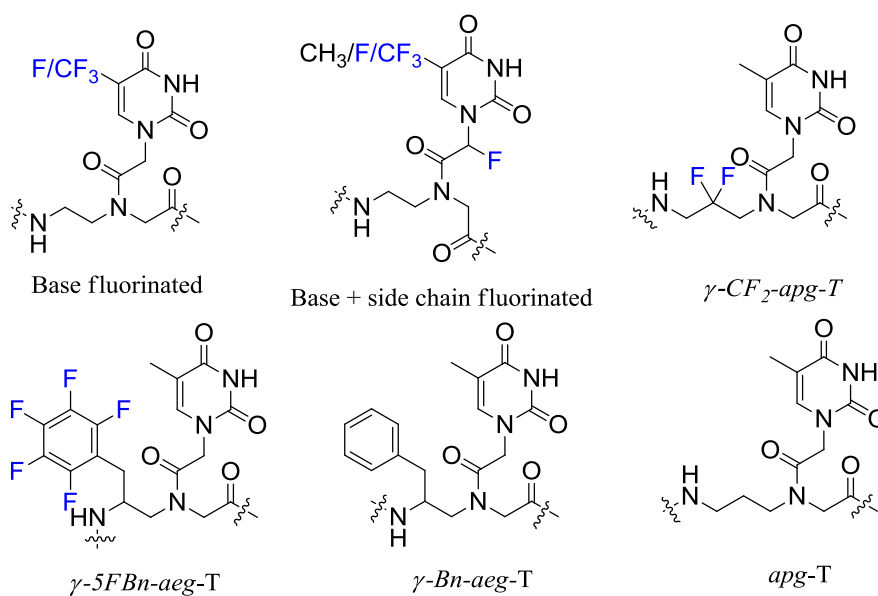
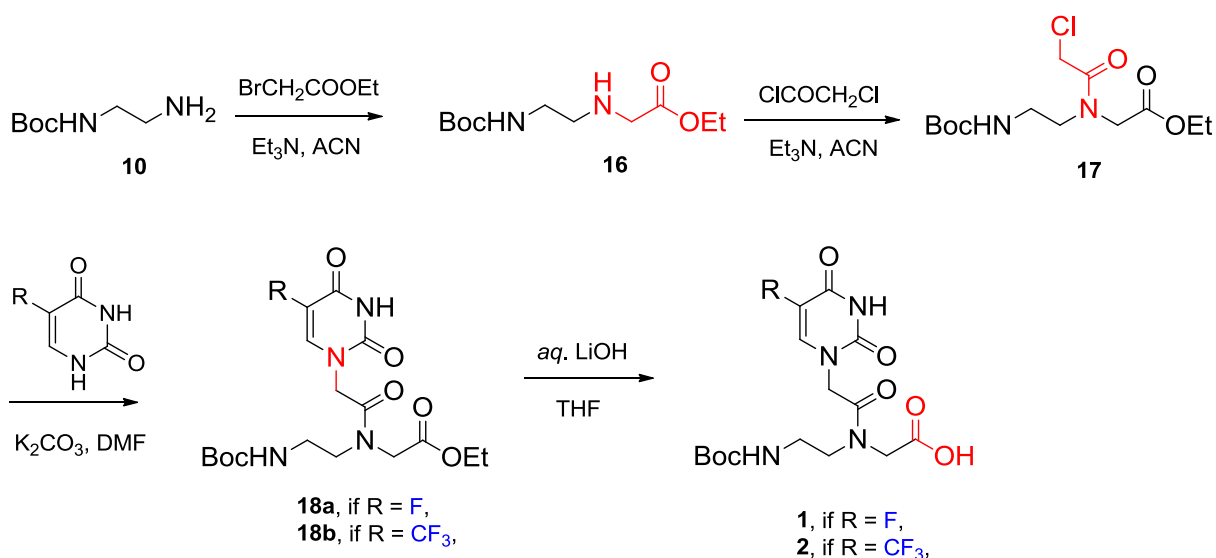


Figure 1 Fluorinated and their control non-fluorinated PNA units

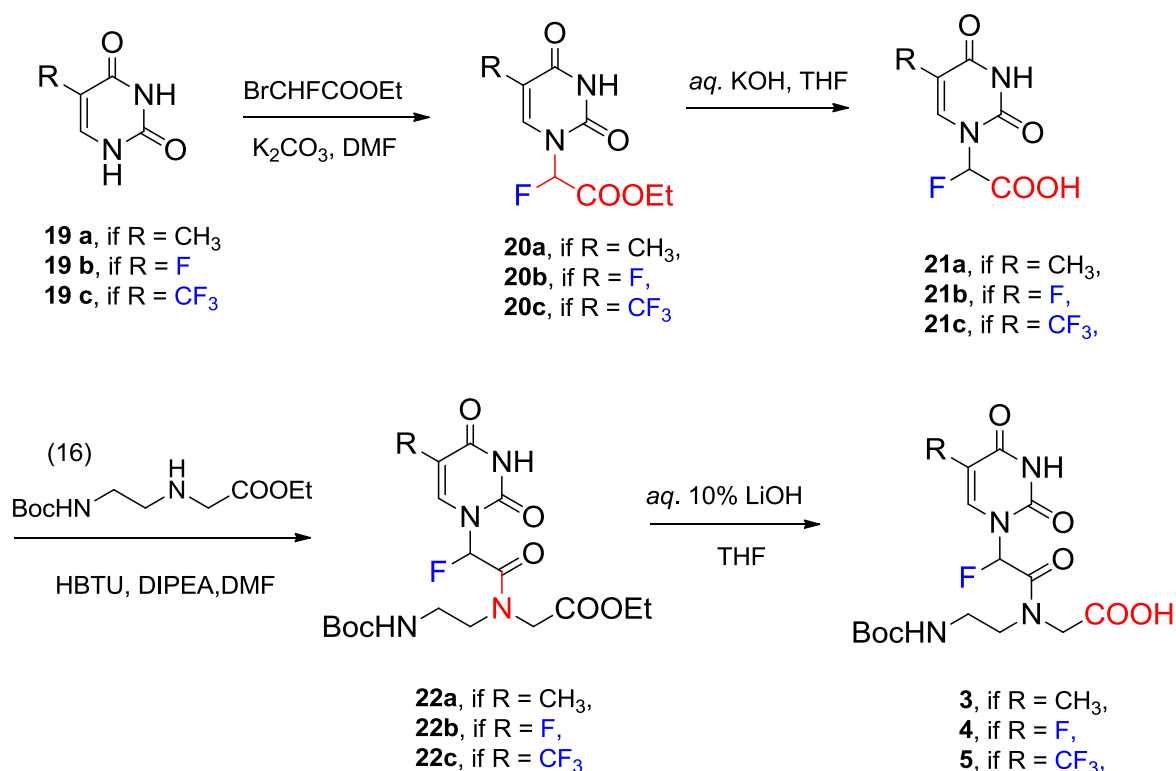
Scheme 1 Synthesis of nucleobase modified (5FU-aeg, 5CF₃U-aeg) PNA monomers

The Boc-protected ethylenediamine **10** was N-alkylated with ethyl bromoacetate to compound **16** (Scheme 4) which was N-acylated with chloroacetyl chloride to give the chloro derivative **17**. This was coupled with 5(F/CF₃)-substituted uracil (5-FU and 5-CF₃U) to yield the ester **18a/b** and the ester was hydrolyzed to acid monomer **1** and **2** respectively.



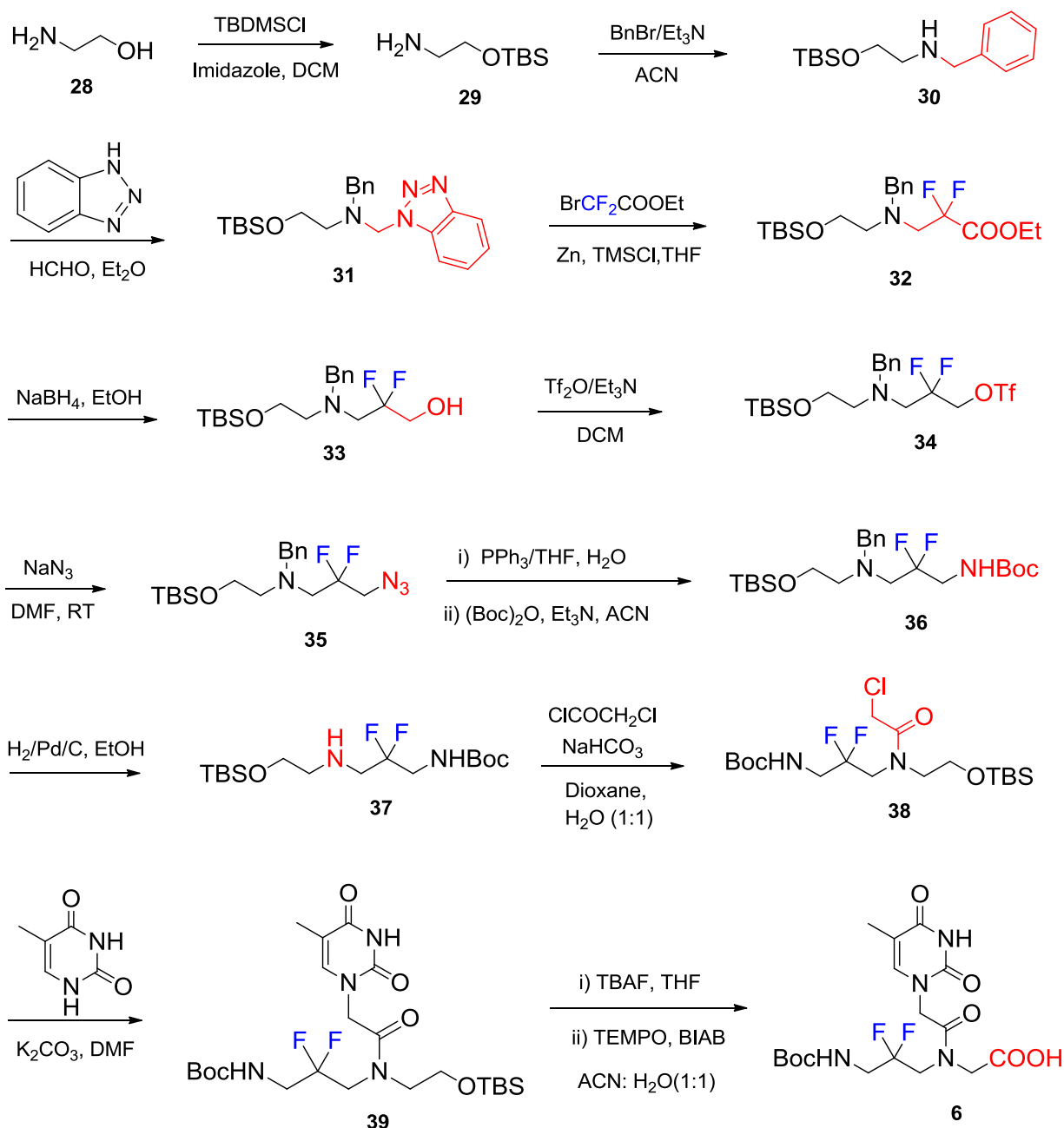
Scheme 2 Schematic representation of the synthesis of nucleobase plus side chain modified PNAs

The 5-substituted uracil nucleobases (5-methyluracil/5-fluorouracil/5-trifluoromethyl uracil) were individually treated with ethyl bromoacetate in presence of K₂CO₃ to obtain N¹-fluoroalkylated product **20a/b/c** respectively. These were hydrolyzed to corresponding acid compounds **21a/b/c** followed by coupling with N-Boc-2-aminoethyl glycine ethylester, to get the PNA ester monomers **22a/b/c**. The esters were hydrolysed to respective acids to obtain the desired fluorinated PNA monomers **3/4/5**.



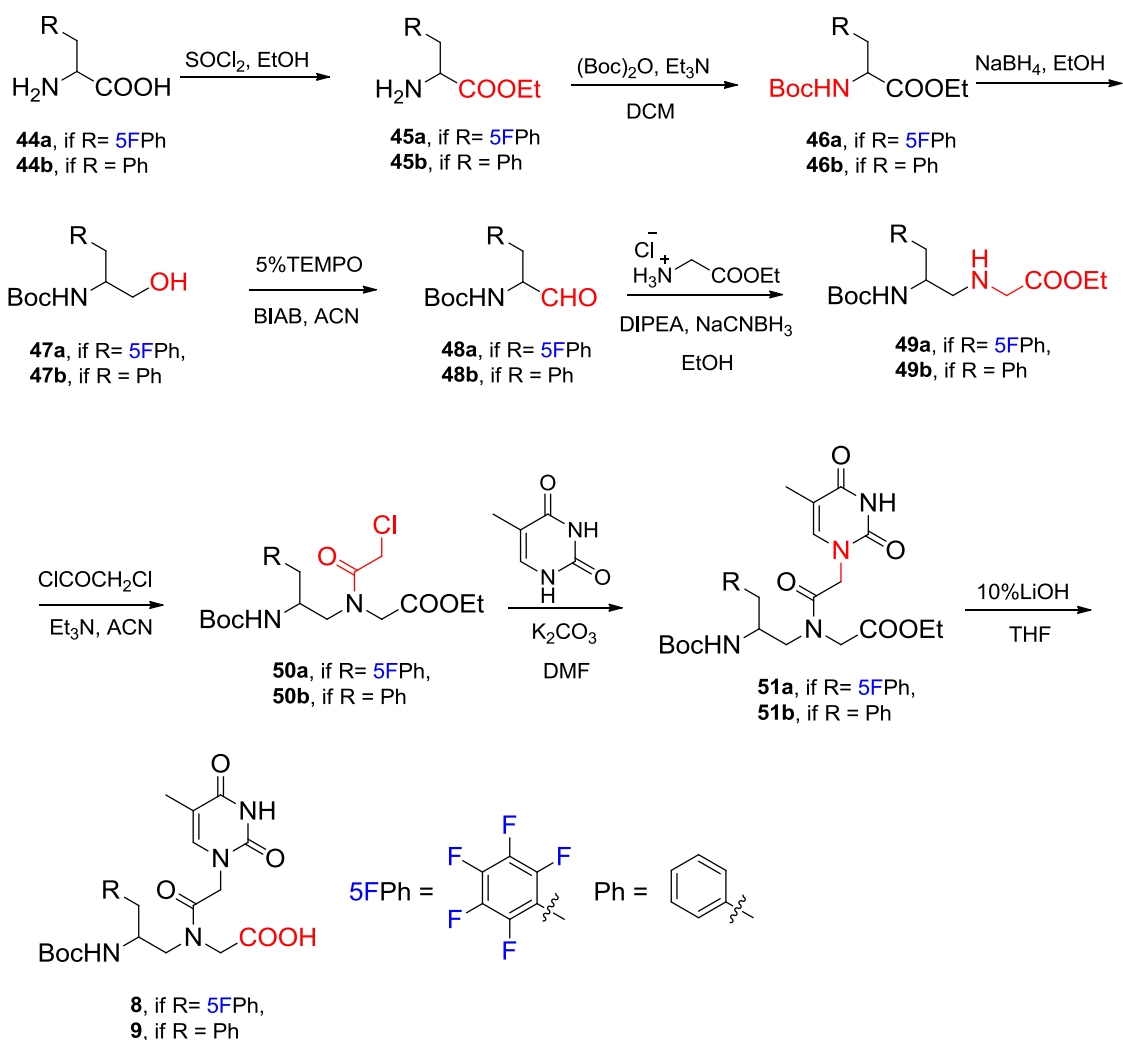
Scheme 3 Synthesis of backbone modified (γ -CF₂-apg) PNA monomer

Backbone modification: Synthesis of difluorinated γ -CF₂-apg PNA monomer **6** was done by reaction of ethyl bromodifluoroacetate under Reformatsky reaction conditions as a key step to get compound **32**. The ester in **32** was sequentially converted to amine through reduction, azidation and protected as NHBoc to afford **36**. The benzyl group of the compound **36** was deprotected under hydrogenation conditions, followed by N-acylation and coupling with thymine to give compound **39**. The silyl protecting group from compound **39** was removed selectively and further oxidation resulted in the γ -CF₂-apg PNA monomer **6**.



Scheme 4 Synthesis of backbone modified (γ -5F*Bn*-*aeg*, γ -*Bn*-*aeg*) PNA monomers

The introduction of methylene pentafluorophenyl group into PNA backbone was achieved starting from the commercially available pentafluoro D-phenylalanine **44a**. The acid and amine groups of the compound **44a** were protected as ester and –NH*Boc* respectively to obtain **46a**. Reduction of the ester to alcohol and subsequent oxidation of the alcohol gave aldehyde **48a**, which was coupled with glycine ethyl ester under reductive amination conditions to get **49a**. N-acylation of **49a** with chloroacetyl chloride and coupling with thymine resulted in the ester monomer **51a**, which was hydrolyzed to acid monomer **8**. Its control PNA monomer γ -*Bn*-*aeg* (**9**) was synthesized by employing similar methodology.



A.2B Section 2B: Solid phase Synthesis, Purification and Characterization of Fluorinated and Control PNA oligomers

A.2B.1 Synthesis of homooctamers

To demonstrate the lipophilic (hydrophobic) character of fluorinated PNA oligomers, homooligomers of various fluoro PNA monomers were synthesized. The sequence used for the study was H-TTTTTTTT-Lys and monomers used in the sequence were (*aeg-T*, *5FU-aeg*, δ -*F-5FU-aeg*, δ -*F-aeg-T*, *5CF₃U-aeg*, *apg*, γ -*CF₂-apg*; Figure 2). The homooligomers (octamers) were synthesized on a MBHA resin as solid support using HBTU/HOBt as coupling reagent, cleaved from resin and purified using reverse phase HPLC followed by characterization using MALDI-TOF spectrometry. The PNA sequences are shown in Table 1.

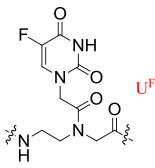
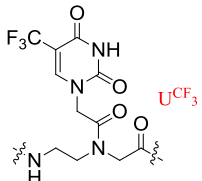
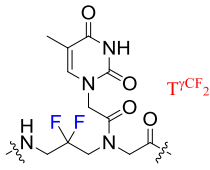
Table 1 Synthesis of homo oligomers

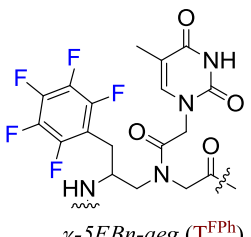
Sr. No.	PNA	PNA sequence	Monomer used
1	PNA 1	H-TTTTTTTT-Lys	<i>aeg-T</i>
2	PNA 2	H-T ^F T ^F T ^F T ^F T ^F T ^F T ^F T ^F -Lys	δ - <i>F-aeg-T</i>
3	PNA 3	H-U ^{CF₃} U ^{CF₃} U ^{CF₃} U ^{CF₃} U ^{CF₃} U ^{CF₃} U ^{CF₃} U ^{CF₃} -Lys	<i>5CF₃U-aeg</i>
4	PNA 4	H-U ^F U ^F U ^F U ^F U ^F U ^F U ^F U ^F -Lys	<i>5FU-aeg</i>
5	PNA 5	H-U ^F _F U ^F _F U ^F _F U ^F _F U ^F _F U ^F _F U ^F _F U ^F _F -Lys	δ - <i>F-5FU-aeg</i>
6	PNA 6	H-TTTTTTTT-Lys	<i>apg-T</i>
7	PNA 7	H-T ^{γCF₂} T ^{γCF₂} T ^{γCF₂} T ^{γCF₂} T ^{γCF₂} T ^{γCF₂} T ^{γCF₂} T ^{γCF₂} -Lys	γ - <i>CF₂ apg</i>

A.2B.2 Synthesis of mixed purine: pyrimidine PNA decamers

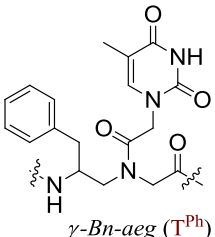
To study PNA:DNA/RNA duplex formation, mixed PNA decamers were synthesized by solid phase peptide synthesis protocol using Boc strategy (Table 2). The designed fluorinated PNA monomers were incorporated at specific positions in the *aeg* PNA sequence (PNA 8) using MBHA (4-methyl-Benzhydryl amine) resin as solid support. The fidelity of duplex formation of the fluorinated and their control PNA oligomers were tested using the complementary and mismatch DNA/RNA sequences.

Table 2 Synthesis of mixed purine:pyrimidine PNA oligomers

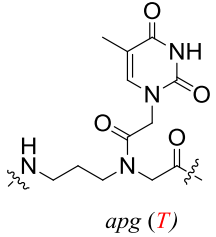
Sr.No.	Seq. code	PNA sequence	Fluorinated PNA oligomer
8	PNA 8	H-TTACCTCAGT-Lys	
9	PNA 9	H-TU ^F ACCTCAGT-Lys	
10	PNA 10	H-TTACCU ^F CAGT-Lys	
11	PNA 11	H-TTACCTCAGU ^F -Lys	
12	PNA 12	H-TU ^F ACCU ^F CAGT-Lys	
13	PNA 13	H-TU ^F ACCU ^F CAGU ^F -Lys	
14	PNA 14	H-TU ^{CF₃} ACCT CAGT-Lys	
15	PNA 15	H-TTACCU ^{CF₃} CAGT-Lys	
16	PNA 16	H-TTACCT CAGU ^{CF₃} -Lys	
17	PNA 17	H-TU ^{CF₃} ACCU ^{CF₃} CAGT-Lys	
18	PNA 18	H-TU ^{CF₃} ACCU ^{CF₃} CAGU ^{CF₃} -Lys	
19	PNA 19	H-TT ^{γCF₂} ACCTCAGT-Lys	
20	PNA 20	H-TTACCT ^{γCF₂} CAGT-Lys	
21	PNA 21	H-TTACCTCAGT ^{γCF₂} -Lys	
22	PNA 22	H-TT ^{γCF₂} ACCT ^{γCF₂} CAGT-Lys	
23	PNA 23	H-TT ^{γCF₂} ACCT ^{γCF₂} CAGT ^{γCF₂} -Lys	
24	PNA 24	H-TTACCTCAGT-Lys	
25	PNA 25	H-TTACCTCAGT-Lys	<i>apg-T (T)</i>
26	PNA 26	H-TTACCTCAGT-Lys	
27	PNA 27	H-T ^{FPh} ACCT ^{FPh} CAGT ^{FPh} -Lys	<i>γ-5FBn-aeg-T (T^{FPh})</i>
28	PNA 28	H-T ^{Ph} ACCT ^{Ph} CAGT ^{Ph} -Lys	<i>γ-Bn-aeg-T (T^{Ph})</i>



γ-5FBn-aeg (T^{FPh})



γ-Bn-aeg (T^{Ph})



apg (T)

All the modified PNA oligomers were purified by reverse phase-HPLC and characterized by MALDI-TOF mass spectrometry. The purified PNA oligomers were used for biophysical studies discussed in the next chapter.

A.3 Chapter 3: Biophysical Evaluation of Fluorinated PNA Oligomers

This chapter describes qualitative hydrophobicity studies of homooligomers, the thermal stability and sequence specificity of mixed purine-pyrimidine fluorinated PNA oligomers with their cDNA and cRNA.

A.3.1 Hydrophobicity studies

To examine the hydrophobic effects of replacing hydrogen with fluorine in a PNA oligomer retention times on reverse phase HPLC was used as a guide. The retention times of

all homooligomers on a reverse phase HPLC column were measured under identical conditions using a linear gradient method and the results were compared with their respective non-fluorinated control PNAs (Table 3). The fluorinated homooligomers showed higher retention times compared to the corresponding non-fluorinated control PNAs. The extent of hydrophobicity depends on the site of fluorine substitution and number of fluorines present in the PNA.

Table 3 Comparison of octamers retention times with respect to No. of fluorines present in the PNA

PNA	PNA sequence	No. of F's	Rt	ΔRt
PNA 1	H-TTTTTTTT-Lys	0	10.10	---
PNA 2	H-U ^{CF₃} U ^{CF₃} U ^{CF₃} U ^{CF₃} U ^{CF₃} U ^{CF₃} U ^{CF₃} U ^{CF₃} -Lys	24	17.7	7.6
PNA 3	H-T ^F T ^F T ^F T ^F T ^F T ^F T ^F T ^F -Lys	8	14.2	4.2
PNA 4	H-U ^F U ^F U ^F U ^F U ^F U ^F U ^F U ^F -Lys	8	10.0	---
PNA 5	H-U ^F _F U ^F _F U ^F _F U ^F _F U ^F _F U ^F _F U ^F _F U ^F _F -Lys	16	14.3	4.3
PNA 6	H-TTTTTTTT-Lys	0	11.0	---
PNA 7	H-T ^{γCF₂} T ^{γCF₂} T ^{γCF₂} T ^{γCF₂} T ^{γCF₂} T ^{γCF₂} T ^{γCF₂} T ^{γCF₂} -Lys	16	13.4	2.4

ΔRt is difference in HPLC retention time between modified and control PNA octamers

A.3.2 Biophysical evaluation of fluorinated PNA Oligomers

This section deals with the temperature dependent UV-spectroscopic studies to determine the thermal stability of fluorinated PNA oligomers with complementary DNA and RNA. The results of the thermal stabilities for the PNA oligomers are shown in Table 4. The specificity of these PNA oligomers was also investigated by challenging them to hybridise with a mismatch DNA/RNA carrying single base mismatch in the middle of the sequence.

The studies showed that the base fluorinated PNAs are binding to their complementary DNA/RNA, better with RNA compared to DNA (ΔT_m range of 1.1 to -13.3 °C in case of DNA and -0.4 to -17.8 °C in case of RNA). The base modified PNAs showed a slightly lower thermal melting (T_m) when compared to unmodified *aeg* PNA:DNA/RNA hybrids.

In case of backbone modified PNAs, γ -CF₂-*apg* PNAs binding with their complementary DNA and RNA and showed almost equal T_m values compared to their respective *apg* PNAs indicating that replacing hydrogen with fluorine does not alter the duplex stability much (Table 5). Thus fluorinated PNAs, although are more hydrophobic, they form hybrids with cDNA/RNA with insignificant change in their stability (except PNA 16)

Table 4 UV- T_m values of fluorinated PNA oligomers with complementary DNA and RNA

Entry	Seq. code	PNA sequence	DNA	ΔT_m	RNA	ΔT_m
			UV- T_m (°C)		UV- T_m (°C)	
1	PNA 8	H-TTACCTCAGT-Lys	48.6	---	60.6	---
2	PNA 9	H-TU ^F ACCTCAGT-Lys	49.7	1.1	60.2	-0.4
3	PNA 10	H-TTACCU ^F CAGT-Lys	45.9	-2.7	56.4	-4.2
4	PNA 11	H-TTACCTCAGU ^F -Lys	46.9	-1.7	58.5	-2.1
5	PNA 12	H-TU ^F ACCU ^F CAGT-Lys	44.3	-4.3	55.8	-4.8
6	PNA 13	H-TU ^F ACCU ^F CAGU ^F -Lys	45.0	-3.6	54.0	-6.6
7	PNA 14	H-TU ^{CF₃} ACCTCAGT-Lys	43.1	-5.5	58.1	-2.5
8	PNA 15	H-TTACCU ^{CF₃} CAGT-Lys	41.2	-7.4	50.2	-10.4
9	PNA 16	H-TTACCTCAGU ^{CF₃} -Lys	35.3	-13.3	42.8	-17.8
10	PNA 17	H-TU ^{CF₃} ACCU ^{CF₃} CAGT-Lys	45.9	-2.7	55.9	-4.7
11	PNA 18	H-TU ^{CF₃} ACCU ^{CF₃} CAGU ^{CF₃} -Lys	49.4	0.8	60.0	-0.6

ΔT_m indicates the difference in T_m of fluorinated PNA:DNA 1/RNA 1 and unmodified PNA 8:DNA 1/RNA 1; The values are accurate to ± 0.5 °C. DNA 1 = 3'AATGGTGTCA5', RNA 1 = 3'AAUGGTGUCA5'.

Table 5 UV- T_m values of backbone fluorinated γ -CF₂-apg PNAs

Entry	Seq. code	PNA sequence	DNA	ΔT_m	RNA	ΔT_m
			UV- T_m (°C)		UV- T_m (°C)	
12	PNA 19	H-TT ^{γCF₂} ACCTCAGT-Lys	50.6	---	60.0	---
13	PNA 21	H-TTACCTCAGT ^{γCF₂} -Lys	48.8	---	59.7	---
14	PNA 24	H-TTACCTCAG T-Lys	42.6	---	53.1	---
15	PNA 20	H-TTACCT ^{γCF₂} CAG T-Lys	38.2	-4.4	51.1	-2.0
16	PNA 25	H-TTACCTCAGT-Lys	42.1	---	49.1	---
17	PNA 22	H-TT ^{γCF₂} ACCT ^{γCF₂} CAGT-Lys	39.9	-2.2	48.3	-0.8
18	PNA 26	H-TTACCTCAGT-Lys	38.8	---	48.3	---
19	PNA 23	H-TT ^{γCF₂} ACCT ^{γCF₂} CAGT ^{γCF₂} -Lys	38.4	-0.4	47.9	-0.4

ΔT_m indicates the difference in T_m of γ -CF₂-apg PNA:DNA 1/RNA 1 and respective control apg PNA:DNA 1/RNA 1; The values are accurate to ± 0.5 °C. DNA 1 = 3'AATGGTGTCA5', RNA 1 = 3'AAUGGTGUCA5'.

A.4 Chapter 4: Cell Permeation Studies of Fluorinated PNAs and Nanoparticles

Formation of PNA:DNA/RNA Duplexes

In order to gain insight on cellular uptake properties of fluorinated PNAs, selected PNA oligomers (PNA 32-37) were tagged with 5(6)-carboxyfluorescein at the N-terminus of the PNA for visualization in the cells and are shown in Table 6. PNAs conjugated with fluorocarbon and hydrocarbon chain were synthesized for comparative evaluation of the effect of fluorine on cell uptake. Carboxyfluorescein was attached at the N-terminus of the sequence in order to ascertain the site of localization of the tagged PNAs within the cells.

Table 6 Carboxy fluorescein tagged and per-fluorocarbon/hydrocarbon chain linked PNA oligomers

Entry	PNA	PNA sequence
1	PNA 32-CF	CF-Lys-TTACCTCAGT-Lys
2	PNA 33-CF	CF-Lys-TT ^{γCF₂} ACT ^{γCF₂} CAGT ^{γCF₂} -Lys
3	PNA 34-CF	CF-Lys-TT ^{Ph} ACCT ^{Ph} CAGT ^{Ph} -Lys
4	PNA 35-CF	CF-Lys-TT ^{FPh} ACCT ^{FPh} CAGT ^{FPh} -Lys
5	PNA 36-CF	(CF, HCc)-LysTTACCTCAGT-Lys
6	PNA 37-CF	(CF, FAc)-LysTTACCTCAGT-Lys

The cell permeation ability of these modified PNA oligomers was investigated by live cell imaging in HeLa and NIH 3T3 cells using confocal microscopy. The confocal microscopy images showed that fluorinated PNA as well as respective control PNAs penetrate into both cell lines and the PNA oligomers were localized in the cytoplasm with some of the PNA cited in ER as indicated by experiments with ER tracker. The representative confocal microscopy images for cell permeation of three γ -CF₂-ap_g modified PNA in HeLa cells are shown in Figure 3.

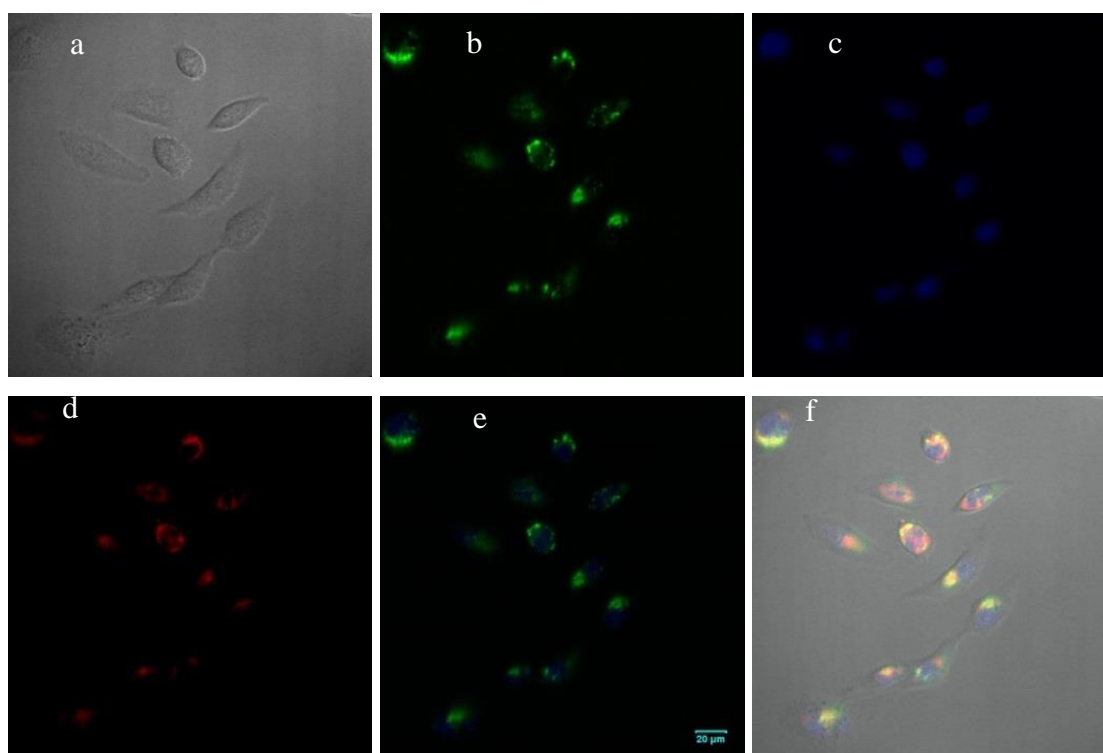


Figure 3 Confocal microscopy images for PNA 33-CF (a) bright field image of HeLa cells; (b) Green fluorescent image; (c) Hoechst 33342 stained image; (d) ER-red stained image and (e) Superimposed image of (b) and (c); (f) Superimposed image of (a) – (d).

The quantification of differential cellular uptake was carried out using fluorescence activated cell sorter (FACS) analysis. In this technique, the quantitative estimation of number

of percentage positive cells is possible and the extent of PNA taken by the cells reflected by the intensity of fluorescent signal. Thus, FACS data would provide quantitative estimation of cell permeability of the PNA oligomers. These studies with fluorinated PNAs showed that PNA modified with three units of γ -CF₂-apg showed remarkable increase in the efficiency of cell penetration in both cell lines used for the study.

Fluorocarbon chain attached PNA showed higher cellular uptake compared to corresponding hydrocarbon chain attached PNA in both the cell lines. Surprisingly the methylene-pentafluoro substituted γ -PNA showed a slight decrease in cell uptake efficiency as compared to corresponding non-fluorinated benzyl substituted γ -PNA. The FACS analysis data for NIH 3T3 cells shown in Figure 4 indicates the relative % positive cells that have taken up the PNA.

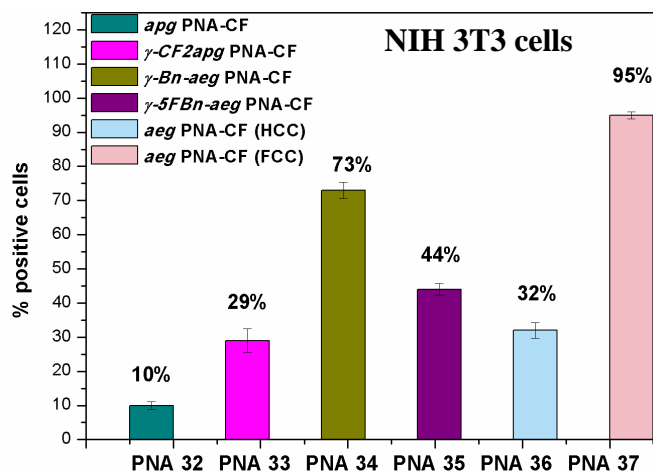


Figure 4. Comparative study of cellular uptake in terms of % percentage positive cells of fluorinated PNAs with their control non-fluorinated PNAs in NIH 3T3 cells.

A.4.1 PNA based Nanoparticles Formation and their Cell Uptake Studies

Nanoparticles are well known systems for drug delivery including that of nucleic acids. Self-assembling peptides organise into well-ordered nanostructures such as nano fibrils, nanotubes, nano spheres or vesicles, depending on the constituent peptide and environmental conditions during assembly and are used as drug delivery systems. It was surmised that the self-assembling and hydrophobic properties of peptides and the base pairing properties of nucleic acids present in PNA may synergistically lead to form nanostructures. With this idea, formation of nanoparticles from the hydrophobic PNAs derived from D-phenyl alanine and pentafluoro D-phenylalanine substitution at C_γ was studied with their complementary DNA/RNA using FESEM and DLS. The DNA/RNA duplexes derived from the hydrophobic γ -substituted PNAs form spherical assemblies (Figure 5). The cell uptake studies of the derived PNA:DNA/RNA duplexes were also studied using confocal microscopy. A

representative FESEM images of γ -*Bn-aeg* PNA:DNA and γ -*Bn-aeg* PNA:RNA at 2 μ M concentration are shown in Figure 5. It was observed that at low concentration of 2 - 10 μ M, these formed nanoparticles in the range of 50-300 nm while at higher concentrations (30 μ M), the nanoparticles grew into microspheres.

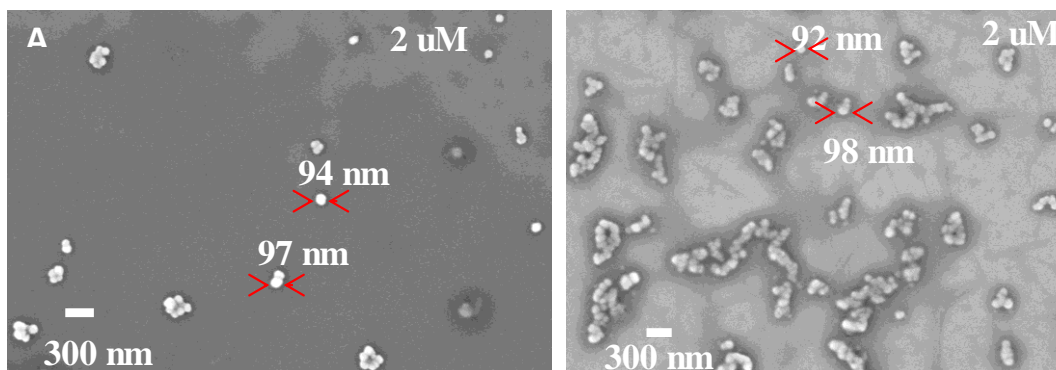


Figure 5 FESEM images of (A) γ -*Bn-aeg* PNA:DNA and (B) γ -*Bn-aeg* PNA:RNA.

A.5 Summary of thesis

- Rationally designed fluorinated and non-fluorinated control PNA monomers have been synthesized using commercially available fluorinated building blocks.
- Fluorinated PNA monomers were incorporated into *aeg* PNA sequence at desired positions by solid phase peptide synthesis protocol using Boc strategy. The synthesized PNA oligomers were purified by RP-HPLC and characterized by MALDI-TOF spectrometry.
- The thermal stability of fluorinated PNA oligomers with complementary DNA and RNA was investigated by temperature dependent UV-visible spectroscopy. The specificity of these PNA oligomers was also investigated by challenging them to mismatch DNA and RNA carrying a single base mismatch in the middle of the sequence.
- The effect of hydrogen substitution with fluorine in the PNA on the conformation of PNA:DNA/RNA duplexes was studied by CD spectroscopy.
- The cell permeation ability of 5(6)-carboxyfluorescein labelled PNA oligomers was investigated by live cell imaging using confocal microscopy.
- The quantification of cell penetration of fluorinated PNA oligomers was carried out by fluorescence activated cell sorter (FACS) analysis.
- The self-assembling properties of the hydrophobic PNA:DNA/RNA duplexes were studied using FESEM and DLS

Chapter 1: Introduction to Peptide Nucleic Acids

1.1 Introduction to Nucleic Acids

Nucleic acids play the most important role in the life of a cell. They store and transmit genetic information required for the execution of essential steps for survival and reproduction of cells: transcription to make RNA and translation to make proteins. Nucleic acids are polymers composed of monomeric units called nucleotides which consist of three components, a nitrogenous heterocyclic base (a purine or a pyrimidine); a pentose sugar; and a phosphate group (Figure 1.1). Nucleic acids can be differentiated into deoxyribonucleic acid (DNA) and ribonucleic acid (RNA) based on the consistent pentose sugar and the bases. DNA contains 2'-deoxyribose while RNA contains ribose. DNA is composed of the bases (Adenine (A), Guanine (G), Cytosine (C), and Thymine (T)) whereas RNA has bases A, G, C but uracil (U) instead of thymine (T) (Figure 1.1).

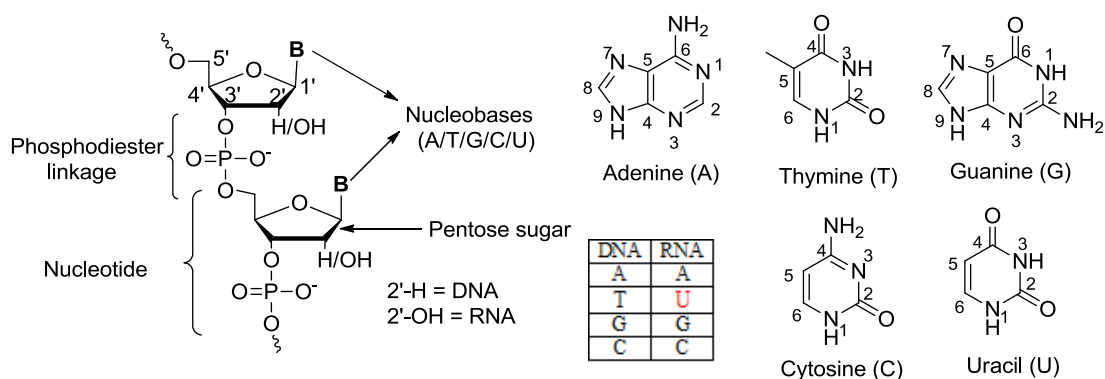


Figure 1.1 Chemical structures of components of DNA/RNA

A very rare exception is a bacterial virus called PBS1 that contains uracil (U) in its DNA.¹ Watson and Crick first proposed the molecular architecture of DNA to be composed of two helical chains each coiled around the same axis with a right handed twist.² The phosphodiester group joins the β -D-deoxyribose residues through 3'-5' linkage forming a helical chain where they are pointed to outside of the helix (Figure 1.2a). The two DNA strands are held together by specific Watson-Crick hydrogen bonding pairs A:T and G:C to form antiparallel double helical structure.

1.2 Base Pairing via Hydrogen Bonding

1.2.1 Watson-Crick hydrogen bonding

The chemical structure alone cannot credit for the unique properties of the nucleic acids. It was found in the first half of the 20th century that the amount of adenine in DNA is equal to the amount of thymine, and the amount of cytosine to that of guanine. This important discovery made perfect sense to Watson and Crick who proposed double helix structure for DNA to be formed from two nucleic acid strands bound in an antiparallel orientation.^{2a} The double helix is stabilized by hydrogen bonds between complementary nucleobase pairs A:T and G:C positioned inside the helices and sugar phosphates backbone on the outside. (Figure 1.2a). The ability of nucleic acids to form duplexes with their complementary counterparts is the key to the storage and transmission of the genetic information. The N-H groups of the bases are potent hydrogen bond donors while the electron pairs on carbonyl oxygen (C=O) and ring nitrogens of the bases are hydrogen bond acceptors. In Watson-Crick pairing, there are two hydrogen bonds in an A:T base pair and three in a C:G base pair^{2a} (Figure 1.2b).

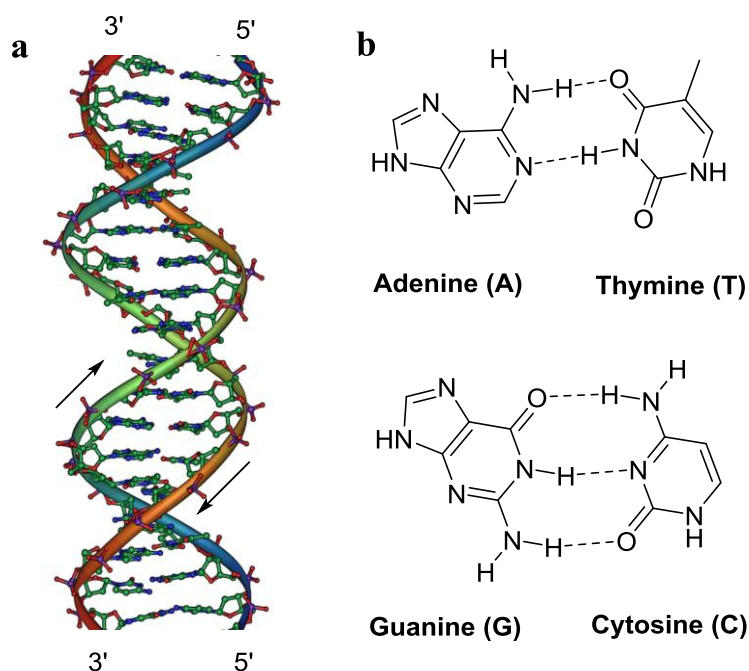


Figure 1.2 (a) DNA structure^{2b}; (b) Watson-Crick hydrogen bonding: A-T base pair and G-C base pair

While Watson-Crick base pairing is the dominant pattern between the nucleobases, other significant pairings are Hoogsteen (HG)³ and Wobble base pairings.⁴

1.2.2 Hoogsteen base pairing

In Hoogsteen base-pairing (Figure 1.3), thymine base can form two additional hydrogen bonds with adenine already engaged in Watson-Crick A:T base pair. Protonated cytosine can form two hydrogen bonds with guanine of Watson-Crick C:G base pair.

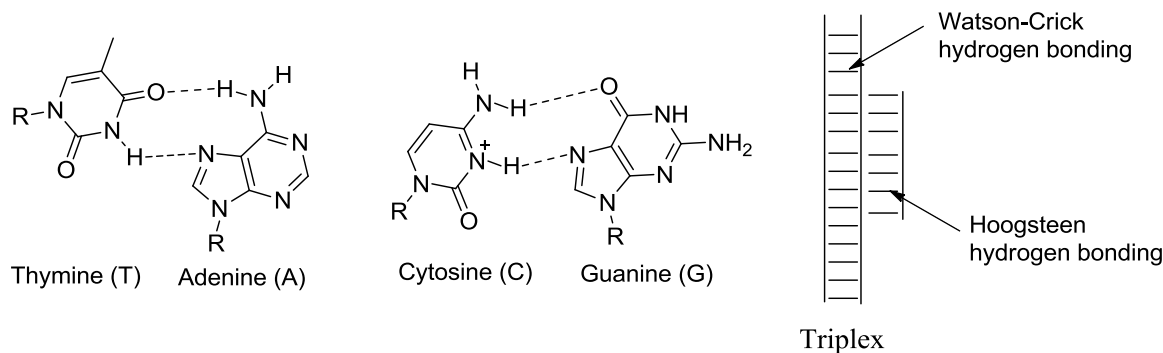


Figure 1.3 Hoogsteen hydrogen bonding; Triplex formation.

The third oligo pyrimidine strand present in a parallel orientation in the major groove of Watson-Crick purine: pyrimidine duplexes lead to formation of triple-helical structures.

1.2.3 Wobble base pairing

A purine base is able to recognize a non-complementary pyrimidine (e.g. G:U) through wobble base pairing which has importance in the interaction of messenger RNA (m-RNA) with transfer RNA (t-RNA) on the ribosome for codon-anticodon interactions during protein synthesis. Several anomalous hydrogen bonding patterns have been seen in X-ray studies of synthetic oligodeoxynucleotides⁵ (Figure 1.4).

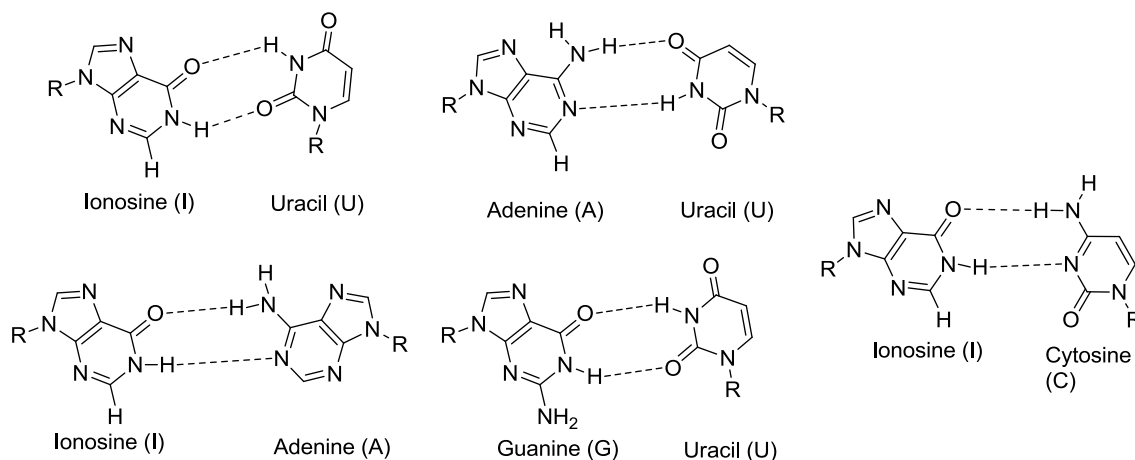


Figure 1.4 Wobble base pairing

1.3 Antisense Technology

The concept of base complementarity principle has led to development of many applications, mainly for therapeutic drugs and as diagnostic tools. The central dogma of biology is the flow of information from gene sequence to protein achieved by DNA replication to give daughter DNA strands which transcribe to RNA that translates into proteins⁶ (Figure 1.5a).⁷ When the sequence of a particular gene is mutated, it may subsequently lead to a disease causing protein. Designing a small drug molecule against the disease causing proteins requires structural knowledge of the protein and binding site. However, the base complementarity principle assists in designing a nucleic acid sequence (antisense strand) for a mutated RNA. Such a complementary strand (antisense strand) binds sequence specifically to the target strand (sense strand) and stops the translation process, so that the disease causing mutant protein cannot be expressed (Figure 1.5b).

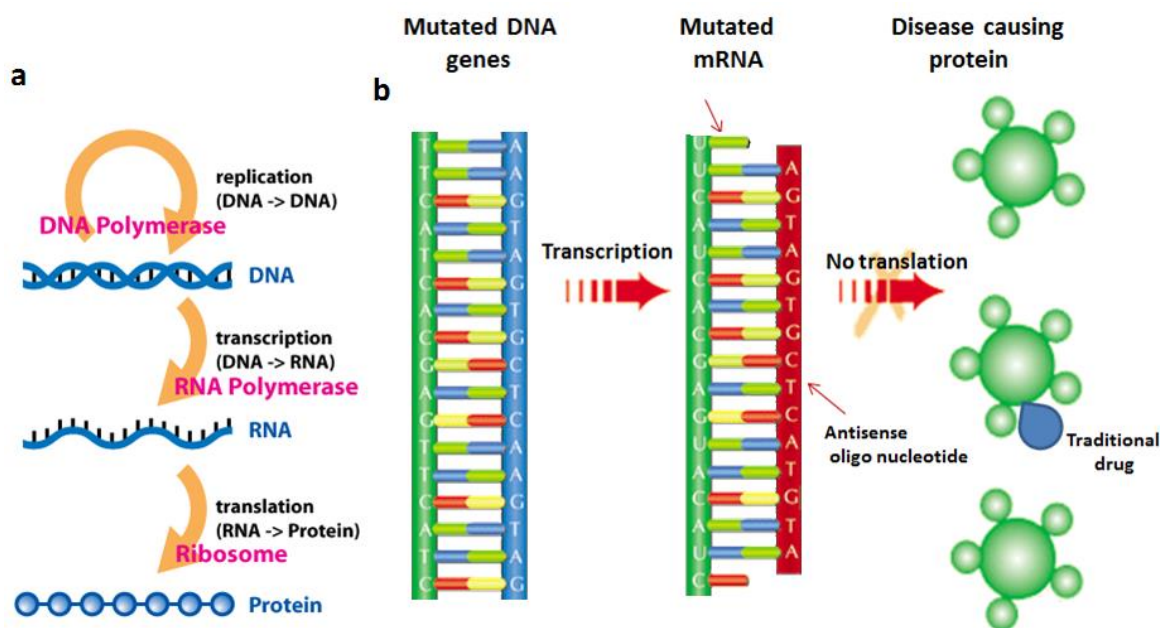


Figure 1.5 (a) Central dogma of biology; (b) Antisense technology.

Vitravene⁸ is the first FDA approved antisense drug developed by ISIS pharmaceuticals in 1998 for the treatment of cytomegalovirus (CMV) retinitis in AIDS patients. Mipomersen⁹ is the second FDA approved antisense drug which is a cholesterol-reducing drug candidate that targets the mRNA for Apo lipoprotein B. There are many antisense drugs which are in clinical trials at different phases some examples are tabulated in the Table 1.1.

Table 1.1 Examples of antisense drugs

Disease	Drug	Chemistry	Target	Clinical phase	Ref.
Retinitis	Fomivirsen	PS DNA	CMV IE2	Approved	8
Cardiovascular	KYNAMRO	2'-MOE, PS DNA	ApoB-100	Approved	9
DMD	IsisG Eteplirsen (AVI-4658)	PMO	Exon 51	Phase II	10
DMD	Drisapersen	2'-OMePS	Exon 51	Phase III	10
SMA	ISIS-SMNRx	2'-MOE	Exon 7	Phase II	10
Cancer	Custirsen	2'-MOE, PS DNA	Clusterin	Phase III	11
Antibacterial	---	PNA (CPP=KFF)3K	SD site	<i>in vivo</i> (Mice)	12
Antibacterial	---	PNA (CPP=KFF)3K	16S rRNA	<i>in vitro</i>	13

For successful antisense inhibition, specific Watson-Crick base pairing between an antisense oligonucleotide and its target mRNA is essential. Hence selection of an appropriate target site from the mRNA is crucial to the success of antisense effect. RNAs are single stranded molecules, known to fold into secondary structures, rendering most of the RNA inaccessible to intermolecular base pairing with antisense DNA. The design of an effective antisense oligonucleotide is hence a formidable technical challenge. However, there are several computational and experimental methods to design effective antisense oligonucleotide sequences.

1.4 Design of Antisense Oligonucleotides

Several design strategies have emerged in literature to design optimal oligodeoxynucleotide (ODN) antisense sequences.¹⁴ Random 'shot-gun' or sequence walking approach,^{15a} reverse transcription with random oligodeoxynucleotide libraries (RT-ROL),^{15b} mRNA accessible site tagging (MAST),^{15c} oligonucleotide arrays,^{15d} MALDI-TOF mass spectrometry based analysis,¹⁶ mRNA antisense-accessible sites library (MASL)¹⁷ are some of the techniques accessible to design effective antisense oligonucleotide sequences for target mRNA.

Antisense oligonucleotide sequences designed from these methods have shown high affinity and selectivity for the target mRNA *in vitro* and many of them are effective *in vivo* also.

1.4.1 Random 'shot-gun' or sequence walking approach

Synthetic oligonucleotides, normally around 50-100 are targeted to various regions of desired mRNA. The accessibility of the target site of these antisense oligonucleotides is measured based on their antisense activity. This method does not give an exhaustive picture of the accessibility of all possible sites on a target mRNA and only 2-5% of oligonucleotides are generally found to be good antisense reagents.^{15a}

1.4.2 MALDI-TOF mass spectrometry based analysis

MALDI-TOF mass spectrometry was used in the analysis of accessible RNA sites to antisense oligonucleotides and RNase H *in vivo*. First the RNase H mediated cleavage was performed on the full-length transcript (pre-mRNA) under native conditions, and then subjected the transcript for degradation in a sequence-specific manner by RNase T1. The produced sub small fragment RNAs are analysed using MALDI-TOF mass spectrometry.¹⁶

1.4.3 mRNA antisense-accessible sites library (MASL) method

The MASL method uses a modified reverse transcriptase random oligodeoxynucleotide (RT-ROL) assay. A random 9-mer oligodeoxynucleotide library terminating in a specific base X (T/G/A/C) on the 3'-end and a PCR tag on the 5'-end is prehybridized with an oligonucleotide complementary to the tag sequence and then allowed to hybridize with total mRNA transcript. This method mainly involves three steps:

1. Amplification of complementary DNA by target mRNA using specific forward PCR primers.
2. Amplification of resulting cDNA template by PCR tag using a reverse primer.
3. Electrophoretic separation of the products of these two processes on a denaturing gel.

The resulting PCR products assigned to specific sequences of the mRNA based on their size enables identification of the antisense-accessible sites after deducing the primer binding sites.¹⁷

1.5 Antisense Mechanism of Action

There are at least 4 well-known mechanisms to inhibit the translation function of the RNA and modulate the gene expression after the binding of oligonucleotide to the target RNA.¹⁸

1.5.1 RNase H dependent antisense mechanism

RNase H dependent antisense mechanism results in the cleavage of the targeted RNA by endogenous cellular nucleases, such as RNase H. RNase H is a ubiquitously expressed enzyme that cleaves the target RNA strand of an RNA-DNA heteroduplex.¹⁹ Synthetic single stranded oligonucleotides are transported across the plasma membrane and once they enter in the cytoplasm, single-stranded oligonucleotides rapidly accumulate in the cell nucleus, where they bind to their targeted RNA. The double stranded oligonucleotide/RNA duplex is recognized by RNase H as a substrate, cleaving the target RNA strand and releasing the antisense oligonucleotide (Figure 1.6). RNase H is also present in the cytosol, allowing the cleavage of the RNA in the cellular compartment as well.²⁰

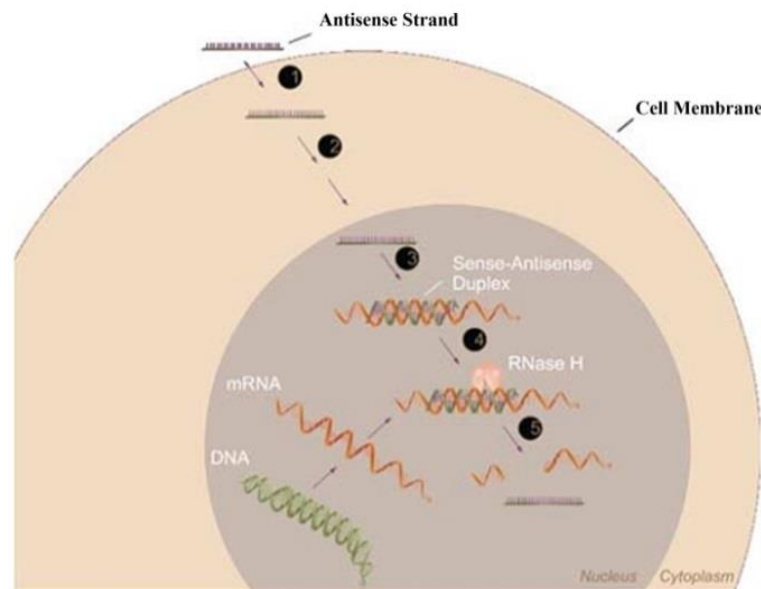


Figure 1. 6 RNase H dependent antisense mechanism²¹

1.5.2 siRNA dependent antisense mechanism

In RNA interference (RNAi) mechanism of action, a single-strand RNA molecule (siRNA) binds to the target RNA by Watson-Crick base pairing and recruits a ribonuclease complex that degrades the target RNA.²² However, in case of siRNA dependent antisense mechanism,

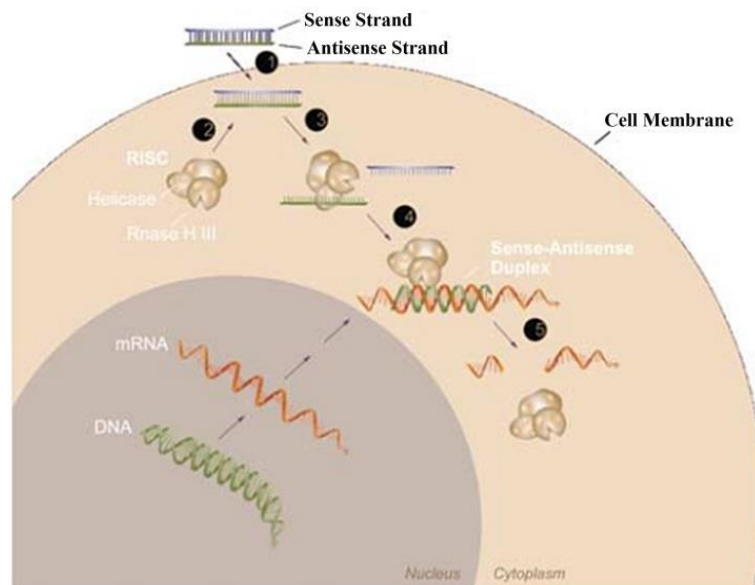


Figure 1.7 siRNA dependent antisense mechanism²¹

siRNA duplexes of 20-21 nucleotides long are directly transfected into mammalian cells and bind to a protein complex, called RNA-induced silencing complex (RISC). This has associated helicase activity that unwinds the two RNA strands facilitating the antisense strand to bind to the targeted RNA. The RISC also contains an endonuclease activity, which hydrolyses the target mRNA at the site where the antisense strand is bound (Figure 1.7).

1.5.3 Translation arrest

This is a steric blockage mechanism which physically inhibits the progression of the translation on ribosomal machinery. Oligonucleotides with right sequence bind to the translational initiation codon and to several other regions. Successful applications include inhibition of HIV,²³ vesicular stomatitis virus (VSV),²⁴ n-myc,²⁵ HBV²⁶ and a number of normal cellular genes.²⁷⁻³⁰ The oligonucleotides used for translational arrest must be RNase H resistant. Peptide nucleic acids (PNAs), morpholino oligonucleotides, methyl phosphonates, and 2'-O-methyl RNAs etc. have utility as RNase H independent oligonucleotides.

1.5.4 Splice correction

Splicing is a critical step in the processing of pre-messenger RNA (pre-mRNA) to mature RNA (mRNA) in eukaryotic cells, in which introns are removed and exons are joined by spliceosome, an enzyme associated with small nuclear ribonucleoproteins (snRNPs) (Figure 1.8). Aberration in splicing is caused by mutations in introns leading to defect proteins. In splice-correction strategy molecular manipulation of pre-messenger RNA for correct splicing

is engineered for therapeutic applications of genetic diseases. The mRNA is restored for right frame for translation process to yield a functional protein.³¹

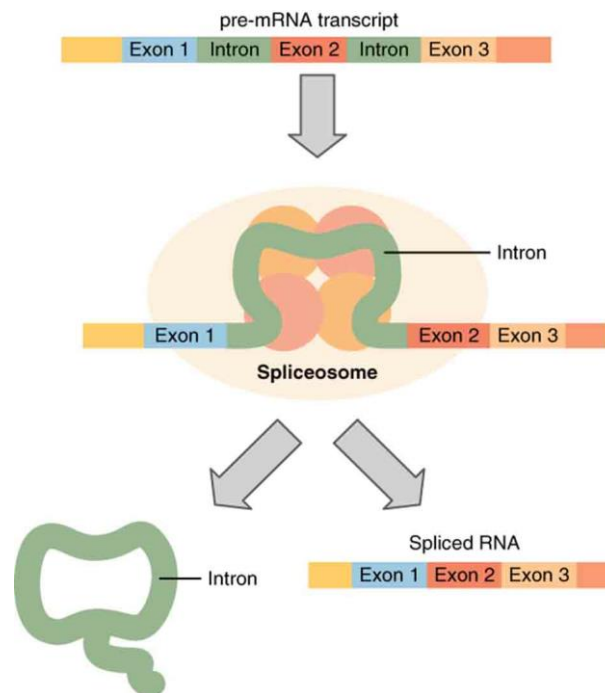


Figure 1.8 Splice mechanism

Restoration of gene activity can be accomplished by targeting the splice sites created or activated by several mutations with antisense oligonucleotides. Thus, modification of splicing by treatment with antisense oligonucleotides provides a potential alternative to gene therapy protocols involving the replacement of defective genes.³²⁻³⁵ This approach to novel therapies has been used for inherited diseases like cystic fibrosis,³⁶ β -thalassemia³⁷ and Duchenne's muscular dystrophy.^{38,39}

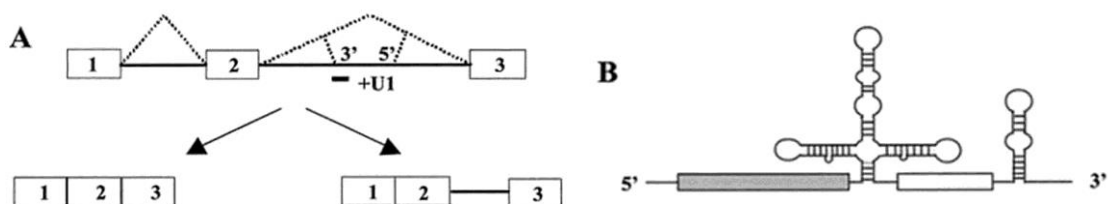


Figure 1.9 A) Schematic diagram of splice correction of IVS2-705 gene by modified U1snRNA (B).⁴⁰

1.6 Chemical Modifications of Nucleic Acids

For effective biological response, antisense oligonucleotides delivered must be sufficiently absorbed from the site of administration, distributed to various tissues and should possess sufficient residence time and concentration at the site of action. To be effective, the

oligonucleotides must be resistant to chemical or enzymatic degradation throughout this process. Unmodified nucleic acids are not stable in biological systems because of the ubiquitously present nucleases that cleave the phosphodiester linkage. They are also not efficient in entering the cell due to the negatively charged membrane as barrier. To address the combined tasks of improving the rate, affinity or specificity of oligonucleotide recognition, enhancing membrane permeability and resistance to nuclease digestion, several chemical modifications of DNA/RNA have been attempted. These chemical modifications can be broadly classified based on the site of modifications i) sugar and ii) sugar-phosphate backbone (Figure 1.10).

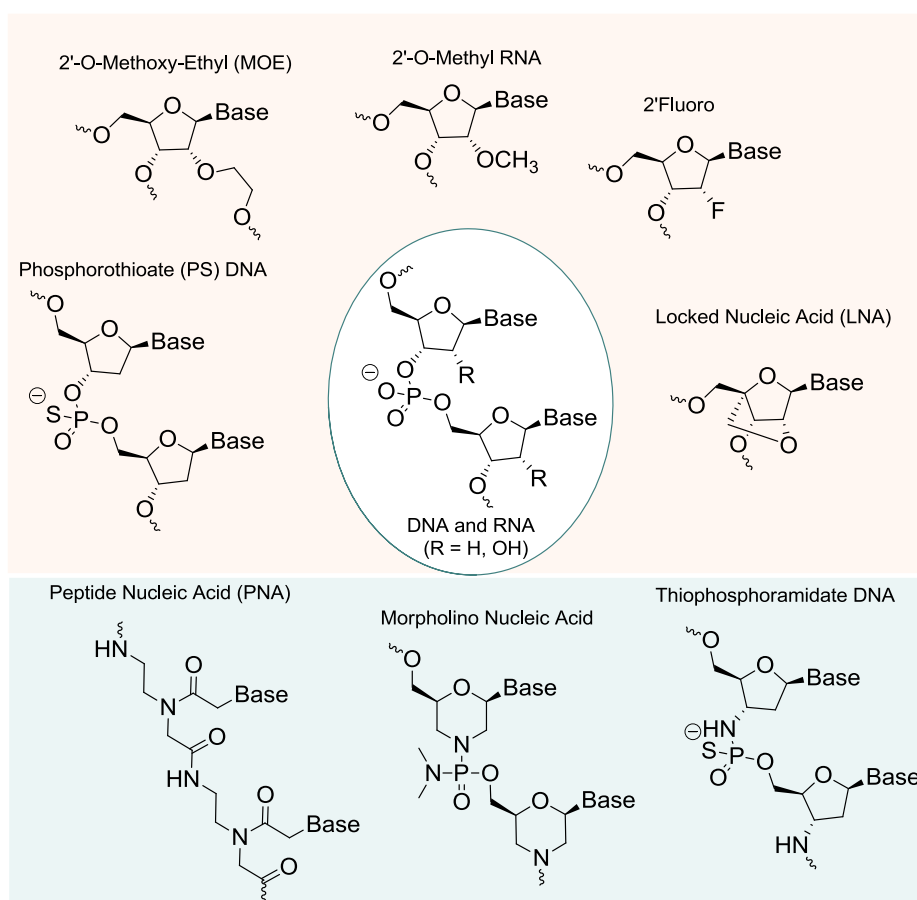


Figure 1.10 Examples of chemically modified antisense oligonucleotides⁴¹

1.6.1 Sugar Modifications

Nucleic acids modified at 2'-position of the sugar moiety have provided the most enhanced value in the drug like properties of the oligo nucleic acids. The 2'-sugar modification organises the sugar into 3'-*endo* puckered RNA like conformation which increases the binding affinity with complementary RNA sequences.⁴² This also enhances its nuclease resistance property, but unfortunately, almost all 2'-modified nucleic acids have less or no ability to

induce RNase H activity to cleave the target RNA strand. This drawback was addressed by the use of 2'-modifications through gapmer strategy where regions of 2'-modified nucleic acid residues flank a central DNA region of the oligonucleotide (Figure 1.11).

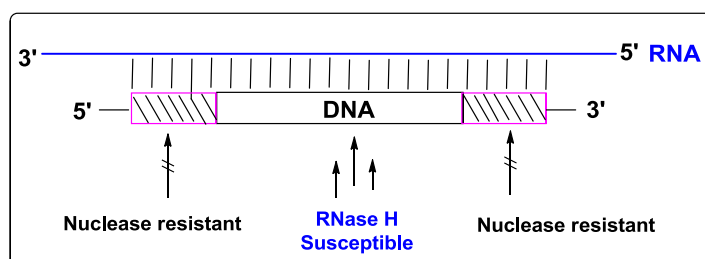
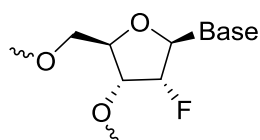


Figure 1.11 Gapmer strategy

The 2'-modified wings help to increase binding affinity and nuclease resistance, whereas the central gap region allows RNase H-mediated cleavage of the target RNA.

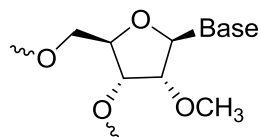
1.6.1a 2'-Fluoro ribonucleic acid



2'-Fluoro RNA

The more electronegative fluorine substituent at 2'-position of the sugar modulates the sugar conformation and thereby increases the binding affinity. Among all the 2'-class of modifications 2'-fluoro analogues imparted highest binding affinity for the target RNA designed for duplex siRNA oligonucleotides.⁴³⁻⁴⁵ This provides RNA duplexes with increased stability and potency to act *via* activation of RNAi pathway.⁴⁶

1.6.1b 2'-OMe ribonucleic acid

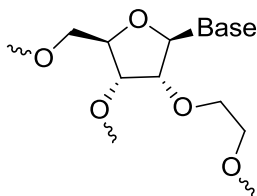


2'-O-Methyl RNA

2'-O-Methyl nucleosides have proved very useful in gapmer strategy for antisense oligonucleotides and these designs have advanced to human trials.⁴⁷ Bulkier modifications at 2'-position restrict the RNAi machinery for recognition of the antisense strand whereas the smaller 2'-O-methyl substitution is often well tolerated.⁴⁸ Minimal use of these nucleosides

has been employed to reduce the off-target effects to limit their ability to serve as microRNA agonists.⁴⁹

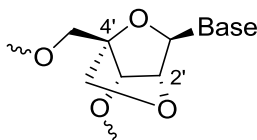
1.6.1c 2'-MOE-Ribonucleic acid



2'-O-Methoxy-Ethyl (MOE) RNA

The 2'-O-methoxyethyl (MOE) modification is one of the most advanced of the 2'-class of modifications and has entered into clinical trials for multiple indications. MOE increases resistance to nucleases and reduces nonspecific protein binding and reduced toxicity.⁵⁰ 2'-MOE substitution induces a C3'-*endo* conformation and in gauche orientation traps water of hydration shell around the adjacent phosphate residue. This increases the rigidity of the C3'-*endo* sugar conformation, organizing the oligonucleotide into an A-form geometry for increased binding affinity for the RNA. These attributes have translated the MOE-modified antisense drugs to enter in to the clinic.

1.6.1d Locked nucleic acid (LNA)



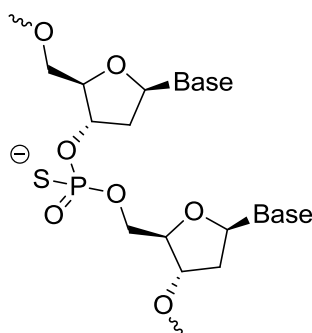
Locked Nucleic Acid (LNA)

The bicyclic modification LNA is a constrained analog of 2'-O-methyl RNA, where in the 2'-substituent is tethered to the 4'-C atom, enforcing a northern sugar pucker identical to that adopted by RNA in A-form.⁵¹⁻⁵⁴ LNA shows enhanced hybridization properties relative to a DNA:RNA duplex improving the nuclease resistance. LNA oligonucleotides do not support RNase H mechanism thus a gapmer strategy has been employed with LNA-modified oligonucleotides.⁵⁵ Optimally designed LNA-modified antisense drugs have shown better potency than other 2'-modifications.⁵⁶ LNA analogs have improved activity and/or toxicity profiles in animals.^{57,58} LNA offers attractive combination of properties, such as nuclease stability, high target affinity, potent biological activity and lack of acute toxicity with great potential as future antisense drugs.

1.6.2 Modifications of phosphate linkage

The phosphodiester linkage in oligonucleotide backbone is susceptible to nucleases. Hence the chemical modification of the backbone is an obvious target to improve the required nuclease resistance of antisense molecules. As a result, extensive medicinal chemistry research has focused on finding backbone modifications that increase the nuclease resistance and improve the affinity and specificity to the target RNA.

1.6.2a Phosphorothioate (PS) oligonucleotides

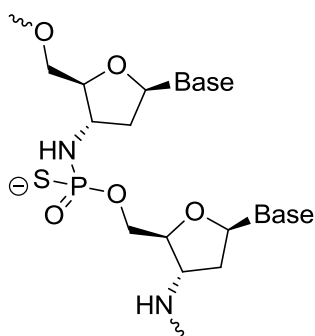


Phosphorothioate (PS) DNA

Phosphorothioate (PS)-containing oligonucleotides are designed by replacing one of the nonbridging phosphate oxygen atoms with a sulfur atom. The sulfur substitution offers several properties onto PS-oligonucleotides that are crucial for their use as systemic antisense drugs.⁵⁹ Foremost, the PS linkage is stable to nucleolytic degradation,⁶⁰ with sufficient stability in plasma, tissues, and cells to avoid metabolism prior to reaching the target RNA. PS-oligodeoxynucleotides are able to elicit RNase H dependent cleavage of the target RNA, and confer substantial pharmacokinetic benefit through increased binding to plasma proteins. This prevents rapid renal excretion and facilitate uptake to tissues. PS modification in combination with other is the most successful modification to date in oligonucleotide therapeutics.⁶¹⁻⁶⁵

1.6.2b N3'--->P5' Phosphoramidate oligodeoxynucleotides

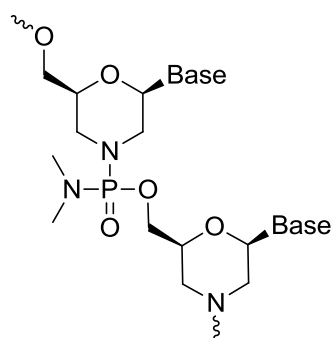
In N3'--->P5' Phosphoramidate oligodeoxynucleotides the 3'-oxygen in the deoxyribose ring is substituted with a 3'-NH-group.⁶⁶



Thiophosphoramidate DNA

These phosphoramidates exhibit high binding affinity toward the complementary RNA and possess nuclease resistance.⁶⁷ Thiophosphoramidate analogs designed by introducing sulfur in place of one of the nonbridging oxygen atoms show higher binding affinity with complementary RNA and have higher stability to acid upon incorporation into oligonucleotides.⁶⁸ Substitution of the phosphodiester linkage with groups such as amides,^{69,70} hydroxylamines,⁷¹ and acetals^{72,73} has been done to maintain or increase the binding affinity, but no improvements over the phosphorothioate backbone have been demonstrated.

1.6.3 Morpholino oligonucleotides



Morpholino Nucleic Acid

Morpholino oligonucleotides have been devised by replacing furanose ring of the DNA with morpholine ring and phosphate backbone with neutral phosphorodiamidate linkage. Because the morpholino oligonucleotides are neutral, their binding affinity is similar to DNA:DNA duplexes and are stable to nucleases. However, they lack ability to activate RNase H and are primarily used in translation arrest or other steric blocking mechanisms. Morpholino oligonucleotides have shown promise for modulating splicing and translation arrest.⁷⁴⁻⁷⁶

1.7 Peptide Nucleic Acids (PNAs)

1.7.1 Introduction

Peptide nucleic acids (PNAs) are radically a different class of nucleic acid analogs pioneered by Buchardt and Nielsen in 1991.⁷⁷ PNAs are DNA analogs where the negatively charged sugar phosphate backbone is replaced with a pseudo peptide backbone (2-aminoethyl-glycine unit) and the nucleobase is attached to the backbone through a conformationally rigid tertiary acetamide linker group. (Figure 1.12) The PNA backbone is constituted by six atoms distance for each repeating unit which is conserved with backbone distances in DNA.⁷⁸ The inter nucleobase distance in PNA are same as in DNA which allows its binding to the target DNA and RNA sequences by obeying Watson-Crick base pairing rule.^{79,80} Since the PNA backbone is neutral in nature, the duplex stability of PNA:DNA is stronger than that of DNA:DNA duplexes, due to absence of interstrand electrostatic repulsion. PNAs are highly specific to their complementary sequences being very sensitive to mismatch in base pairing, with single mismatch base pairing resulting in a reduction of T_m value of 8-20 °C.⁸¹

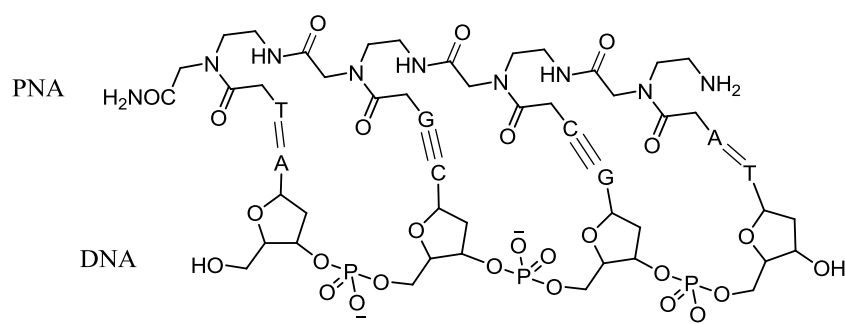


Figure 1.12 Schematic diagram of PNA:DNA duplex

In DNA:DNA duplexes the two strands are in an antiparallel orientation whereas PNA:DNA adducts can form either in antiparallel or parallel orientations (Figure 1.13), With the antiparallel orientation showing higher stability than parallel orientation.⁸²

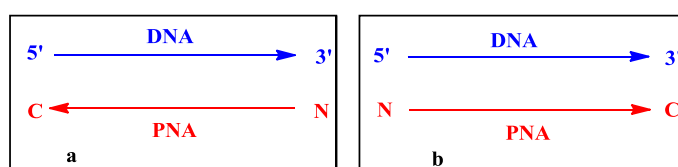


Figure 1.13 Antiparallel and parallel modes of PNA:DNA duplex

PNAs being neither true peptides or nucleic acids are resistant to degradation by both nucleases and proteases, but do not activate RNase H. Hence, they are suitable primarily for

translation inhibition⁸³ and splicing modulation antisense mechanisms.⁸⁴⁻⁸⁶ However, the DNA/PNA chimeras are capable of stimulating RNA cleavage by RNase H *via* formation of chimeric- RNA duplex. RNA cleavage occurs at the ribonucleotides which base pair with the DNA part of the chimera but not PNA part of the chimera (Figure 1.14).⁸⁷

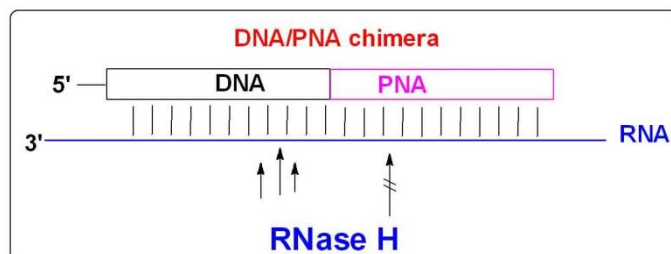


Figure 1.14 PNA/DNA chimera

1.7.2 Secondary structure formation of PNA with DNA/RNA

1.7.2a Strand invasion by PNA

The unique property of PNAs to displace one strand of *dsDNA* to form strand invasion complexes, is a favourable attribute for their application as gene therapeutic agents and will have important implications in gene diagnostics and molecular biology. Homopyrimidine PNAs can invade *dsDNA* to form PNA₂:DNA triplex structures and purine rich PNAs can also invade *dsDNA* *via* PNA:DNA duplexes through Watson-Crick base pairing principle (Figure 1.15a).⁸⁸ Mixed purine-pyrimidine PNA sequences do not provide sufficient free energy to invade *dsDNA*, however, the required free energy can be gained if both DNA strands are targeted simultaneously. Two PNAs or oligonucleotides, complementary to each other would quench each other by forming a stable duplex. This problem was solved by Nielsen *et al.*⁸⁸ using modified nucleobases (2,6-diaminopurine, thiouracil) that are pseudo complementary to each other. These modified nucleobases can recognize their natural A:T or G:C counterparts, but not be able to recognize each other due to steric clash between diaminopurine and thiouracil (see Figure 1.15b). They concluded that any sequence having at least 40% A:T content can be targeted by double duplex invading PNAs, and this would statistically cover more than 83% of all 10-mer targets.⁸⁹

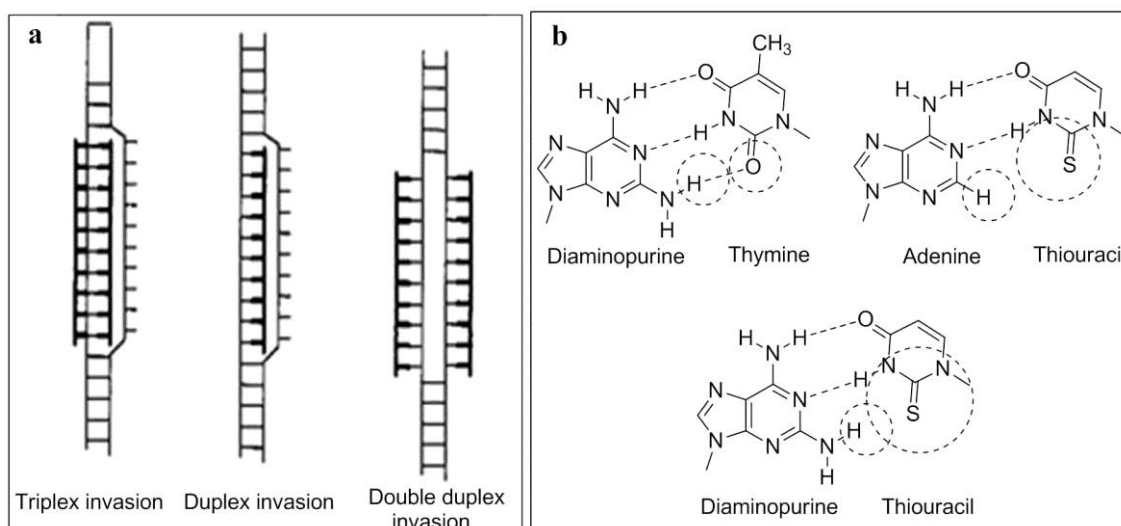


Figure 1.15 (a) Strand invasion by PNAs; (b) Schematic drawing showing extra hydrogen bonding between diaminopurine and thymine; and a steric clash between diaminopurine and thiouracil⁸⁹

The high affinity of PNA for DNA and RNA lead to form triplexes or quadruplexes through canonical Watson-Crick hydrogen bonding and Hoogsteen hydrogen bonding patterns.⁹⁰

1.7.2b Duplex and Triplex Formation by PNA

NMR and X-ray crystallography have been used to derive the three-dimensional structures of PNA:RNA,⁹¹ PNA:PNA,⁹² PNA:DNA duplexes,⁹³ and PNA₂:DNA triplexes.⁹⁴

PNA:DNA/RNA duplex: Brown *et al.*⁹¹ determined the structure of a PNA:RNA duplex with nuclear magnetic resonance. A hexameric PNA (H-GAACTC-NH₂) formed a 1:1 complex with a complementary RNA (5'-r(GAGUUC)-3') that is an antiparallel, right-handed double helix with Watson-Crick base pairing similar to the “A” form structure of RNA duplexes (Figure 1.16b).

Magdalena and Nielsen carried^{92a} out a ¹H-NMR study on 8-mer PNA (H-GCTATGTC-NH₂) and its complementary DNA 5'-d(GACATAGC)-3' and found that it forms an antiparallel duplex. The PNA:DNA duplex adopts conformation that has elements of both A- and B-form DNA, demonstrating the conformational flexibility of PNA. Recently, Ly *et al.*^{93c} reported the crystal structure of chiral γ -PNA with complementary DNA strand. The crystal structure is a uniquely preorganized γ -PNA:DNA duplex, containing a chiral PNA strand organized into a right-handed helix with a helical twist of 23.6 Å, a rise of 3.1 Å, and a pitch of 15 base-pairs per turn (Figure 1.16a).

PNA:PNA duplex: The crystal structure of PNA:PNA duplex revealed that PNAs prefer to form its own structure, termed P-form helix. The P-form helix constitutes a wide PNA duplex (28 Å diameter) with a large base pair helical displacement and pitch covering 18 base pairs. Also, the base pairs are displaced away from the P-form helix leaving a central tunnel in the helix (Figure 1.16c).

PNA₂:DNA triplex: Polypyrimidine PNAs are able to form stable PNA₂:DNA triplexes with complementary polypurine DNA through Watson-Crick and Hoogsteen hydrogen bonding.⁹⁴ The crystal structure of the triplex revealed that it is a P-form helix for PNA duplex (Figure 1.16d) with a large cavity along the helix axis and an average base displacement of 6.8 Å compared with 4.5 Å for A-form DNA. The deoxyribose sugars have a C3'-endo conformation with an average inter phosphate distance of 6.0 Å similar to A-form DNA. The relative orientation of the Watson-Crick (WC) strand is such that the NH₂-terminus of the PNA is aligned with the 3' end of the DNA strand (antiparallel orientation) consistent with studies of mixed base sequences and hairpin polypyrimidine PNAs.

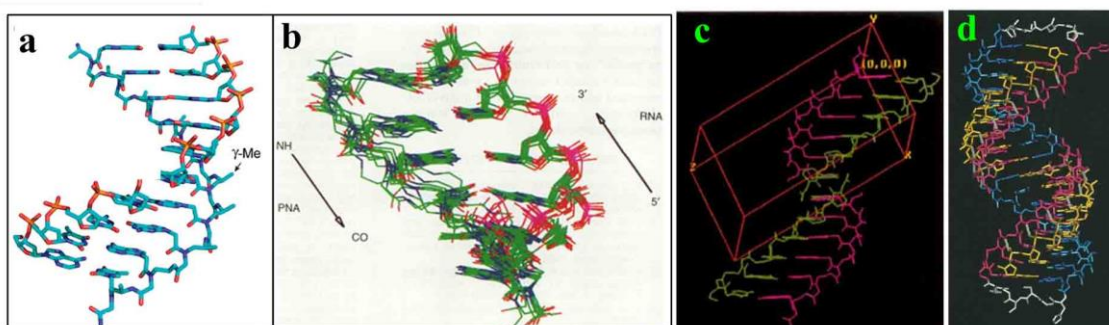


Figure 1.16 (a) Crystal structure of γ -PNA:DNA duplex;^{93c} (b) NMR model for PNA:RNA duplex;⁹¹ (c) Crystal structure of PNA:PNA duplex;⁹² (d) Crystal structure of PNA₂:DNA triplex.⁹⁴

The Hoogsteen (HG) strand of the PNA is antiparallel to the WC PNA strand parallel orientation to the DNA strand. These structures suggest that PNA can adapt well to its nucleic acid partners with high affinity and specificity.

1.7.2c Quadruplex and i-motif formation by PNA

DNA and RNA oligomers that contain multiple stretches of consecutive guanine (G) nucleotides are able to fold into a stable secondary structure known as G-quadruplex^{95,96} that is gaining increasing attention due to its implication in regulation of gene expression.⁹⁷ Balasubramanian *et al.*⁹⁸ have shown the formation of quadruplex composed entirely of PNA (Q-PNA) (Figure 1.17b). A homologous PNA (i.e., a PNA having the same sequence as the

target) forms a stable PNA₂:DNA₂/RNA₂ hybrid quadruplex by disrupting a bimolecular DNA/RNA G-quadruplex (Figure 1.17a).⁹⁹ Ganesh *et al.*¹⁰⁰ demonstrated the formation of C-C⁺ tetraplex (i-motif) with unmodified PNAs TC₄ and TC₈ in acidic pH. The tetraplex formation was monitored using UV-thermal melting at 295 nm, show a reverse sigmoidal pattern, which is characteristic of C-C⁺ tetraplex formation (Figure 1.17c).

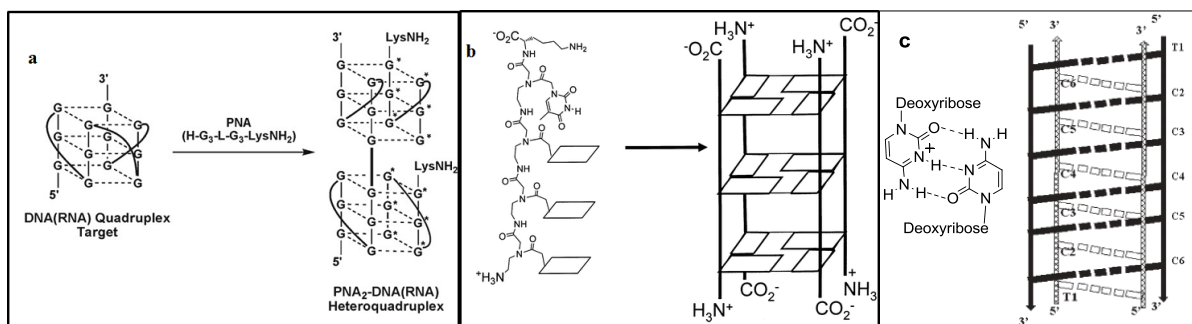


Figure 1.17 (a) Schematic drawing for PNA:DNA/RNA homologous quadruplex;⁹⁹ (b) Schematic diagram for PNA-Q⁴ quadruplex;⁹⁸ (c) Schematic diagram of i-motif formation¹⁰⁰

1.7.3 Solubility of PNA

PNA possesses neutral backbone and has poor water solubility compared with anionic DNA. The neutral PNA molecules have a tendency to aggregate, depending on the sequence of the oligomer. PNA solubility is related to the length of the oligomer and also to the purine/pyrimidine ratio.^{101,102} Some of the recent modifications, including the incorporation of positively charged lysine or guanidino residues have shown improvements in solubility of the PNA.^{103,104}

1.7.4 Cellular uptake of PNA

Although, PNA binds to complementary DNA and RNA with high affinity, specificity and stability in biological systems, the exploration of PNA as antisense or antigene agents has been hampered by their poor cellular uptake. Hence, efficient cellular delivery methods are required to develop PNAs as antisense and antigene drugs. PNA-peptide conjugates can be internalized into cells,¹⁰⁵ with the major fraction of the PNA localizing to endosomal compartments and not available for DNA/RNA targeting. Additives like calcium ions and chloroquine are used to release the PNA-peptide conjugates from endosome. However the potency of PNA-peptide conjugates improved to only a small extent and these exhibited pronounced toxicity.^{106,107} PNA suffers from other drawbacks like poor solubility, ambiguity

in orientational binding to its complementary sequence. To successfully address these problems, PNA has been chemically modified in many ways as described below.

1.7.5 Chemical modifications of PNA

The antisense antigene potential of PNAs can be improved by enhancing the binding affinity for DNA and RNA by suitable conformational preorganization. One approach for improving DNA binding affinity is the design and synthesis of preorganized PNAs that prefer a right-handed helical conformation which can be achieved by adding substituents to the backbone or by cyclization of the PNA backbone (Figure 1.18).^{108,109}

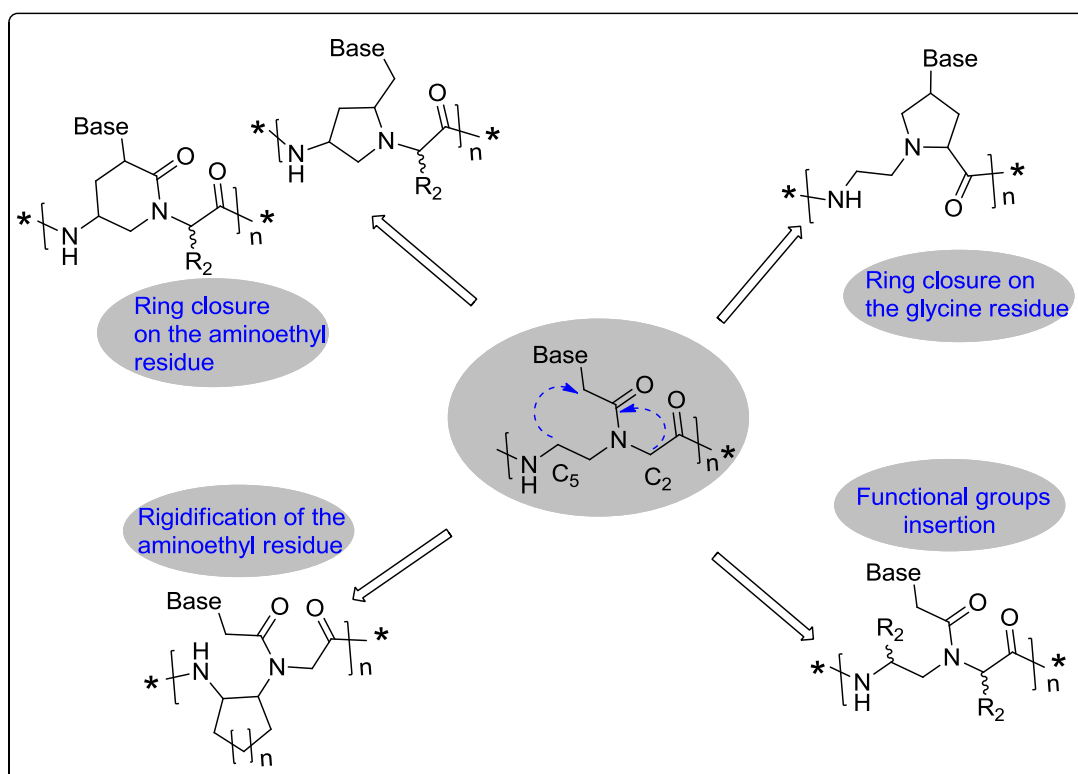


Figure 1.18 Strategies for inducing preorganization in the PNA structure

1.7.5a Preorganization of acyclic PNAs

The N-(2-aminoethyl) glycine unit in PNA backbone is a versatile motif for the modification of the PNA. Replacement of glycine by other α -substituted amino acids and substitution in ethylenediamine results in chiral PNAs that bear substituents at different positions (α , β , γ).

α -PNAs: The first α -PNAs were reported by Nielsen *et al.*¹¹⁰ in 1994, derived from both L and D alanine (Figure 1.19a). PNA:DNA duplex stability derived from D-alanine in PNA is almost equal to unmodified PNA whereas C α -substituted PNA derived from L-alanine drastically destabilised the duplex stability. PNAs derived from D-lysine (Figure 1.19b) in

place of glycine exhibited higher T_m than that from the corresponding PNA derived from L-lysine, with T_m more than that with unmodified PNAs.¹¹¹ C_α -substituted PNAs derived from D-amino acids prefer P-helix formation and mismatch discrimination ability is more than those of unmodified PNAs.¹¹² PNA oligomer containing three units of Lys-D-PNA and its peptide conjugate tested for cellular uptake ability, were found to be taken in most of the tested cells.¹¹³

D-Arginine in place of glycine leads to α -guanidinium PNAs (GPNAs, Figure 1.19c) that showed destabilization of the derived PNA:DNA duplex. However, incorporation of multiple α -guanidinium PNA units (α -GPNA) in a PNA decamer improved the binding affinity, partly from electrostatic interactions between guanidinium group and phosphates.¹¹⁴ C_α -PNAs with negatively charged side chains (derived from glutamic acid and aspartic acid) destabilized the PNA:DNA duplex stability due to electrostatic repulsions between negatively charged PNA backbone and polyanionic DNA backbone.¹¹⁵

C_α -substituted PNAs derived from α -amino acids having bulky side chains such as tyrosine, histidine, tryptophan, phenyl alanine and valine showed lower T_m values due to steric hindrance.¹¹⁶ 1-(2,2-Dimethylcyclobutyl)ethanone containing α -PNA (Figure 1.19e) showed almost equal binding affinity with DNA and RNA.¹¹⁷ Gem-dimethyl substitution at C_α increases the T_m of derived PNA:DNA duplexes,¹¹⁸ and the homologous aminopropyl-(α,α -dimethyl)glycine (*apdmg*) PNAs improved the binding affinity to DNA. These gem-dimethyl substituted PNAs have showed preferential binding to DNA than to RNA.

C_β -PNAs: In 2011, Sugiyama *et al.*¹¹⁹ reported the first C_β -substituted PNA bearing a methyl group at β -position using D and L enantiomers of alanine (Figure 1.19f). C_β -PNA oligomer derived from L-alanine showed similar binding affinity as that of unmodified *aeg* PNAs, whereas the corresponding C_β -PNA derived from D-alanine did not bind to DNA. Circular dichroism revealed that C_β -S-PNA exhibited a right handed helical structure whereas C_β -R-PNA exhibited left handed helical structure.¹¹⁹

properties considerably. The cellular uptake of a fully modified alternate C_γ -GPNA decamer by HeLa cells is comparable to that of TAT transduction domain. Recently, Manicardi *et al.*¹³¹ reported the inhibition of micro-RNA by GPNA carrying an arginine side chain. Anti-miR-210 activity of PNAs in leukemic K562 cells was examined using a series of modified 18-mer PNAs (α or γ , PNAs conjugated with arginine octamer and unmodified PNAs). The best anti-miR-210 activity was observed with γ -GPNAs with consecutive placement.

Ganesh *et al.*^{103,132} have reported the design and synthesis of chiral C_α - and C_γ -aminoethyl PNAs (*am*-PNAs) with substitutions in the PNA backbone (Figure 1.19 l and m). The *am*-PNAs formed stable PNA:DNA duplexes and the order of stabilization was, γ -(*S*)-*am*-PNA > α -(*R*)-*am*-PNA > α -(*S*)-*am*-PNA. The *am*-PNAs are taken up by HeLa cells, with the decreasing order of uptake efficiency as γ -(*S*)-*am*-PNA > α -(*R*)-*am*-PNA > α -(*S*)-*am*-PNA. Recently it was shown γ -GPNAs (Figure 1.19 n, n = 2) and γ -azido PNAs (Figure 1.19 o) that side chain lengths is important for hybridization with DNA. The guanidinium PNAs with shorter spacer chain increased the PNA:DNA duplex stability. These PNAs taken up in 3T3 and HeLa cells were visualized by confocal microscopy and quantified using fluorescence assisted cell sorter (FACS).¹⁰⁶ The azido functionality of C_γ -substituted methylene/butylene azido PNAs enable the attachment of multisite labelling and introduction of fluorophores in a single step through click reaction without any protection/deprotection steps. The azido fluorescent PNA oligomers have been shown to accumulate around the nuclear membrane in 3T3 cells.¹³³

1.7.5b Preorganization through cyclic PNAs

The PNA, being acyclic, is conformationally flexible and formation of ordered PNA:DNA/RNA complexes is accompanied by enthalpic advantage through hydrogen bonding and base stacking interactions, but has undesirable loss in entropy of the PNA strand.¹³⁴ A high rotation barrier is encountered in the interconversion of *cis* and *trans* rotamers around the tertiary amide linkage in PNA leads to different PNA:DNA/RNA hybridization kinetics in parallel and antiparallel hybrids.^{135,136} Ganesh *et al.*⁴¹ have synthesized many modified cyclic PNAs that can potentially preorganize PNA to form PNA:DNA/RNA complexes and achieved hybridization preferences (decreased loss in entropy) for either DNA or RNA complementation and parallel or antiparallel orientation.

Many strategies have been developed to enrich populations of single stranded PNAs that have the favourable, pre-organised conformation for binding to complementary

DNA/RNA. The preorganized conformers could trigger a shift in equilibrium toward the desired complexation because of the net reduced entropy loss upon complexation. The strategies to conformational preorganization are based on introduction of methylene/ethylene groups to bridge the aminoethyl-glycyl backbone and methylene carbonyl side chain to generate diverse five- or six-membered nitrogen heterocyclic analogues. Some of these strategies are described below in detail.

Aminoprolyl PNA (ap-PNA): 4(*R/S*)-aminoprolyl PNA synthesized by the introduction of a methylene bridge between β -carbon atom of the aminoethyl segment and the α' -carbon of the glycine segment on *aeg*-PNA backbone (Figure 1.20).¹³⁷ None of the homochiral aminoprolyl thymynyl PNAs corresponding to any of the diastereomers bound to target DNA sequences,¹³⁸ and this might be attributed to high rigidity in the backbone resulting in structural incompatibility.¹³⁹

Aminoethylprolyl PNA (aep-PNA): Chimeric aminoethylprolyl PNA (*aep*-PNA) analogues arise from connecting the glycine on backbone with side chain to give 4(*S*)-2(*SR*)-*aep*-T oligomers that showed strong and specific binding properties toward target DNA sequences.¹⁴⁰ The homooligomer *aep*-PNA-T8 with (*2R,4R*) stereochemistry displayed significant stabilization of the complexes with poly rA,¹⁴¹ while the adenine A8 homooligomer with (*2S,4S*) stereochemistry showed improved binding to the target DNA.¹⁴² Nucleobase dependent binding and orientation selectivity were observed with these analysis.

Aminoethylpyrrolidinone PNA (aepone-PNA): The aminoethylprolyl-5-one thymine (*aepone*) monomers contain cyclic amide and were incorporated into *aeg*-PNA-T8 backbone at different positions.¹⁴³ The *aepone*-PNAs showed remarkable stabilization of derived PNA₂:DNA triplexes compared to *aeg*-PNA.¹⁴⁴ The homooligomers of *aepone*-PNA T8 bound to the complementary 12-mer DNA more strongly than that of cRNA. This suggested that the structurally preorganized PNA can discriminate their binding efficacy to DNA over RNA.

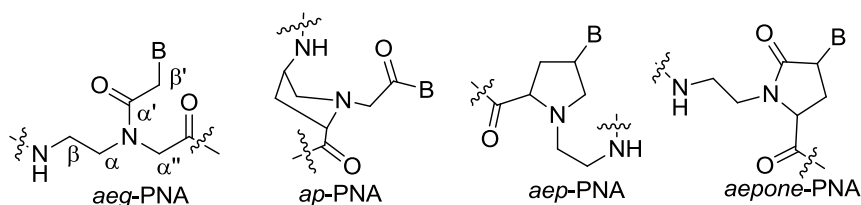


Figure 1.20 Cyclic PNAs: *ap*-PNA, *aep*-PNA and *aepono*-PNA

Pyrrolidine PNAs: Deletion of the *endo* cyclic carbonyl group in pyrrolidinone PNA gave the pyrrolidine PNA¹⁴⁵ (Figure 1.21a). The derived (2*R*,4*S*) stereomeric homo adenylate chimeric *aeg*-PNA oligomer formed a stable complex with both DNA and RNA.¹⁴⁶ The (2*R*,4*R*) version of this PNA analogue was shown to bind target DNA and RNA with high affinity and kinetic selectivity toward RNA.¹⁴⁷ (2*S*,4*S*) pyrrolidine PNA analogue, and its thymynyl oligomer resulted in a decreased binding efficiency with target DNA and RNA sequences.¹⁴⁸ PNA:DNA dimer prepared from (2*R*,4*R*) pyrrolidine PNA-T, which when placed in a PNA-DNA chimera lead to decreased DNA triplex stability.¹⁴⁸

Introduction of the α' - β -methylene bridge led to another pyrrolidine-PNA (Figure 1.21b)¹⁴⁹ having the nucleobase away from the pyrrolidine ring by one carbon. The (2*R*,4*S*) pyrrolidine-T monomer when introduced into the middle of the *aeg*-PNA-T8, bound to the target DNA better than the diastereomeric (2*S*,4*S*) PNA. This is an example of stereochemical discrimination effects in PNA:DNA recognition. The 4*R* pyrrolidine-T PNA sequences stabilized the PNA:DNA duplex with a significant difference in parallel/antiparallel binding compared to *aeg*-PNA:DNA duplexes,¹⁵⁰ while the PNAs with 4*S* modifications destabilized the duplexes without much parallel/antiparallel binding differences as compared to the unmodified hybrids. The enantiomeric pairs (2*S*,4*S*) and (2*R*,4*R*) formed antiparallel complexes with RNA much stronger than that of *aeg*-PNA or other diastereomers.

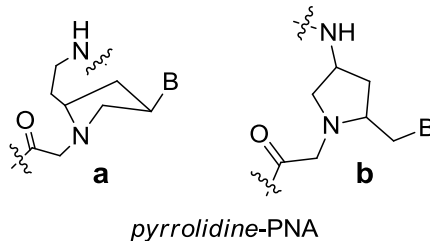


Figure 1.21 Pyrrolidine PNAs

Pipecolic and Piperidinyl PNAs: The pipecolyl PNA monomers (1 and 2) were synthesized by introducing a methylene, or an ethylene bridge between the C_{γ} - or C_{β} -carbon of the aminopropyl segment and the α'' -carbon of the glycyl segment into an aminopropyl-glycyl

PNA analogue (Figure 1.22) respectively.¹⁵¹ The modified PNA-T10 oligomer (*pip*-PNA-1) carrying the *trans* (2*S*,4*S*) monomer destabilized the PNA₂:DNA triplex formation. However, the homothymine mixed *aeg*-PNA sequences incorporating the 5-aminopipercolyl unit (*pip*-PNA-2) form stable complexes with target DNA oligomers.

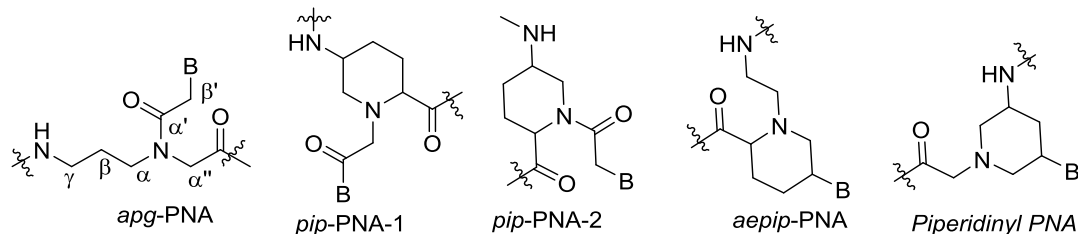


Figure 1.22 Pipercolic and Piperidinyl PNAs¹⁵¹

The chiral six-membered analogues (2*S*,5*R*) *aepip*-PNA and the *trans* (3*S*,5*S*)-piperidinyl PNA-T upon incorporation into the *aeg*-PNA-T8 homooligomer at different positions stabilized the corresponding PNA₂:DNA triplexes.¹⁵²

Cyclohexyl PNA: One of the earliest PNA modifications was to constrain the flexibility in the aminoethyl segment around a single C-C bond by introducing a cyclohexyl ring (Figure 1.23).¹⁵³ The derived *trans*-(*S,S*)-cyclohexyl PNA oligomer hybridized with complementary DNA as good as the unmodified *aeg*-PNA, while the enantiomeric *trans*-(*R,R*)-cyclohexyl PNA oligomers lacked such a property. Significant stereo differentiation was observed with *SR*- and *RS*-*ch*-PNAs, the *SR* isomer was more destabilizing than the *RS* isomer in *ch*-PNA:DNA complexes while In case of RNA complexes *RS* being more destabilizing than *SR*. From T_m values it was observed that (*R,S*)-*ch*-PNAs bound to RNA with higher affinity than to DNA. This is attributed to the inherent rigidity of the *cis*-*ch*-PNAs that forbids structural readjustments to bind to DNA (PNA:DNA $\beta \sim 140^\circ$) and prefers binding to RNA (PNA:RNA). This discrimination was achieved *via* the concept of preorganization.

Cyclopentyl PNAs: Ganesh *et al.*¹⁵⁴ also synthesized *cis*-(1*S*,2*R*/1*R*,2*S*)-cyclopentyl PNA-T monomers in which the characteristic *endo-exo* puckering that dictates the pseudoaxial/pseudoequatorial dispositions of substituents may allow better torsional adjustments to attain the necessary hybridization-competent conformations. These monomers were incorporated into homothymine *aeg*-PNA-T10 sequence at defined positions and studied their binding affinity with DNA and RNA. It was observed that the *RS*-*cp*-PNA enantiomer showed higher affinity for DNA as compared to *SR*-*cp*-PNA isomer and in case of RNA this was reversed.

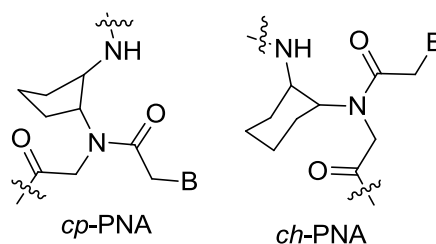


Figure 1.23 Cyclohexyl and cyclopentyl PNAs

The all-modified homooligomers of both enantiomers exhibited significant stabilization of their triplexes with DNA and poly rA without sacrificing the base specificity. *ch*-PNA and *cp*-PNA-T monomers of both (*S,R*) and (*R,S*) enantiomers were introduced into mixed sequences, in all the cases PNA:RNA hybrids were more stable than the corresponding PNA:DNA hybrids, and significantly, *cp*-PNA oligomers showed much higher T_m 's compared to *ch*-PNA.

1.7.6 Biological applications of PNA as antisense and antigene agents

The significant properties of PNAs such as high binding affinity, sequence specificity and strand invasion has made it a versatile candidate in designing gene therapeutic drugs.¹⁵⁵

1.7.6a Translation Arrest

PNAs cannot activate PNA:RNA duplex as substrates for RNase H and hence the antisense effect of the PNA is mainly based on the steric blocking of the translation machinery with the usual targets in the coding region of mRNA. Duplex as well as triplex-forming PNAs targeted towards sequences adjacent to the AUG start codon could efficiently block the translation of CAT mRNA by physically blocking the assembly of the 80S ribosome initiation complex.^{156,157} DNA/PNA chimeras are able to stimulate RNA cleavage by RNase H on formation of chimera RNA double strand. PNA/DNA chimeras taken up by NIH 3T3 cells and the degree and kinetics of cellular uptake are similar to that of an oligonucleotide of the same sequence.¹⁵⁸ Hence, duplex and triplex forming PNAs can serve as better antisense agents in future medicinal chemistry.

1.7.6b Inhibition of Gene Transcription

Nielsen *et al.*¹⁵⁹ have demonstrated that an 8-mer PNA-T8 is capable of blocking phage T3 polymerase activity. The presence of a PNA target within the promoter region of IL-2Ra gene has been used to understand the effect of PNA binding to its target on the gene expression.¹⁶⁰ The formation of PNA₂-DNA triplex arrests transcription *in vitro* and is capable of acting as

an antigene agent. Ottonello *et al.*¹⁶¹ also demonstrated that a T₁₀ PNA strongly and specifically inhibits the RNA polymerase III transcription *in vitro*. DNA ligand H-T₁₀-D-Lys-NH₂ PNA, in which the D-lysine at the C terminus is known to favour DNA binding and the formation of right handed helices. These results suggest that oligothymine PNAs strongly and specifically inhibit polymerase transcription and useful for *in vivo* exploitation of these polymerase terminator ligands for pharmacological purposes.

1.7.7 PNA tools for molecular biology and functional genomics

1.7.7a PCR clamping

Point mutations in the ras proto-oncogenes are amongst the most frequent changes found in human malignancies.¹⁶² A variety of methods have been reported for the detection of the ras mutations.¹⁶³ However, even the most frequently used assays are also limited in their sensitivity for the detection of ras mutations, or require radioactive labelling.^{163a,b} The PCR clamping method for the detection of point mutations¹⁶⁴ using PNAs is based on three factors (i) PNA/DNA-hybrids have a higher thermal stability compared with the corresponding DNA/DNA hybrids (ii) PNA/DNA hybrids are more destabilized by single base pair mismatches than the corresponding DNA/DNA hybrids¹⁶⁴ and (iii) PNAs could not serve as primer molecules in PCR. Discrimination of point mutations in the Ki-ras gene has been carried out by PCR clamping.¹⁶⁵ A PNA oligomer complementary to wild-type Ki-ras DNA strongly inhibits amplification of the wild-type gene, relative to the mutated gene, to which the PNA binds with lower affinity (see Figure 1.24).

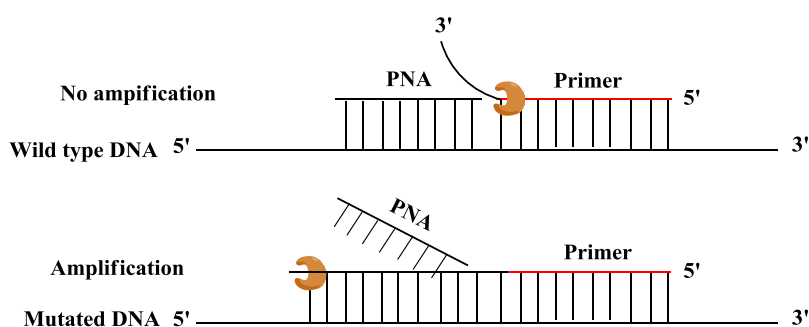


Figure 1.24 Schematic illustration of PNA mediated PCR clamping.¹⁶⁴

1.7.7b PNA- based artificial restriction DNA cutter

Site-selective scission of genomes is quite important for future biotechnology. However, naturally occurring restriction enzymes cut huge DNAs at too many sites and cannot cut the genomes at one desired site, since their site-specificity is too low. Recently, Komiyama *et*

*al.*¹⁶⁶ have developed a completely chemistry-based artificial restriction DNA cutter (ARCUT) by combining a pair of pseudo-complementary PNA strands (*pcPNA*, sequence recognition moiety) and Ce(IV)/EDTA complex (molecular scissors) (Figure 1.25).

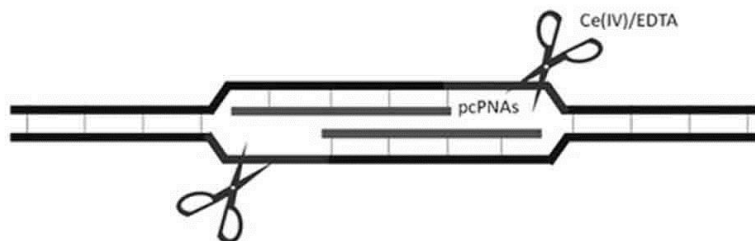


Figure 1.25 Strategy of artificial restriction DNA cutter (ARCUT). The phosphodiester linkages in the single-stranded portions are hydrolyzed by Ce(IV)/EDTA¹⁶⁶

The scission site of ARCUT and its scission specificity can be easily modulated in terms of the sequences and lengths of the *pcPNA* strands so that even huge genomes can be selectively cut at only one predetermined site. Pseudo-complementary PNAs are employed by replacing adenine and thymine with modified bases 2,6-diaminopurine (D) and 2-thiouracil (U).¹⁶⁷ The steric repulsion between D and U suppresses the formation of *pcPNA:pcPNA* duplex, and allows invasion of double-stranded DNA to form double-duplex invasion complex.

1.7.7c PNA microarray

Microarrays consist of a solid support like glass or silicon slide containing an array of small spots with well-defined DNA or PNA probes. These probes are capable of binding complementary DNA or RNA target molecules. After successful hybridisation experiments, the target cDNA/RNA molecules are detected *via* a label (in general a fluorescence dye). Peptide nucleic acid (PNA) microarrays have been used for the analysis of unlabelled DNA molecules using a time-of-flight secondary mass spectrometry (TOF-SIMS). After DNA hybridisation, the PNA microarray is performed with a TOF-SIMS imaging. The resulting mass spectra enabled the visualisation of molecular distribution for PO_2^- (63 amu) and PO_3^- (79 amu) secondary ions.¹⁶⁸ These specific signals are detected only on spots at which DNA bound to complementary PNA probes, as phosphorous is an integral part of the nucleic acids (Figure 1.26).

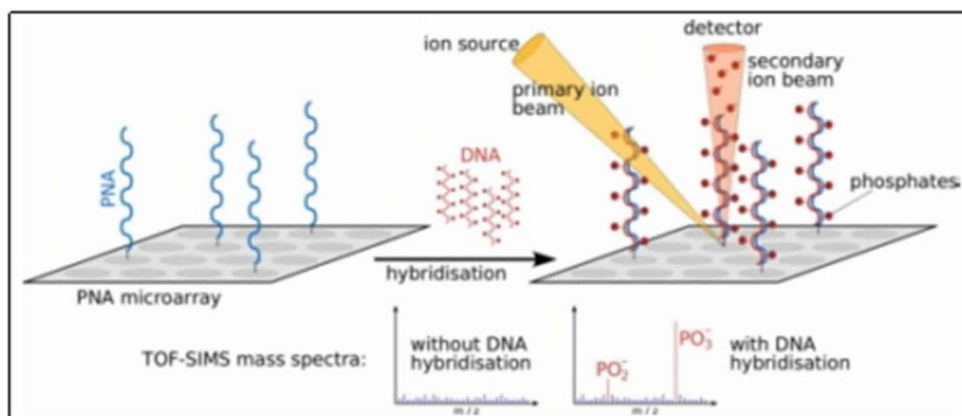


Figure 1.26 PNA microarray.

1.8 Scope of Present Work

The preceding section has given an overview on modified nucleic acids especially, peptide nucleic acid (PNA) which is emerging as a promising DNA mimic. The superior properties of PNAs like high binding affinity, strand invasion, stability in biological systems etc., are important for the development of therapeutics in the form of antisense/antigene oligonucleotides. In spite of these advantages, PNA has few drawbacks like poor water solubility, inefficient cellular uptake, self-aggregation and ambiguity in directional selectivity of binding and restrict its applications in terms of PNA-based gene targeted drugs. Hence, various modifications of PNA as described in this chapter have been employed in order to overcome these limitations by different research groups as described in previous section.

The work presented in this thesis deals with an entirely new approach to modulate the PNA biological activity without any structural/conformational constraint but by introduction of electronegative, lipophilic fluorine at different positions of PNA structure, on the nucleobase, in the backbone and in the side chain (Figure 1.27).

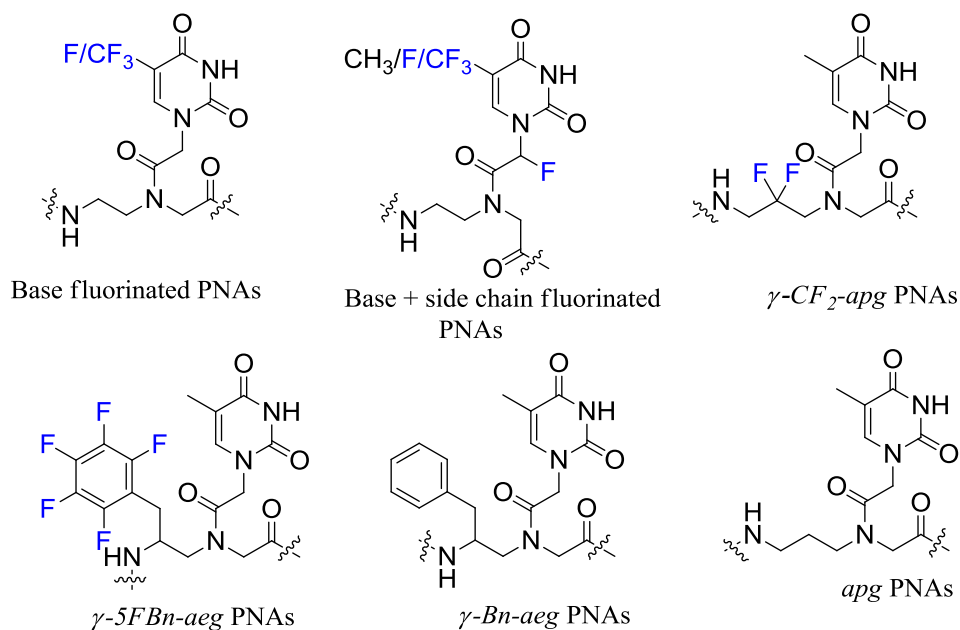
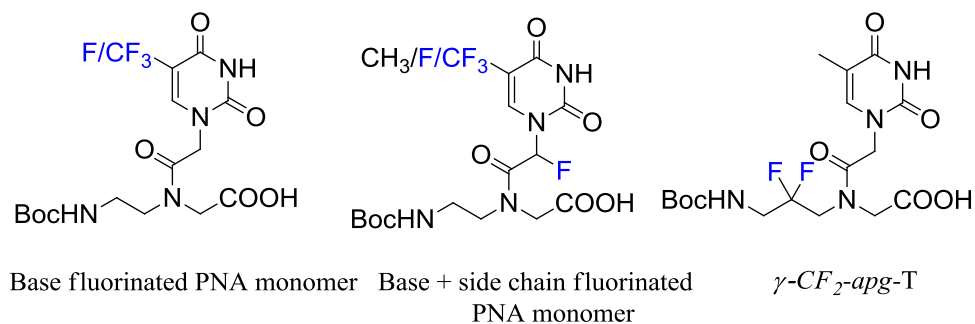


Figure 1.27 Fluorinated and non-fluorinated PNA structures

Chapter 2 of the thesis describes synthesis of sequence specific fluorinated PNA analogs using fluorinated PNA monomers. The structural presence of fluorine in PNA may change physicochemical properties of the PNA oligomers and thereby may lead to improve their binding affinity towards complementary sequences and cell penetration.

The design, synthesis and characterization of novel fluorinated PNA monomers (Figure 1.28) is followed by the incorporation of various fluorinated PNA monomers at various positions in the homopyrimidine and mixed purine: pyrimidine sequences using solid phase peptide synthesis. The cleavage of PNA from the solid support and purification of the fluorinated oligomers by RP -HPLC and characterization by MALDI-TOF spectrometry are described.



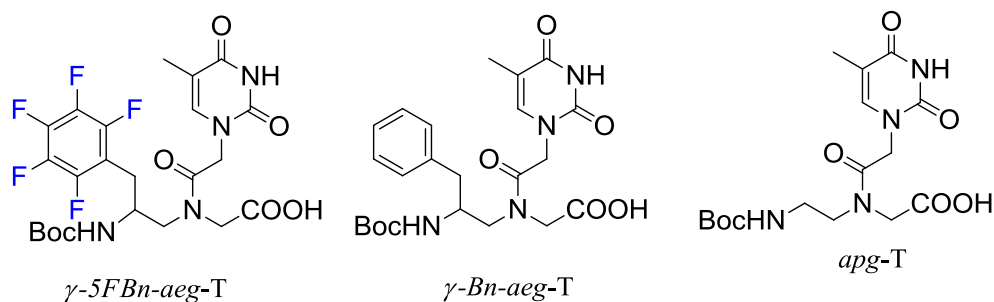


Figure 1.28 Fluorinated and non-fluorinated PNA monomers

Chapter 3 reports on the biophysical evaluation of various fluorinated PNA oligomers, employing temperature dependent UV absorbance. The thermal stabilities of the derived PNA:DNA/RNA duplexes with complementary and mismatch sequences indicate uncompromising specificity of these fluorinated PNAs towards their complementary sequences. Circular Dichroism (CD) studies suggested no major conformational alterations to fluorinated PNA:DNA/RNA duplexes.

Chapter 4 deals with cell permeation studies of the fluorescently labelled fluorinated PNA analogs in NIH 3T3 and HeLa cell lines. The cell permeation ability of various fluorinated PNA oligomers quantitatively studied by fluorescence activated cell sorter (FACS) analysis indicated facile cell permeation compared to non-fluorinated PNAs. Interestingly, the fluorinated PNA analogues induced nanoparticle formation of the corresponding DNA/RNA duplexes.

Overall, the work presented in this thesis has shown new designs of PNA analogues by introduction of fluorine and the biological utility of this is seen in terms of selectivity, thermal stability, better cell permeability and nanoparticle formation by the derived DNA/RNA complexes.

1.9 References

1. Takahashi, I.; Marmur, J. *Nature* **1963**, *197*, 794.
2. a) Watson, J. D.; Crick, F. H. C. *Nature* **1953**, *171*, 737-738.
b) http://swift.cmbi.ru.nl/gv/students/mtom/DRNA_7.html
3. Hoogsteen, K. *Acta. Cryst.* **1963**, *65*, 907.
4. Crick, F. H. C. *J. Mol. Biol.* **1966**, *19*, 548.
5. Seeman, N. C.; Rosenberg, J. M.; Rich, A. *Proc. Natl. Acad. Sci. USA* **1976**, *73*, 804.
6. Crick, F. H. *Nature* **1970**, *227*, 561-563.
7. http://en.wikipedia.org/wiki/Central_dogma_of_molecular_biology

8. Kurreck. J. *Eur. J. Biochem.* **2003**, 270, 1628-1644.
9. Isis Pharmaceuticals /Genzyme
10. Lee, J. J.; Yokota, T. *J. Pers. Med.* **2013**, 3,144-176.
11. Isis Pharmaceuticals /Teva/oncogenex
12. Tan, X. X.; Actor, J. K.; Chen, Y. (2005). *Antimicrobial Agents and Chemotherary* **2005**, 49, 3203-3207.
13. Hatamoto, M.; Ohashi, A.; Imachi, H. *Applied Microbiology and Biotechnology* **2010**, 86, 397-402
14. Sohail, M.; Southern, E.M. *Advanced Drug Delivery Reviews* **2000**, 44, 23-34.
15. Peyman, A.; Helsing, M.; Kretschmar, G.; Mag, M.; Grabley, S.; Uhlmann, E. *Biol. Chem. Hoppe-Seyler* **1995**, 376, 195-198. b) Allawi, H. T.; Dong, F.; IP, H. S.; Neri, B. P.; and Lyamichev, V. I. *RNA* **2001**, 7, 314-327. c) Zhang, H.; Mao¹, J.; Zhou¹, D.; Xu¹, Y.; Thonberg¹, H.; Liang¹, Z.; and Wahlestedt, C. *Nucleic Acids Research*, **2003**, 31, 14e72. d) Sun, Y.; Duan, M.; Lin, R.; Wang, D.; Li, C.; Bo, X.; Wang, S. *Molecular Vision* **2006**; 12,1364-71.
16. Angelika Gabler *Nucleic Acids Res.* **2003**, 31, e79
17. Fang *et al.* *RNA* **2010**, 16, 1429-1435.
18. Dominski, Z.; Kole. *Proc. Natl. Acad. Sci. U.S.A* **1993**, 90, 8673-8676.
19. Lima, W. F.; Wu, H.; and Crooke, S. T. *Methods Enzymol.* **2001**, 341,430-440.
20. Monia, B. P.; Lesnik, E. A.; Gonzalez, C.; Lima, WF.; McGee, D.; Guinosso, C. J.; Kawasaki, A. M.; Cook, P. D.; Freier, S. M. *J Biol Chem.* **1993**, 268, 14514-14522.
21. Dean, N. M.; Bennett, C. F. *Oncogene* **2003**, 22, 9087-9096.
22. a) Fire, A.; Xu, S.; Montgomery, M. K.; Kostas, S. A.; Driver, S. E.; Mello, C. C. b) *Nature* **1998**, 391, 806-811. b) Hutvagner, G.; Zamore, PD. *Science* **2002**, 297, 2056-2060.
23. a) Agrwal, A.; Goodchild, J.; Civeira, M. P.; Thornton, A. H.; Sarin, P. S.; Zamecnik, P. C. b) *Proc. Natl. Acad. Sci. U.S.A* **1989**, 86, 1504. b) *Proc. Natl. Acad. Sci.U.S.A* **1988**, 85, 7079-7083.
24. Lemaitre, M.; Bayard, B.; Lebleu, B.; *Proc. Natl. Acad. Sci. U.S.A* **1987**, 84, 648-652.
25. Rosolen, A.; Whitesell, L.; Ikegaki, N.; Kennett, R. H.; Neckers, L. M.; *Cancer Res.* **1990**, 50, 6316-6322.
26. J. Summerton, D.; Stein, S.; Huang, P.; Matthews, D.; Weller, M.; Partridge. *Antisense Nucleic Acid Drug Dev.* **1997**, 7, 63-70.

27. a) Vasanthakumar, G.; Ahmed, N. K.; *Cancer Commun.* **1990**, *2*, 295. b) *Cancer, Commun.* **1989**, *1*, 225-232.
28. Sburlati, A. R.; Manrow, R. E.; Berger, S. L.; *Proc. Natl. Acad. Sci. U.S.A* **1991**, *88*, 253-257.
29. Zheng, H.; Sahai, B. M.; Kilgannon, P.; Fotedar, A.; Green, D. R. *Proc. Natl. Acad. Sci. U.S.A* **1989**, *86*, 3758-3762.
30. Maier, J. A. M.; Voulalas, P.; Roeder, D.; Maciag, T. *Science* **1990**, *249*, 1570-1574
31. Crick F. *Science* **1979**, *204*, 264-271.
32. Sierakowska, H.; Sambade, M. J.; Agrawal, S.; Kole, R. *Proc. Natl. Acad. Sci. U.S.A* **1996**, *93*, 12840-12844.
33. Dominski, Z.; and Kole, R. *Proc. Natl. Acad. Sci. U.S.A* **1993**, *90*, 8673-1677.
34. Schmajuk, G.; Sierakowska, H.; and Kole, R. *J. Biol. Chem.* **1999**, *274*, 21783-21789.
35. Sierakowska, H.; Sambade, M. J.; Schumperli, D.; and Kole, R. *RNA* **1999**, *5*, 369-377.
36. Friedman, K. J.; Kole, J.; Cohn, J. A.; Knowles, M. R.; Silverman, L. M.; Kole, R. *J. Biol. Chem.* **1999**, *274*, 36193-36199.
37. Busslinger, M.; Moschonas, N.; Flavell, R. A. *Cell* **1981**, *27*, 289-298.
38. Koenig, M.; Beggs, A. H.; Moyer, M.; Scherpf, S.; Heindrich, K.; Bettecken, T.; Meng, G.; Muller, C. R.; Lindlof, M.; Kaariainen, H. *et al. Am. J. Hum. Genet.* **1989**, *45*, 498-506.
39. Guterstam, P.; Lindgren, M.; Johansson, H.; Tedebark, U.; Wengel, J.; E. L Andaloussi, S.; Langel, U. *Biochem. J.* **2008**, *412*, 307-313.
40. Gorman, L.; Mercatante, D. R.; Kole, R. *J. Boil. Chem.* **2000**, *275*, 35914-35919.
41. Bennett, C. F.; Swayze, E. E. *Annu. Rev. Pharmacol. Toxicol.* 2010. *50*:259-93
42. Altona, C.; Sundaralingam, M. *J. Am. Chem. Soc.* **1972**, *94*, 8205-12.
43. Freier, S. M.; Altmann, K. H. *Nucleic Acids Res.* **1997**, *25*, 4429-43.
44. Chiu, Y. L.; Rana, TM. *RNA* **2003**, *9*, 1034-48.
45. Morrissey, D. V.; Lockridge, J. A.; Shaw, L.; Blanchard, K.; Jensen, K.; *et al. Nat. Biotechnol.* **2005**, *23*, 1002-7.
46. Allerson, C. R.; Sioufi, N.; Jarres, R.; Prakash, T. P.; Naik, N.; *et al. J. Med. Chem.* **2005**, *48*, 901-904.
47. Goel, S.; Desai, K.; Macapinlac, M.; Wadler, S.; Goldberg, G.; *et al. Invest. New Drugs* **2006**, *24*, 125-34.
48. Prakash, T. P.; Allerson, C. R.; Dande, P.; Vickers, T. A.; Sioufi, N.; *et al. J. Med. Chem.* **2005**, *48*, 4247-53.

49. Jackson, A. L.; Burchard, J.; Leake, D.; Reynolds, A.; Schelter, J.; et al. *RNA* **2006**, *12*, 1197-205.
50. Teplova, M.; Minasov, G.; Tereshko, V.; Inamati, G. B.; Cook, P. D.; et al. *Nat. Struct. Biol.* **1999**, *6*, 535-39.
51. Koshkin, A. A.; Singh, S. K.; Nielsen, P.; Rajwanshi, V. K.; Kumar, R.; et al. *Tetrahedron* **1998**, *54*, 3607-30.
52. Wengel, J. *Acc. Chem. Res.* **1999**, *32*, 301-10.
53. Petersen, M.; Bondensgaard, K.; Wengel, J.; Jacobsen, J. P. *J. Am. Chem. Soc.* **2002**, *124*, 5974-82.
54. Nielsen, K. E.; Spielmann, H. P. *J. Am. Chem. Soc.* **2005**, *127*, 15273-82.
55. Kurreck, J.; Wyszko, E.; Gillen, C.; Erdmann, V. A. *Nucleic Acids Res.* **2002**, *30*, 1911-18.
56. Swayze, E. E.; Siwkowski, A. M.; Wancewicz, E. V.; Migawa, M. T.; Wyrzykiewicz, T. K. et al. *Nucleic Acids Res.* **2007**, *35*, 687-700.
57. Seth, P. P.; Siwkowski, A.; Allerson, C. R.; Vasquez, G.; Lee, S. et al. *J. Med. Chem.* **2009**, *52*, 10-13.
58. Koizumi, M. *Curr. Opin. Mol. Ther.* **2006**, *8*, 144-149.
59. Eckstein F. *Antisense Nucleic Acid Drug Dev.* **2000**, *10*, 117-21.
60. Stein, C. A.; Subasinghe, C.; Shinozuka, K.; Cohen, J. S. *Nucleic Acids Res.* **1998**, *16*, 3209-21.
61. Stein, C. A.; Cheng, Y-C. *Science* **1993**, *261*, 1004-12.
62. Stein, C. A. *Nat. Med.* **1995**, *1*, 1119-21.
63. Krieg, A. M.; Stein, C. A. *Antisense Res. Dev.* **1995**, *5*, 241.
64. Stein, C. A. *Trends Biotechnol.* **1996**, *14*, 147-49.
65. Roehr, B. J. *Int. Assoc. Physicians AIDS Care* **1998**, *4*, 14-16.
66. Gryaznov, S. M.; Lloyd, D. H.; Chen, J. K.; Schultz, R. G.; DeDionisio, L. A. et al. *Proc. Natl. Acad. Sci. USA* **1995**, *92*, 5798-802.
67. Gryaznov, S.; Skorski, T.; Cucco, C.; Nieborowska-Skorska, M.; Chiu, C. Y.; et al. *Nucleic Acids Res.* **1996**, *24*, 1508-14.
68. Pongracz, K.; Gryaznov, S. *Tetrahedron Lett.* **1999**, *40*, 7661-64.
69. DeMesmaeker, A.; Waldner, A.; Leberton, J.; Homann, P.; Fritsch, V. et al. *Angew. Chem. Int. Ed. Engl.* **1994**, *33*, 226.
70. Leberton, J.; Waldner, A.; Fritsch, V.; Wolf, R. M.; DeMesmaeker, A. *Tetrahedron Lett.* **1994**, *35*, 5225-28.

71. Sanghvi, Y. S.; Swayze, E. E.; Peoc'h, D.; Bhat, B.; Dimock, S. *Nucleosides Nucleotides* **1997**, *16*, 907-16.
72. Jones, R. J.; Lin, K. Y.; Milligan, J. F.; Wadwani, S.; Matteucci, M. D. *J. Org. Chem.* **1993**, *58*, 2983-91.
73. Zhang, J.; Shaw, J. T.; Matteucci, M. D. *Bioorg. Med. Chem. Lett.* **1999**, *9*, 319-22.
74. Alter, J.; Lou, F.; Rabinowitz, A.; Yin, H.; Rosenfeld, J.; *et al.* *Nat. Med.* **2006**, *12*, 175-177.
75. Summerton, J. *Biochim. Biophys. Acta* **1999**, *1489*, 141-58.
76. Wu, B.; Moulton, H. M.; Iversen, P. L.; Jiang, J.; Li, J.; *et al.* *Proc. Natl. Acad. Sci. USA* **2008**, *105*, 14814-19131.
77. Nielsen, P. E.; Egholm, M.; Berg, R.H.; Buchardt, O. *Science* **1991**, *254*, 1497-1500.
78. Egholm, M.; Buchardt, O.; Nielsen, P. E.; Berg, R. H. *J. Am. Chem. Soc.* **1992**, *114*, 1895-1897.
79. Tomac, S.; Sarkar, M.; Ratilainen, T.; Wittung, P.; Nielsen, P. E.; Norden, B.; Graslund, A. *J. Am. Chem. Soc.* **1996**, *118*, 5544.
80. Knudsen, H.; Nielsen, P. E. *Nucleic Acid Res.* **1996**, *24*, 494.
81. Egholm, M.; Buchardt, O.; Christensen, L.; Behrens, C.; Freier, S. M.; Driver, D. A.; Berg, R. H.; Kim, S. K.; Norden, B.; Nielsen, P. E. *Nature* **1993**, *365*, 566.
82. Uhlmann, E.; Will, D. W.; Breipohl, G.; Langner, D.; Rytte, A. *Angew. Chem. Int. Ed. Engl.* **1996**, *35*, 2632- 2635.
83. Nulf, C. J.; Corey, D. *Nucleic Acids Res.* **2004**, *32*, 3792-3798.
84. Sazani, P.; Gemignani, F.; Kang, S. H.; Maier, M. A.; Manoharan, M.; *et al.* *Nat. Biotechnol.* **2002**, *20*, 1228-1233.
85. Siwkowski, A. M.; Malik, L.; Esau, CC.; Maier, M. A.; Wancewicz, EV. *et al.* *Nucleic Acids Res.* **2004**, *32*, 2695-2706.
86. Abes, S.; Turner, J. J.; Ivanova, G. D.; Owen, D.; Williams, D. *et al.* *Nucleic Acids Res.* **2007**, *35*, 4495-4502.
87. Uhlmann, E.; Peyman, A.; Breipohl, G.; Will, D. W. *Angew. Chem. Int. Ed.* **1998**, *37*, 2796-2823.
88. Wittung, P.; Nilsen, P. E.; Norde'n, B. *Biochemistry* **1997**, *36*, 7973-7979.
89. Lohse, J.; Dahl, O.; Nielsen, P. E. *Proc. Natl. Acad. Sci. U S A* **1999**, *96*, 11804-11808.
90. Egholm, M.; Buchardt, O.; Christensen, L.; Behrens, C.; Freier, S. m.; Driver, D. A.; Berg, R. H.; Kim, S. K.; Norden, B.; Nielsen, P. E. *Nature* **1993**, *365*, 566-568.
91. Brown, S. C.; Thomson, S. A.; Veal, J. M.; Davis, D. G. *Science* **1994**, *265*, 777-780.

92. (a) Rasmussen, H.; Kastrup, J. S.; Nielsen, J. N.; Nielsen, J. M.; Nielsen, P. E. *Nat. Struct. Biol.* **1997**, *4*, 98-101. (b) Eldrup, A. B.; Nielsen, B. B.; Haaima, G.; Rasmussen, H.; Kastrup, J. S.; Christensen, C.; Nielsen, P. E. *Eur. J. Org. Chem.* **2001**, 1781-1790. (c) Haaima, G.; Rasmussen, H.; Schmidt, G.; Jensen, D. K.; Kastrup, J. S.; Stafshede, P. W.; Norden, B.; Buchardt, O.; Nielsen, P. E. *New J. Chem.* **1999**, *23*, 833-840. (d) Brown, S. C.; Thomson, S. A.; Veal, J. M.; Davis, D. G. *Science* **1994**, *265*, 777-780. (e) He, W.; Hatcher, E.; Balae, A.; Beratan, D. N.; Gil, R. R.; Madrid, M.; Achim, C. *J. Am. Chem. Soc.* **2008**, *130*, 13264-13273. (f) He, W.; Crawford, M. J.; Rapireddy, S.; Madrid, M.; Gil, R. R.; Ly, D. H.; Achim, C. *Mol. Biol. Syst.* **2010**, DOI: 10.1039/c002254c.
93. (a) Eriksson, M.; Nielsen, P. E. *Nat. Struct. Biol.* **1996**, *3*, 410-413. (b) Menchise, V.; De Simone, G.; Tedeschi, T.; Corradini, R.; Sforza, S.; Marchelli, R.; Capasso, D.; Saviano, M.; Pedone, C. *Proc. Natl. Acad. Sci. U.S.A* **2003**, *100*, 12021-12026. (c) Yeh, J.I.; Boris Shivachev, B.; Rapireddy, S.; Crawford, M.J.; Gil, R.R.; Du, S.; Madrid, M.; Ly, D. H. *J. Am. Chem. Soc.* **2010**, *132*, 10717-10727.
94. Betts, L.; Josey, J. A.; Veal, J. M.; Jordan, S. R. *Science* **1995**, *270*, 1838-1841.
95. Davis, J. T. *Angew. Chem., Int. Ed.* **2004**, *43*, 668-698.
96. Simonsson, T. *Biol. Chem.* **2001**, *382*, 621-628.
97. Egholm, M.; Buchardt, O.; Christensen, L.; Behrens, C.; Freier, S. M.; Driver, D. A.; Berg, R. H.; Kim, S. K.; Norden, B.; Nielsen, P. E. *Nature* **1993**, *265*, 566-568.
98. Krishnan-Ghosh, Y.; Stephens, E.; Balasubramanian, S. *J. Am. Chem. Soc.* **2004**, *126*, 5944-5945.
99. Datta, B.; Schmitt, C.; Armitage, B. A. *J. Am. Chem. Soc.* **2003**, *125*, 4111-4118. (b) Marin, V. L.; Armitage, B. A. *J. Am. Chem. Soc.* **2005**, *127*, 8032-8033.
100. Sharma, N. K.; Ganesh, K. N. *Chem. Commun.*, **2005**, 4330-4332.
101. Nielsen, P. E. *Pure Appl. Chem.* **1998**, *70*, 105-110.
102. Hyrup, B.; Nielsen, P. E. *Bioorg. Med. Chem.* **1996**, *4*, 5-23.
103. Mitra, R.; Ganesh, K. N. *Chem. Commun.* **2011**, *47*, 1198-1200.
104. Jain, D. R.; Anandi, L. V.; Lahiri, M.; Ganesh, K. N. *J. Org. Chem.* **2014**, *79*, 9567-9577.
105. Nielsen, P. E. *Q. Rev. Biophys.* **2005**, *38*, 345-350.
106. Shiraishi, T.; Pankratova, S.; Nielsen, P. E. *Chem. Biol.* **2005**, *12*, 923-929.
107. Hu, J.; Corey, D. R. *Biochemistry* **2007**, *46*, 7581-7589.
108. Kumar, V. A.; Ganesh, K. N. *Acc. Chem. Res.* **2005**, *38*, 404-412.

109. Corradini, R.; Sforza, S.; Tedeschi, T.; Totsingan, F.; Manicardi, A.; Marchelli, R. *Curr. Top. Med. Chem.* **2011**, *11*, 1535-1554.
110. Dueholm, K. L.; Petersen, K. H.; Jensen, D. K.; Egholm, M.; Nielsen, P. E.; Buchardt, O. *Bioorg. Med. Chem. Lett.* **1994**, *4*, 1077-1080.
111. Sforza, S.; Corradini, R.; Ghirardi, S.; Dossena, A.; Marchelli, R. *Eur. J. Org. Chem.* **2000**, *2000*, 2905-2913.
112. Menchise, V.; de Simone, G.; Tedeschi, T.; Corradini, R.; Sforza, S.; Marchelli, R.; Capasso, D.; Saviano, M.; Pedone, C. *Proc. Natl. Acad. Sci. USA* **2003**, *100*, 12021-12026.
113. Koppelhus, U.; Awasthi, S. K.; Zachar, V.; Holst, H. U.; Ebbesen, P.; Nielsen, P. E. *Antisense Nucleic Acid Drug Dev.* **2002**, *12*, 51-63.
114. Zhou, P.; Dragulescu-Andrasi, A.; Bhattacharya, B.; O'Keefe, H.; Vatta, P.; Hyldig-Nielsen, J. J.; Ly, D. H. *Bioorg. Med. Chem. Lett.* **2006**, *16*, 4931-4935.
115. Haaima, G.; Lohse, A.; Buchardt, O.; Nielsen, P. E. *Angew. Chem. Int. Ed. Engl.* **1996**, *35*, 1939-1942.
116. Puschl, A.; Sforza, S.; Haaima, G.; Dahl, O.; Nielsen, P. E. *Tetrahedron Lett.* **1998**, *39*, 4707-4710.
117. Aguado, G. P.; Rua, F.; Branchadell, V.; Nielsen, P. E.; Ortuno, R. M. *Tetrahedron: Asymmetry* **2006**, *17*, 2499-2503.
118. Gourishankar, A.; Ganesh, K. N. *Artificial DNA PNA XNA* **2012**, *3*, 5-13.
119. Sugiyama, T.; Imamura, Y.; Demizu, Y.; Kurihara, M.; Takano, M.; Kittaka, A. *Bioorg. Med. Chem. Lett.* **2011**, *21*, 7317-7320.
120. Kosynkina, L.; Wang, W.; Liang, T. C. *Tetrahedron Lett.* **1994**, *35*, 5173-5176.
121. Tedeschi, T.; Sforza, S.; Corradini, R.; Marchelli, R. *Tetrahedron Lett.* **2005**, *46*, 8395-8399.
122. Englund, E. A.; Appella, D. H. *Org. Lett.* **2005**, *7*, 3465-3467.
123. Dose, C.; Seitz, O. *Org. Lett.* **2005**, *7*, 4365-4368.
124. Ficht, S.; Dose, C.; Seitz, O. *ChemBioChem.* **2005**, *6*, 2098-2103.
125. Englund, E. A.; Wang, D.; Fujigaki, H.; Sakai, H.; Micklitsch, C. M.; Ghirlando, R.; Martin-Manso, G. *Nat. Commun.* **2012**, doi: 10.1038/ncomms1629.
126. Sforza, S.; Tedeschi, T.; Corradini, R.; Marchelli, R. *Eur. J. Org. Chem.* **2007**, *2007*, 5879-5885.
127. Avitabile, C.; Moggio, L.; Malgieri, G.; Capasso, D.; Gaetano, S. D.; Saviano, M.; Pedone, C.; Romanelli, A. *PLoS One* **2012**, *7*, e35774.

128. Dragulescu-Andrasi, A.; Rapireddy, S.; Frezza, B. M.; Gayathri, C.; Gil, R. R.; Ly, D. H. *J. Am. Chem. Soc.* **2006**, *128*, 10258-10267.
129. Yeh, J. I.; Boris Shivachev, B.; Rapireddy, S.; Crawford, M. J.; Gil, R. R.; Du, S.; Madrid, M.; Ly, D. H. *J. Am. Chem. Soc.* **2010**, *132*, 10717-10727.
130. Crawford, M. J.; Rapireddy, S.; Bahal, R.; Sacui, I.; Ly, D. H. *J. Nucleic Acids* **2011**, *2011*, doi:10.4061/2011/652702.
131. Manicardi, A.; Fabbri, E.; Tedeschi, T.; Sforza, S.; Nicoletta Bianchi, N.; Brognara, E.; Gambari, R.; Marchelli, R.; Corradini, R. *Chem. Bio. Chem.* **2012**, *13*, 1327-1337.
132. Mitra, R.; Ganesh, K. N. *J. Org. Chem.* **2012**, *77*, 5696-5704.
133. Jain, D. R and Ganesh, K. N. *J. Org. Chem.* **2014**, *79*, 6708-6714.
134. Tomac, S.; Sarkar, M.; Ratilainen, T.; Wittung, P.; Nielsen, P. E.; Norden, B.; Graslund, A. *J. Am. Chem. Soc.* **1996**, *118*, 5544-5549.
135. Hollenstein, M.; Leumann, C. *J. Org. Lett.* **2003**, *5*, 1987-1990.
136. Rose, D. *J. Anal. Chem.* **1993**, *65*, 3545-3549.
137. Gangamani, B. P.; Kumar, V. A.; Ganesh, K. N. *Tetrahedron* **1996**, *52*, 15017-15030.
138. Gangamani, B. P.; D'Costa, M.; Kumar, V. A.; Ganesh, K. N. *Nucleosides Nucleotides* **1999**, *18*, 1409-1011.
139. Gangamani, B. P.; Kumar, V. A.; Ganesh, K. N. *Tetrahedron* **1999**, *55*, 177-192.
140. D'Costa, M.; Kumar, V. A.; Ganesh, K. N. *Org. Lett.* **1999**, *1*, 1513-1516.
141. Vilaivan, T.; Khongdeesameor, C.; Harnyuttanokam, P.; Westwell, M. S.; Lowe, G. *Bioorg. Med. Chem. Lett.* **2000**, *10*, 2541-2545.
142. D'Costa, M.; Kumar, V. A.; Ganesh, K. N. *Org. Lett.* **2001**, *3*, 1281-1284.
143. Sharma, N.; Ganesh, K. N. *Tetrahedron Lett.* **2004**, *45*, 1403-1406.
144. Sharma, N.; Ganesh, K. N. *Chem. Commun.* **2003**, 2484-2485.
145. Puschl, A.; Boesen, T.; Zuccarello, G.; Dahl, O.; Pitsch, S.; Nielsen, P. E. *J. Org. Chem.* **2001**, *66*, 707-712.
146. Hickman, D. T.; King, P. M.; Cooper, M. A.; Slater, J. M.; Mickelfield, J. *Chem. Commun.* **2000**, 2251-2252.
147. Kumar, V. A.; Pallan, P. S.; Meena,; Ganesh, K. N. *Org. Lett.* **2001**, *3*, 1269-1272.
148. Kumar, V. A.; Meena. *Nucleosides Nucleotides Nucleic acids* **2003**, *22*, 1101-1104.
149. D'Costa, M.; Kumar, V. A.; Ganesh, K. N. *Tetrahedron. Lett.* **2002**, *43*, 883-886.
150. Lonkar, P.; Ganesh, K. N.; Kumar, V. A. *Org. Biomol. Chem.* **2004**, *2*, 2604-2611
151. Lonkar, P. S.; Kumar, V. A.; Ganesh, K. N. *Nucleosides, Nucleotides Nucleic Acids* **2001**, *20*, 1197-1200.

152. Lescrinier, E.; Froeyen, M.; Herdewijn, P. *Nucleic Acids Res.* **2003**, *31*, 2975-2989.
153. Lagrioule, P.; Wittung, P.; Eriksson, M.; Jensen, K. K.; Norden, B.; Buchardt, O.; Nielsen, P. E. *Chem. Eur. J.* **1997**, *3*, 912-919.
154. a) Govindaraju, T.; Kumar, V. A.; Ganesh, K. N. *J. Org. Chem.* **2004**, *69*, 1858-1865. b) Govindaraju, T.; Kumar, V. A.; Ganesh, K. N. *J. Org. Chem.* **2004**, *69*, 5725-5734.
155. (a) Knudsen, H.; Nielsen, P. E. *Nucleic Acid Res.* 1996, *24*, 494. (b) Bentin, T.; Larsen, H. J.; Nielsen, P. E. *Biochemistry* **2003**, *42*, 13987.
156. Boiziau, C.; Kurfurst, R.; Cazenave, C.; Roig, V.; Thuong, N. T.; Toulme, J.J. *Nucleic Acids Res.* **1991**, *19*, 1113-1119.
157. Knudsen, H.; Nielsen, P. E. *Nucleic Acid Res.* **1996**, *24*, 494.
158. (a) Uhlmann, E.; Will, D. W.; Breipohl, G.; Langner, D.; Rytte, A. *Angew. Chem. Int. Ed. Engl.* 1996, *108*, 2793-2797; (b) *Angew. Chem. Int. Ed. Engl.* 1996, *35*, 2632-2635.
159. Dieci, G.; Corradini, R.; Sforza, S.; Marchelli, R.; Ottonello, S. *J. Biol. Chem.* **2001**, *276*, 5720.
160. (a) Knudsen, H.; Nielsen, P. E. *Nucleic Acid Res.* **1996**, *24*, 494. (b) Bentin, T.; Larsen, H. J.; Nielsen, P. E. *Biochemistry* **2003**, *42*, 13987.
161. (a) Sforza, S.; Haaima, G.; Marchelli, R.; and Nielsen, P. E. *Eur. J. Org. Chem.* **1999**, 197-204. (b) Lagrioule, P.; Wittung, P.; Eriksson, M.; Jensen, K. K.; Norden, B.; Buchardt, O.; and Nielsen, P. E. *Chem. Eur. J.* **1997**, *3*, 912-919.
162. Bos, J. L. *Cancer Res.* **1989**, *49*, 4682-4689.
163. (a) Farr, C. J.; Saiki, R. K.; Ehrlich, H. A.; Mc Cormick, F.; Marshall, C. *J. Proc. Natl Acad. Sci. USA* **1988**, *85*, 1629-1633. (b) Suzuki, Y.; Orita, M.; Shiraishi, M.; Hayashi, K.; Sekiya, T. *Oncogene* **1990**, *5*, 1037-1043. (c) Haliassos, A.; Chomel, J. C.; Grandjouan, S.; Kaplan, J. C.; Kitzis, A. *Nucleic Acids Res.* **1989**, *17*, 8093-8099.
164. Oerum, H.; Nielsen, P. E.; Egholm, M.; Berg, R. H.; Buchardt, O.; Stanley, C. *Nucleic Acids Res.* **1993**, *21*, 5332-5336.
165. Thiede, C.; Bayerdoerer, E.; Blasczyk, R.; Wittig, B.; Neubauer, A. *Nucleic Acids Res.* **1996**, *24*, 983-984.
166. Komiyama, M.; Aiba, Y.; Yamamoto, Y.; Sumaoka, J. *Nat Protoc* **2008**, *3*, 655-662.
167. Lohse, J.; Dahl, O.; Nielsen, P. E. *Proc. Natl. Acad. Sci. U S A* **1999**, *96*, 11804-11808.
168. Brandt, O.; Feldner, J.; Stephan, A.; Schroder, M.; Schnolzer, M.; Arlinghaus, H. F.; Hoheisel, J. D.; Jacob, A. *Nucleic Acids Research*, **2003**, *31*, e119.

Chapter 2

Design, Synthesis and Characterization of Fluorinated PNA Monomers and Their Oligomerization

PNAs fluorinated at various positions in the nucleobase, side chain and backbone have been synthesized and characterized in this chapter.

2.1 Introduction

The major limitations of the therapeutic applications of PNA as described in chapter 1 are poor solubility in aqueous media due to self-aggregation, insufficient cellular uptake and ambiguity in orientational selectivity of binding. To address these limitations of PNA several modifications have been introduced into the classical PNA, (chapter 1) generally based on conformational preorganization through cross linking the backbone atoms or backbone with side chain to generate cyclic PNAs, making them chiral and cationic. *The present work departs from these approaches and involves introduction of fluorine (F) into backbone, side chain and/or nucleobases to make PNAs intrinsically lipophilic and hence better propensity for cell penetration.*

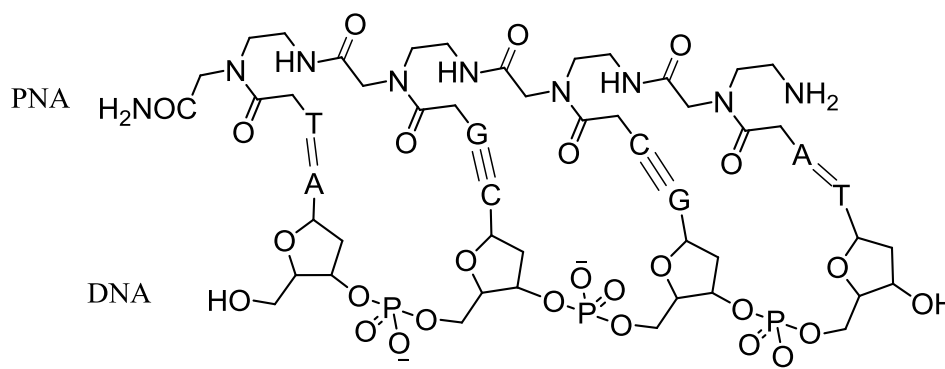


Figure 2.1 PNA:DNA duplex

As expected from its position in the periodic table of elements, fluorine possesses high electronegativity and a small atomic radius. Fluorine is the smallest substituent that can be used as replacement for the H atom in the C-H bond.¹ Introducing a F atom in an organic molecule is known to generally increase the lipophilicity, metabolic stability and bioavailability. Metabolic stability is one of the key factors in determining the bioavailability of a compound. Rapid oxidative metabolism by the liver enzymes, in particular the P450 cytochromes, is often found to limit bioavailability. A frequently employed strategy to circumvent this problem is to block the reactive site by the introduction of a fluorine atom. There are many examples illustrating the replacement of an oxidizable C-H bond by a C-F bond increasing the metabolic stability of the molecule.² Thus the incorporation of fluorine into a drug allows simultaneous modulation of electronic, lipophilic and metabolic stability, all of which can critically influence both the pharmacodynamics and pharmacokinetic properties of drugs. Bioisosteric substitution of hydrogen by fluorine is therefore an important strategy for incorporation of a group capable of reinforcing drug-receptor interactions, aiding translocation across lipid bilayers and inducing conformational change/blocking metabolism.³

Fluorinated compounds are least abundant of natural organic halides but interestingly 20-25% of drugs in the pharmaceutical pipeline contain at least one fluorine atom.¹ One of the earliest synthetic fluorinated drugs was 5-fluorouracil, an antimetabolite first synthesized in 1957.⁴ It showed high anticancer activity by inhibiting the enzyme thymidylate synthase, thereby preventing the cellular synthesis of thymidine. Since then, fluorine substitution is commonly used in contemporary medicinal chemistry to improve metabolic stability, bioavailability and protein-ligand interactions.¹

The strong basic groups on drugs may have good affinity for receptors but reduce the bioavailability. Fluorine substitution reduces the basicity of neighbouring amines and thereby enhances bioavailability. The strong basic indole derivatives are selective to 5HT_{1D} receptor ligands but they have low bioavailability and cannot transverse through membranes. The basicity and bioavailability have been optimized by introducing fluorine⁵ (Figure 2.2).

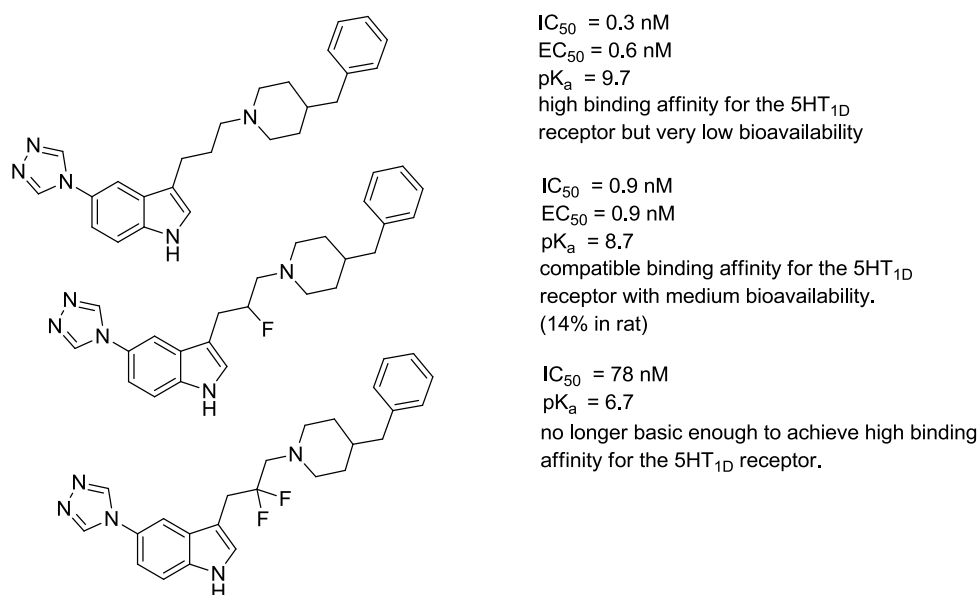


Figure 2.2 Fluorine effect on basicity of neighbouring amines and bioavailability⁵

The replacement of an oxidizable C-H group by a C-F group increases the metabolic stability of the drug and this approach is often employed to design many successful drugs.⁶⁻¹⁰ This happens via lowering the susceptibility of nearby groups to cytochrome P450 enzymatic oxidation.⁶ The potent cholesterol absorption inhibitor Ezetimibe having fluorine substituents has increased metabolic stability compared to its non-fluorinated analog SCH 48461 (Figure 2.3). The introduction of fluorine on phenyl ring and replacing the methoxy group by fluorine prevents the oxidation of the phenyl ring to phenol and dealkylation of the methoxy group.^{8,9}

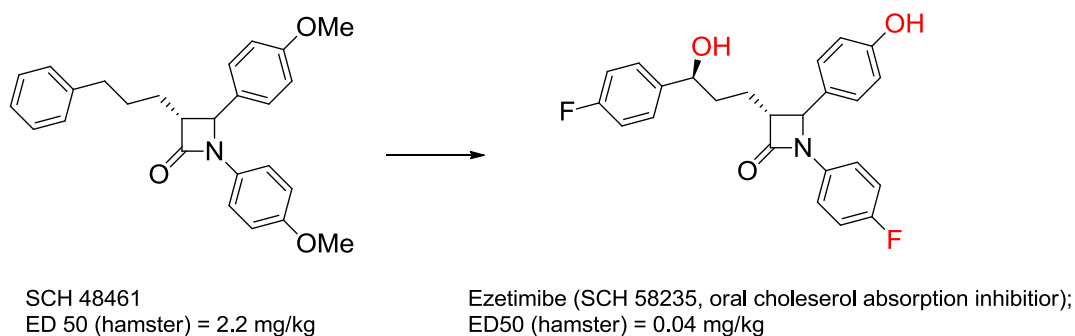


Figure 2.3 Metabolic stability of Ezetimibe increased by blocking metabolically labile sites of the compound SCH48461 by fluorine substituents⁸

Another interesting and reverse example is the design of the cyclooxygenase 2 (COX 2) inhibitor celecoxib.¹¹ In this case, the lead compound celecoxib is metabolically highly stable with a very long biological half-life. The half-life is reduced to acceptable levels by replacing a fluorine atom by a methyl group (Figure 2.4).

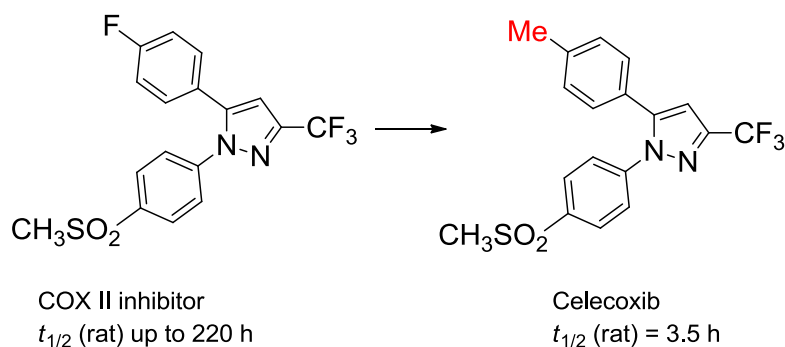
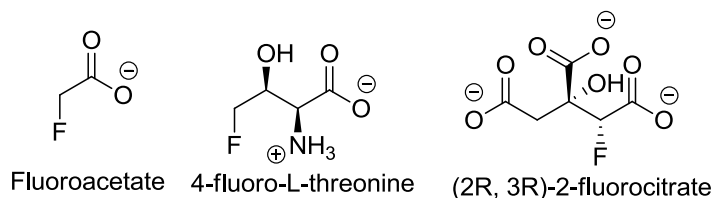


Figure 2.4 Replacement of a fluorine group by a methyl group reduces the long half-life of celecoxib to an acceptable level.¹¹

The physical properties of the fluoride ion appear to limit the evolution of fluorine biochemistry; however, in nature a few rare fluoro metabolites have been identified, and are shown in Figure 2.5.¹² Interestingly, even out of these five naturally occurring fluoro metabolites, two are antibiotics (Nucleocidin¹³ and 4-fluorothreonine¹⁴, Figure 2.5).



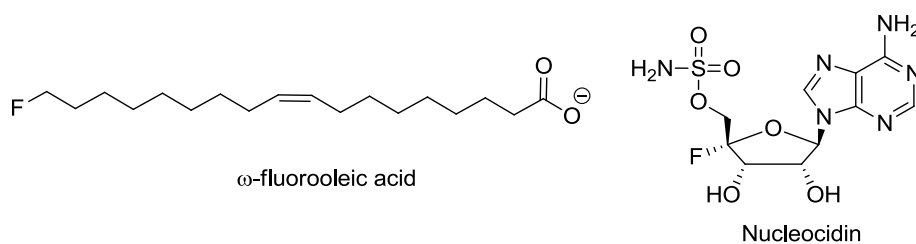


Figure 2.5 Naturally occurring fluorinated compounds.¹²

Fluorination enzyme has been identified in bacteria, the first of which was isolated from the soil bacterium *Streptomyces cattleya*.¹⁵ Only five fluorination enzyme are known so far and are involved in secondary metabolism, and thus synthesizing bioactive fluorinated natural products when bacterium is grown in a medium containing fluoride.¹⁴ It is an exciting concept that *flA* genes and their associated biosynthetic and regulatory genes are successfully used in engineering the biosynthesis of novel fluoro metabolites. The fluorinase enzyme is also utilized in the synthesis of a range of [¹⁸F]-labelled compounds for positron emission tomography (PET) experiments.¹²

These are some illustrative examples of fluorine containing drugs where fluorine has played a major role in tuning the medicinal properties. Thus there is a great deal of interest in the synthesis of fluorinated organic compounds.

2.1.1 Selective fluorinating agents

Although the preparation of elemental fluorine was discovered in 1886 by Moisson, use of fluorine as reagent was limited due to its extreme reactivity. The introduction of safe and selective fluorinating reagents around 1970 has seen an increase in the number of commercial fluorinating agents. Currently, there are three types of fluorinating reagents available in the form of nucleophilic, electrophilic and trifluoromethylating reagents¹⁶⁻¹⁸ (Figure 2.6). Employing these, many fluorine based building blocks are available for synthesis of oligo peptides and carbohydrates. Recognising the important role played by fluorine in medicinal chemistry, this chapter is devoted to the synthesis of fluorinated analogues PNAs are hitherto unknown, except for a single example at the time this work was initiated.

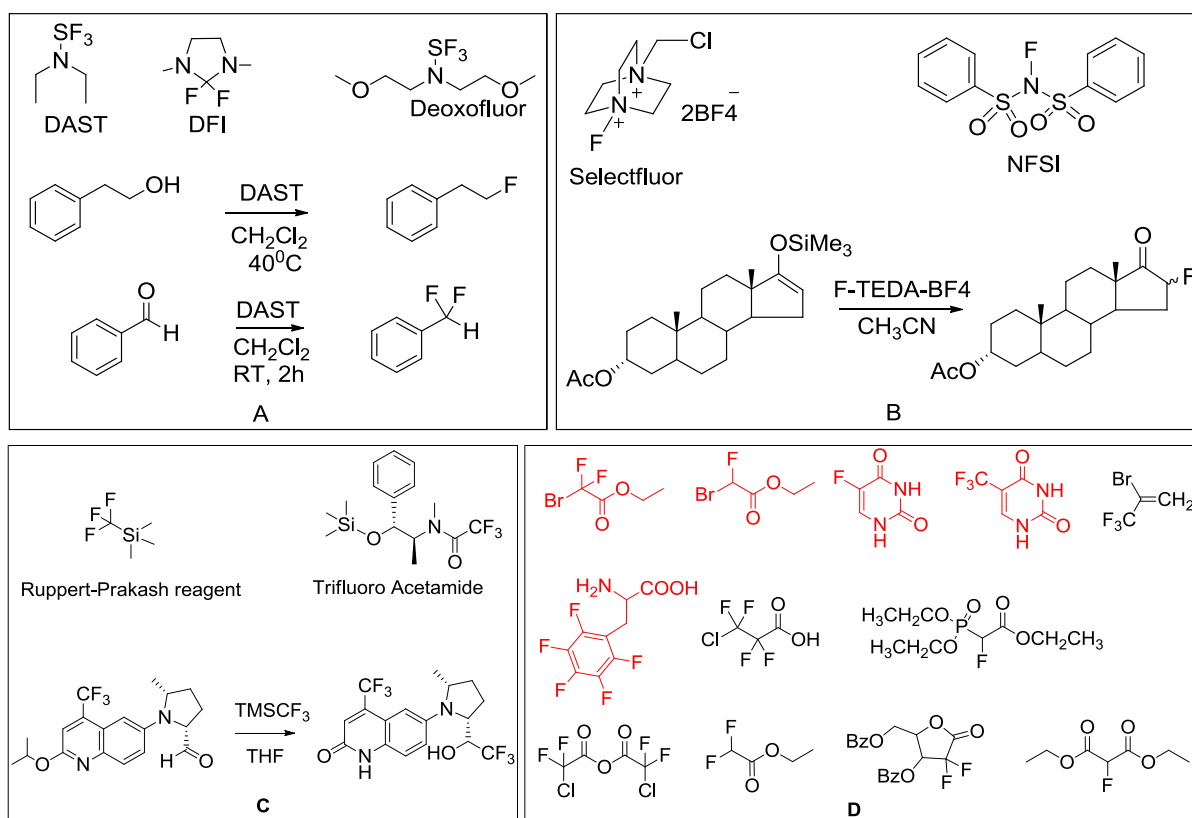


Figure 2.6 A) Nucleophilic fluorinating reagents¹⁶ B) Electrophilic fluorinating reagents¹⁷ C) reagents to introduce CF_3 groups¹⁸ and D) Fluorinating building blocks

Leumann *et al.*¹⁹ synthesized the fluorinated olefinic peptide nucleic acid monomer (F-OPA) in which methylene carbonyl linker carrying the base was replaced with an isostructural fluorinated C-C double bond (Figure 2.7). This was done to understand the role of tertiary amide function in PNA fixing the base orientation for DNA recognition. It was concluded that the central amide bond in PNA provided steric control as an important element in recognition of cDNA.¹⁹

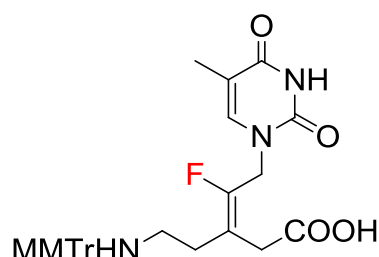


Figure 2.7 Olefinic fluorinated PNA monomer

Barthelemy *et al.*²⁰ conjugated per-fluorinated C8 chain to a 17-mer oligonucleotide to study its cellular uptake (Figure 2.8). The fluorinated oligo could be successfully delivered into three different human cell lines (hepatic Huh7, gastric epithelial NCI-N87 and embryonic kidney HEK293 cells).²⁰

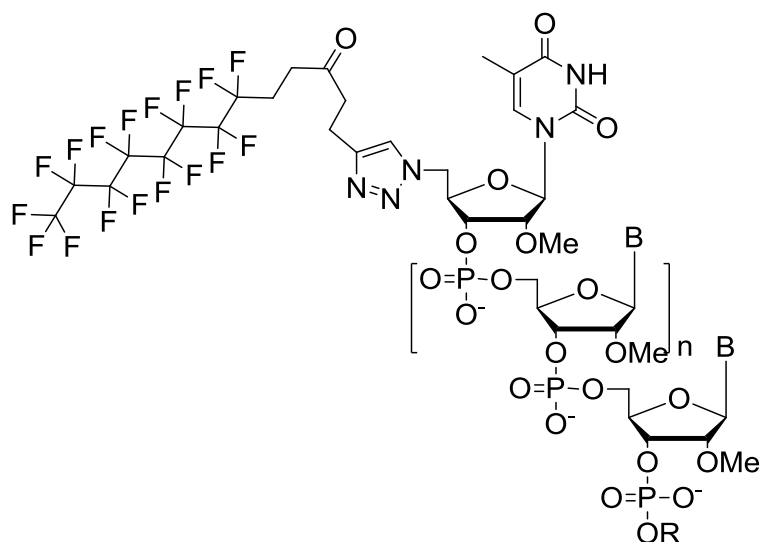


Figure 2.8 Oligoribonucleotide conjugated with perfluoro alkyl chain ²⁰

While the present work was in progress Virta *et al.*²¹ reported 5-[3,3-bis(trifluoromethyl)-4,4,4-trifluorobut-1-ynyl]uracil- and 5-(trifluoromethyl)uracil-derived PNAs containing fluorine on base (Figure 2.9). The base fluorinated monomers were incorporated into PNA and the duplex formation with complementary DNA and RNA was monitored by ¹⁹F-NMR spectroscopy, demonstrating the merit of fluorine as a sensor to probe PNA:DNA/RNA hybridization.²¹

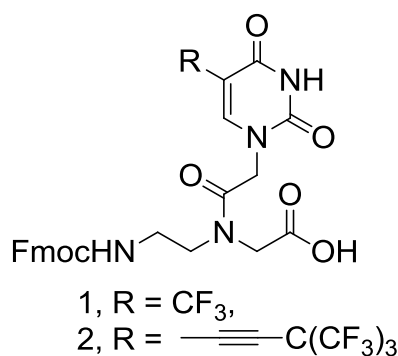


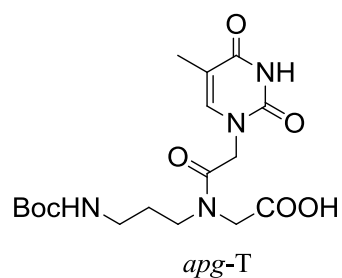
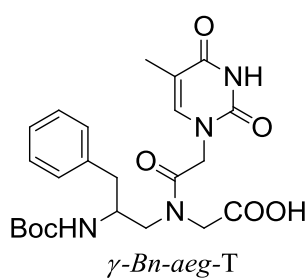
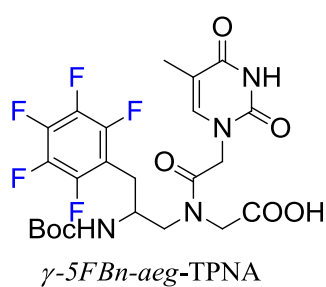
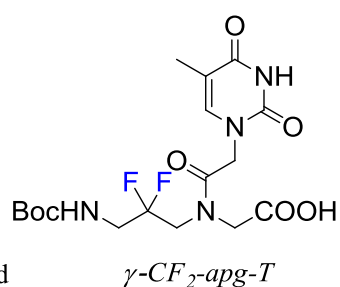
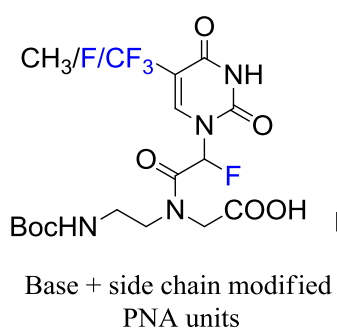
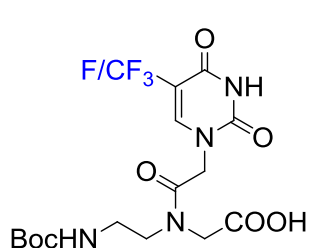
Figure 2.9 Fluorinated building blocks for ¹⁹F-NMR sensing²¹

The next section (Section 2A) deals with the synthesis of monomers containing fluorine at various possible positions (base, side chain and backbone) on PNA (Figure 2.10). This is followed by incorporation of the various fluorinated monomers into PNA oligomers by solid phase synthesis (Section 2B).

Section 2A

Synthesis and Characterization of Fluorinated PNA

Monomers



The objectives of the chapter are to synthesise fluorinated PNA monomers (base, side chain and backbone substituted) their incorporation at specific sites in PNA sequence to generate fluorinated PNA oligomers in order to improve their cell permeation abilities. The various positions possible for the incorporation of fluorine in a PNA unit are illustrated in the Figure 2.10.

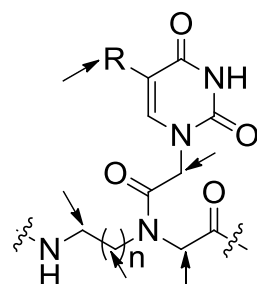
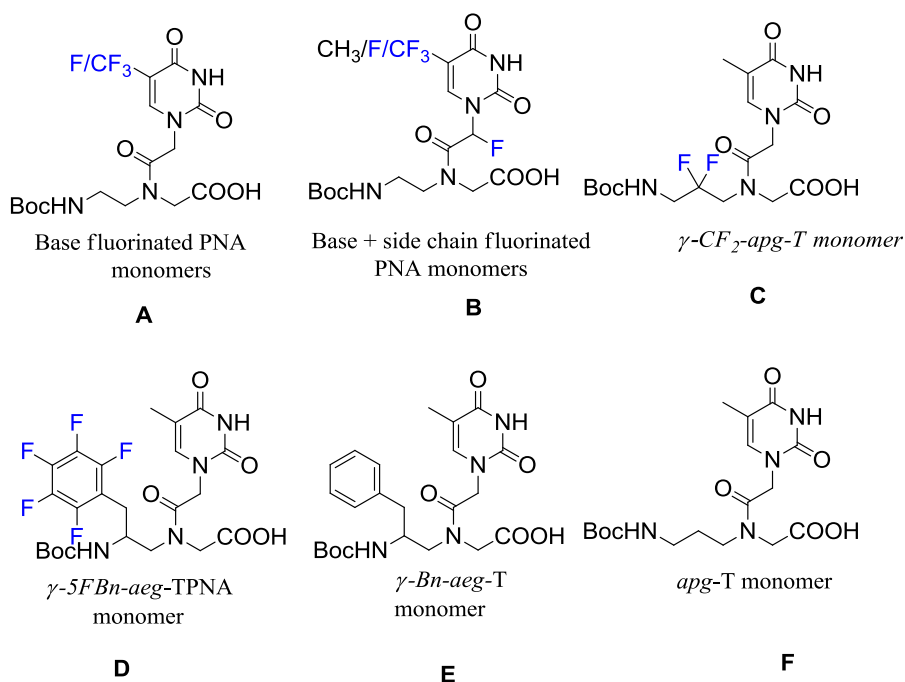


Figure 2.10 Possible sites for fluorination in PNA units

2A.1 Aim of the present work

Synthesis and characterization of PNA monomers fluorinated in

- Nucleobase (C5, F/CF₃), [A]
- Side chain (Fluoro acetyl (-CHF-CO-)), [B]
- Side chain + nucleobase (Fluoro acetyl + C5 nucleobase), [B]
- Backbone (-CH₂CF₂-CH₂-, -CH₂-5FPh), [C, D]



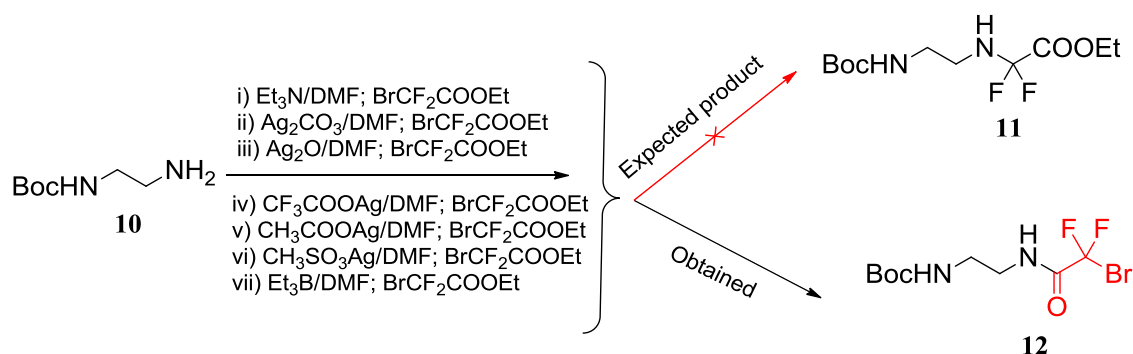
2A.2 Synthesis of fluorinated PNA monomers

This section describes the synthesis of designed fluorinated PNA monomers and their characterisation using appropriate spectroscopic techniques.

2A.2.1 Attempts towards the synthesis of α -fluorinated PNA monomer

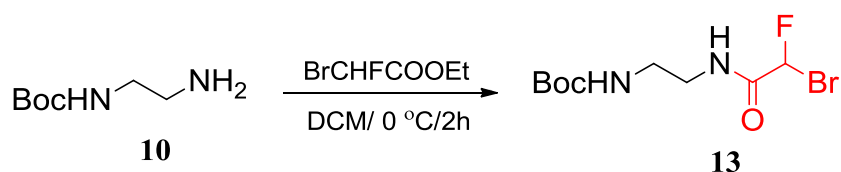
The first fluorinated PNA monomer attempted was α -fluoroglycinated monomer from the fluorinated reagent ethyl bromodifluoroacetate (Scheme 1). The commercially available ethylene diamine was reacted with Boc-anhydride (Boc)₂O in presence of Et₃N to obtain mono N-Boc-ethylene diamine **10**. Attempts to N-alkylate compound **10** with ethyl bromodifluoroacetate to obtain compound **11** interestingly resulted in N-acylation to yield product **12**. All efforts to achieve N-alkylation under different reaction conditions always resulted in the formation of the N-acylated product **12**.

Scheme 1 Attempt towards the synthesis of α -difluorinated PNA monomer



As difluorinated reagent BrCF₂COOEt was failed to give N-alkylation, the monofluoro agent ethyl bromofluoroacetate was tried for N-alkylation of N-Boc-ethylenediamine **10** (Scheme 2). However this again resulted in the formation of the corresponding N-acylated product **13** instead of the desired N-alkylated product.

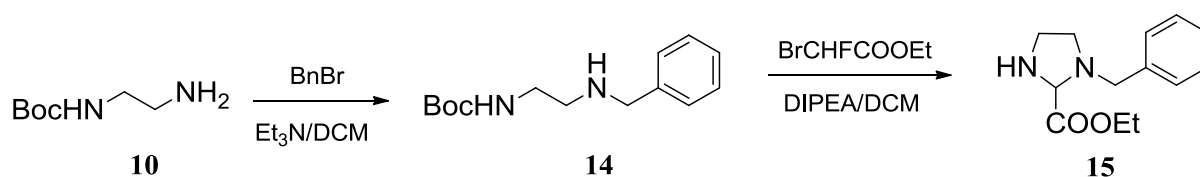
Scheme 2 Attempt towards the synthesis of α -monofluorinated PNA monomer



Thus, the reaction of both monofluoro- and difluoro ethylbromoacetate with primary amine lead to N-acylation but not N-alkylation. In view of these reactions with a primary

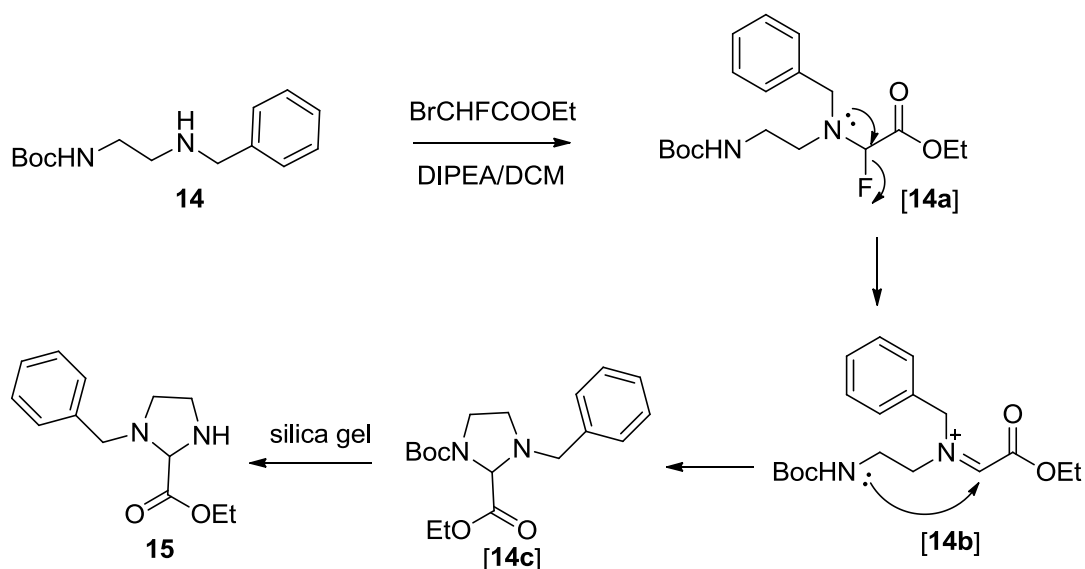
amine to N-acylation, possibility of N-alkylation was attempted with a secondary amine (Scheme 3). The mono Boc-ethylene diamine **10** was treated with benzyl bromide to get the secondary amine **14** which was treated with ethyl bromofluoroacetate. This led to the formation of a non-fluorinated cyclized product **15** which was characterized by ^1H , ^{13}C and DEPT.

Scheme 3 Attempt towards the synthesis of α -monofluorinated PNA monomer from 2 $^\circ$ -amine



The formation of compound **15** can be explained by the mechanism shown below. The initial N-alkylated product [**14a**] undergoes F^- elimination to give the α,β -unsaturated cationic imine [**14b**] which undergoes intramolecular cyclization to give the cyclized product [**14c**] and that gets N-protected during column chromatography to yield the cyclized compound **15**. Hence attempts to obtain α -fluoro glycinated PNA monomer were abandoned.

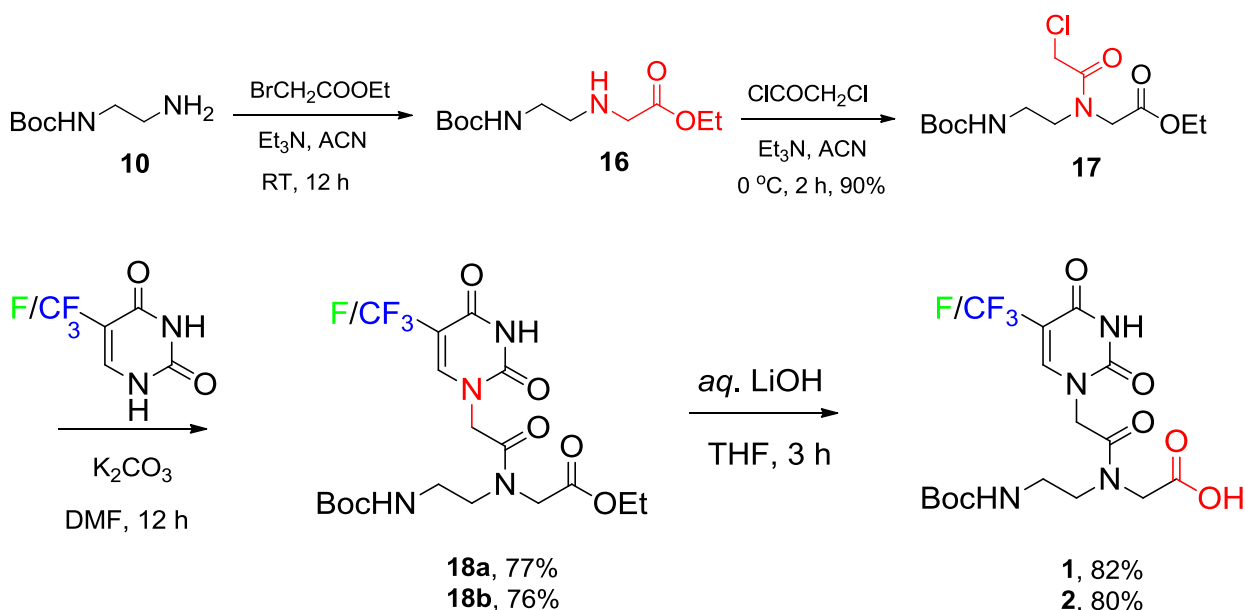
Proposed mechanism



2A.2.2 Synthesis of nucleobase modified (5FU-aeg, 5CF₃U-aeg) PNA monomers 1 & 2

The Boc-protected ethylenediamine **10** was N-alkylated with ethyl bromoacetate in acetonitrile using Et₃N as base to obtain compound **16** (Scheme 4) which was N-acylated with chloroacetyl chloride in acetonitrile in presence of Et₃N to give the chloro derivative **17**. This was coupled with 5(F/CF₃)-substituted uracil (5-FU and 5-CF₃U) in presence of K₂CO₃ as base in DMF to yield the ester **18a/b**. The ester was hydrolyzed to acid monomer **1** and **2** respectively.

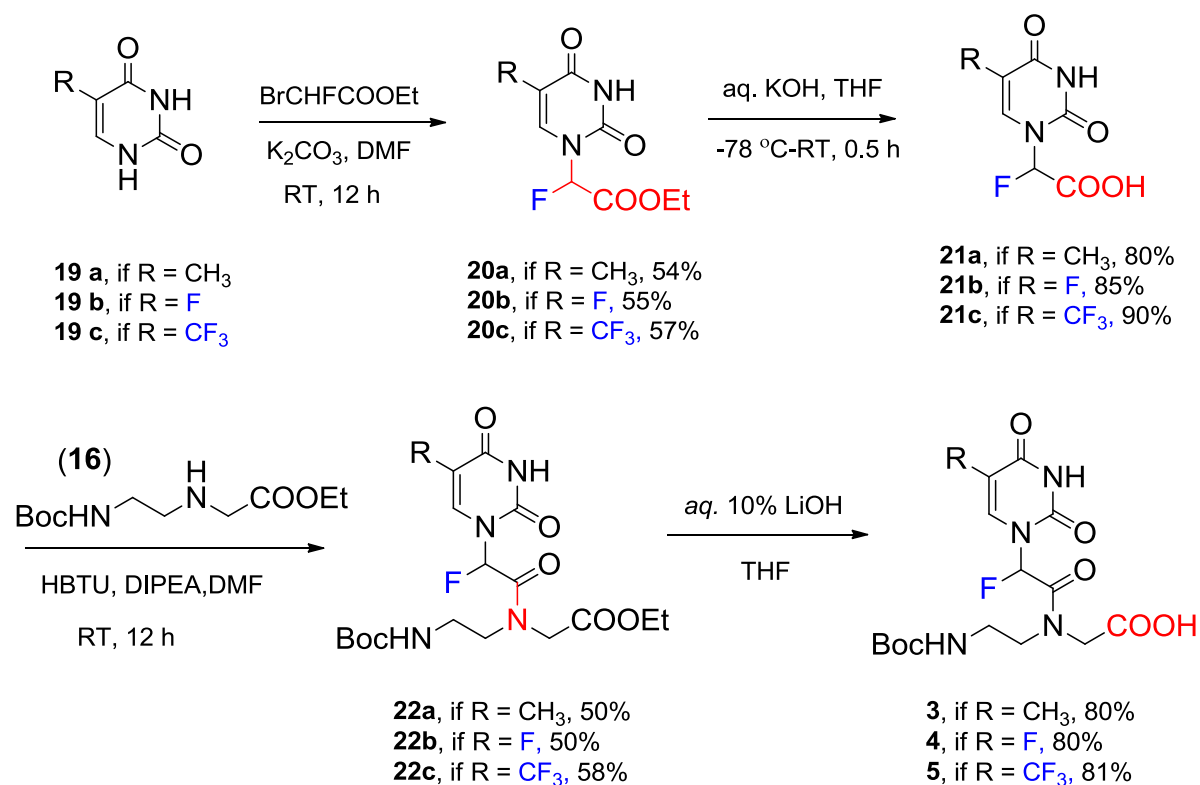
Scheme 4 Synthesis of 5FU-aeg, 5CF₃U-aeg PNA monomers 1 & 2



2A.2.3 Synthesis of nucleobase and side chain fluorinated (δ -F-aeg-T), (δ -F-5FU-aeg), and (δ -F-5CF₃U-aeg) PNA monomers 3, 4 & 5

The nucleobase and side chain fluorinated PNA monomers were synthesized from the commercially available 5-substituted uracil nucleobase (5-methyluracil/5-fluorouracil/5-trifluoromethyluracil). These were individually treated with ethyl bromofluoroacetate in presence of K₂CO₃ to obtain N¹-fluoroalkylated product **20a/b/c** respectively. These were hydrolyzed to corresponding acid compounds **21a/b/c** using aq. KOH, followed by coupling with N-Boc-2-aminoethyl glycine ethylester in presence of HBTU/DIPEA to obtain the PNA ester monomers **22a/b/c**. interestingly this gave the N-alkylated product rather than the N-acylated product as seen with the aliphatic amines. The esters were hydrolysed to respective acids to obtain the desired fluorinated PNA monomers **3/4/5** required for later synthesis of fluorinated PNA oligomers (Scheme 5).

Scheme 5 Synthesis of δ -F-*ae*-T, δ -F-5FU-*ae*g, and δ -F-5CF₃U-*ae*g PNA monomers 3, 4 & 5

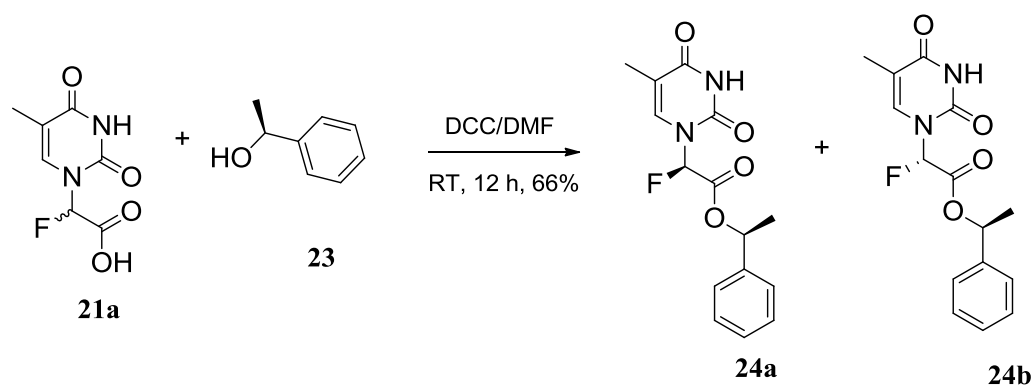


All compounds were characterized by ¹H-NMR and ¹⁹F-NMR. Since all the free acid monomers **1-3** are racemic, approaches to resolve the same through conversion to diastereomeric mixture is presented in next section.

2A.2.3a Resolution of racemic mixture of compound **21a**

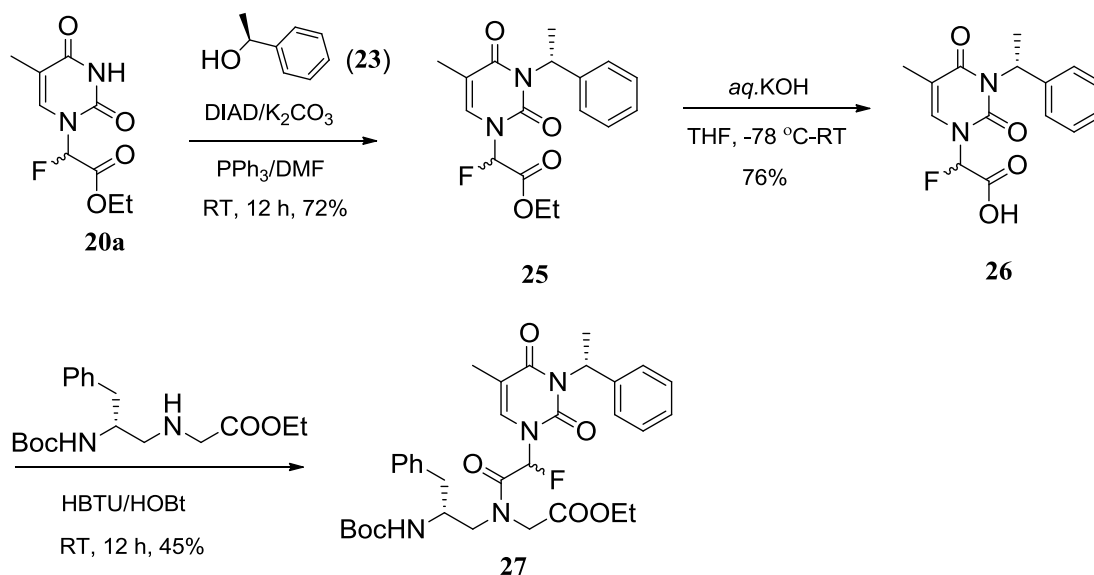
Attempt 1: The racemic **21a** was treated with (*S*)-1-phenylethanol **23** in presence of DCC using DMF as solvent to obtain the diastereomeric mixture of **24a** and **24b** (Section 5a). These could not be separated using either regular column chromatography or by crystallization. The crystals obtained had both the diastereomers and the packing diagrams indicated that they were held together by thymine-thymine hydrogen bonding (Experimental section, page no 103).

Scheme 5a Synthesis of diastereomeric mixture for compound 21a



Attempt 2: In second approach (Scheme 5b), compound **20a** was treated with (*S*)-1-phenylethanol **23** in presence of DIAD/ PPh_3 and K_2CO_3 in DMF to obtain mixtures of the diastereomeric *N*-alkylated compounds **25**. The mixture **25** also could not be separated under regular column chromatography. It was hydrolyzed to acid mixture **26** and coupled with γ -benzyl-aminoethyl glycine ethylester (γ -*Bn*-*aeg*) backbone **50b** (for synthesis see section 2A.2.6) using HBTU/HOBt to obtain the diastereomeric mixture **27** which also could not be separated by column chromatography or crystallization.

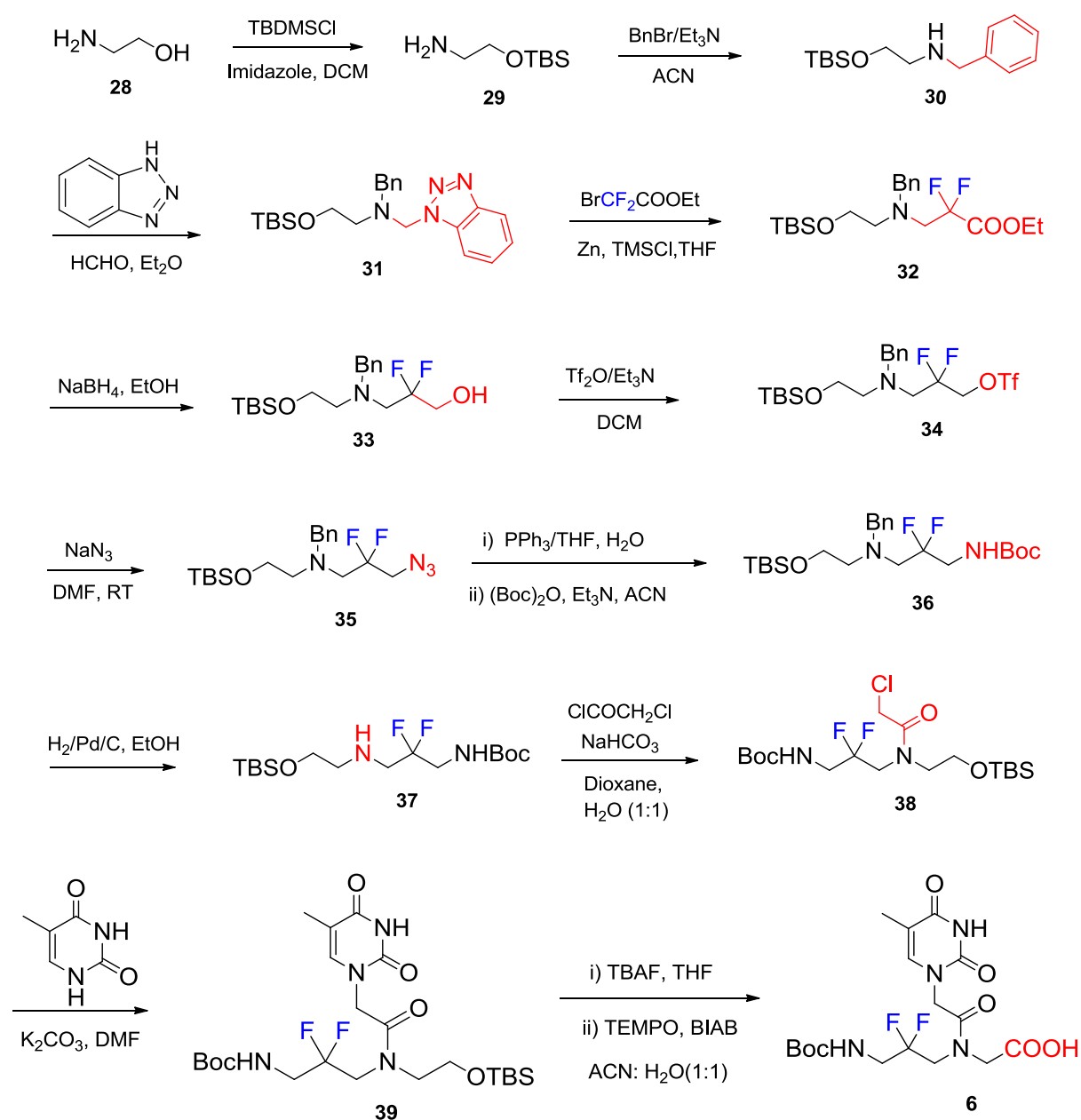
Scheme 5b Synthesis of diastereomeric mixtures for compound 21a

2A.2.4 Synthesis of backbone modified (γ - CF_2 -*apg*) PNA monomer 6

Synthesis of difluorinated γ - CF_2 -*apg* PNA monomer **6** that has an extended backbone (propylene in place of ethylene) was done by reaction of ethyl bromodifluoroacetate under Reformatsky reaction conditions as the key step (Scheme 6). The commercially available

ethanolamine **28** was protected at hydroxyl group with TBDMSCl to obtain compound **29**, which was N-alkylated with benzyl bromide in presence of Et₃N to give compound **30**. This was treated with formaldehyde and benzotriazole to yield **31** that was used for the Reformatsky reaction with ethyl bromodifluoroacetate in presence of zinc and trimethylsilyl chloride. The reaction gave the N-dialkylated difluoro compound **32**, whose ester group was reduced to the alcohol **33** with sodium borohydride. The hydroxyl group was converted to triflate derivative by reaction with triflic anhydride and then to azide **35** by reaction with sodium azide. The reaction gave the N-dialkylated difluoro compound **35**, whose ester group was reduced to the alcohol **33** with sodium borohydride. The hydroxyl group was converted to triflate derivative by reaction with triflic anhydride and then to azide **35** by reaction with sodium azide.

Scheme 6 Synthesis of γ -CF₂-apg PNA monomer **6**

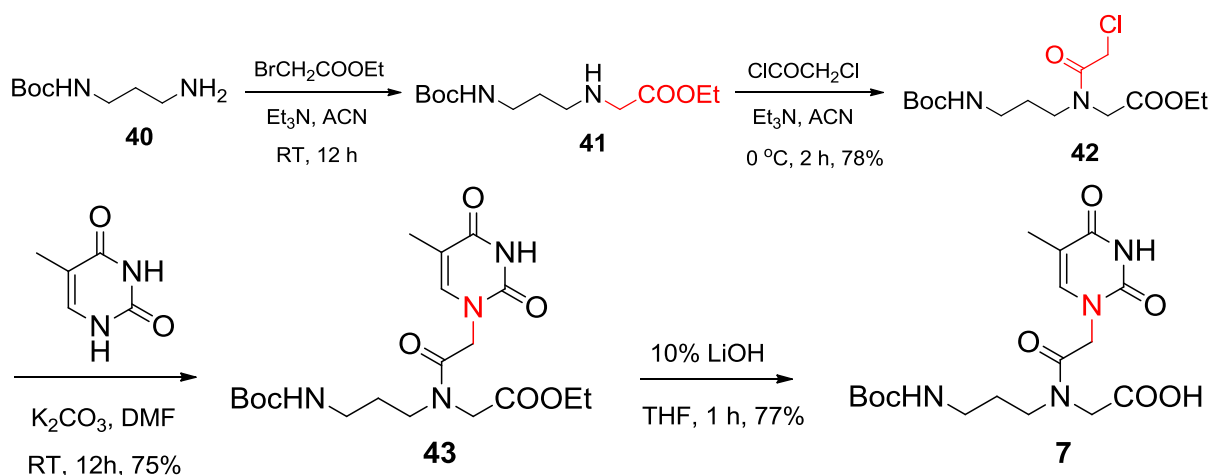


The azide was transformed to amine using Staudinger reaction conditions and in situ protected as -NHBoc using Boc-anhydride to get compound **36** which was debenzylated by hydrogenation over Pd/C to the amine **37**. This was N-acylated with chloroacetyl chloride to yield compound **38** that was coupled with thymine using K_2CO_3 as base to obtain precursor monomer **39**. The O-TBDMS in **39** was deprotected using TBAF and subsequently oxidized to acid using TEMPO (2,2,6,6-tetramethyl-piperidin-1-yl)oxyl) and BIAB (bis(acetoxy)iodobenzene) to reach the desired acid PNA monomer **6**, having difluoromethylene group in the extended backbone.

2A.2.5 Synthesis of N-(3-aminopropyl)glycine (*apg*) PNA monomer 7

The commercially available 1,3-diaminopropane was treated with Boc-anhydride to yield mono N-Boc compound **40** which was N-alkylated using ethylbromoacetate to obtain compound **41** (Scheme 7). This was N-acylated with chloroacetyl chloride to get **42** which was coupled with thymine to yield the ester **43**. Saponification of ester **43** to acid gave the target *apg* PNA monomer **7** needed to synthesise the control *apg* PNA oligomers.

Scheme 7 Synthesis of *apg* PNA monomer 7

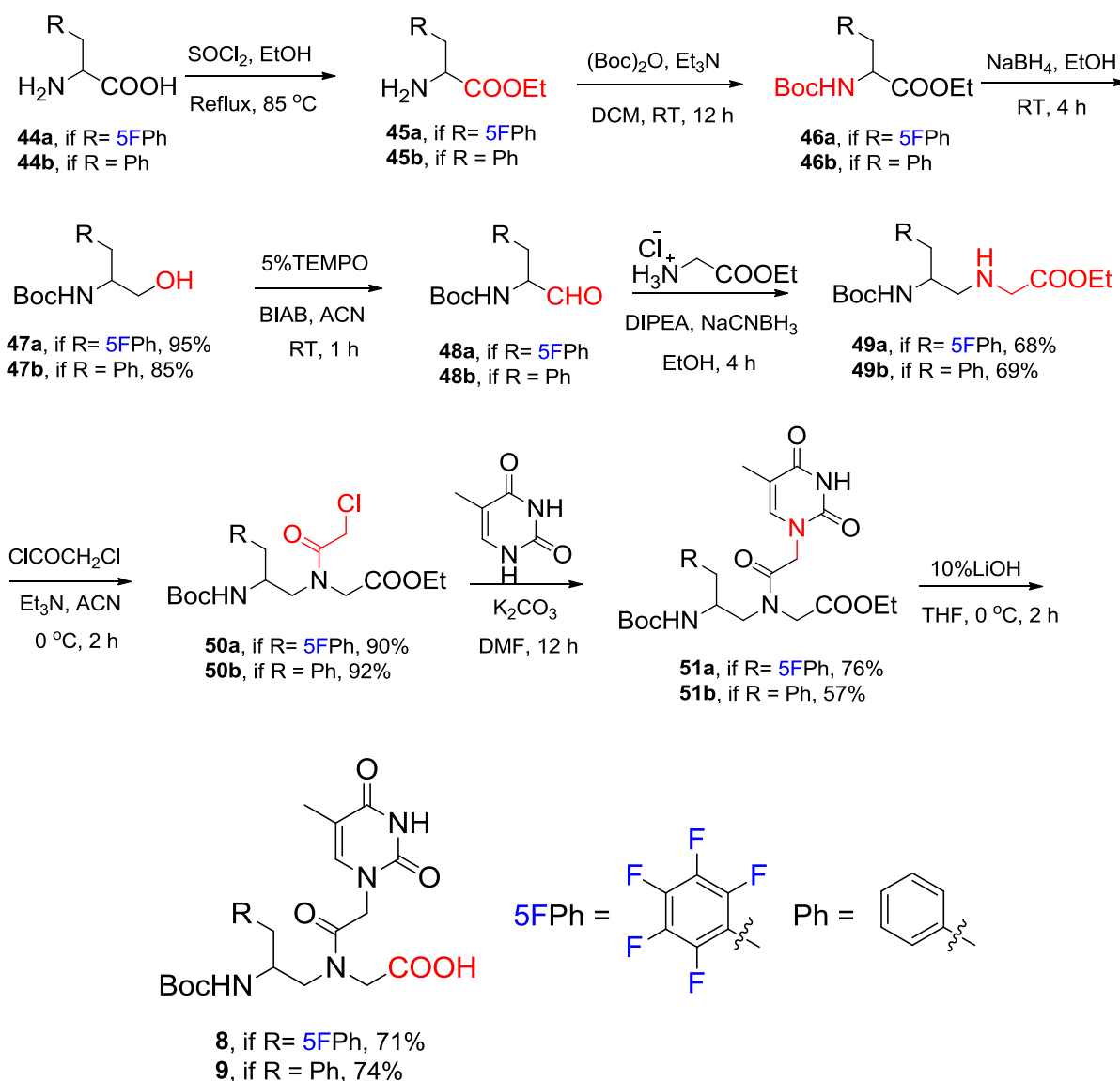


2A.2.6 Synthesis of backbone modified (γ -5*F*Bn-*aeg*, γ -Bn-*aeg*) PNA monomers 8 & 9

A useful method for introduction of multiple fluorine into PNA is by incorporation of pentafluorophenyl group into the molecule. This was achieved starting from the commercially available pentafluoro D-phenylalanine **44a**, which was treated with thionylchloride in ethanol to obtain corresponding ester **45a**. The amine was protected as -NHBoc to obtain **46a**, followed by reduction of the ester to alcohol **48a** using $NaBH_4$. Subsequent oxidation of alcohol to aldehyde **48a** and coupling with glycine ethyl ester under reductive amination conditions gave ethyl 2-((2-((*t*-Boc)amino)-3-(perfluorophenyl) propyl)amino)acetate **49a**.

This was N-acylated with chloroacetyl chloride to get **50a** and coupled with thymine to result in the ester monomer **51a**. Final hydrolysis of the ester monomer **51a** to acid yielded the γ -methylene pentafluorophenyl substituted monomer **8**. Its control PNA monomer γ -Bn-*aeg* (**9**) was synthesized by employing similar methodology.

Scheme 8 Synthesis of γ -5FBn-*aeg*, γ -Bn-*aeg* PNA monomers **8** & **9**



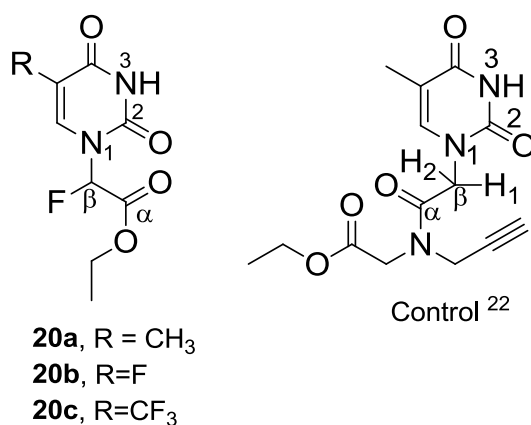
Calculation of rotameric population

Side chain modified fluoro derivatives δ -F-*aeg*-T, δ -F-5FU-*aeg* and δ -F-5CF₃U-*aeg* showed ~ 69%, ~ 68% and ~ 70% major rotameric populations respectively whereas *aeg*-T showed 62% major rotameric population. This clearly indicates that introducing fluorine in side chain of the *aeg* PNA backbone slightly decreases the rotation of amide bond over central

tertiary amide. In case of *apg* PNA monomer the major rotameric population is ~57% whereas its fluorinated derivative γ -CF₂ *apg* showed 77% major rotameric population. This also indicates that fluorine substitution in the backbone of the *apg* PNA monomer restricted the amide bond rotation significantly. Thus fluorine substitution in a PNA monomer increases one rotameric population considerably over other rotamer. In case of *5FBn-aeg* and *5Bn-aeg* PNA monomers, the rotameric population was almost equal and it was ~ 55%. Introducing pentafluorophenyl/benzyl group in the side chain of the *aeg* backbone decreased the rotameric population as compared to unmodified *aeg* PNA monomer (62%).

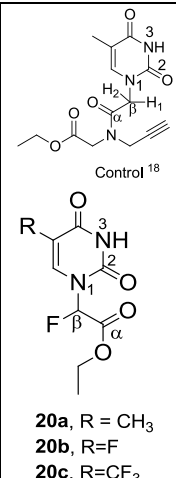
2A.3 Crystal details of racemic compounds 20a, 20b and 20c

From crystal packing diagrams it was observed that the two enantiomers were held together by hydrogen bonding. Crystal packing details of each compound is given below. A theoretical study was also employed on compounds **20a-c** in order to compare fluorine effect on dihedral angles of F-C_β-N1-C₂, F-C_β-C_α-O and the angle of N1-C_β-F at ground-state energy to the values of obtained from crystal structure. The dihedral angles were also compared with that of non-fluorinated analog ethyl 2-(2-(5-methyl-2,4-dioxo-3,4-dihydropyrimidin-1(2H)-yl)-N-(prop-2-yn-1-yl)acetamido)acetate which are obtained from its crystal structure. Structures of fluorinated and non-fluorinated analogs are shown below and the dihedral angles are tabulated in Table 2.1.



Numerical simulations have been performed within density functional theory (DFT) using Gaussian 09 package²³ for compounds **20a**, **20b** and **20c**. The Becke three-parameter hybrid (B3)²⁴ functional was used along with Lee-Yang-Parr (LYP)²⁵ correction. For all optimization and harmonic vibrational frequency calculations, 6-31 G* basis set of Pople has been employed. The structures derived from theoretical study are given in Figure 2.11, 2.12 and 2.13 respectively.

Table 2.1 Tri angle and torsion angles of compounds 20a, 20b and 20c

Compound	N1-C _β - F/H ₁ /H ₂ angle	H ₁ \F-C _β - N1-C ₂ torsion angle	F-C _β -C _α -O torsion angle	Hydrogen bonding N-H...O=C	 <p>Control¹⁸</p> <p>20a, R = CH₃ 20b, R = F 20c, R = CF₃</p>
Control/H ₁	109.68	41.43	-129.89		
Control/H ₂	109.62	160.29	111.59		
20aR	109.60	72.02	19.98	2.923, 2.759	
20aS	109.93	-71.51	-19.37		
20bR	108.83	67.63	-150.03	2.860	
20bS	108.83	109.86	150.03		
20cR	109.65	73.77	24.49	2.820	
20cS	109.65	-73.77	-24.49		
20aR	110.48	80.03	11.77	----	
DFT calculations					
20bS	109.61	116.15	99.44	----	
20cS	110.14	-78.88	-13.98	----	

2A.3.1 Crystal, DFT calculated structure and data of compound 20a

Crystals were grown by slow evaporation from a solution of ethylacetate/petroleumether mixture. A single crystal (0.45 x 0.35 x 0.30 mm) was mounted on loop with a small amount of the paraffin oil. The X-ray data were collected at 200K temperature on a Bruker APEX DUO CCD diffractometer using Mo K α radiation ($\lambda = 0.71073 \text{ \AA}$), ω -scans ($2\theta = 60.86$), for a total of 6506 independent reflections. Space group P 2₁/n $a = 13.527(2) \text{ \AA}$, $b = 11.7083(16) \text{ \AA}$, $c = 14.304(2) \text{ \AA}$, $\alpha = 90^\circ$, $\beta = 104.702(3)^\circ$, $\gamma = 90^\circ$; $V = 2191.4(5) \text{ \AA}^3$, Monoclinic, $Z = 8$ for chemical formula C₉H_{11.5}F N₂O₄, $\rho_{\text{calcd.}} = 1.399 \text{ gcm}^{-3}$, $\mu = 0.121 \text{ mm}^{-1}$, $F(000) = 964$, $R_{\text{int}} = 0.0373$. The final R value was 0.0457 ($wR_2 = 0.0981$) 2145 observed reflections ($F_0 \geq 4\sigma(|F_0|)$) and 146 variables, $S = 0.990$. The structure was obtained by direct methods using SHELXS-97.1 All non-hydrogen atoms were refined anisotropically. The hydrogen atoms were fixed geometrically in the idealized position and refined in the final cycle of refinement as riding over the atoms to which they are bonded. The largest difference peak and hole were 0.321 and -0.223 e \AA^3 , respectively.

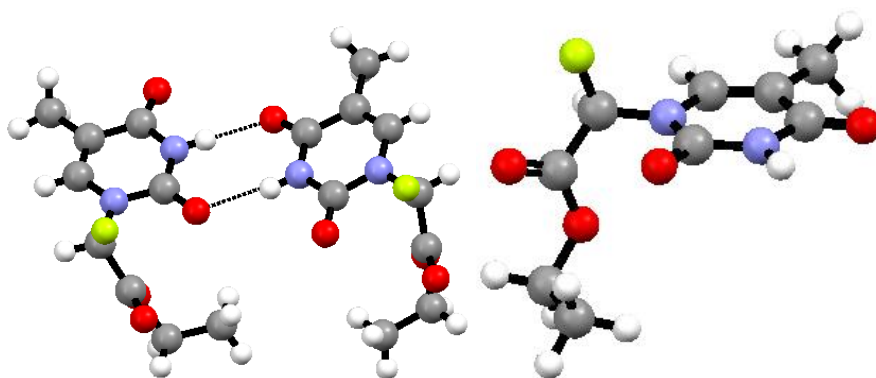


Figure 2.11 (left) Crystal structure; (right) DFT calculated structure of compound **20a**

In the crystal structure a reverse Watson-Crick Hydrogen bonding was observed between the two enantiomers. The hydrogen bonds are formed between NH (at 3rd position), carbonyl oxygen (at 4th position) of one enantiomer (N3-H---C4-O) and carbonyl oxygen (at 2nd position), NH (at 3rd position) (C2-O---H-N3) of the second molecule with a distance of 2.923 Å and 2.759 Å respectively.

2A.3.2 Crystal, DFT calculated structure and data of compound **20b**

Crystals were grown by slow evaporation from a solution of chloroform. A single crystal (0.2 x 0.12 x 0.5 mm) was mounted on loop with a small amount of the paraffin oil. The X-ray data were collected at 200K temperature on a Bruker APEX DUO CCD diffractometer using Mo K α radiation ($\lambda = 0.71073$ Å), ω -scans ($2\theta = 55.90$), for a total of 2145 independent reflections. Space group P-1 $a = 5.0538(17)$ Å, $b = 8.982(3)$ Å, $c = 10.635(3)$ Å, $\alpha = 88.176(7)^\circ$, $\beta = 83.300(7)^\circ$, $\gamma = 78.466(6)^\circ$; $V = 469.8(3)$ Å³, Triclinic, $Z = 2$ for chemical formula C₁₈H₂₄NO₄, with one molecule in asymmetric unit; $\rho_{\text{calcd.}} = 1.168$ gcm⁻³, $\mu = 0.085$ mm⁻¹, $F(000) = 240$, $R_{\text{int}} = 0.0172$. The final R value was 0.0597 ($wR2 = 0.1610$) 2145 observed reflections ($F_0 \geq 4\sigma(|F_0|)$) and 146 variables, $S = 1.009$. The structure was obtained by direct methods using SHELXS-97.1 All non-hydrogen atoms were refined anisotropically. The hydrogen atoms were fixed geometrically in the idealized position and refined in the final cycle of refinement as riding over the atoms to which they are bonded. The largest difference peak and hole were 0.412 and -0.452 eÅ⁻³, respectively.

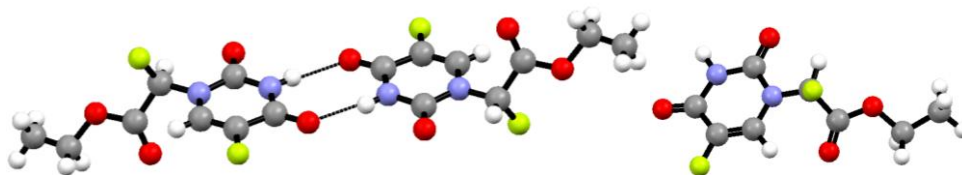


Figure 2.12 (left) Crystal structure; (right) DFT calculated structure of compound **20b**

In the crystal packing diagram of the compound **20b** a reverse Watson-crick Hydrogen bonding (2.860 Å) observed between the two enantiomers and are formed between NH group (at 3rd position), carbonyl oxygen (at 4th position) (N3-H---C4-O) of one enantiomer and carbonyl oxygen (at 4th position), NH (at 3rd position) (C2-O---H-N3) of the second enantiomer respectively with a distance 2.860Å.

2A.3.3 Crystal, DFT calculated structure and data of compound **20c**

Crystals were grown by slow evaporation from a solution of chloroform. A single crystal (0.4 x 0.4 x 0.2 mm) was mounted on loop with a small amount of the paraffin oil. The X-ray data were collected at 200K temperature on a Bruker APEX DUO CCD diffractometer using Mo K α radiation ($\lambda = 0.71073$ Å), ω -scans ($2\theta = 55.90$), for a total of 2145 independent reflections. Monoclinic space group $P21/n$ $a = 13.754(3)$ Å, $b = 5.4127(12)$ Å, $c = 15.330(4)$ Å, $\alpha = 90^\circ$, $\beta = 93.349(5)^\circ$, $\gamma = 90^\circ$; $V = 1139.4(5)$ Å³; $T = 296(2)$ K; $Z = 4$ for chemical formula C₉H₈F₄N₂O₄, with one molecule in asymmetric unit; $\rho_{\text{calcd}} = 1.657$ gcm⁻³, $\mu = 0.170$ mm⁻¹, $F(000) = 576$, $R_{\text{int}} = 0.0316$. The final R value was 0.0539 ($wR2 = 0.1339$) 2470 observed reflections ($F_0 \geq 4\sigma(|F_0|)$) and 173 variables, $S = 1.052$. The structure was obtained by direct methods using SHELXS-97.1 All non-hydrogen atoms were refined anisotropically. The hydrogen atoms were fixed geometrically in the idealized position and refined in the final cycle of refinement as riding over the atoms to which they are bonded. The largest difference peak and hole were 0.961 and -0.454 eÅ⁻³, respectively.

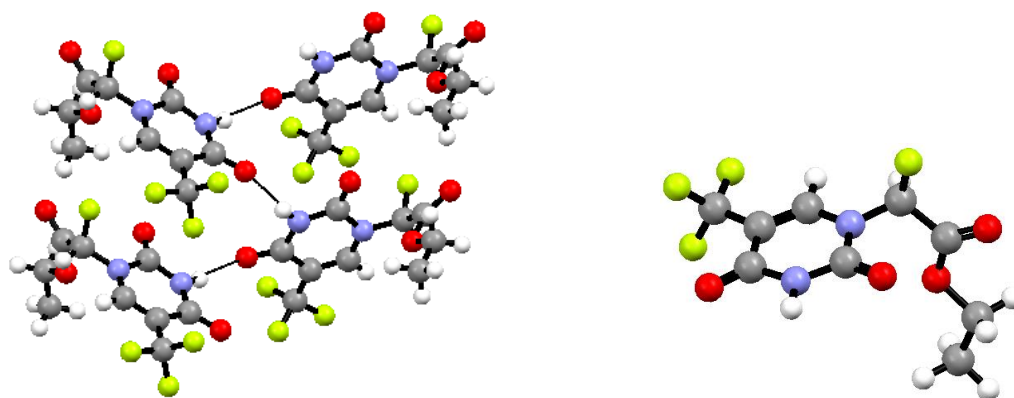


Figure 2.13 (left) Crystal structure; (right) DFT calculated structure of compound **20c**

In the crystal structure of compound **20c** a criss-cross hydrogen bonding (2.820 Å) was observed between the enantiomers between the NH group (at 3rd position) and carbonyl oxygen (at 4th position) of the first enantiomer with the carbonyl oxygen (at 4th position) and NH group (at 3rd position) of the second enantiomer respectively. Angles between N1-C β -F

and torsion angles (F-C_β-N-C₂, F-C_β-C_α-O) of each compound (**20a**, **20b** and **20c**) from crystal packing diagram and DFT calculated structure are shown in Table 2.1.

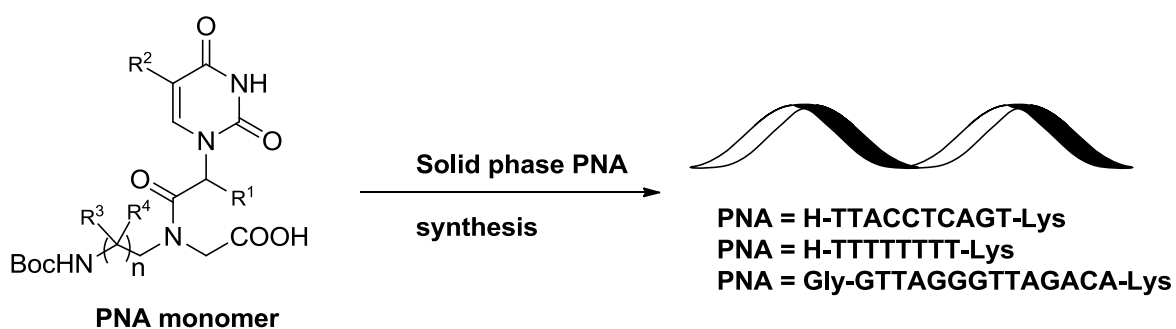
2A.4 Summary

This section describes the synthesis and characterization of rationally designed fluorinated PNA monomers by incorporating fluorine at different sites (nucleobase, side chain and the backbone).

All the intermediates have been characterized by ¹H and ¹³C NMR spectroscopy, mass spectral analysis and other appropriate analytical data (see Appendix-I). All attempts made to resolve the racemic mixture, met with failure. The next section deals with the incorporation of these fluorinated PNA monomer units into oligomers at various desired positions using solid phase peptide synthesis.

Section 2B

Solid phase Synthesis, Purification and Characterization of Fluorinated and control PNA oligomers



In this section, the synthesized fluorinated PNA monomers were site-specifically incorporated into oligomers along with the unmodified *aeg* PNA monomers by solid phase peptide synthesis.

2B.1 Solid phase peptide synthesis

Since Emil Fischer synthesized the first peptide in solution phase in 1901, the laborious and time-consuming method has been revolutionised by introduction of solid phase synthesis by Merrifield in 1963.²⁶ The method involves coupling of the desired N-protected amino acid to solid resin bound amino acid (free NH₂) employing suitable coupling reagent. After the coupling reaction, the excess amino acid and reagents are washed out, and the deprotection/coupling reactions are repeated in that order until the desired peptide is achieved. The need to purify the intermediates at every step as in solution phase is omitted. The resin bound peptide and the side chain protecting groups are cleaved in one final step. Merrifield's technique has undergone a series of modifications and improvements to overcome the physicochemical incompatibility of the growing peptide chain on the solid support. This has led to design of new types of solid supports to suit both Boc and Fmoc chemistries. Some resins which are frequently employed in solid phase peptide synthesis are shown in Figure 2.14. The big advantage is the amenability of Merrifield technique of solid phase synthesis to automation, resulting in development of several brands of automated peptide synthesizers, including microwave reactor for difficult couplings.

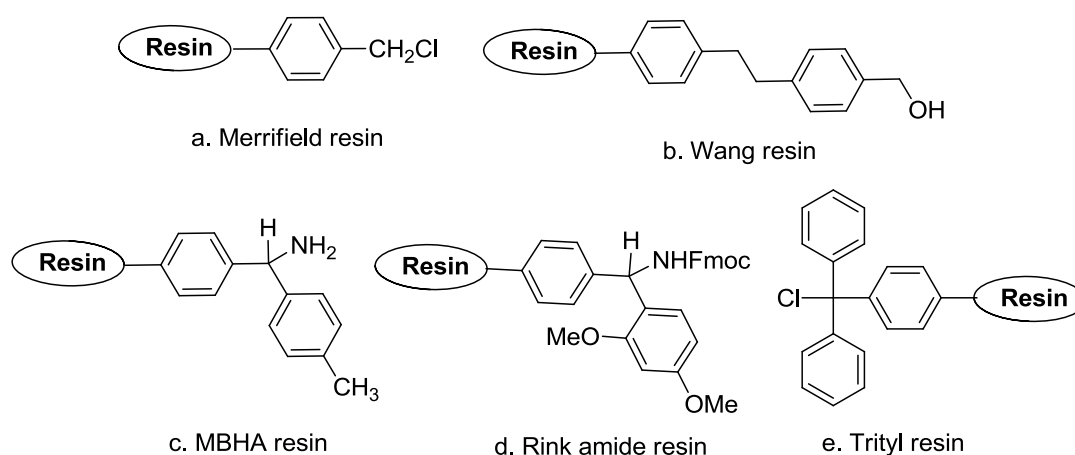
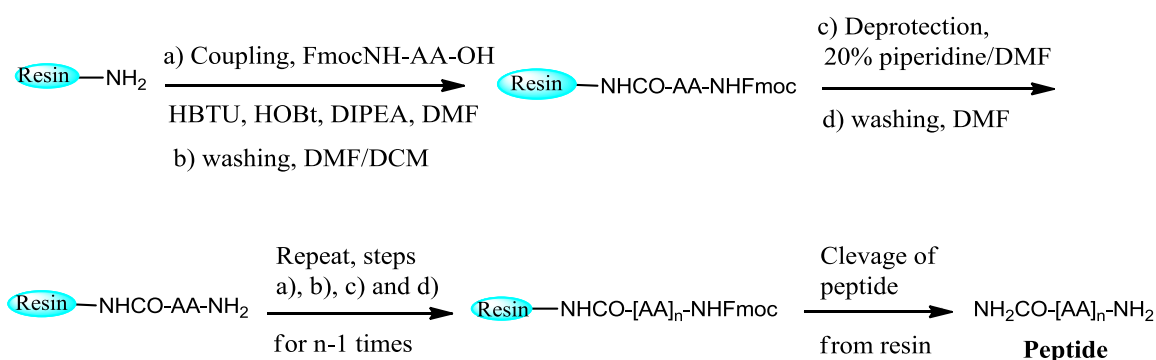


Figure 2.14 Resins commonly used for solid phase peptide synthesis

There are two standard chemical strategies for solid phase peptide synthesis, depending on the type of temporary protecting group used in every cycle: (i) Fmoc strategy that uses base labile protecting group and (ii) the Boc strategy that uses acid labile protecting group (Figure 2.15). Solid-phase peptide synthesis proceeds in C-terminus to N-terminus

direction. The monomeric amino acid protected either as -NHFmoc or -NHBoc with free acid is coupled on the solid support having free amino group. In the first protocol, fluorenylmethyloxycarbonyl (Fmoc) group used for N-protection is stable to acidic conditions and can be cleaved efficiently at the end of every cycle with the base piperidine and the side chain amino groups are protected as acid labile groups (*t*-Boc, Cbz). The final peptide and side chain protecting groups are then cleaved with acid (50% TFA). The second protocol uses *t*-butoxycarbonyl (*t*-Boc) group for N-protection removed by acid conditions such as 50% TFA in DCM at the end of each cycle. The reactive side chains are protected with groups that are stable for normal acid and finally removed under strong acidic conditions using HF in dimethylsulfide or TFMSA in TFA (Figure 2.15).

A) Fmoc-chemistry:



B) Boc-chemistry:

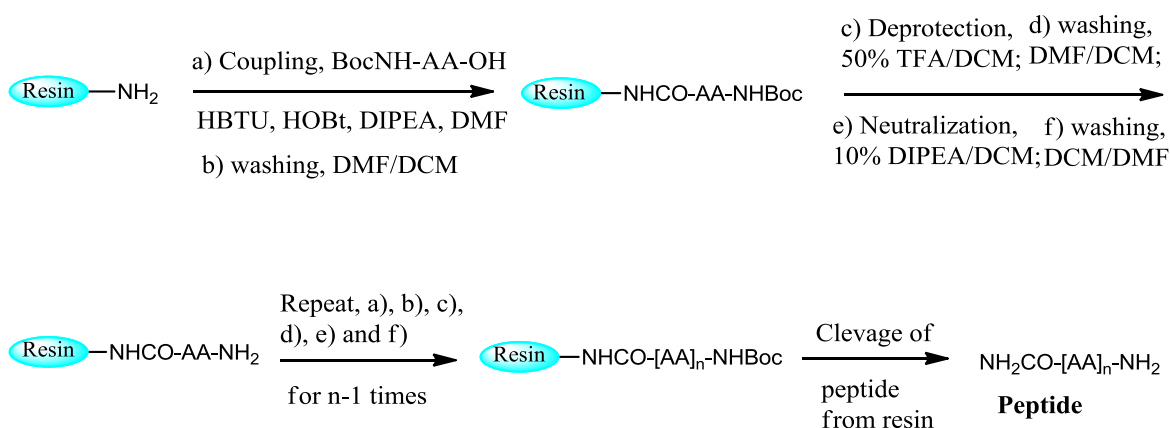


Figure 2.15 General protocols for solid phase peptide synthesis: (A) Fmoc-chemistry and (B) Boc-chemistry

2B.2 Aim of the present work

The specific objectives of this section are

1. Incorporation of *aeg* PNA monomers (A/T/G/C) and fluorinated PNA (T) monomers at various sites in PNA sequence by solid phase peptide synthesis
2. Synthesis of fluorescent PNA oligomers by conjugating the fluorescein at the N-terminus of the PNA
3. Purification and characterization of the PNA oligos by HPLC and MALDI-TOF spectrometry.

2B.3 Solid phase synthesis of PNA oligomers

The fluorinated PNA monomers were incorporated at desired positions in the selected *aeg* PNA sequence by solid phase peptide synthesis (SPPS) protocol using Boc strategy. MBHA resin (4-methyl-benzhydryl amine resin) was chosen as solid support as it is stable to acid conditions. All PNA monomers preactivated with HBTU/HOBt were successfully coupled with the growing chain on solid support under microwave conditions (25 watts, 75 °C, for 5 min.). In the synthesis of all oligomers, orthogonally protected (Boc/Cl-Cbz) L-lysine was selected as the C-terminal spacer-amino acid linked to the resin through amide bond. The amine content on the resin was suitably lowered from 0.67 mmol/g to 0.35 mmol/g by partial coupling of (Boc/Cl-Cbz) L-lysine to the free amines on solid support followed by capping with acetic anhydride. The deprotection of the N-t-Boc protecting group and the completion of coupling reaction were monitored by Kaiser's test. Small amounts of resin beads taken in a test tube and heated with Kaiser's solution resulting in a blue colour indicate the presence of free amine (complete deprotection of the t-Boc group). On the other hand, low colour or colourless resin beads after addition of reagent indicates incomplete deprotection.

2B.3.1 Synthesis of homooligomers (octamers)

To demonstrate the lipophilic (hydrophobic) character of fluorinated PNA oligomers, homooligomers having all fluoro PNA units were synthesized and analysed by HPLC using same mobile phase (system A: 5% ACN/water and system B: 50% ACN/water) and gradient for all homo oligomers. It was seen that the retention time became longer with increase in the number of fluorinated units in a PNA sequence, indicating enhanced hydrophobicity of fluorinated PNAs.

The PNA reference sequence used for the hydrophobicity study was H-TTTTTTTT-Lys and the different fluorinated monomers (*aeg*, *5FU-aeg*, (δ -*F-5FU-aeg*), (δ -*F-aeg-T*), *5CF₃U-aeg*, *apg*, γ -*CF₂-apg*) were used individually to make analogous fluorinated PNAs (Figure 2.16). Homooligomers (octamers) corresponding to all fluorinated PNA monomers were synthesized on solid support (MBHA resin) (Table 2.2). The PNAs were cleaved and purified using reverse phase HPLC and characterized by MALDI- TOF spectrometry.

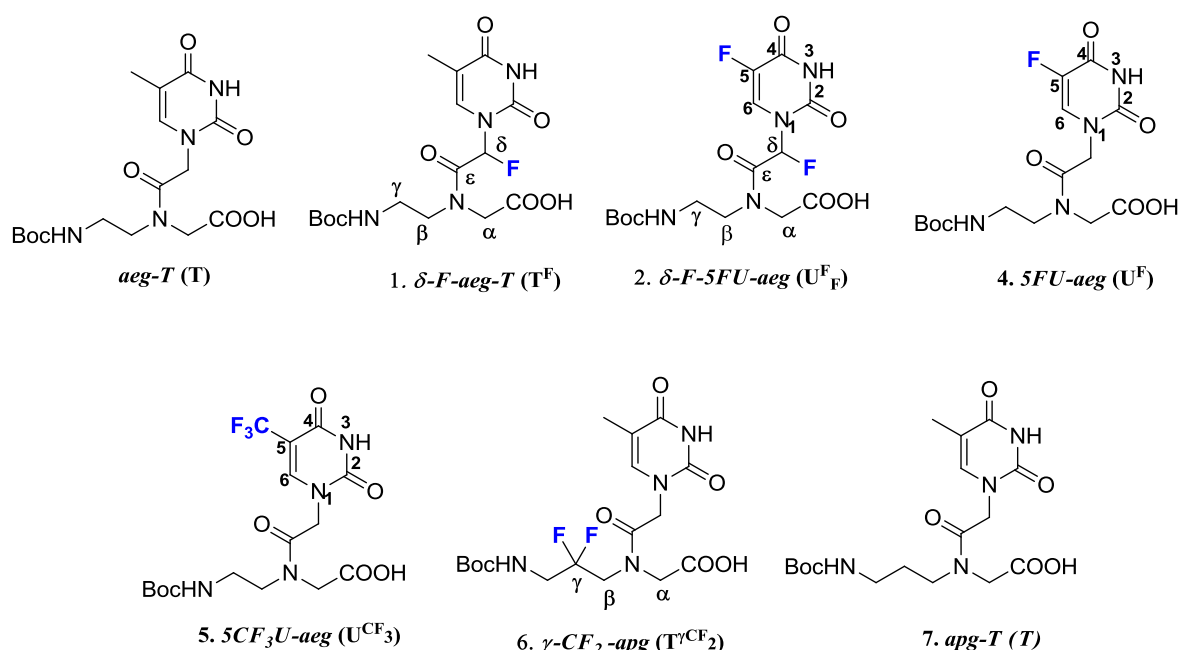


Figure 2.16 PNA Monomers used for the synthesis of homooligomers

Table 2.2 Synthesis of homo oligomers

Sr.No.	PNA	PNA sequence	Monomer used
1	PNA 1	H-TTTTTTTT-Lys	<i>aeg-T</i>
2	PNA 2	H-T ^F T ^F T ^F T ^F T ^F T ^F T ^F T ^F -Lys	δ - <i>F-aeg-T</i> (1)
3	PNA 3	H-U ^{CF₃} U ^{CF₃} U ^{CF₃} U ^{CF₃} U ^{CF₃} U ^{CF₃} U ^{CF₃} U ^{CF₃} -Lys	<i>5CF₃U-aeg</i> (5)
4	PNA 4	H-U ^F U ^F U ^F U ^F U ^F U ^F U ^F U ^F -Lys	<i>5FU-aeg</i> (4)
5	PNA 5	H-U ^F _F U ^F _F U ^F _F U ^F _F U ^F _F U ^F _F U ^F _F U ^F _F -Lys	δ - <i>F-5FU-aeg</i> (2)
6	PNA 6	H-TTTTTTTT-Lys	<i>apg-T</i> (7)
7	PNA 7	H-T ^{γCF₂} T ^{γCF₂} T ^{γCF₂} T ^{γCF₂} T ^{γCF₂} T ^{γCF₂} T ^{γCF₂} T ^{γCF₂} -Lys	γ - <i>CF₂ apg</i> (6)

2B.3.2 Synthesis of mixed purine-pyrimidine PNA oligomers

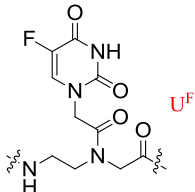
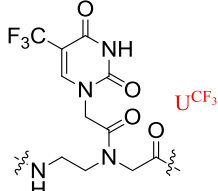
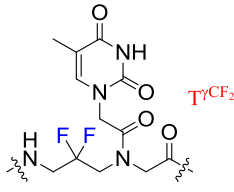
The mixed purine-pyrimidine PNA sequences were synthesized to study the duplex stability and the sequence specificity of the derived PNA:DNA and PNA:RNA hybrids. The PNA

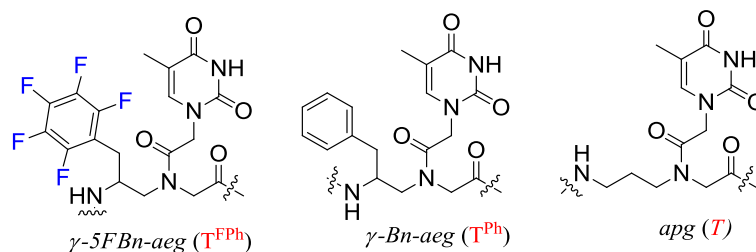
mixed oligomers bearing both fluorinated Ts and unmodified (A/T/G/C) units were synthesized to study the duplex stability and their cell uptake efficiencies.

The antisense oligonucleotide sequence ON-705 (CCUCUUACCUCAGUUACA) corresponds to the region containing the mutated intron which interrupts the coding sequence of luciferase gene in the construct by Kole *et al.*²⁷ It can target the aberrant splice site and restore the correct splicing pattern to enable the expression of luciferase gene. The central 10-mer sequence of the antisense ON-705 (CCUCUUACCUCAGUUACA) was chosen for synthesis and evaluation of fluorinated PNA oligomers

Various PNAs corresponding to above decamer incorporating different fluorinated units at N-terminus (H-TTACCTCAGT-Lys); middle (H-TTACCTCAGT-Lys); C-terminus (H-TTACCTCAGT-Lys); doubly-modified (H-TTACCTCAGT-Lys) and Triply-modified (H-TTACCTCAGT-Lys) were synthesized (Table 2.3).

Table 2.3 Synthesis of PNA oligomers for biophysical evaluation

Sr.No.	Seq. code	PNA sequence	Fluorinated unit in PNA oligomer
8	PNA 8	H-TTACCTCAGT-Lys	
9	PNA 9	H-TU ^F ACCTCAGT-Lys	
10	PNA 10	H-TTACCU ^F CAGT-Lys	
11	PNA 11	H-TTACCTCAGU ^F -Lys	
12	PNA 12	H-TU ^F ACCU ^F CAGT-Lys	
13	PNA 13	H-TU ^F ACCU ^F CAGU ^F -Lys	
14	PNA 14	H-TU ^{CF₃} ACCT CAGT-Lys	
15	PNA 15	H-TTACCU ^{CF₃} CAGT-Lys	
16	PNA 16	H-TTACCT CAGU ^{CF₃} -Lys	
17	PNA 17	H-TU ^{CF₃} ACCU ^{CF₃} CAGT-Lys	
18	PNA 18	H-TU ^{CF₃} ACCU ^{CF₃} CAGU ^{CF₃} -Lys	
19	PNA 19	H-TT ^{γCF₂} ACCTCAGT-Lys	
20	PNA 20	H-TTACCT ^{γCF₂} CAGT-Lys	
21	PNA 21	H-TTACCTCAGT ^{γCF₂} -Lys	
22	PNA 22	H-TT ^{γCF₂} ACCT ^{γCF₂} CAGT-Lys	
23	PNA 23	H-TT ^{γCF₂} ACCT ^{γCF₂} CAGT ^{γCF₂} -Lys	
24	PNA 24	H-TTACCTCAGT-Lys	apg-T (T)
25	PNA 25	H-TTACCTCAGT-Lys	
26	PNA 26	H-TTACCTCAGT-Lys	
27	PNA 27	H-T ^{FPh} ACCT ^{FPh} CAGT ^{FPh} -Lys	γ-5FBn-aeg-T (T ^{FPh})
28	PNA 28	H-T ^{Ph} ACCT ^{Ph} CAGT ^{Ph} -Lys	γ-Bn-aeg-T (T ^{Ph})



2B.3.3 Fluorinated PNAs for the inhibition of telomerase activity

Another target sequence chosen for synthesis is the one corresponding to the RNA of human telomerase which is Lys-ACAGATTGGGATTG-Gly.²⁸ In this sequence the aeg-T units were replaced by γ -CF₂-apg PNA-T units along with normal unmodified aeg units for A, C and G.

Table 2.4 Synthesis of PNA oligomers for telomerase inhibition

Sr.No.	Seq. code	PNA sequence	Monomer used
29	PNA 29	Gly-GTTAGGGTTAGACA-Lys	aeg-T
30	PNA 30	Gly-GTTAGGGTTAGACA-Lys	δ -F, aeg-T
31	PNA 31	Gly-GT ^{γCF₂} T ^{γCF₂} AGGGT ^{γCF₂} T ^{γCF₂} AGACA-Lys	γ -CF ₂ apg

2B.4 Cleavage of the PNA oligomers from the solid support

The PNA oligomers were cleaved from the solid support (MBHA resin), using trifluoromethane sulphonic acid (TFMSA) and trifluoroacetic acid (TFA) in presence of scavengers thioanisole and 1, 2-ethanedithiol. During this cleavage process all orthogonal protecting groups were also removed. After removal of excess TFA, the PNA oligomers were precipitated out by the addition of cold diethyl ether and the precipitate was dissolved in water for further analysis. Using the protocol, all the PNA oligomers of desired sequence were synthesized by incorporating fluorinated as well as unmodified PNA monomers at the desired positions.

2B.5 Purification and characterization of PNA oligomers

The free PNA oligomers were purified by reverse phase high performance liquid chromatography (RP-HPLC) on a semi-preparative C18 column using acetonitrile/water gradient elution. The purity of PNA oligomers was checked by reinjecting the sample on analytical C18 column. The integrity of the synthesized PNA oligomers was confirmed by MALDI-TOF mass spectrometry using 2,5-dihydroxybenzoic acid (DHB) as matrix. The calculated and observed molecular weights for all PNAs with their molecular formula and

HPLC retention times are shown in Table 2.7. The HPLC and MALDI-TOF spectra of the PNA oligomers are shown in Appendix-I.

Table 2.7 MALDI-TOF spectral analysis of the synthesized PNA oligomers

Sr.No.	PNA	Mol.formula	Calcd. mass	Obsvd. mass	HPLC Rt (min.)
1	PNA 1	C ₉₄ H ₁₂₈ N ₃₅ O ₃₃	2274.9414	2276.2155	10.1
2	PNA 2	C ₉₄ H ₁₂₀ F ₈ N ₃₅ O ₃₃	2418.8660	2419.1062	14.2
3	PNA 3	C ₉₄ H ₁₀₄ F ₂₄ N ₃₅ O ₃₃	2706.7153	2706.7990	17.7
4	PNA 4	C ₈₆ H ₁₀₄ F ₈ N ₃₅ O ₃₃	2306.7408	2306.9862	9.9
5	PNA 5	C ₈₆ H ₉₆ F ₁₆ N ₃₅ O ₃₃	2450.6654	2450.7821	14.2
6	PNA 6	C ₁₀₂ H ₁₄₄ N ₃₅ O ₃₃	2387.0666	2387.1919	11.0
7	PNA 7	C ₁₀₂ H ₁₂₈ F ₁₆ N ₃₅ O ₃₃	2674.9158	2675.9289	13.4
8	PNA 8	C ₁₁₃ H ₁₄₉ N ₅₅ O ₃₃	2804.1672	2805.2516	9.9
9	PNA 9	C ₁₁₂ H ₁₄₆ FN ₅₅ O ₃₃ Na	2831.1319	2831.5495	9.8
10	PNA 10	C ₁₁₂ H ₁₄₆ FN ₅₅ O ₃₃ Na	2831.1319	2831.4927	9.7
11	PNA 11	C ₁₁₂ H ₁₄₇ FN ₅₅ O ₃₃	2809.1499	2809.5801	9.8
12	PNA 12	C ₁₁₁ H ₁₄₄ FN ₅₅ O ₃₃	2794.1265	2794.5619 (M-F)	9.8
13	PNA 13	C ₁₁₀ H ₁₄₀ F ₃ N ₅₅ O ₃₃	2816.0920	2816.9088	9.7
14	PNA 14	C ₁₁₃ H ₁₄₇ F ₃ N ₅₅ O ₃₃	2859.1467	2859.4169	10.4
15	PNA 15	C ₁₁₃ H ₁₄₇ F ₃ N ₅₅ O ₃₃	2859.1467	2859.3951	10.3
16	PNA 16	C ₁₁₃ H ₁₄₇ F ₃ N ₅₅ O ₃₃	2859.1467	2859.9595	10.4
17	PNA 17	C ₁₁₃ H ₁₄₃ F ₆ N ₅₅ O ₃₃	2912.1107	2912.8851	10.8
18	PNA 18	C ₁₁₃ H ₁₄₀ F ₉ N ₅₅ O ₃₃ Na	2989.0722	2989.3088	10.7
19	PNA 19	C ₁₁₄ H ₁₅₀ F ₂ N ₅₅ O ₃₃	2855.1718	2856.0429	10.1
20	PNA 20	C ₁₁₄ H ₁₅₀ F ₂ N ₅₅ O ₃₃	2855.1718	2855.5370	10.1
21	PNA 21	C ₁₁₄ H ₁₅₀ F ₂ N ₅₅ O ₃₃	2855.1718	2855.4285	10.0
22	PNA 22	C ₁₁₅ H ₁₅₀ F ₄ N ₅₅ O ₃₃	2905.1686	2905.6612	10.3
23	PNA 23	C ₁₁₆ H ₁₅₀ F ₆ N ₅₅ O ₃₃	2955.1654	2955.5978	10.5
24	PNA 24	C ₁₁₄ H ₁₅₂ N ₅₅ O ₃₃	2819.1907	2819.6793	9.9
25	PNA 25	C ₁₁₅ H ₁₅₄ N ₅₅ O ₃₃	2833.2063	2833.3549	10.0
26	PNA 26	C ₁₁₆ H ₁₅₆ N ₅₅ O ₃₃	2847.2220	2847.4982	10.1
27	PNA 27	C ₁₃₄ H ₁₅₂ F ₁₅ N ₅₅ O ₃₃ Na	3367.1565	3367.2075	15.6
28	PNA 28	C ₁₃₄ H ₁₆₇ N ₅₅ O ₃₃	3074.3080	3074.6116	13.8
29	PNA 29	C ₁₆₁ H ₂₀₅ N ₈₈ O ₄₄	4074.6509	4076.2310	15.6
30	PNA 30	C ₁₆₅ H ₂₁₃ N ₈₈ O ₄₄	4130.7135	4132.9210	15.6
31	PNA 31	C ₁₆₅ H ₂₀₅ F ₈ N ₈₈ O ₄₄	4274.6381	4275.7353	16.5

2B.6 ¹⁹F-NMR shifts of various fluorinated compounds

The ¹⁹F-NMR chemical shifts depend upon the chemical environments of fluorine in a compound. The ¹⁹F-NMR values for fluorine in side chain of the thymine fluoroacetate derivatives varied from -155.2 to -157.6 ppm (entry 1-6). In case of 5-fluorouracil fluoroacetate derivatives, the ¹⁹F-values for fluorine in side chain varied from -150.1 to -156.8 ppm (entry 7-12). For the 5-trifluoromethyluracil fluoroacetate derivatives, the ¹⁹F-values for fluorine at the same position varied from -153.9 to -158.3 ppm (entry 13-18). ¹⁹F-NMR values for the Boc-ethylenediamine bromodifluoroacetate and Boc-ethylenediamine monofluoroacetate appeared at -60.4 and 148.6 ppm respectively (entry 19,20). In case of

difluorination in backbone by replacing two hydrogens by two fluorines, the ^{19}F values varied from -107.3 to -109.6 ppm (entry 19-28) whereas the insertion of methylene pentafluoro phenyl group at γ -position in the PNA backbone showed three peaks at \sim -144, \sim -158 and \sim -164 ppm (entry 29-33). The ^{19}F -NMR shifts are shown in Table 2.8a-c.

Table 2.8a ^{19}F -NMR shifts of base and side chain fluorinated compounds.

Entry	Compound	Structure No.	Fluorine in side chain	Fluorine on nucleobase
1		24	-156.0	--
2		25	-155.7	--
3		27	-155.4- (-157.2)	--
4		20a	-157.6	--
5		21a	-156.3	--
6		22a	-155.2	--
7		20b	-156.8	-161.1
8		21b	-154.6	-167.1
9		22b	-155.6	-163.4
10		4	-150.8	-161.5
11		18a	--	-165.9
12		1		-170.3
13		20c	-158.3	-65.1
14		21c	-155.0	-62.7
15		22c	-155.5	-62.4

16		5	-153.9	-62.8
17		18b	--	-64.6
18		2		-62.0

Table 2.8b ¹⁹F-NMR shifts of backbone fluorinated compounds.

Entry	Compound	Structure No.	Fluorine in backbone
19		12	-60.4
20		13	-148.6
21		32	-109.2
22		33	-107.3
23		35	-106.4
24		36	-106.6
25		37	-109.6
26		38	-107.3
27		39	-107.5
28		6	-107.3

Table 2.8c ¹⁹F-NMR shifts γ -methylene pentafluorophenyl substituted compounds.

Entry	Compound	Structure No.	Pentafluorophenyl methylene at C γ in PNA backbone		
29		47a	-144.2,	-157.8,	-163.7
30		49a	-143.9,	-158.0,	-163.8
31		50a	-142.7,	-156.3,	-162.2
32		51a	-142.6,	-158.7,	-164.3
33		8	-142.2,	-158.1,	-163.4

2B.7 ^{19}F -NMR of PNA 14 & 17

The ^{19}F -NMR of the PNAs **14** and **17** were recorded on 500 MHz instrument at 30 μM concentration of each in D_2O (Table 2.9). The N-terminus modified PNA **14** corresponding to 5- CF_3U showed a peak at -75.5 ppm (entry 1) whereas the double modified (N-terminus and middle) PNA **17** showed two peaks, one at -75.4 ppm and the other at -78.7 ppm (entry 2). The first peak corresponds to N-terminus modification and the later one corresponds to middle modification. Thus the interior fluorinated 5- CF_3U shows 3.3 ppm up field shift compared to the one at N-terminus. Thus the successful incorporation of fluorinated PNA monomers into oligomers and retention of the fluorine were checked by ^{19}F -NMR in the selected PNAs (**14** & **17**). Compared to monomer 5 CF_3U -*ae*g the oligomer shows ~ 15.0 ppm up field (Table 2.9, Figure 2.17).

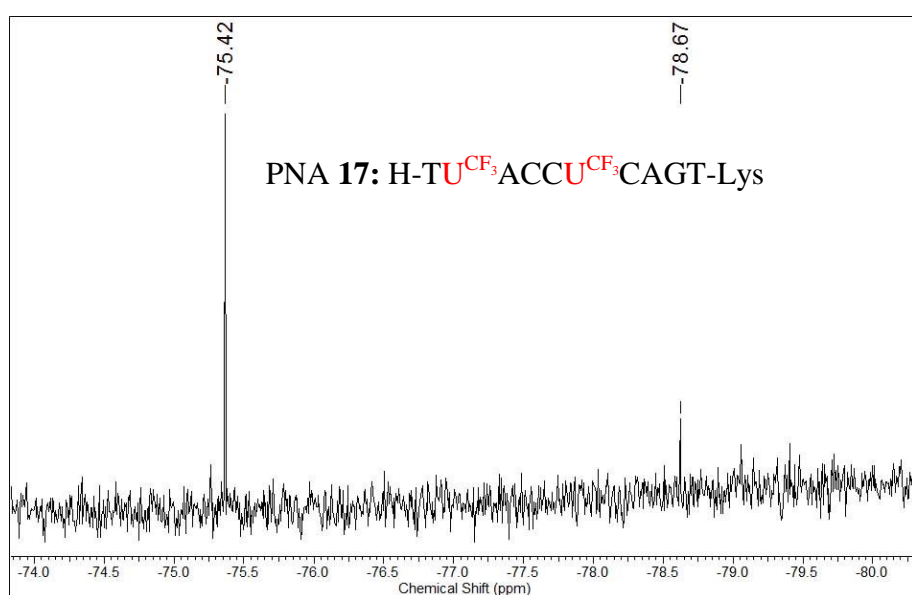
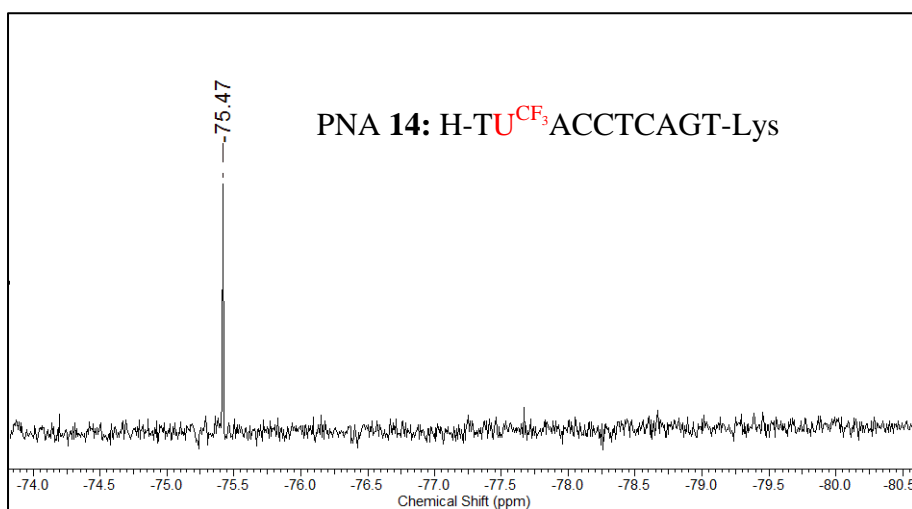


Figure 2.17 ^{19}F -NMR of PNA 14 and 17Table 2.9 ^{19}F -NMR shifts of PNAs 14 and 17

Entry	PNA oligomer	PNA oligomer ^{19}F -NMR	$5\text{CF}_3\text{U}$ -aeg Monomer ^{19}F -NMR
1	PNA 14 (N)	-75.5 ppm	-62.0 ppm
2	PNA 17 (N, M)	-75.4, -78.7 ppm	

2B.8 Summary

To summarize,

This section describes the incorporation various fluorinated PNA-T monomers into homopyrimidine PNA-T sequence (octamer), mixed purine:pyrimidine PNA 10-mer and 14-mer sequences. The PNA oligomers after cleavage from resin were purified by RP-HPLC and characterized by MALDI-TOF spectrometry.

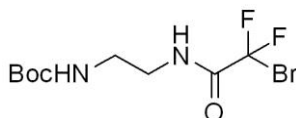
The next chapter deals with the investigation of biophysical properties of PNA oligomers.

2.2 Experimental section

This section describes the detailed synthetic procedures and spectral characterization of the rationally designed PNA monomers.

General: All reactions were conducted in oven-dried glassware under argon atmosphere. Low temperature experiments were carried out by cooling down the flasks with an acetone bath frozen by dry ice. The flasks were equipped with septum caps. All commercial solvents were distilled prior to use. THF was distilled over sodium/ benzophenone under nitrogen atmosphere, CH₂Cl₂ over CaH₂ and DMF over P₂O₅. Analytical thin layer chromatography (TLC) was performed on precoated 250 μm layer thickness silica gel GF254 (Merck 5554) plates. Visualization was performed by ultraviolet light and staining with a solution of ninhydrin. Column chromatography was performed using 100-200 μm silica gel. ¹H NMR, ¹³C NMR, and ¹⁹F NMR were recorded using JEOL 400 MHz NMR spectrometer at 400, 100, and 376.6 MHz respectively. The delta (δ) values for chemical shifts are reported in ppm and are referred to internal standard TMS or deuterated NMR solvents. Hexafluorobenzene was used as internal reference for ¹⁹F NMR. IR spectra were recorded on Bruker's Fourier transform infra-red spectrometer. Mass spectra for PNA oligomers were obtained by Applied Biosystems 4800 Plus MALDI-TOF/TOF mass spectrometry using DHB as matrix. High resolution mass spectra for all reaction intermediates were recorded on Synapt G2 High Definition Mass Spectrometry. PNA oligomers were purified on Dionex ICS 3000 HPLC system using semi-preparative BEH130 C18 (10X250 mm) column.

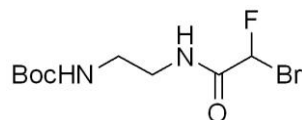
tert-Butyl (2-(2-bromo-2,2-difluoroacetamido)ethyl)carbamate (**12**)



To a solution of N-Boc-ethylenediamine (130 mg, 0.81 mmol) and triethylamine (0.11 mL, 0.81 mmol) in anhydrous ACN (15 mL), ethyl bromodifluoroacetate (0.1 mL, 0.81 mmol) was added at RT and the stirring was continued for 12 h at the same temperature. After completion of reaction, (monitored by TLC) water (20 mL) was added to the reaction mixture and extracted with ethyl acetate (3 x 15 mL). The organic layer was washed with brine solution and dried over anhydrous Na₂SO₄. The solvent was removed under reduced pressure and the product was purified by column chromatography, eluting with EtOAc/petroleum ether (15:85) to afford the compound **12**. (Yield 170 mg, 66%). ¹H-NMR (400 MHz, CDCl₃) δ:

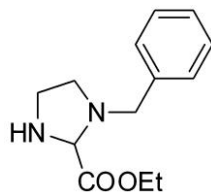
1.43 (s, 9H), 3.36-3.61 (m, 4H), 5.12 (bs, 1H), 7.82 (bs, 1H); ^{19}F -NMR (376.6 MHz, CDCl_3) δ : -60.38 (s); ^{13}C -NMR (100 MHz, CDCl_3) δ : 28.2, 39.1, 42.2, 80.4, 111.7 (t, $J = 15$ Hz), 157.6, 160.6. HRMS (ESI-TOF) m/z Calcd for $\text{C}_9\text{H}_{15}\text{BrF}_2\text{N}_2\text{NaO}_3$ [$\text{M} + \text{Na}$] $^+$ 339.0132, found 339.0141.

***tert*-Butyl (2-(2-bromo-2-fluoroacetamido)ethyl)carbamate (13)**



To a solution of N-Boc-ethylenediamine (500 mg, 3.125 mmol) in anhydrous DCM (1.0 mL), ethyl bromofluoroacetate (0.37 mL, 3.125 mmol) was added at ice-cold condition and the stirring was continued for 1 h at the same temperature. After completion of reaction, (monitored by TLC) water (15 mL) was added to the reaction mixture and extracted with ethyl acetate (3 x 10 mL). The organic layer was washed with brine solution and dried over anhydrous Na_2SO_4 . The solvent was removed under reduced pressure and the product was purified by column chromatography, eluting with EtOAc/petroleum ether (1:9) to afford the compound **13**. (Yield 754 mg, 81%). ^1H -NMR (400 MHz, CDCl_3) δ : 1.45 (s, 9H), 3.37-3.47 (m, 4H), 4.94 (bs, 1H), 6.61 (d, 1H, $J = 52$ Hz), 7.32 (bs, 1H); ^{19}F -NMR (376.6 MHz, CDCl_3) δ : -148.06 (d, $J = 45.2$ Hz); ^{13}C -NMR (100 MHz, CDCl_3) δ : 28.4, 39.6, 41.6, 80.4, 84.57 (d, 265 Hz), 157.2, 165.5, (d, $J = 20$ Hz). HRMS (ESI-TOF) m/z Calcd for $\text{C}_9\text{H}_{16}\text{BrFN}_2\text{NaO}_3$ [$\text{M} + \text{Na}$] $^+$ 321.0226, found 321.0235.

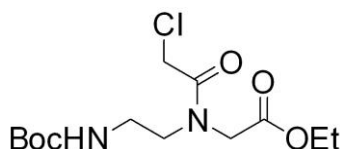
Ethyl 1-benzylimidazolidine-2-carboxylate (15)



To a solution of N-Boc-ethylenediamine (250 mg, 1.562 mmol) in anhydrous ACN (10 mL), benzyl bromide (0.39 mL, 1.562 mmol) and triethylamine (0.2 mL, 1.562 mmol) were added at ice-cold condition and the stirring was continued for 12 h at the same temperature. After completion of reaction, (monitored by TLC) water (15 mL) was added to the reaction mixture and extracted with ethyl acetate (3 x 20 mL). The organic layer was washed with brine solution and dried over anhydrous Na_2SO_4 , and the organic layer was concentrated and the product purified using column chromatography to get product **14**. The product was eluted at a

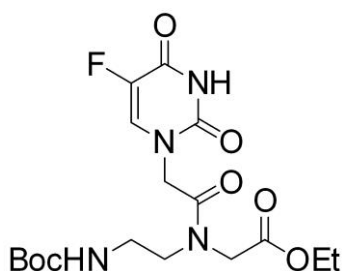
percentage of (3:1) EtOAc/petroleum ether. The compound **14** (200 mg, 0.8 mmol) was treated with ethylbromofluoroacetate (0.1 mL, 0.8 mmol) and DIPEA (0.3 mL, 1.6 mmol) in ACN to afford the N-alkylated product but interestingly, a cyclized product **14c** was obtained. The same workup procedure employed to remove the salts and the solvent was evaporated under reduced pressure and the product was purified by column chromatography, eluting with EtOAc/petroleum ether (20:80) yield the compound **15**. (Yield 351 mg, 75%). $^1\text{H-NMR}$ (400 MHz, CDCl_3) δ : 1.24 (t, 3H, $J = 8$ Hz), 2.82-2.88 (m, 1H), 3.16-3.22 (m, 1H), 3.72 (d, 1H, $J = 12$ Hz), 3.92 (d, 1H, $J = 15$ Hz), 3.96-3.99 (m, 1H), 4.04-4.09 (m, 1H), 4.15 (q, 2H), 4.73 (s, 1H), 7.21-7.34 (m, 5H); $^{13}\text{C-NMR}$ (100 MHz, CDCl_3) δ : 14.1, 50.9, 58.4, 61.0, 65.6, 92.1, 127.3, 128.3, 138.0, 170.2; DEPT: 14.2, 51.1 ($-\text{CH}_2$) 58.6 ($-\text{CH}_2$) 61.2 ($-\text{CH}_2$), 65.8 ($-\text{CH}_2$), 92.3, 127.5, 128.5, 128.9.

Ethyl 2-(N-(2-((tert-butoxycarbonyl) amino) ethyl)-2-chloroacetamido) acetate (17)



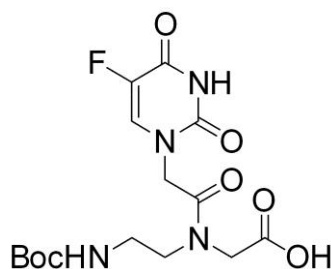
To a solution of the compound **16** (5 g, 20 mmol) in acetonitrile (10 mL), triethylamine (2.76 mL, 20 mmol) and chloroacetylchloride (1.6 mL, 20 mmol) were added at 0 °C drop wise, and stirring was continued for 5 h, monitoring the completion of reaction by TLC. After completion of reaction, water was added and extracted with ethyl acetate (3 x 15 mL). The organic layer was dried over anhydrous Na_2SO_4 . The solvent was removed in vacuo and product was purified by column chromatography, eluting with petroleum ether/ EtOAc (1:1) to obtain the compound **17**. (Yield 5.5 g, 90%). $^1\text{H-NMR}$ (400 MHz, CDCl_3) δ : 1.24 (t, 3H), 1.39 (s, 9H), 3.23 (m, 2H), 3.48 (t, 2H), 3.98 (s, 2H), 4.11 (s, 2H), 4.17 (q, 2H), 5.49 (bs, 1H); $^{13}\text{C-NMR}$ (100 MHz, CDCl_3) δ : 14.1, 28.3, 38.7, 49.7, 61.7, 80.0, 156.1, 167.7.

Ethyl 2-(N-(2-((tert-butoxycarbonyl) amino) ethyl)-2-(5-fluoro-2, 4-dioxo-3, 4-dihydropyrimidin-1(2H)-yl) acetamido) acetate (18a)



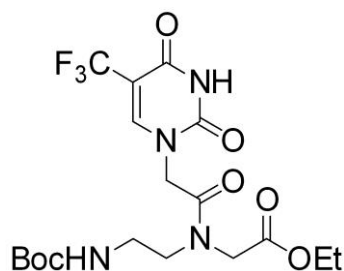
To a solution of compound **17** (2 g, 6.21 mmol) in DMF (5.0 mL), 5-fluorouracil (0.83 g, 6.21 mmol) and K_2CO_3 (0.85 g, 6.21 mmol) were added at RT and stirring was continued at same temperature for 12 h, monitoring the completion of reaction by TLC, after completion of reaction, water was added and extracted with ethyl acetate (3x25 mL). The organic layer was dried over anhydrous Na_2SO_4 . The solvent was removed under reduced pressure and product was purified by column chromatography, eluting with petroleum ether/EtOAc (1:1) to obtain the compound **18a**. (Yield 2.1 g, 77%). 1H -NMR (400 MHz, $CDCl_3$) δ : 1.26-1.34 (m, 3H), 1.44 (s, 9H), 3.2-3.33 (m, 2H), 3.52 (t, 2H, $J = 8$ Hz), 4.06 (s, 2H), 4.18-4.27 (m, 2H), 4.46 (min) 4.60 (maj) (s, 2H), 5.66 (bs, 1H) 7.-7.34 (m, 1H), 9.69 (bs, 1H); ^{19}F -NMR (376.6 MHz, $CDCl_3$) δ : -165.9; ^{13}C -NMR (100 MHz, $CDCl_3$) δ : 14.1, 28.4, 38.7, 48.3, 48.8, 61.9, 80.2, 129.55 (d, $J = 36$ Hz, 139.2, 141.6, 149.8, 156.1, 157.3, 157.5, 167.0, 169.3, 169.7; HRMS (ESI-TOF) m/z Calcd for $C_{17}H_{25}FN_4NaO_7$ [M + Na] 439.1605, found 439.1606.

2-(N-2((tert-butoxycarbonyl)amino)ethyl)-2-(5-fluoro-2,4-dioxo-3,4-dihydropyrimidin-1(2H)-yl)acetamido)acetic acid (1)



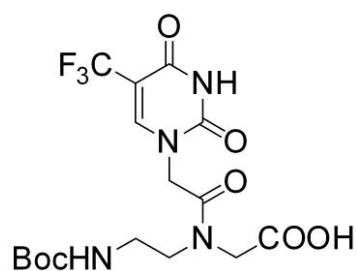
To the ester compound **18a** (2.1 g, 5.05 mmol) in THF (5 ml), 10% LiOH was added at 0 °C and stirred for 3 h. After completion of reaction, the mixture was acidified with *sat. aq.* $KHSO_4$ solution extracted with ethyl acetate and dried over Na_2SO_4 . The solvent was evaporated under reduced pressure to obtain the desired monomer **1** in good yields. 1H -NMR (400 MHz, $DMSO-d_6$) δ : 1.35 (maj) 1.37 (min) (s, 9H), 2.99-3.13 (m, 2H), 3.27-3.32 (t, 2H, $J = 8$ Hz), 3.65 (s, 2H), 4.43 (maj) 4.57 (min) (s, 2H), 7.01 (maj) 7.18 (min) (t, 1H), 7.76-7.85 (m, 1H), 8.42 (bs, 1H); ^{19}F -NMR (376.6 MHz, $CDCl_3$) δ : -170.3; ^{13}C -NMR (100 MHz, $DMSO-d_6$) δ : 28.7, 38.1, 47.9, 48.5, 52.9, 78.0, 131.4 (d, $J = 31$ Hz, 1F), 138.6, 140.9, 150.6, 156.1, 158.0, 166.7, 167.8, 171.4; HRMS (ESI-TOF) m/z Calcd for $C_{15}H_{21}FN_4NaO_7$ [M + Na] $^+$ 411.1292, found 411.1285.

Synthesis of ethyl-2-(N-2((tert-butoxycarbonyl)amino)ethyl)-2-(2,4-dioxo-5-(trifluoromethyl)-3,4-dihydropyrimidin-1(2H)-yl)acetamido)acetate (18b)



To a solution of the compound **17** (1.0 g, 3.10 mmol) in DMF (5 ml), K_2CO_3 (428 mg, 3.10 mmol) and 5-trifluoromethyluracil (560 mg, 3.10 mmol) were added at RT and stirring was continued at same temperature for 12 h, monitoring the completion of reaction by TLC, after completion of reaction, water and *aq.* $KHSO_4$ were added and extracted with ethyl acetate (3x25 mL). The organic layer was dried over anhydrous Na_2SO_4 . The solvent was removed in vacuo and product was purified by column chromatography, eluting with petroleum ether/EtOAc (1:1) to obtain the compound **18b**. (Yield 1.10 mg, 76%). 1H -NMR (400 MHz, $CDCl_3$) δ : 1.25-1.33 (m, 3H), 1.43 (s, 9H), 3.25-3.34 (m, 2H), 3.52 (m, 2H), 4.07 (s, 2H), 4.17 - 4.27 (m, 2H), 4.56(min) 4.71 (maj)(s, 2H), 5.11(min) 5.61 (maj) (br d, 1H), 7.68-7.73 (m, 1H), 9.78 (maj) 9.85 (min) (bs,1H); ^{19}F -NMR (376.6 MHz, $CDCl_3$, C_6F_6 as internal reference) δ : -64.60 (s, 3F); ^{13}C -NMR (100 MHz, $CDCl_3$) δ : 14.1, 28.4, 29.7, 38.7, 48.8, 61.9, 62.5, 80.2, 105.13 (q, $J = 32$ Hz) 120.5, 123.2, 146.3, 150.1, 156.3, 159.2, 162.9, 166.8, 167.2, 169.5. HRMS (ESI-TOF) m/z Calcd for $C_{18}H_{25}F_3N_4NaO_7$ $[M + Na]^+$ 489.1573, found 489.1571.

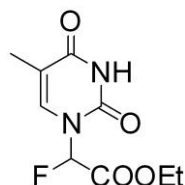
Synthesis of 2-(N-(2-((tert-butoxycarbonyl)amino)ethyl)-2-(2,4-dioxo-5-(trifluoromethyl)-3,4-dihydropyrimidin-1(2H)-yl)acetamido)acetic acid (2)



The ester compound **18b** (1.0 g, 2.14 mmol) in THF was saponified with 10% LiOH at 0 °C for 3 h. After completion of reaction, the mixture was acidified with *sat. aq.* $KHSO_4$ solution and then the acid compound was extracted with ethyl acetate, dried over Na_2SO_4 and evaporated under reduced pressure to obtain the desired monomer **2** in good yields. (Yield 750 mg, 80%). 1H -NMR (400 MHz, $DMSO-d_6$) δ : 1.31(min) 1.33 (maj) (s, 9H), 2.96-3.15 (m, 2H), 3.25-3.35 (m, 2H), 3.93 (maj) 4.04 (min) (s, 2H), 4.58 (min) 4.76 (maj) (s, 2H), 6.73

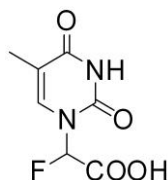
(min) 6.89 (maj) (br, 1H), 8.18 (min) 8.24 (maj) (s, 1H), 11.81 (bs, 1H) ; ^{19}F -NMR (376.6 MHz, DMSO- d_6 , C_6F_6 as internal reference) δ : -62.0 (s) ; ^{13}C -NMR (100 MHz, DMSO- d_6) δ : 28.6, 38.5, 47.3, 48.3, 48.8, 78.2, 78.5, 99.9, 121.5, 121.8, 124.5, 148.5, 150.6, 156.1, 156.2, 159.8, 167.1, 167.6, 170.9 ; HRMS (ESI-TOF) m/z . Calcd for $\text{C}_{16}\text{H}_{21}\text{F}_3\text{N}_4\text{NaO}_7$ [$\text{M} + \text{Na}$] $^+$ 461.1260, found 461.1264.

Ethyl 2-fluoro-2-(5-methyl-2, 4-dioxo-3, 4-dihydropyrimidin-1(2H)-yl) acetate (20a)



To a solution of thymine **19a** (2 g, 15.90 mmol) and K_2CO_3 (2.2 g, 15.90 mmol) in anhydrous DMF (10 mL), ethyl bromofluoroacetate (1.9 mL, 15.90 mmol) was added at RT and the stirring was continued for 12 h at the same temperature. Yellow coloured precipitate was observed, after completion of reaction, (monitored by TLC) water (15 mL) was added to the reaction mixture and the product was extracted with ethyl acetate (3 x 30 mL). The organic layer was washed with brine solution and dried over anhydrous Na_2SO_4 . The solvent was removed under reduced pressure and the product was purified by column chromatography, eluting with EtOAc/petroleum ether (3:7) to afford the compound **20a**. (Yield 1.97 g, 54%). ^1H -NMR (400 MHz, CDCl_3) δ : 1.36 (t, 3H, $J = 8$ Hz), 1.96 (s, 3H), 4.36 (q, 2H, $J = 8$ Hz), 6.64 (d, 1H, $J = 48$ Hz), 7.11 (s, 1H), 9.23 (bs, 1H); ^{19}F -NMR (376.6 MHz, CDCl_3 , C_6F_6 as internal reference) δ : -157.61 (d, $J = 48.9$ Hz); ^{13}C -NMR (100 MHz, CDCl_3) δ : 12.4, 14.0, 63.5, 87.3 (d, 215 Hz), 113.2, 135.3, 150.2, 163.8, 163.9, 64.3; HRMS (ESI-TOF) m/z Calcd for $\text{C}_9\text{H}_{12}\text{FN}_2\text{O}_4$ [$\text{M} + \text{H}$] $^+$ 231.0781, found 231.0780.

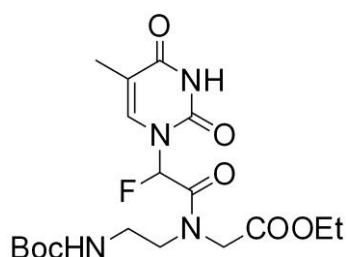
2-fluoro-2-(5-methyl-2, 4-dioxo-3,4-dihydropyrimidin-1(2H)-yl) acetic acid (21a)



To a solution of the compound **20a** (2 g, 8.7 mmol) in THF (10 mL), 2.5M KOH (1.0 ml, 7.4 mmol) was added at -78 °C. After 20 min stirring, reaction mixture was warmed to room temperature and monitored by TLC. After completion of reaction, proton exchange resin Dowex-H $^+$ was added in order to acidify the reaction mixture. Then the acid compound was

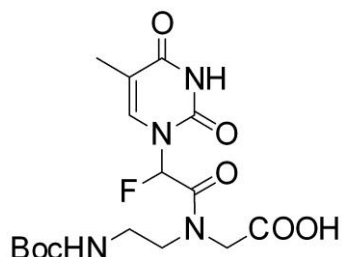
filtered, and the solvent was removed under vacuo to obtain the compound **21a**. (Yield 1.4 g, 80%): $^1\text{H-NMR}$ (400 MHz, D_2O) δ : 1.57 (s, 3H), 6.13 (d, 1H, $J = 52$ Hz), 7.15 (s, 1H), 11.04 (bs, 1H) $^{19}\text{F-NMR}$ (376.6 MHz, D_2O , C_6F_6 as internal reference) δ : -156.3 (d, $J = 60$ Hz) ; $^{13}\text{C-NMR}$ (100 MHz, D_2O) δ : 11.3, 90.5 (d, $J = 217$ Hz), 112.2, 139.4, 151.5, 166.5, 169.2; HRMS (ESI-TOF) m/z Calcd for $\text{C}_7\text{H}_8\text{FN}_2\text{O}_4$ 203.0468 $[\text{M} + \text{H}]^+$, found 203.0468.

Ethyl 2-(N-(2-((tert-butoxycarbonyl) amino) ethyl)-2-fluoro-2-(5-methyl-2,4-dioxo-3,4-dihydropyrimidin-1(2H)-yl) acetamido) acetate (22a)



To the acid compound **21a** (1.4 g, 6.93 mmol) in anhydrous DMF (4 mL), secondary amine (*aeg*) **16** (1.4 g, 6.93 mmol) was added and cooled to 0 °C. After 5 min stirring, HBTU (2.88 g, 7.62 mmol) and DIPEA (3.6 mL, 20.79 mmol) were added to the reaction mixture and stirred for 12 h at RT. After completion of reaction, reaction mixture was poured into water (25 ml), neutralized with *sat.aq.* KHSO_4 (10 mL), and extracted with ethyl acetate (3 x 20 mL). The organic layer was dried over anhydrous Na_2SO_4 . The solvent was removed under reduced pressure and product was purified by column chromatography, eluting with petroleum ether/EtOAc (1:1) to afford the compound **22a**. (Yield 1.5 g, 50%). $^1\text{H-NMR}$ (400 MHz, CDCl_3) δ : 1.28 (m, 3H), 1.42 (s, 9H), 1.94 (maj) 1.95 (min) (s, 3H), 3.29-3.34 (comp, 2H), 3.42-3.67 (comp, 2H), 4.10-4.25 (comp, 4H), 4.94 (min.) 5.29 (maj) (bs 1H), 6.97 (min) (maj) 7.17 (d, 1H), 7.32 (min) 7.37 (maj) (s, 1H), 9.16 (bs, 1H); $^{19}\text{F-NMR}$ (376.6 MHz, CDCl_3 , C_6F_6 as internal reference) δ : -155.55 (d, 1F); $^{13}\text{C-NMR}$ (100 MHz, CDCl_3) δ : 12.5, 14.1, 28.3, 29.7, 38.5, 48.9, 61.9, 80.1 (d, $J = 209$ Hz), 112.7, 135.5, 150.1, 156.1, 163.2, 164.3, 168.6, 168.8; HRMS (ESI-TOF) m/z Calcd for $\text{C}_{18}\text{H}_{27}\text{FN}_4\text{NaO}_7$ $[\text{M} + \text{Na}]^+$ 453.1761, found 453.1766.

2-(N-(2-((tert-butoxycarbonyl)amino)ethyl)-2-fluoro-2-(5-methyl-2,4-dioxo-3,4-dihydropyrimidin-1(2H)-yl)acetamido)acetic acid (3)



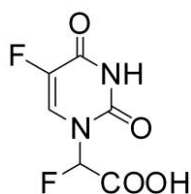
To the ester compound **22a** (1.5 g, 3.48 mmol) in THF (5 ml), 10% LiOH was added at 0 °C and stirred for 3 h. After completion of reaction, the mixture was acidified with *sat. aq.* KHSO₄ solution. The product was extracted with ethyl acetate and dried over anhydrous Na₂SO₄. The organic layer was evaporated under reduced pressure to obtain the desired monomer **3** in good yields. (Yield 1.15 g, 82%). ¹H-NMR (400 MHz, CDCl₃) δ: 1.37 (s, 9H), 1.83 (s, 3H), 3.19-3.52(m, 4H), 3.94-4.19 (m, 2H), 5.47 (min) 5.59 (maj) (bs, 1H), 6.93 (min) 7.08 (maj) (d, 1H), 7.32 (s, 1H), 9.77 (s, 1H); HRMS (ESI-TOF) *m/z* Calcd for C₁₆H₂₃FN₄O₇ [M + Na]⁺ 425.1448, found 425.1436.

Ethyl 2-fluoro-2-(5-fluoro-2, 4-dioxo-3,4-dihydropyrimidin-1(2H)-yl)acetate (**20b**)



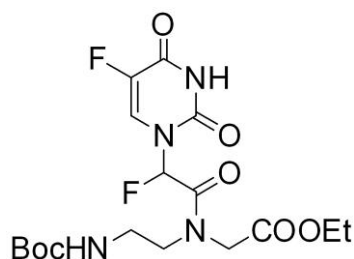
To a solution of 5-fluorouracil **19b** (2 g, 15.38 mmol) in anhydrous DMF (10 mL), K₂CO₃ (2.19 g, 15.38 mmol) and ethyl bromofluoroacetate (1.9 mL, 15.38 mmol) were added at RT and stirring was continued at RT for 12 h, pink coloured precipitate was observed. After completion of reaction, water (15 mL) and *aq.* KHSO₄ (10 mL) were added and the product was extracted with ethyl acetate (3 x 25 mL). The organic layer was dried over anhydrous Na₂SO₄. The solvent was removed under reduced pressure and product was purified by column chromatography, eluting with petroleum ether/EtOAc (7:3) to obtain the compound **20b**. (Yield 1.94 g, 55%). ¹H-NMR (400 MHz, CDCl₃) δ: 1.38 (t, 3H, *J* = 8 Hz), 4.37 (m, 2H), 6.67 (d, 1H, *J* = 48 Hz), 7.425 (d, 1H, *J* = 4 Hz), 9.50 (bs, 1H) ; ¹⁹F-NMR (376.6 MHz, CDCl₃) δ: -158.63 (d, *J* = 45.2 Hz); ¹³C-NMR (100 MHz, CDCl₃) δ: 14.0, 63.9, 87.34 (d, *J* = 217 Hz), 123.9 (d, *J* = 34 Hz), 139.9, 142.3, 148.6, 156.2, 156.5, 163.4, 163.7; HRMS (ESI-TOF) *m/z* Calcd for C₈H₉F₂N₂O₄ [M + H]⁺ 235.0531, found 235.0527.

2-fluoro-2-(5-fluoro-2,4-dioxo-3,4-dihydropyrimidin-1(2H)-yl)aceticacid (**21b**)



To a solution of compound **20b** (1.94 g, 8.43 mmol) in THF (10 mL,) 2.5 M KOH (1 mL, 16.86 mmol) was added at -78 °C. After 20 min stirring, reaction was brought to room temperature and monitored by TLC. After completion of reaction, proton exchange resin Dowex-H+ was added in order to acidify the reaction mixture. Then the acid was filtered and solvent was removed under vacuo to obtain the compound **21b**. (Yield 1.45 g, 85%). ¹H-NMR (400 MHz, DMSO-d₆) δ: 6.40 (d, 1H, *J* = 44 Hz), 8.25 (d, 1H, *J* = 4 Hz), 12.20 (bs, 1H); ¹⁹F-NMR (DMSO-d₆, C₆F₆ as internal reference 376.6 MHz) δ: -154.57 (d, *J* = 12 Hz), -167.11 (s). HRMS (ESI-TOF) *m/z* Calcd C₆H₅F₂N₂O₄ [M + H] 207.0217 found 207.0212.

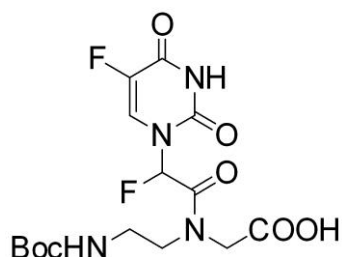
Ethyl-2-(N-(2-((tert-butoxycarbonyl) amino) ethyl)-2-fluoro-2-(5-fluoro-2,4-dioxo-3,4-dihydropyrimidin-1(2H)-yl)acetamido)acetate (22b)



To the acid compound **21b** (1.45g, 7.04 mmol) in anhydrous DMF (4 mL), secondary amine (*aeg*) **16** (1.73g, 7.04 mmol) was added and cooled to 0 °C. After 5 min stirring, HBTU (2.66g, 7.04 mmol) and DIPEA (3.1mL, 17.60 mmol) were added to the reaction mixture and stirred for 12 h at RT. After completion of reaction, reaction mixture was poured into water (25 ml), neutralized with *sat.aq.* KHSO₄ (10 mL), and extracted with ethyl acetate (3 x 20 mL). The organic layer was dried over anhydrous Na₂SO₄. The solvent was removed under reduced pressure and product was purified by column chromatography, eluting with petroleum ether/EtOAc (1:1) to obtain the compound **22b**. (Yield 1.52 g, 50%). ¹H-NMR (400 MHz, CDCl₃) δ: 1.23-1.28 (m, 3H), 1.39 (s, 9H), 3.29-3.65 (comp, 4H), 4.05-4.24 (comp, 4H), 5.15 (min) (maj) 5.46 (bs, 1H), 7.01 (min) (maj) 7.16 (d, 1H), 7.615 (min) (maj) 7.64 (d, 1H, *J* = 8 Hz), 10.29 (bs, 1H); ¹⁹F-NMR (376.6 MHz, CDCl₃, C₆F₆ as internal reference) δ: -163.33 (min) (maj) -163.45 (s), -155.68 (maj) (min) (d, *J* = 45.2 Hz); ¹³C-NMR (100 MHz, CDCl₃) δ: 14.1, 28.2, 38.4, 48.9, 62.0, 80.2, 85.0 (maj) 86.0 (min) (d, *J* = 210 Hz),

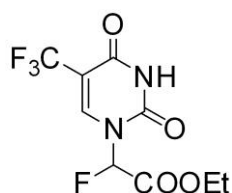
124.4 (d, $J = 35$ Hz), 139.7, 142.1, 148.9, 156.3, 156.8, 157.1, 163.6, 163.9, 168.7; HRMS (ESI-TOF) m/z Calcd for $C_{17}H_{24}F_2N_4NaO_7$ $[M + Na]^+$ 457.1511, found 457.1506.

2-(N-(2-((tert-butoxycarbonyl)amino)ethyl)-2-fluoro-2-(5-fluoro-2,4-dioxo-3,4-dihydropyrimidin-1(2H)-yl)acetamido)acetic acid (4)



To the ester compound **22b** (1.52 g, 3.50 mmol) in THF (5 ml), 10% LiOH was added at 0 °C and stirred for 3 h. After completion of reaction, the mixture was acidified with *sat. aq.* $KHSO_4$. The product was extracted with ethyl acetate and dried over Na_2SO_4 . The solvent was evaporated under reduced pressure to obtain the desired monomer **4**. Yield (1.13 g, 80%). 1H -NMR (400 MHz, $ACN-d_3$) δ : 1.38 (s, 9H), 3.21 -3.47 (m, 4H), 3.94 (m, 2H), 5.39 (min) 5.53 (maj) (bs, 1H), 6.93 (min) 7.09 (maj) (d, 1H, $J = 48$ Hz), 7.63 (bs, 1H), 9.72 (bs, 1H); ^{19}F -NMR (376.6 MHz, $CDCl_3$, C_6F_6 as internal reference) δ : -150.33 (maj) -151.37 (min) (d, $J = 45.19$ Hz), -161.36 (min) -161.70 (maj) (s); HRMS (ESI-TOF) m/z Caclcd for $C_{15}H_{20}F_2N_4NaO_7$ $[M + Na]$ 429.1198, found 429.1198.

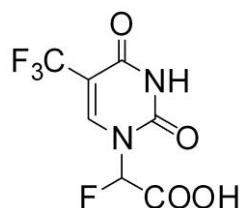
Synthesis of ethyl 2-(2,4-dioxo-5-(trifluoromethyl)-3,4-dihydropyrimidin-1(2H)-yl)-2-fluoroacetate (20c)



To the solution of 5-fluoromethyluracil **19c** (500 mg, 2.78 mmol) in anhydrous DMF (2 mL), K_2CO_3 (383 mg, 2.78 mmol) and ethyl bromofluoroacetate (0.3 mL, 2.78 mmol) were added at RT and stirring was continued at RT for 12 h, pink coloured precipitate was observed. After completion of reaction, water (15 mL) and *aq.* $KHSO_4$ (10 mL) were added and extracted with ethyl acetate (3 x 25 mL). The organic layer was dried over anhydrous Na_2SO_4 . The solvent was removed under reduced pressure and product was purified by column chromatography, eluting with petroleum ether/EtOAc (7:3) to obtain the compound **20c**. (Yield 470 mg, 60%). 1H -NMR (400 MHz, $CDCl_3$) δ : 1.38 (t, $J = 8$ Hz, 3H), 4.41 (qd, $J = 4$

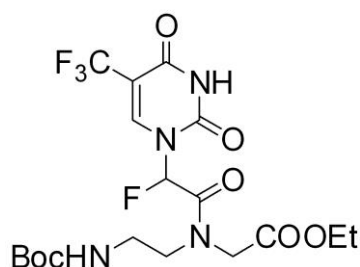
Hz, 2H), 6.65 (d, $J = 44$ Hz, 1H), 7.84 (s, 1H), 9.17 (bs, 1H); ^{19}F -NMR (376.6 MHz, CDCl_3 , C_6F_6 as internal reference) δ : -158.26 (d, $J = 4.5$ Hz), -65.12 (s); ^{13}C -NMR (100 MHz, CDCl_3) δ : 13.9, 64.1, 87.6 (d, $J = 220$ Hz), 108.8 (q, $J = 34$ Hz), 119.7, 122.4, 141.8 (q, $J = 11$ Hz), 148.4, 157.5, 163.0, 163.3; HRMS (ESI-TOF) m/z Calcd for $\text{C}_9\text{H}_8\text{F}_4\text{N}_2\text{NaO}_4$ [$\text{M} + \text{Na}$] 307.0318, found 307.0320.

Synthesis of 2-(2,4-dioxo-5-(trifluoromethyl)-3,4-dihydropyrimidin-1(2H)-yl)-2-fluoroacetic acid (21c)



To a solution of compound **20c** (470 mg, 1.65 mmol) in THF (2 mL), 2.5 M KOH (1 mL, 9.9 mmol) was added at -78 °C. After 20 min stirring, reaction was brought to room temperature and monitored by TLC. After completion of reaction, proton exchange resin Dowex-H⁺ was added in order to acidify the reaction mixture. Then the acid was filtered and solvent was removed under vacuo to obtain the compound **21c**. (Yield 380 mg, 90%). ^1H -NMR (400 MHz, DMSO-d_6) δ : 6.42 (d, $J = 48$ Hz, 1H), 8.54 (s, 1H), 12.24 (s, 1H); ^{19}F -NMR (376.6 MHz, DMSO-d_6 , C_6F_6 as internal reference) δ : -158.2 (d, $J = 45.2$ Hz), -62.7 (s). HRMS (ESI-TOF) m/z Calcd for $\text{C}_7\text{H}_5\text{F}_4\text{N}_2\text{O}_4$ [$\text{M} + \text{H}$]⁺ 257.0185, found 257.0204.

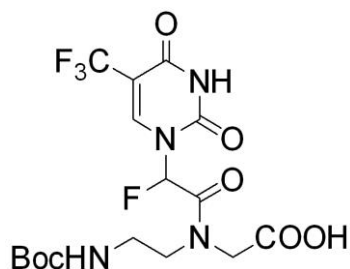
Synthesis of ethyl-2-(N-(2-((tert-butoxycarbonyl)amino)ethyl)-2-(2,4-dioxo-5-(trifluoromethyl)-3,4-dihydropyrimidin-1(2H)-yl)-2-fluoroacetamido)acetate (22c)



To the acid compound **21c** (380 mg, 1.48 mmol) in anhydrous DMF (2.5 mL), secondary amine *aeg* backbone **16** (365 mg, 1.48 mmol) was added and cooled to 0 °C. After 5 min stirring, HBTU (560 mg, 1.48 mmol) and DIPEA (0.77 mL, 4.45 mmol) were added to the reaction mixture and stirred for 12 h at RT. After completion of reaction, reaction mixture was poured into water (25 mL), neutralized with *sat.aq.* KHSO_4 (10 mL), and extracted with ethyl

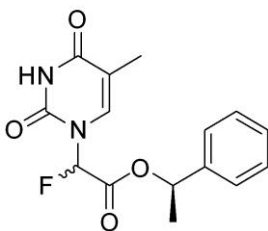
acetate (3 x 20 mL). The organic layer was dried over anhydrous Na₂SO₄. The solvent was removed under reduced pressure and product was purified by column chromatography, eluting with petroleum ether/EtOAc (1:1) to obtain the compound **22c**. (Yield 420 mg, 58%). ¹H-NMR (400 MHz, CDCl₃) δ: 1.26 (m, 3H), 1.40 (s, 9H), 3.26- 3.57 (m, 4H), 4.04 (min) 4.11(maj) (s, 2H), 4.18-4.28 (m, 2H), 5.13 (min) 5.48 (maj) (bs, 1H), 7.05 (min) 7.23 (maj) (d, 1H, *J* = 44 Hz), 7.37 (q, 1H, *J* = 4 Hz), 8.03 (bs, 1H); ¹⁹F-NMR (376.6 MHz, CDCl₃, C₆F₆ as internal reference) δ: -155.5 (d, *J* = 45.2 Hz), -62.4 (s); ¹³C-NMR (100 MHz, CDCl₃) δ: 14.0, 28.3, 38.7, 49.1, 62.1, 62.5, 80.3, 85.1 (maj) 86.3 (min) (d, *J* = 211 Hz), 106.9 (q, *J* = 34Hz), 141.7 (d, *J* = 6Hz), 149.1, 156.4, 158.3, 163.4, 163.7, 168.7; HRMS (ESI-TOF) *m/z* Calcd for C₁₈H₂₄F₄N₄NaO₇ [M + Na]⁺ 507.1479, found 507.1479.

Synthesis of 2-(N-(2-((tert-butoxycarbonyl)amino)ethyl)-2-(2,4-dioxo-5-(trifluoromethyl)-3,4-dihydropyrimidin-1(2H)-yl)-2-fluoroacetamido)acetic acid (5)



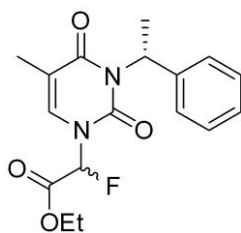
To the ester compound **22c** (420 mg, 0.867 mmol) in THF (5 ml), 10% LiOH was added at 0 °C and stirred for 3 h. After completion of reaction, the mixture was acidified with *sat. aq.* KHSO₄ solution and product was extracted with ethyl acetate and dried over Na₂SO₄. The solvent was evaporated under reduced pressure to obtain the desired monomer **5**. Yield (320 mg, 81 %). ¹H-NMR (400 MHz, MeOH-d₄) δ: 1.40 (s, 9H), 3.24-3.27 (m, 2H), 3.45-3.60 (m, 2H), 4.03 (min.) 4.07 (bs, 1H), 4.22-4.35 (m, 2H), 7.15 (min) 7.27 (maj) (d, *J* = 44 Hz, 1H) 8.15 (s, 1H); ¹⁹F-NMR (376.6 MHz, DMSO-d₆, C₆F₆ as internal reference) δ: -155.5 (d, *J* = 45.2 Hz), -62.8 (s); ¹³C-NMR (100 MHz, MeOH-d₄) δ: 27.1, 29.8, 37.3, 37.9, 79.3, 85.9 (d, *J* = 110 Hz), 106.2 (d, *J* = 110 Hz), 123.2, 141.9 (maj) 142.0 (min) (d, *J* = 6 Hz), 149.2, 157.0, 157.1, 158.9, 164.1, 170.5; HRMS (ESI-TOF) *m/z* Calcd for C₁₆H₂₀F₄N₄NaO₇ [M + Na]⁺ 479.1166, found 479.1173.

(S)-1-phenylethyl 2-fluoro-2-(5-methyl-2,4-dioxo-3,4-dihydropyrimidin-1(2H)-yl)acetate (24)



To a solution of acid compound **21a** (300 mg, 1.49 mmol) and (*S*)-1-phenylethanol (0.36 mL, 2.98 mmol) in anhydrous DMF (10 mL), DCC predissolved in DMF (369 mg, 1.79 mmol) was added at RT and stirring was continued at the same temperature for 12 h. After completion of reaction, DCU was filtered and water (15 mL) was added to the filtrate and the product was extracted with ethyl acetate (3 x 25 mL). The organic layer was dried over anhydrous Na₂SO₄. The solvent was removed under reduced pressure and product was purified by column chromatography, eluting with petroleum ether/EtOAc (1:9) to obtain the compound **24**. (Yield 250 mg, 55%). ¹H-NMR (400 MHz, CDCl₃) δ: 1.63 (t, 3H, *J* = 8 Hz), 1.80-1.90 (dd, 3H), 6.01-6.08 (m, 1H, *J* = 8 Hz), 6.61-6.77(dd, 1H, *J* = 16 Hz), 6.76-6.70 (d, 1H), 7.31-7.40 (m, 5H); 9.11-9.15 (bd, 1H); ¹⁹F-NMR (376.6 MHz, CDCl₃) δ: -155.99 (d, 1F, *J* = 49 Hz); ¹³C-NMR (100 MHz, CDCl₃) δ: 12.3, 12.4, 21.6, 21.7, 76.2, 85.8 (d, *J* = 39 Hz), 87.96 (d, *J* = 40 Hz), 113.0, 113.1, 126.3, 128.7, 134.9, 135.0, 139.7, 149.9, 163.1, 163.5. HRMS (ESI-TOF) *m/z* Calcd for C₁₅H₁₅FN₂NaO₄ [M + Na]⁺ 329.0914, found 329.0921.

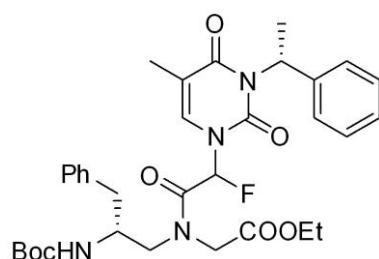
Ethyl 2-fluoro-2-(5-methyl-2,4-dioxo-3-((*R*)-1-phenylethyl)-3,4-dihydropyrimidin-1(2H)-yl)acetate (25**)**



To a solution of *S*-phenyl alcohol (0.21 mL, 1.74 mmol) in DMF, DIAD (0.32 mL, 1.74 mmol) and PPh₃ (456 mg, 1.74 mmol) were added at ice-cold condition and stirred for 15 min., after the formation of active intermediate, compound **20a** (200 mg, 0.87 mmol) and K₂CO₃ (120 mg, 0.87 mmol) were added at the same temperature, and stirring was continued at RT for 12 h. After completion of reaction (monitored by TLC), water (20 mL) was added to the reaction mixture and the product was extracted with ethyl acetate (3 x 10 mL). The organic layer was dried over anhydrous Na₂SO₄. The solvent was removed under reduced pressure and product

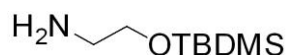
was purified by column chromatography, eluting with EtOAc/petroleum ether (15:85) to obtain the compound **25**. (Yield 131 mg, 45%). ¹H-NMR (400 MHz, CDCl₃) δ: 1.30-1.34 (m, 3H) 1.82 (dd, 2H, *J* = 8 Hz), 1.94 (d, 1H, *J* = 4 Hz), 4.26-4.36 (m, 2H), 6.25-6.29 (m, 1H), 6.49 (dd, 1H), 7.07 (s, 1H), 7.23-7.43 (m, 5H); ¹⁹F-NMR (376.6 MHz, CDCl₃) δ: -155.69 (dd, *J* = 45.2 Hz); ¹³C-NMR (100 MHz, CDCl₃) δ: 13.3, 13.9, 14.0, 51.3, 51.4, 63.3, 87.2, 89.4, 89.6, 112.4, 112.5, 127.3, 127.4, 128.1, 128.7, 133.7, 133.9, 139.7, 163.0, 163.9, 164.3. HRMS (ESI-TOF) *m/z* Calcd for C₁₇H₁₉FN₂NaO₄ [M + Na]⁺ 357.1227, found 357.1229.

Ethyl 2-(N-((R)-2-((tert-butoxycarbonyl)amino)-3-phenylpropyl)-2-fluoro-2-(5-methyl-2,4-dioxo-3-((R)-1-phenylethyl)-3,4-dihydropyrimidin-1(2H)-yl)acetamido)acetate (27)



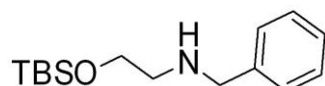
To the acid compound **26** (730 mg, 2.38 mmol) in anhydrous DMF (2 mL), secondary amine **49b** (800 mg, 2.38 mmol) was added and cooled to 0 °C. After 5 min stirring, HBTU (900 mg, 2.38 mmol) and DIPEA (0.8 mL, 4.76 mmol) were added to the reaction mixture and stirred for 12 h at RT. After completion of reaction, reaction mixture was poured into water (25 ml), neutralized with *sat.aq.* KHSO₄ (10 mL), and extracted with ethyl acetate (3 x 20 mL). The organic layer was dried over anhydrous Na₂SO₄. The solvent was removed under reduced pressure and product was purified by column chromatography, eluting with petroleum ether/EtOAc (1:1) to obtain the compound **27**. (Yield 475 mg, 32%). ¹H-NMR (400 MHz, CDCl₃) δ: 1.25 (min) (maj) 1.26 (s, 9H) , 1.29-1.31 (m, 3H), 3.39-1.46 (m, 2H), 1.56-1.64 (m, 2H), 1.79-1.95 (m, 2H) 4.90-5.11 (m, 2H), 5.95-6.34 (m, 1H), 6.47-6.71 (m, 1H), 6.75-6.95 (m, 1H), 7.26-7.44 (m, 5H); ¹⁹F-NMR (376.6 MHz, CDCl₃) δ: -157.18 – (-155.40 (m)); ¹³C-NMR (100 MHz, CDCl₃) δ: 13.1, 14.1, 15.7, 21.6, 21.7, 22.1, 28.3, 29.7, 39.0, 51.3, 53.4, 69.6, 70.1, 71.2, 72.2, 75.8, 77.2, 86.5, 112.3, 126.2, 127.3, 128.1, 128.6, 129.2, 133.1, 133.3, 139.6, 140.8, 155.1; HRMS (ESI-TOF) *m/z* Calcd for C₂₈H₃₃FN₄O₅ [M-Boc + Na]⁺ 547.2333, found 547.2382.

Synthesis of 2-((tert-butyldimethylsilyl)oxy)ethanamine (29)



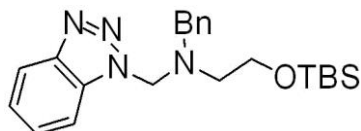
To a solution of ethanolamine **28** (10 mL, 163.93 mmol) in anhydrous DCM (300 mL), TBDMSCl (27.05 g, 180.32 mmol) and imidazole (27.86 g, 409.82 mmol) were added, and stirred for 12 h. After completion of reaction (monitored by TLC), water and *sat.aq.* NH₄Cl were added and extracted with DCM and dried over anhydrous Na₂SO₄. The solvent was removed under reduced pressure to obtain product **29**.

Synthesis of N-benzyl-2-((tert-butyldimethylsilyl)oxy)ethanamine (**30**)



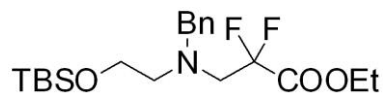
To the solution of compound **29** (10 g, 57.30 mmol) in ACN (100 mL), bromobenzene (5.0 mL, 40.10 mmol), and Et₃N (19.4 mL, 28.64 mmol) were added and stirring was continued at RT for 12 h, monitoring the completion of reaction by TLC, after completion of reaction, water was added and extracted with ethyl acetate (3 x 50 mL). The organic layer was dried over anhydrous Na₂SO₄. The solvent was removed under reduced pressure and product was purified by column chromatography, eluting with petroleum ether/EtOAc (1:1) to obtain the compound **30**.

Synthesis of N-((1H-benzo[d][1,2,3]triazol-1-yl)methyl)-N-benzyl-2-((tert-butyldimethylsilyl)oxy)ethanamine (**31**)



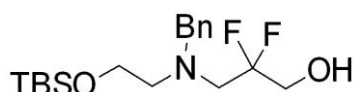
To a solution of compound **30** (5 g, 18.86 mmol) in diethyl ether (50.0 mL), benzotriazole (3.36 g, 28.30 mmol) and formalin (2 mL of 35% formalin, 22.64 mmol) were added at 0 °C and stirring was continued at RT for 12 h, after completion of reaction (monitored by TLC), the solid formed in the reaction mixture was filtered and filtrate was concentrated. The product was purified by column chromatography, eluting with petroleum ether/EtOAc (3:1) to obtain the compound **31**. (Yield 5.97 g, 80%). ¹H-NMR (400 MHz, CDCl₃) δ: 0.02 (min) 0.05 (maj) (s, 6H), 0.87 (min) 0.89 (maj) (s, 9H), 2.84 (t, 2H, *J* = 4 Hz), 3.77 (t, 2H, *J* = 8 Hz), 3.82 (s, 2H), 5.59 (s, 2H), 7.24-8.06 (m, 9H); ¹³C-NMR (100 MHz, CDCl₃) δ: -5.2, 26.0, 53.5, 53.7, 56.8, 62.4, 66.7, 110.4, 118.4, 119.8, 123.8, 126.2, 127.2, 127.4, 128.4, 128.8, 129.0, 133.8, 138.4, 145.9; MALDI-TOF : *m/z* Calcd for C₂₂H₃₂KN₄OSi 435.1982 [M + K] 435.1982, found 435.0692. HRMS (ESI-TOF) *m/z* Calcd for C₁₅H₂₈NOSi [M-CH₂Bt + H] 266.1940, found 266.1938.

Synthesis of ethyl 3-(benzyl(2-((tert-butyldimethylsilyl)oxy)ethyl)amino)-2,2-difluoropropanoate (**32**)



Zinc (4.1 g, 63.13 mmol) was placed into a 250 mL round-bottom flask, to this 25 mL of freshly distilled THF, and TMSCl (1.6 mL, 12.62 mmol) were added, and the mixture was stirred vigorously at 50 °C for 15 min. Then, ethyl bromodifluoroacetate (6.4 mL, 50.50 mmol) was added and stirred at the same temperature for 20 min. The mixture was cooled to RT, and then compound **31** (5 g, 12.62 mmol) previously dissolved in 10 mL of THF was added and stirred at RT for 1h. After completion of reaction the reaction mixture was filtered through celite pad and filtrate was concentrated under vacuo. The crude product was purified by column chromatography, eluting with pet ether /ethyl acetate to obtain pure compound **32**. Yield (2.25 g, 45%): ¹H NMR (CDCl₃, 400 MHz) δ: 0.00 (s, 6H), 0.86 (s, 9H), 1.30 (t, 3H, *J* = 8 Hz), 2.68 (t, 2H, *J* = 8 Hz), 3.30 (t, 2H, *J* = 12 Hz), 3.62 (t, 2H, *J* = 8 Hz), 3.80 (s, 2H), 4.27 (q, 2H, *J* = 8 Hz), 7.22-7.28 (m, 5H); ¹⁹F-NMR (376.6 MHz, CDCl₃, C₆F₆ as internal reference) δ: -109.2 (s); ¹³C-NMR (100 MHz, CDCl₃) δ: -5.3, 14.0, 25.9, 55.6, 57.3 (t, *J* = 40 Hz), 59.4, 61.1, 62.7, 127.1, 128.3, 128.8, 138.8; HRMS (ESI-TOF) *m/z* Calcd for C₂₀H₃₄F₂NO₃Si [M + H] 402.2276, found 402.2322.

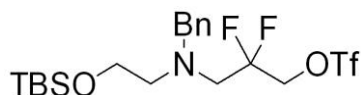
Synthesis of 3-(benzyl(2-((tert-butyldimethylsilyl)oxy)ethyl)amino)-2,2-difluoropropan-1-ol (**33**)



To the solution of ester compound **32** (2.25 g, 5.6 mmol) in ethanol (20.0 mL), sodiumborohydride (0.85 g, 22.44 mmol) was added at 0 °C and then warmed to room temperature, stirred at the same temperature for 12 h. After completion of reaction, water was added and extracted with ethyl acetate (3x25 mL). The organic layer was dried over anhydrous Na₂SO₄ and the solvent was removed under reduced pressure. The product was purified by column chromatography, eluting with petroleum ether/EtOAc (3:1) to obtain the compound **33**. (Yield 1.91 g, 95%). ¹H NMR (CDCl₃, 400 MHz) δ: 0.04 (s, 6H), 0.90 (s, 9H), 2.66 (t, 2H, *J* = 8 Hz), 3.07 (t, 2H, *J* = 12 Hz), 3.73 (t, 2H, *J* = 8 Hz), 3.74 (s, 2H), 3.83 (t, 2H, *J* = 12 Hz), 4.02 (maj) 4.12 (min) (t, 1H, *J* = 8 Hz) 7.30 (m, 5H); ¹⁹F-NMR (376.6 MHz, CDCl₃, C₆F₆ as internal reference) δ: -107.3 (s); ¹³C-NMR (100 MHz, CDCl₃) δ: -5.4, 18.3,

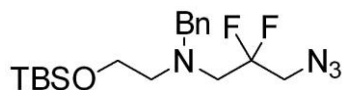
25.9, 55.4 (t, $J = 32$ Hz), 56.2, 60.1, 61.3, 63.5 (t, $J = 32$ Hz), 123.0 (t, $J = 244$ Hz) 127.45, 128.5, 129.0, 138.2; HRMS (ESI-TOF) m/z Calcd for $C_{18}H_{32}F_2NO_2Si$ [M + H] 360.2170, found 360.2216.

Synthesis of 3-(benzyl(2-((tert-butyldimethylsilyl)oxy)ethyl)amino)-2,2-difluoropropyl trifluoromethanesulfonate (34)



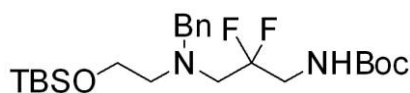
To the solution of hydroxyl compound **33** (1.9 g, 5.29 mmol) in DCM, triethylamine (0.8 mL, 5.82 mmol) and triflic anhydride (10 mL, 5.82 mmol) were added at -78 °C and stirred at same temperature for 1 h. After completion of reaction, reaction mixture was poured into water and extracted with DCM, dried over Na_2SO_4 , concentrated under vacuo to obtain the compound **34** and was used for further reaction without purification.

Synthesis of 3-azido-N-benzyl-N-(2-((tert-butyldimethylsilyl)oxy)ethyl)-2,2-difluoropropan-1-amine (35)



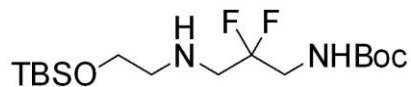
To a solution of compound **34** (2.59 g, 5.29 mmol) in DMF (5.0 mL), sodiumazide (1.37 g, 21.16 mmol) was added at RT and stirred for 12 h. After completion of reaction, water was added and the product was extracted with ethyl acetate (3x25 mL) and the organic layer was dried over anhydrous Na_2SO_4 . The solvent was removed under reduced pressure and product was purified by column chromatography, eluting with petroleum ether/EtOAc (3:1) to obtain the compound **35**. (Yield 1.62 g, 80%). 1H NMR ($CDCl_3$, 400 MHz) δ : 0.06 (s, 6H), 0.91 (s, 9H), 2.73 (t, 2H, $J = 8$ Hz), 3.07 (t, 2H, $J = 12$ Hz), 3.58 (t, 2H, $J = 12$ Hz), 3.65 (t, 2H, $J = 8$ Hz), 3.80 (s, 2H), 7.31-7.34 (m, 5H); ^{19}F -NMR (376.6 MHz, $CDCl_3$, C_6F_6 as internal reference) δ : -106.36 (s); ^{13}C -NMR (100 MHz, $CDCl_3$) δ : -5.3, 18.3, 25.9, 52.2 (t, $J = 28$ Hz), 56.2 (t, $J = 27$ Hz), 56.5, 56.5, 60.1, 61.5, 123.1 (t, $J = 243$ Hz), 127.3, 128.4, 128.8, 138.9; HRMS (ESI-TOF) m/z Calcd for $C_{18}H_{31}F_2N_4OSi$ [M + H] $^+$ 385.2235, found 385.2247.

Synthesis of tert-butyl(3-(benzyl(2-((tert-butyldimethylsilyl)oxy)ethyl)amino)-2,2-difluoropropyl)carbamate (36)



The azide compound **35** was converted to amine using Staudinger reaction conditions. To the solution of azide compound **35** (1.6 g, 4.16 mmol) in THF (15 mL), triphenylphosphine (1.09 g, 4.16 mmol) was added and stirred at RT for 12 h, then water was added to the reaction mixture and warmed to 45 °C for 4 h. After completion of reaction, THF was evaporated under reduced pressure and then water was added and product was extracted with ethyl acetate (3x15 mL). The organic layer was dried over anhydrous Na₂SO₄ and the solvent was removed under reduced pressure to obtain free amine which was used for further reaction without purification. To the solution of the amine compound (1.49 g, 4.16 mmol) in ACN (10.0 mL), triethylamine (0.6 mL, 4.57 mmol) and Boc-anhydride (0.99 g, 4.57 mmol) were added. The reaction mixture stirred at RT for 12 h, after completion of reaction, water was added and extracted with ethyl acetate (3x20mL). The organic layer was dried over anhydrous Na₂SO₄. The solvent was removed under reduced pressure and product was purified by column chromatography, eluting with petroleum ether/EtOAc (3.5:0.5) to obtain the compound **36**. (Yield 1.42 g, 75%). ¹H NMR (CDCl₃, 400 MHz) δ: 0.04 (s, 6H), 0.89 (s, 9H), 1.44 (s, 9H), 2.70 (t, 2H, *J* = 8 Hz), 2.97 (t, 2H, *J* = 12 Hz), 3.6 (m, 2H), 3.72 (t, 2H, *J* = 8 Hz), 3.76 (s, 2H), 5.04 (t, 1H, *J* = 8 Hz), 7.32-7.34 (m, 5H); ¹⁹F-NMR (376.6 MHz, CDCl₃, C₆F₆ as internal reference) δ: -106.57 (s); ¹³C-NMR (100 MHz, CDCl₃) δ: -5.3, 18.3, 26.0, 28.4, 43.4 (t, *J* = 29 Hz), 55.98 (t, *J* = 27 Hz), 56.5, 60.3, 61.5, 79.6, 122.9 (t, *J* = 244 Hz), 127.3, 128.5, 129.0, 129.1 138.8, 155.9; HRMS (ESI-TOF) *m/z* Calcd for C₂₃H₄₁F₂N₂O₃Si [M + H]⁺ 459.2855, found 459.2852.

Synthesis of tert-butyl(3-((2-((tert-butyldimethylsilyl)oxy)ethyl)amino)-2,2-difluoropropyl)carbamate (**37**)



The compound **36** (1.42 g, 3.12 mmol) was taken in ethanol (10.0 mL), and subjected to hydrogenation using Pd/C (0.05 g, 10% mmol) as catalyst at RT for 1 h. After completion of reaction, the reaction mixture was filtered through celite pad and the filtrate was concentrated on vacuo. The product was purified by column chromatography, eluting with petroleum ether/EtOAc (3:1) to obtain the compound **37**. (Yield 0.91 g, 80%). ¹H-NMR (400 MHz, CDCl₃) δ: 0.07 (s, 6H), 0.90 (s, 9H), 1.45 (s, 9H), 1.84 (bs, 1H), 2.77(t, 2H, *J* = 4 Hz), 3.01 (t, 2H, *J* = 12 Hz), 3.56-3.65 (m, 2H), 3.70 (t, 2H, *J* = 4 Hz), 5.03 (bs, 1H); ¹⁹F-NMR(CDCl₃, 376.6 MHz, C₆F₆ as internal reference) δ: -109.55 (s); ¹³C-NMR (100 MHz, CDCl₃) δ: -5.2,

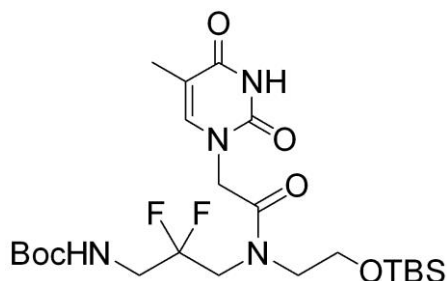
18.3, 25.9, 28.3, 29.7, 43.5 (t, $J = 30$ Hz), 51.2, 51.5, 51.8, 62.3, 80.0, 122.0 (t, $J = 242$ Hz), 155.8; HRMS (ESI-TOF) m/z Calcd for $C_{16}H_{35}F_2N_2O_3Si$ $[M + H]^+$ 369.2385, found 369.2383.

Synthesis of tert-butyl(3-(N-(2-((tert-butyldimethylsilyl)oxy)ethyl)-2-chloroacetamido)-2,2-difluoropropyl)carbamate (38)



To a solution of compound **37** (0.91 g, 2.49 mmol) in (1:1 water, Dioxane, 5.0 mL), sodium bicarbonate (0.46 g, 5.47 mmol) and chloroacetylchloride (0.2 mL, 2.73 mmol) were added at 0 °C and stirred for 2 h, monitoring the completion of reaction by TLC, after completion of reaction, water was added and extracted with ethyl acetate (3 x 15 mL). The organic layer was dried over anhydrous Na_2SO_4 . The solvent was removed under reduced pressure and product was purified by column chromatography, eluting with petroleum ether/EtOAc (3:1) to obtain the compound **38**. (Yield 1.1 g, 85%). 1H NMR ($CDCl_3$, 400 MHz) δ : 0.05 (s, 6H), 0.88 (s, 9H), 1.45 (s, 9H), 3.46-3.51 (m, 2H), 3.62-3.67 (m, 2H), 3.76-3.86 (m, 2H), 4.09 (min) 4.12 (maj) (s, 1H), 4.34 (maj) 4.37 (min) (s, 1H), 5.45 (min) 5.63 (maj) (bs, 1H); ^{19}F -NMR (376.6 MHz, $CDCl_3$, C_6F_6 as internal reference) δ : -107.31 (s); ^{13}C -NMR ($CDCl_3$, 100 MHz) δ : -5.5, 18.2, 25.8, 28.4, 29.7, 41.3, 46.6, 50.8, 59.8, 79.9, 121.4, 156.0, 169.7; HRMS (ESI-TOF) m/z Calcd for $C_{18}H_{35}ClF_2N_2NaO_4Si$ $[M + Na]^+$ 467.1920, found 467.1920, $[M + 2 + Na]$ 469.1920, found 469.1901.

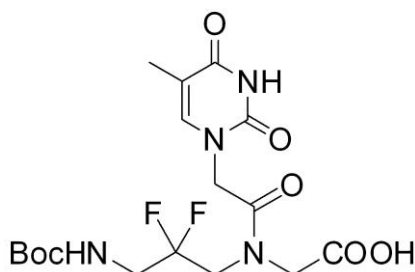
Synthesis of tert-butyl(3-(N-(2-((tert-butyldimethylsilyl)oxy)ethyl)-2-(5-methyl-2,4-dioxo-3,4-dihydropyrimidin-1(2H)-yl)acetamido)-2,2-difluoropropyl)carbamate (39)



To a solution of compound **38** (1.1 g, 2.47 mmol) in DMF, thymine (0.31 g, 2.47 mmol) and K_2CO_3 (0.34 g, 2.47 mmol) were added at 0 °C and stirred at RT for 12 h, monitoring the completion of reaction by TLC, after completion of reaction, water and *sat. aq.* $KHSO_4$ solution were added and extracted with ethyl acetate (3 x 20 mL). The organic layer was dried

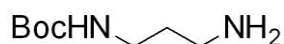
over anhydrous Na_2SO_4 . The solvent was removed under reduced pressure and product was purified by column chromatography, eluting with petroleum ether/EtOAc (1:1) to obtain the compound **39**. (Yield 1.06 g, 80%). δ : 0.09 (s, 6H), 0.09 (s, 9H), 1.43 (s, 9H), 1.93 (s, 3H), 3.41-3.49 (m, 2H), 3.63 (t, 2H, $J = 8$ Hz), 3.75-3.84 (m, 4H), 4.51 (min) 4.68 (maj) (s, 2H), 5.41 (t, 1H, $J = 8$ Hz), 6.91 (s, 1H), 8.86 (bs, 1H); ^{19}F -NMR (376.6 MHz, CDCl_3 , C_6F_6 as internal reference) δ : -107.52 (maj) -108.69 (min) (s); ^{13}C -NMR (100 MHz, CDCl_3) δ : -5.3, 12.5, 18.4, 26.0, 28.3, 29.7, 42.3 (t, $J = 30$ Hz), 46.9 (t, $J = 31$ Hz), 48.7, 50.3, 60.2, 79.9, 110.9, 121.49, 140.8, 151.0, 155.8, 164.1, 169.0; HRMS (ESI-TOF) m/z Calcd for $\text{C}_{23}\text{H}_{40}\text{F}_2\text{N}_4\text{NaO}_6\text{Si}$ [$\text{M} + \text{Na}$] $^+$ 557.2583, found 557.2572.

Synthesis of 2-(N-(3-((tert-butoxycarbonyl)amino)-2,2-difluoropropyl)-2-(5-methyl-2,4-dioxo-3,4-dihydropyrimidin-1(2H)-yl)acetamido)acetic acid (6)

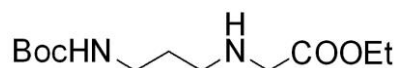


To a solution of compound **39** (1.06 g, 1.98 mmol) in THF(1.0 mL), TBAF (1.6 mL of 1.0 M, 5.94 mmol) was added at 0 °C and stirred at RT for 3 h, after completion of reaction, THF was evaporated, water was added and extracted with ethyl acetate (4 x 25 mL). The organic layer was dried over anhydrous Na_2SO_4 . The solvent was removed under reduced pressure and product was purified by column chromatography, eluting with DCM/MeOH (9:1) to obtain the alcoholic compound. To the solution of the alcoholic compound (0.62 g, 1.47 mmol) in (1:1 water, ACN), TEMPO (23 mg, 0.147 mmol) and BIAB (0.52 g, 1.61 mmol) were added at RT, stirred for 2 h, after completion of reaction, acetonitrile was evaporated, *aq.* sodium carbonate was added to the reaction mixture and washed with diethyl ether (2x5 mL) in order to remove byproducts. Then the water layer was neutralized with *aq. sat.* KHSO_4 solution and extracted with ethyl acetate and dried over anhydrous Na_2SO_4 . The solvent was removed under reduced pressure to afford the difluoro PNA monomer **6**. (Yield 0.38 g, 60%). ^1H -NMR (400 MHz, DMSO-d_6) δ : 1.38 (maj) 1.40 (min) (s, 9H), 1.75 (s, 3H), 3.47-3.55 (m, 2H), 3.77-3.96 (m, 2H), 4.01 (maj) 4.29 (min) (s, 2H), 4.56 (maj) 4.63 (min) (s, 2H), 7.08 (t, 1H, $J = 8$ Hz), 7.33-7.40 (m, 1H), 11.31 (bs, 1H); ^{19}F -NMR (376.6 MHz, DMSO-d_6 , C_6F_6 as internal reference) δ : -106.70 (min) -107.31 (maj) (s); ^{13}C -NMR (100

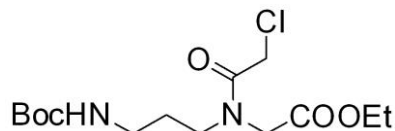
MHz, DMSO-d₆) δ : -12.4, 28.6, 43.0, 48.4, 49.8, 50.2, 78.9, 108.6, 119.6, 122.3, 124.5, 142.5, 151.4, 156.1, 164.9, 168.8, 169.5, 170.2, 170.7; HRMS (ESI-TOF) m/z Calcd for C₁₇H₂₄F₂N₄NaO₇ [M + Na]⁺ 457.1511, found 457.1509.

Synthesis of tert-butyl (3-aminopropyl)carbamate (40)

To a solution of excess propylene 1,3-diamine (10 g, 135 mmol) in dichloromethane (250 mL), Boc-anhydride (15 mL previously dissolved in 50 ml DCM, 135 mmol) was added at 0 °C drop wise and stirred at RT for 12 h. After completion of reaction, water was added and extracted with dichloromethane (3 x 50 mL). The organic layer was washed with *aq.* NaHCO₃ solution and dried over anhydrous Na₂SO₄. The organic solvent was removed under reduced pressure to obtain the crude compound **40**.

Synthesis of ethyl 2-((3-((tert-butoxycarbonyl)amino)propyl)amino)acetate (41)

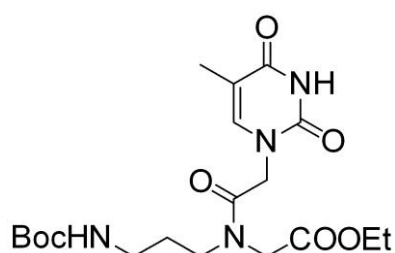
To a solution of compound **40** (15 g, 86.20 mmol) in acetonitrile (50 mL), triethylamine (23.3 mL, 86.20 mmol) and ethyl bromoacetate (9.59 mL previously dissolved in 20 mL ACN, 86.20 mmol) were added at 0 °C drop wise and stirring was continued at RT for 12 h. The reaction was monitored by TLC, after completion of the reaction, acetonitrile was evaporated on rota and then water was added and extracted with ethyl acetate (3 x 50 mL). The organic layer was washed with brine solution and then dried over anhydrous Na₂SO₄. The solvent was removed under reduced pressure to obtain the product **41** and the product was used for further reaction without purification.

Ethyl 2-(N-(3-((tert-butoxycarbonyl)amino)propyl)-2-chloroacetamido)acetate (42)

To a solution of the compound **41** (20 g, 76.92 mmol) in water, Dioxane (1:1, 50mL), sodium bicarbonate (14.2 g, 169.2 mmol) was added at RT. After 5 min stirring chloroacetylchloride (6.8 mL, 84.61 mmol) was added at 0 °C drop wise, and stirring was continued for 5 h, after completion of reaction, water was added and product was extracted with ethyl acetate (3 x 50 mL). The organic layer was dried over anhydrous Na₂SO₄. The solvent was removed in vacuo

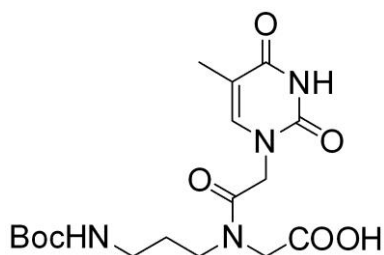
and product was purified by column chromatography, eluting with petroleum ether/ EtOAc (1:1) to obtain the compound **42**. (Yield 20.16 g, 78%). $^1\text{H-NMR}$ (400 MHz, CDCl_3) δ : 1.21-1.27 (m, 3H) 1.38 (maj) 1.39 (min) (s, 9H), 1.59-1.83(m, 2H), 3.03-3.14 (m, 2H), 3.42 (q, 2H, $J = 8$ Hz), 4.00 (maj) 4.01 (min) (s, 2H), 4.09-4.22 (m, 4H), 4.91 (bs, 1H); $^{13}\text{C-NMR}$ (100 MHz, CDCl_3) δ : 14.1, 28.4, 29.1, 37.0, 37.9, 40.8, 41.1, 45.3, 47.2, 48.0, 49.9, 53.5, 61.4, 62.1, 76.8, 77.1, 77.5, 79.0, 79.5; HRMS (ESI-TOF) m/z Calcd for $\text{C}_{14}\text{H}_{25}\text{ClKN}_2\text{O}_5$ [$\text{M} + \text{K}$] $^+$ 375.1089, found 375.1090.

Synthesis of ethyl-2-(N-(3-((tert-butoxycarbonyl)amino)propyl)-2-(5-methyl-2,4-dioxo-3,4-dihydropyrimidin-1(2H)-yl)acetamido)acetate (43)



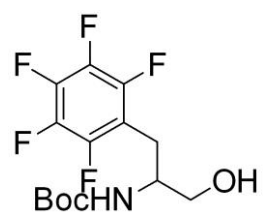
To a solution of the compound **42** (10 g, 29.76 mmol) in DMF (20 ml), K_2CO_3 (4.1 g, 29.76 mmol) and thymine (3.75 g, 29.76 mmol) were added at RT and stirring was continued at same temperature for 12 h. After completion of reaction, *aq.* KHSO_4 was added and extracted with ethyl acetate (3 x 25 mL). The organic layer was dried over anhydrous Na_2SO_4 . The solvent was removed under reduced pressure and the product was purified by column chromatography, eluting with petroleum ether/ EtOAc (1:1) to obtain the compound **43**. (Yield 9.5 g, 75%). $^1\text{H-NMR}$ (400 MHz, CDCl_3) δ : 1.2-1.27 (m, 3H), 1.37 (s, 9H), 1.84(s, 3H), 2.82-3.41 (m, 8H), 4.0-4.57 (m, 4H), 5.25 (bs, 1H), 7.04 (s, 1H), 9.92 (bs, 1H); $^{13}\text{C-NMR}$ (100 MHz, CDCl_3) δ : 12.4, 14.1, 28.4, 31.5, 36.5, 46.1, 47.6, 47.9, 48.0, 49.5, 61.4, 62.2, 79.0, 110.6, 141.4, 151.5, 156.5, 162.7, 164.6, 167.1, 168.9, 169.3; HRMS (ESI-TOF) m/z Calcd for $\text{C}_{19}\text{H}_{30}\text{N}_4\text{NaO}_7$ [$\text{M} + \text{Na}$] $^+$ 449.2012, found 449.2003.

Synthesis of 2-(N-(3-((tert-butoxycarbonyl)amino)propyl)-2-(5-methyl-2,4-dioxo-3,4-dihydropyrimidin-1(2H)-yl)acetamido)acetic acid (7)



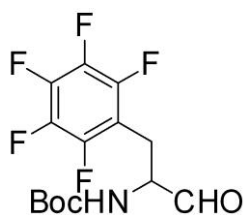
The ester compound **43** (9.0 g, 21.12 mmol) in THF was saponified with 10% LiOH at 0 °C for 3 h. After completion of reaction, the mixture was acidified with *sat. aq.* KHSO₄ solution and then the acid compound was extracted with ethyl acetate, dried over Na₂SO₄ and evaporated under reduced pressure to obtain the desired monomer **7** in good yields. (Yield 6.20 g, 77%). ¹H-NMR (400 MHz, DMSO-d₆) δ: 1.36 (min) 1.37 (maj) (s, 9H), 1.74 (s, 3H), 1.49-1.72 (m, 2H) 2.86-3.01 (m, 2H), 3.23-3.35 (m, 2H), 3.95 (maj) 4.18 (min) (s, 2H), 4.45(min) 4.60 (maj) (s, 2H), 6.82 (bs, 1H), 7.30 (min) 7.39 (maj) (s, 1H); ¹³C-NMR (100 MHz, DMSO-d₆) δ: 12.4, 27.8, 28.7, 37.7, 45.7, 47.8, 48.2, 78.0, 108.4, 142.7, 151.4, 156.0, 164.9, 167.3, 167.8, 170.8, 171.3; HRMS (ESI-TOF) *m/z* Calcd for C₁₇H₂₇N₄O₇ [M + H]⁺ 399.1880, found 399.1873.

Synthesis of tert-butyl (1-hydroxy-3-(perfluorophenyl)propan-2-yl)carbamate (**47a**)



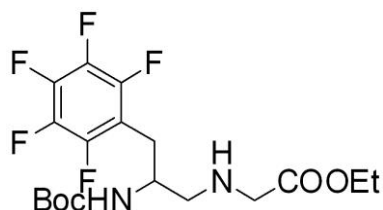
To the solution of ester compound **46a** (1.3 g, 3.39 mmol) in ethanol (8 mL), sodiumborohydride (513 mg, 13.57 mmol) was added at ice cold condition and stirred at RT for 3 h. After completion of reaction, ethanol was evaporated and product was extracted with ethylacetate and the organic layer was concentrated and purified by column chromatography, eluted with 30% EtOAc: pet-ether to obtain compound **47a**. Yield (1.1 g, 95%); ¹H-NMR (400 MHz, CDCl₃) δ: 1.37 (s, 9H), 2.95 (d, 2H, J = 8 Hz), 3.67-3.78 (m, 2H), 3.91 (bm, 1H), 4.87 (bs, 1H); ¹⁹F-NMR (376.6 MHz, CDCl₃, C₆F₆ as internal reference) δ: -144.19 (d), -157.80 (t), -163.73 (t); ¹³C-NMR (100 MHz, CDCl₃) δ: 24.9, 28.2, 51.9, 64.7, 80.0, 111.7, 138.7, 144.2, 146.7, 155.6; HRMS (ESI-TOF) *m/z* Calcd for C₉H₉F₅NO [M-Boc + H]⁺ 242.0604, found 242.0609.

Synthesis of tert-butyl (1-oxo-3-(perfluorophenyl)propan-2-yl)carbamate (**48a**)



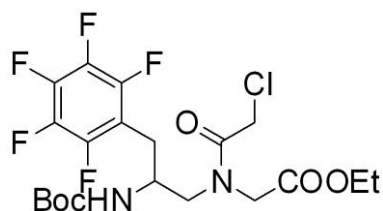
To the solution of compound **47a** (1.1 g, 3.22 mmol) in acetonitrile, TEMPO (100 mg, 0.644 mmol) and BIAB (1.036 g, 3.22 mmol) were added at RT and stirred for half an hour and the reaction mixture was concentrated and the oxidized product aldehyde **48a** and was used for next reaction without any further purification.

Synthesis of ethyl 2-((2-((tert-butoxycarbonyl)amino)-3-(perfluorophenyl)propyl)amino)acetate (49a**)**



To the solution of the aldehyde **48a** (1.05 g, 3.09 mmol) and glycine ethylester hydrochloride (1.55 g, 12.36 mmol) in ethanol, DIPEA (2.2 mL, 12.36 mmol) was added at ice cold condition and stirred for 5-10 min, and then sodiumcyanoborohydride (791 mg, 12.36 mmol) was added in small portions at the same temperature and stirred at RT for 4 h. After completion of reaction (monitored by TLC), ethanol was evaporated and the product was extracted with ethylacetate. The organic layer was concentrated and subjected for column chromatography and the product **49a** was eluted with 35% EtOAc: pet-ether. Yield (900 mg, 68%); $^1\text{H-NMR}$ (400 MHz, CDCl_3) δ : 1.26 (t, 3H, $J = 8$ Hz), 1.34 (s, 9H), 2.52 (bs, 1H), 2.69-2.94 (m, 4H), 3.41 (dd, 2H, $J = 20$ Hz), 3.90 (, 1H), 4.18 (q, 2H, $J = 8$ Hz), 4.99 (bs, 1H); $^{19}\text{F-NMR}$ (376.6 MHz, CDCl_3 , C_6F_6 as internal reference) δ : -143.94 (s), -157.95 (s), 163.82 (s); $^{13}\text{C-NMR}$ (100 MHz, CDCl_3) δ : 14.1, 26.5, 28.1, 50.1, 50.8, 52.2, 60.9, 79.5, 111.8, 155.4, 136.1, 138.6, 141.5, 144.3, 146.7, 155.5, 172.3; HRMS (ESI-TOF) m/z Calcd for $\text{C}_{18}\text{H}_{24}\text{F}_5\text{N}_2\text{O}_4$ $[\text{M} + \text{H}]^+$ 427.1656, found 427.1657.

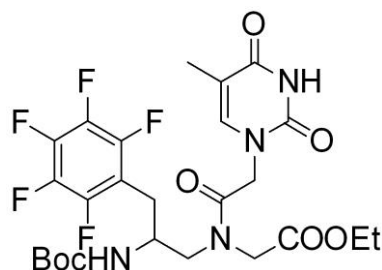
Synthesis of ethyl 2-(N-(2-((tert-butoxycarbonyl)amino)-3-(perfluorophenyl)propyl)-2-chloroacetamido)acetate (50a**)**



To the solution of secondary-amine compound **49a** (900 mg, 2.11 mmol) in acetonitrile (5 mL), triethylamine (0.42 mL, 3.165 mmol) and chloroacetylchloride (0.2 mL, 2.11 mmol)

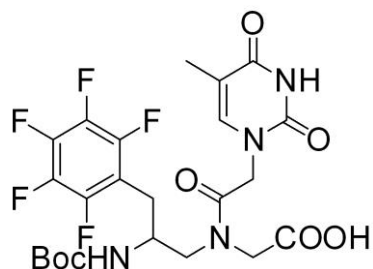
were added at ice cold condition and stirred at same temperature for 1h, after completion of reaction, acetonitrile was evaporated and the product was extracted with ethyl acetate. The organic layer was concentrated and purified with EtOAc: petroleum ether (1:4) to obtain compound **50a**. Yield (950 mg, 89%); $^1\text{H-NMR}$ (400 MHz, CDCl_3) δ : 1.24-1.32 (m, 3H), 1.33 (maj) 1.36 (min) (s, 9H), 2.82-2.95 (m, 2H), 3.34-3.92 (m, 2H), 4.03-4.28 (m, 7H), 4.85-4.98 (bs, 1H); $^{19}\text{F-NMR}$ (376.6 MHz, CDCl_3 , C_6F_6 as internal reference) δ : -142.74, -156.20, -162.17; $^{13}\text{C-NMR}$ (100 MHz, CDCl_3) δ : 14.1, 26.1, 28.1, 40.9, 49.3, 50.0, 50.3, 62.2, 79.8, 136.3, 141.3, 144.2, 146.8, 155.6, 168.4, 168.7; MALDI-TOF m/z : Calcd for $\text{C}_{20}\text{H}_{24}\text{ClF}_5\text{KN}_2\text{O}_5$ $[\text{M} + \text{K}]^+$ 541.0931, found 541.1498.

Synthesis of ethyl-2-(N-(2-((tert-butoxycarbonyl)amino)-3-(perfluorophenyl)propyl)-2-(5-methyl-2,4-dioxo-3,4-dihydropyrimidin-1(2H)-yl)acetamido)acetate (51a)



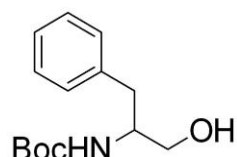
To the solution of chloro compound **50a** (950 mg, 1.89 mmol) in dimethylformamide DMF (2 mL), thymine (240 mg, 1.89 mmol) and K_2CO_3 (260 mg, 1.89 mmol) were added at RT and stirred at the same temperature for 12 h. After completion of reaction (monitored by TLC), water was added to the reaction mixture and the product was extracted with ethyl acetate, and the organic layer was concentrated and subjected for column chromatography, eluted with 100% EtOAc to obtain compound **51a**. Yield (850 mg, 76%); $^1\text{H-NMR}$ (400 MHz, CDCl_3) δ : 1.17 (t, 3H, $J = 8$ Hz), 1.24 (maj) 1.25 (min) (s, 9H), 1.74 (s, 3H), 2.60-3.01 (m, 2H), 3.45-3.87 (m, 2H), 3.97- 4.19 (m, 2H), (m, 2H), 4.36-4.82 (m, 3H), 6.88-6.99 (m, 1H), 7.28 (bs, 1H); $^{19}\text{F-NMR}$ (376.6 MHz, CDCl_3 , C_6F_6 as internal reference) δ : -142.62, -158.74, -164.3; $^{13}\text{C-NMR}$ (100 MHz, CDCl_3) δ : 12.3, 14.4, 28.3, 48.3, 49.3, 50.0, 50.5, 50.8, 60.9, 61.6, 78.3, 78.7, 108.7, 135.8, 138.5, 142.4, 144.4, 146.8, 151.4, 155.5, 155.7, 164.9, 168.2, 168.7, 169.0, 169.6; HRMS (ESI-TOF) m/z . Calcd for $\text{C}_{20}\text{H}_{22}\text{F}_5\text{N}_4\text{O}_5$ $[\text{M-Boc} + \text{H}]^+$ 493.1510, found 493.1516.

Synthesis of 2-(N-(2-((tert-butoxycarbonyl)amino)-3-(perfluorophenyl)propyl)-2-(5-methyl-2,4-dioxo-3,4-dihydropyrimidin-1(2H)-yl)acetamido)acetic acid (8)



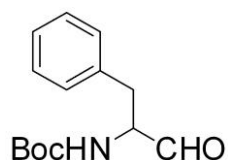
The ester compound **51a** (850 mg, 1.43 mmol) in THF was saponified with 10% LiOH at 0 °C for 3 h. After completion of reaction, the mixture was acidified with *sat. aq.* KHSO₄ solution and then the acid compound was extracted with ethyl acetate, dried over Na₂SO₄ and evaporated under reduced pressure to obtain the desired monomer **8** in good yields. (Yield 600 mg, 71%); ¹H-NMR (400 MHz, CDCl₃) δ: 1.24 (maj) 1.26 (min) (s, 9H), 1.75 (s, 3H), 2.61-2.87 (m, 2H), 2.97-3.05 (m, 1H), 3.37-3.63 (m, 2H), 3.76-3.90 (m, 2H), 3.94-4.82 (m, 4H), 6.89-7.0 (m, 1H), 7.29 (s, 1H), 11.30 (d, 1H); ¹⁹F-NMR (376.6 MHz, CDCl₃, C₆F₆ as internal reference) δ: -163.4, -158.1, -142.2; ¹³C-NMR (100 MHz, CDCl₃) δ: 12.4, 28.3, 48.0, 48.3, 49.2, 50.0, 50.3, 50.8, 78.3, 78.7, 108.6, 142.5, 151.5, 155.6, 155.7, 164.9, 168.1, 168.7, 170.6, 171.1; HRMS (ESI-TOF) *m/z* Calcd for [M + Na]⁺ 587.1541, found 587.1528 and Calcd for C₁₈H₁₈F₅N₄O₅ [M-Boc + H] 465.1197, found 465.1192.

Synthesis of tert-butyl (1-hydroxy-3-phenylpropan-2-yl)carbamate (**47b**)



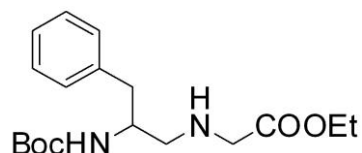
To the solution of compound **46b** (2.2 g, 7.5 mmol) in ethanol (15 mL), sodiumborohydride (1.14 g, 30 mmol) was added at ice cold condition and stirred at RT for 3 h. After completion of reaction ethanol was evaporated and product was extracted with ethylacetate and the organic layer was concentrated and purified by column chromatography, eluted with 30% EtOAc: petroleum ether to obtain compound **47b**. Yield (1.6 g, 85%); ¹H-NMR (400 MHz, CDCl₃) δ: 1.42 (s, 9H), 2.85 (d, 2H, J = 8 Hz), 3.55-3.69 (m, 2H), 3.88 (m, 1H), 4.80 (bs, 1H), 7.21- 7.33 (m, 5H); ¹³C-NMR (100 MHz, CDCl₃) δ: 28.4, 37.5, 53.7, 64.4, 79.7, 126.6, 128.6, 129.3, 137.8, 156.2.

Synthesis of tert-butyl (1-oxo-3-phenylpropan-2-yl)carbamate (**48b**)



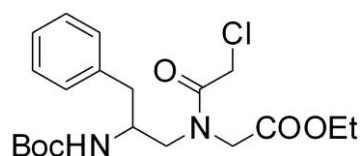
To the solution of compound **47b** (1.6 g, 6.425 mmol) in dry acetonitrile, TEMPO (200 mg, 1.285 mmol) and BIAB (2.68 g, 6.425 mmol) were added at RT and stirred for half an hour and the reaction mixture was concentrated and the product aldehyde **48b** was used for further reaction without any purification.

Synthesis of ethyl 2-((2-((tert-butoxycarbonyl)amino)-3-phenylpropyl)amino)acetate (**49b**)



To the solution of the aldehyde **48b** in ethanol, glycine ethylester hydrochloride (3.22 g, 25.70 mmol) was added and then neutralized with DIPEA (4.4 mL, 25.07 mmol) at ice cold condition and stirred for 5-10 min, and then sodiumcyanoborohydride (1.64 g, 25.70 mmol) was added pinch wise at the same temperature and stirred for 4 h. After completion of reaction (monitored by TLC), ethanol was evaporated and the product was extracted with ethylacetate. The organic layer was concentrated and subjected for column chromatography, and the product was eluted with 35% EtOAc: pet-ether to obtain compound **49b**. Yield (1.5 g, 69%); $^1\text{H-NMR}$ (400 MHz, CDCl_3) δ : 1.24 (t, 3H, $J = 8$ Hz), 1.40 (s, 9H), 2.62(d, 2H, $J = 4$ Hz), 2.72-2.84 (m, 2H), 3.29-3.43 (m, 2H, $J = 16$ Hz), 3.88 (bs, 1H), 4.15 (q, 2H, $J = 8$ Hz), 4.94 (bs, 1H), 7.2 (d, 1H), 7.15-7.25 (m, 5H); $^{13}\text{C-NMR}$ (CDCl_3 , 100 MHz) δ : 14.2, 28.4, 39.1, 50.8, 51.5, 60.8, 79.2, 126.4, 128.4, 129.4, 138.0, 155.7, 172.4; HRMS (ESI-TOF) m/z Calcd for $\text{C}_{18}\text{H}_{29}\text{N}_2\text{O}_4$ $[\text{M} + \text{H}]^+$ 337.2127, found 337.2127.

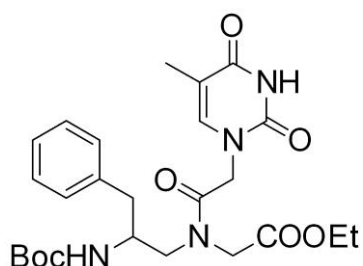
Synthesis of ethyl 2-(N-(2-((tert-butoxycarbonyl)amino)-3-phenylpropyl)-2-chloroacetamido)acetate (**50b**)



To the solution of amine compound **49b** (750 mg, 2.232 mmol) in acetonitrile, triethylamine (0.45 mL, 3.348 mmol) and chloroacetylchloride (1.8 mL, 2.232 mmol) were added at ice

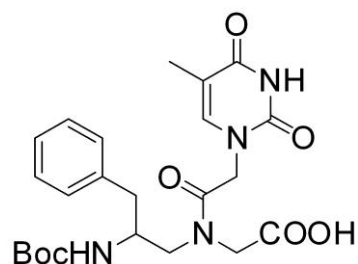
cold condition and stirred at same temperature for 1h. After completion of reaction, acetonitrile was evaporated and the product was extracted with ethyl acetate. The organic layer was concentrated and purified with 25% EtOAc: pet-ether to obtain compound **50b**. Yield (850 mg, 92%); $^1\text{H-NMR}$ (400 MHz, CDCl_3) δ : 1.26 (t, 3H, $J = 8$ Hz) ; 1.37 (min) 1.38 (maj) (s, 9H), 2.75-2.90 (m, 2H), 3.21-3.64 (comp., 2H), 3.91-4.00 (m, 2H), 4.06-4.12 (m, 1H), 4.18 (q, 2H, $J = 8$ Hz), 4.82 (bs, 1H), 7.18-7.33 (m, 5H); $^{13}\text{C-NMR}$ (100 MHz, CDCl_3) δ : 14.2, 28.3, 40.7, 41.1, 53.5, 60.4, 61.4, 62.0, 79.4, 126.6, 126.9, 128.5, 128.8, 129.0, 129.2, 129.4, 137.5, 155.8, 168.9, 171.3; HRMS (ESI-TOF) m/z Calcd for $\text{C}_{20}\text{H}_{29}\text{ClN}_2\text{NaO}_5$ [$\text{M} + \text{Na}$] $^+$ 435.1663, found 435.1666.

Synthesis of ethyl 2-(N-(2-((tert-butoxycarbonyl)amino)-3-phenylpropyl)-2-(5-methyl-2,4-dioxo-3,4-dihydropyrimidin-1(2H)-yl)acetamido)acetate (51b)



To the solution of chloro compound **50b** (800 mg, 1.94 mmol) in dimethylformamide DMF, thymine (245 mg, 1.94 mmol) and K_2CO_3 (268 mg, 1.94 mmol) were added at RT and stirred at the same temperature for 12 h. After completion of reaction (monitored by TLC), water was added to the reaction mixture and the product was extracted with ethyl acetate, and the organic layer was concentrated and subjected for column chromatography, eluted the product **51b** with 100% EtOAc. Yield (550 mg, 57%); $^1\text{H-NMR}$ (400 MHz, CDCl_3) δ : 1.23-1.31 (m, 3H), 1.36 (maj) 1.39 (min) (s, 9H), 1.89 (min) 1.92 (maj) (s, 3H), 2.81-2.91 (m, 2H), 3.38-3.68 (m, 2H), 3.93-4.02 (m, 2H), 4.14-4.17 (m, 2H), 4.19-4.26 (m, 2H), 4.34-4.46 (m, 1H), 5.30 (bs, 1H), 7.02 (s, 1H), 7.16-7.33 (m, 5H), 9.27 (s, 1H); $^{13}\text{C-NMR}$ (100 MHz, CDCl_3) δ : 12.4, 14.1, 28.3, 38.7, 47.6, 48.9, 49.9, 50.6, 51.1, 51.7, 61.5, 62.2, 79.5, 110.7, 126.6, 126.9, 128.6, 128.8, 129.1, 129.2, 137.2, 137.4, 140.9, 141.2, 151.0, 155.7, 164.3, 167.5, 168.3, 169.1; HRMS (ESI-TOF) m/z Calcd for $\text{C}_{25}\text{H}_{34}\text{N}_4\text{NaO}_7$ [$\text{M} + \text{Na}$] $^+$ 525.2325, found 525.2327.

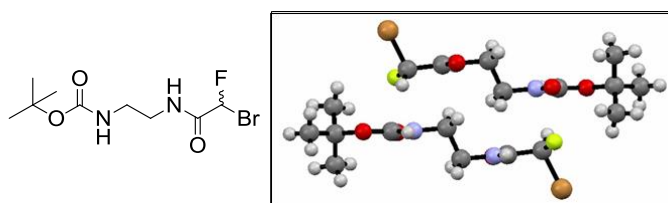
Synthesis of 2-(N-(2-((tert-butoxycarbonyl)amino)-3-phenylpropyl)-2-(5-methyl-2,4-dioxo-3,4-dihydropyrimidin-1(2H)-yl)acetamido)acetic acid (9)



The ester compound **51b** (500 mg, 0.996 mmol) in THF was saponified with 10% LiOH at 0 °C for 3 h. After completion of reaction (monitored by TLC), the mixture was acidified with sat. aq. KHSO₄ solution and then the acid compound was extracted with ethyl acetate, dried over Na₂SO₄ and evaporated under reduced pressure to obtain the desired monomer **9** in good yields. Yield (350 mg, 74%); ¹H-NMR (400 MHz, DMSO-d₆) δ: 1.22 (min) 1.28 (maj) (s, 9H), 1.75 (s, 3H), 2.55-2.87 (m, 2H), 3.31-3.44 (m, 2H), 3.62-4.22 (comp., 5H), 4.44-4.75 (m, 2H), 6.75-6.93 (m, 1H), 7.19- 7.26 (m, 5H), 11.31 (bs, 1H); ¹³C-NMR (100 MHz, DMSO-d₆) δ: 12.4, 28.7, 31.7, 37.7, 48.3, 50.7, 51.8, 78.1, 78.4, 108.6, 126.5, 128.5, 128.6, 129.6, 139.2, 142.3, 151.5, 164.9, 167.8, 168.3, 170.9, 171.3; HRMS (ESI-TOF) *m/z* Calcd for C₂₃H₃₀N₄NaO₇ [M + Na]⁺ 497.2012, found 497.2013.

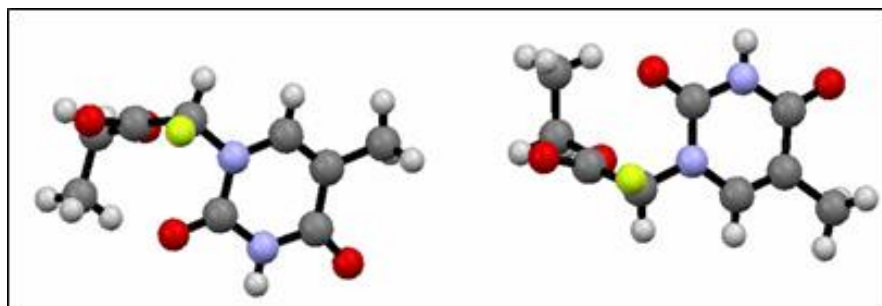
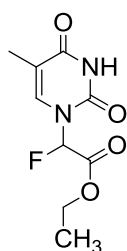
Crystal structure and data of some intermediate compounds:

Compound 13



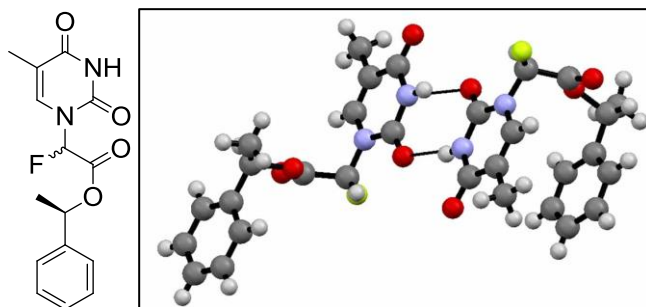
Identification code	es_bocnhester	
Empirical formula	C ₉ H ₁₇ Br F N ₂ O ₃	
Formula weight	300.16	
Temperature	296(2) K	
Wavelength	0.71073 Å	
Crystal system	Triclinic	
Space group	p-1	
Unit cell dimensions	a = 5.0958(18) Å	α = 105.565(7)°.
	b = 9.818(3) Å	β = 95.493(7)°.
	c = 13.453(5) Å	γ = 91.34(2)°.
Volume	644.6(4) Å ³	
Z	2	
Density (calculated)	1.547 Mg/m ³	
Absorption coefficient	3.197 mm ⁻¹	
F(000)	306	
Crystal size	0.5 x 0.4 x 0.25 mm ³	
Theta range for data collection	1.58 to 28.92°.	
Index ranges	-3<=h<=6, -11<=k<=10, -17<=l<=18	
Reflections collected	2102	
Independent reflections	1918 [R(int) = 0.0208]	
Completeness to theta = 25.00°	99 %	
Absorption correction	Semi-empirical from equivalents	
Max. and min. transmission	0.450 and 0.235	
Refinement method	Full-matrix least-squares on F ²	
Data / restraints / parameters	1918 / 0 / 148	
Goodness-of-fit on F ²	0.938	
Final R indices [I>2sigma(I)]	R1 = 0.0610, wR2 = 0.1433	
R indices (all data)	R1 = 0.1086, wR2 = 0.1776	
Largest diff. peak and hole	0.649 and -0.525 e.Å ⁻³	

Compound 20a

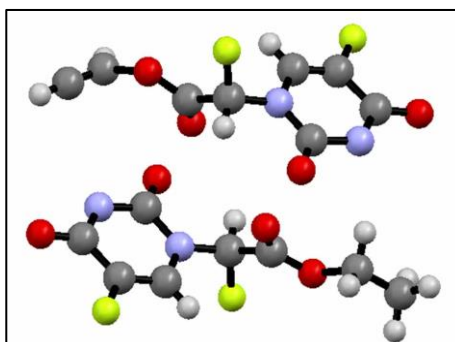
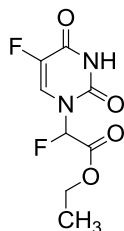


Identification code	a	
Empirical formula	C ₉ H _{11.50} F N ₂ O ₄	
Formula weight	230.70	
Temperature	296(2) K	
Wavelength	0.71073 Å	
Crystal system	'Monoclinic'	
Space group	'P2(1)/n '	
Unit cell dimensions	a = 13.527(2) Å	α = 90°.
	b = 11.7083(16) Å	β = 104.702(3)°.
	c = 14.304(2) Å	γ = 90°.
Volume	2191.4(5) Å ³	
Z	8	
Density (calculated)	1.399 Mg/m ³	
Absorption coefficient	0.121 mm ⁻¹	
F(000)	964	
Crystal size	? x ? x ? mm ³	
Theta range for data collection	1.85 to 30.43°.	
Index ranges	-19 ≤ h ≤ 18, -16 ≤ k ≤ 11, -19 ≤ l ≤ 20	
Reflections collected	22950	
Independent reflections	6506 [R(int) = 0.0373]	
Completeness to theta = 30.43°	97.8 %	
Refinement method	Full-matrix least-squares on F ²	
Data / restraints / parameters	6506 / 0 / 293	
Goodness-of-fit on F ²	1.413	
Final R indices [I > 2σ(I)]	R1 = 0.1088, wR2 = 0.3393	
R indices (all data)	R1 = 0.1591, wR2 = 0.3763	
Largest diff. peak and hole	1.417 and -0.600 e.Å ⁻³	

Compound 24

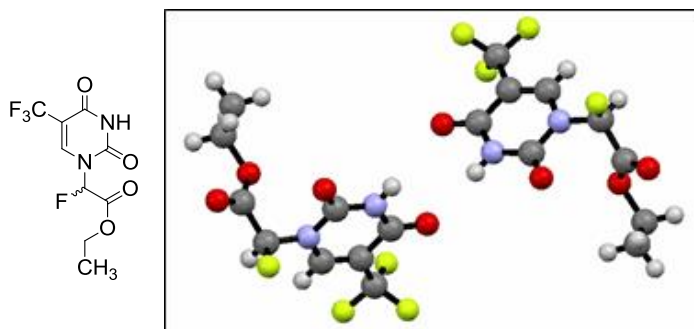


Identification code	trail	
Empirical formula	C ₁₅ H ₁₅ F N ₂ O ₄	
Formula weight	306.79	
Temperature	273(2) K	
Wavelength	0.71073 Å	
Crystal system	Monoclinic	
Space group	P2(1)	
Unit cell dimensions	a = 7.514(5) Å	α = 90°.
	b = 23.183(15) Å	β = 98.615(10)°.
	c = 8.242(5) Å	γ = 90°.
Volume	1419.5(16) Å ³	
Z	4	
Density (calculated)	1.436 Mg/m ³	
Absorption coefficient	0.114 mm ⁻¹	
F(000)	642	
Crystal size	1.85 x 1.30 x 0.80 mm ³	
Theta range for data collection	1.76 to 29.43°.	
Index ranges	-10 ≤ h ≤ 8, -30 ≤ k ≤ 31, -11 ≤ l ≤ 10	
Reflections collected	15456	
Independent reflections	7609 [R(int) = 0.0433]	
Completeness to theta = 29.43°	99.7 %	
Refinement method	Full-matrix least-squares on F ²	
Data / restraints / parameters	7609 / 1 / 401	
Goodness-of-fit on F ²	0.840	
Final R indices [I > 2σ(I)]	R1 = 0.0447, wR2 = 0.1125	
R indices (all data)	R1 = 0.0614, wR2 = 0.1282	
Absolute structure parameter	1.1(6)	
Largest diff. peak and hole	0.202 and -0.198 e.Å ⁻³	

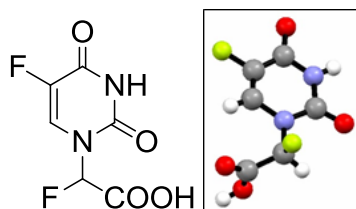
Compound **20b**

Identification code	es1	
Empirical formula	C ₈ H ₈ F ₂ N ₂ O ₄	
Formula weight	234.16	
Temperature	296(2) K	
Wavelength	0.71073 Å	
Crystal system	P-1	
Space group	TRICLINIC	
Unit cell dimensions	a = 5.0538(17) Å	α = 88.176(7)°.
	b = 8.982(3) Å	β = 83.300(7)°.
	c = 10.635(3) Å	γ = 78.463(7)°.
Volume	469.8(3) Å ³	
Z	2	
Density (calculated)	1.655 Mg/m ³	
Absorption coefficient	0.157 mm ⁻¹	
F(000)	240	
Crystal size	0.2 x 0.12 x 0.5 mm ³	
Theta range for data collection	1.93 to 27.95°.	
Index ranges	-6 ≤ h ≤ 4, -11 ≤ k ≤ 10, -13 ≤ l ≤ 11	
Reflections collected	4359	
Independent reflections	2145 [R(int) = 0.0172]	
Completeness to theta = 27.95°	95.0 %	
Refinement method	Full-matrix least-squares on F ²	
Data / restraints / parameters	2145 / 0 / 146	
Goodness-of-fit on F ²	1.009	
Final R indices [I > 2σ(I)]	R1 = 0.0597, wR2 = 0.1610	
R indices (all data)	R1 = 0.0983, wR2 = 0.1868	
Largest diff. peak and hole	0.412 and -0.452 e.Å ⁻³	

Compound 20c

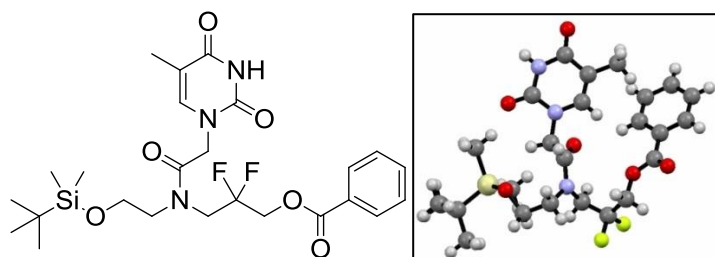


Identification code	mo_es_401_0m	
Empirical formula	C ₉ H ₈ F ₄ N ₂ O ₄	
Formula weight	284.17	
Temperature	296(2) K	
Wavelength	0.71073 Å	
Crystal system	'Monoclinic'	
Space group	P2 ₁ /n	
Unit cell dimensions	a = 13.754(3) Å	α = 90°.
	b = 5.4127(12) Å	β = 93.349(5)°.
	c = 15.330(4) Å	γ = 90°.
Volume	1139.4(5) Å ³	
Z	4	
Density (calculated)	1.657 Mg/m ³	
Absorption coefficient	0.170 mm ⁻¹	
F(000)	576	
Crystal size	0.4 x 0.4 x 0.2 mm ³	
Theta range for data collection	1.93 to 27.05°.	
Index ranges	-17 ≤ h ≤ 16, -6 ≤ k ≤ 6, -15 ≤ l ≤ 19	
Reflections collected	9623	
Independent reflections	2470 [R(int) = 0.0316]	
Completeness to theta = 27.05°	99.3 %	
Refinement method	Full-matrix least-squares on F ²	
Data / restraints / parameters	2470 / 0 / 173	
Goodness-of-fit on F ²	1.052	
Final R indices [I > 2σ(I)]	R1 = 0.0539, wR2 = 0.1339	
R indices (all data)	R1 = 0.0726, wR2 = 0.1452	
Largest diff. peak and hole	0.961 and -0.454 e.Å ⁻³	

Compound **21b**

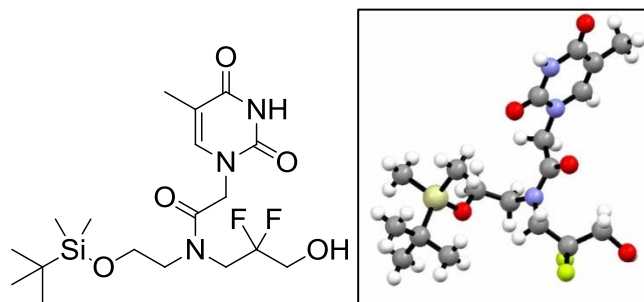
Identification code	moescooh0m	
Empirical formula	C ₂₄ H ₉ F ₉ N ₁₁ O ₁₆	
Formula weight	870.36	
Temperature	273(2) K	
Wavelength	0.71073 Å	
Crystal system	Triclinic	
Space group	P-1	
Unit cell dimensions	a = 5.361(15) Å	α = 90.25(11)°.
	b = 17.80(6) Å	β = 90.45(8)°.
	c = 18.97(6) Å	γ = 98.47(13)°.
Volume	1790(10) Å ³	
Z	2	
Density (calculated)	1.615 Mg/m ³	
Absorption coefficient	0.165 mm ⁻¹	
F(000)	862	
Crystal size	0.5 x 0.15 x 0.04 mm ³	
Theta range for data collection	1.07 to 21.67°.	
Index ranges	-5 ≤ h ≤ 5, -17 ≤ k ≤ 18, -19 ≤ l ≤ 19	
Reflections collected	14919	
Independent reflections	3892 [R(int) = 0.2373]	
Completeness to theta = 21.67°	92.3 %	
Refinement method	Full-matrix least-squares on F ²	
Data / restraints / parameters	3892 / 0 / 248	
Goodness-of-fit on F ²	1.005	
Final R indices [I > 2σ(I)]	R1 = 0.1174, wR2 = 0.2903	
R indices (all data)	R1 = 0.2598, wR2 = 0.3443	
Largest diff. peak and hole	2.230 and -0.463 e.Å ⁻³	

Crystal data of (N-(3-((tert-butyldimethylsilyl)oxy)-2,2-difluoropropyl)-2-(5-methyl-2,4-dioxo-3,4-dihydropyrimidin-1(2H)-yl)acetamido)methyl benzoate



Identification code	sats	
Empirical formula	C ₂₅ H ₃₅ Cl ₃ F ₂ N ₃ O ₆ Si	
Formula weight	646.00	
Temperature	296(2) K	
Wavelength	0.71073 Å	
Crystal system	'Triclinic'	
Space group	'P-1'	
Unit cell dimensions	a = 10.780(3) Å	α = 116.099(5)°
	b = 12.215(3) Å	β = 93.114(5)°
	c = 12.901(3) Å	γ = 91.139(6)°
Volume	1521.5(7) Å ³	
Z	2	
Density (calculated)	1.410 Mg/m ³	
Absorption coefficient	0.396 mm ⁻¹	
F(000)	674	
Crystal size	0.163 x 0.093 x 0.030 mm ³	
Theta range for data collection	1.76 to 28.49°	
Index ranges&	-11 ≤ h ≤ 14, -16 ≤ k ≤ 15, -17 ≤ l ≤ 17	
Reflections collected	27079	
Independent reflections	7605 [R(int) = 0.1496]	
Completeness to theta = 28.49°	98.6 %	
Refinement method	Full-matrix least-squares on F ²	
Data / restraints / parameters	7605 / 0 / 340	
Goodness-of-fit on F ²	1.794	
Final R indices [I > 2σ(I)]	R1 = 0.1423, wR2 = 0.4004	
R indices (all data)	R1 = 0.2526, wR2 = 0.4304	
Largest diff. peak and hole	4.974 and -0.518 e.Å ⁻³	

Crystal data of (N-(2,2-difluoro-3-hydroxypropyl)-2-(5-methyl-2,4-dioxo-3,4-dihydropyrimidin-1(2H)-yl)acetamido)methyl benzoate



Identification code	trail-7	
Empirical formula	C ₁₈ H ₂₉ F ₂ N ₃ O ₅ Si	
Formula weight	433.53	
Temperature	296(2) K	
Wavelength	0.71073 Å	
Crystal system	Monoclinic	
Space group	P2(1)/n	
Unit cell dimensions	a = 19.162(5) Å	α = 90°.
	b = 6.2376(15) Å	β = 96.803(6)°.
	c = 19.488(4) Å	γ = 90°.
Volume	2312.9(10) Å ³	
Z	4	
Density (calculated)	1.245 Mg/m ³	
Absorption coefficient	0.149 mm ⁻¹	
F(000)	920	
Crystal size	? x ? x ? mm ³	
Theta range for data collection	1.41 to 23.46°.	
Index ranges	-21 ≤ h ≤ 21, -6 ≤ k ≤ 6, -21 ≤ l ≤ 21	
Reflections collected	14412	
Independent reflections	3380 [R(int) = 0.0887]	
Completeness to theta = 23.46°	99.8 %	
Refinement method	Full-matrix least-squares on F ²	
Data / restraints / parameters	3380 / 0 / 270	
Goodness-of-fit on F ²	0.837	
Final R indices [I > 2σ(I)]	R1 = 0.0621, wR2 = 0.1617	
R indices (all data)	R1 = 0.1061, wR2 = 0.2035	
Extinction coefficient	0.022(3)	
Largest diff. peak and hole	0.809 and -0.407 e.Å ⁻³	

2.3 References

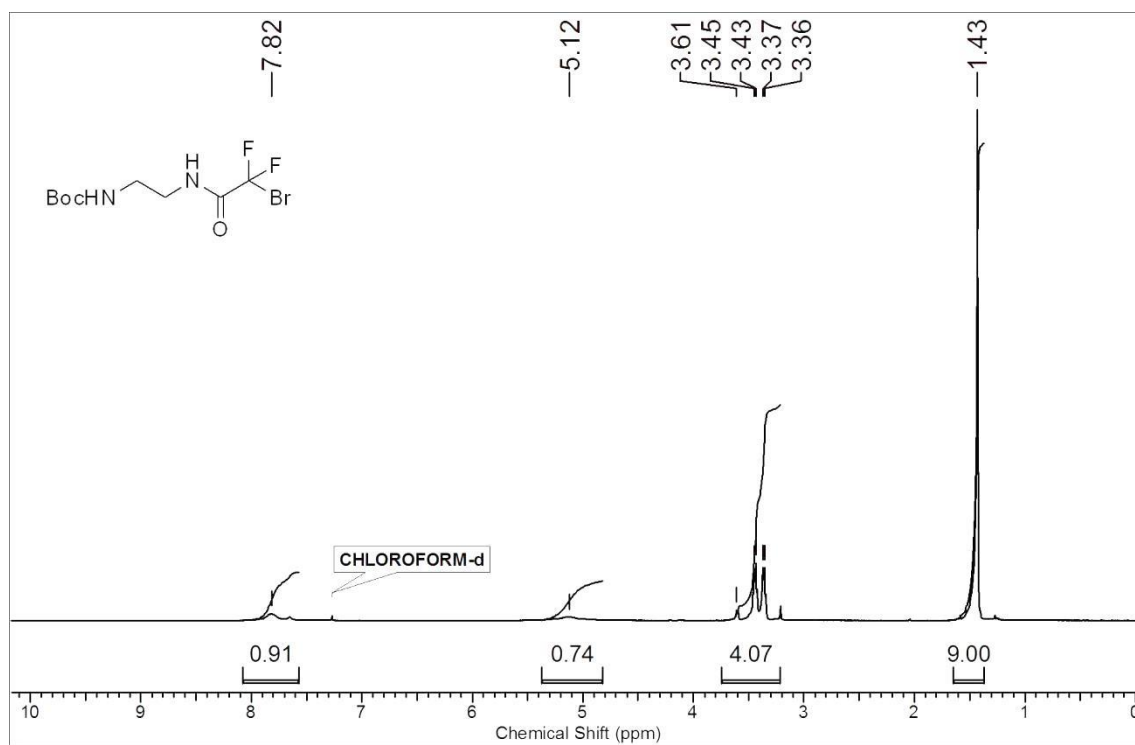
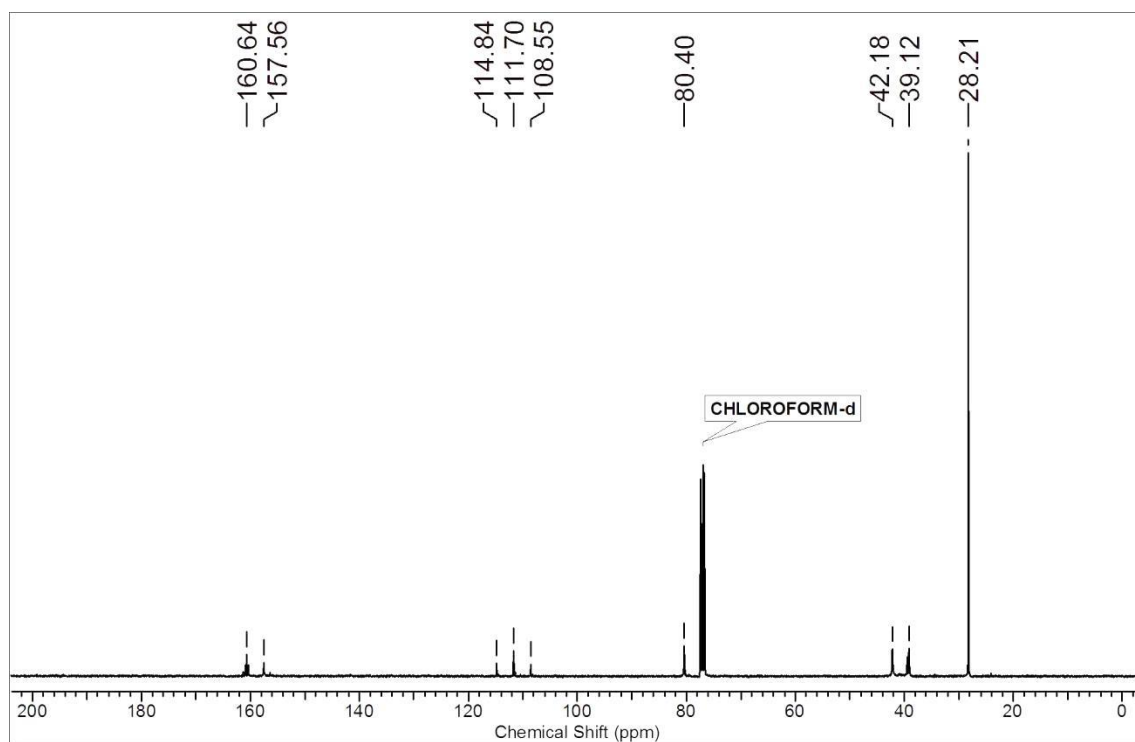
1. Purser, S.; Moore, P. R.; Swallow, S.; Gouverneur, V. *Chemical Society Reviews* **2008**, *37*, 320.
2. Bohm, H. J.; Banner, D.; Bendels, S.; Kansy, M.; Kuhn, B.; Muller, K.; Obst-Sander, U.; Stahl, M. *Chembiochem* **2004**, *5*, 637.
3. Muller, K.; Faeh, C.; Diederich, F. *Science* **2007**, *317*, 1881.
4. Heidelberger, C.; Chaudhuri, N. K.; Danneberg, P.; Mooren, D.; Griesbach, L.; Duschinsky, R.; Schnitzer, R. J. *Nature* **1957**, *179*, 663.
5. Van Niel, M. B.; Collins, I.; Beer, M. S.; Broughton, H. B.; Cheng, S. K. F.; Goodacre, S. C.; Heald, A.; Locker, K. L.; MacLeod, A. M.; Morrison, D.; Moyes, C. R.; O'ZConnor, D.; Pike, A.; Rowley, M.; Russel, M. G. N.; Sohal, B.; Stan-ton J. A.; Thomas, S.; Verrier, H.; Watt, A. P.; Castro, J. L. *J. Med. Chem.* **1999**, *42*, 2087-2104.
6. Park, B. K.; Kitteringham, N. R.; O'Neill, P. M. *Annu. Rev. Pharmacol. Toxicol.* **2001**, *41*, 443.
7. Smith, D. H.; van de Waterbeemd, H.; Walker, D. K. *Pharmacokinetics and Metabolism in Drug Design, Methods and Principles in Medicinal Chemistry, Vol. 13*, Wiley-VCH, Weinheim, **2001**.
8. Barnette, W. E. *CRC Crit. Rev. Biochem.* **1984**, *15*, 201-235.
9. van Heek, M.; France, C. F.; Compton, D. S.; McLeod, R. L.; Yumibe, N. P.; Alton, K. B.; Sybertz, E. J.; Davies, H. R.; *J. Pharmacol. Exp. Therap.* **1997**, *283*, 157-163.
10. Clader, J. W. *J. Med. Chem.* **2004**, *47*, 1-9.
11. Penning, T. D.; Talley, J. J.; Bertenshaw, S. R.; Carter, J. S.; Collins, P. W.; Doc-ter, S.; Graneto, M. J.; Lee, L. F.; Malecha, J. W.; Miyashiro, J. M.; Rogers, R. S.; Rogier, D. J.; Yu, S. S.; Anderson, G. D.; Burton, E. G.; Cogburn, E. G.; Gregory, S. A.; Koboldt, C. M.; Perkins, W. E.; Seibert, K.; Veenhuizen, A. W.; Zhang, A. W.; Isaakson, P. C.; *J. Med. Chem.* **1997**, *40*, 1347-1365.
12. O'Hagan, D.; Deng, H. *Chem. Rev.* **2015**, *115*, 634-649.
13. Morton, G.; Lancaster, J. E.; Van Lear, G. E.; Fulmor, W.; Meyer, W. E. *J. Am. Chem. Soc.* **1969**, *91*, 1535.
14. Sanada, M.; Miyano, T.; Iwadare, S.; Williamson, J. M.; Arison, B. H. J.; Smith, L.; Douglas, A. W.; Liesch, J. M.; Inamine, E. *J. Antibiot.* **1986**, *39*, 259.
15. O'Hagan, D.; Schaffrath, C.; Cobb, S. L.; Hamilton, J. T. G.; Murphy, C. D. *Nature* **2002**, *416*, 279.
16. Middleton, W. J. *J. Org. Chem.* **1975**, *40*, 574-78.

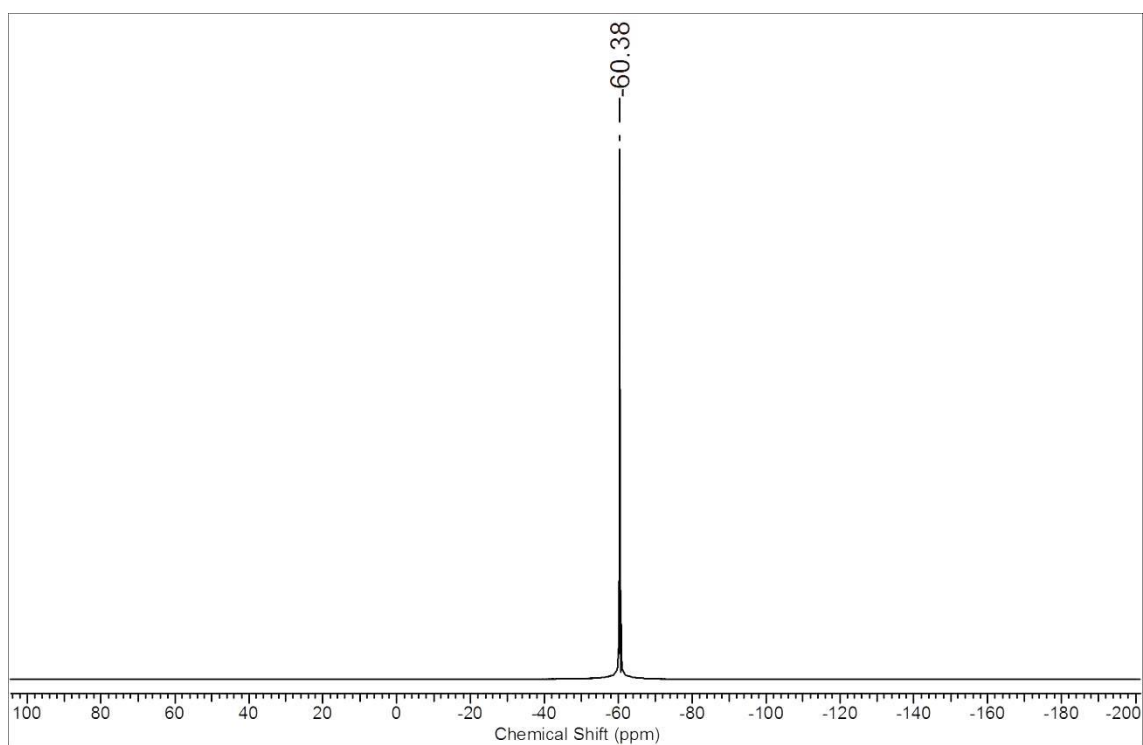
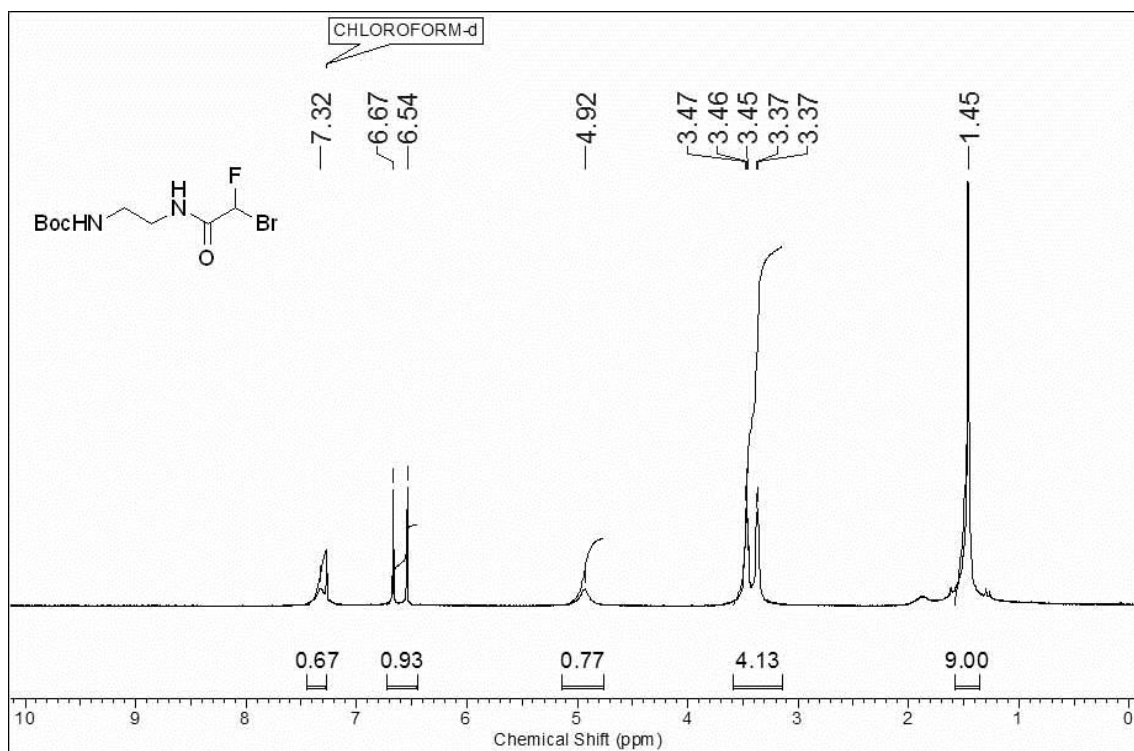
17. Lal, G. S. *J. Org. Chem.* **1993**, *58*, 2791-2796.
18. Ruppert, I.; Schlich, K.; Volbach W.; *Tetrahedron Letters* **1984**, *25*, 2195-2198.
19. Hollenstein, M.; Leumann, C. J. *Organic Letters* **2003**, *5*, 1987.
20. Godeau, G.; Arnion, H.; Brun, C.; Staedel, C.; Barthelemy, P. *Med Chem Comm* **2010**, *1*, 76.
21. Kiviniemi, A.; Murtola, M.; Ingman, P.; Virta, P. *J. Org. Chem.* **2013**, *78*, 5153.
22. Howarth, N. M. Ricci, J. *Tetrahedron* **2011**, *67*, 9588-9594.
23. Gaussian 09, Revision A.1, Frisch, M. J.; Trucks, G. W.; Schlegel, H. B.; Scuseria, G. E.; Robb, M. A.; Cheeseman, J. R.; Scalmani, G.; Barone, V.; Mennucci, B.; Petersson, G. A.; Nakat-suji, H.; Caricato, M.; Li, X.; Hratchian, H. P.; Izmaylov, A. F.; Bloino, J.; Zheng, G.; Sonnenberg, J. L.; Hada, M.; Ehara, M.; Toyota, K.; Fukuda, R.; Hasegawa, J.; Ishida, M.; Nakajima, T.; Honda, Y.; Kitao, O.; Nakai, H.; Vreven, T.; Montgomery, Jr., J. A.; Peralta, J. E.; Ogliaro, F.; Bearpark, M.; Heyd, J. J.; Brothers, E.; Kudin, K. N.; Staroverov, V. N.; Kobayashi, R.; Normand, J.; Raghavachari, K.; Rendell, A.; Burant, J. C.; Iyengar, S. S.; Tomasi, J.; Cossi, M.; Rega, N.; Millam, N. J.; Klene, M.; Knox, J. E.; Cross, J. B.; Bakken, V.; Adamo, C.; Jaramillo, J.; Gom-perts, R.; Stratmann, R. E.; Yazyev, O.; Austin, A. J.; Cammi, R.; Pomelli, C.; Ochterski, J. W.; Martin, R. L.; Morokuma, K.; Zakrzewski, V. G.; Voth, G. A.; Salvador, P.; Dannenberg, J. J.; Dapprich, S.; Daniels, A. D.; Farkas, Ö.; Foresman, J. B.; Ortiz, J. V.; Cioslowski, J.; ox, D. J. *Gaussian, Inc., Wallingford CT*, **2009**.
24. Becke, A. D. *J. Chem. Phys.* **1993**, *98*, 5648.
25. Lee, C.; Yang, W.; Parr, R.G. *Phys. Rev. B* **1988**, *37*, 785.
26. Merrifield, R. B. *J. Am. Chem. Soc.* **1963**, *85*, 2149.
27. Kang, S. H; Cho, M. J; Kole, R. *Biochemistry* **1998**, *37*, 6235-6239.
28. Ishihara, T.; Kano, A.; Obara, K.; Saito, M.; Chen, X.; Park, T. G.; Akaike, T.; Maruyama, A. *J. Control. Release* **2011**, *155*, 34.

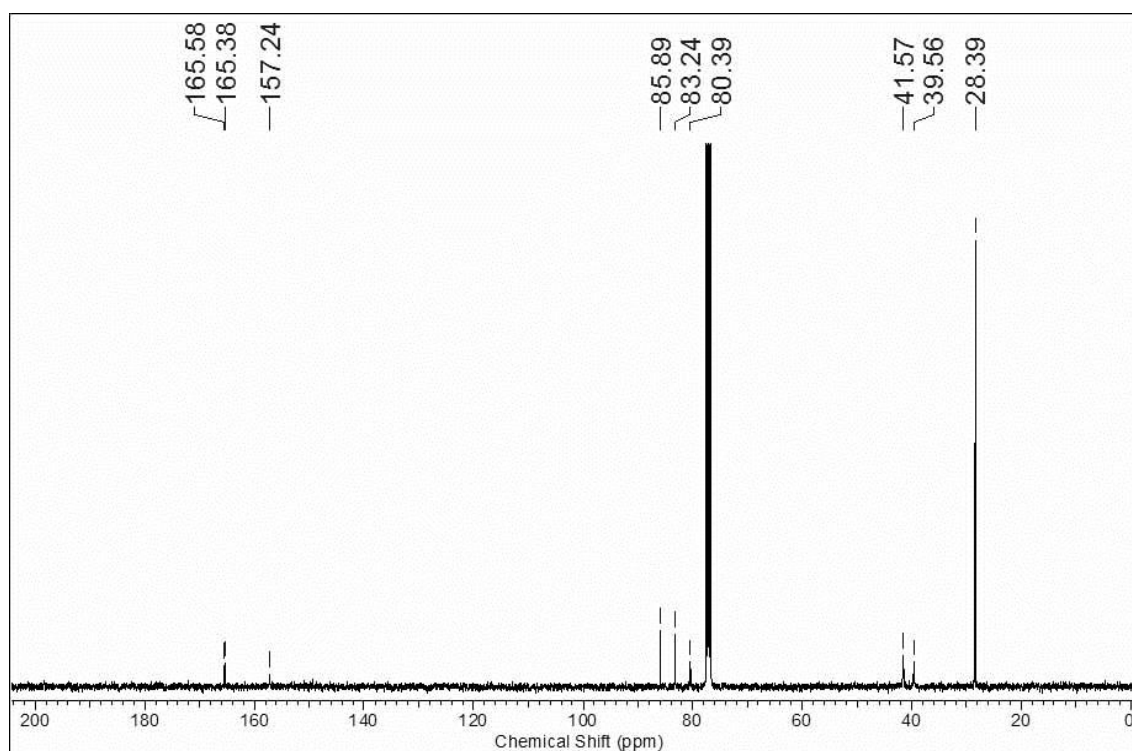
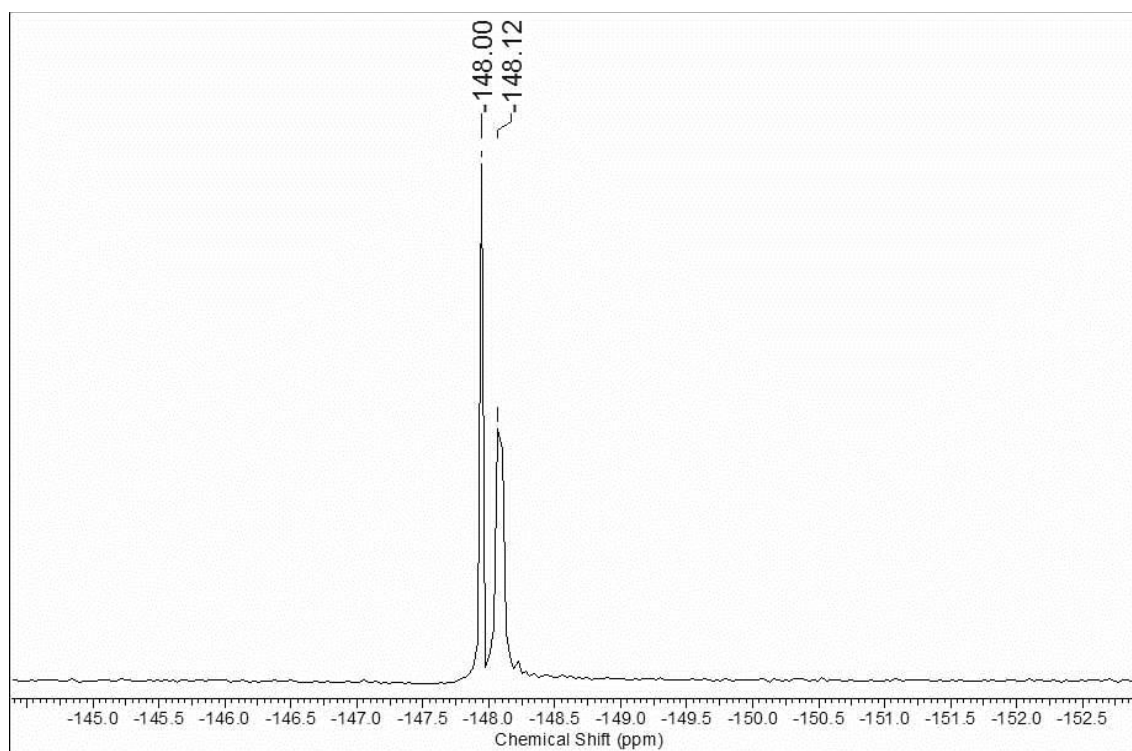
2.4 Appendix-I

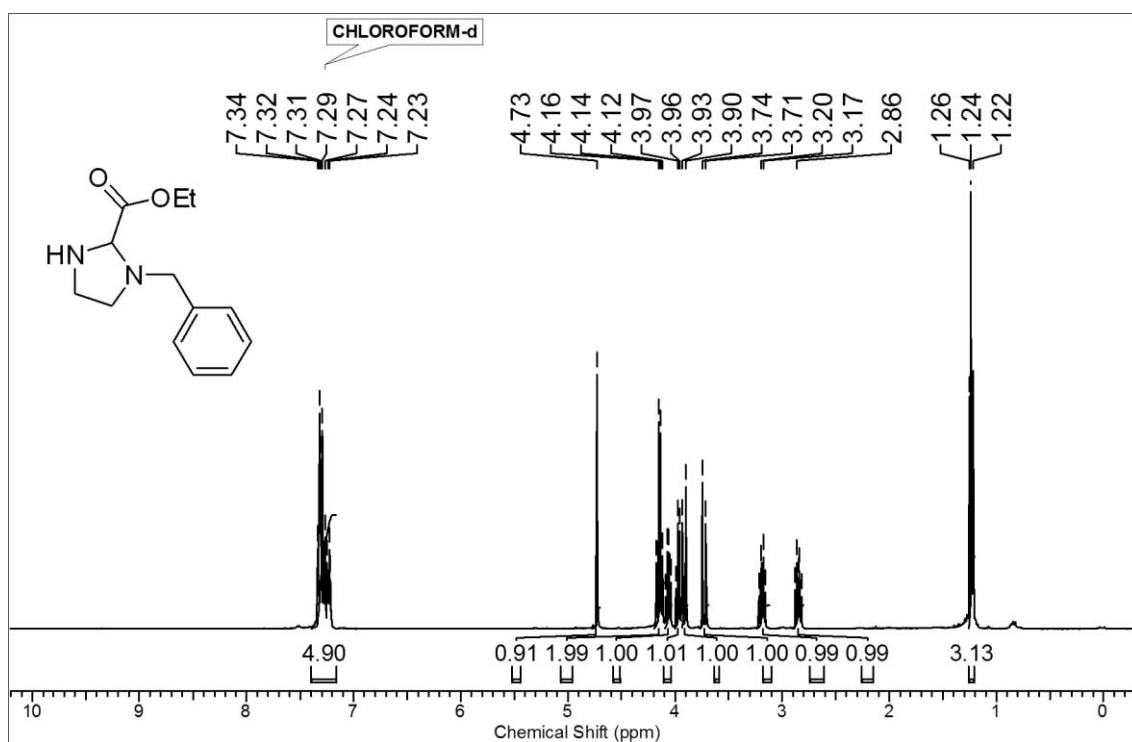
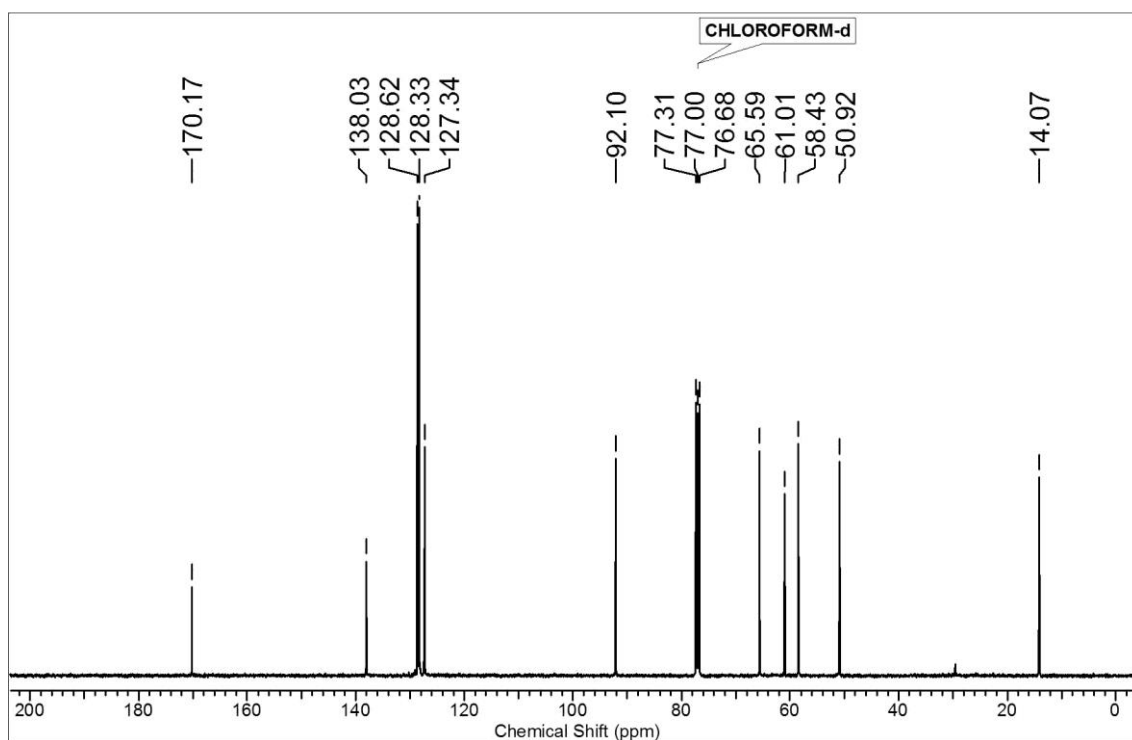
Entry	Table of contents	Page No.
1	¹ H, ¹³ C, and ¹⁹ F NMR spectra of all compounds	118-178
2	HPLC profiles of all synthesized PNA oligomers	179-189
3	MALDI-TOF mass spectra of all synthesized PNA oligomers	189-119

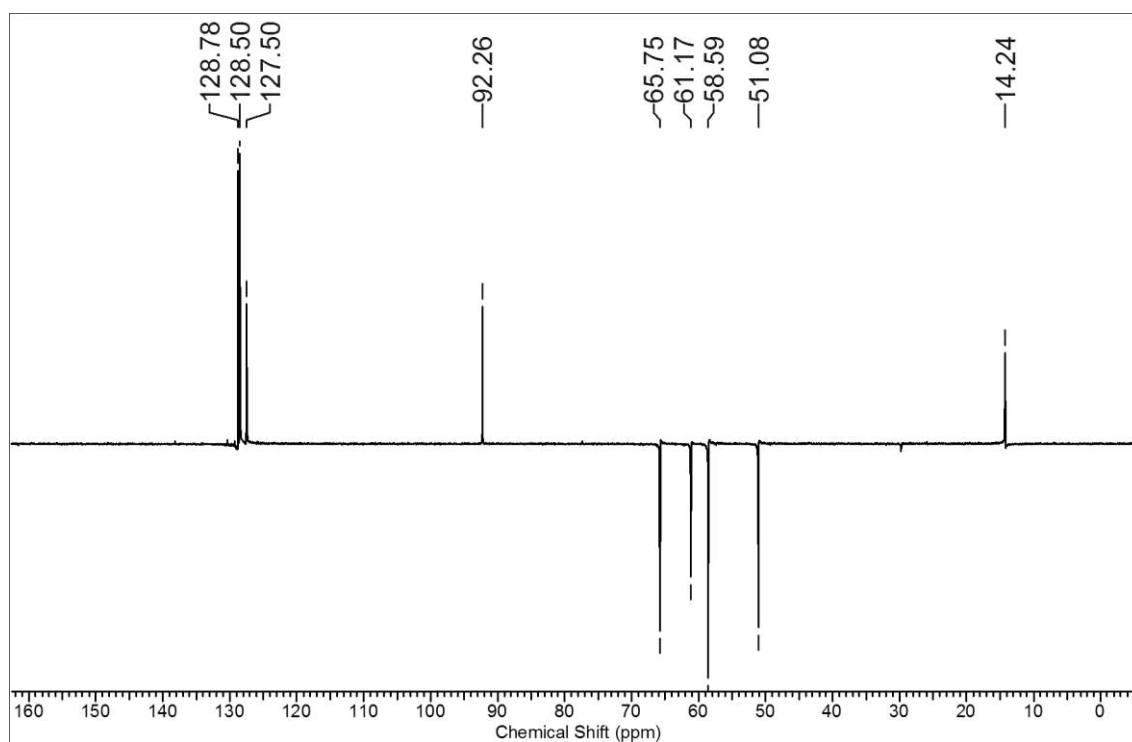
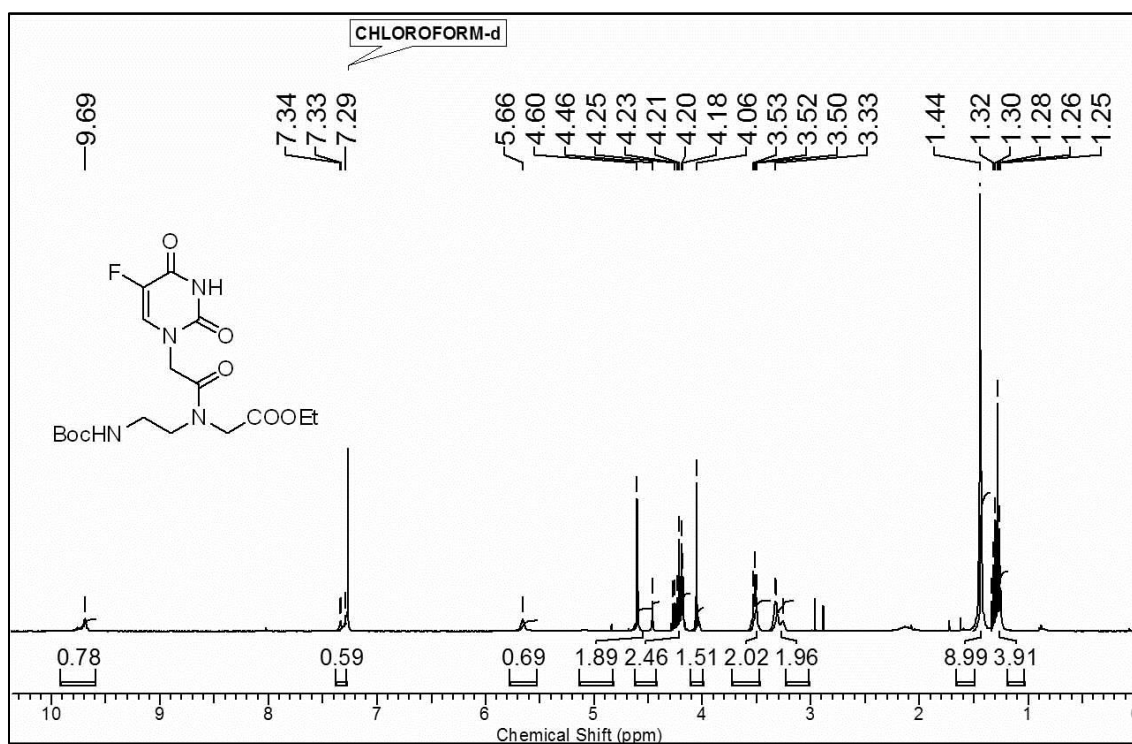
NMR Spectral Data

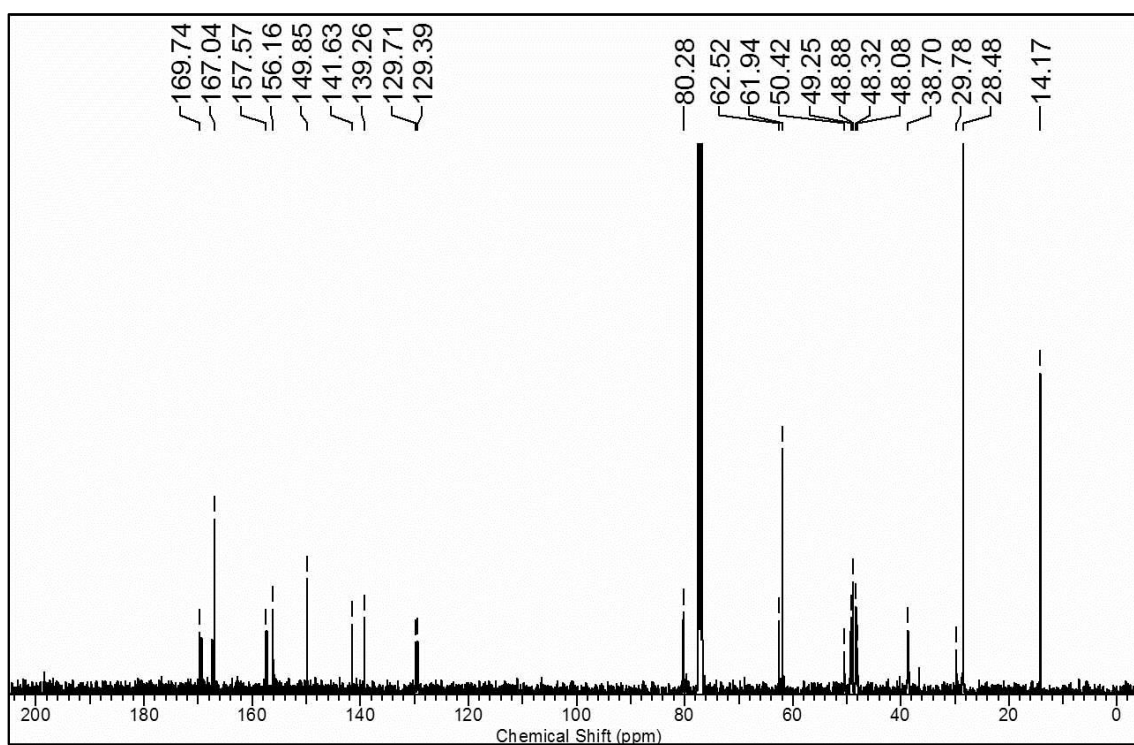
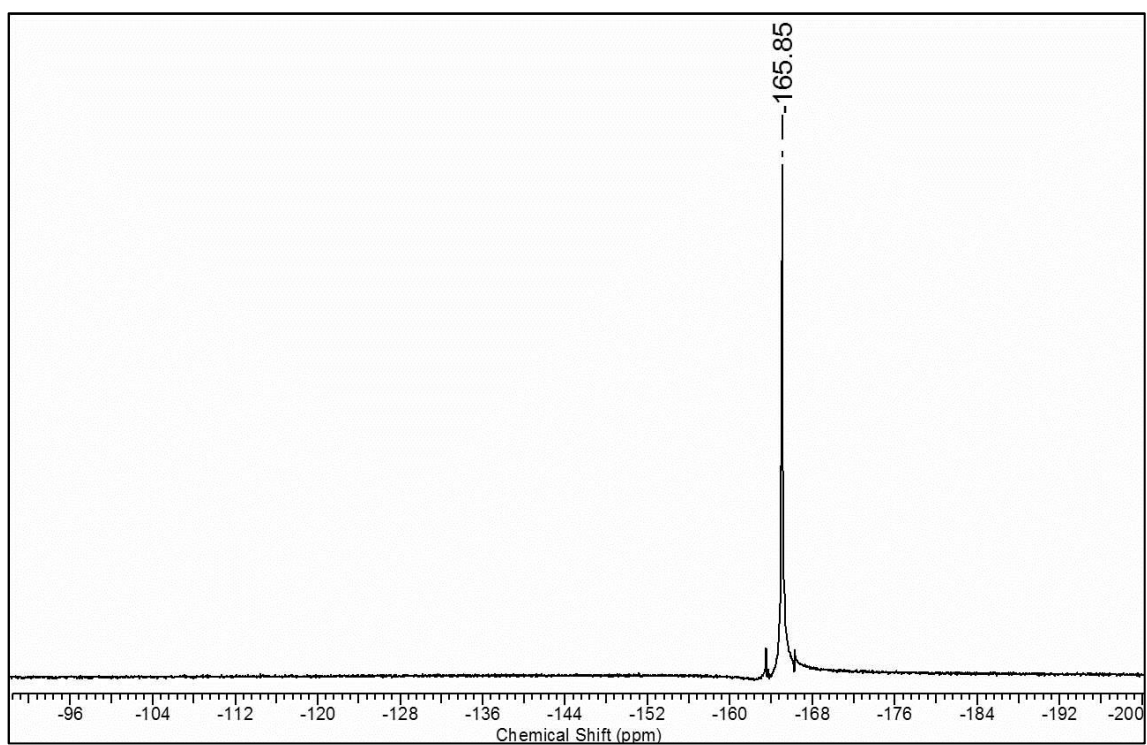
 $^1\text{H-NMR}$ of compound **12** $^{13}\text{C-NMR}$ of compound **12**

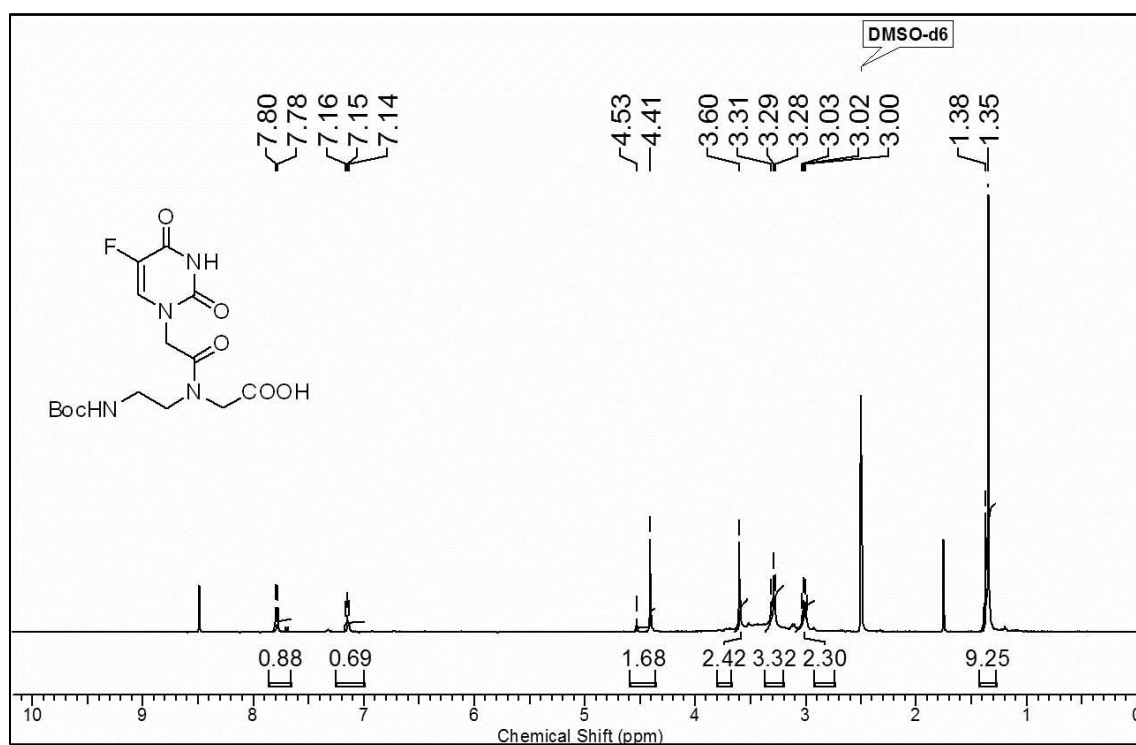
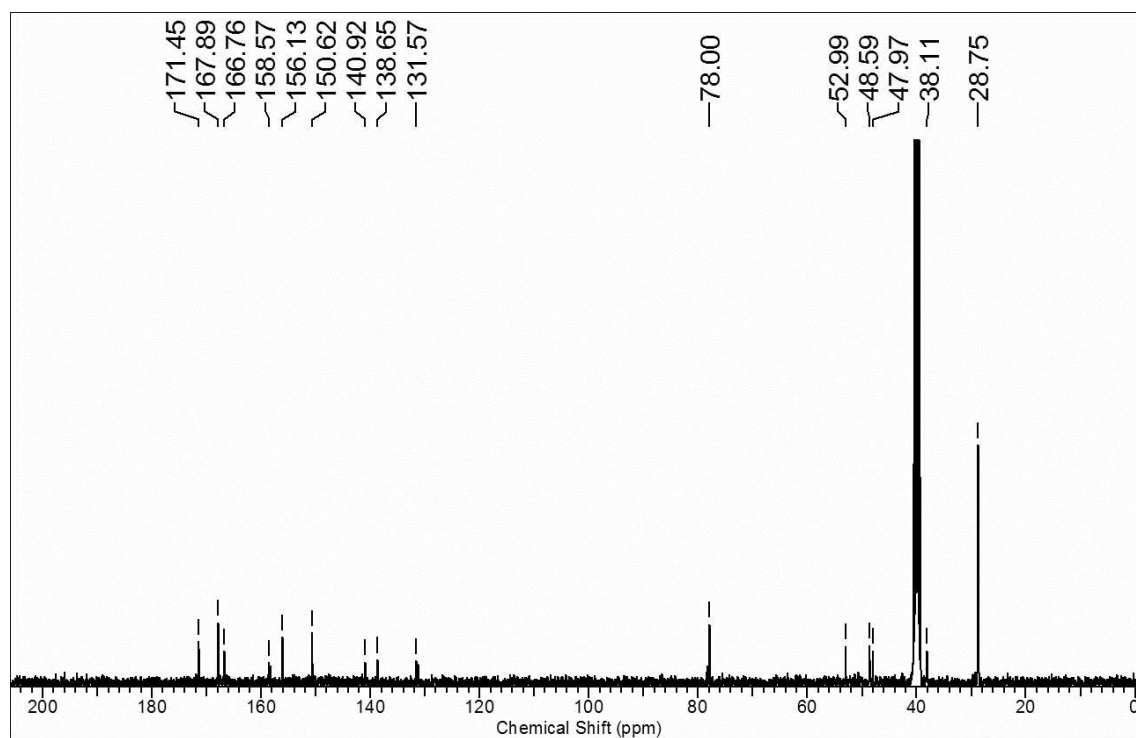
^{19}F -NMR of compound **12** ^1H -NMR of compound **13**

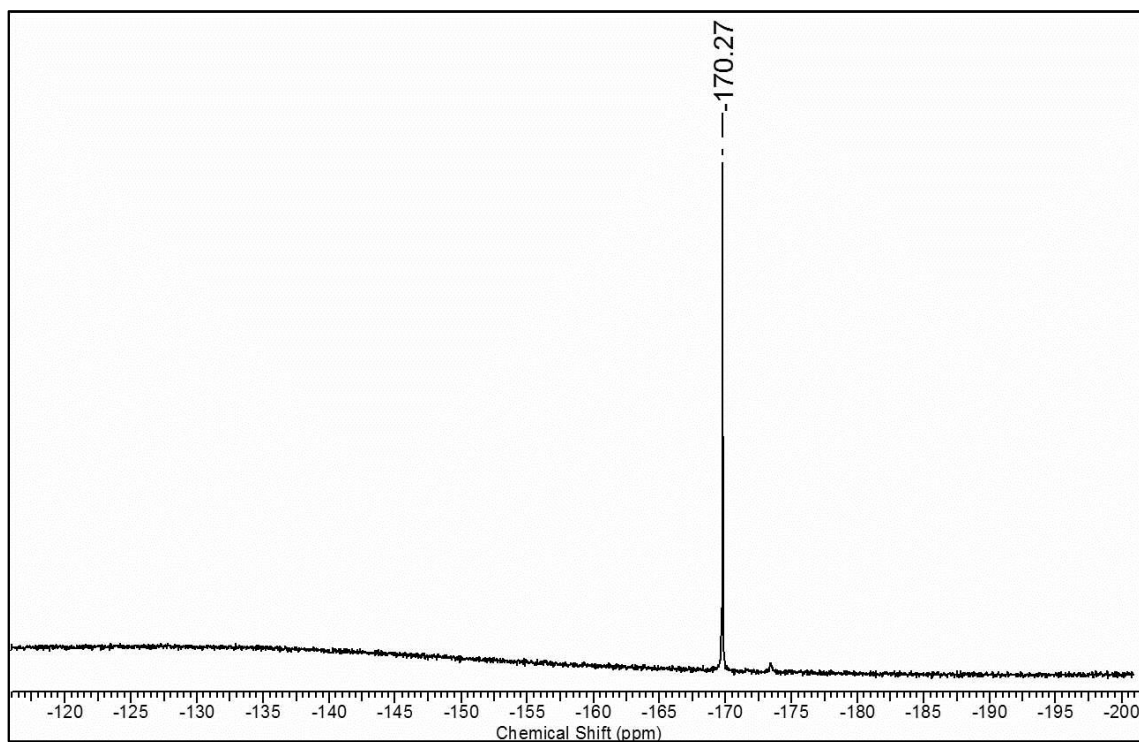
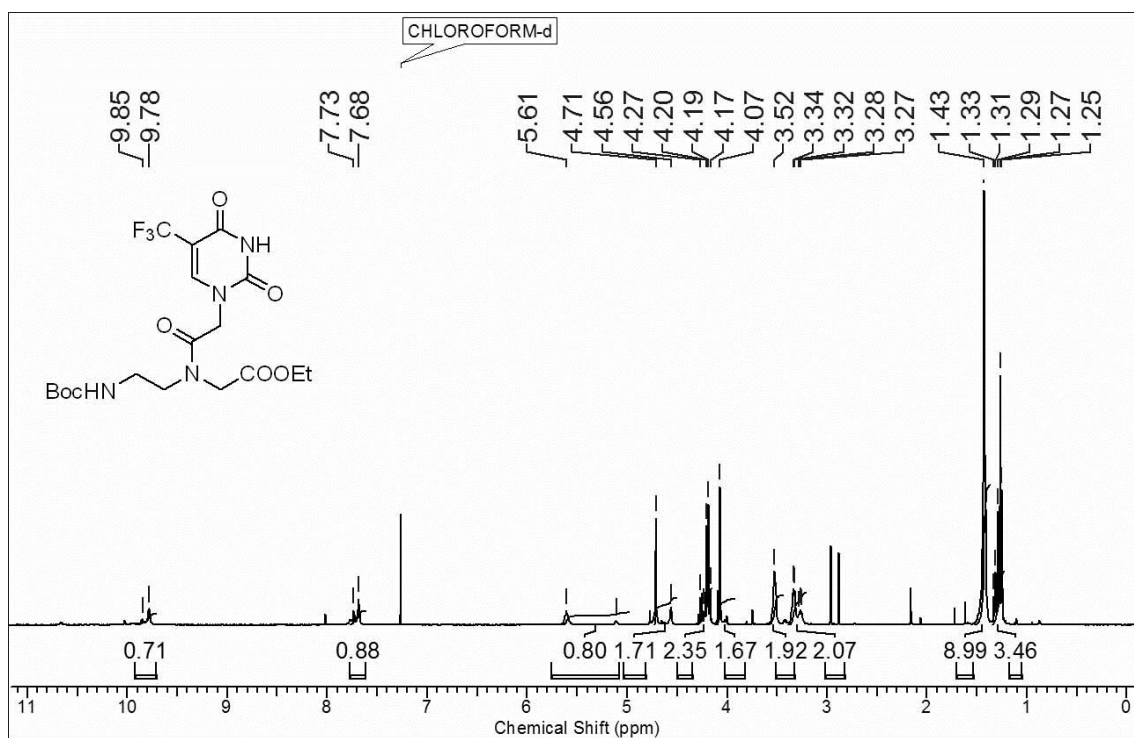
^{13}C -NMR of compound **13** ^{19}F -NMR of compound **12**

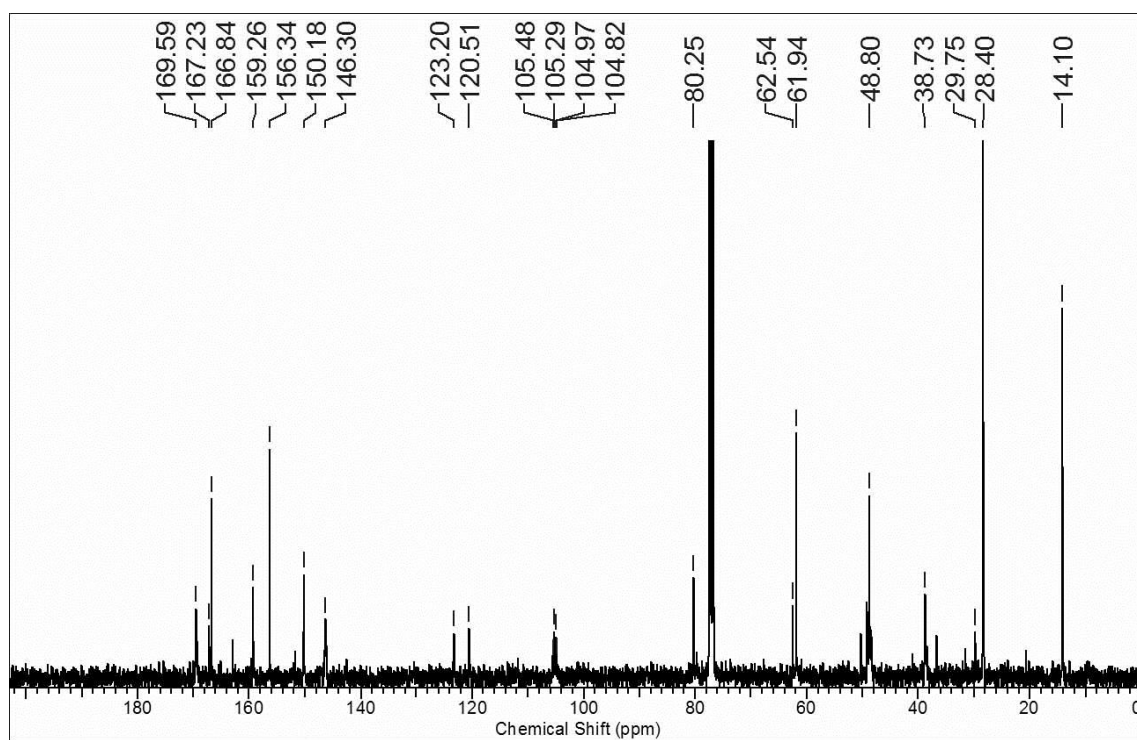
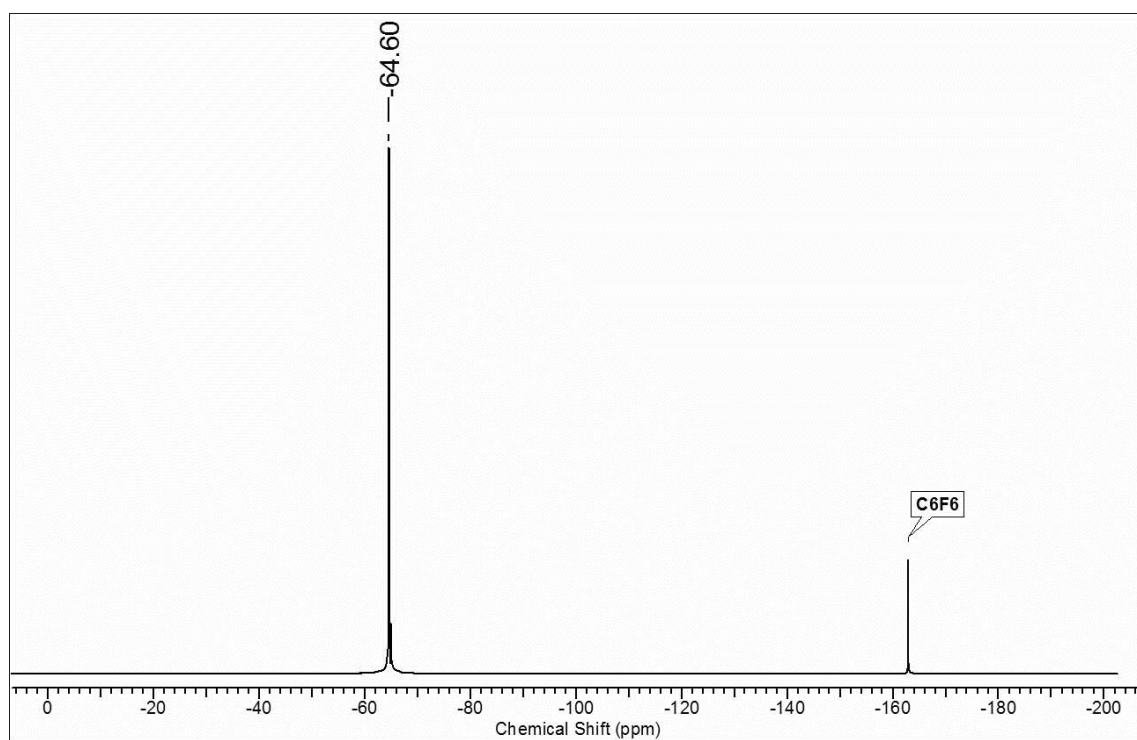
$^1\text{H-NMR}$ of compound **15** $^{13}\text{C-NMR}$ of compound **15**

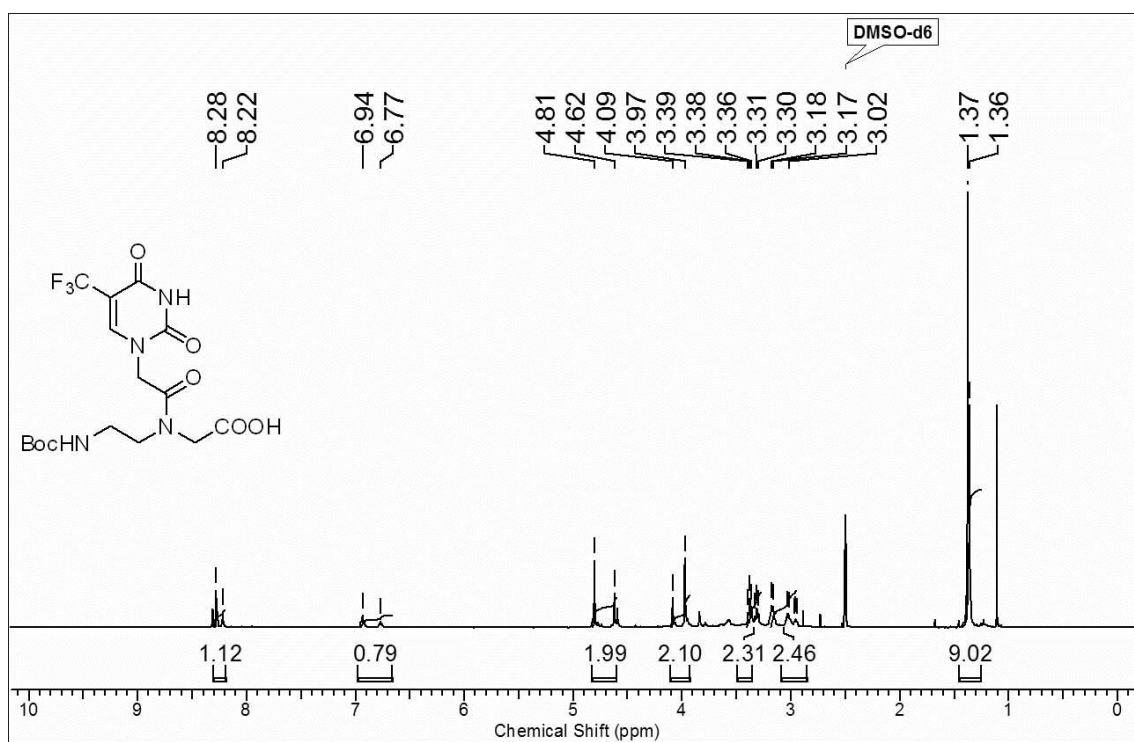
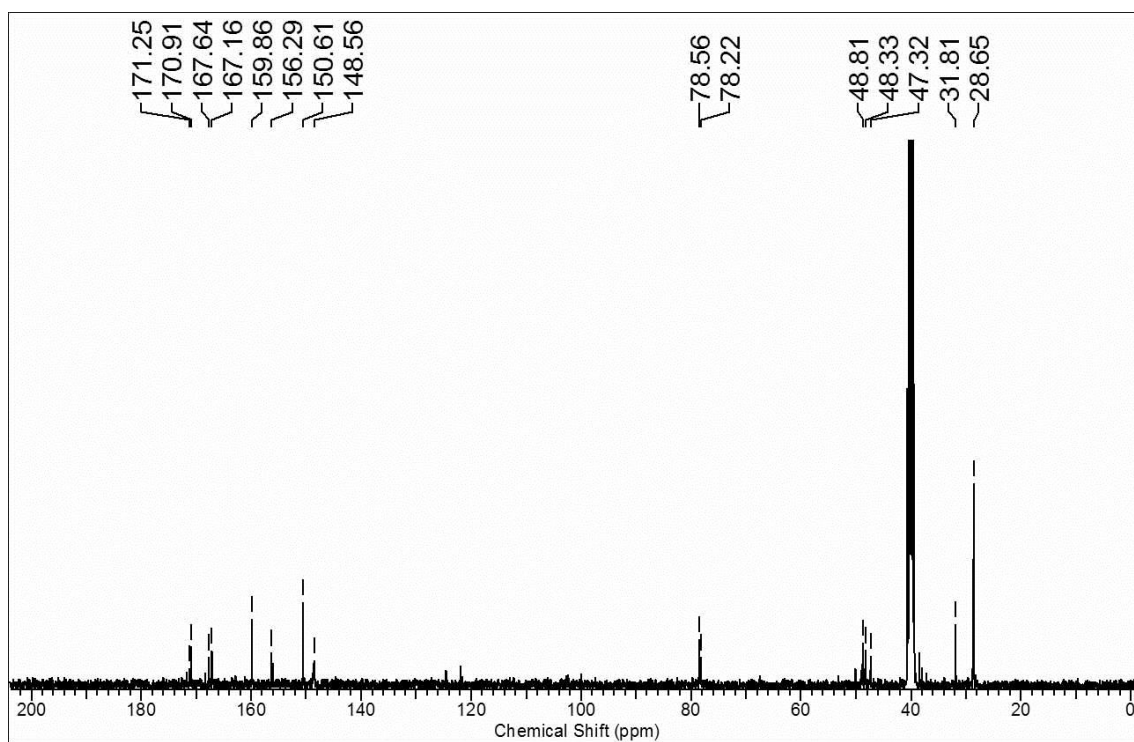
DEPT-NMR of compound **15** ^1H -NMR of compound **18a**

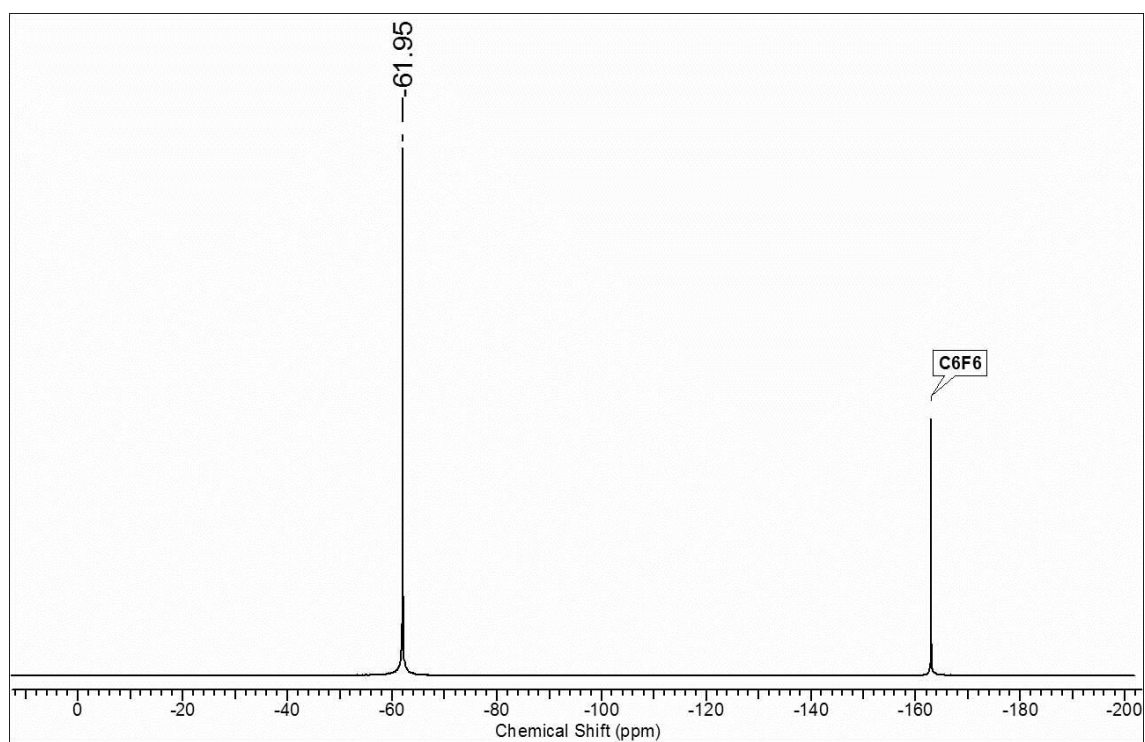
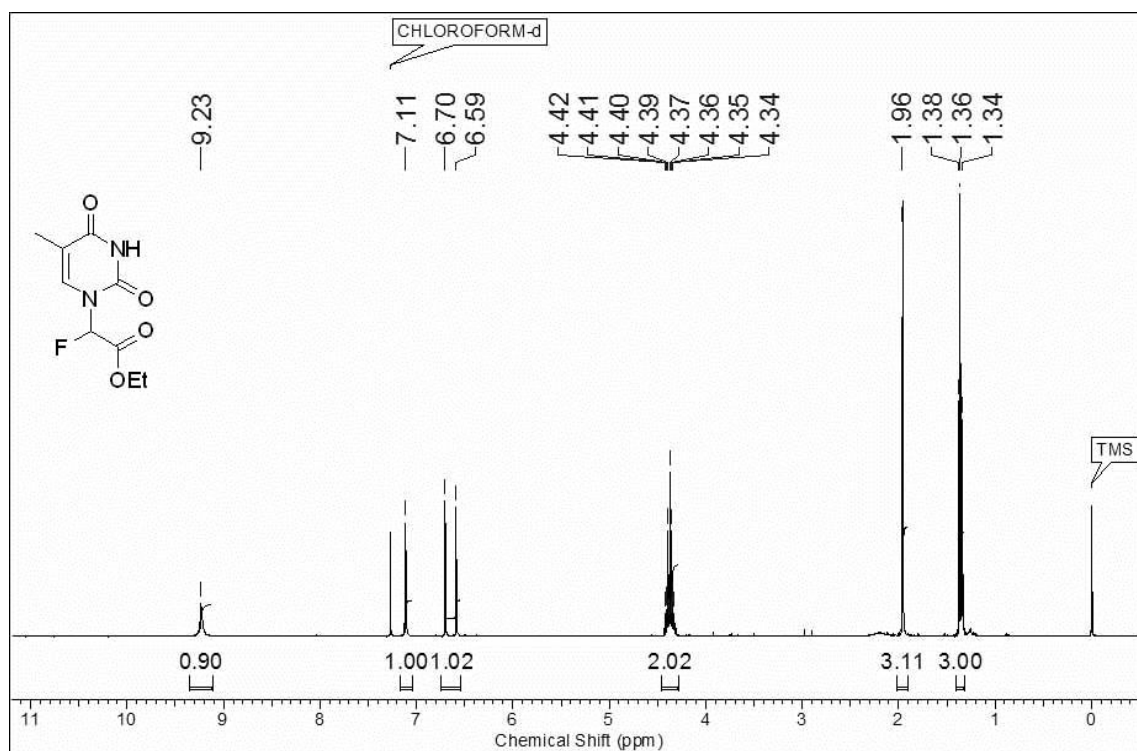
^{13}C -NMR of compound **18a** ^{19}F -NMR of compound **18a**

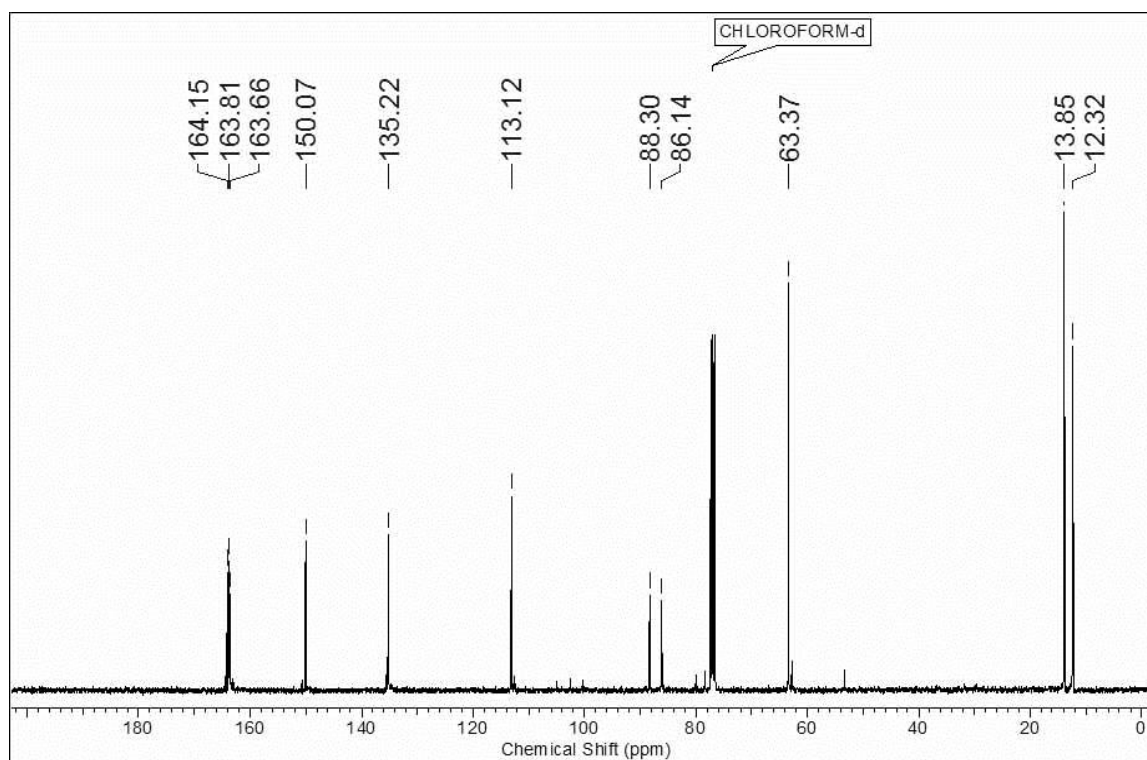
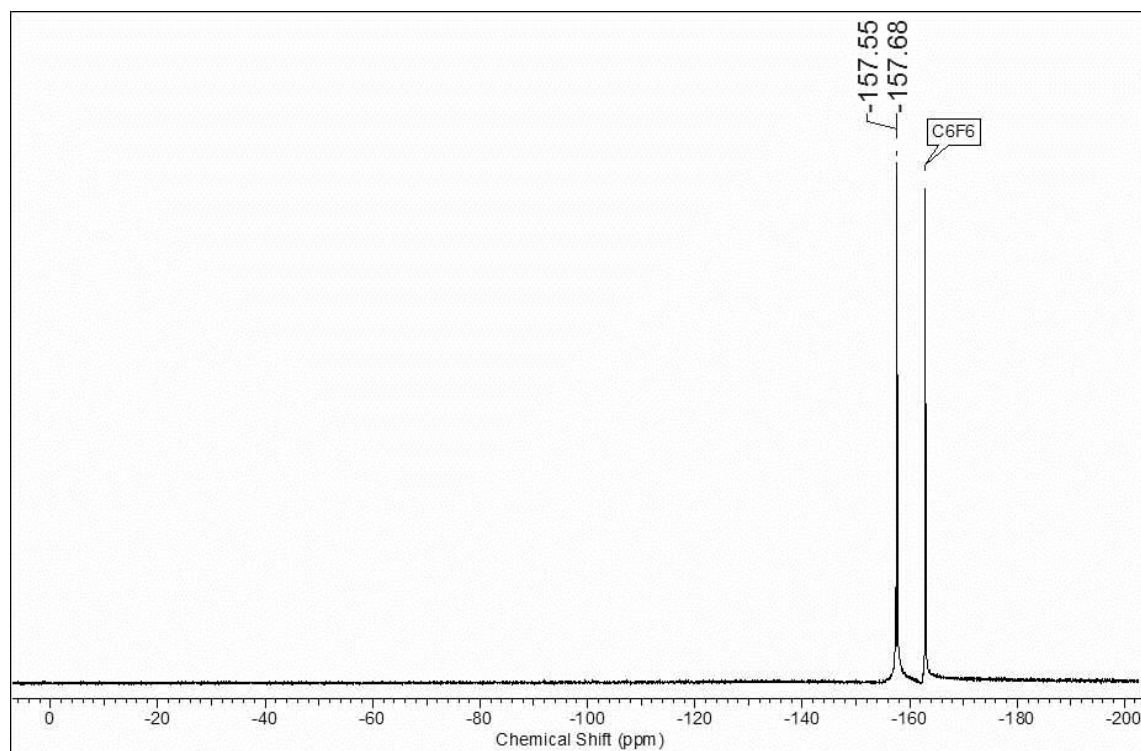
$^1\text{H-NMR}$ of compound **1** $^{13}\text{C-NMR}$ of compound **1**

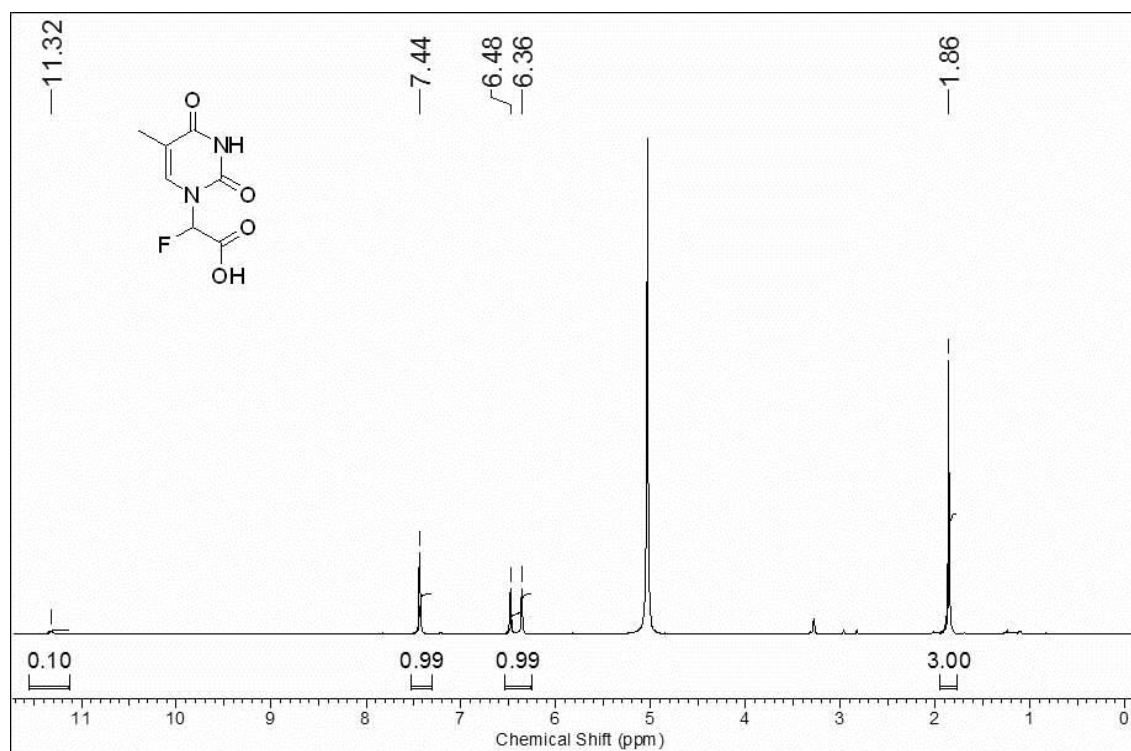
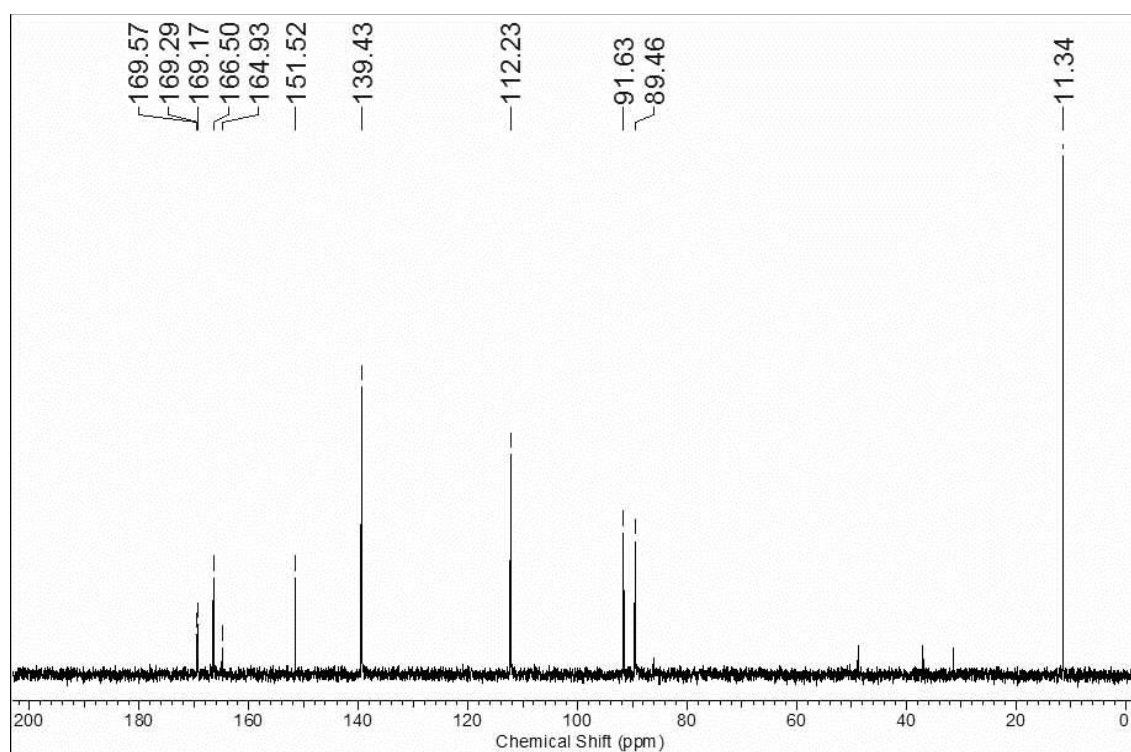
^{19}F -NMR of compound **1** ^1H -NMR of compound **18b**

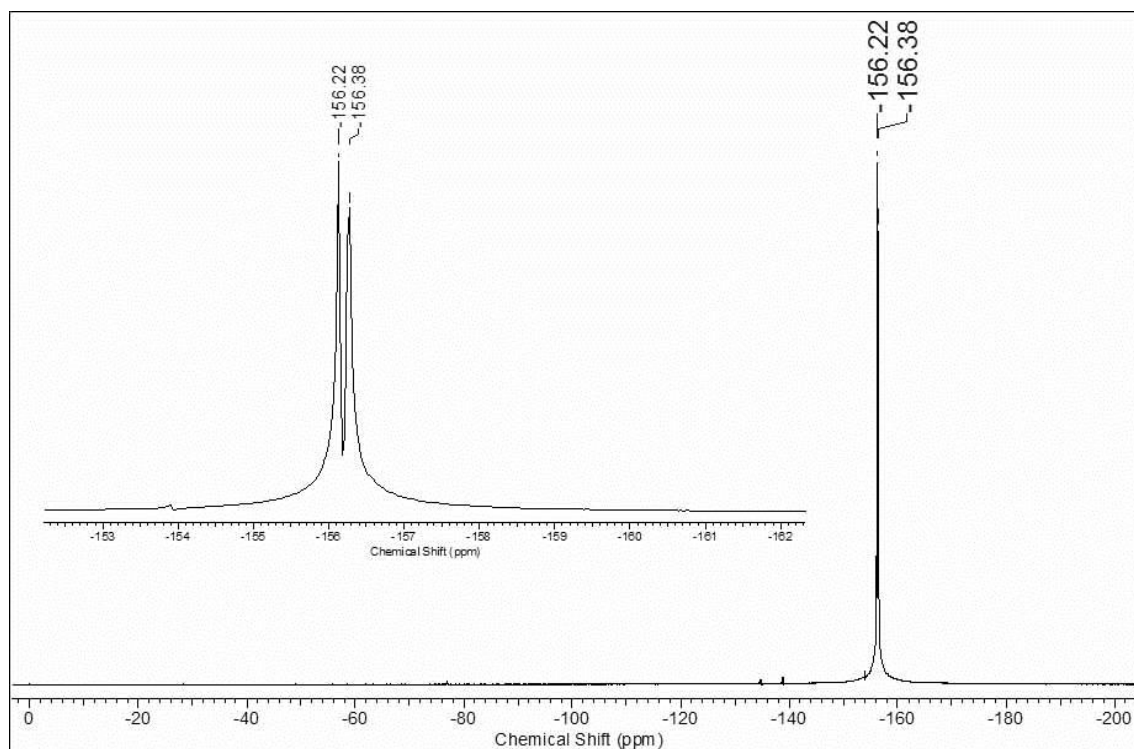
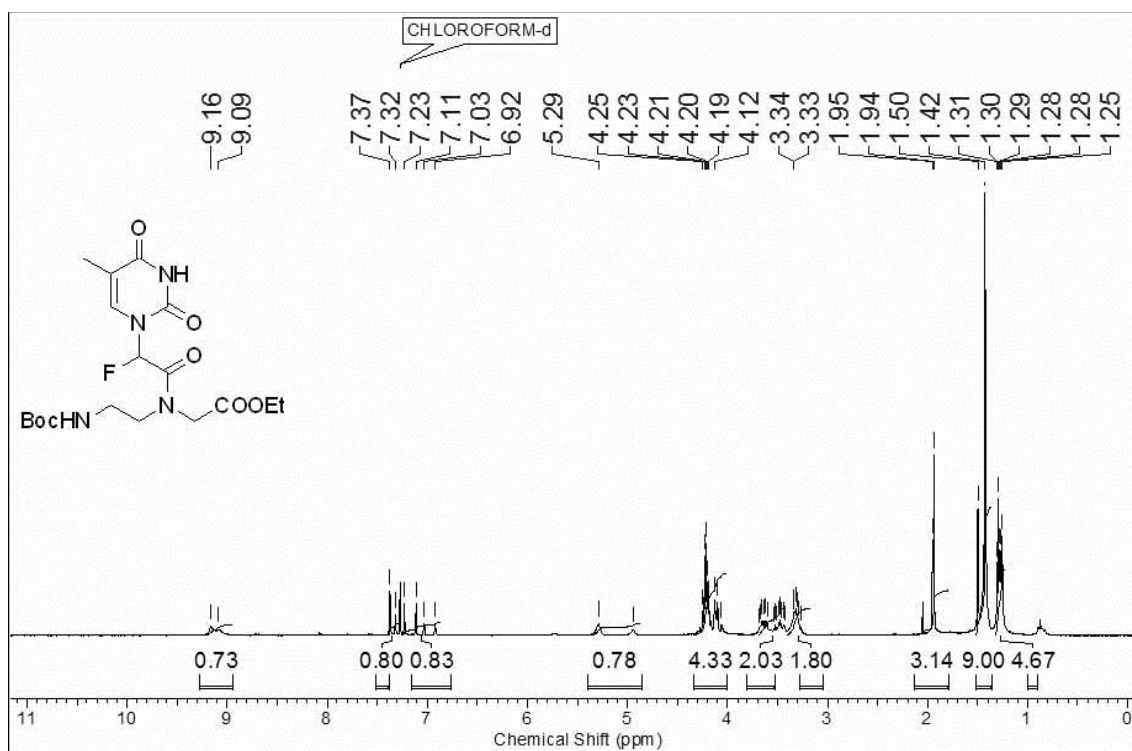
^{13}C -NMR of compound **18b** ^{19}F -NMR of compound **18b**

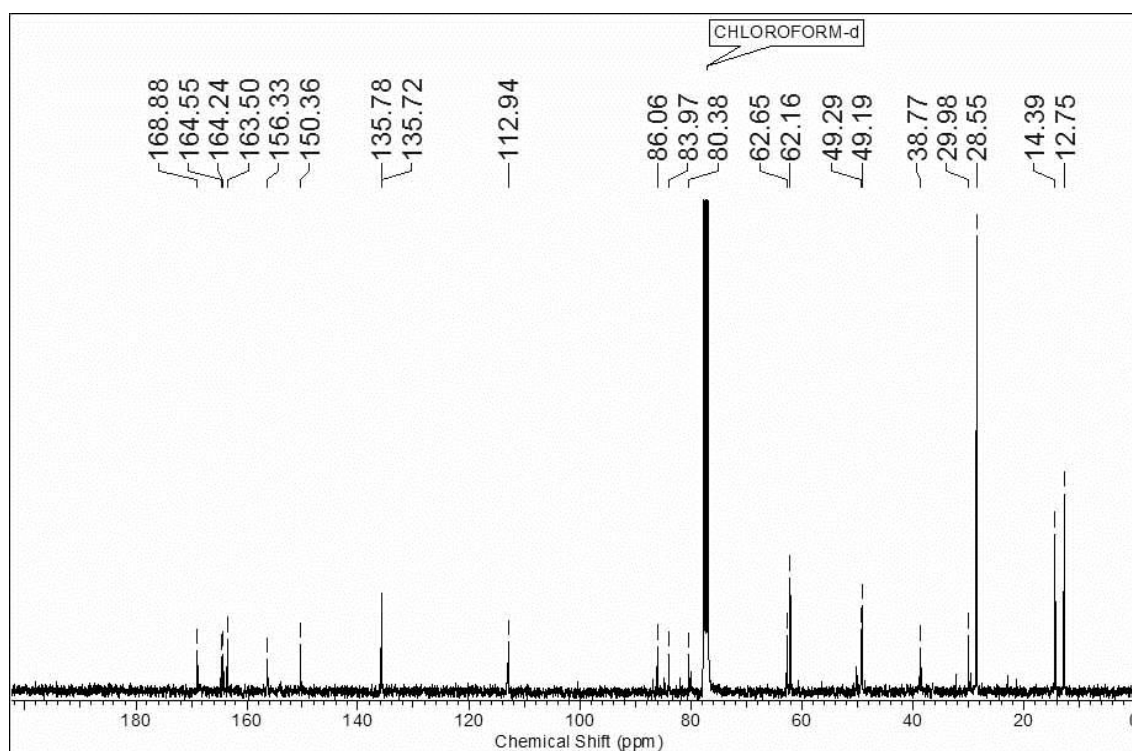
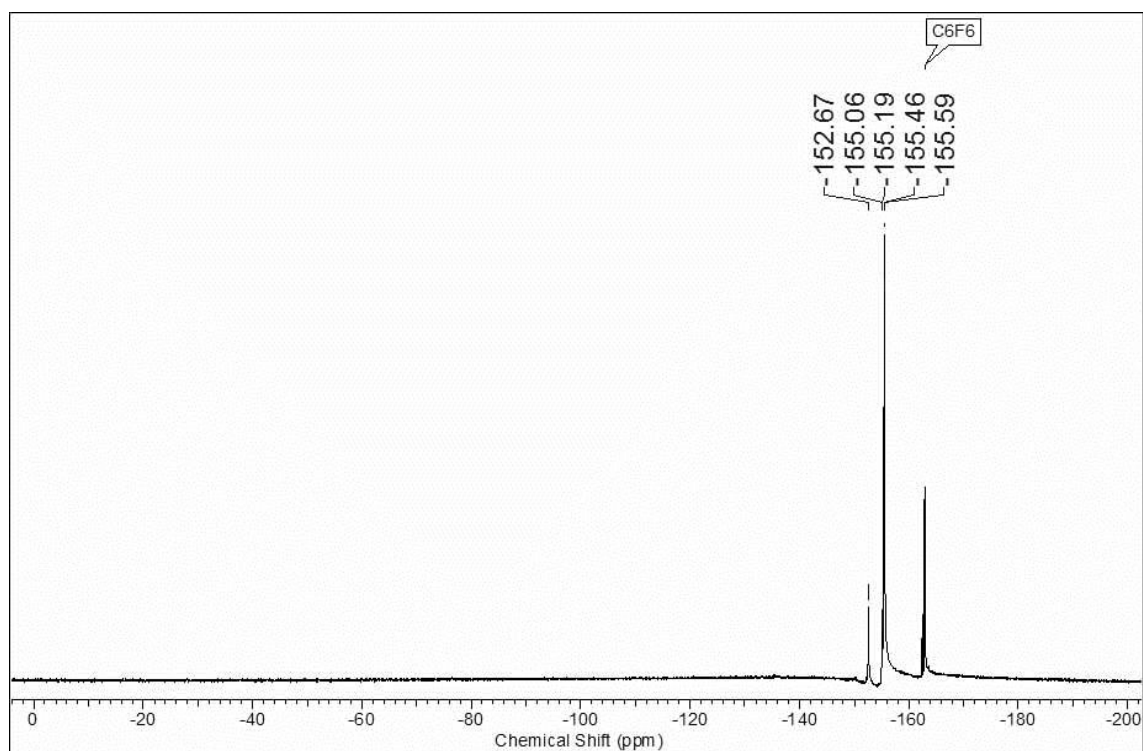
$^1\text{H-NMR}$ of compound **2** $^{13}\text{C-NMR}$ of compound **2**

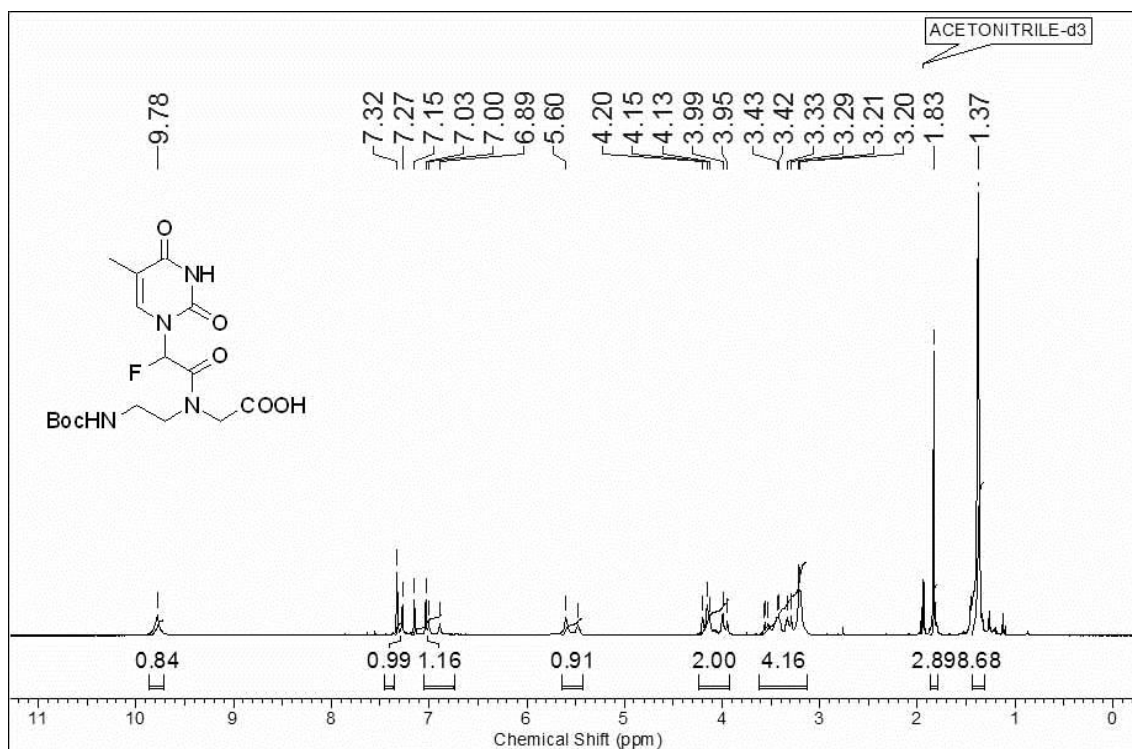
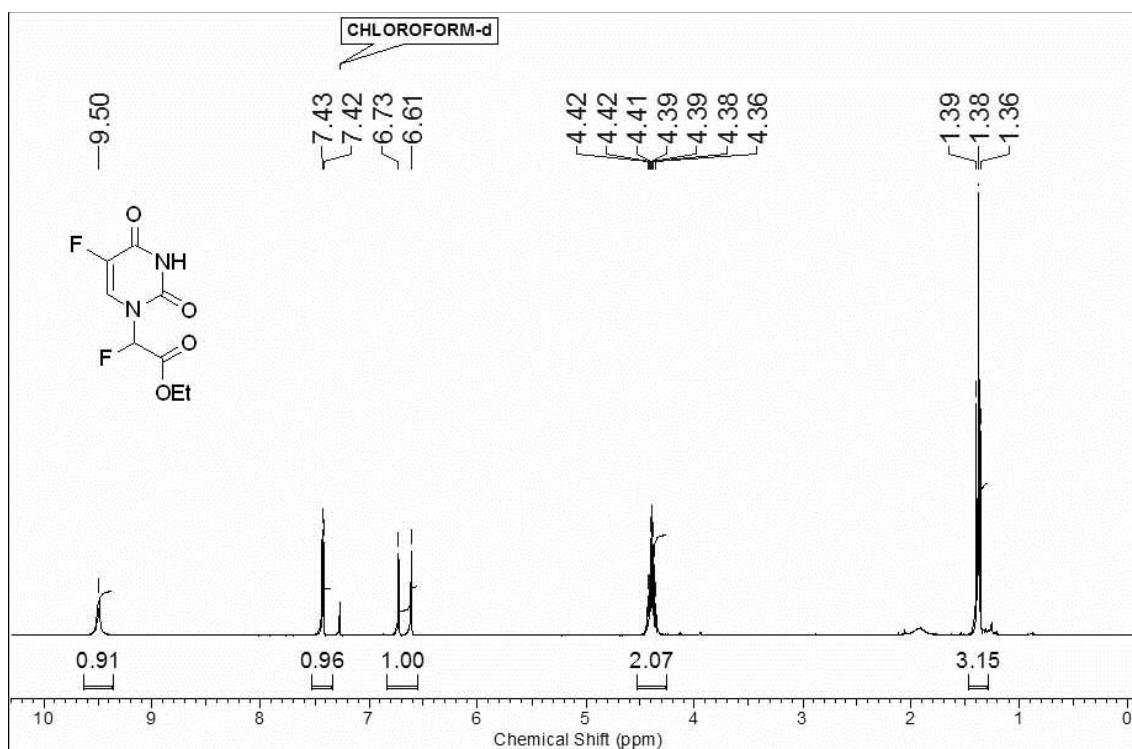
^{19}F -NMR of compound **2** ^1H -NMR of compound **20a**

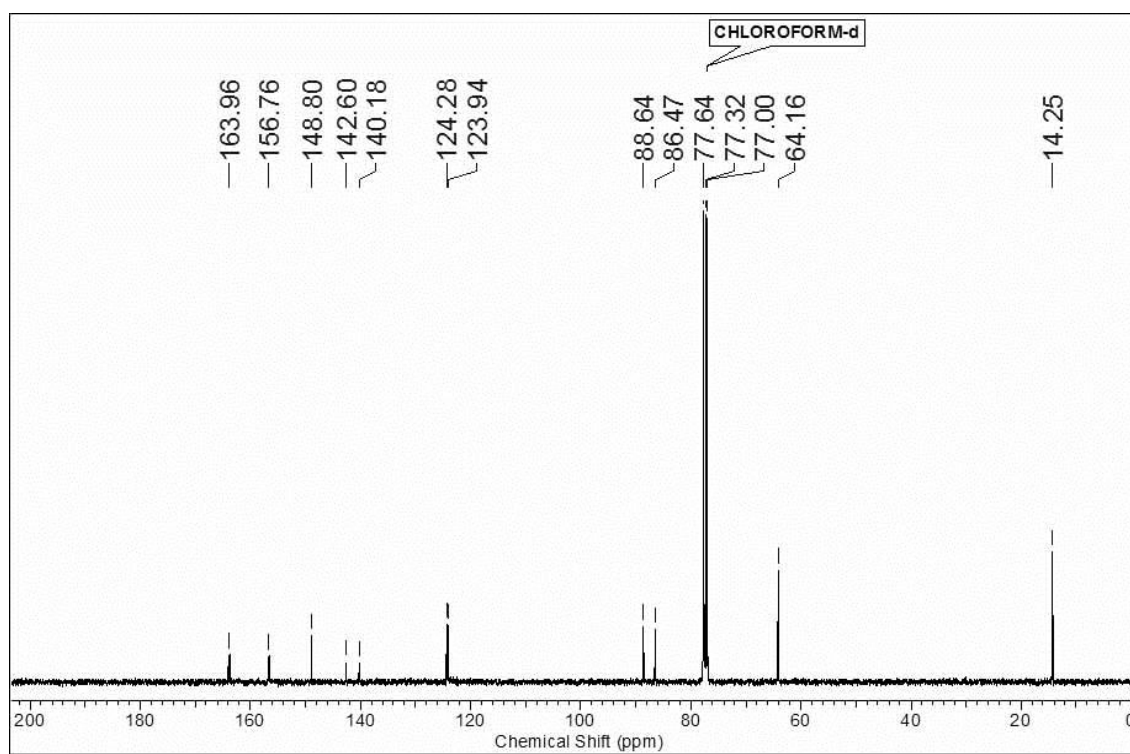
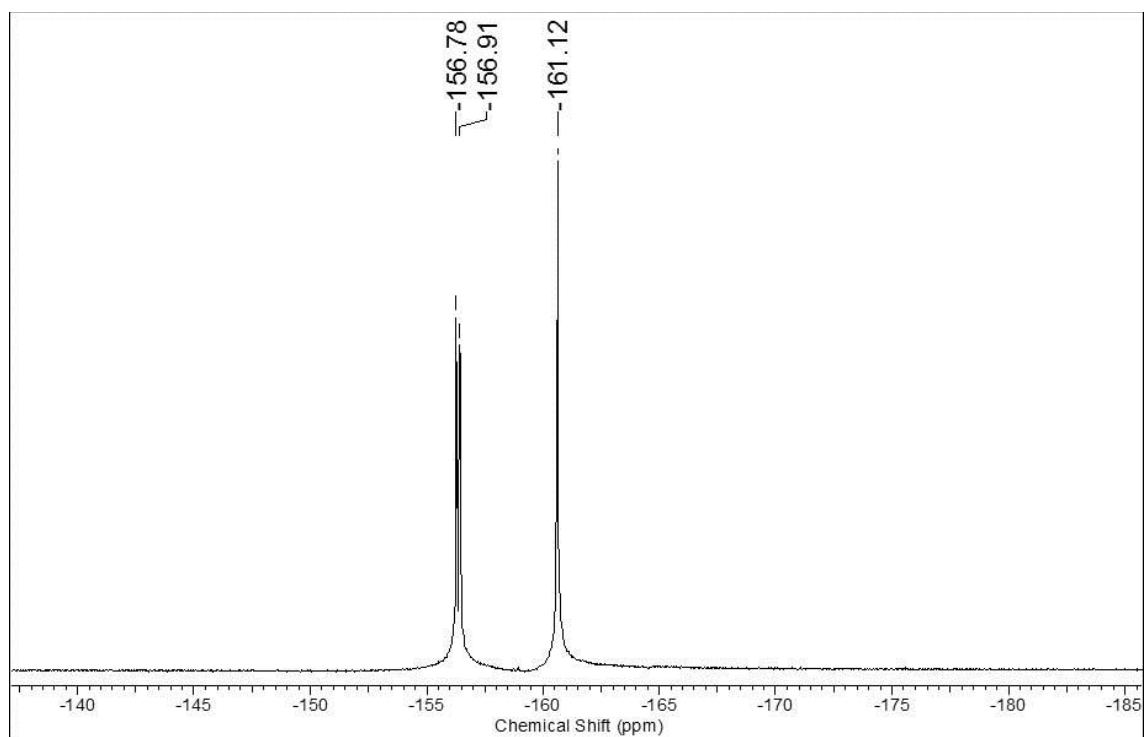
^{13}C -NMR of compound **20a** ^{19}F -NMR of compound **20a**

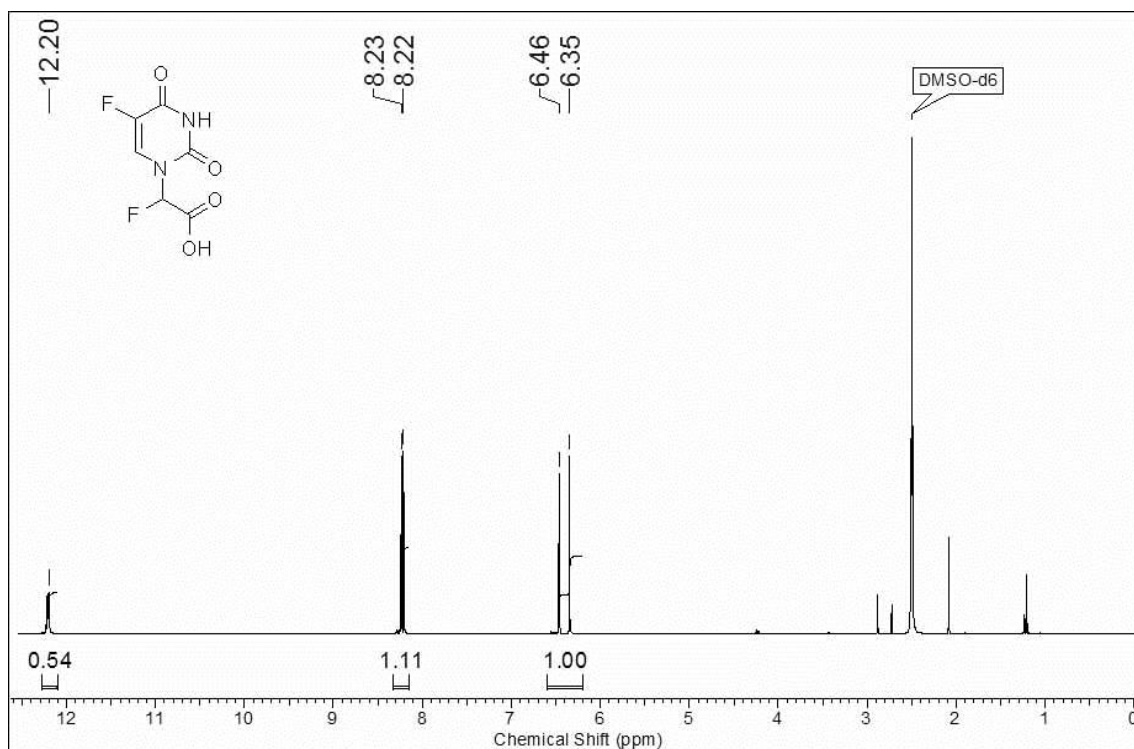
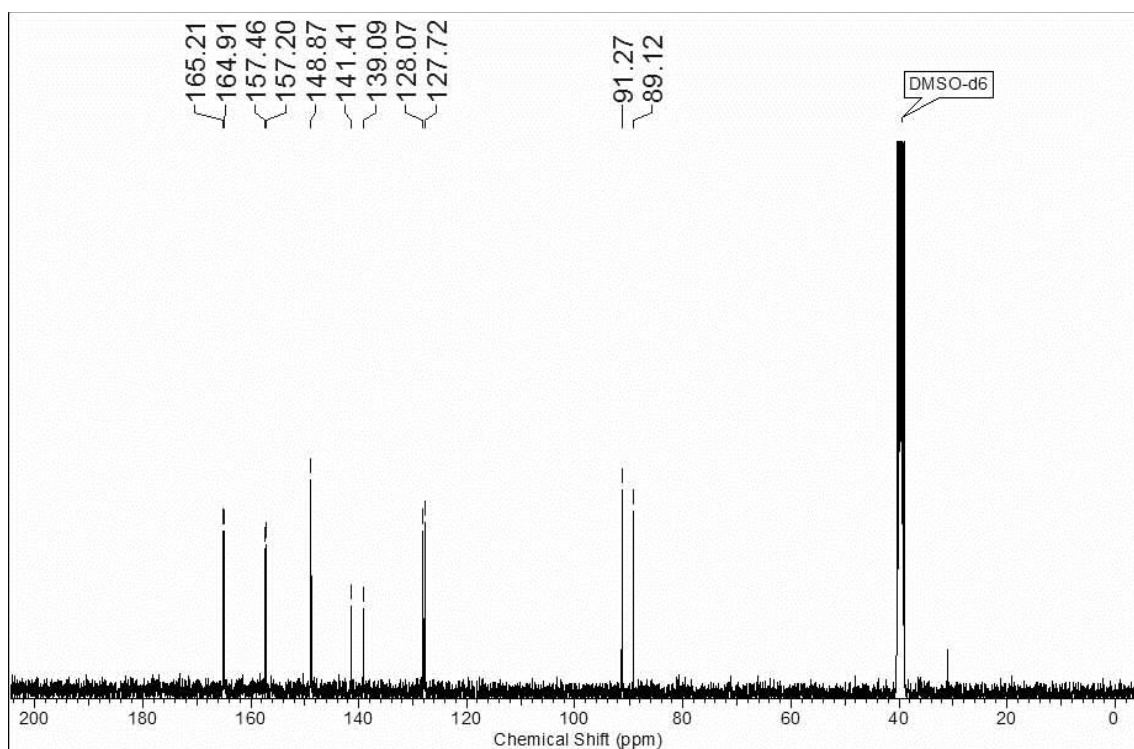
$^1\text{H-NMR}$ of compound **21a** $^{13}\text{C-NMR}$ of compound **21a**

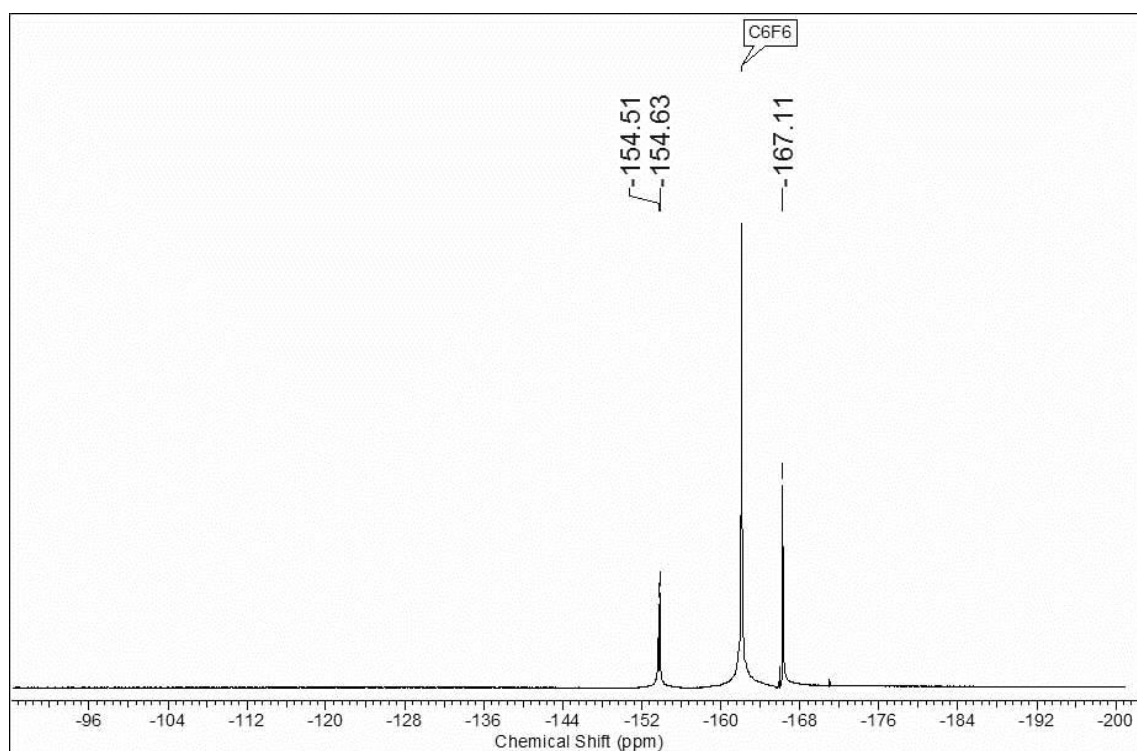
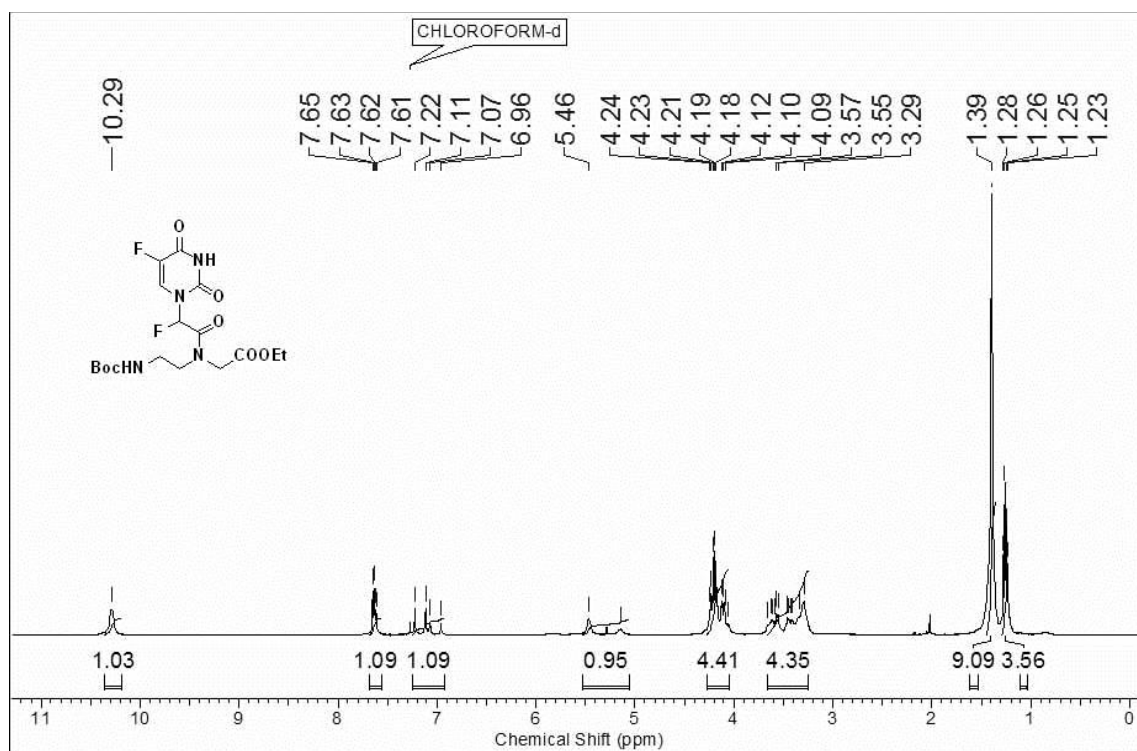
^{19}F -NMR of compound **21a** ^1H -NMR of compound **22a**

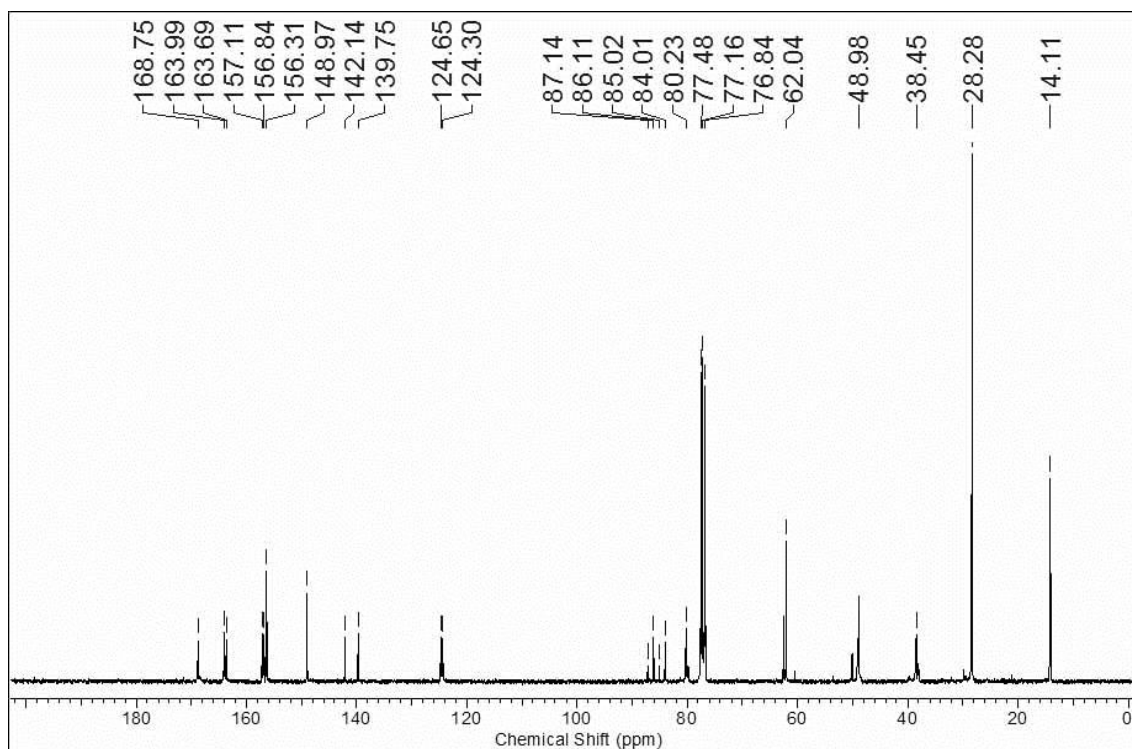
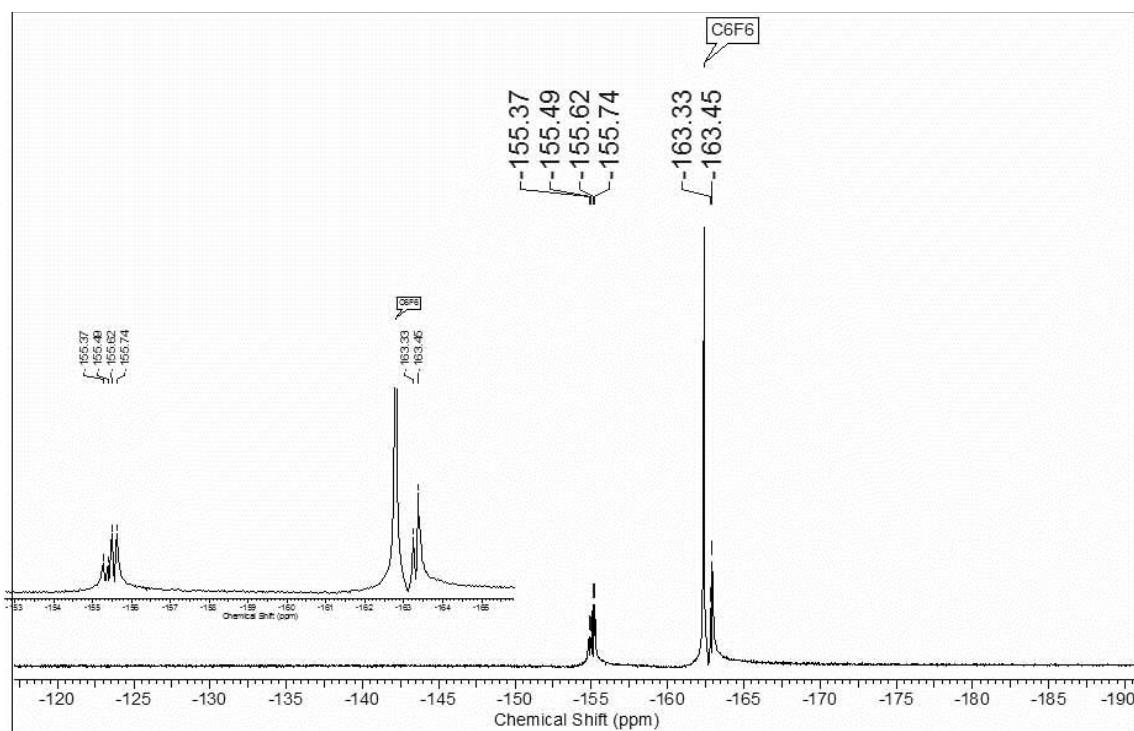
^{13}C -NMR of compound **22a** ^{19}F -NMR of compound **22a**

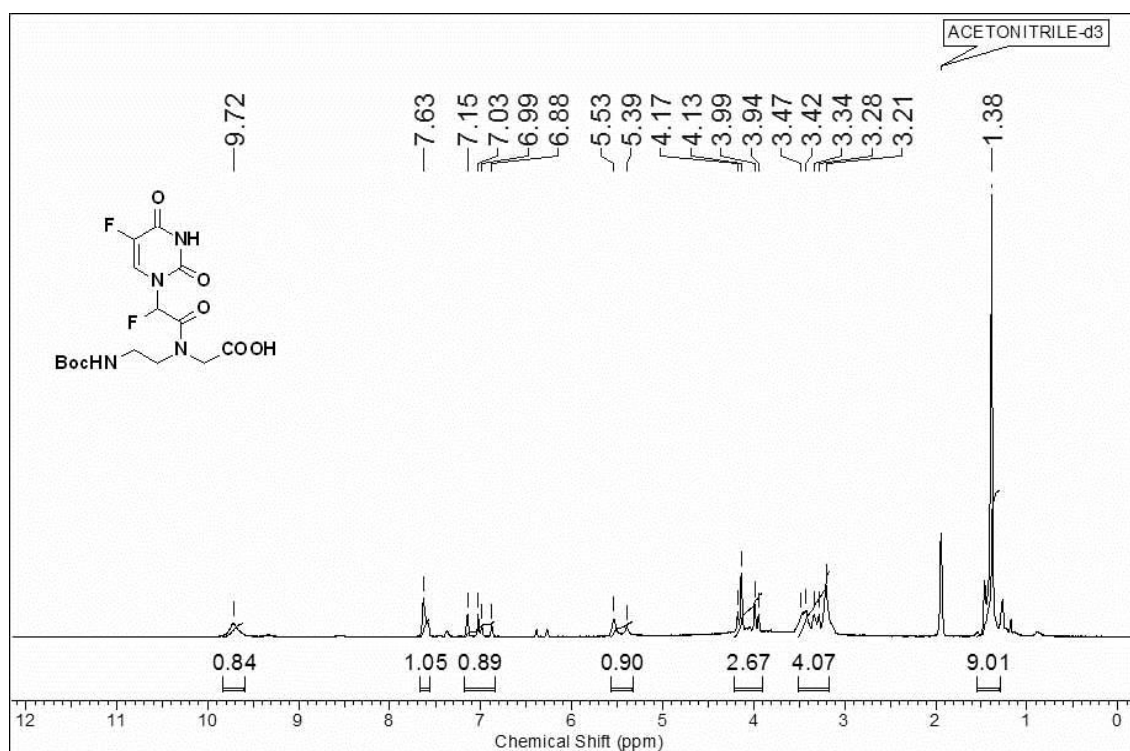
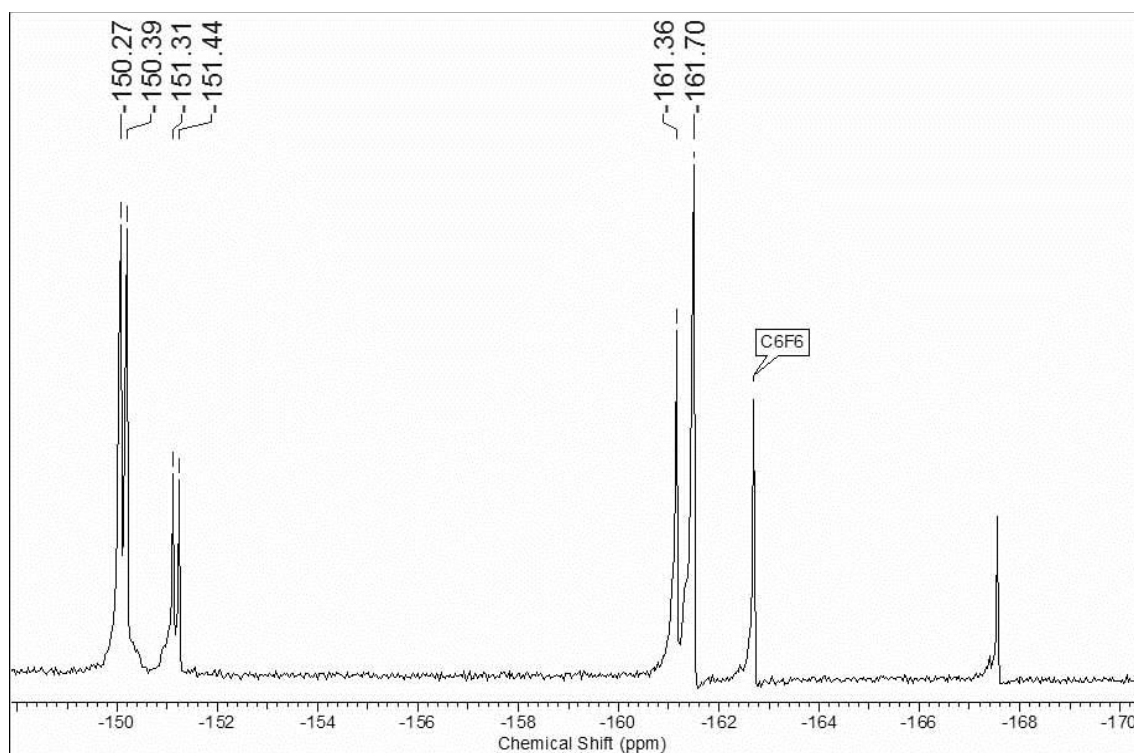
$^1\text{H-NMR}$ of compound **3** $^1\text{H-NMR}$ of compound **20b**

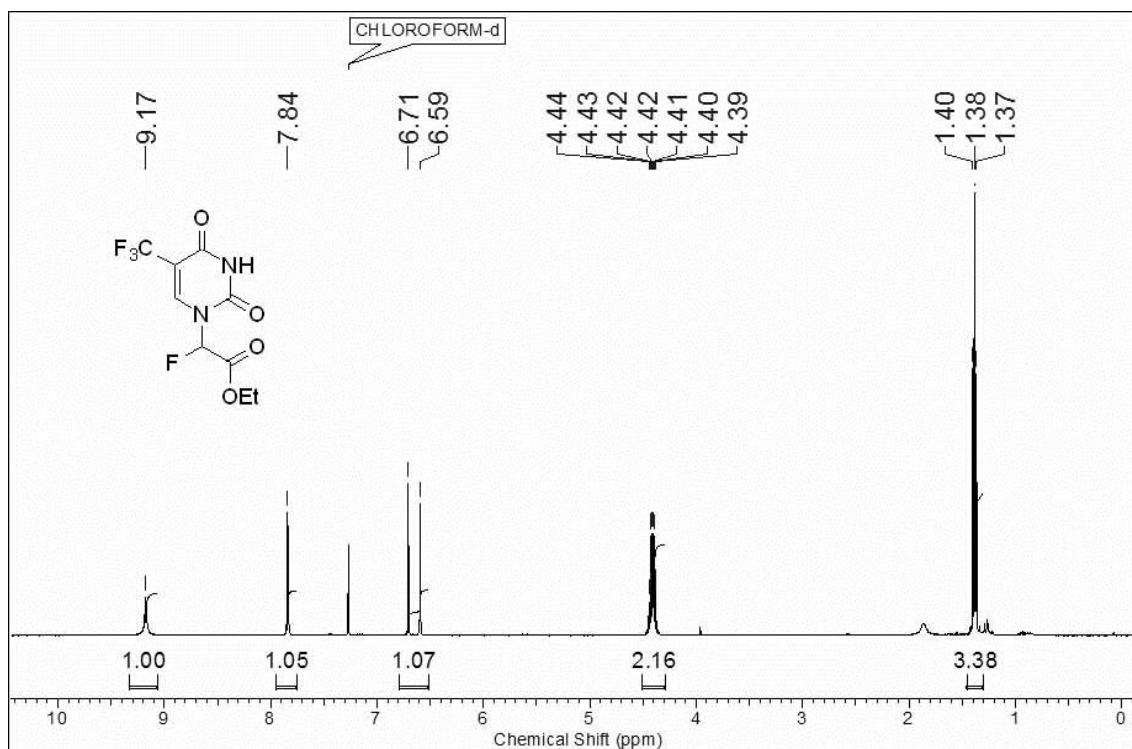
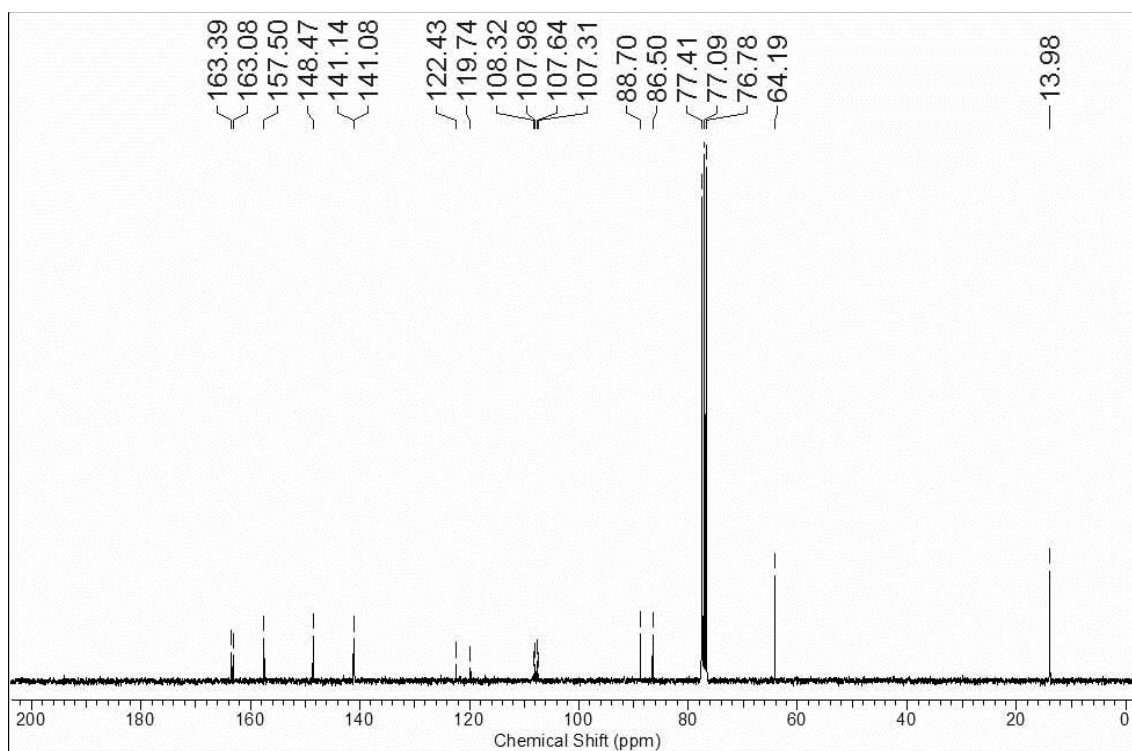
^{13}C -NMR of compound **20b** ^{19}F -NMR of compound **20b**

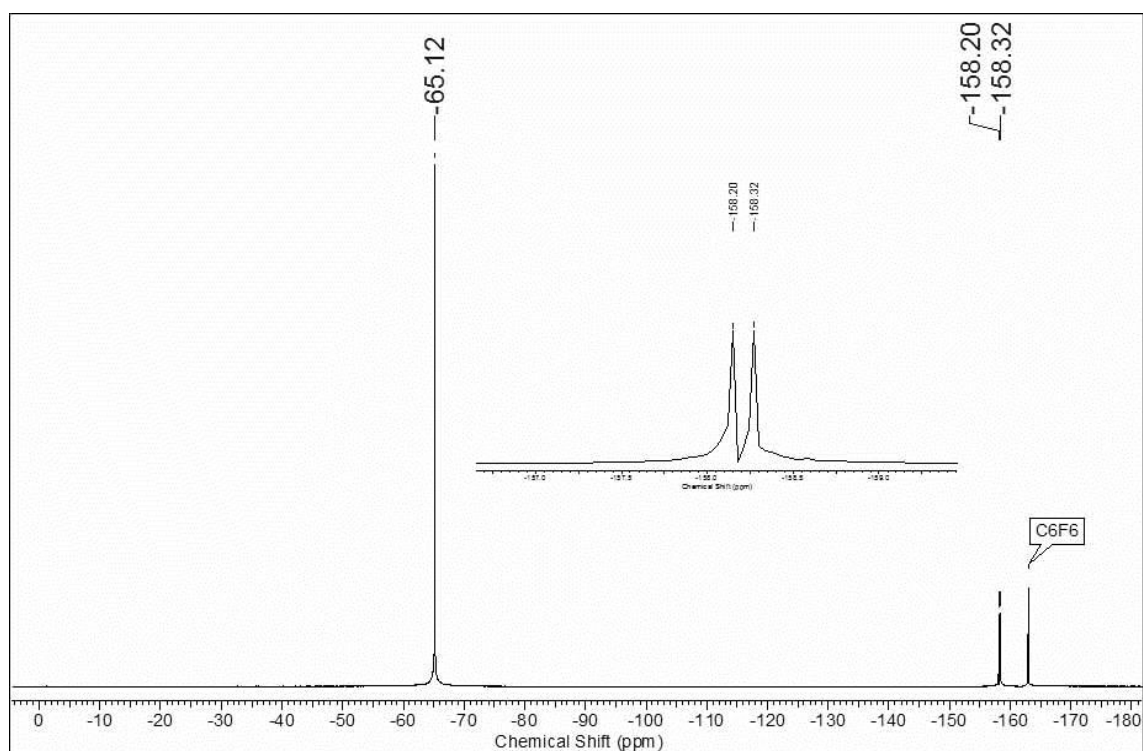
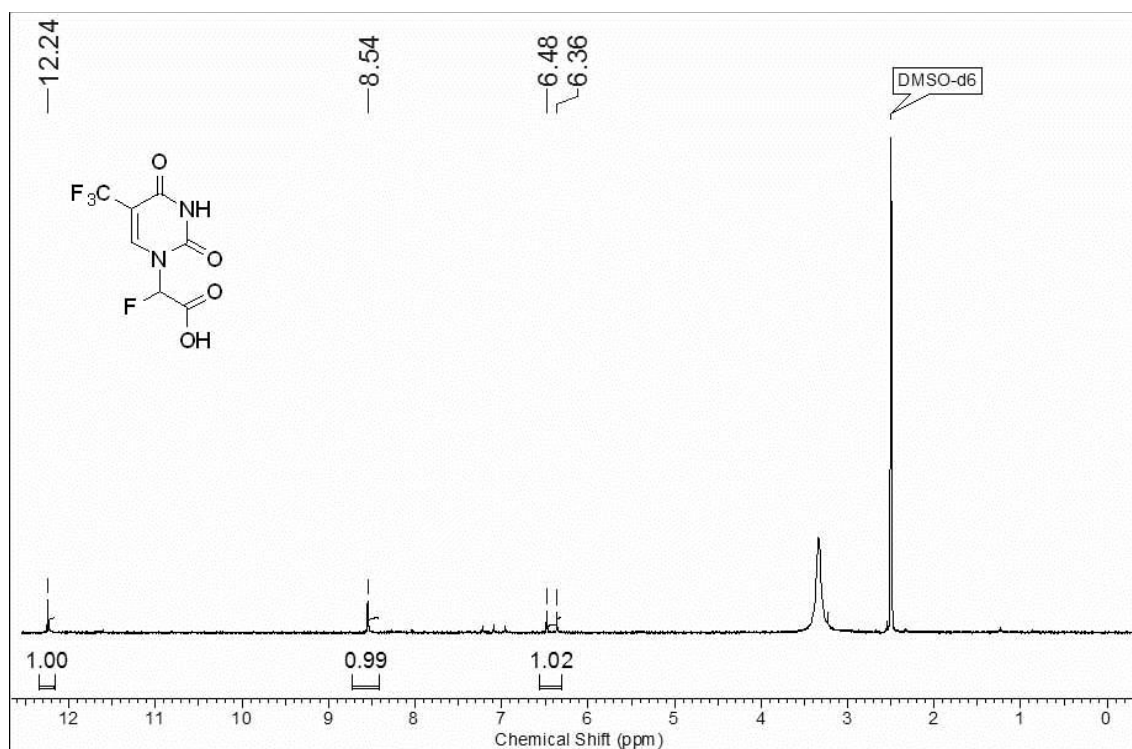
$^1\text{H-NMR}$ of compound **21b** $^{13}\text{C-NMR}$ of compound **21b**

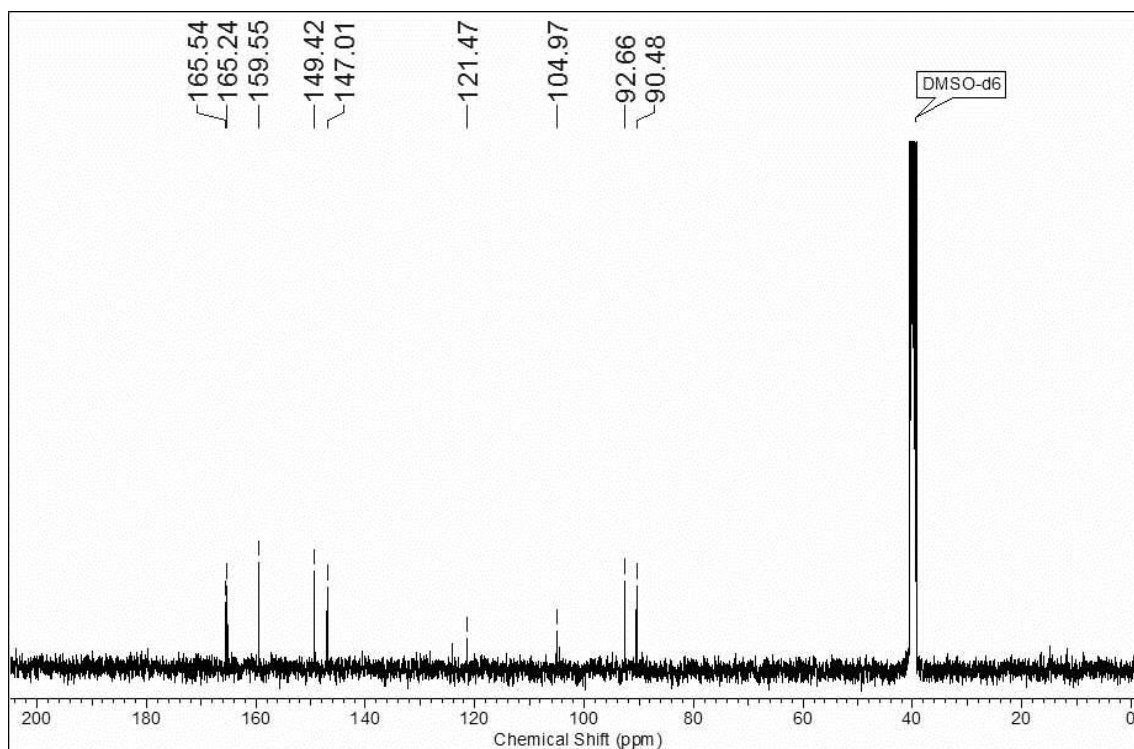
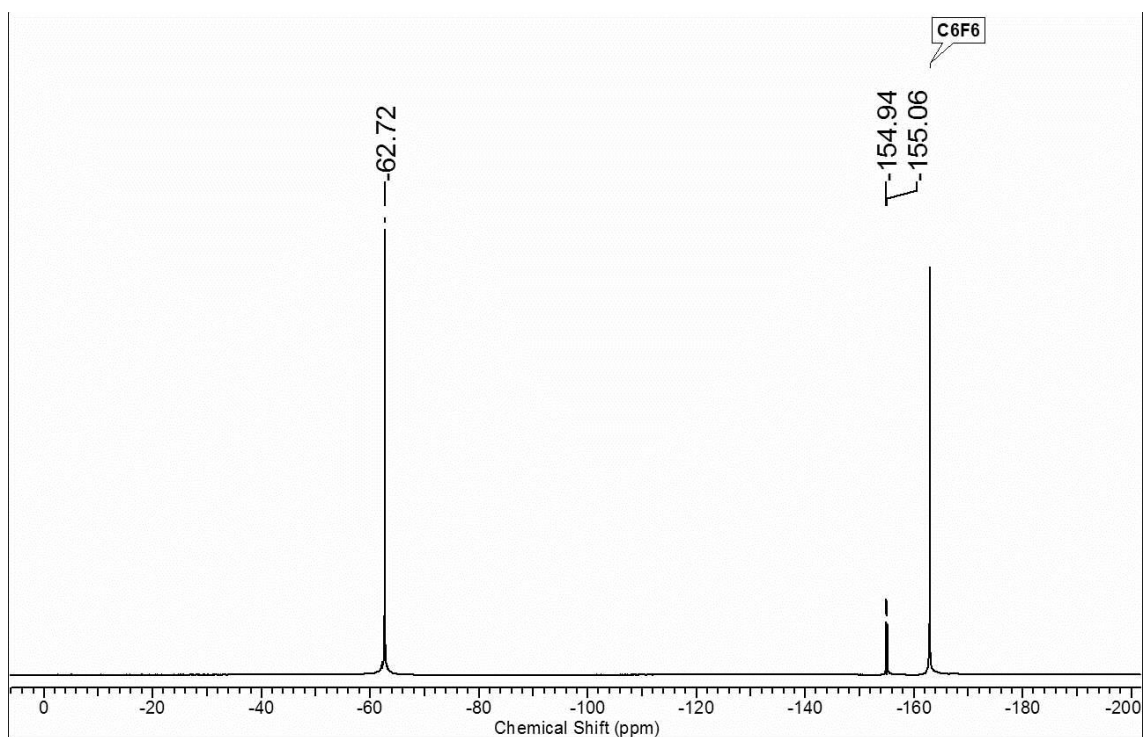
^{19}F -NMR of compound **21b** ^1H -NMR of compound **22b**

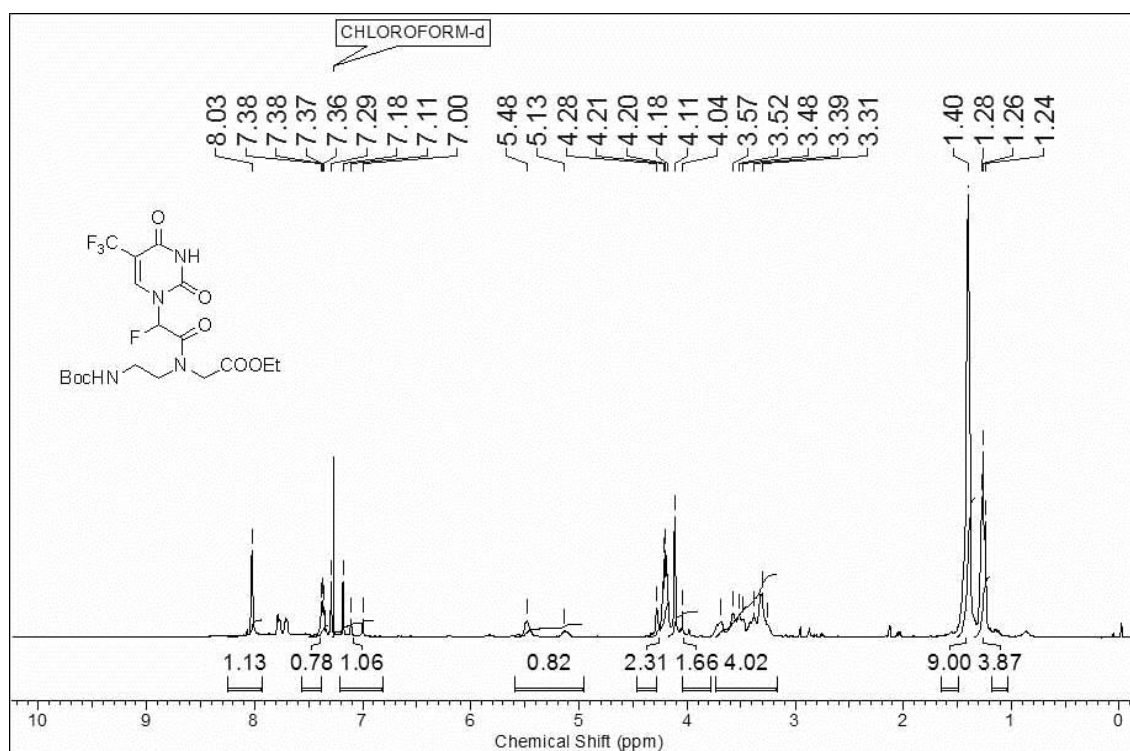
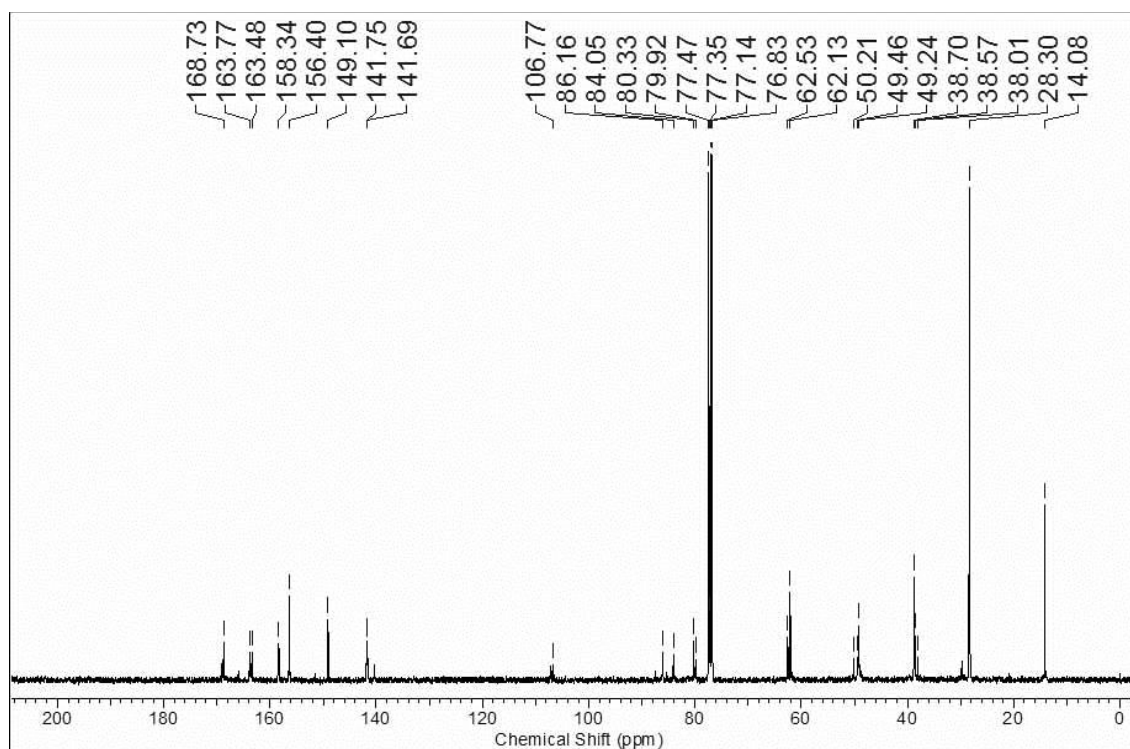
^{13}C -NMR of compound **22b** ^{19}F -NMR of compound **22b**

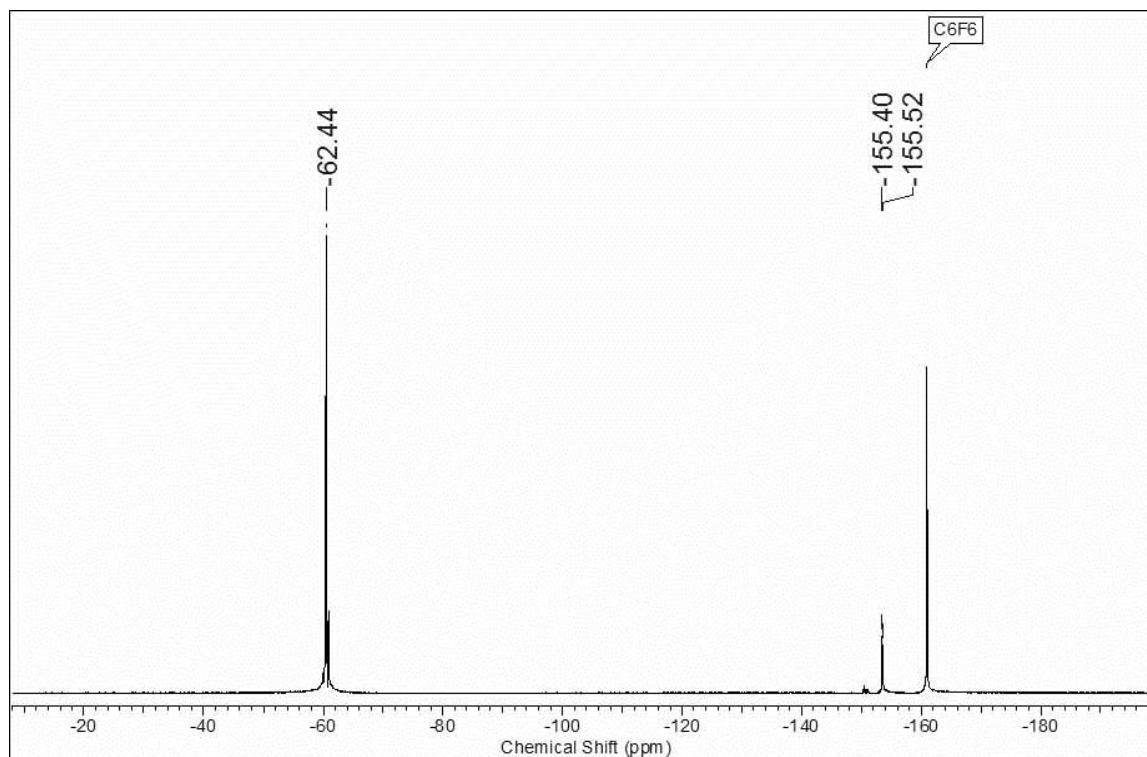
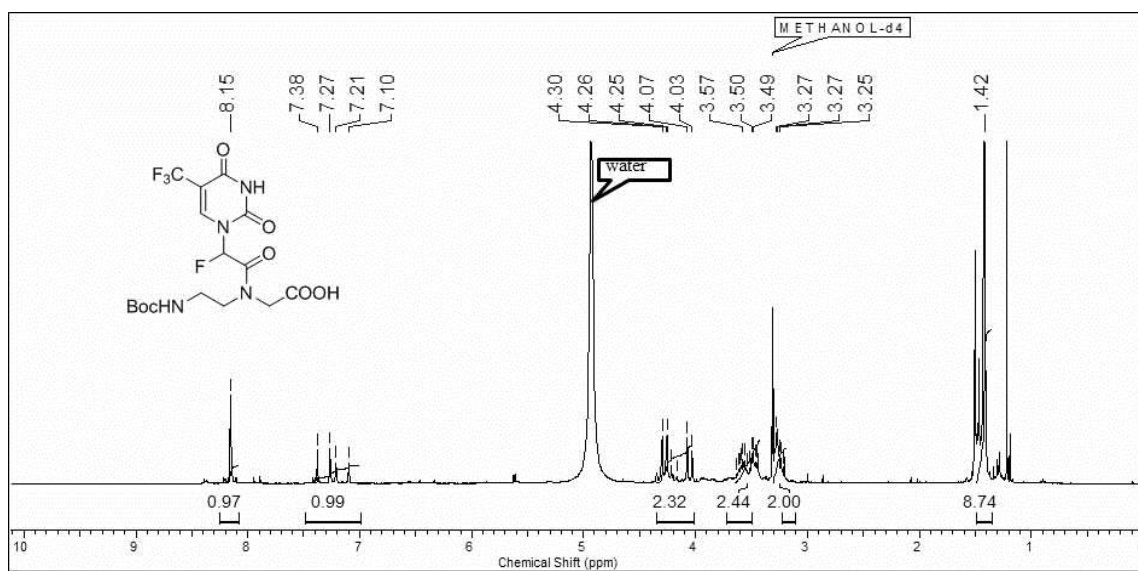
$^1\text{H-NMR}$ of compound 4 $^{19}\text{F-NMR}$ of compound 4

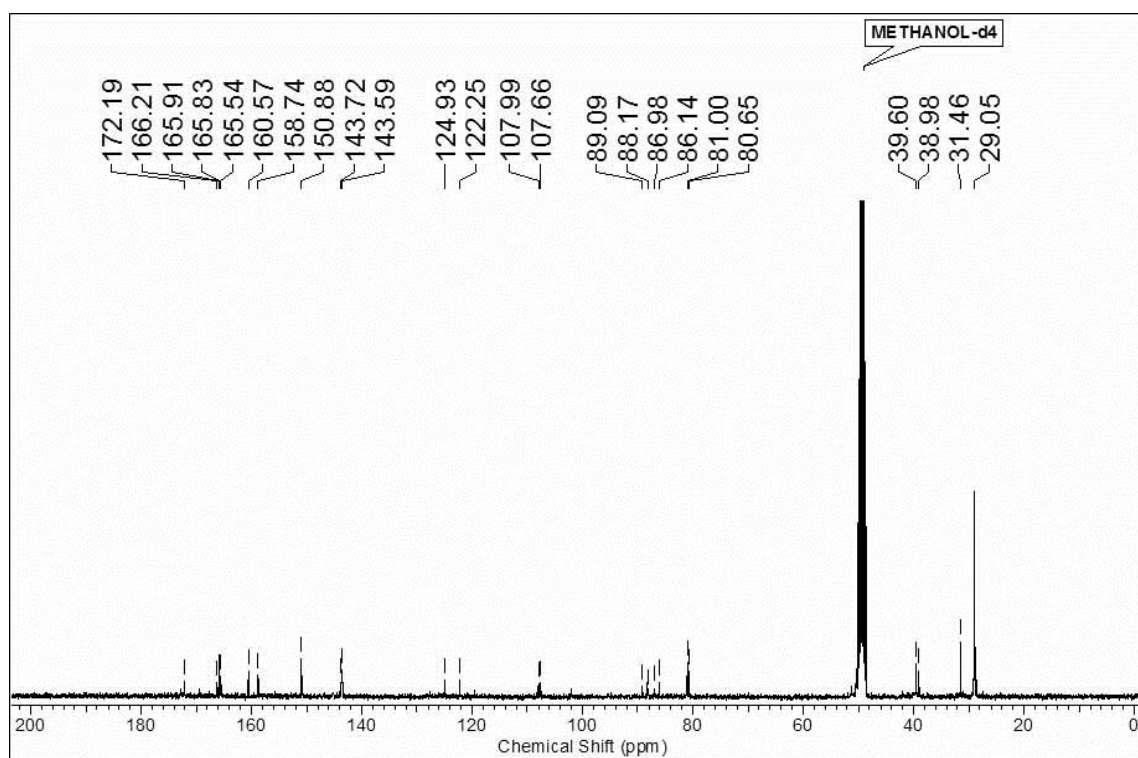
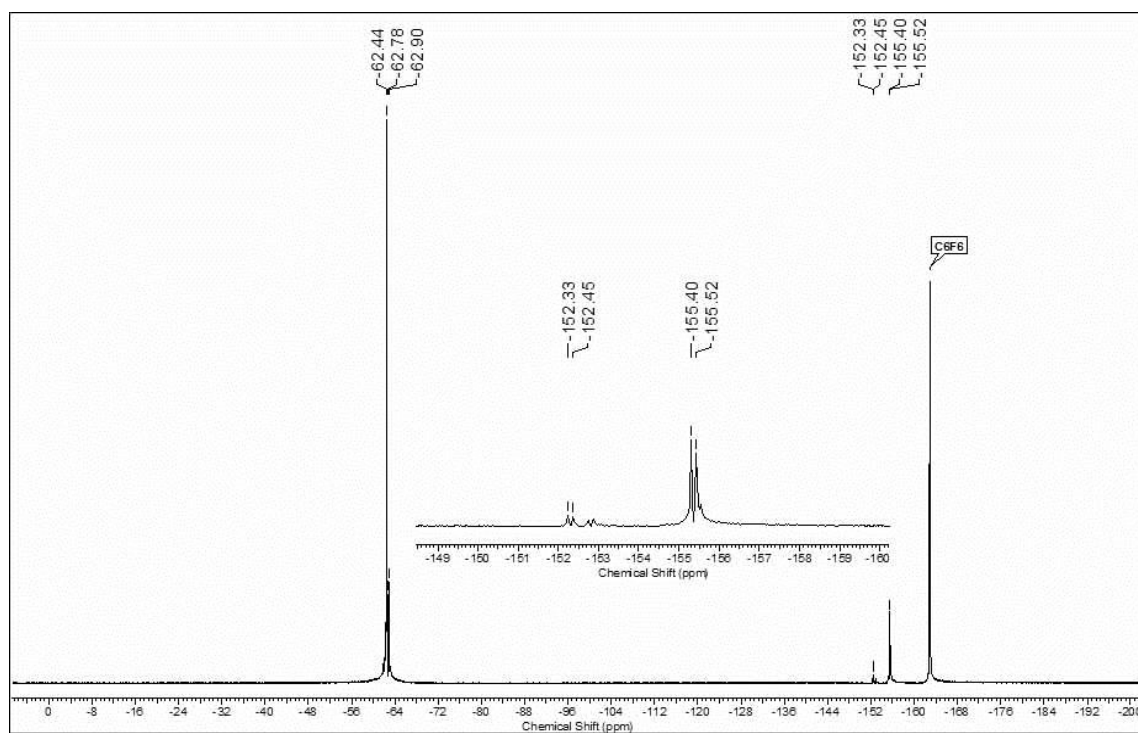
$^1\text{H-NMR}$ of compound **20c** $^{13}\text{C-NMR}$ of compound **20c**

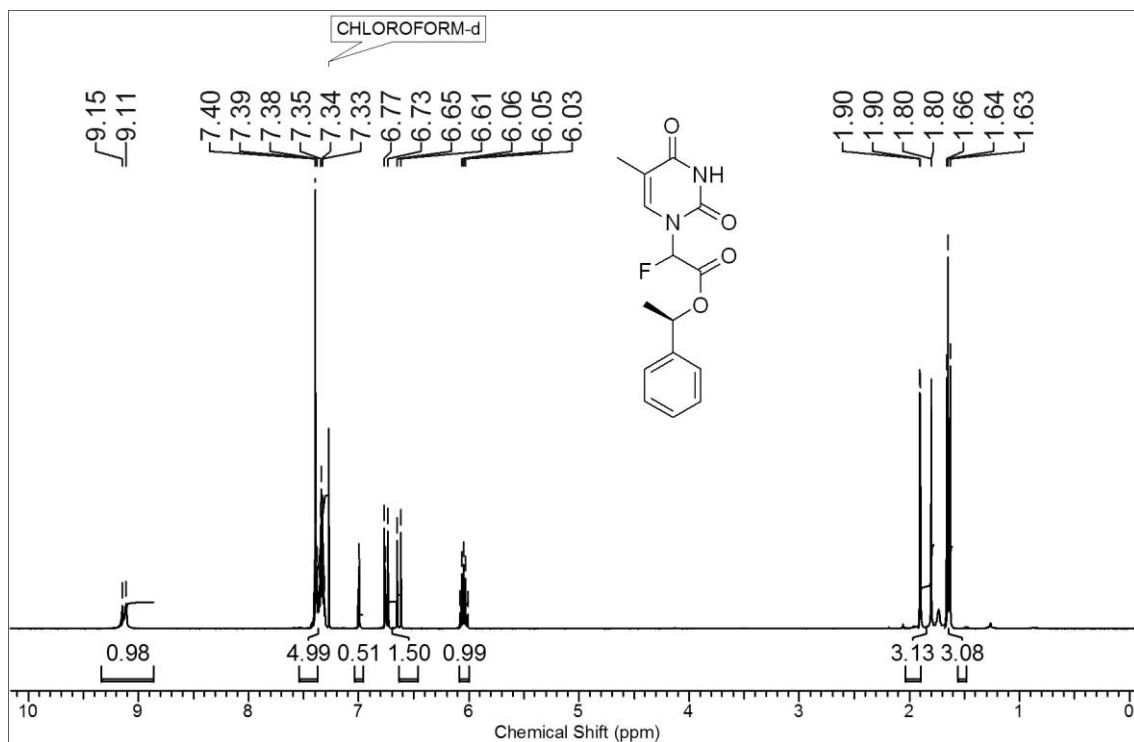
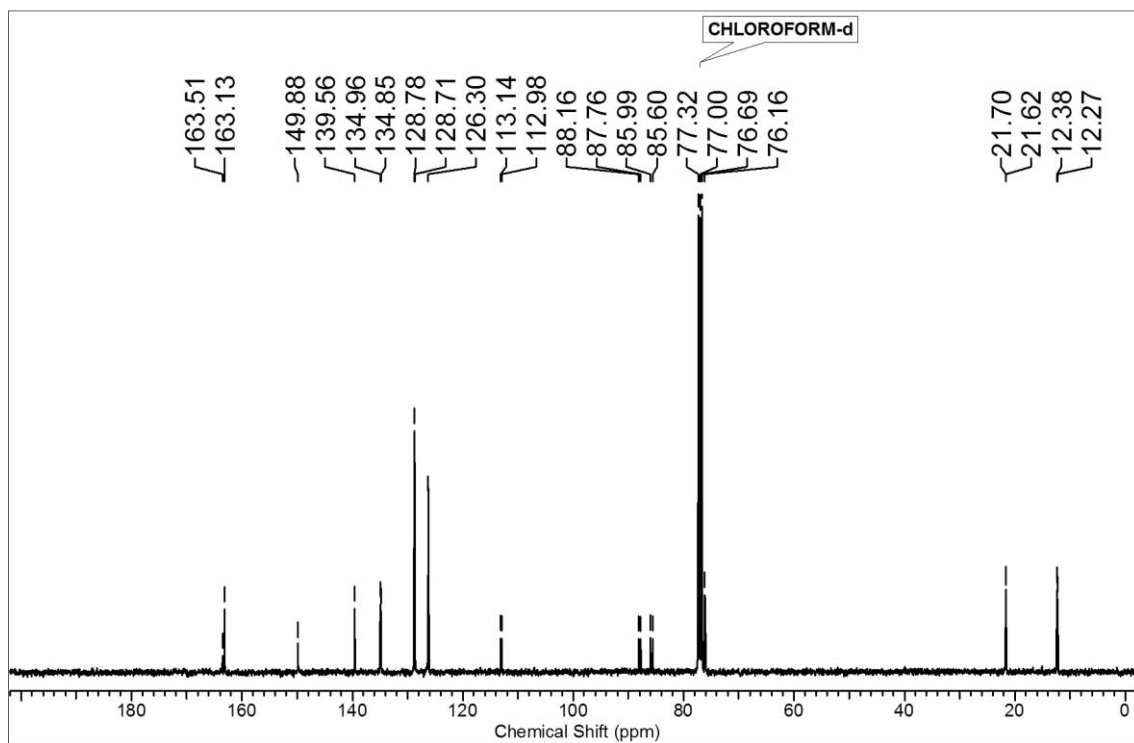
^{19}F -NMR of compound **20c** ^1H -NMR of compound **21c**

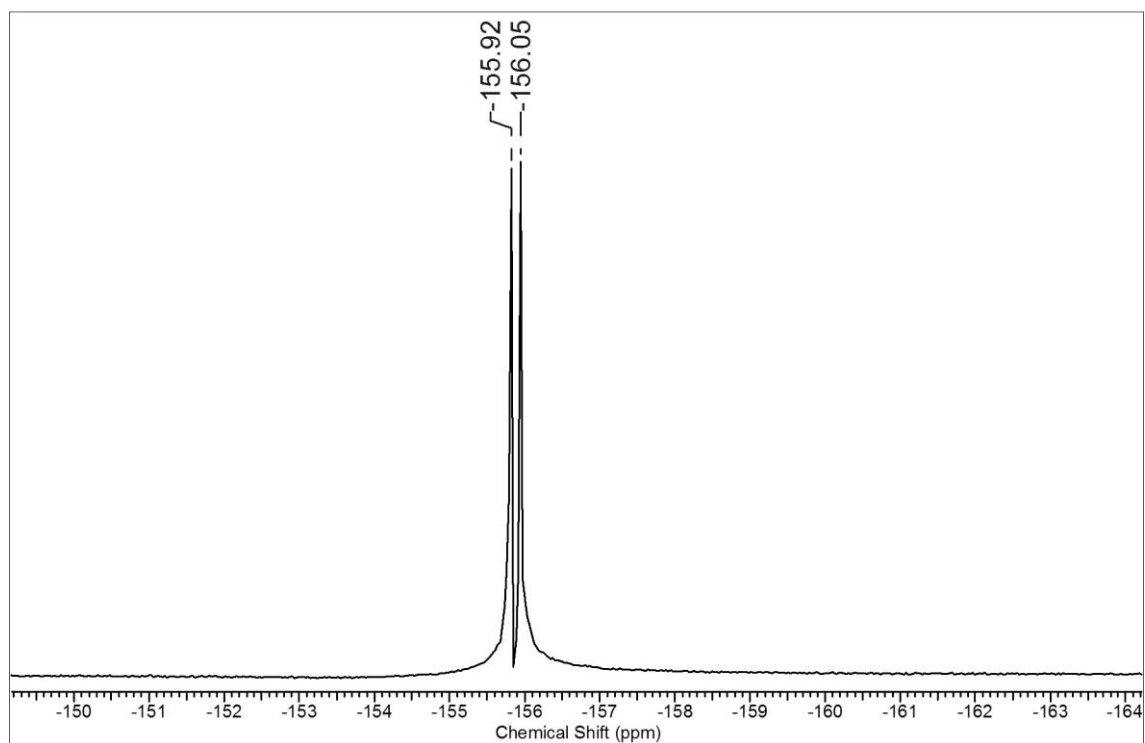
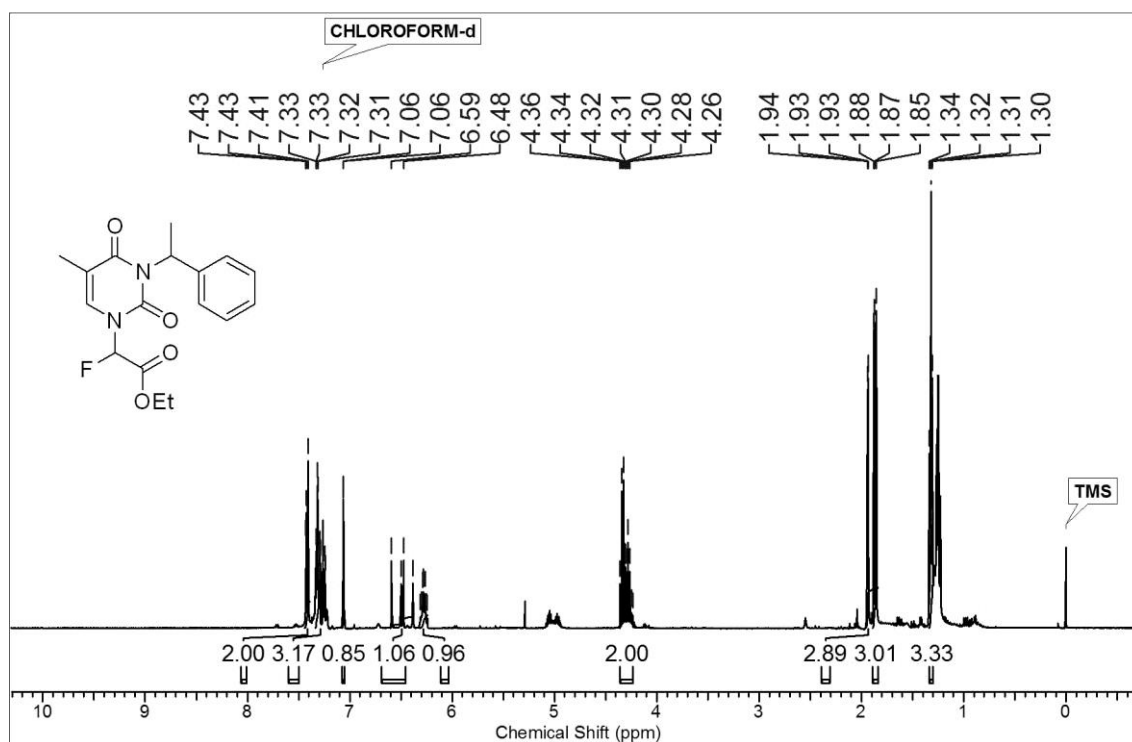
^{13}C -NMR of compound **21c** ^{19}F -NMR of compound **21c**

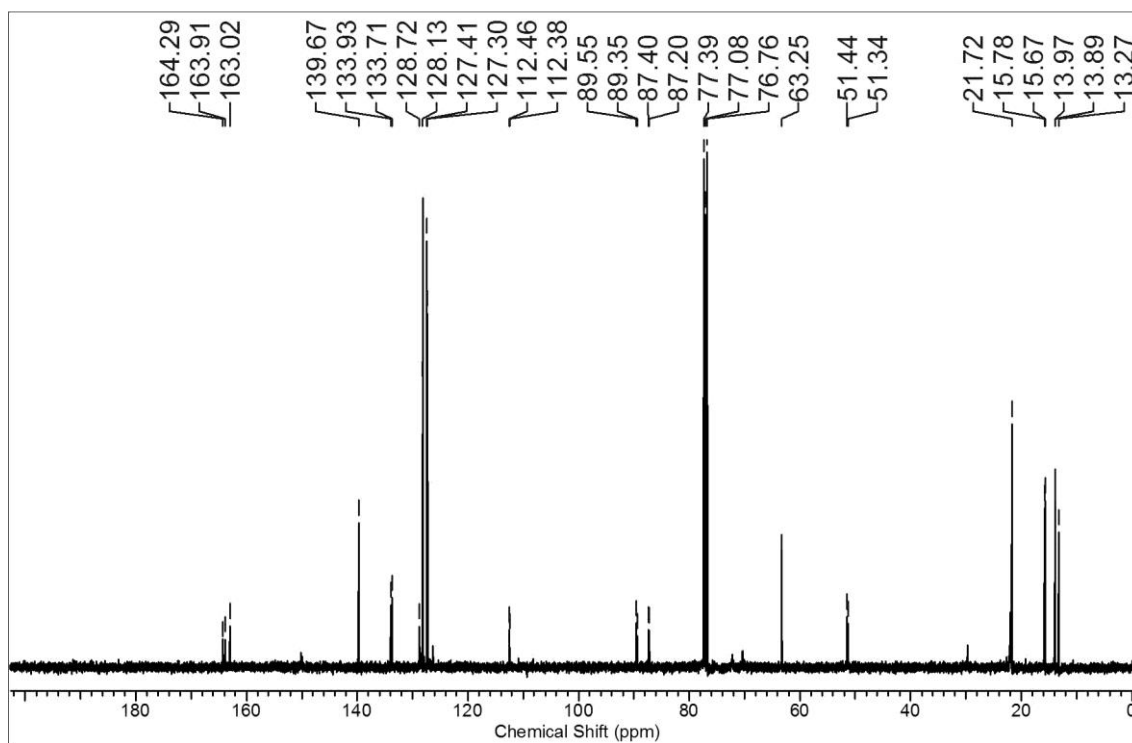
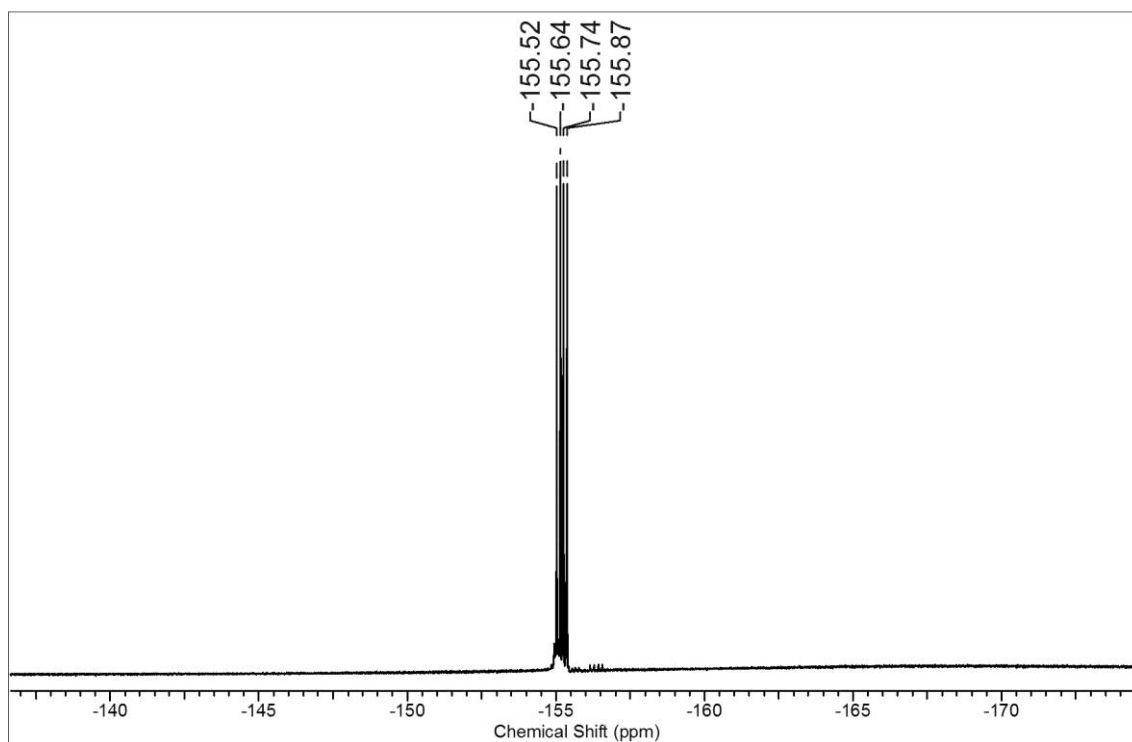
$^1\text{H-NMR}$ of compound **22c** $^{13}\text{C-NMR}$ of compound **22c**

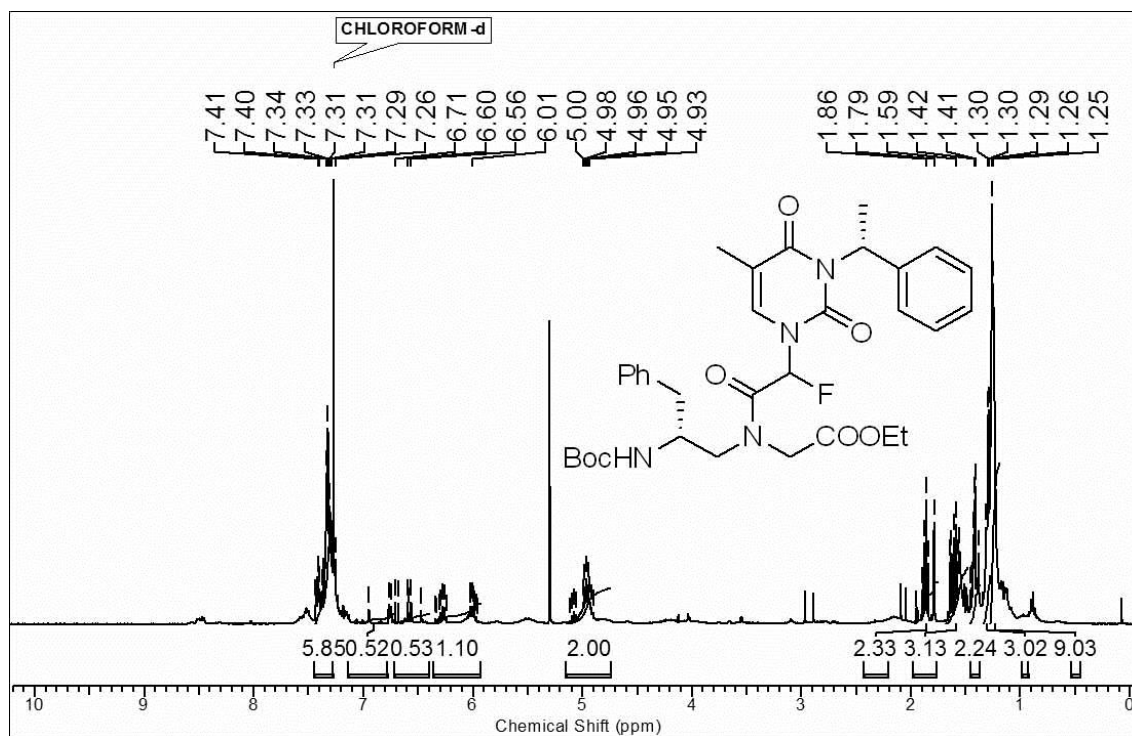
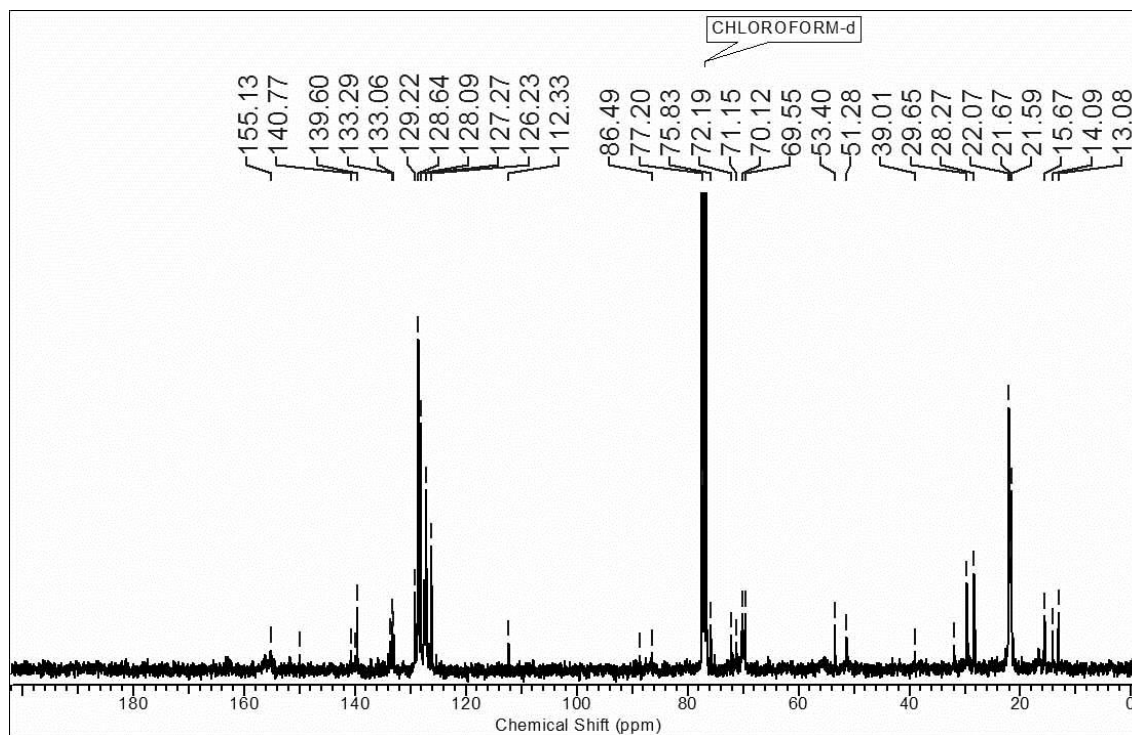
^{19}F -NMR of compound **22c** ^1H -NMR of compound **5**

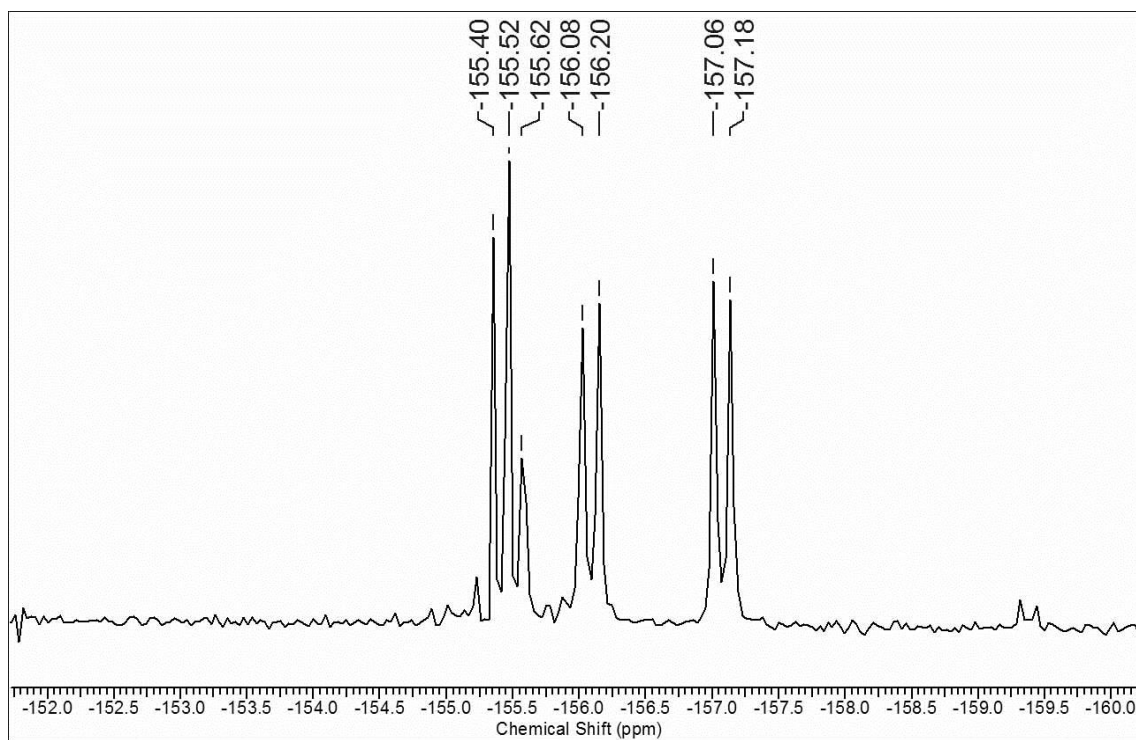
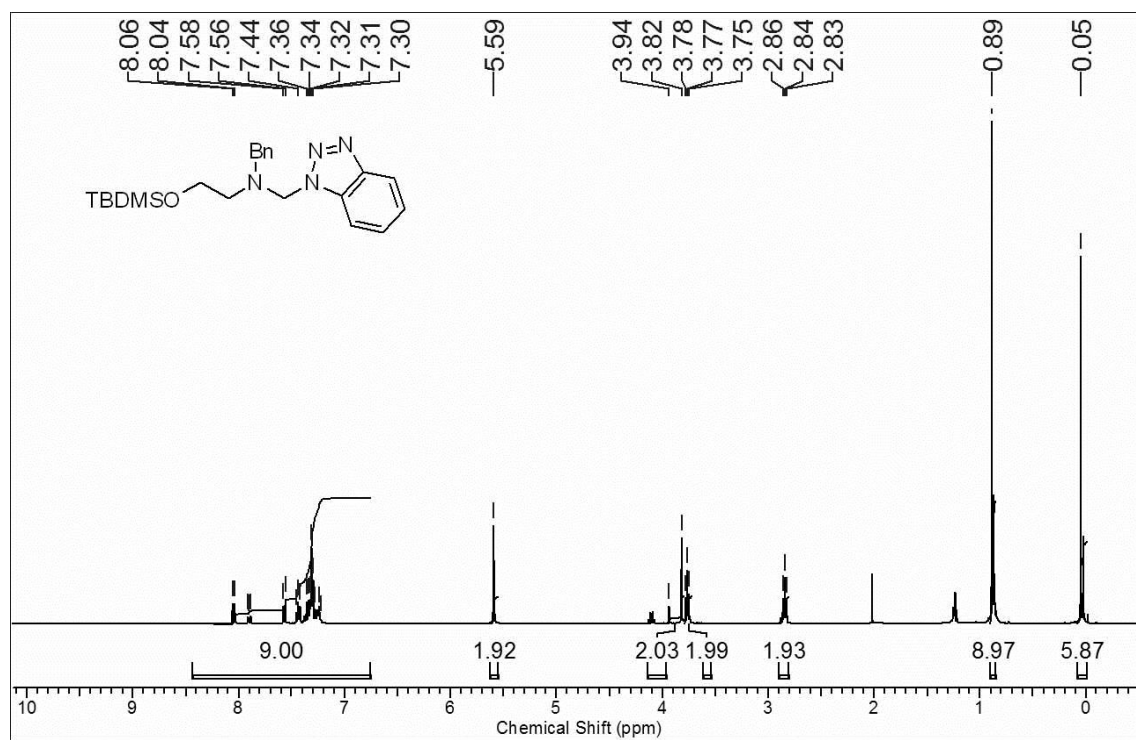
^{13}C -NMR of compound 5 ^{19}F -NMR of compound 5

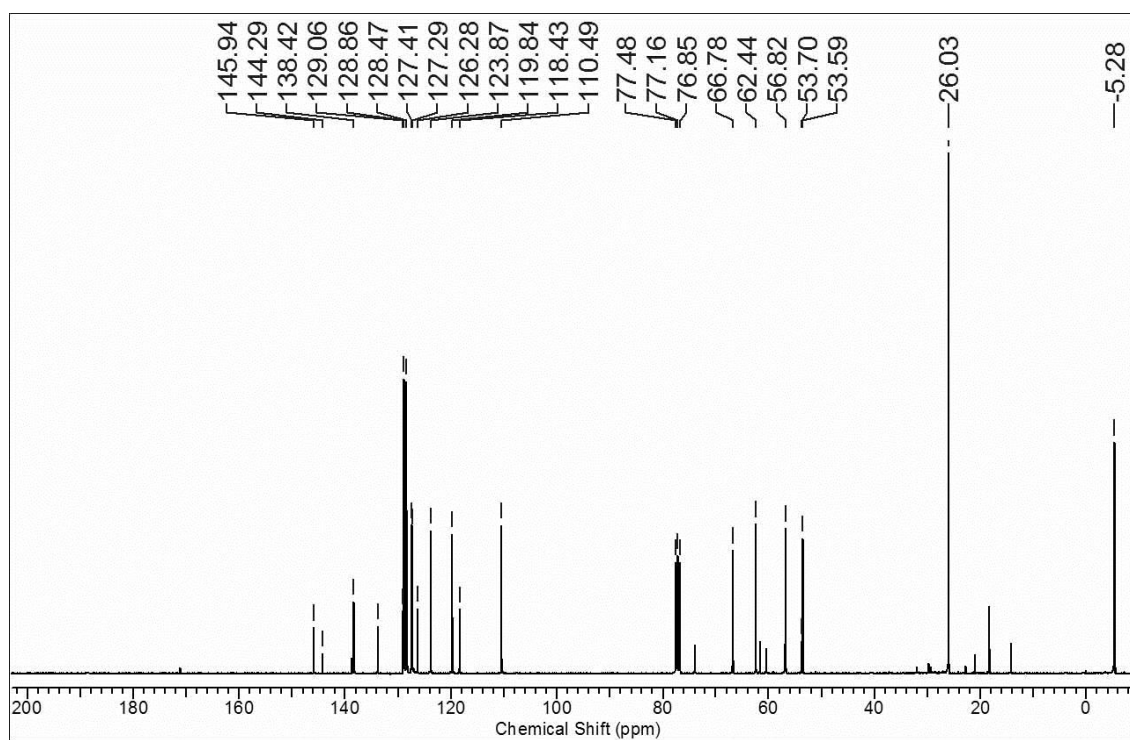
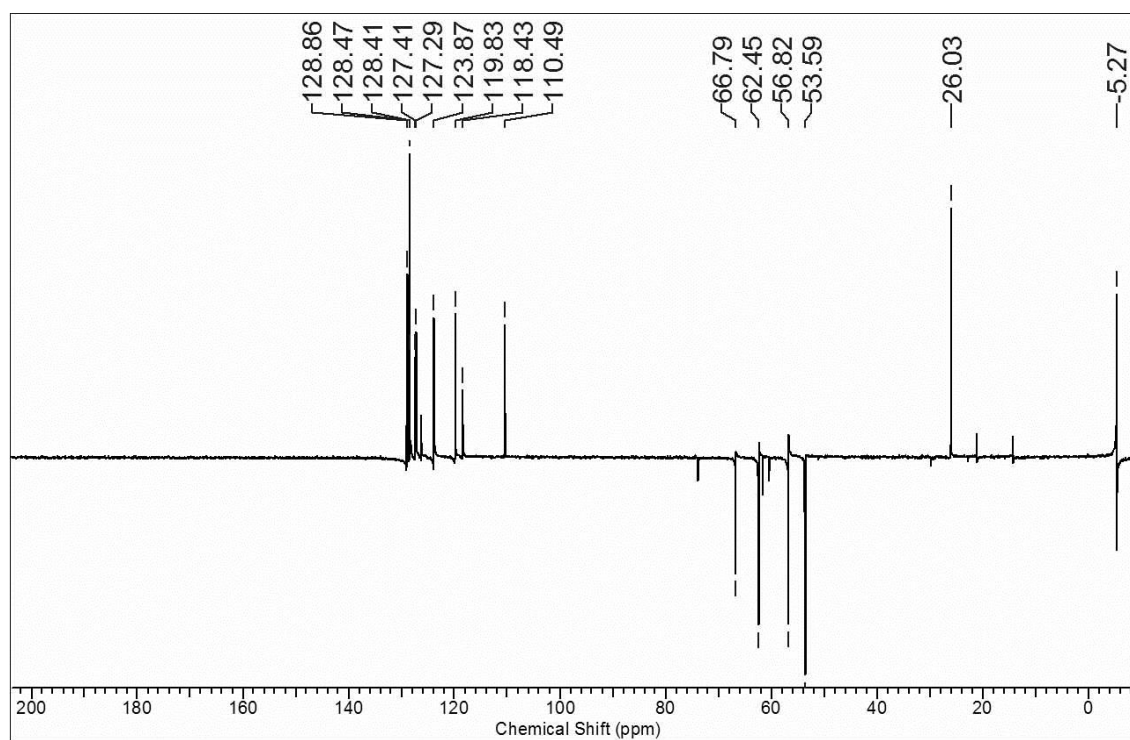
$^1\text{H-NMR}$ of compound **24** $^{13}\text{C-NMR}$ of compound **24**

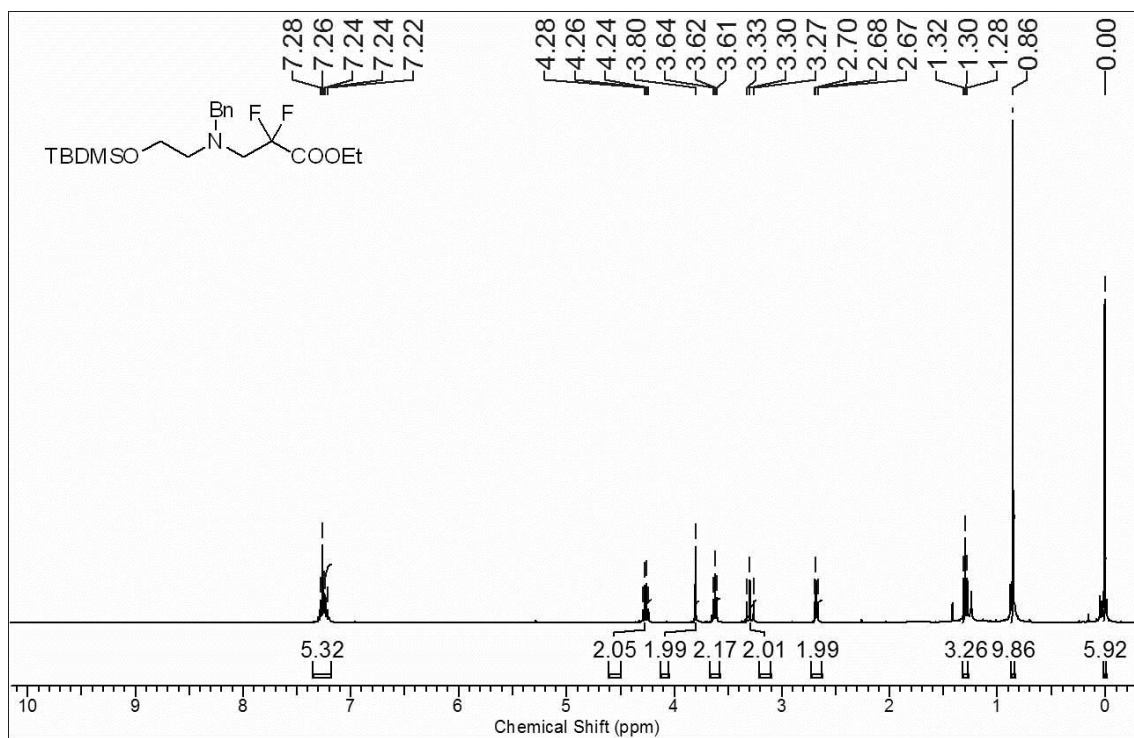
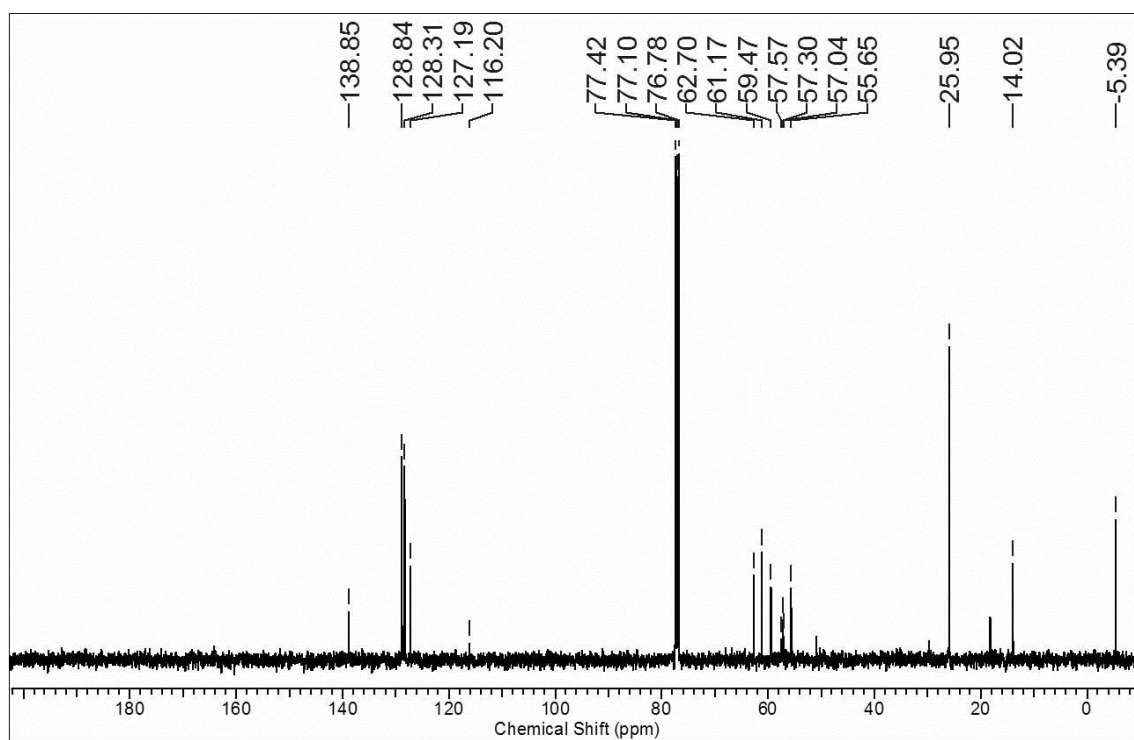
^{19}F -NMR of compound **24** ^1H -NMR of compound **25**

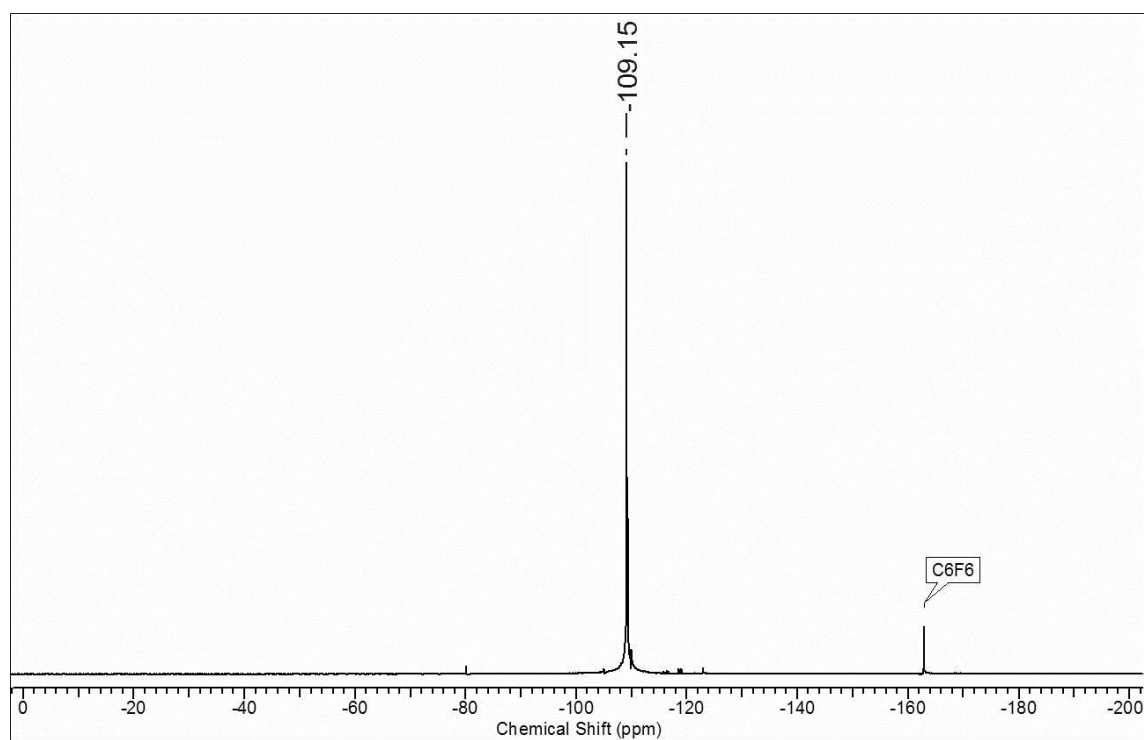
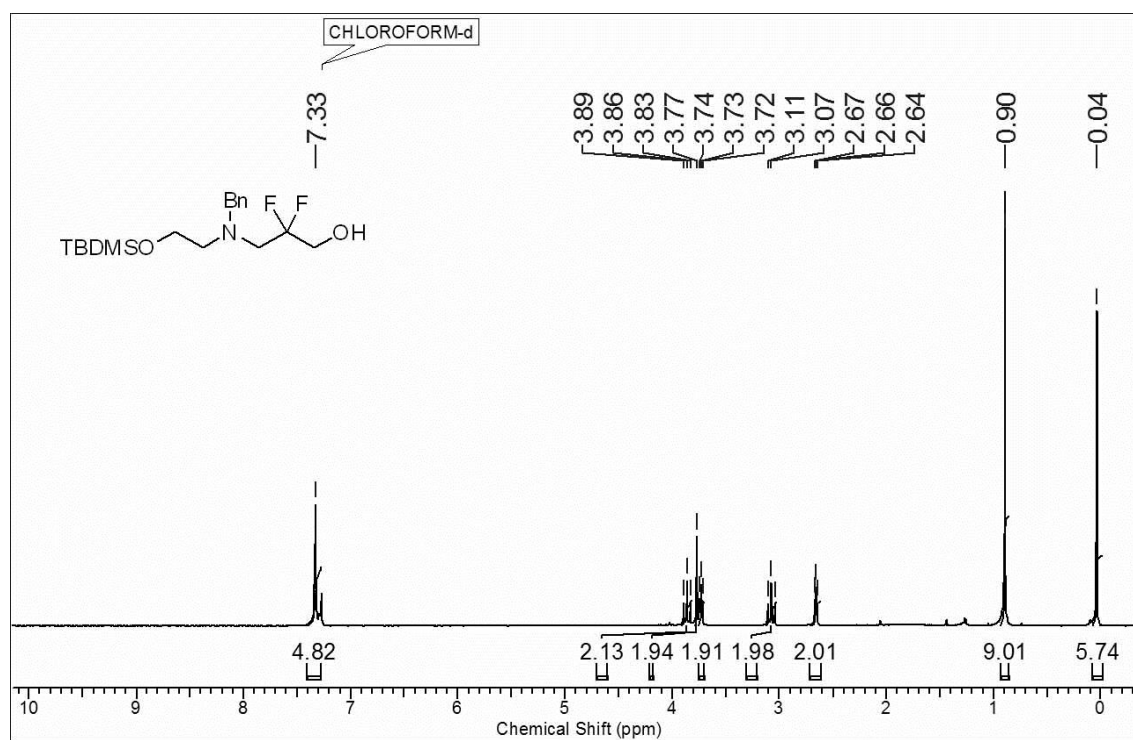
^{13}C -NMR of compound **25** ^{19}F -NMR of compound **25**

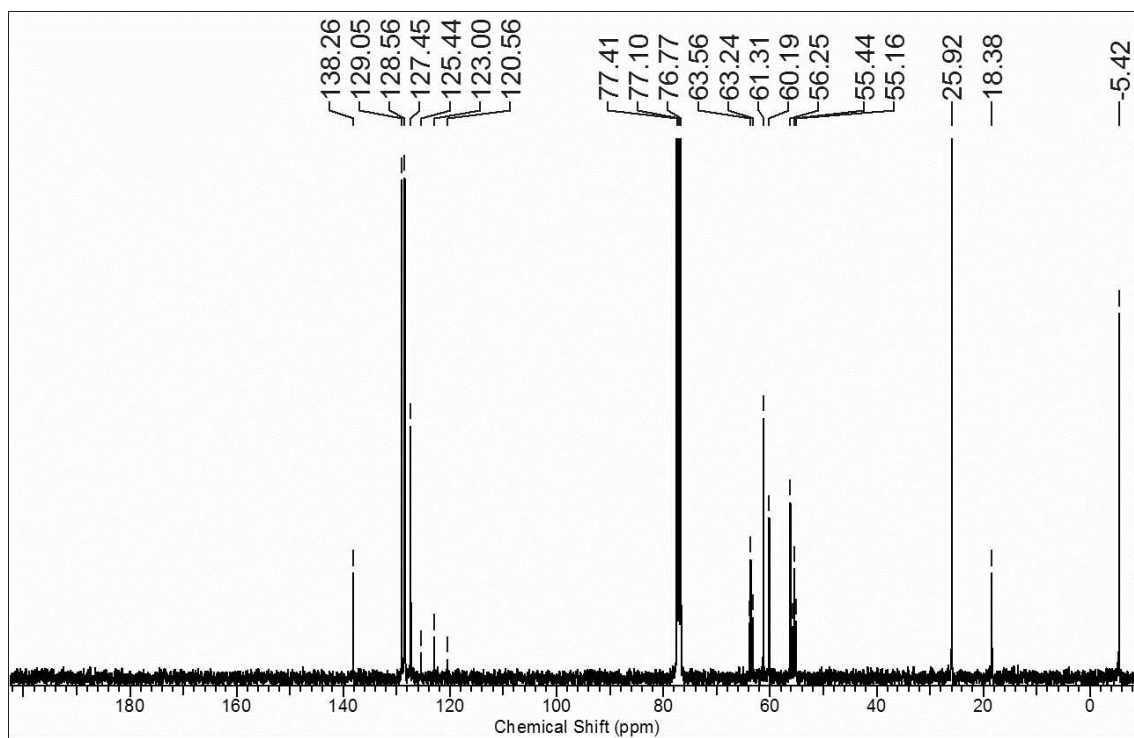
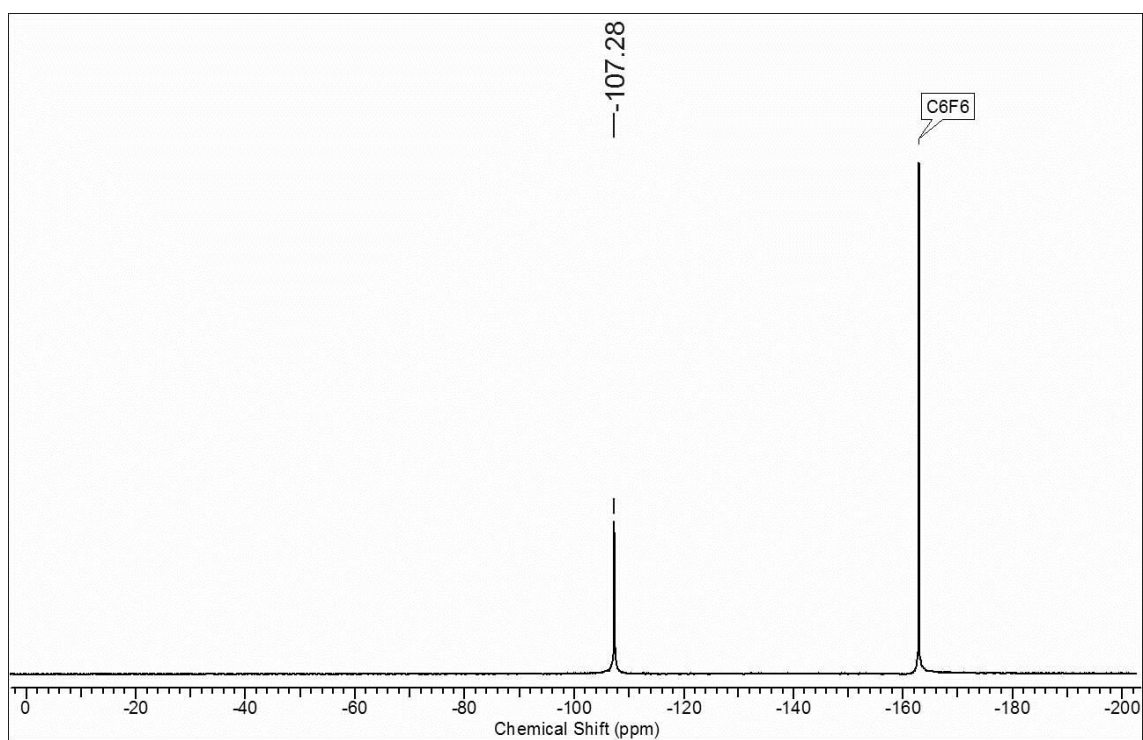
$^1\text{H-NMR}$ of compound **27** $^{13}\text{C-NMR}$ of compound **27**

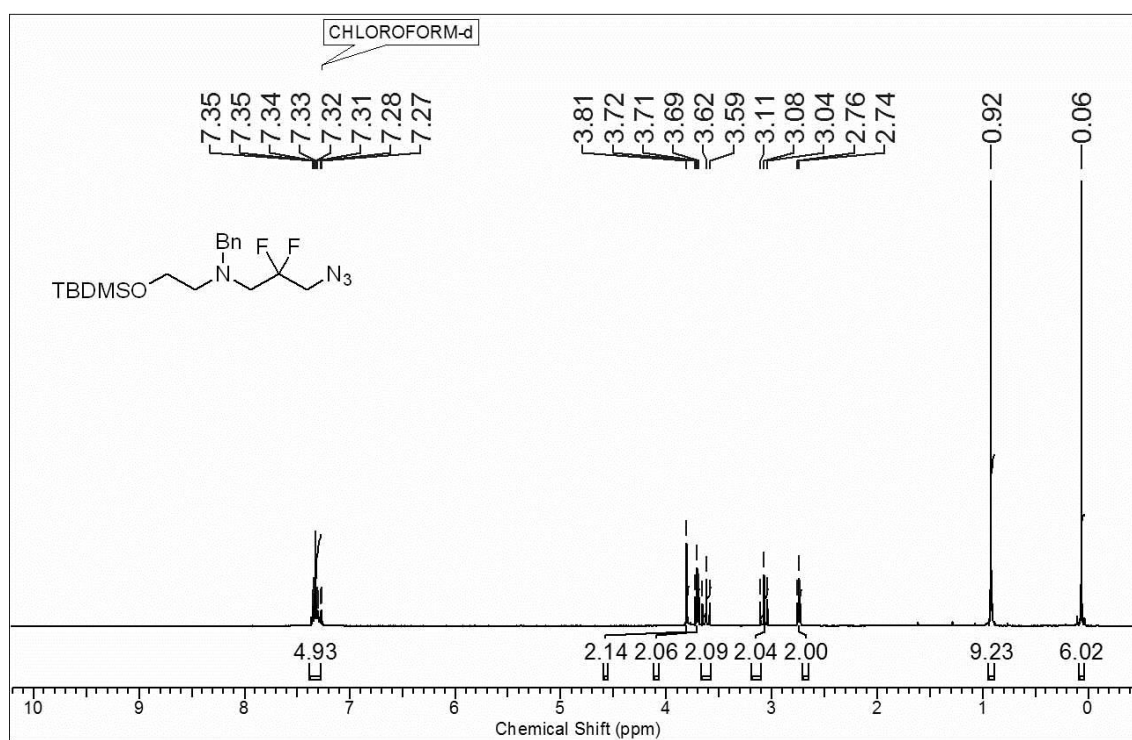
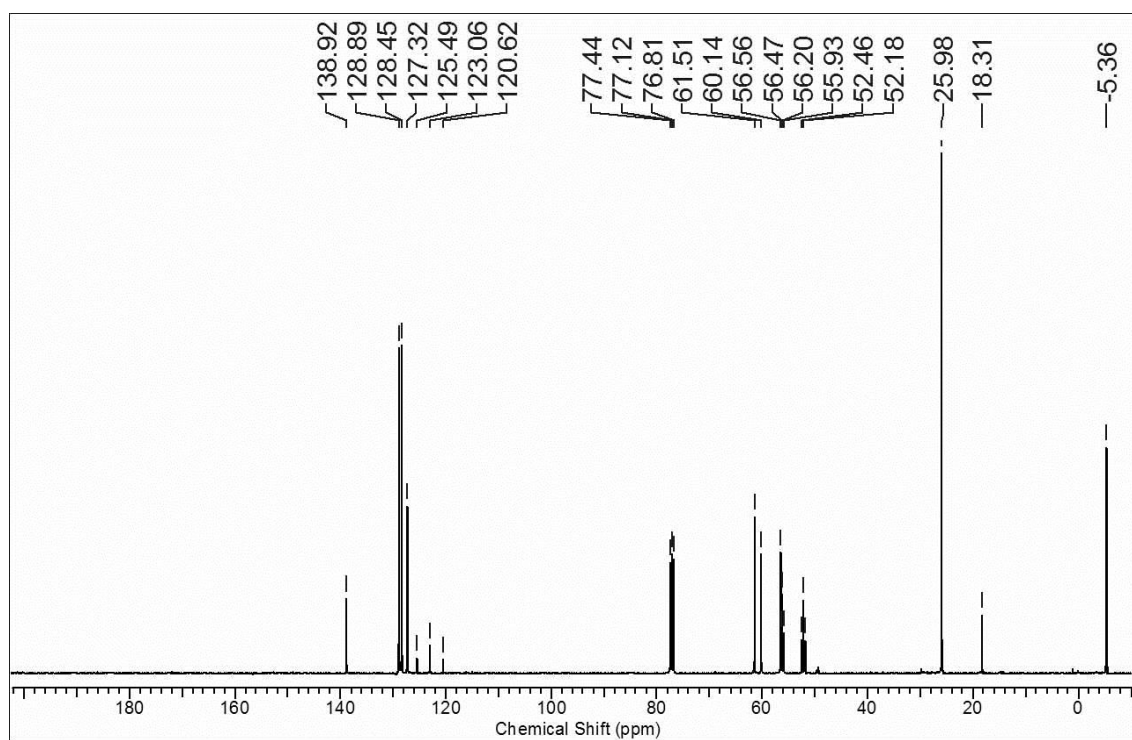
^{19}F -NMR of compound **27** ^1H -NMR of compound **31**

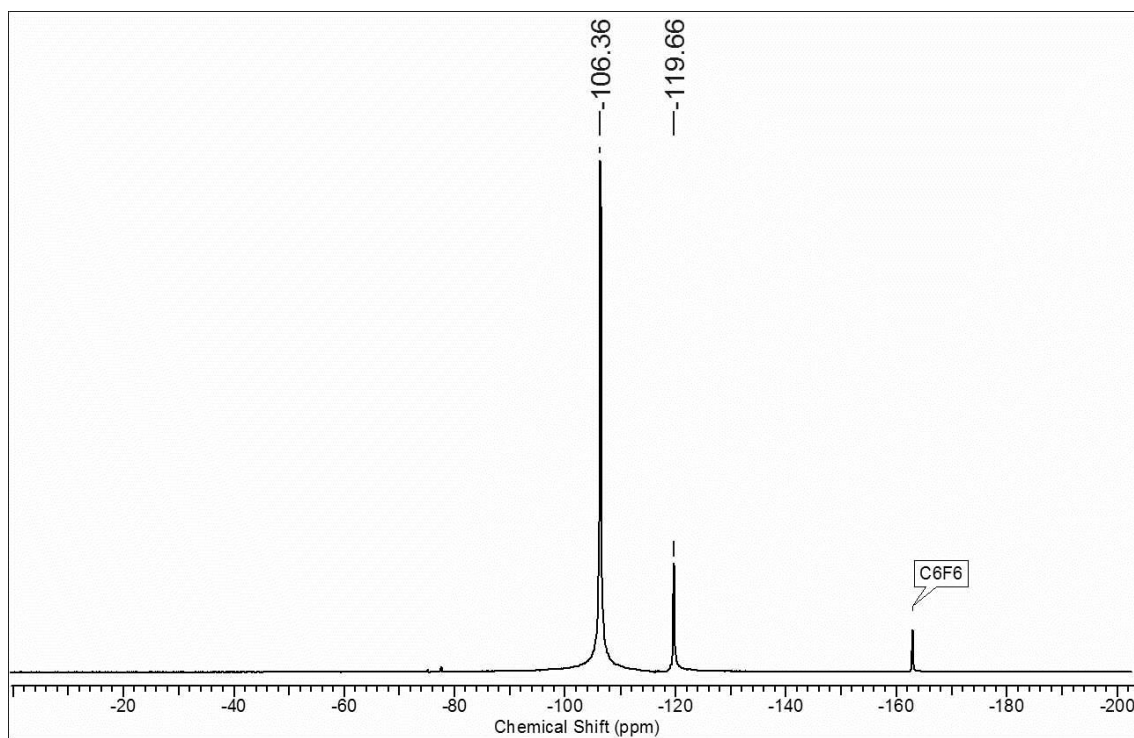
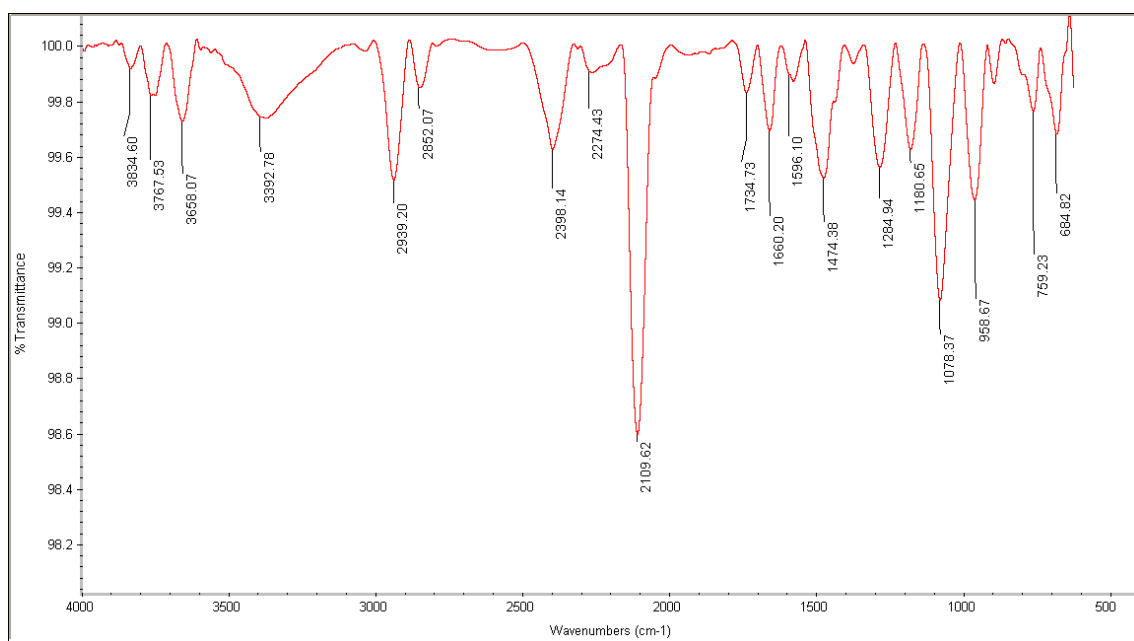
^{13}C -NMR of compound **31** ^{19}F -NMR of compound **31**

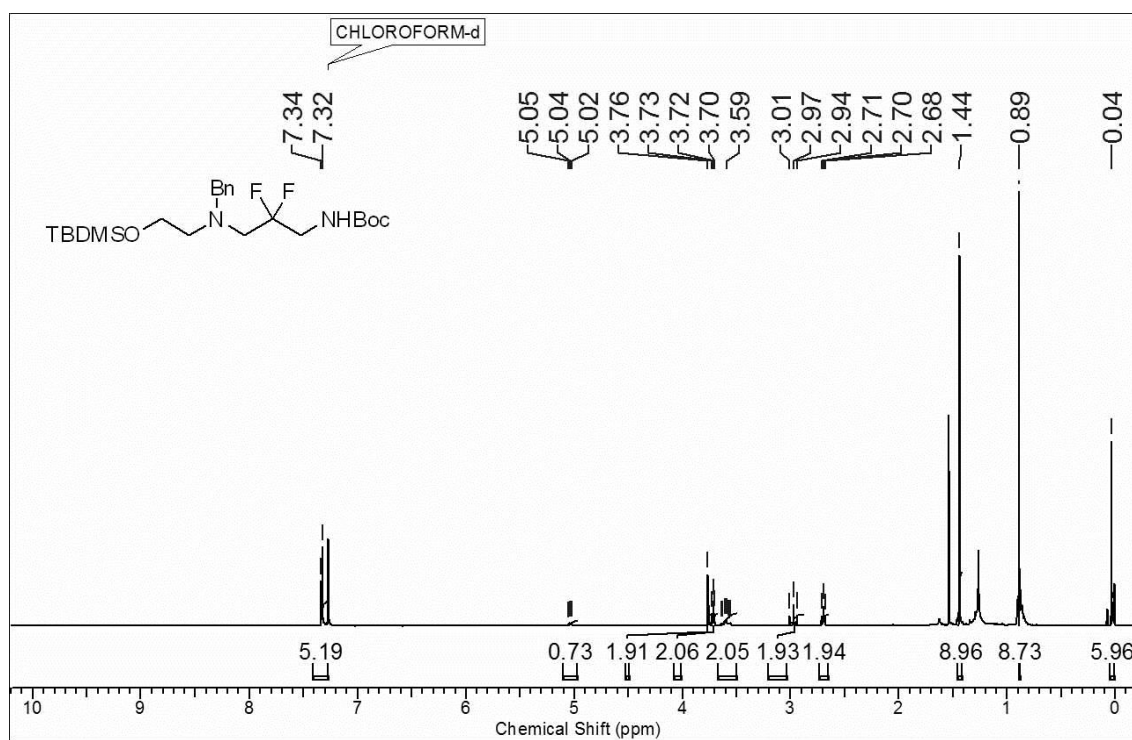
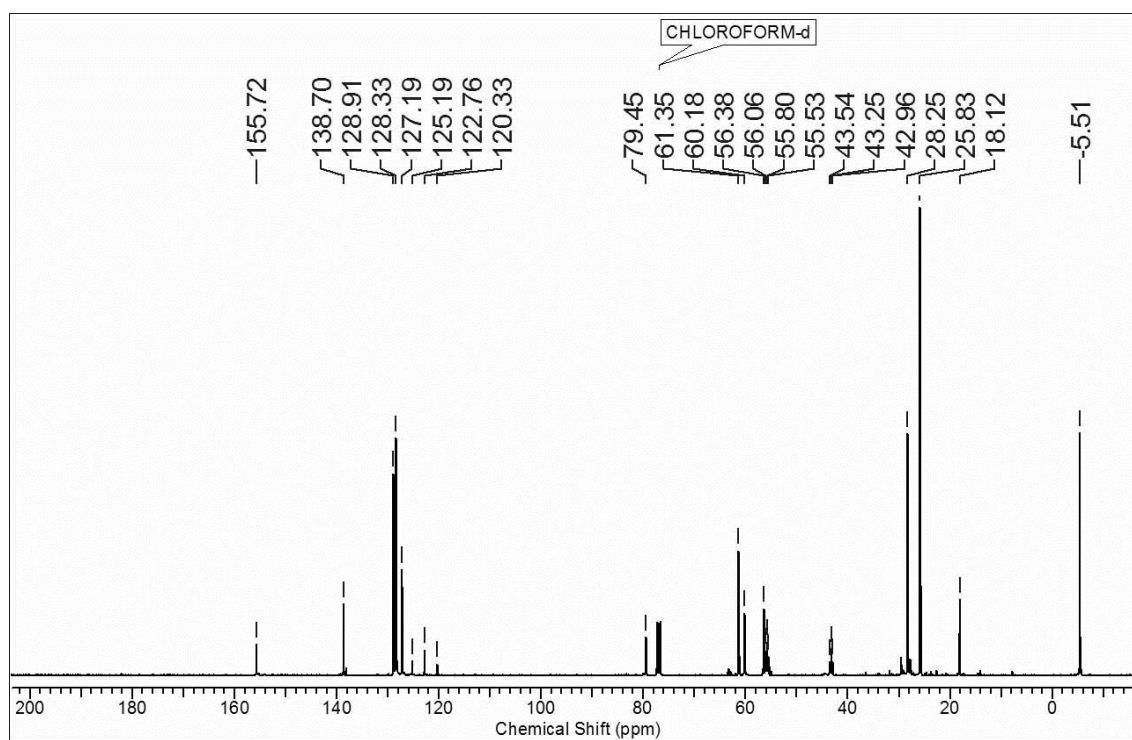
$^1\text{H-NMR}$ of compound **32** $^{13}\text{C-NMR}$ of compound **32**

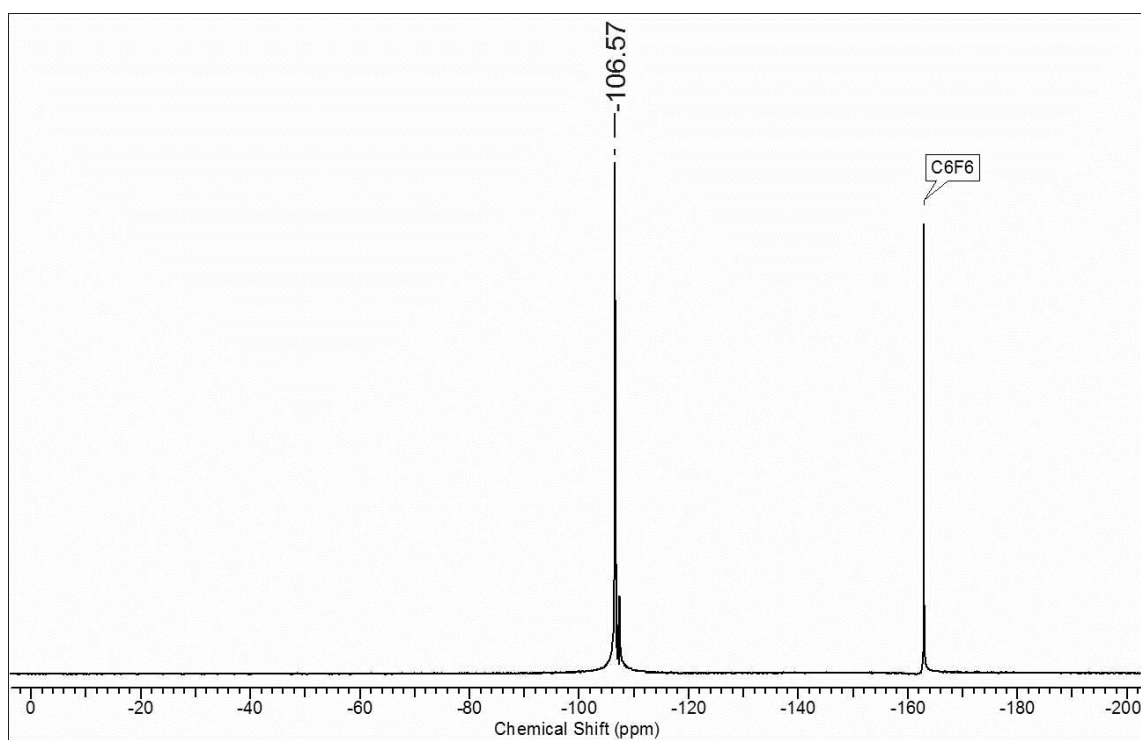
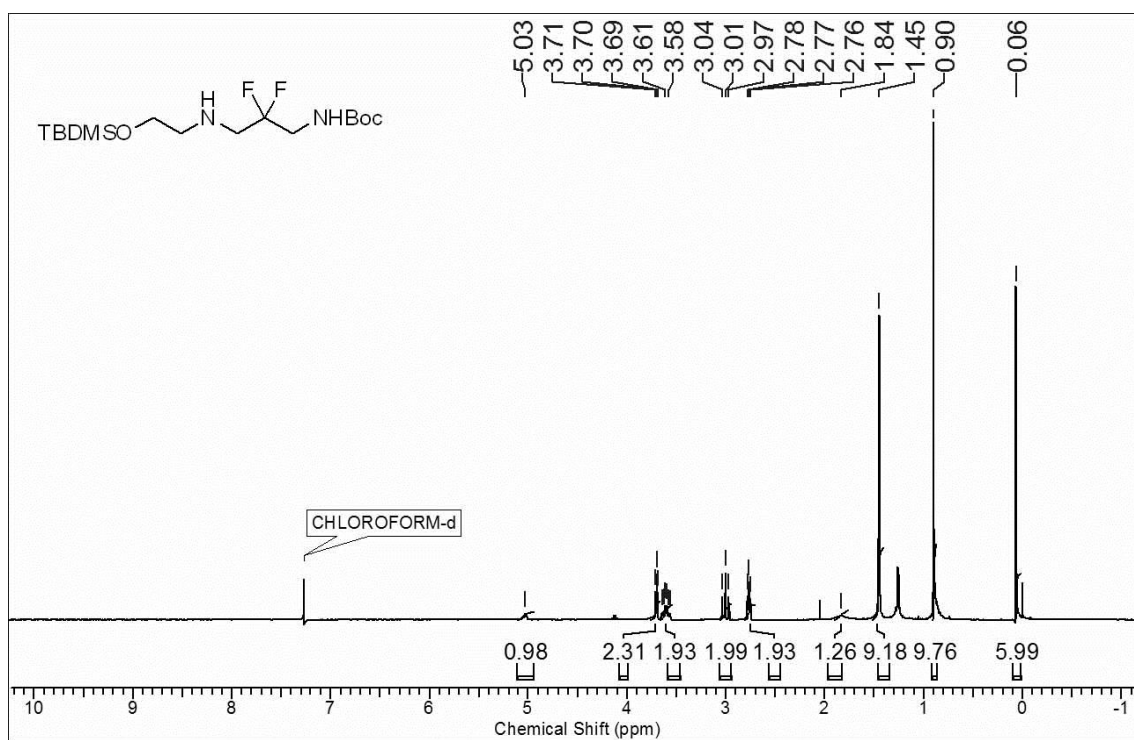
^{19}F -NMR of compound **32** ^1H -NMR of compound **33**

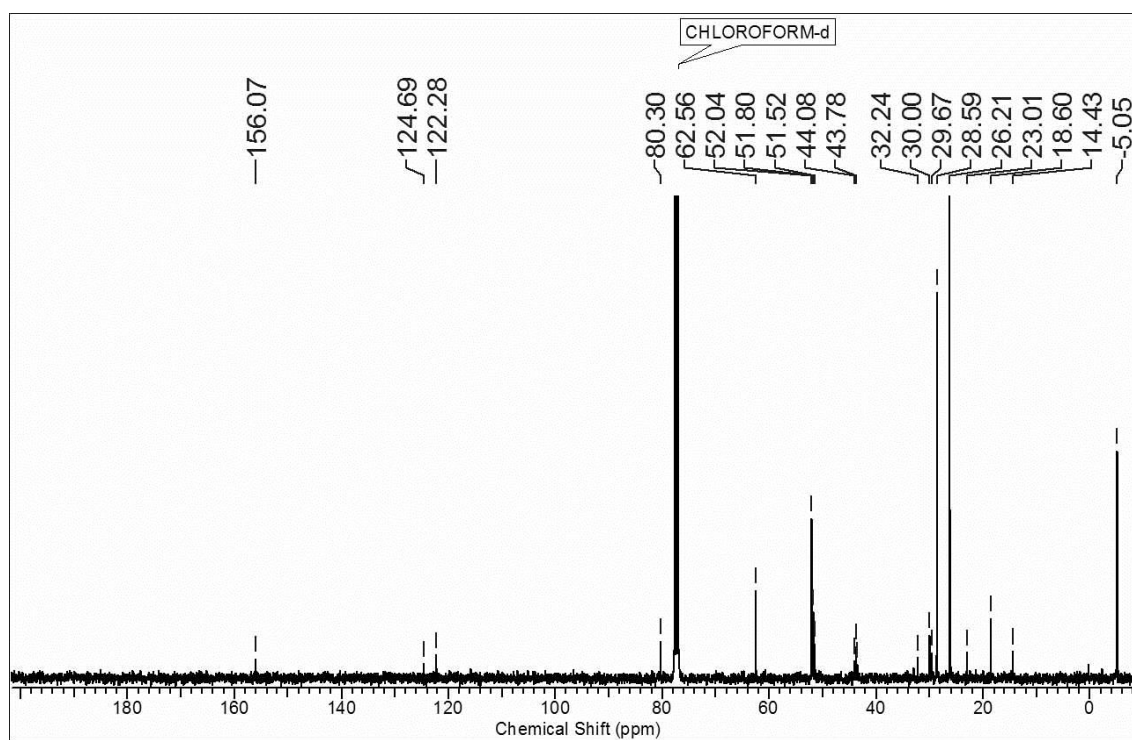
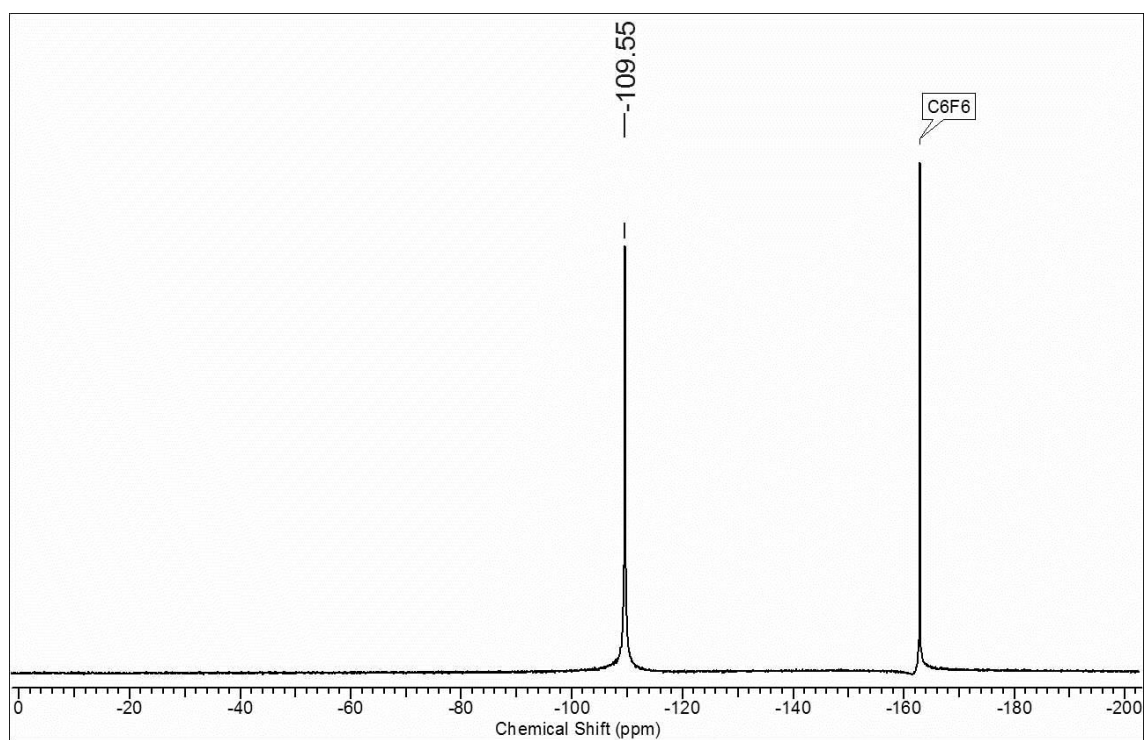
^{13}C -NMR of compound **33** ^{19}F -NMR of compound **33**

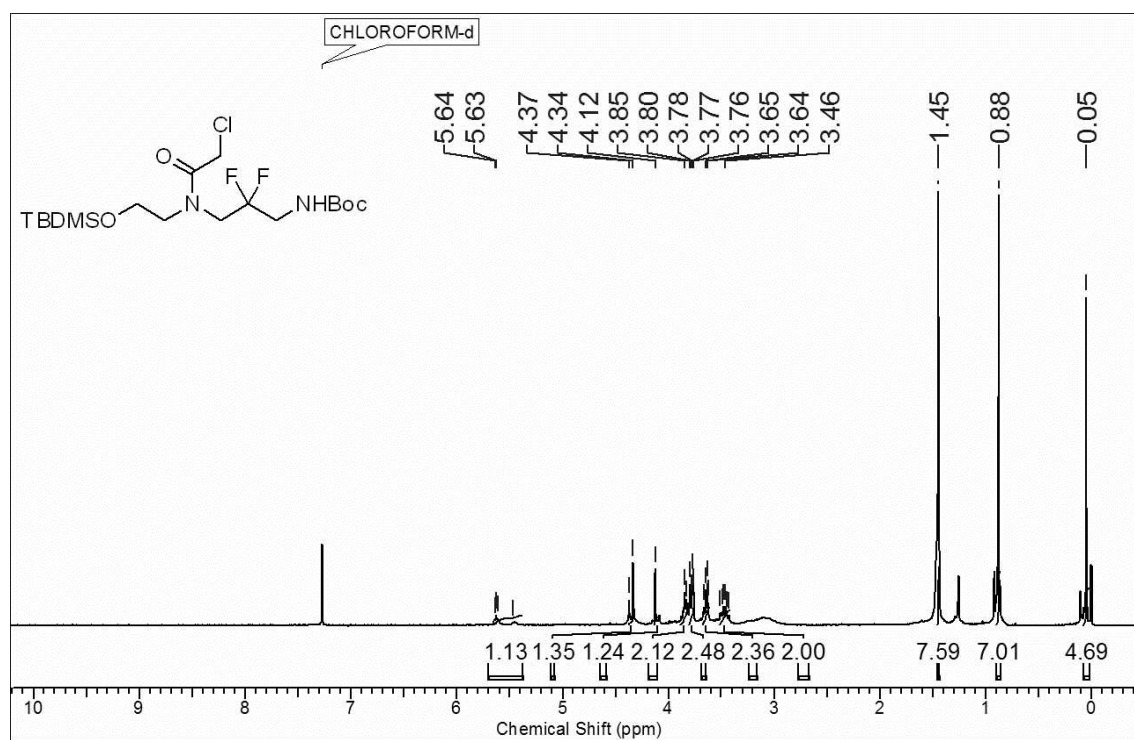
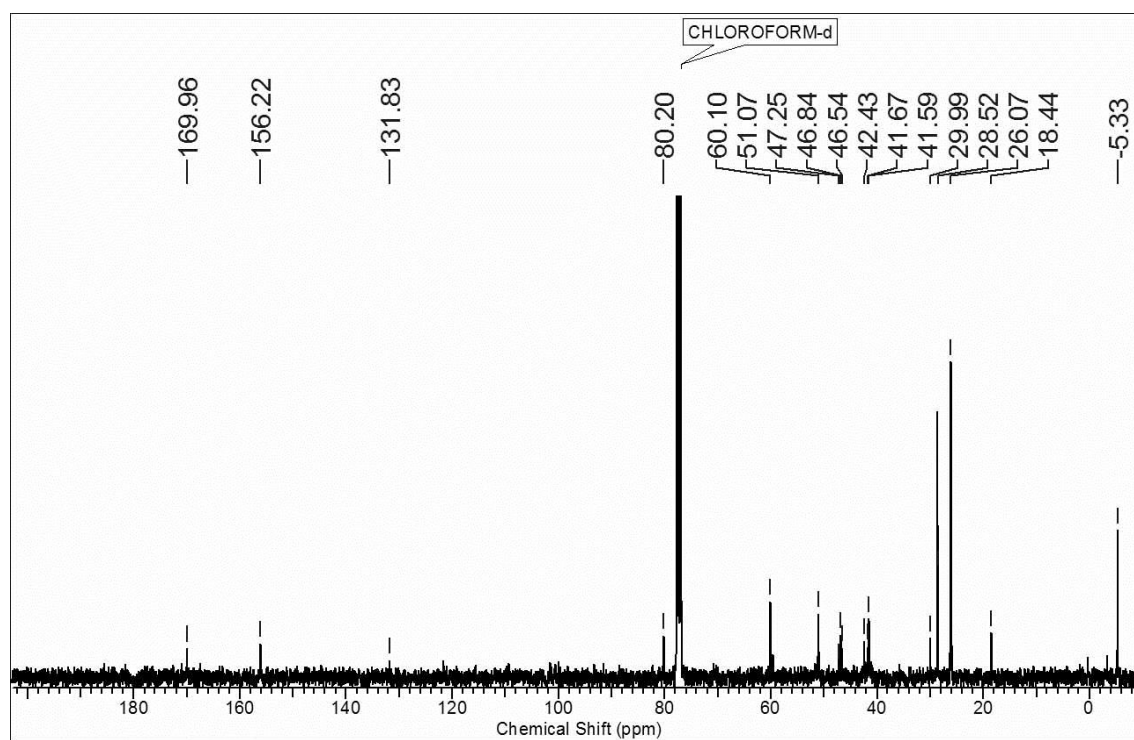
$^1\text{H-NMR}$ of compound **34** $^{13}\text{C-NMR}$ of compound **34**

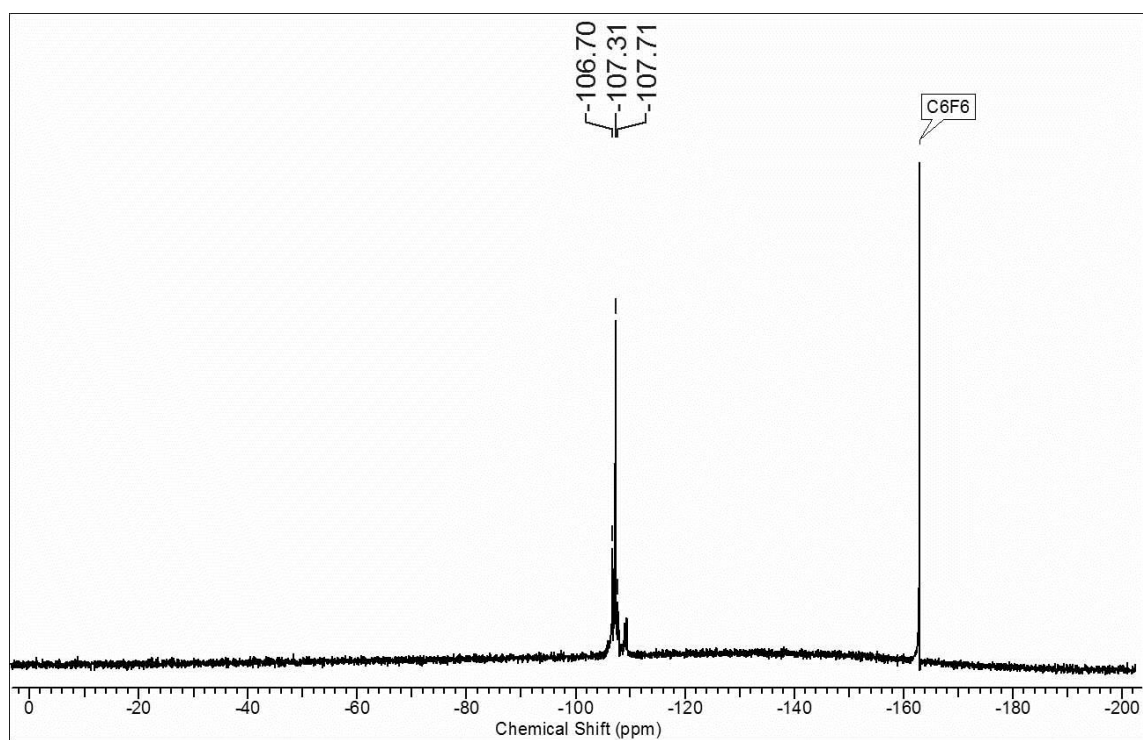
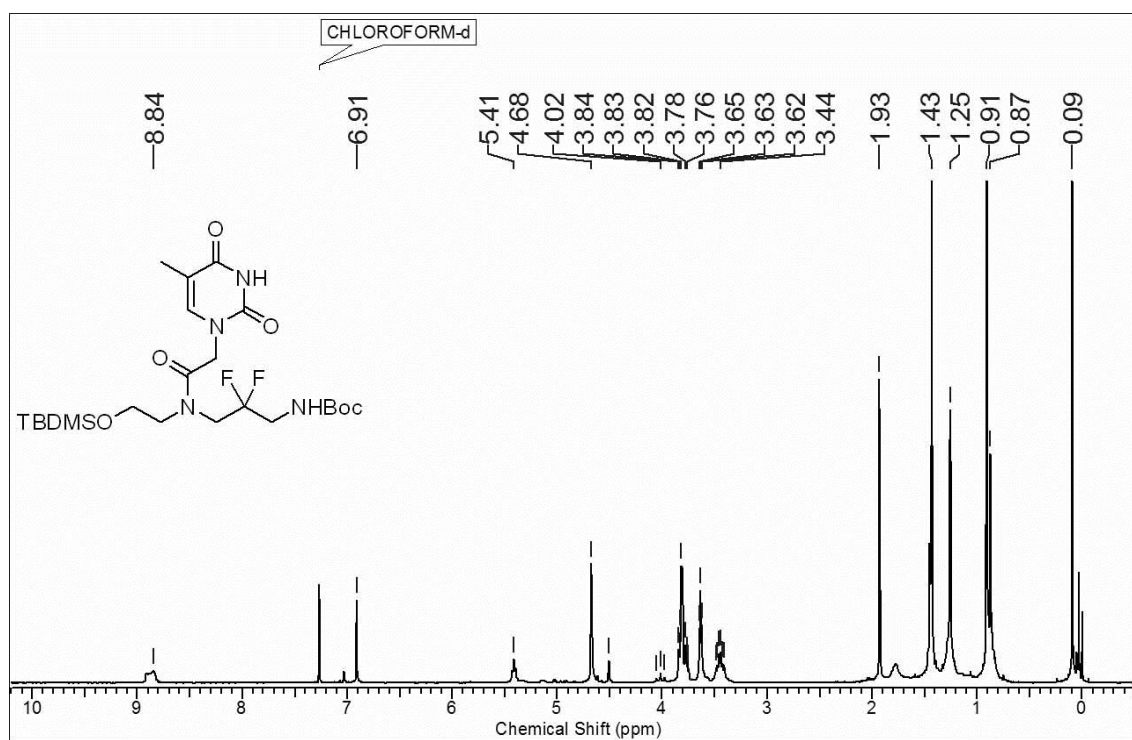
^{19}F -NMR of compound **34**IR of compound **34**

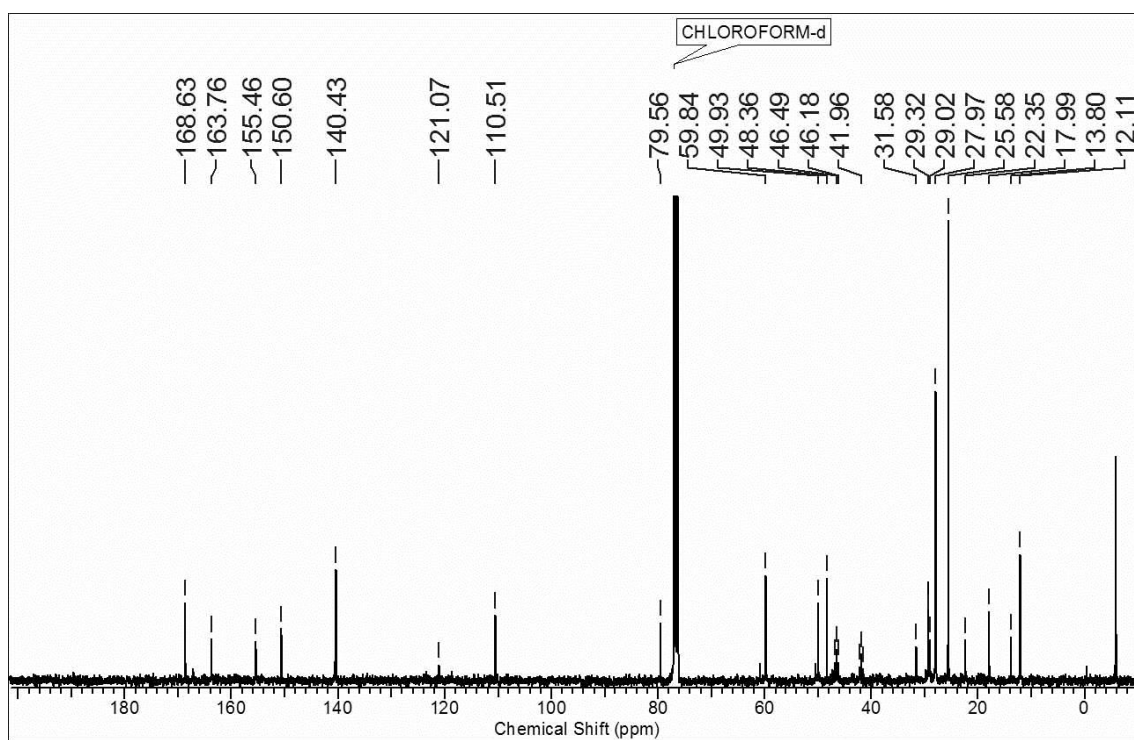
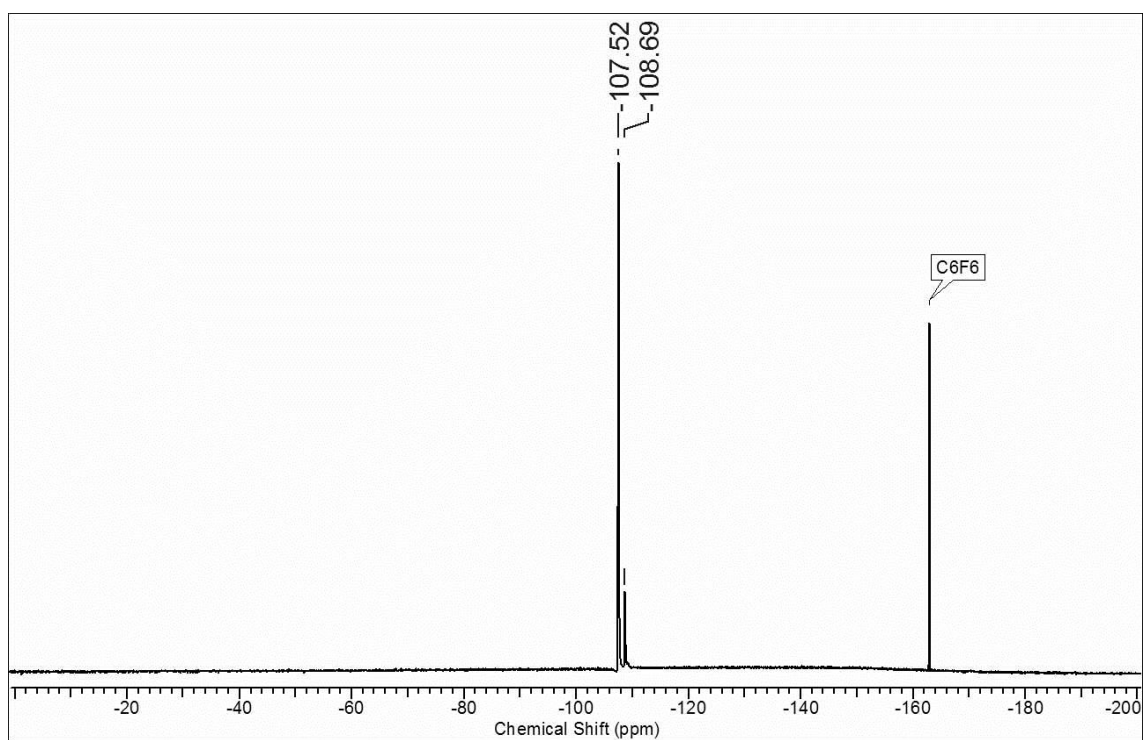
$^1\text{H-NMR}$ of compound **36** $^{13}\text{C-NMR}$ of compound **36**

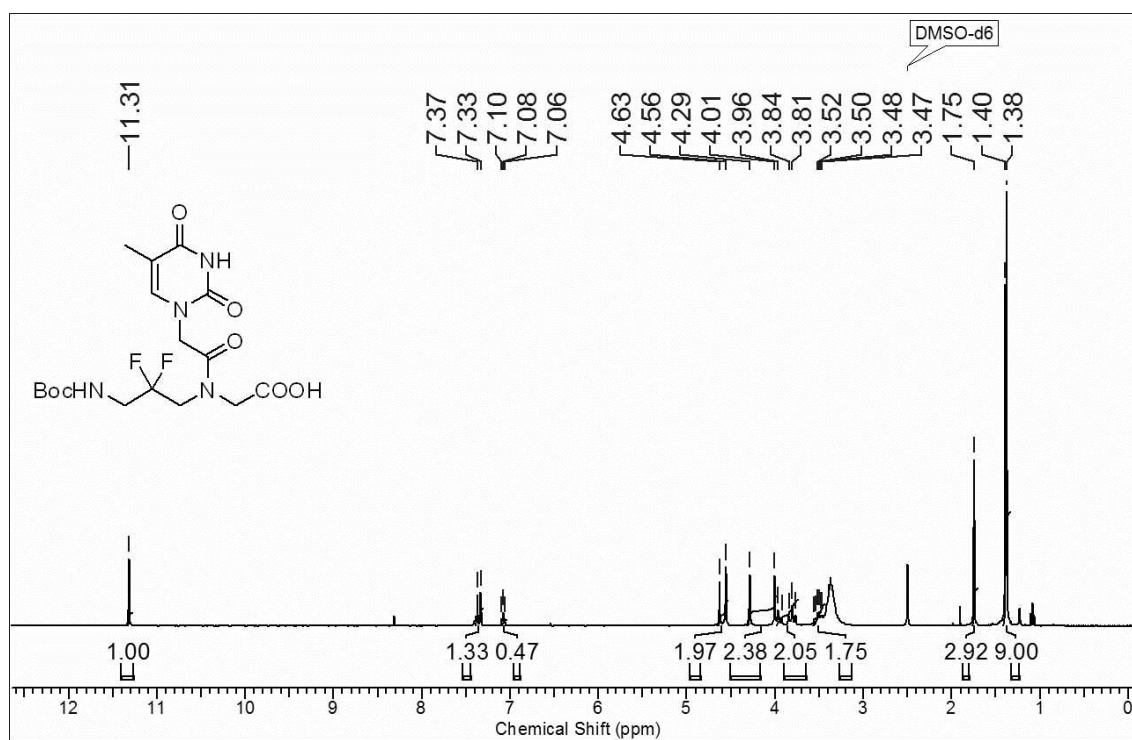
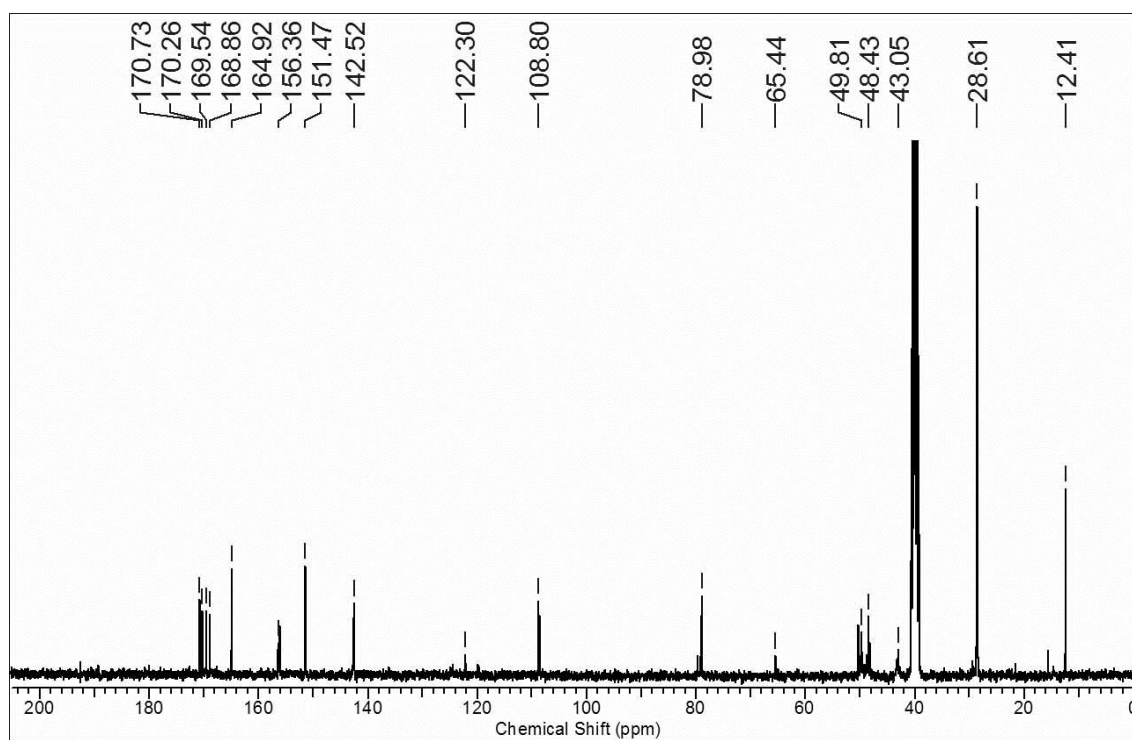
^{19}F -NMR of compound **36** ^1H -NMR of compound **37**

^{13}C -NMR of compound **37** ^{19}F -NMR of compound **37**

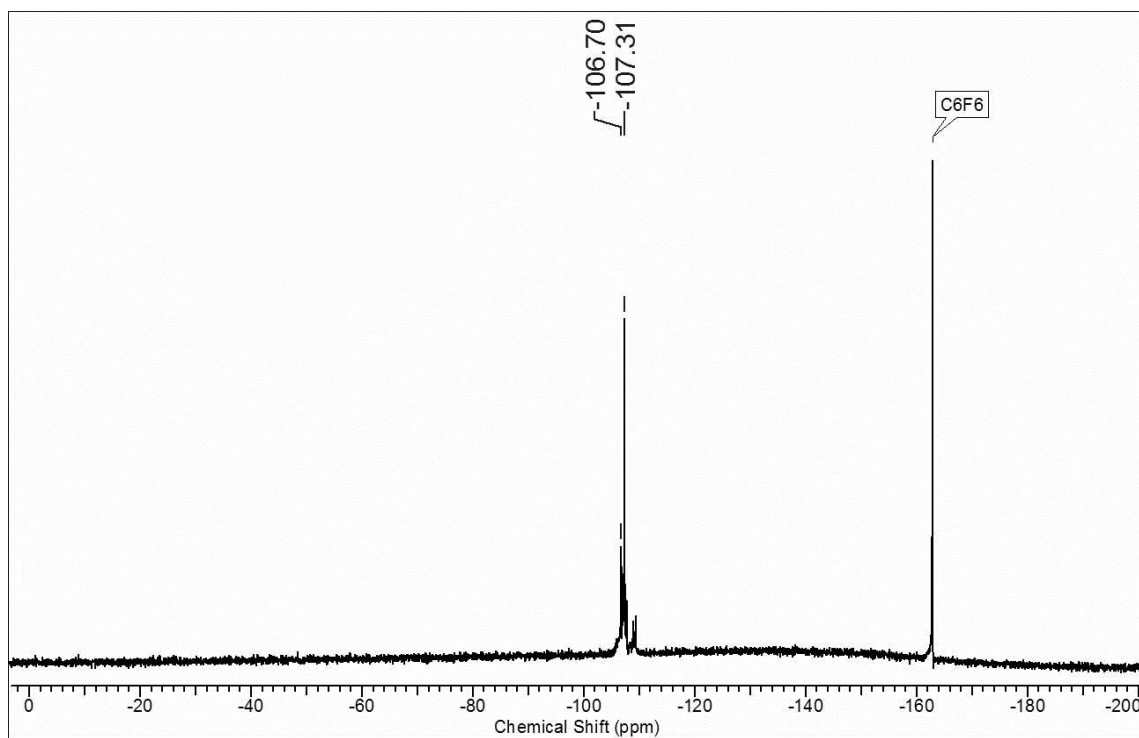
$^1\text{H-NMR}$ of compound **38** $^{13}\text{C-NMR}$ of compound **38**

^{19}F -NMR of compound **38** ^1H -NMR of compound **39**

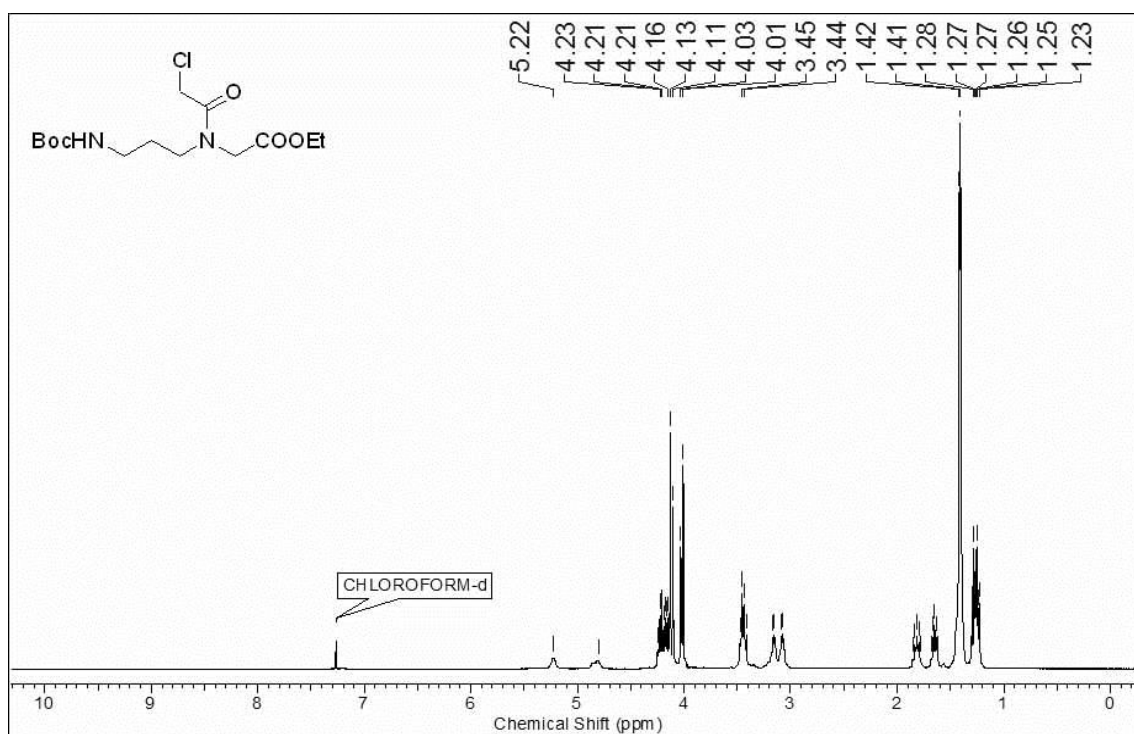
^{13}C -NMR of compound **39** ^{19}F -NMR of compound **39**

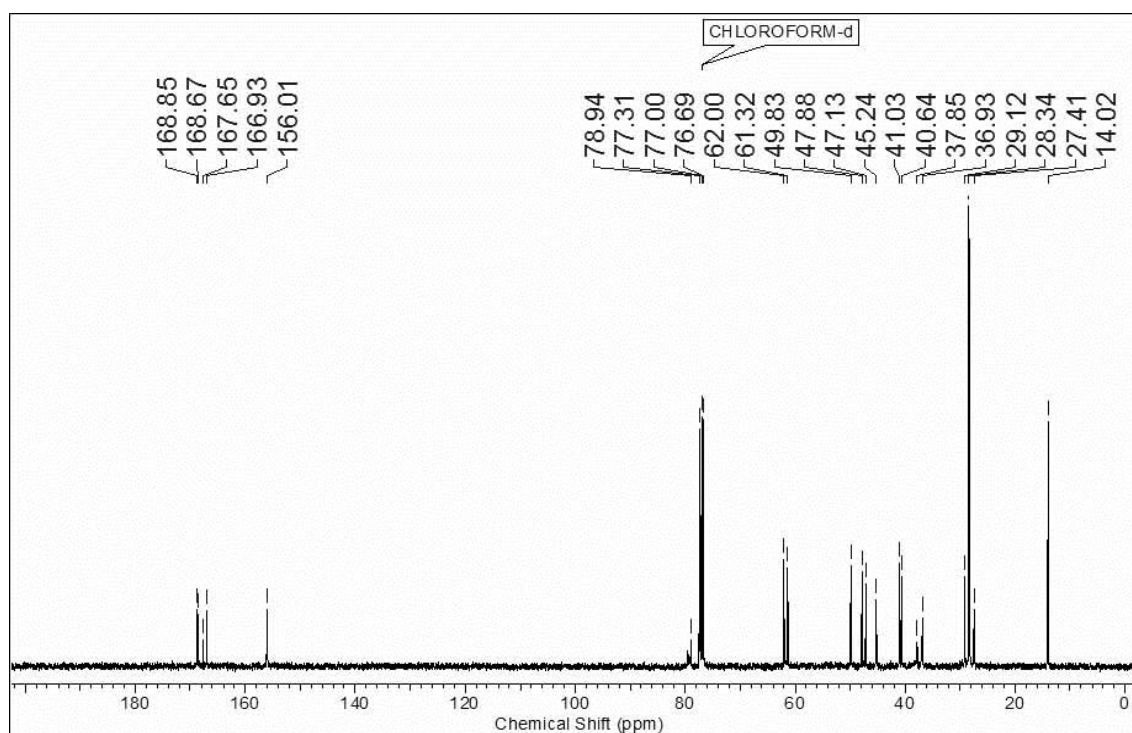
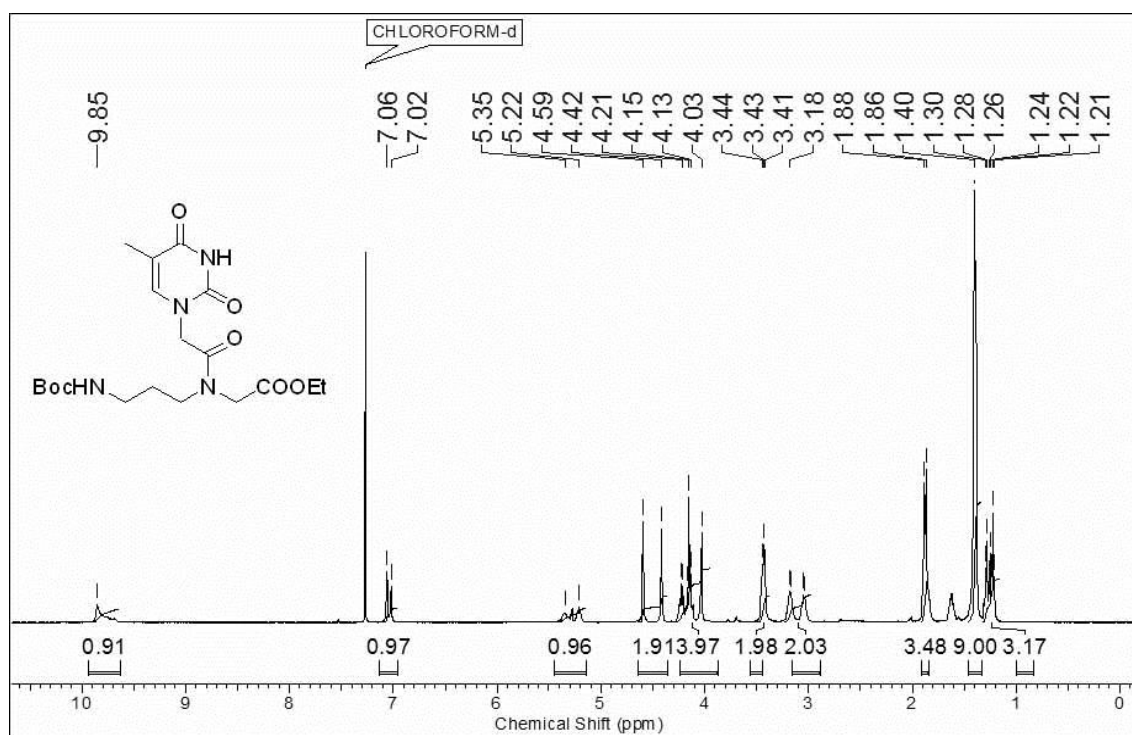
$^1\text{H-NMR}$ of compound **6** $^{13}\text{C-NMR}$ of compound **6**

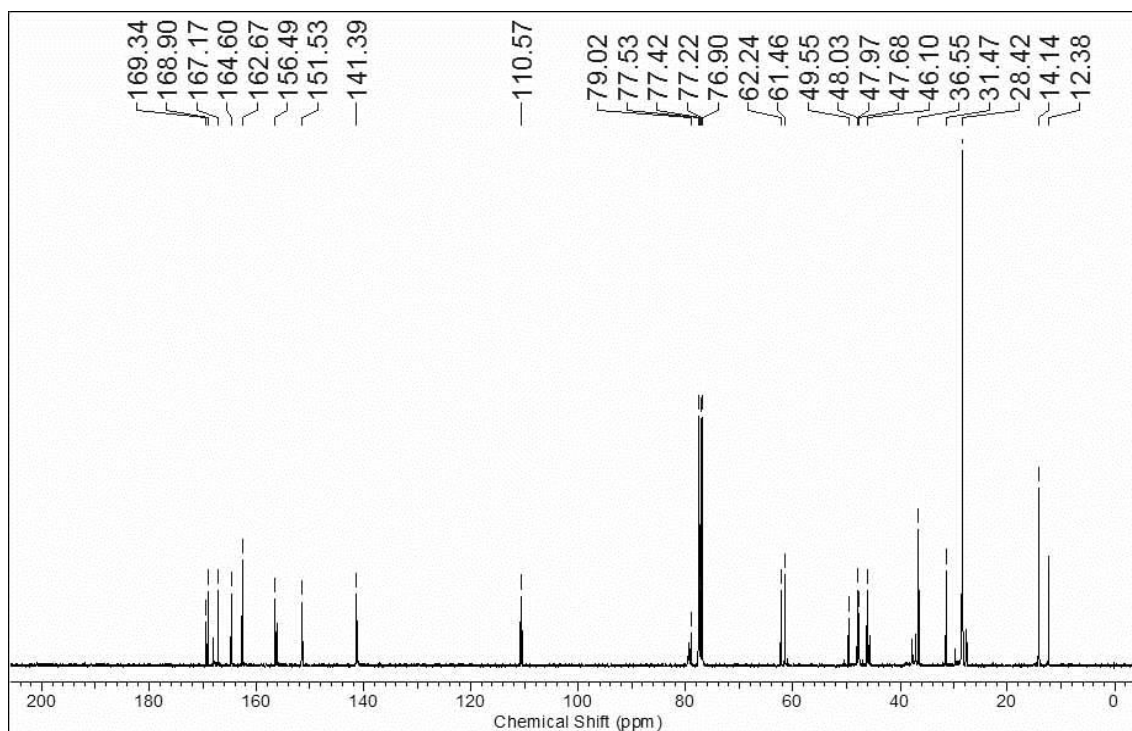
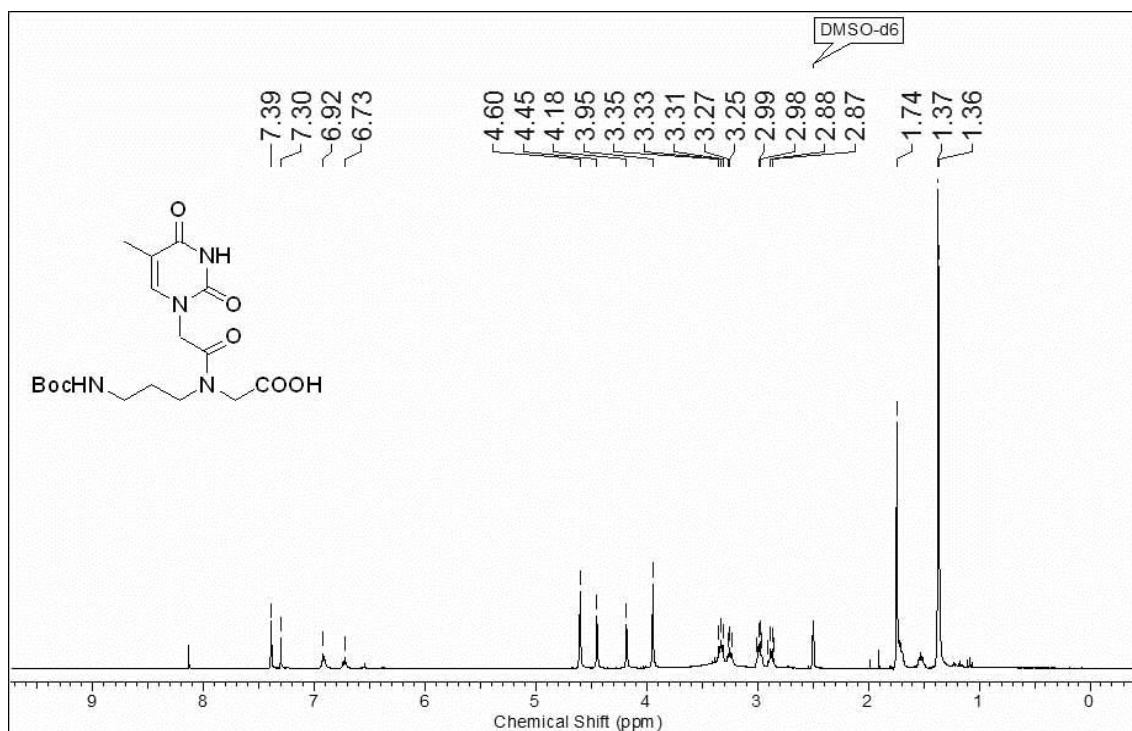
^{19}F -NMR of compound **6**

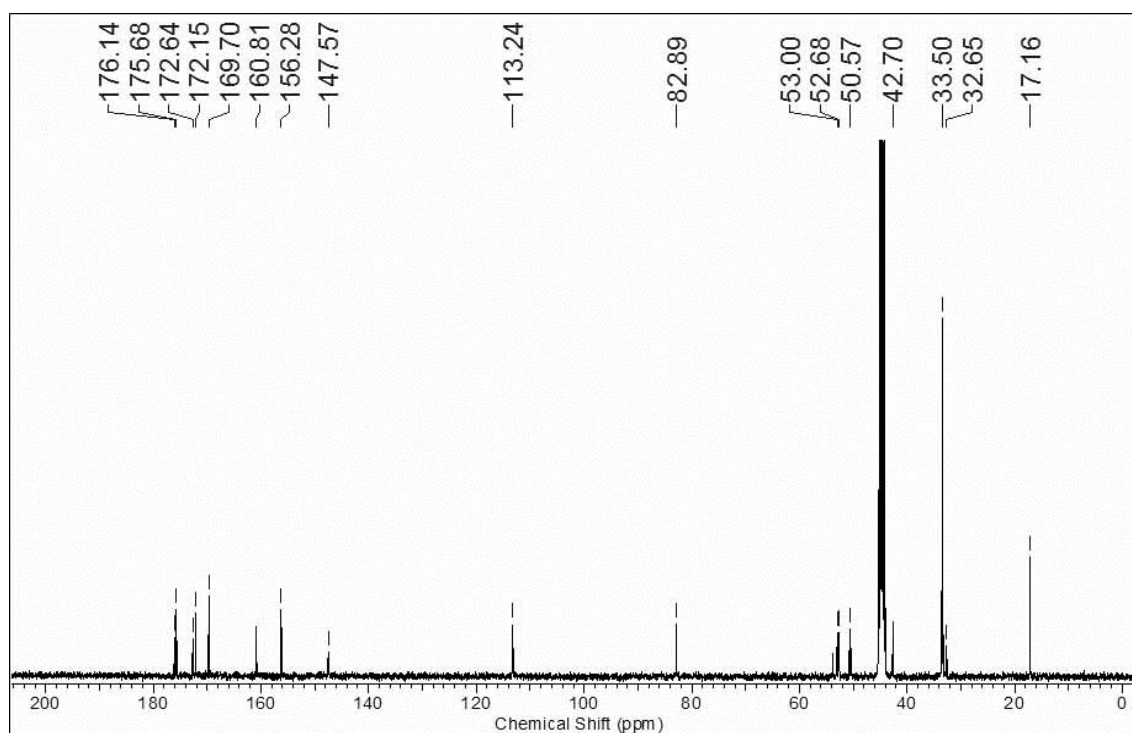
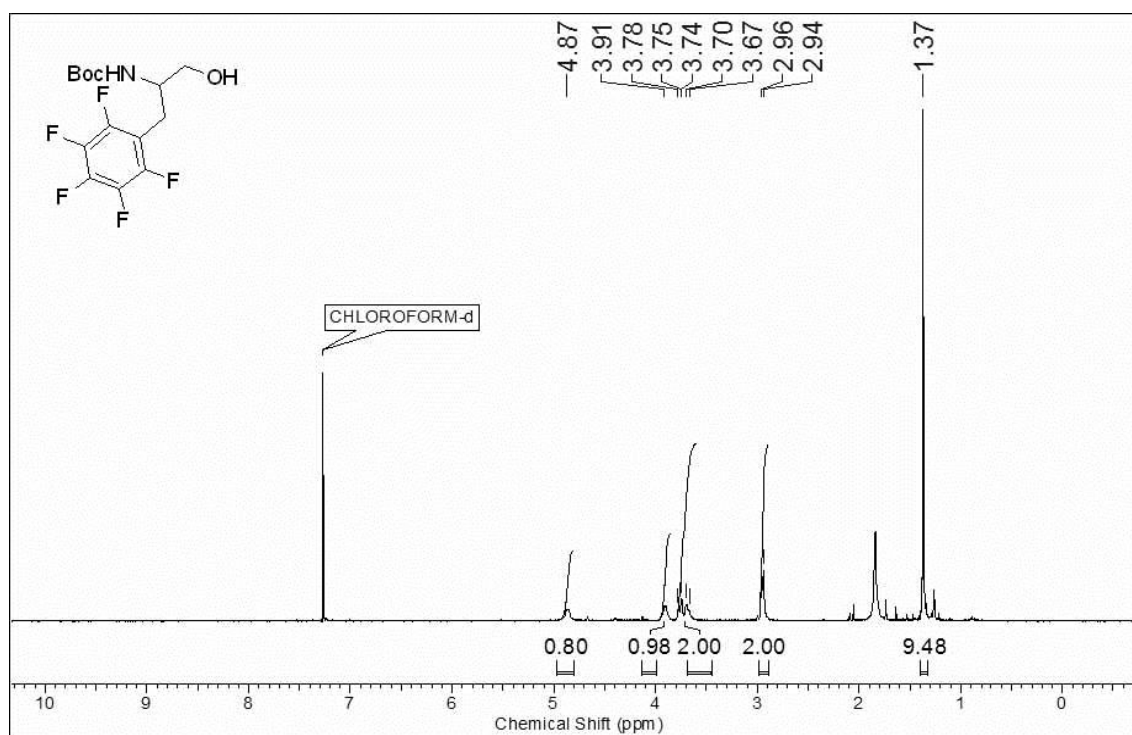


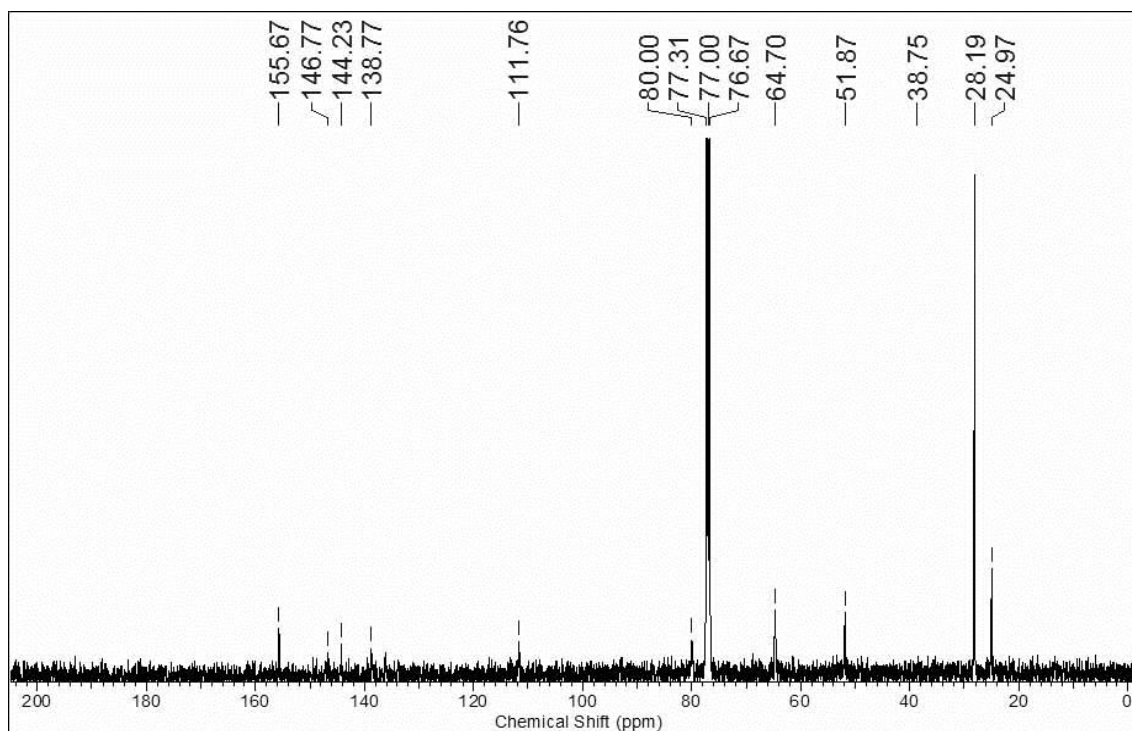
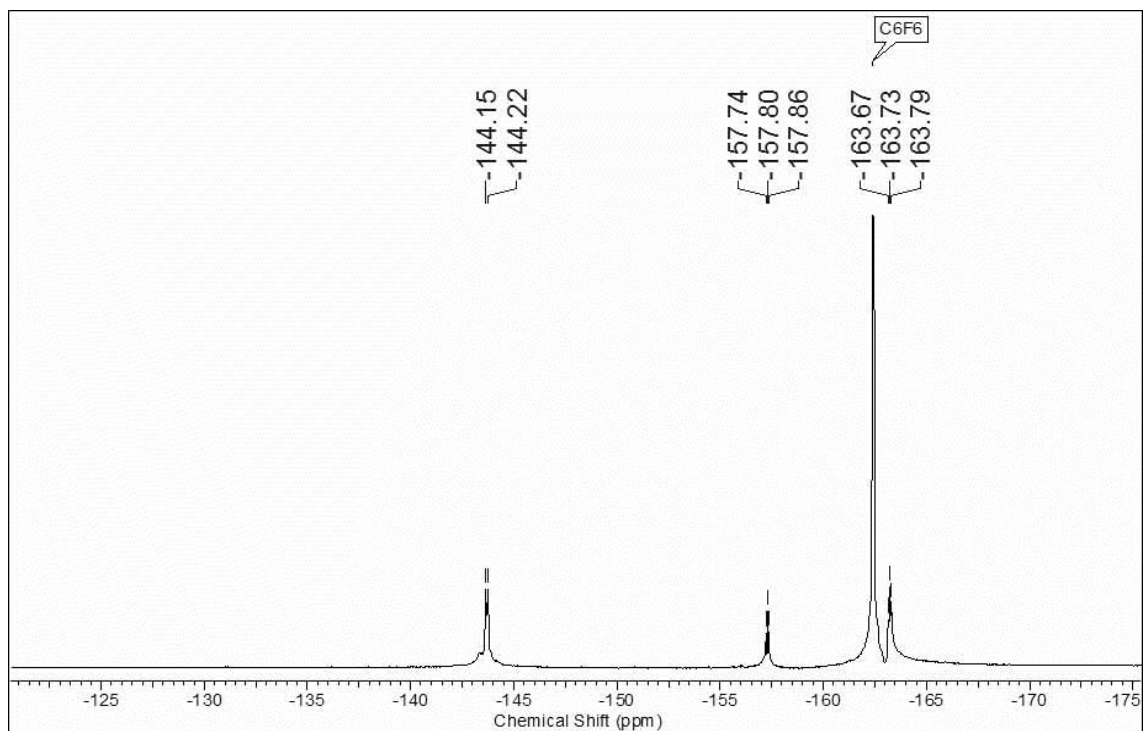
^1H -NMR of compound **42**

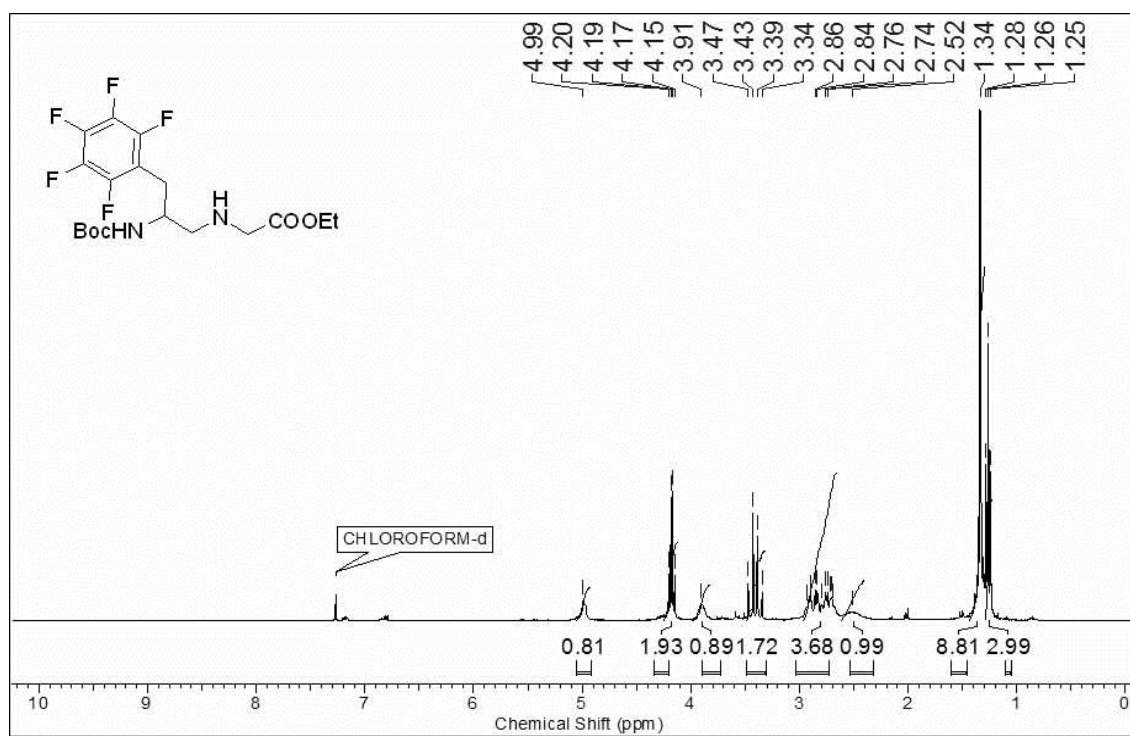
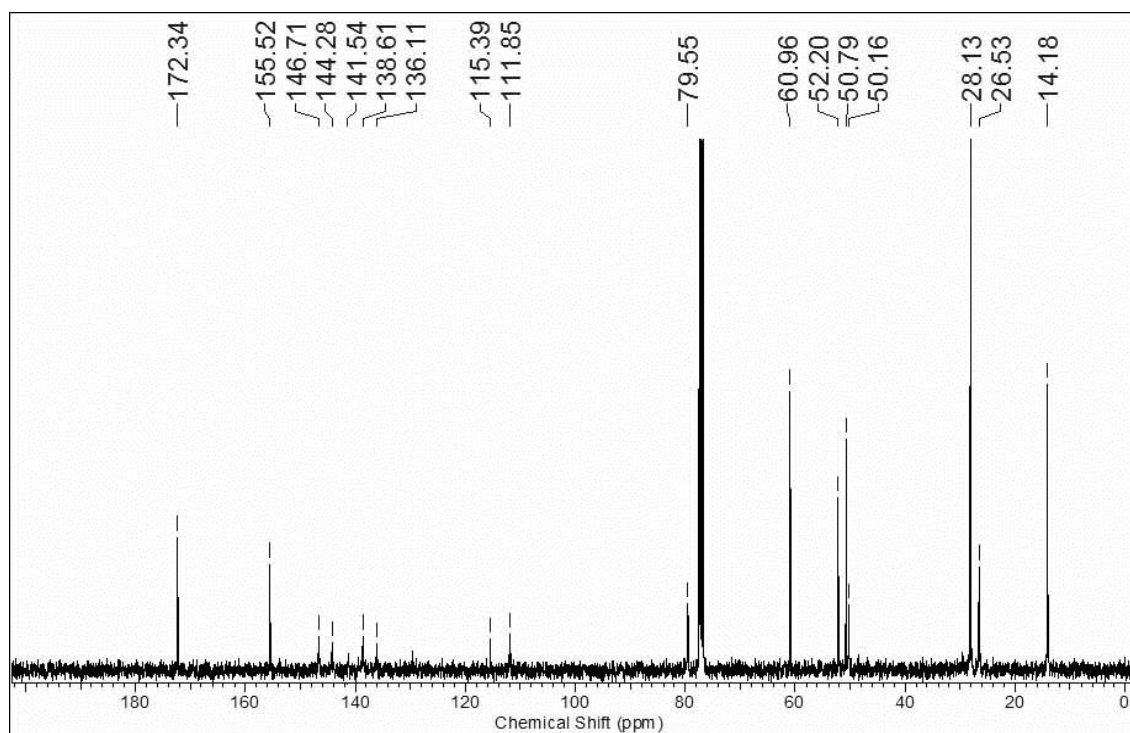


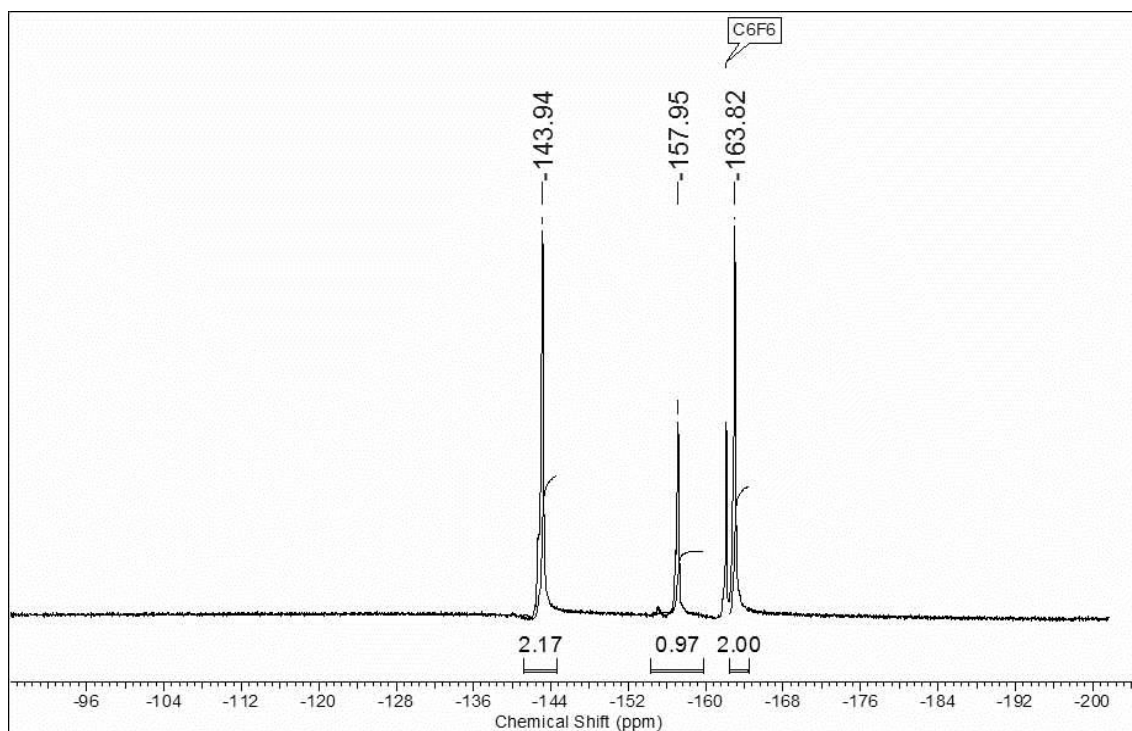
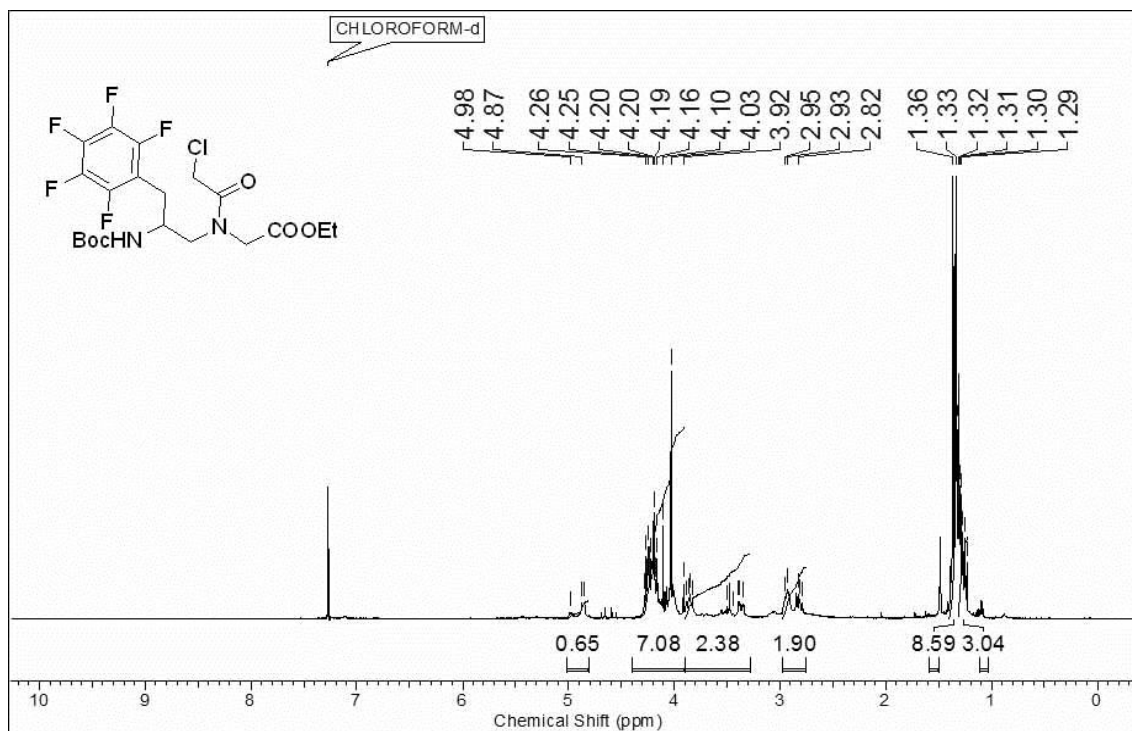
^{13}C -NMR of compound **42** ^1H -NMR of compound **43**

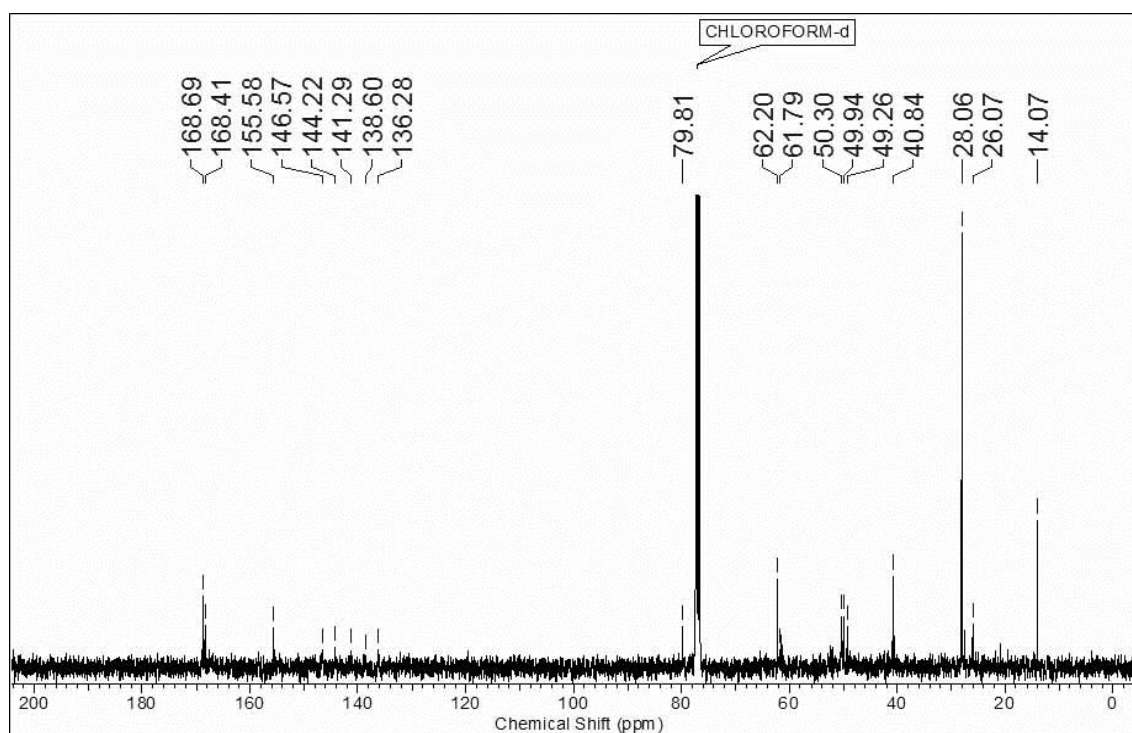
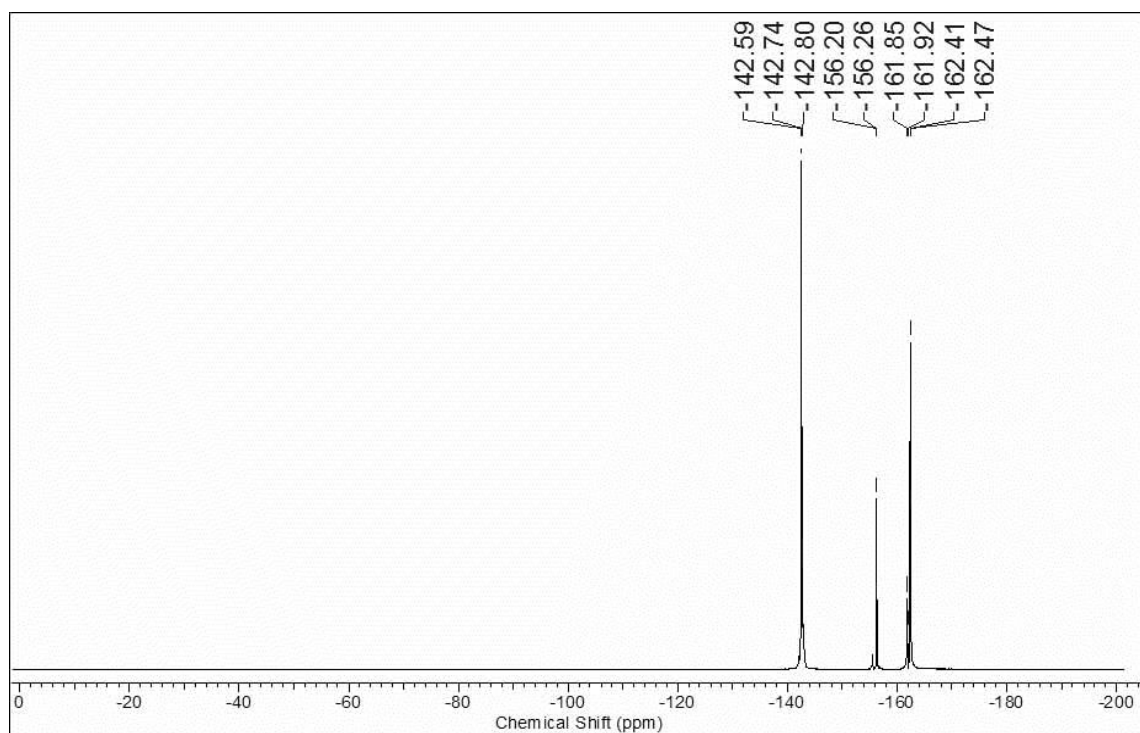
^{13}C -NMR of compound **43** ^1H -NMR of compound **7**

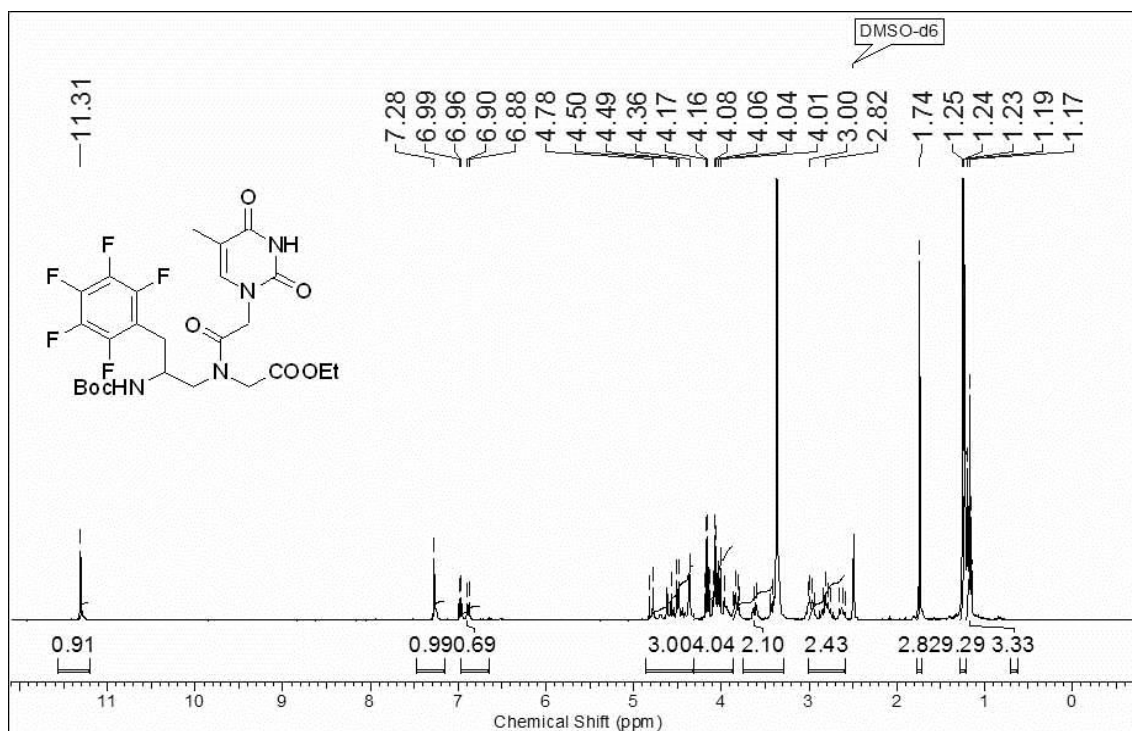
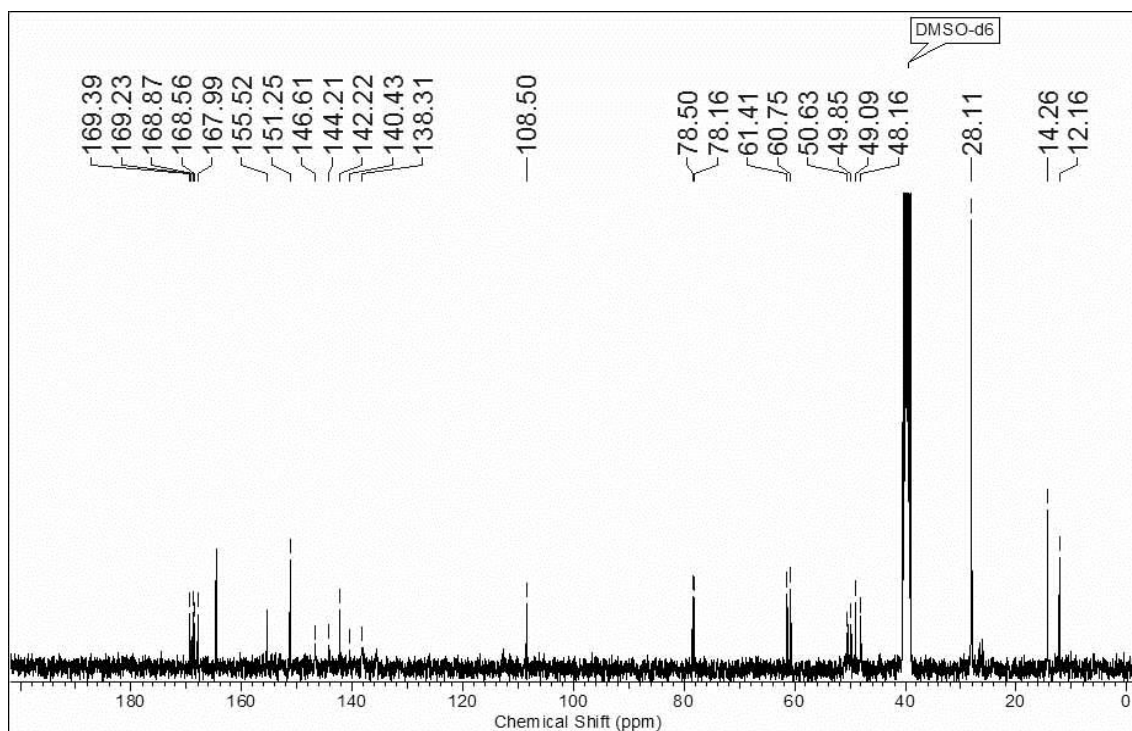
^{13}C -NMR of compound **7** ^1H -NMR of compound **47a**

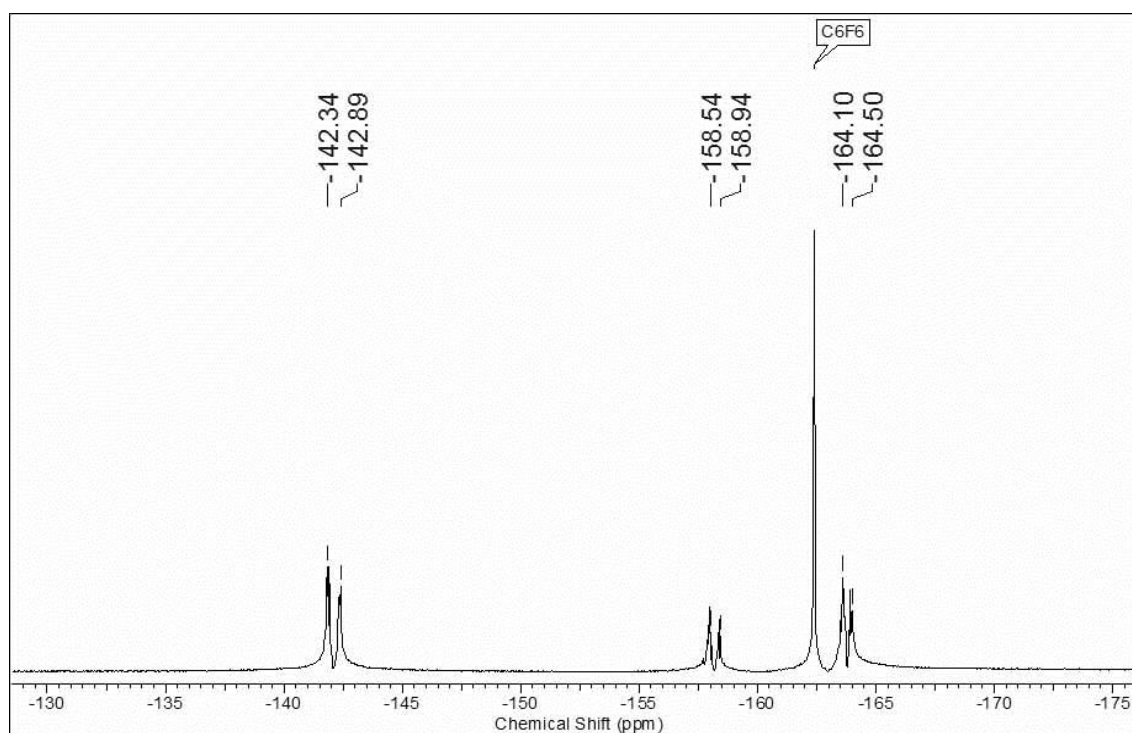
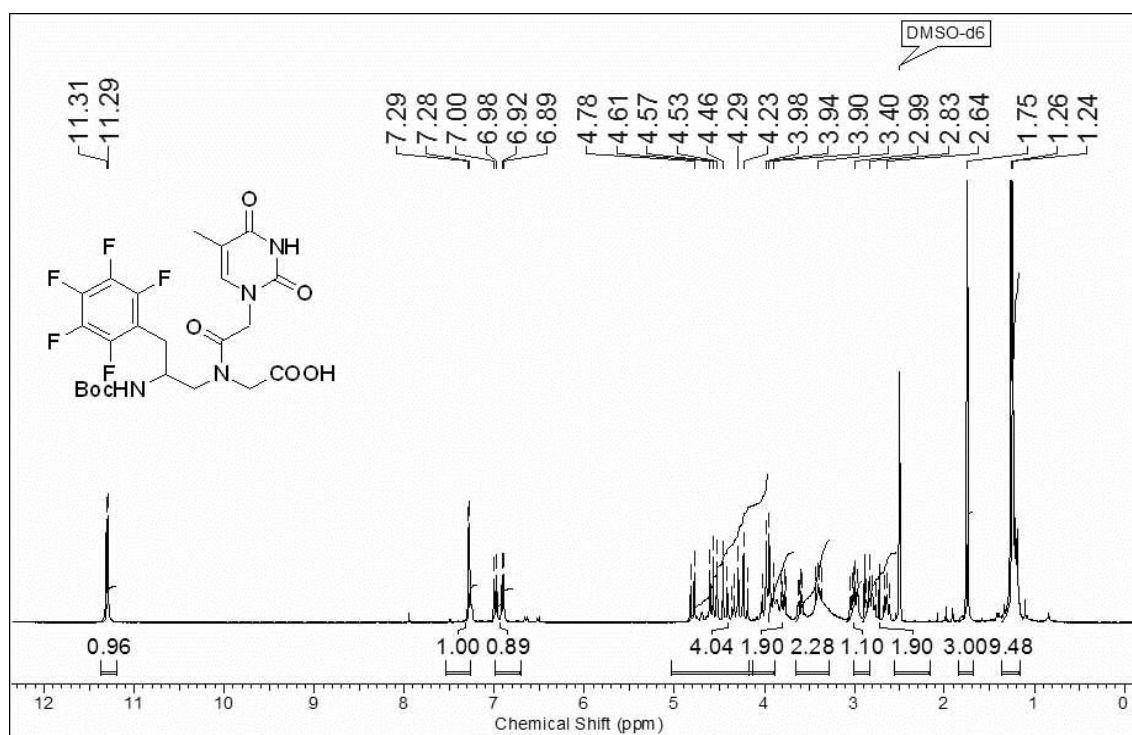
^{13}C -NMR of compound **47a** ^{19}F -NMR of compound **47a**

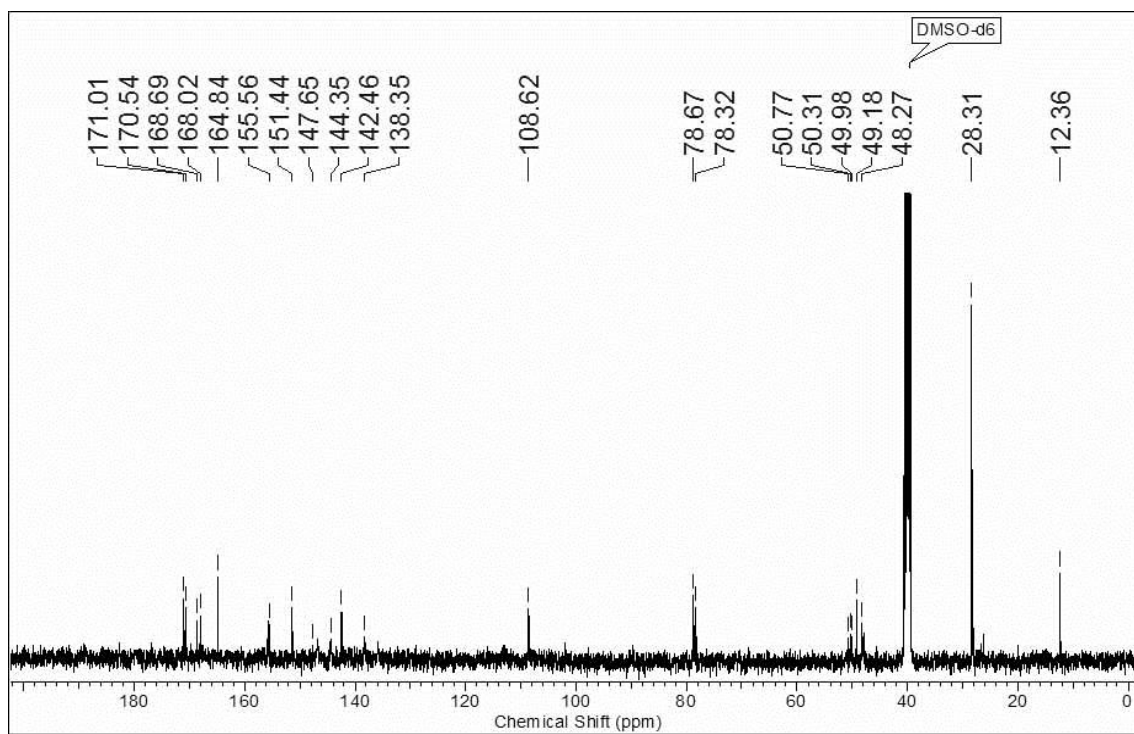
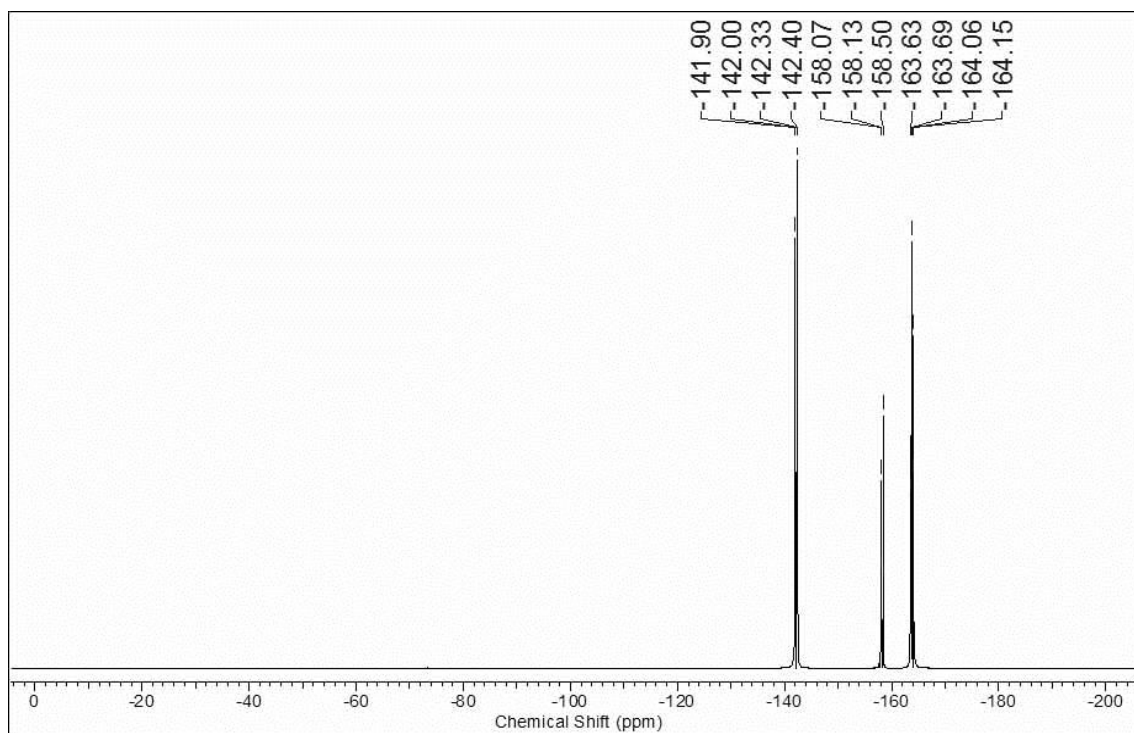
$^1\text{H-NMR}$ of compound **49a** $^{13}\text{C-NMR}$ of compound **49a**

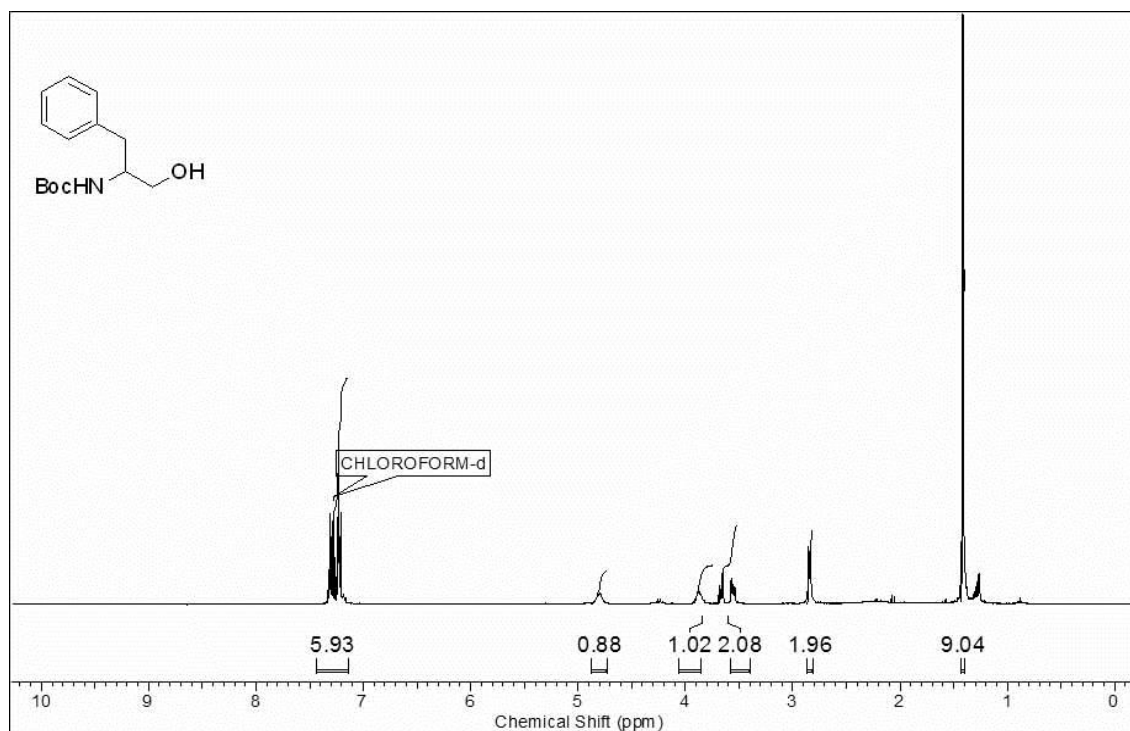
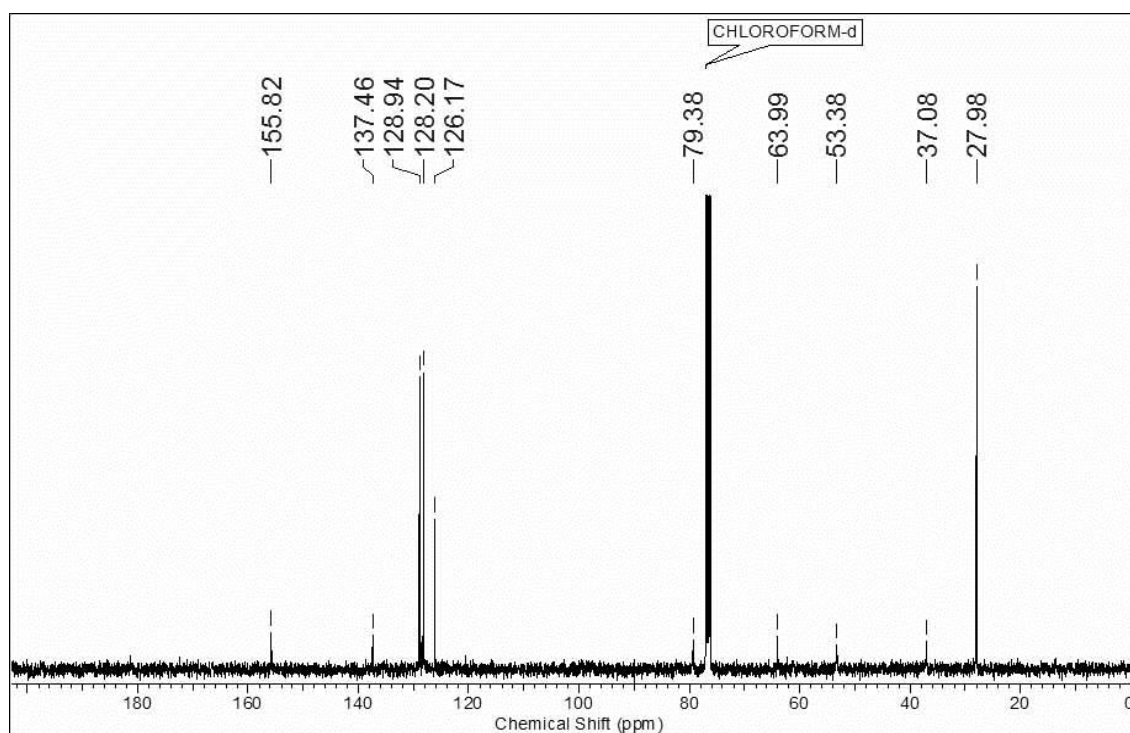
^{19}F -NMR of compound **49a** ^1H -NMR of compound **50a**

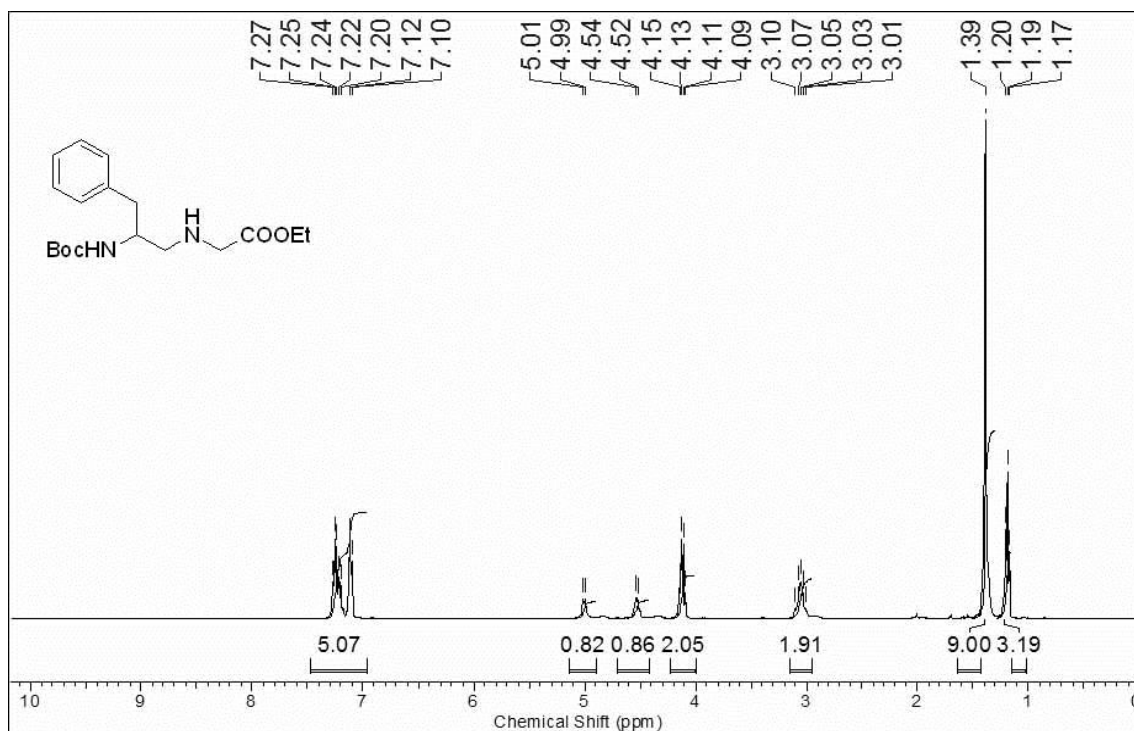
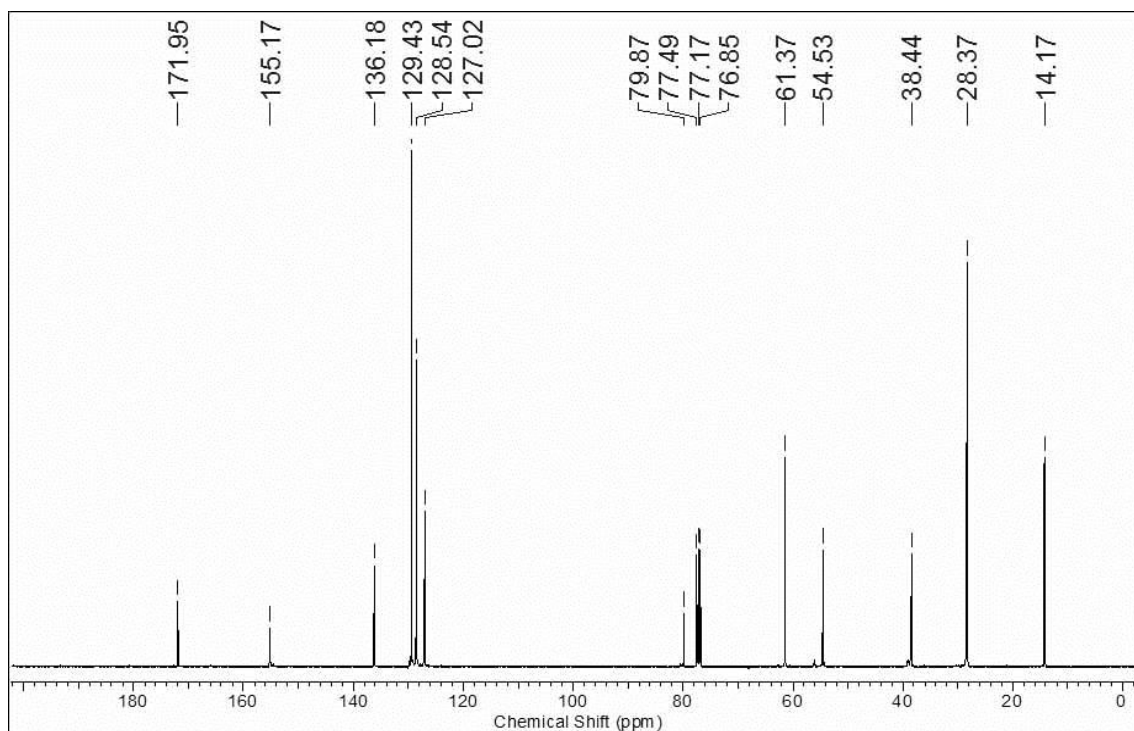
^{13}C -NMR of compound **50a** ^{19}F -NMR of compound **50a**

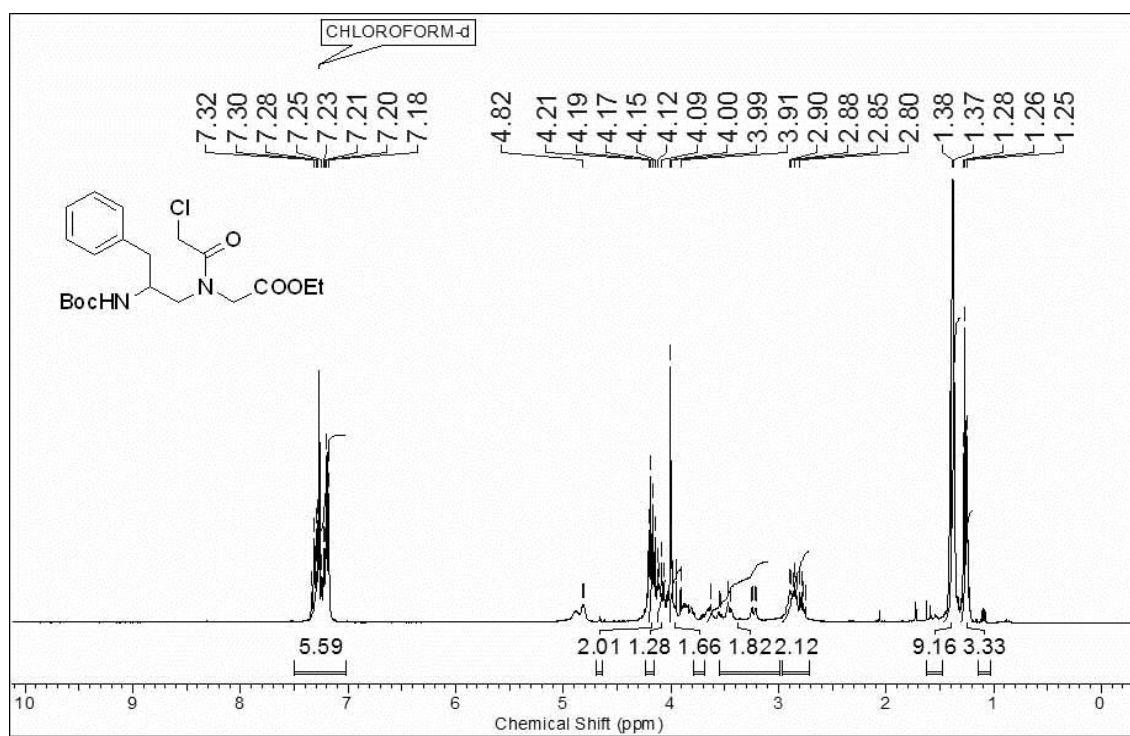
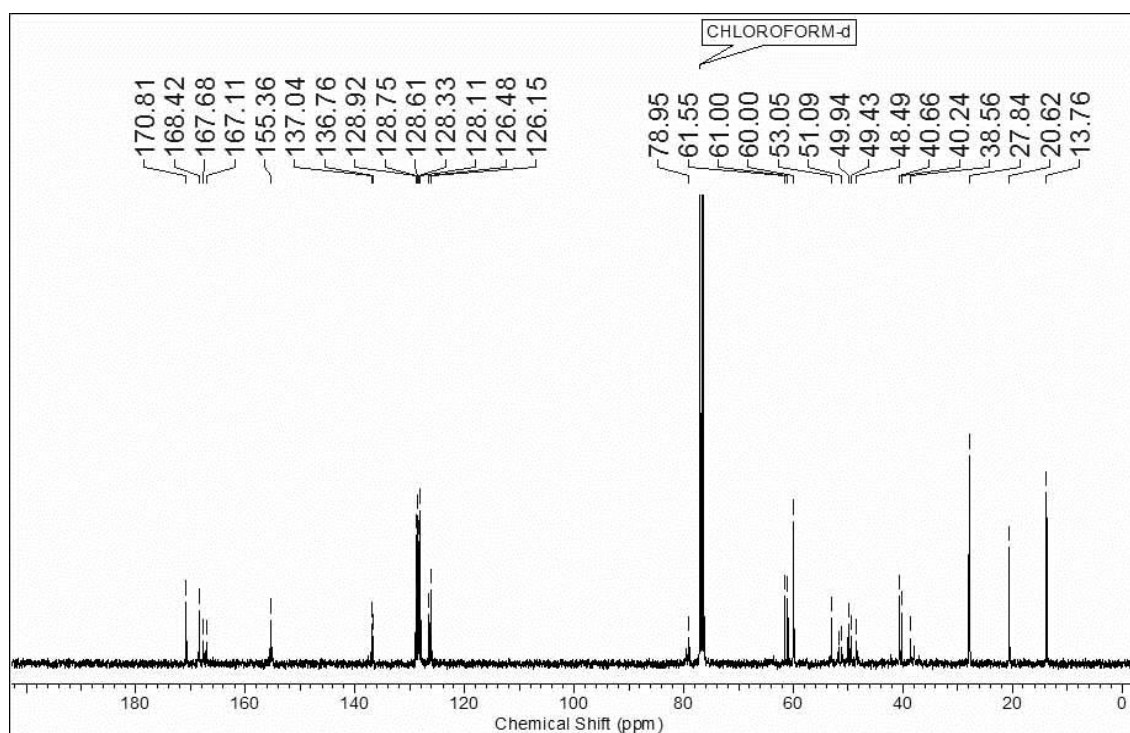
$^1\text{H-NMR}$ of compound **51a** $^{13}\text{C-NMR}$ of compound **51a**

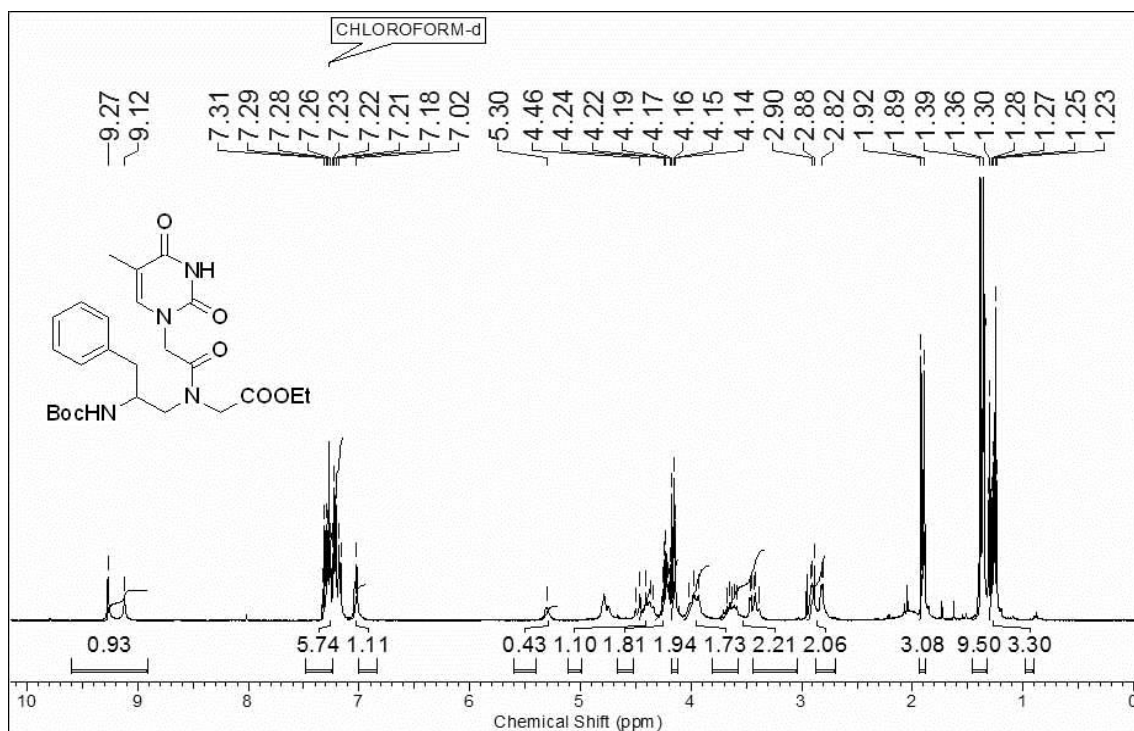
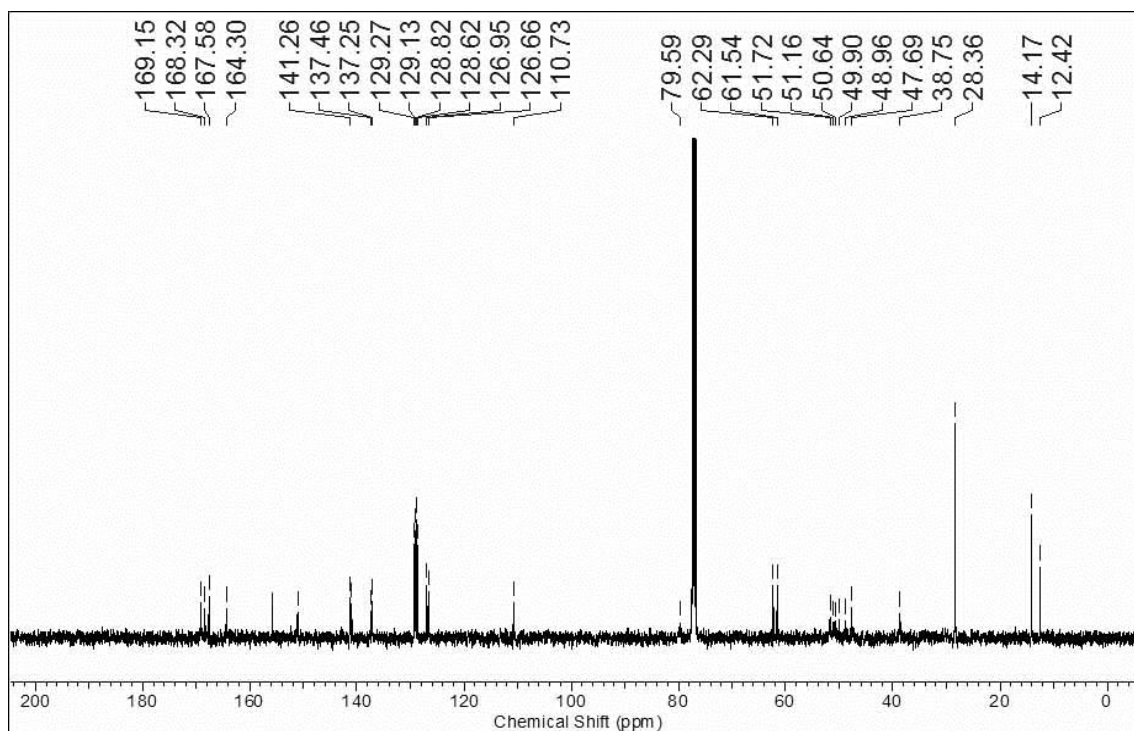
^{19}F -NMR of compound **51a** ^1H -NMR of compound **8**

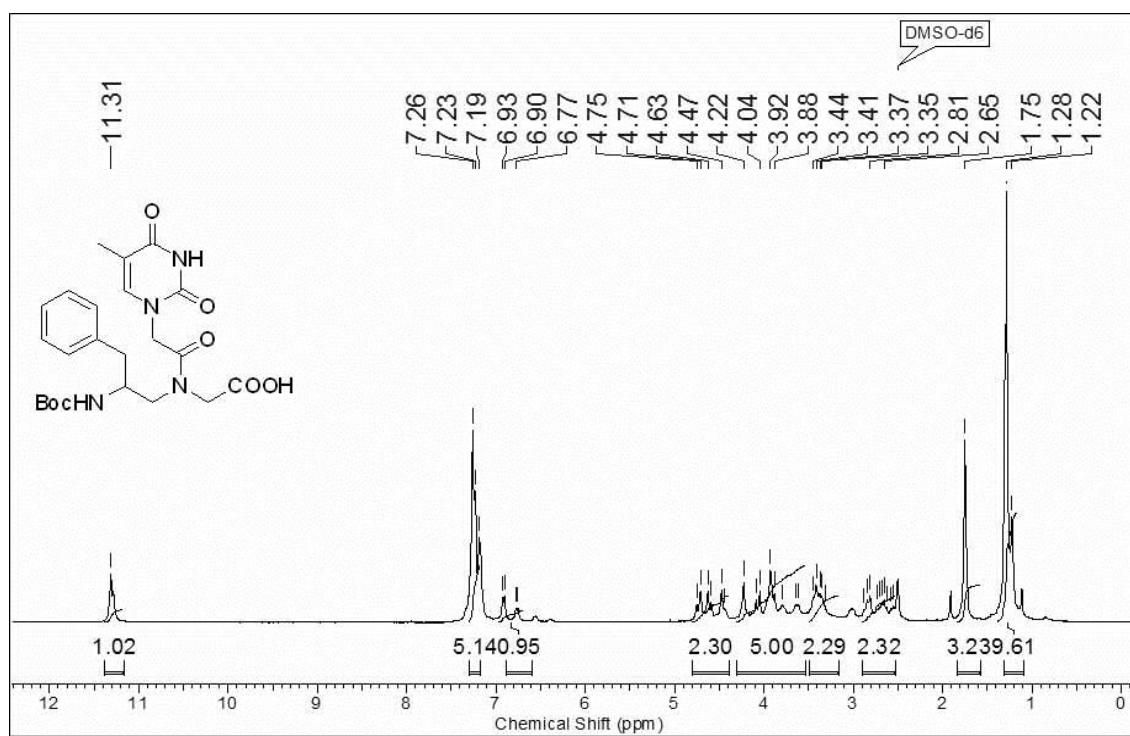
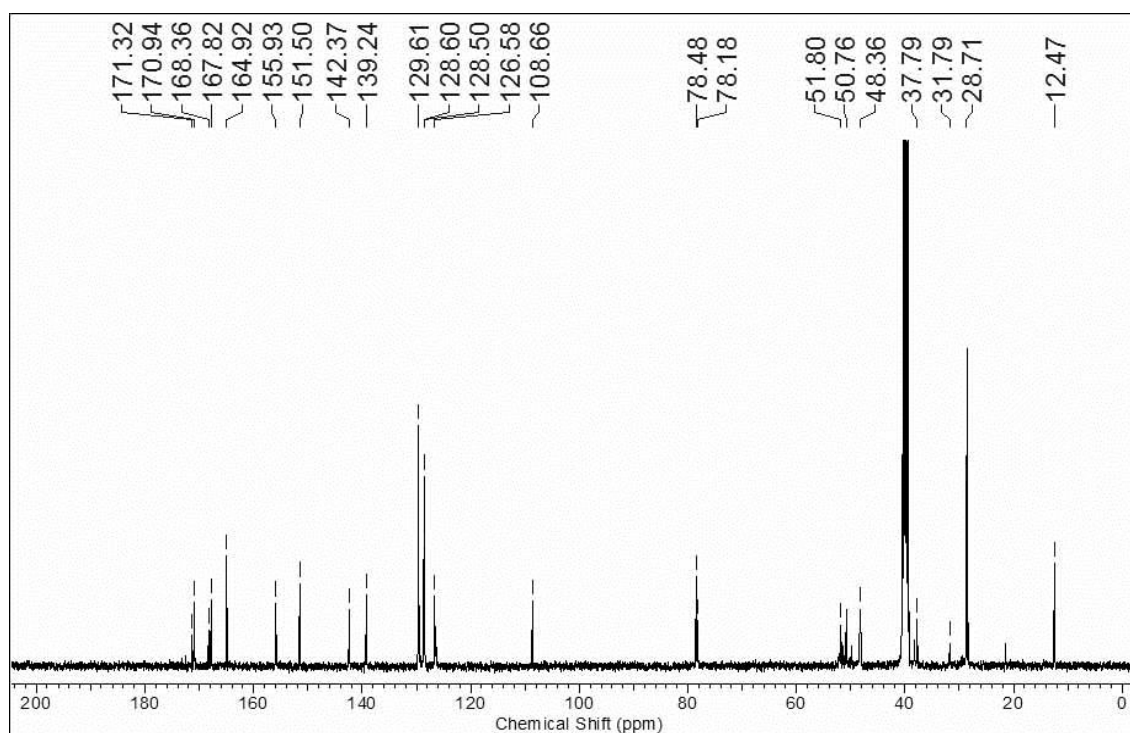
^{13}C -NMR of compound **8** ^{19}F -NMR of compound **8**

$^1\text{H-NMR}$ of compound **47b** $^{13}\text{C-NMR}$ of compound **47b**

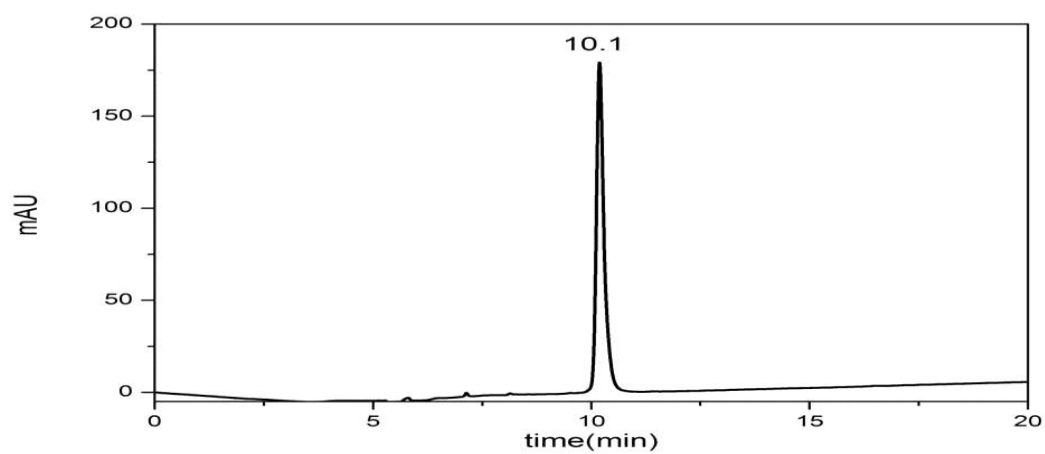
$^1\text{H-NMR}$ of compound **49b** $^{13}\text{C-NMR}$ of compound **49b**

$^1\text{H-NMR}$ of compound **50b** $^{13}\text{C-NMR}$ of compound **50b**

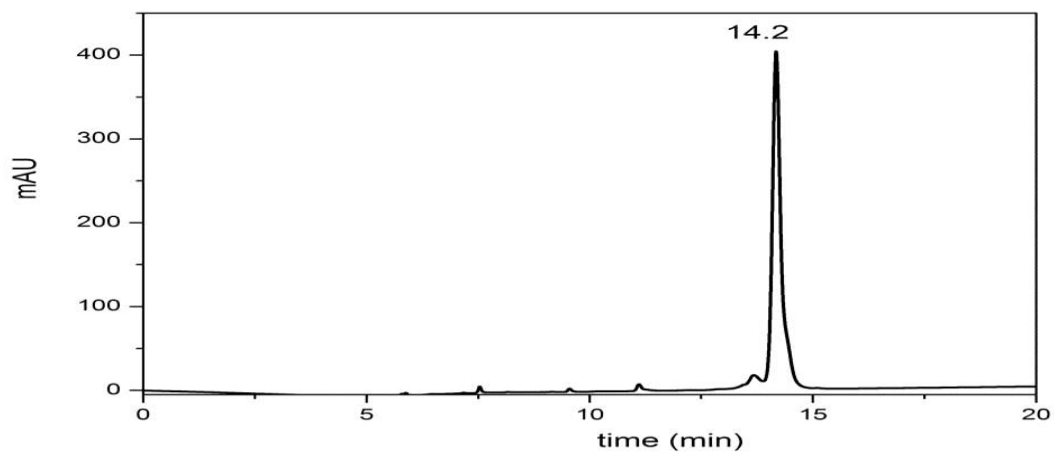
$^1\text{H-NMR}$ of compound **51b** $^{13}\text{C-NMR}$ of compound **51b**

$^1\text{H-NMR}$ of compound **9** $^{13}\text{C-NMR}$ of compound **9**

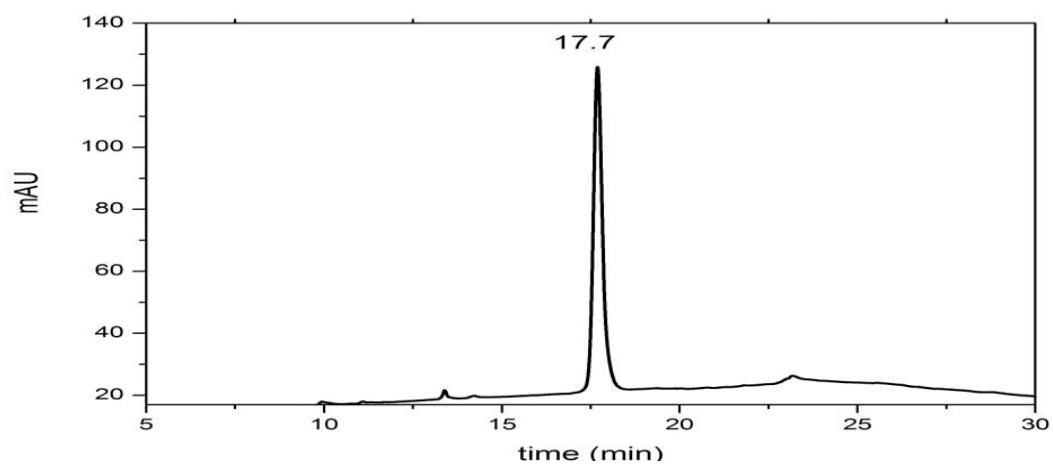
HPLC of PNA 1



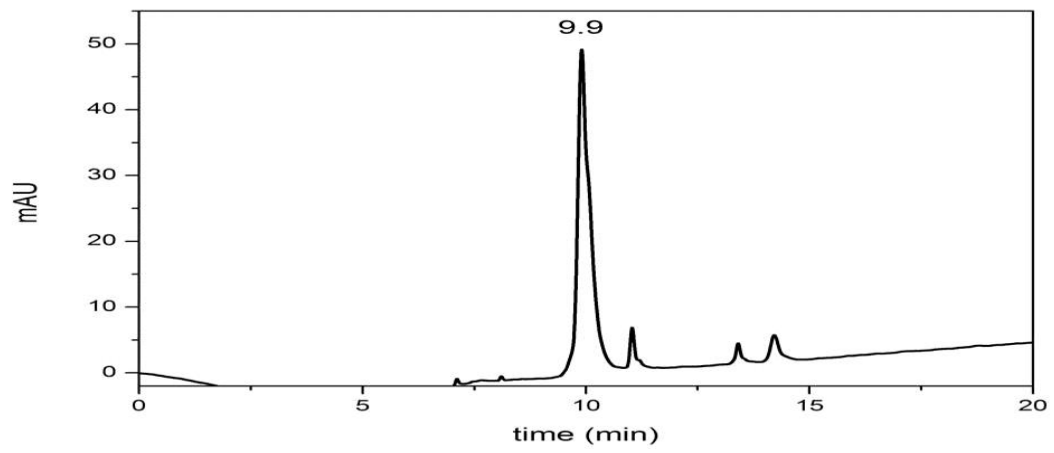
HPLC of PNA 2



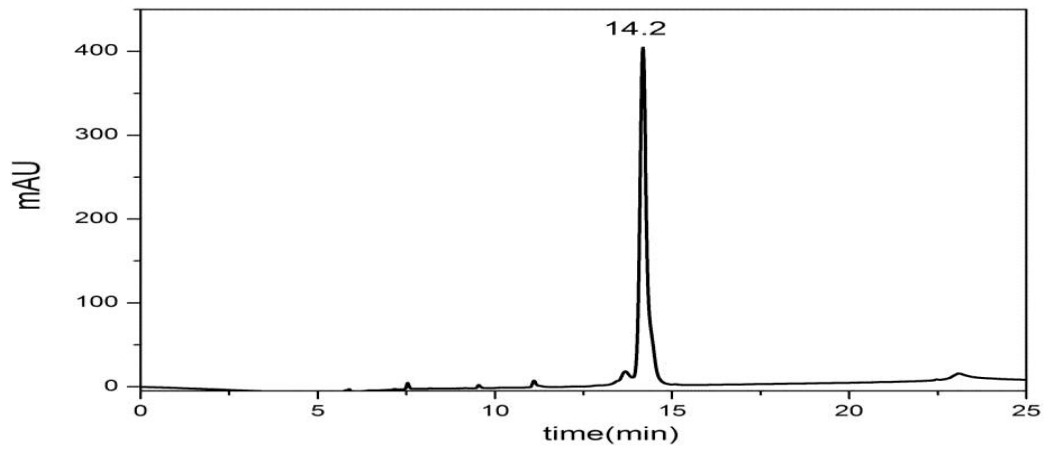
HPLC of PNA 3



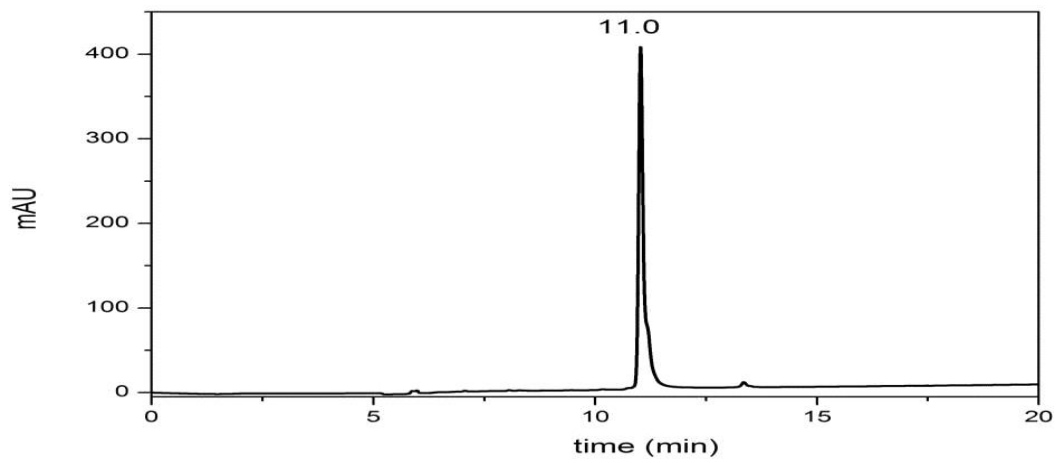
HPLC of PNA 4



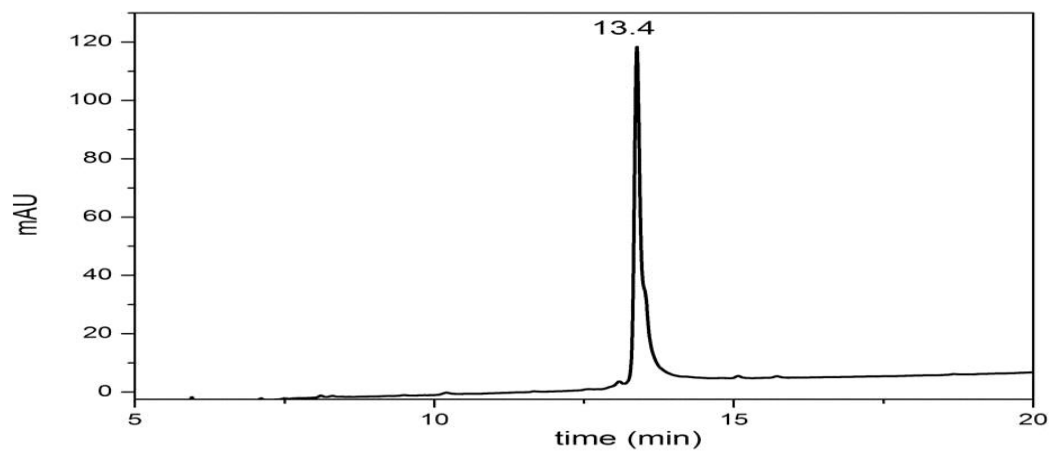
HPLC of PNA 5



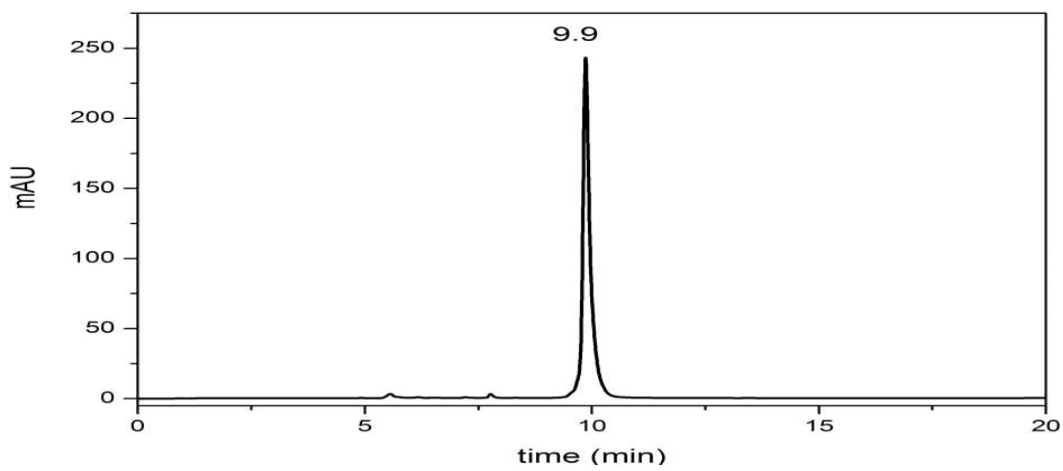
HPLC of PNA 6



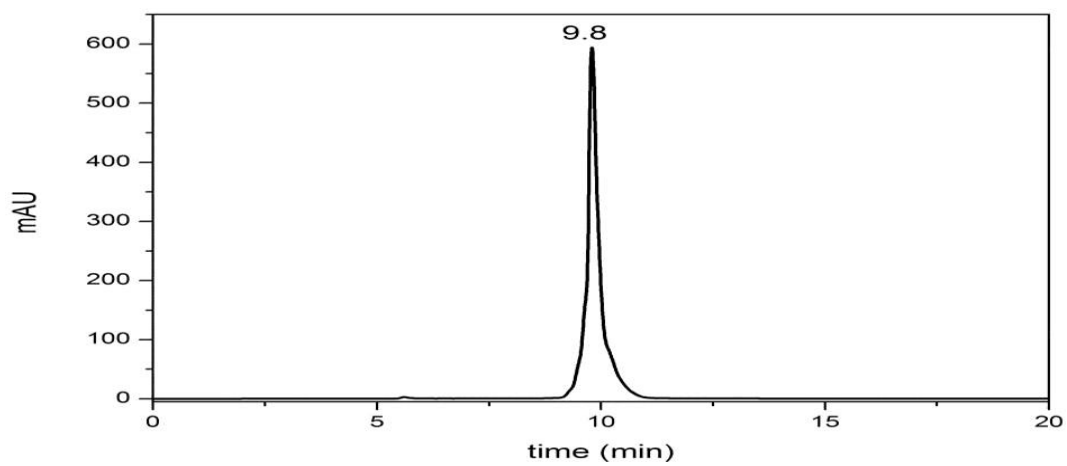
HPLC of PNA 7



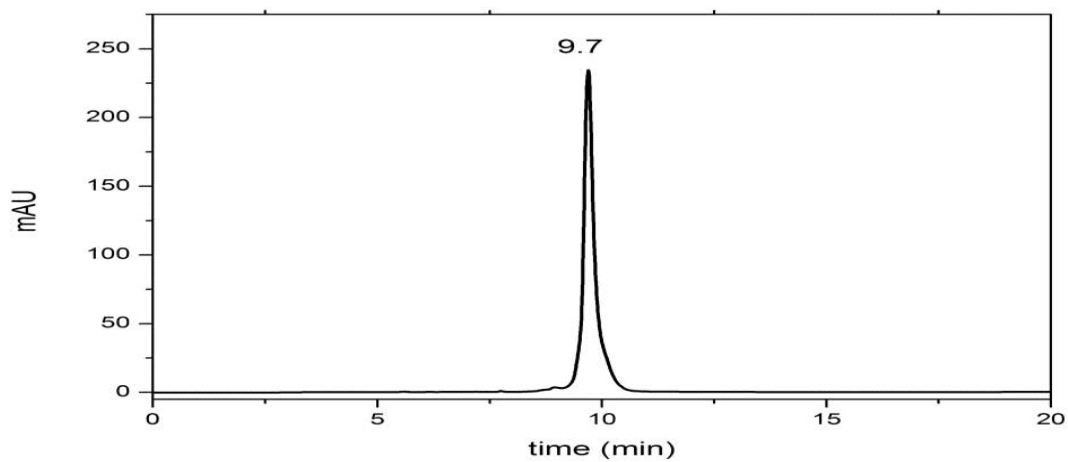
HPLC of PNA 8



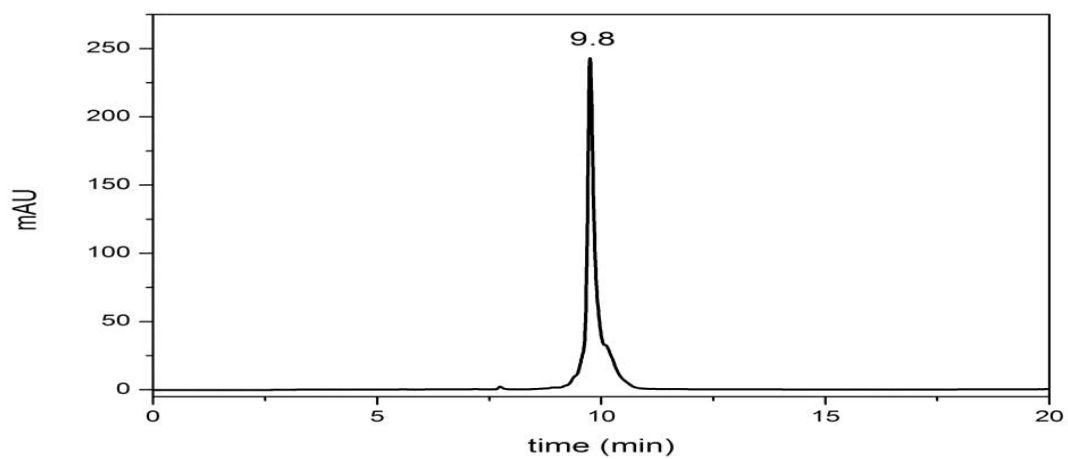
HPLC of PNA 9



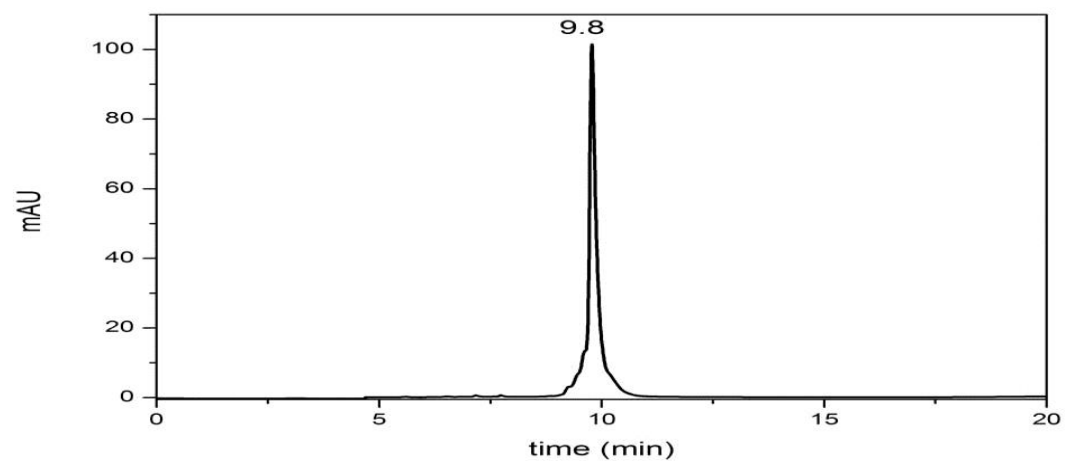
HPLC of PNA 10



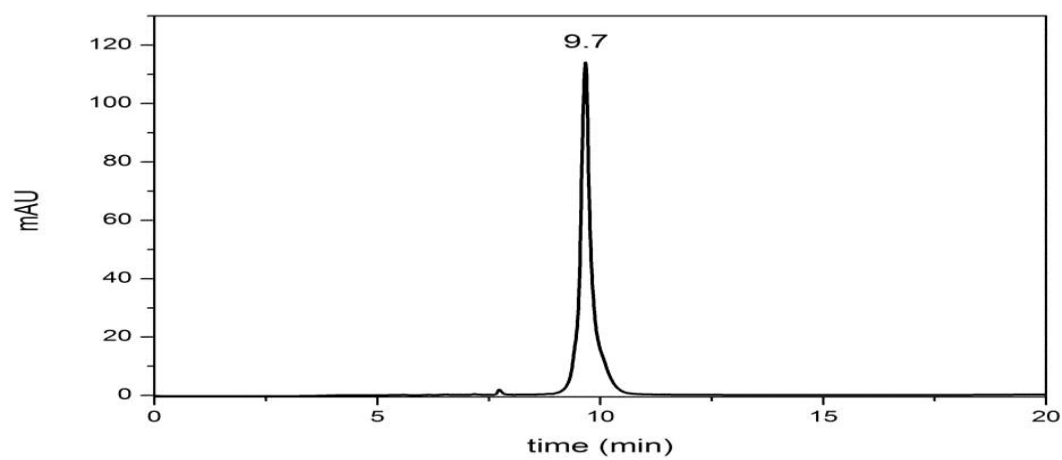
HPLC of PNA 11



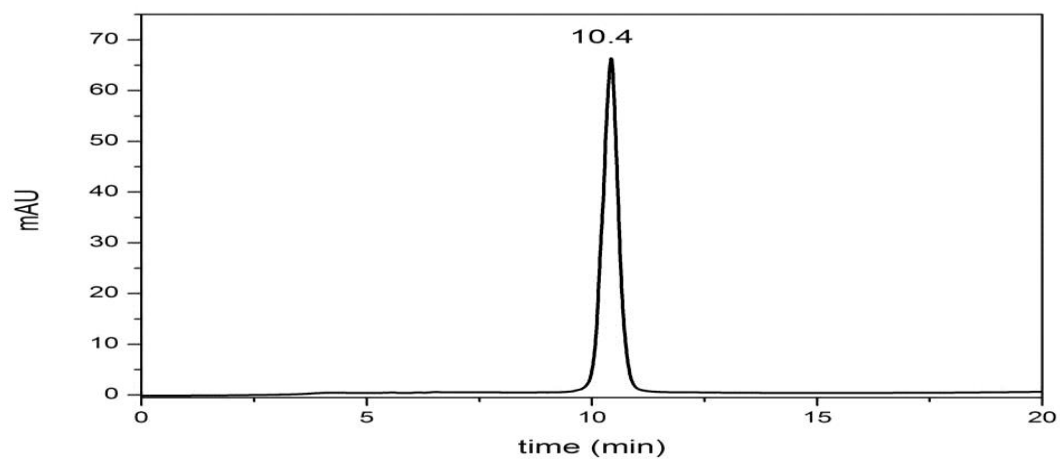
HPLC of PNA 12



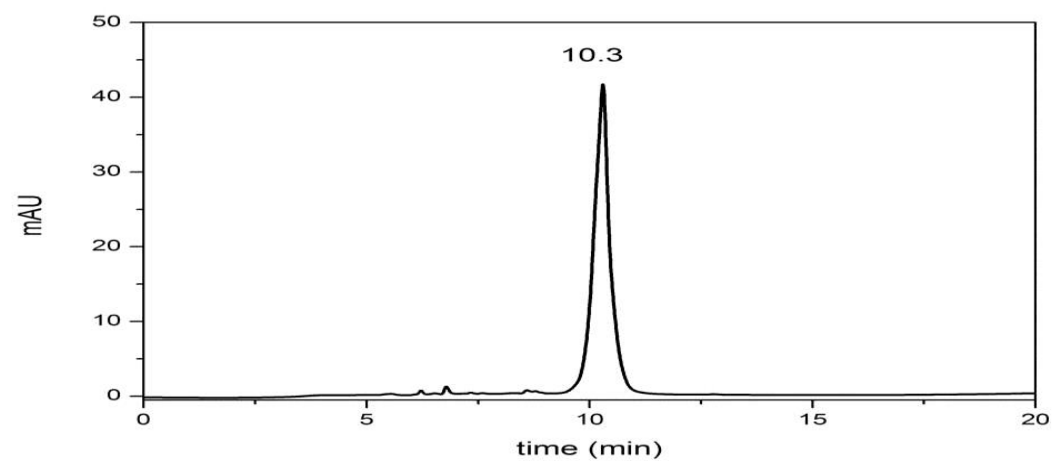
HPLC of PNA 13



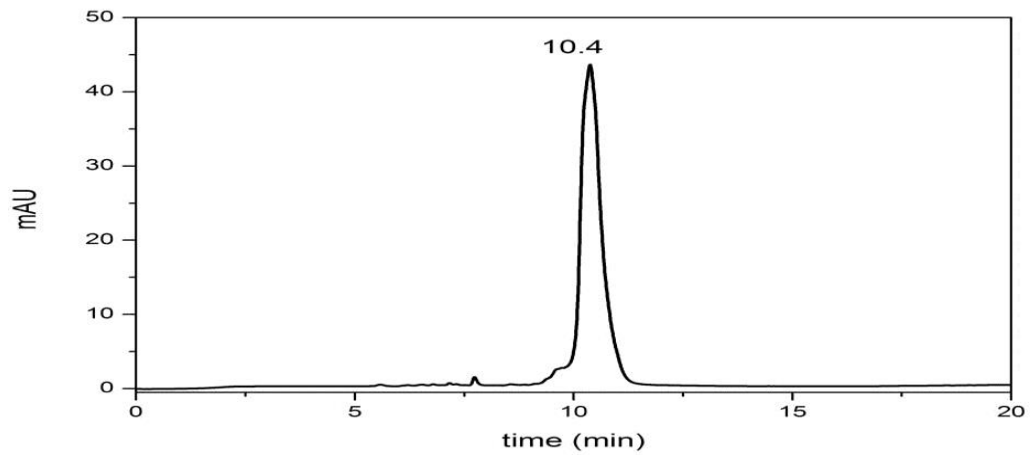
HPLC of PNA 14



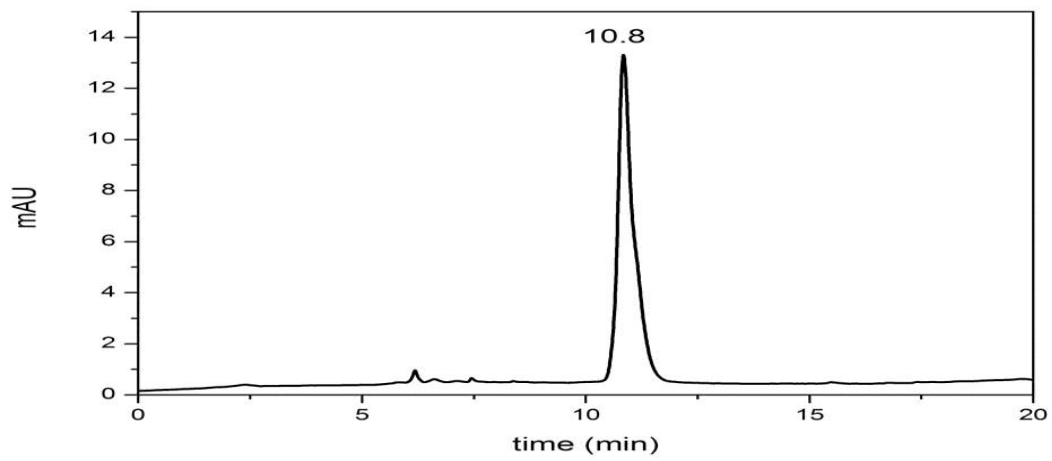
HPLC of PNA 15



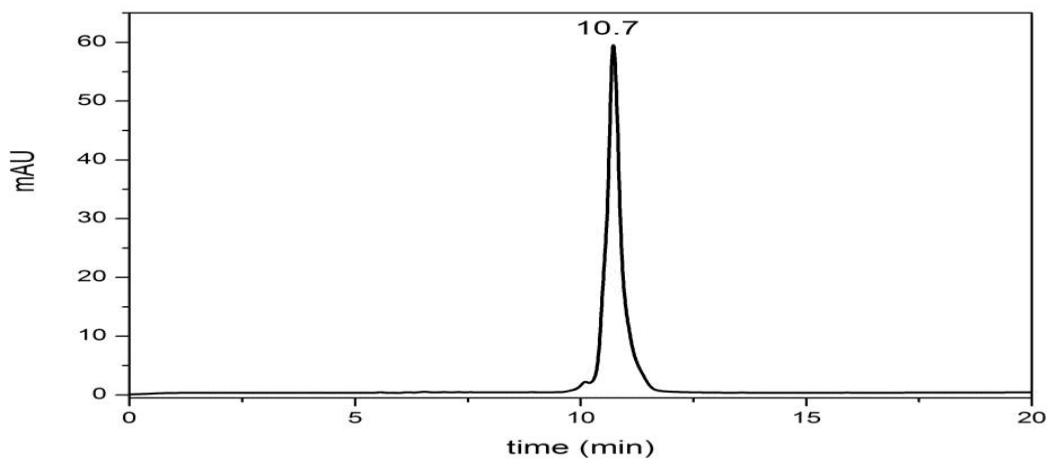
HPLC of PNA 16



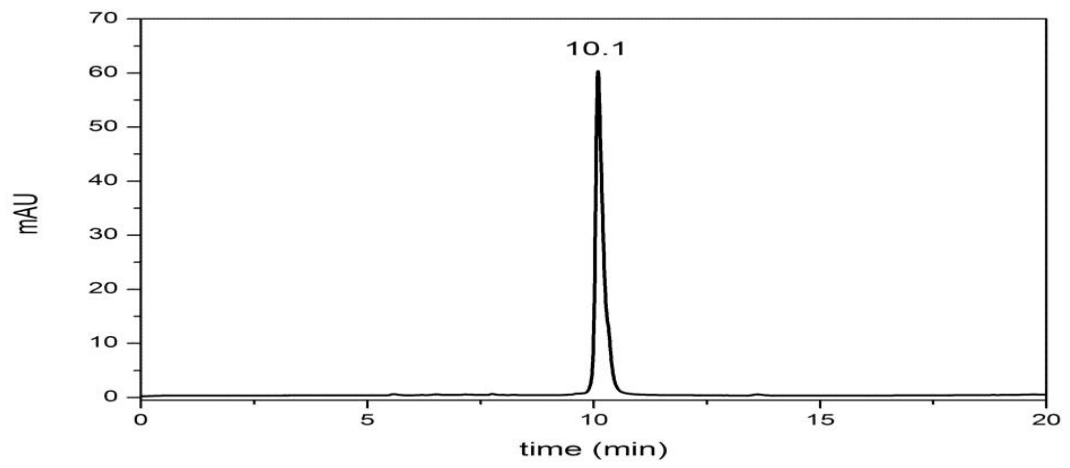
HPLC of PNA 17



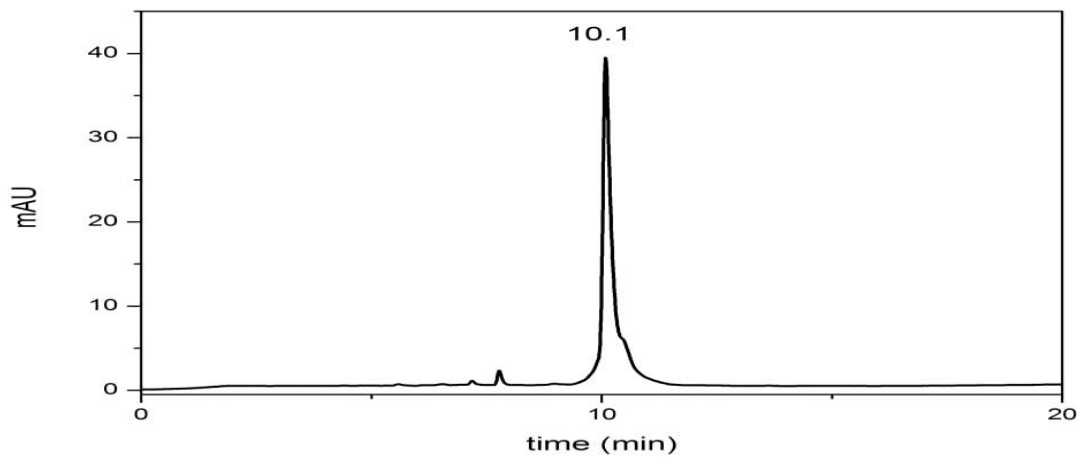
HPLC of PNA 18



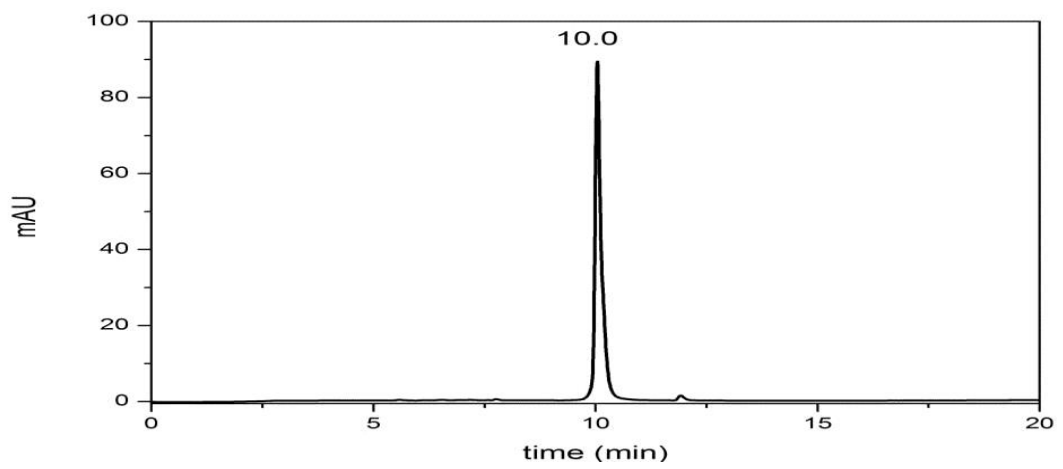
HPLC of PNA 19



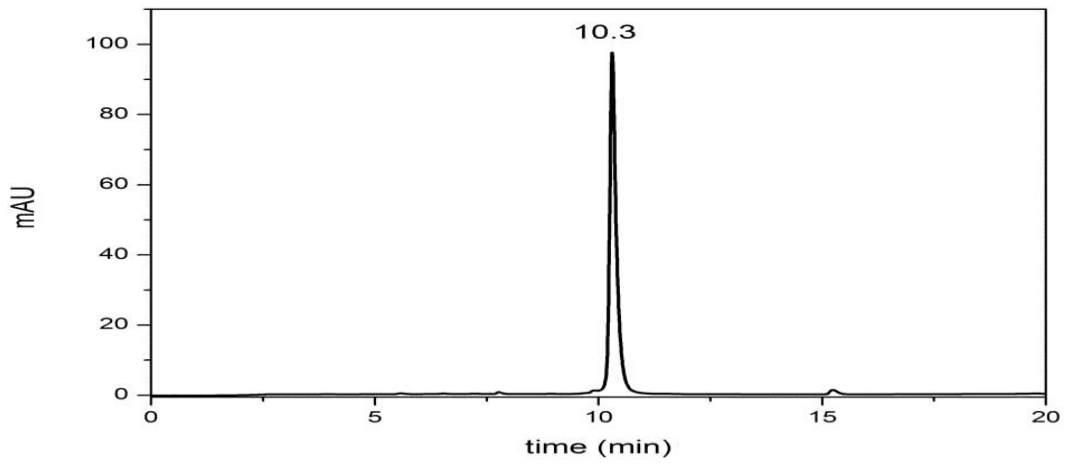
HPLC of PNA 20



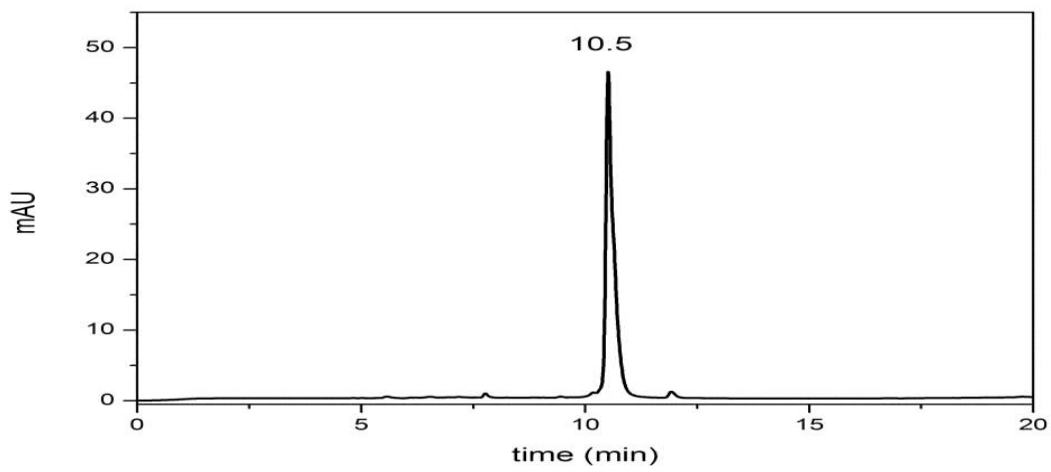
HPLC of PNA 21



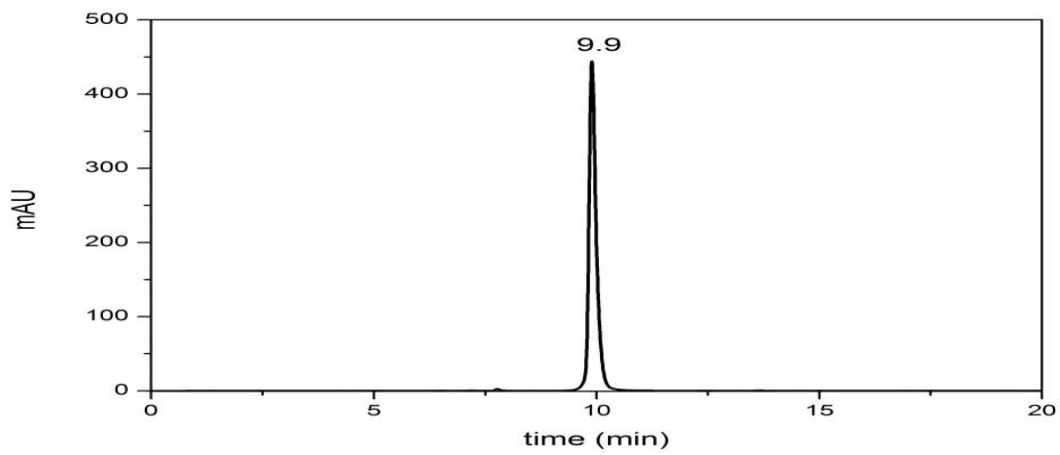
HPLC of PNA 22



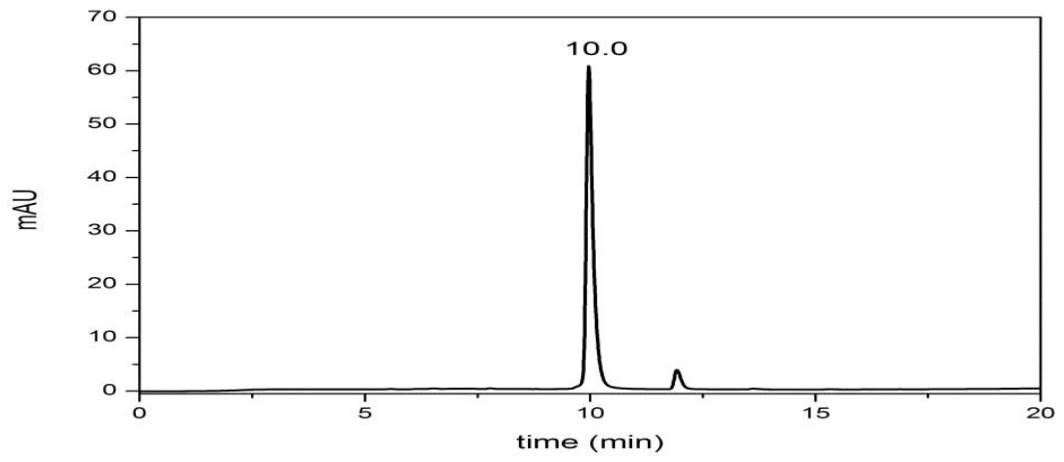
HPLC of PNA 23



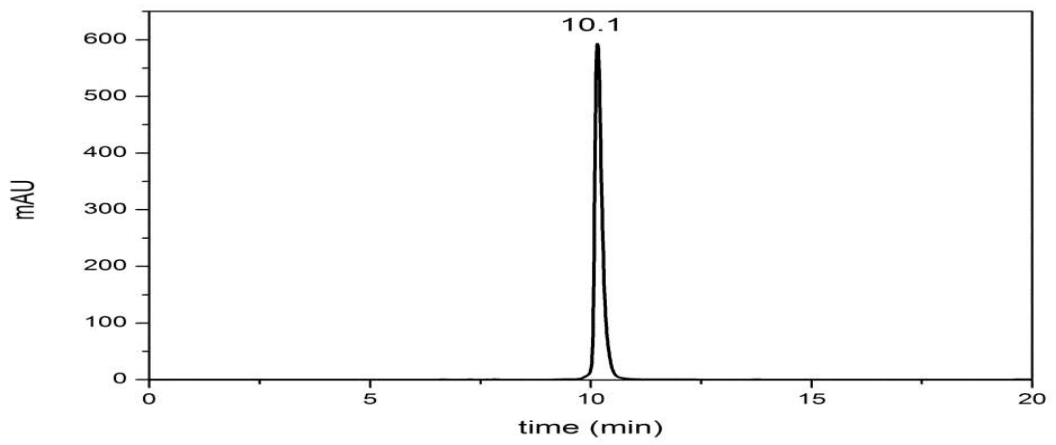
HPLC of PNA 24



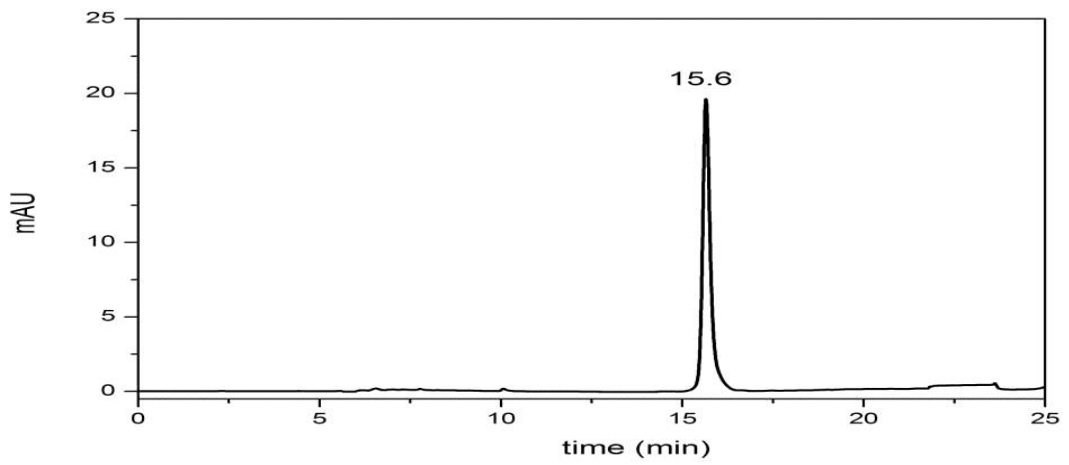
HPLC of PNA 25



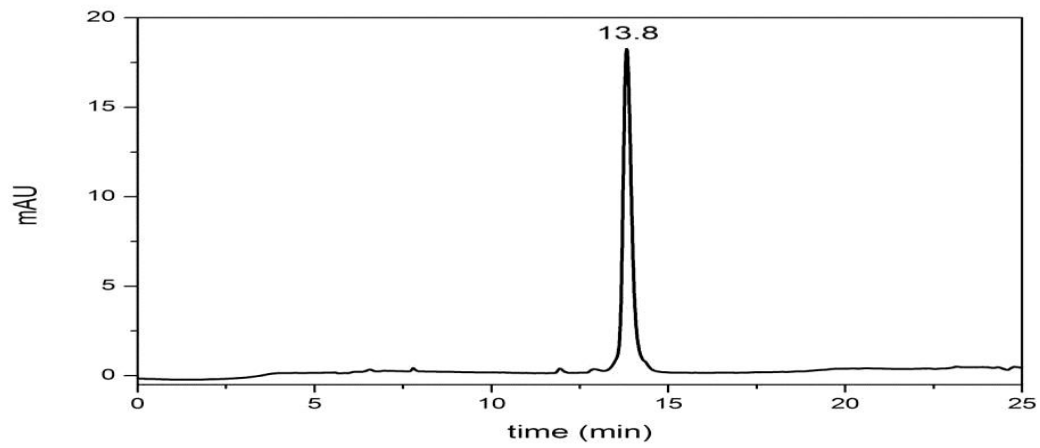
HPLC of PNA 26



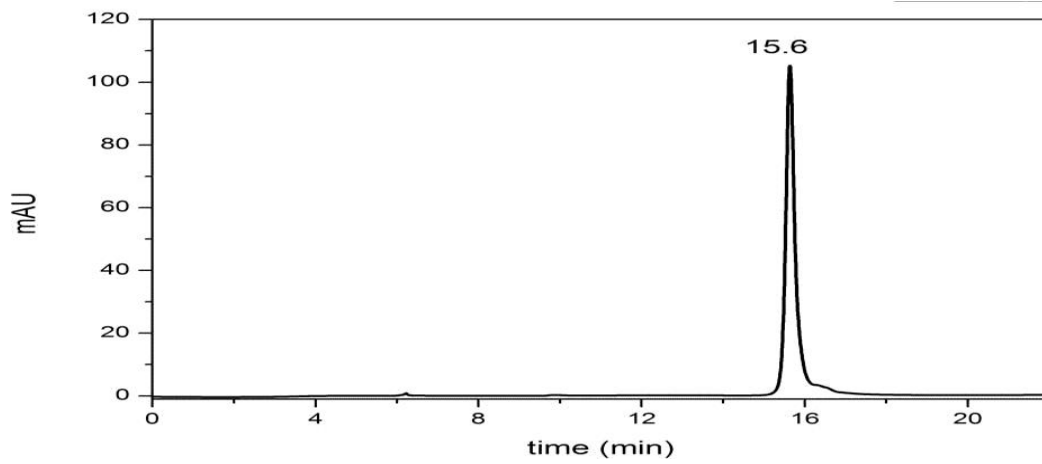
HPLC of PNA 27



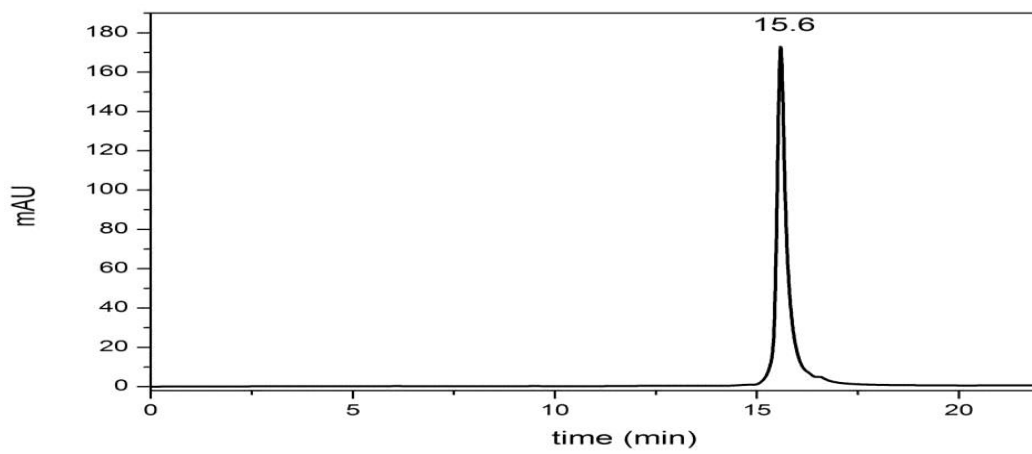
HPLC of PNA 28



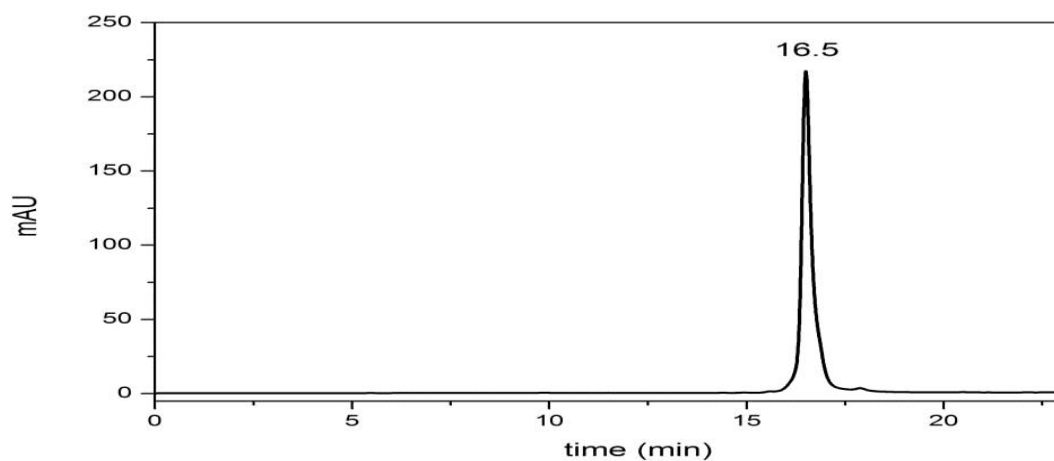
HPLC of PNA 29



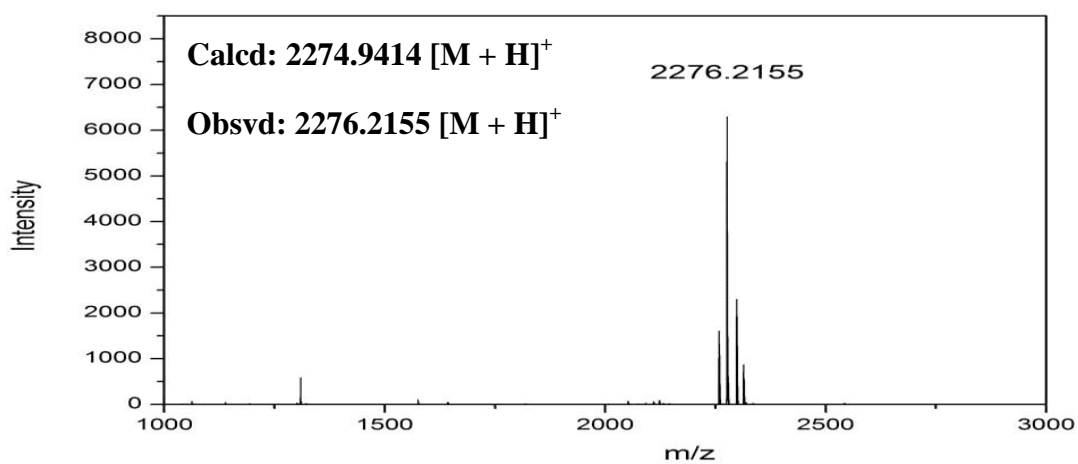
HPLC of PNA 30



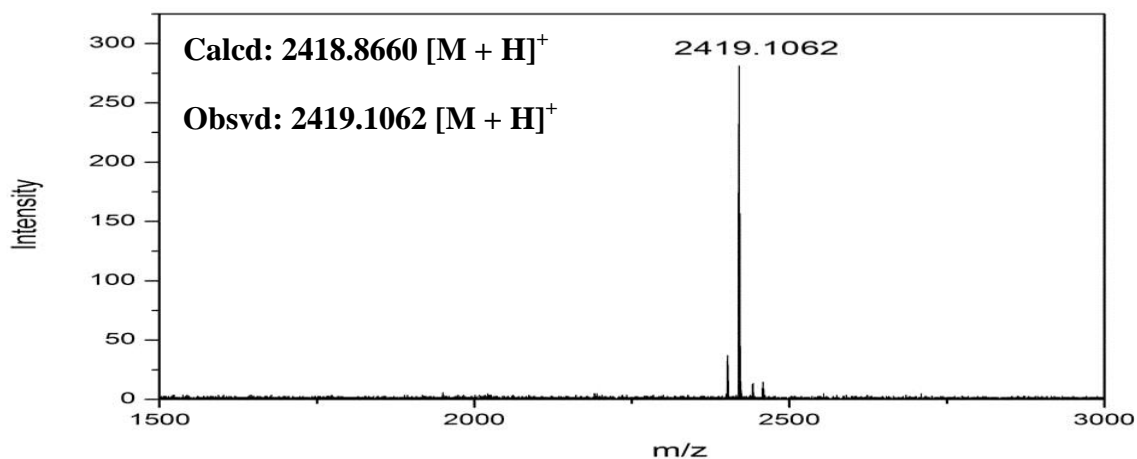
HPLC of PNA 31



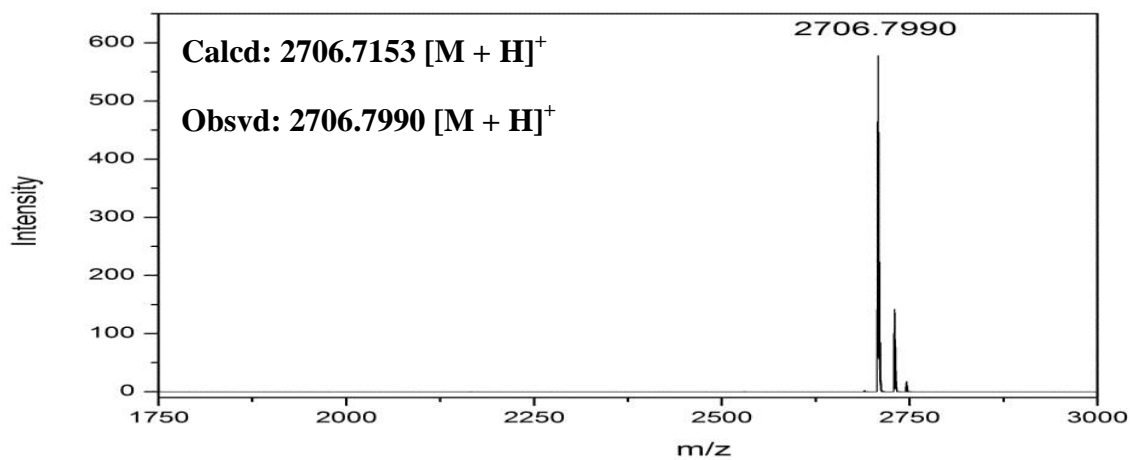
MALDI-TOF PNA 1



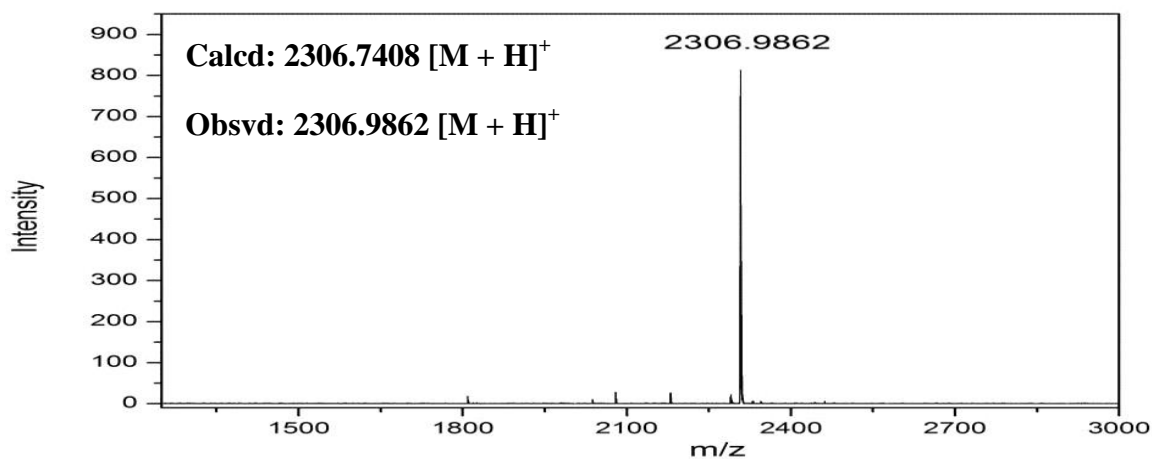
MALDI-TOF PNA 2



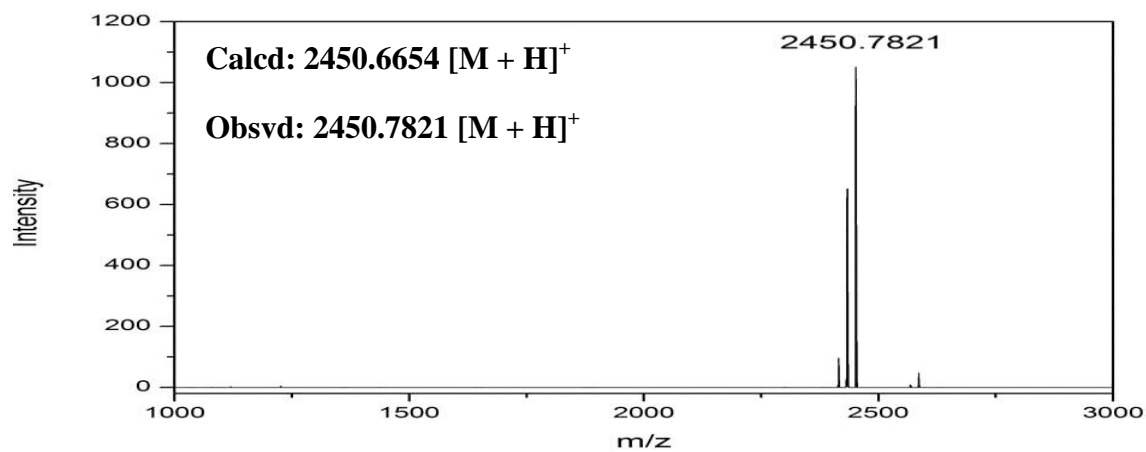
MALDI-TOF PNA 3



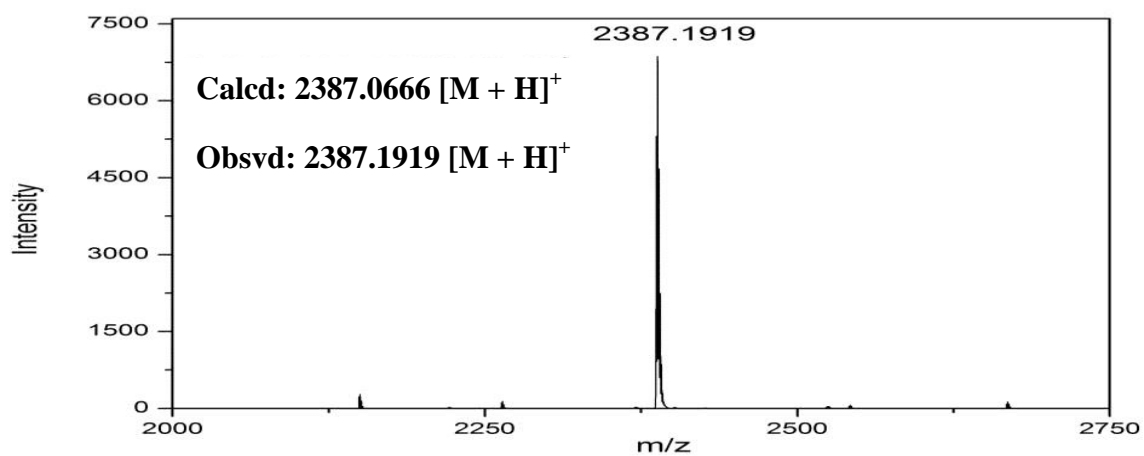
MALDI-TOF PNA 4



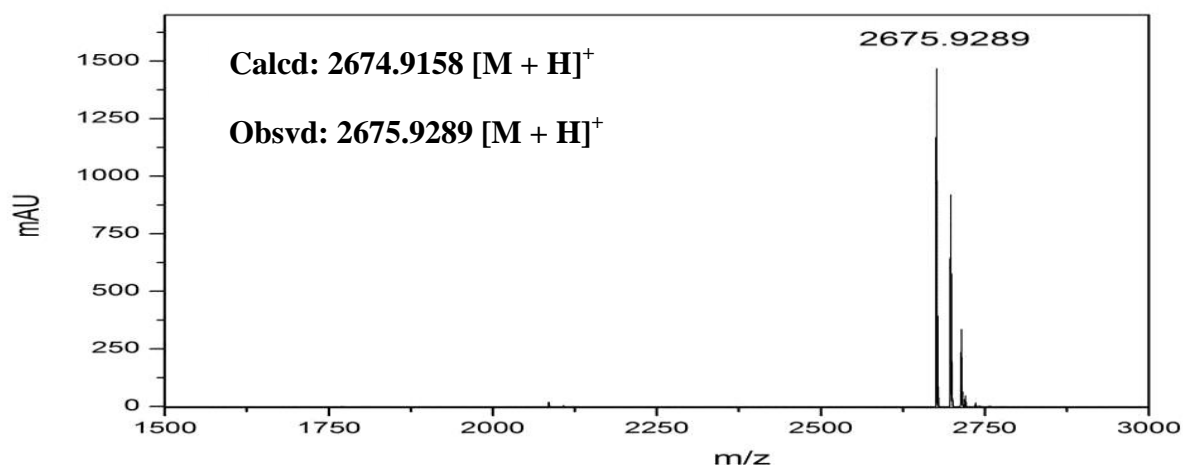
MALDI-TOF PNA 5



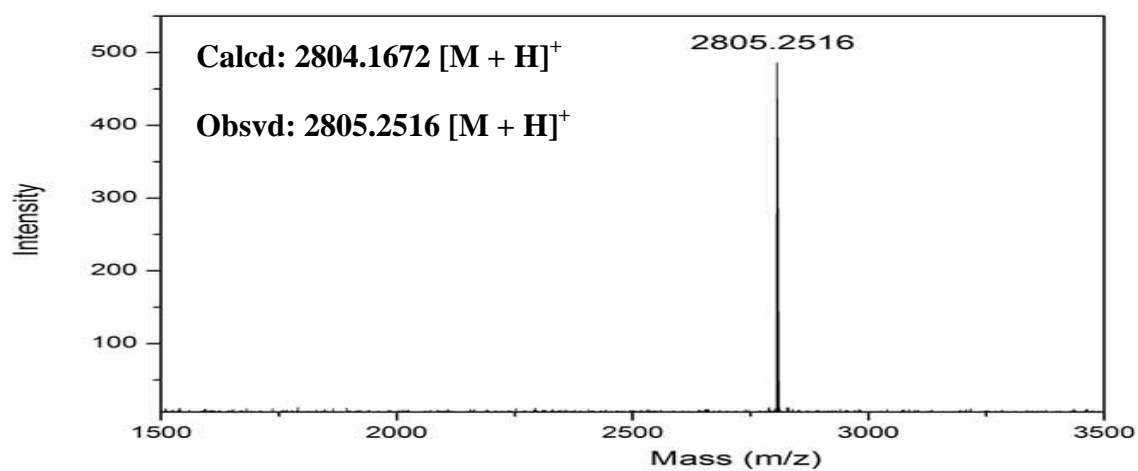
MALDI-TOF PNA 6



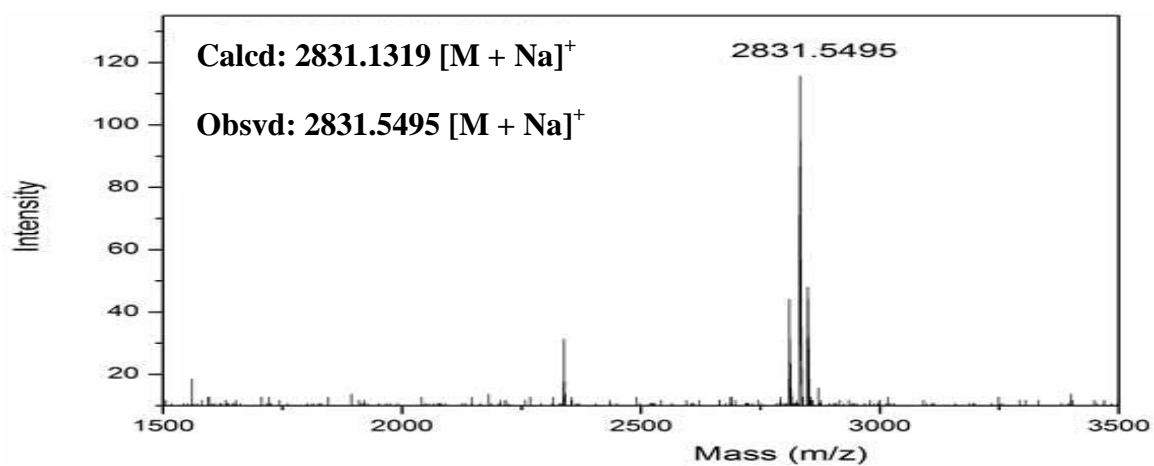
MALDI-TOF PNA 7



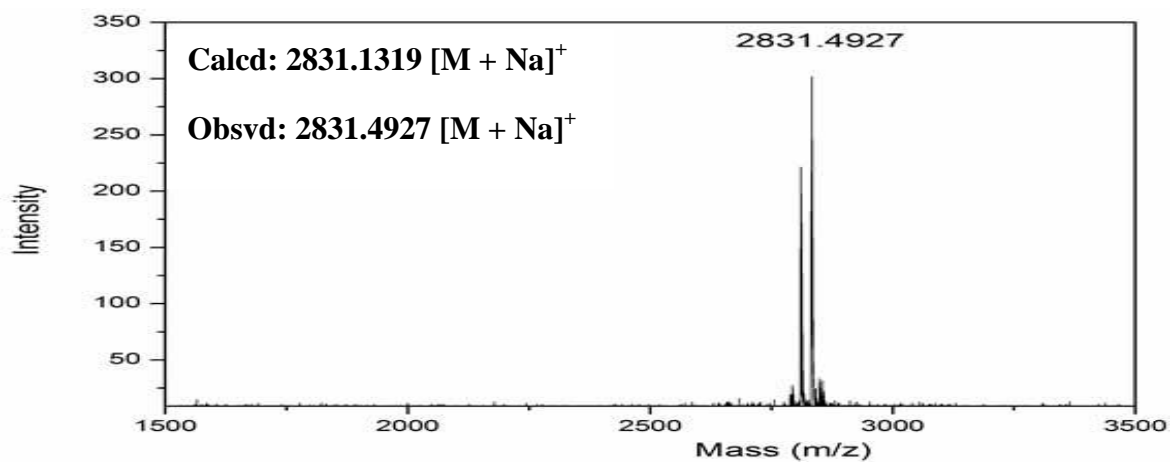
MALDI-TOF PNA 8



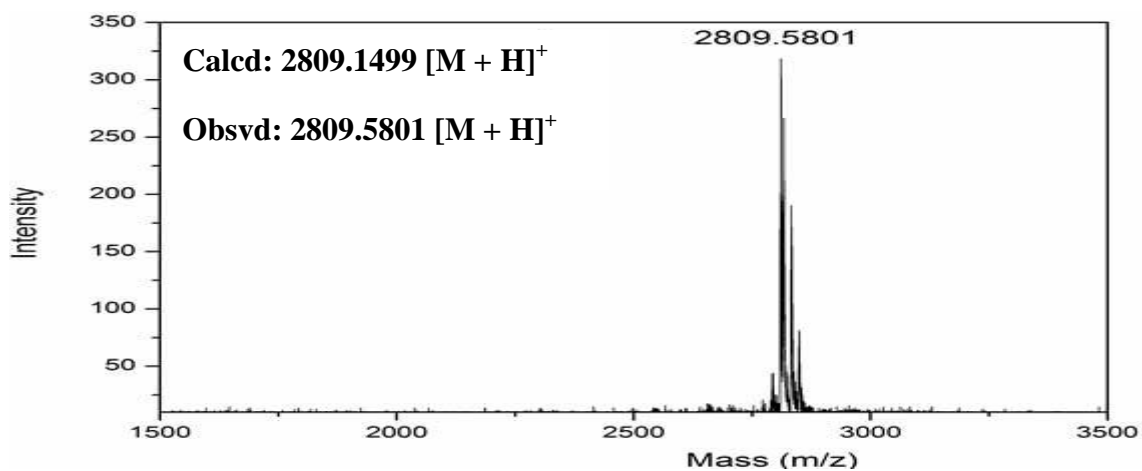
MALDI-TOF PNA 9



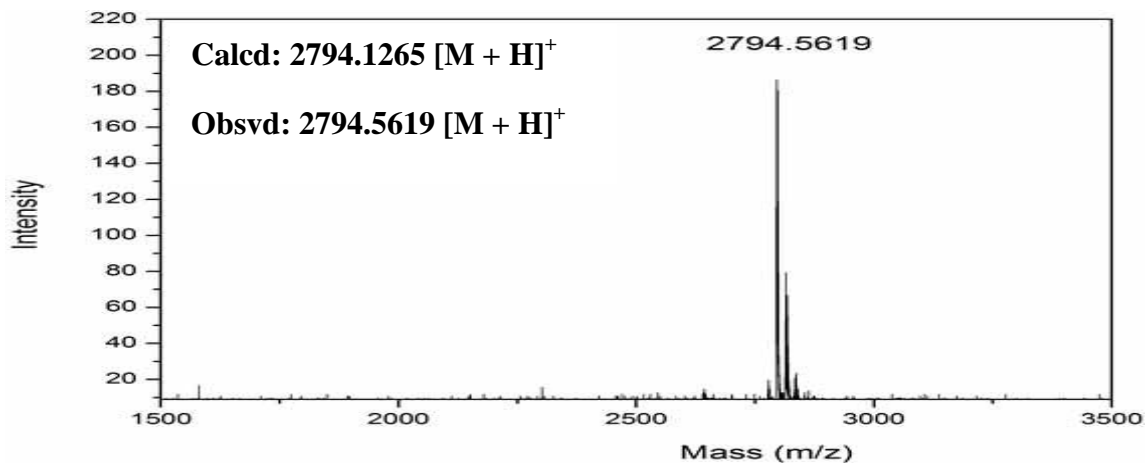
MALDI-TOF PNA 10



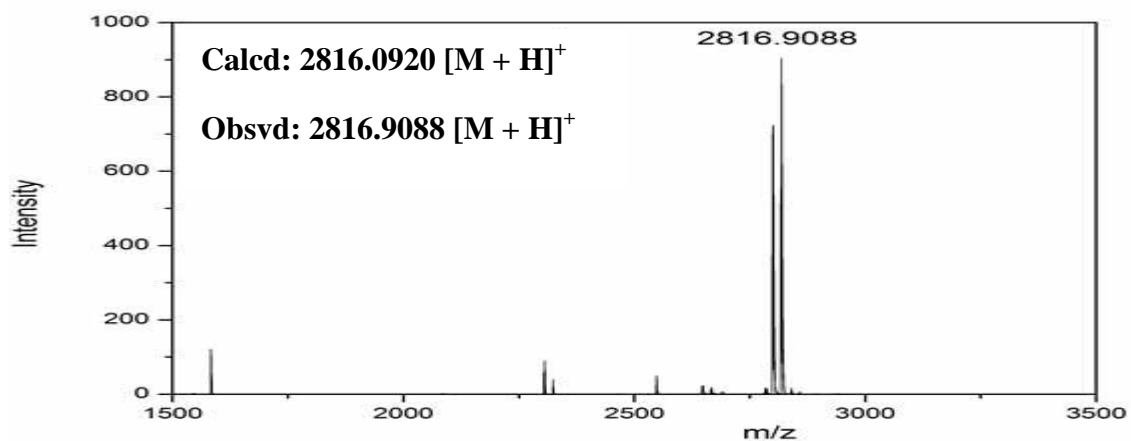
MALDI-TOF PNA 11



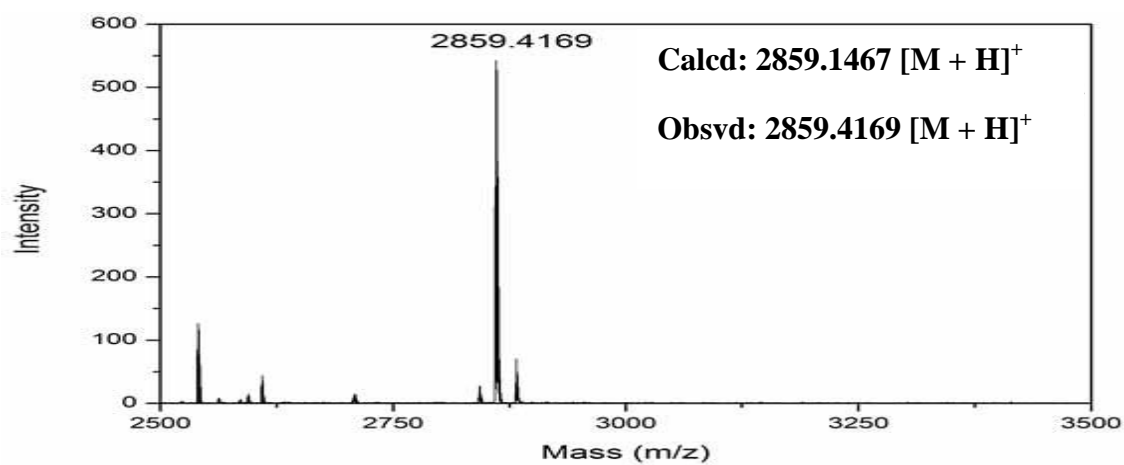
MALDI-TOF PNA 12



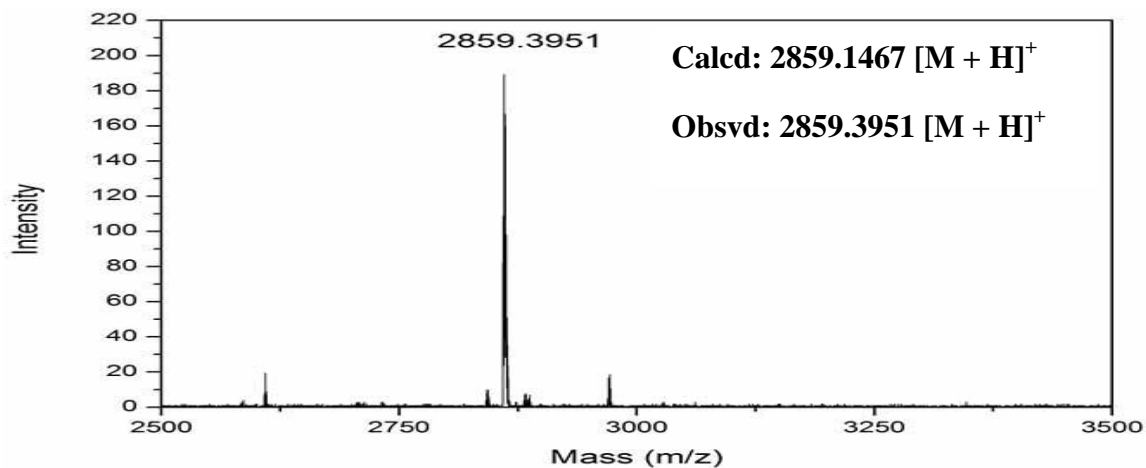
MALDI-TOF PNA 13



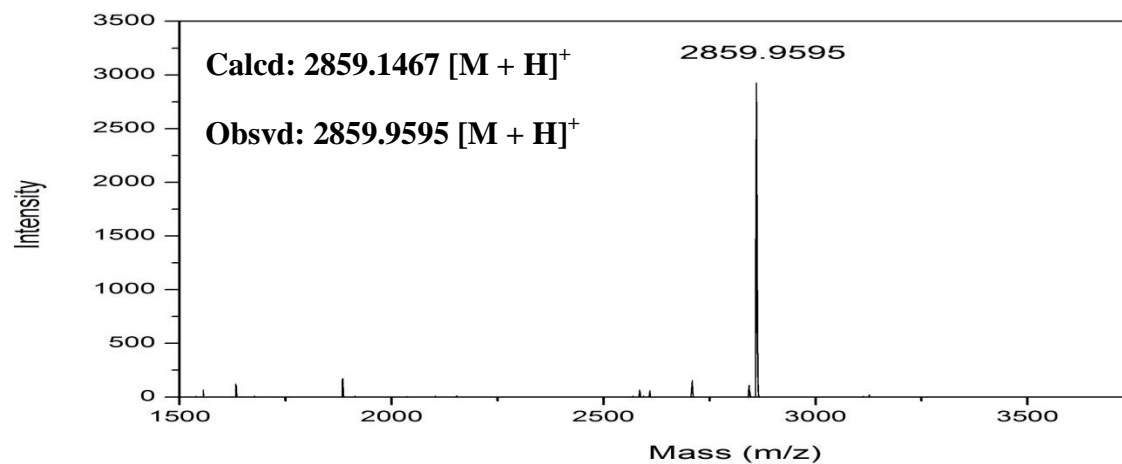
MALDI-TOF PNA 14



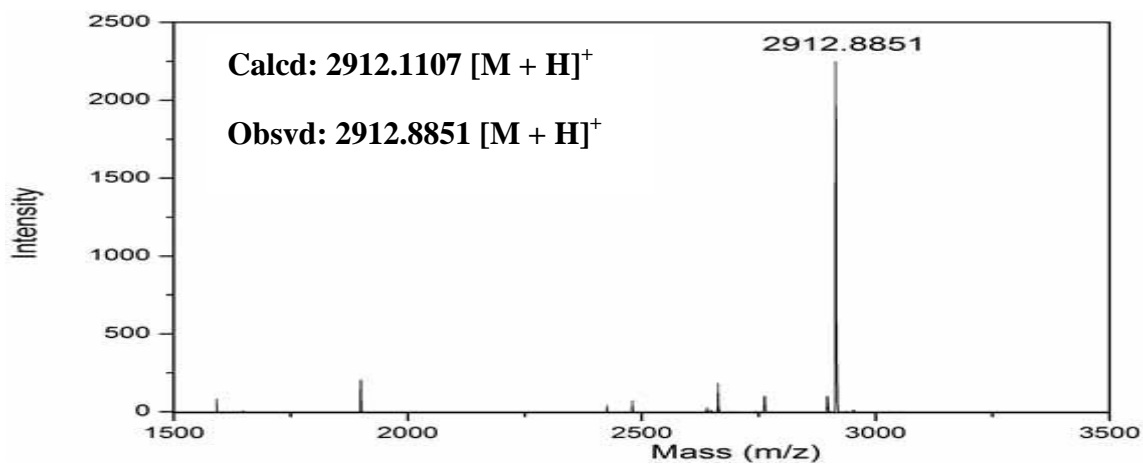
MALDI-TOF PNA 15



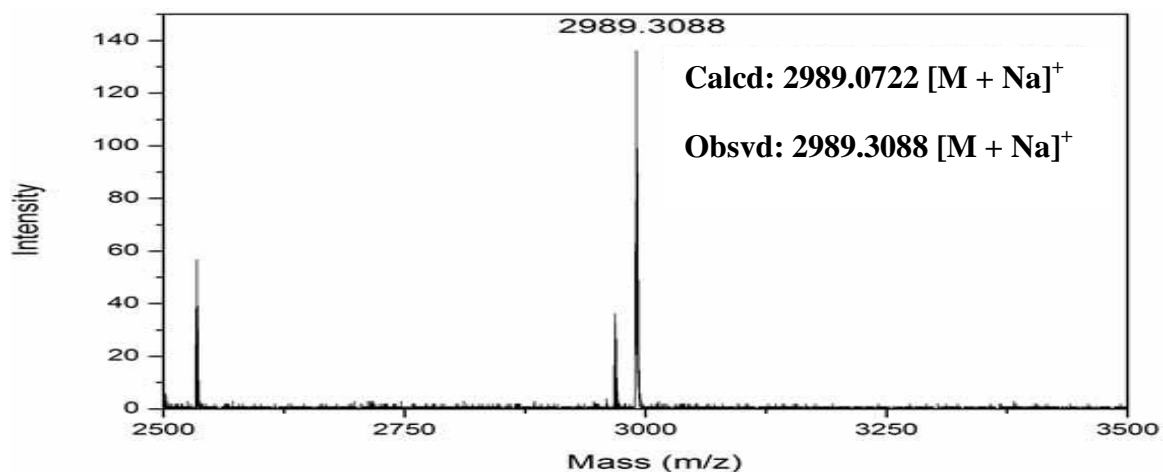
MALDI-TOF PNA 16



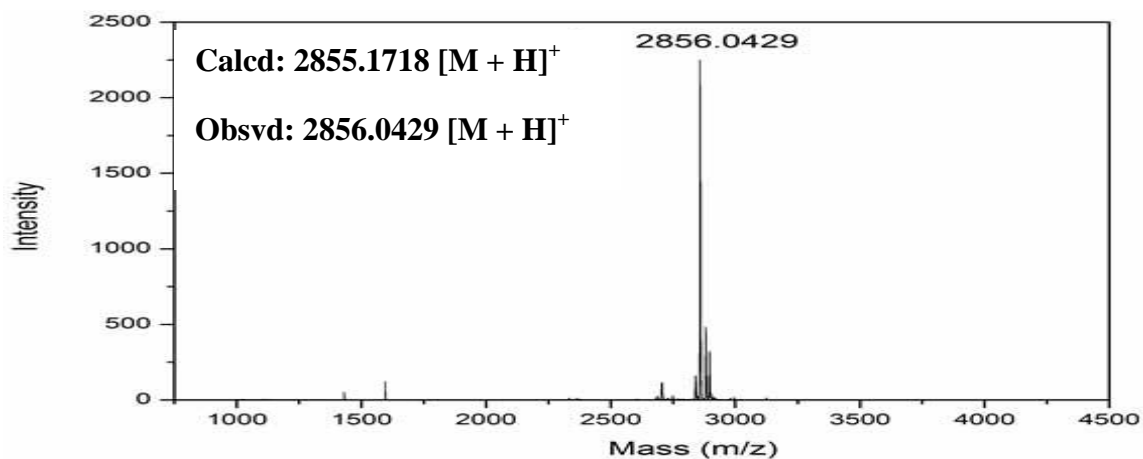
MALDI-TOF PNA 17



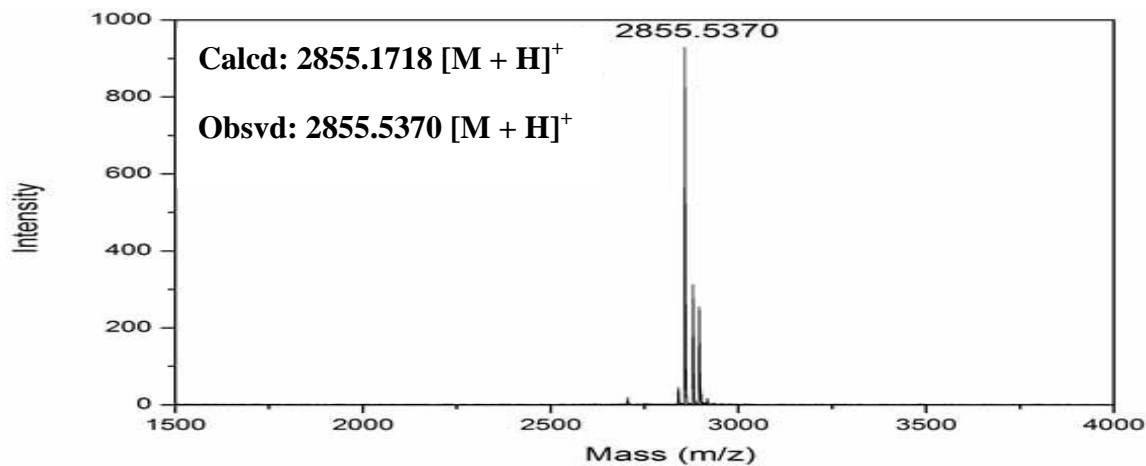
MALDI-TOF PNA 18



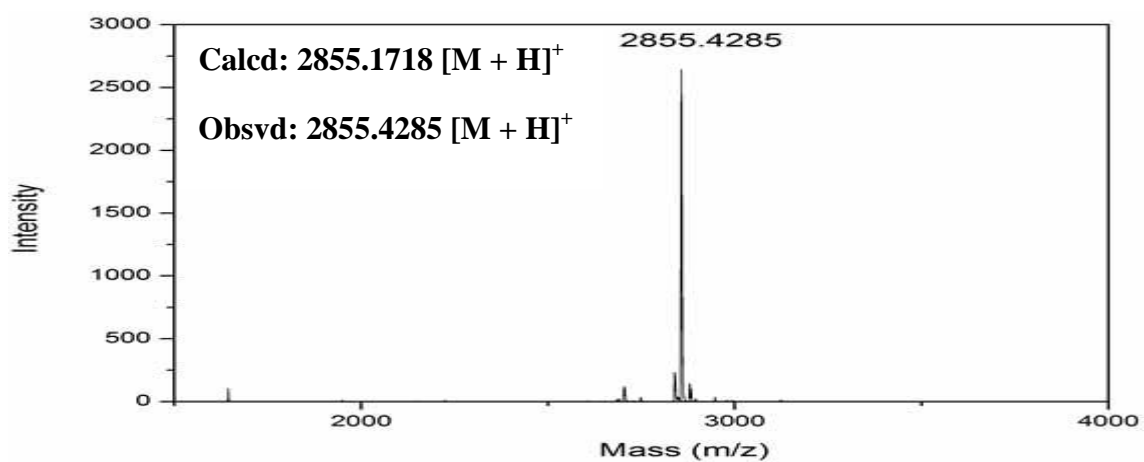
MALDI-TOF PNA 19



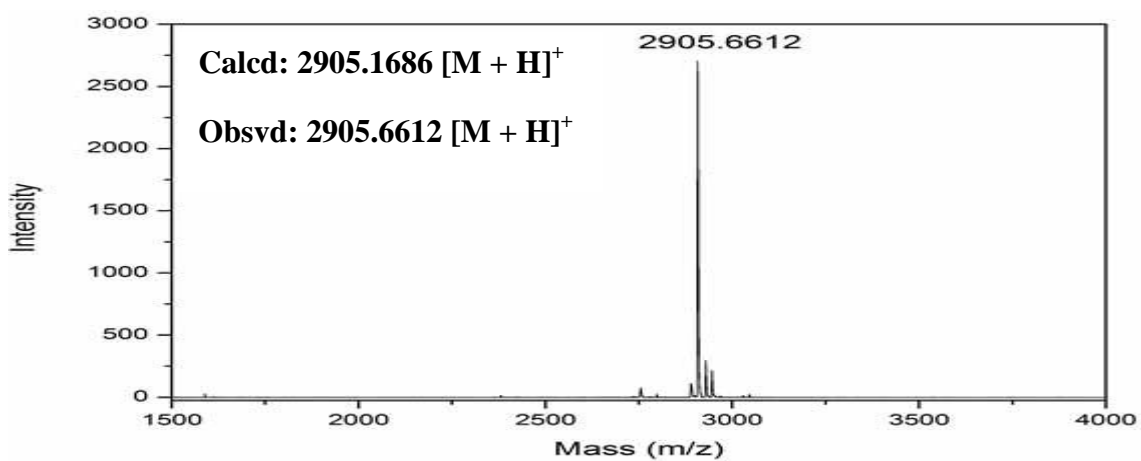
MALDI-TOF PNA 20



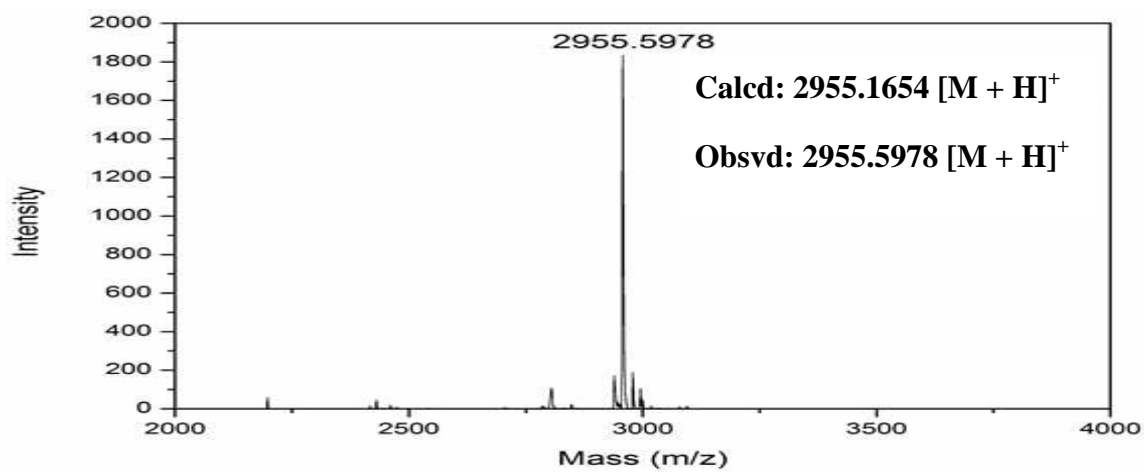
MALDI-TOF PNA 21



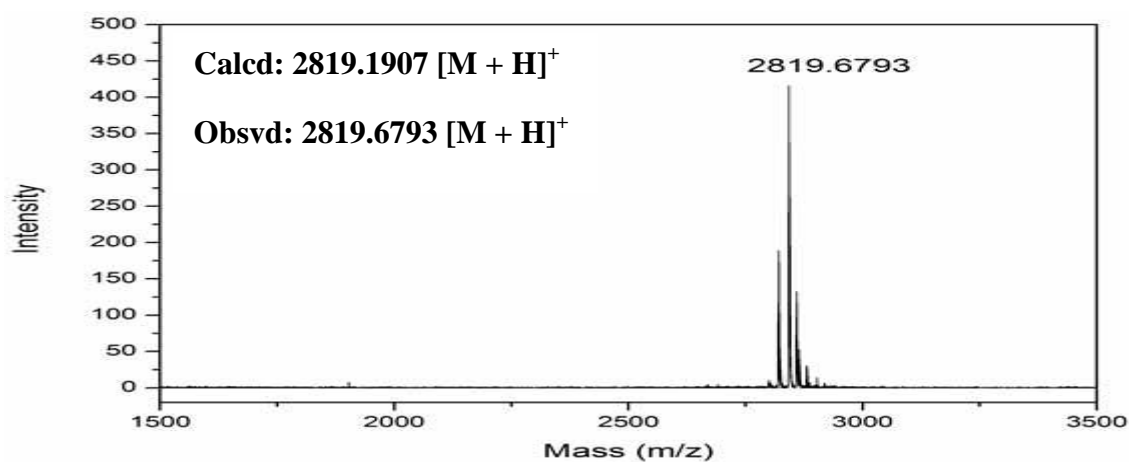
MALDI-TOF PNA 22



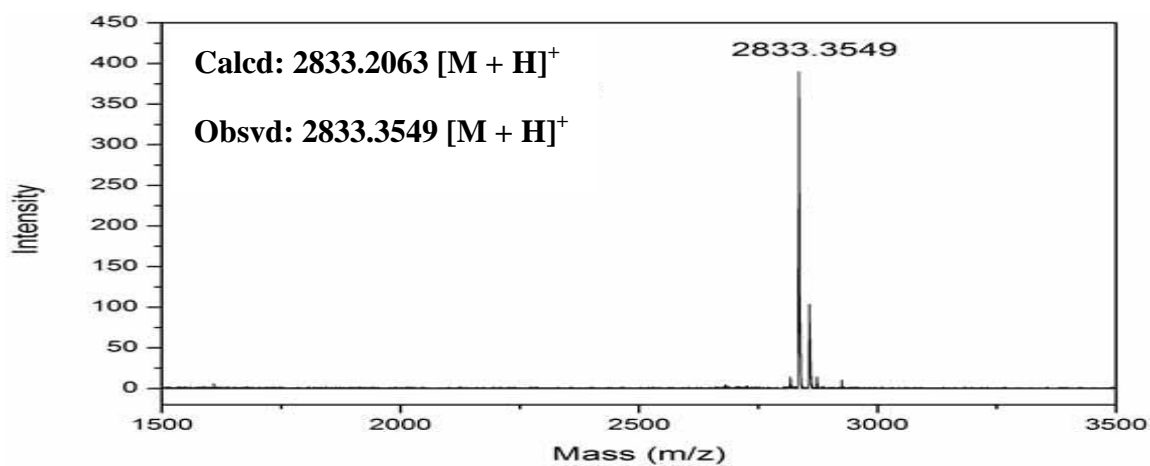
MALDI-TOF PNA 23



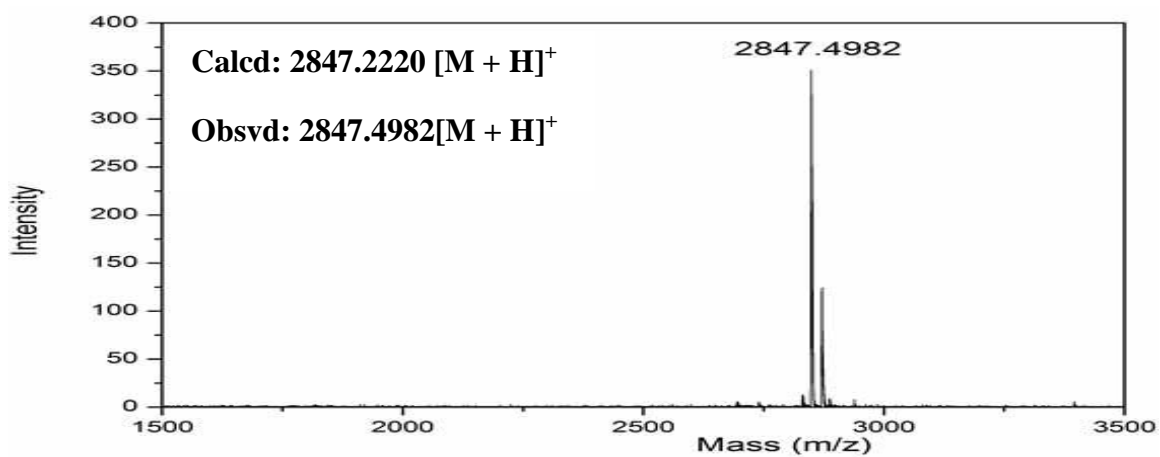
MALDI-TOF PNA 24



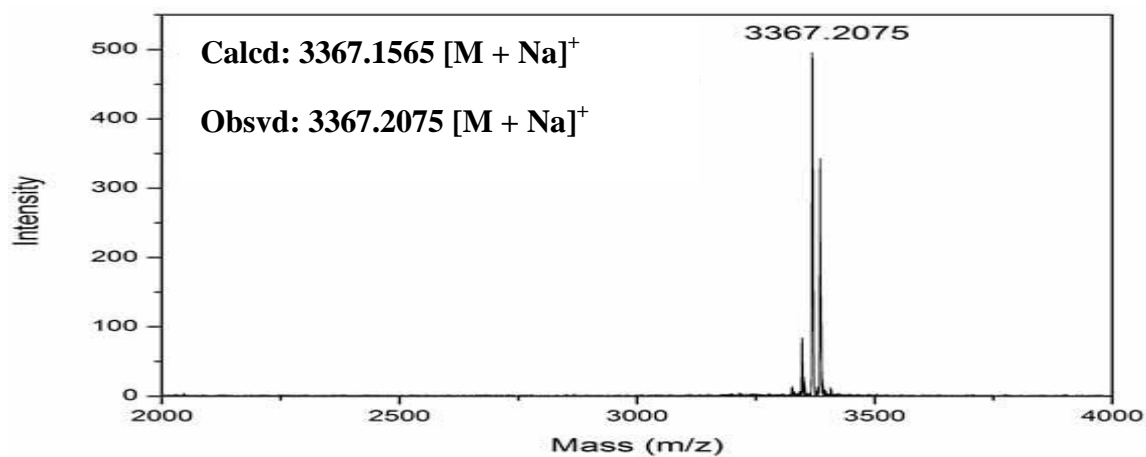
MALDI-TOF PNA 25



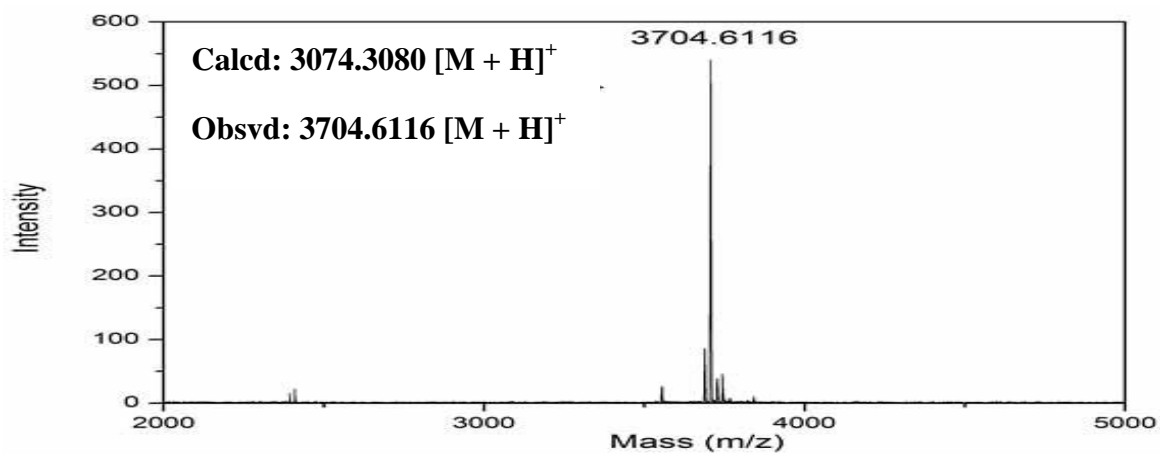
MALDI-TOF PNA 26



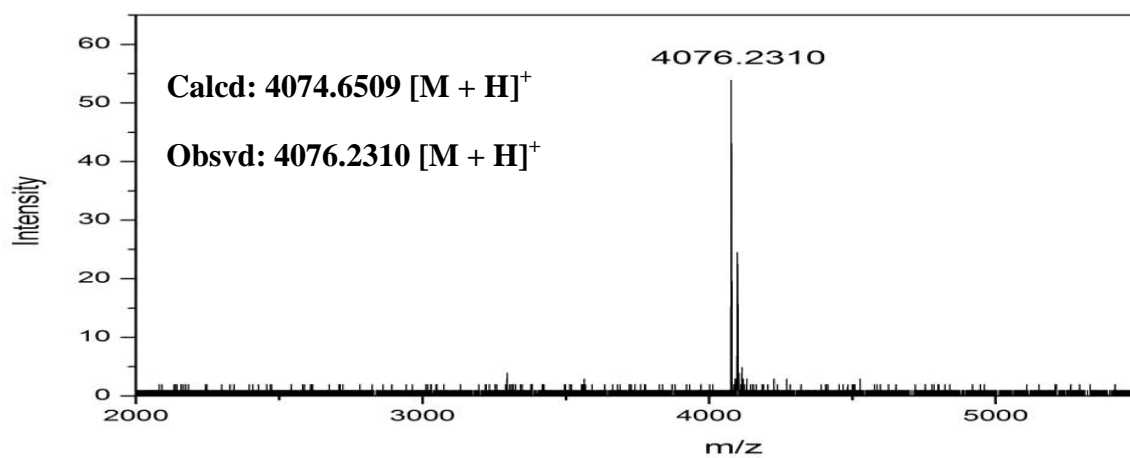
MALDI-TOF PNA 27



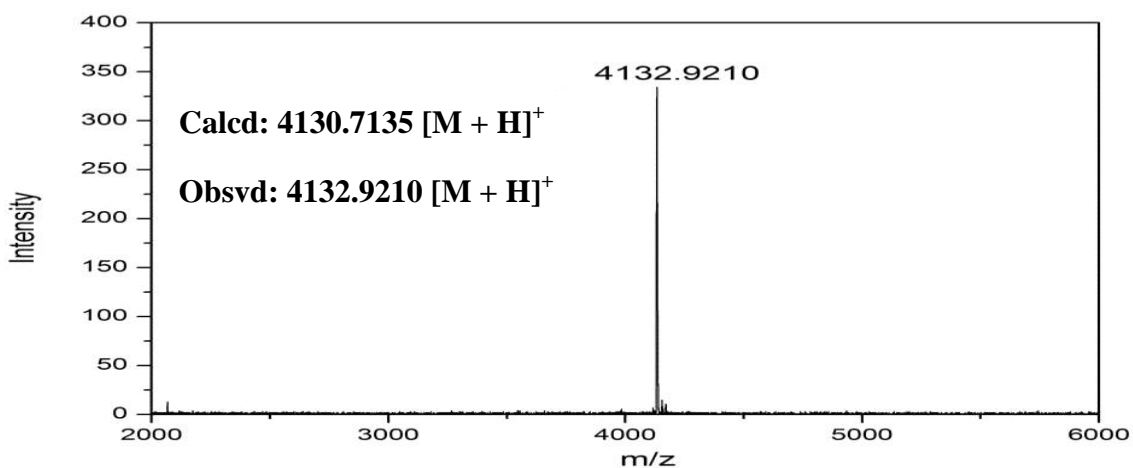
MALDI-TOF PNA 28



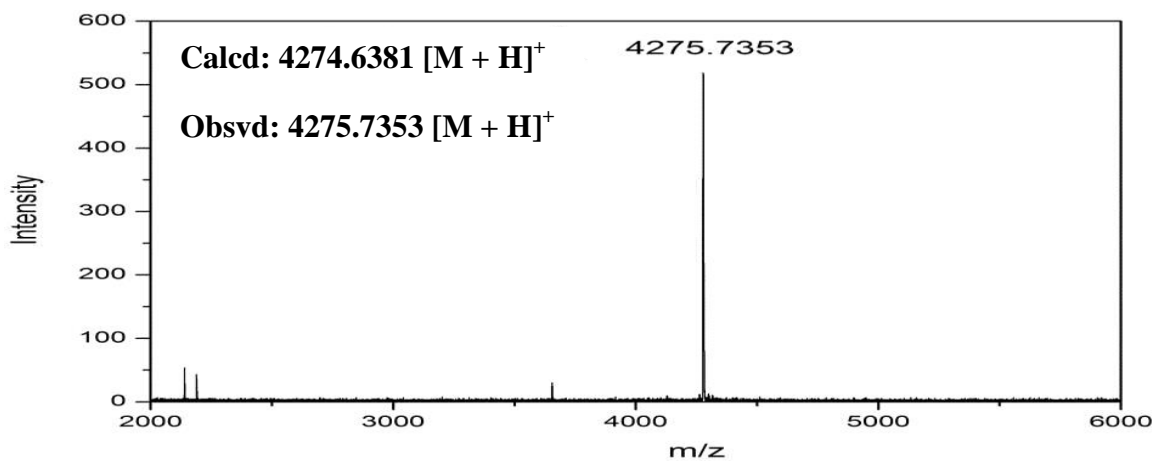
MALDI-TOF PNA 29



MALDI-TOF PNA 30



MALDI-TOF PNA 31



Chapter 3: Biophysical Evaluation of Fluorinated PNA Oligomers

3.1 Introduction

The objective of introduction of fluorine into PNA oligomers was to improve its hydrophobicity character and persuade such fluorinated PNAs to enter into cells better than unsubstituted PNAs. Introduction of fluorine may also affect their base pairing/duplex formation property. This chapter aims to investigate the consequences of fluorine substitution on both these biophysical properties.

3.1.1 Hydrophobicity (lipophilicity) studies of fluorinated homooligomers

Lipophilicity is a physicochemical property that has crucial importance in medicinal chemistry and is an important factor defining the pharmacokinetics and pharmacodynamics of a drug substance. It has emerged as a meaningful parameter in innumerable strategies for successful drug development.

A number of experimental methods exist in literature to determine the lipophilicity in terms of partition coefficient ($\log P/\log D$) which is a ratio of the concentrations of a solute in two immiscible or slightly miscible liquids. The classical method for partition coefficient measurement is shake-flask procedure, which involves a simple extraction with n-octan-1-ol/water system.¹ There are many variations of the shake-flask method. For example, (i) use of a quartet solvent system consisting of four different solvents octanol, chloroform, cyclohexane and propylene glycol dipelargonate (PGDP) instead of only octanol² and (ii) solid-phase microextraction (SPME) method, in which the sample partition between a fused silica fiber coated with a polymer and an aqueous phase.^{3,4} The choice of method depends on the type of substances used for the study. For lipophilicity determination of poorly soluble substances, automated continuous flow (sampling) method can be used, and for the partition of neutral or ion-paired substances into the organic phase the potentiometric titration method can be used.⁵

The shake-flask method has its advantages as well as disadvantages. This method is laborious and useful for a low $\log p$ range of -3 to 3. It can't be used for high hydrophobic or hydrophilic compounds because of solubility issues, emulsion formation and adsorption onto vessel walls and also needs high purity and relatively large amounts of substances.^{6,7}

As a consequence of accessibility, precision, reproducibility of retention data, and partitioning automation, HPLC has become a convenient and standard procedure to estimate lipophilicity ($\log P$) of a compound. The method enables an estimation of the $\log P$ values in the range of 0 to 6, unlike shake-flask method which allows $\log p$ only in the range of -3 to 3.⁸

HPLC method is an indirect approach to measure the relative lipophilicity, involving the use of reference compounds injected onto a C18 column. The retention factors of compounds with known $\log P$ values are used to create a calibration curve and a group of compounds with unknown $\log P$ values injected and their retention factors are used to predict $\log P$ from the calibration curve.⁹

Substitution of hydrogen by fluorine is known to enhance the cell permeability through enhanced overall hydrophobicity.¹⁰ In order to examine the effect of fluorine in modulating hydrophobic character upon substitution of hydrogen with fluorine in a PNA, the various fluorinated PNA homooligomers synthesized with fluorine located at different sites on backbone, side chain and in the nucleobase. The HPLC retention time (R_t) was used as a marker to estimate the effect of fluorinated PNAs on lipophilicity. This is followed by biophysical studies of the fluorinated PNA oligomers to determine the thermal stability of their hybrids with complementary DNA/RNA.

3.1.2 Biophysical techniques used to study the hybridization properties

3.1.2a UV-based thermal melting (T_m)

The two strands of DNA are bound together through the stacking interactions favoured in an aqueous medium and specific hydrogen bonding between complementary base pairs. When the DNA sample is heated, the double helix unwinds into two single strands with the breaking of complementary base pairing and consequently the base-base stacking interaction. This increases the UV absorbance of a DNA solution (hyperchromicity). A similar phenomenon occurs in melting of PNA:DNA and PNA:RNA hybrids. Measuring the UV-absorbance as a function of temperature gives melting curves from which strength of the duplex stability of various hybrids (DNA:DNA, PNA:DNA, PNA:RNA) can be derived. This process termed as melting of DNA is a two state co-operation process with the PNA:DNA strands present either in the duplex form or in completely single stranded form. A plot of absorbance at 260 nm versus temperature gives a sigmoidal curve and midpoint of the transition denotes the T_m (Figure 3.1). The higher the T_m , grater is the stability of the duplex.

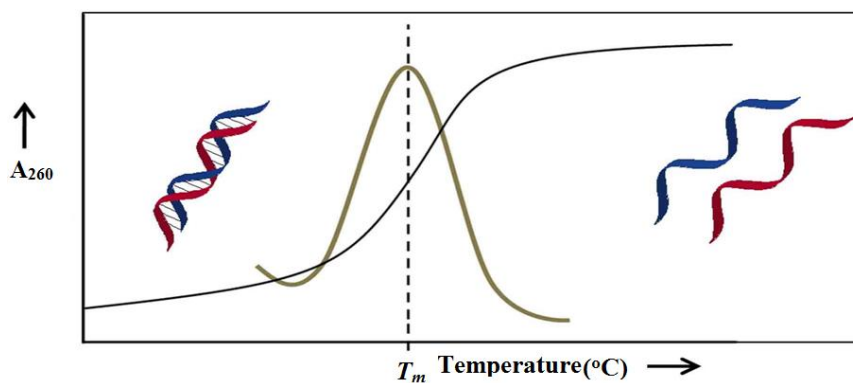


Figure 3.1 Sigmoidal and Derivative plots of PNA:DNA/RNA duplexes

3.1.2b Circular dichroism (CD)

CD refers to the differential absorption of the left and right circularly polarised components of plane-polarised light. This phenomenon arises from structural effects, when light is passed through a sample of chromophore, which is either intrinsically chiral because of its structure linked to an asymmetric center or placed in an asymmetric environment.¹¹ It is an excellent tool for rapid determination of the secondary structures and folding properties of biological macromolecules. The most common applications of CD include probing the structure and conformational analysis of proteins, nucleic acids and interaction with other ligands etc. CD spectra can provide a reliable estimation of the overall conformational state of biopolymers and any structural changes induced by binding to other ligands or interaction with complementary sequences. In case of nucleic acids, the sugar units of the backbone possess chirality and the bases attached to sugars are the chromophores. The single stranded PNA not being chiral does not show CD signal, but upon complexation with DNA or RNA that are chiral, shows CD profiles. The examples of CD-patterns of A- and B-forms of DNA,¹² PNA:DNA and PNA:RNA¹³ duplexes are shown in Figure 3.2.

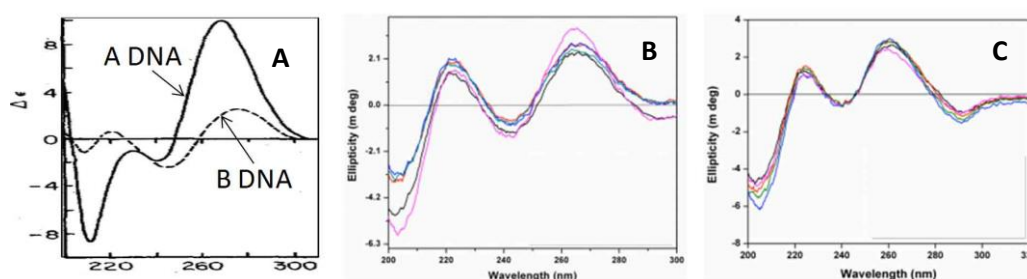


Figure 3.2 CD-signatures of (A) ADNA, BDNA¹²; (B) PNA:DNA duplex and (C) PNA:RNA duplex.¹³

In the present work, this technique has been used to investigate the secondary conformations of single stranded fluorinated PNAs, PNA:DNA and PNA:RNA duplexes.

3.1.2c Mismatch base pair and duplex stability

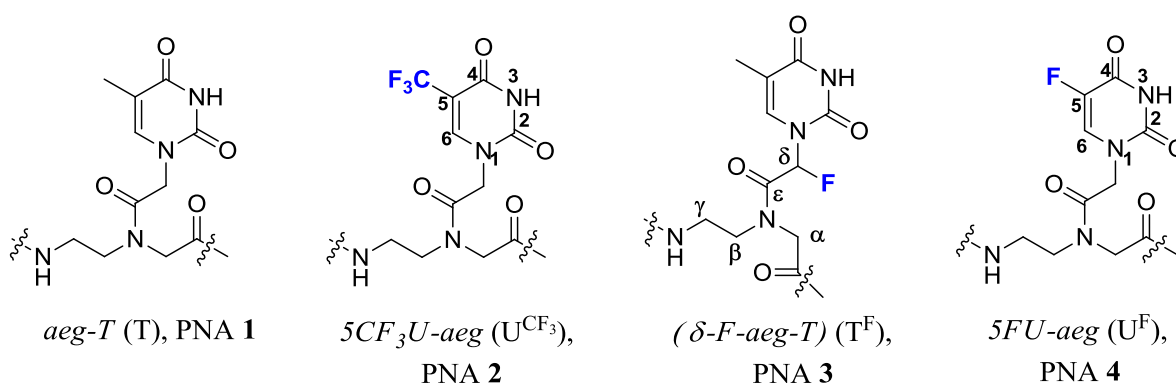
PNA oligomers show greater specificity in binding to complementary DNAs or RNAs; single base mismatch in PNA:DNA or PNA:RNA complexes are more destabilizing than a similar mismatch in a DNA:DNA or DNA:RNA duplex. Hence the extent of decrease in T_m of PNA duplexes with a mismatch DNA or RNA measured using temperature dependent UV absorbance should give evidence of their specificity in the base pairing. The sequence specificity of fluorinated PNAs in hybridizing to cDNA or cRNA was determined by comparing T_m values of their hybrids with that of DNA or RNA sequences carrying single base mismatch in the center of the sequence.

3.2 Results and Discussion

3.2.1 Hydrophobicity studies of fluorinated PNA homooctamers

This section describes evaluation of hydrophobicity of PNA homooligomers arising from substituted fluorines in the PNA and the effect of number and positions of the fluorine present in the PNA.

The sequence used for the hydrophobicity measurements was H-TTTTTTTT-Lys. The HPLC solvent elution used for the study is a linear gradient run for 20 min using acetonitrile/water mixture as a mobile phase using C18-column. The HPLC profiles shown in Figures 3.4 & 3.5 and the retention times are tabulated in Table 3.1.



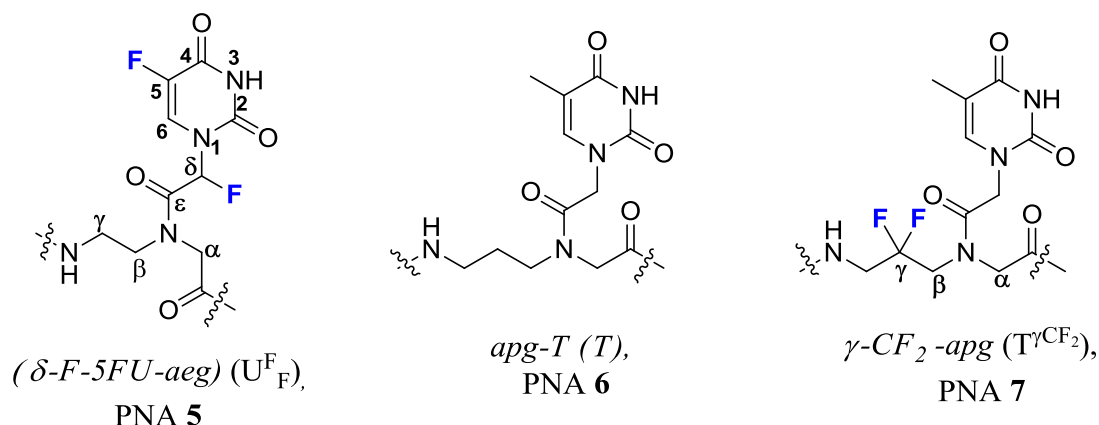


Figure 3.3 Fluorinated PNA and PNA homooligomers.

The homooligomers of *aeg*-T (PNA 1) and nucleobase fluorinated $5\text{CF}_3\text{U-aeg}$ (PNA 2) have retention times of 10.1 min. and 17.7 min. respectively. Replacing the 5-methyl group of thymine in PNA 1 with trifluoromethyl group in PNA 2 octamer with a total of 24 fluorine atoms ($8 \times \text{CF}_3$) resulted in an increase in retention time of 7.6 min. (entry 1,2). This clearly indicated that increasing the number of fluorines in PNA enhances the hydrophobicity of the PNA (see Figure 3.4).

The homooctamer ($\delta\text{-F-aeg-T}$) PNA 3 with one fluorine substitution at δ -carbon in side chain contains a total of 8 fluorine atoms and had retention time (*Rt*) of 14.2 min, to *Rt* of 10.1 min for unsubstituted PNAT-1 (Figure 3.4), an increase of 4.2 min.

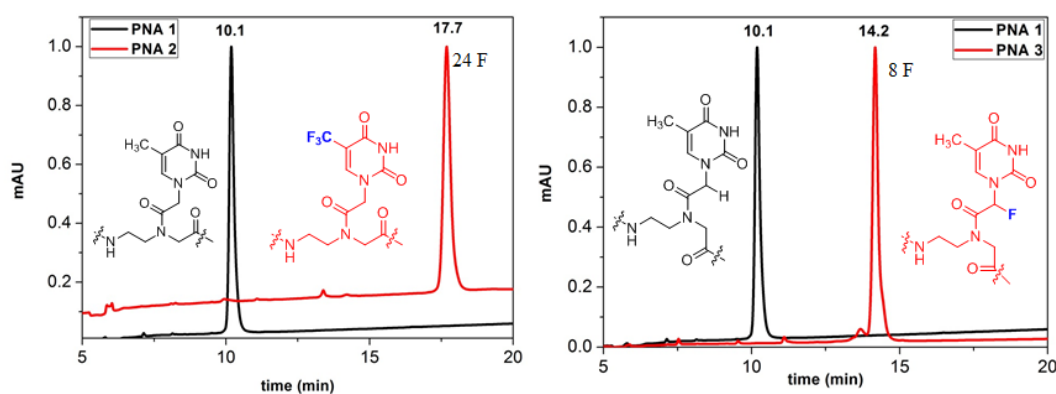


Figure 3.4 Comparison of HPLC retention times (*Rt*) of *aeg*-T and $5\text{CF}_3\text{U-aeg}$ PNA octamers and *aeg*-T and ($\delta\text{-F-aeg-T}$) PNA octamers.

The same trend was observed for homooctamers of 5FU-aeg (PNA 4, entry 4, 8F atoms) and doubly fluorinated $\delta\text{-F-5FU-aeg}$ (PNA 5, entry 5) which has a total of 16 F atoms. $\delta\text{-F-5FU aeg}$ (PNA 5) homooligomer has higher retention time of 14.3 min compared to 5FU-aeg homooligomer (PNA 4) with *Rt* of 10.0 min, with additional 8F atoms increases *Rt*

by 4.3 min. This indicated that introduction of fluorine in the acetyl side chain of the *5FU-aeg* at δ -position also induces more hydrophobicity (Figure 3.5).

Introducing one methylene group in the backbone of *aeg* PNA **1** to give *apg*-PNA **6** enhanced hydrophobicity only slightly by a ΔR_t of 1.0 min (entry 1,6). In case of corresponding fluoro methylene backbone modified γ - CF_2 -*apg* PNA **7** (entry 7), ΔR_t of 2.4 min (with 16 F atoms) was seen compared to the non-fluorinated *apg* PNA **6** (entry 6). This indicated that upon substitution of methylene group with difluoro methylene in the backbone lead to only a slight increase in hydrophobicity (Figure 3.5).

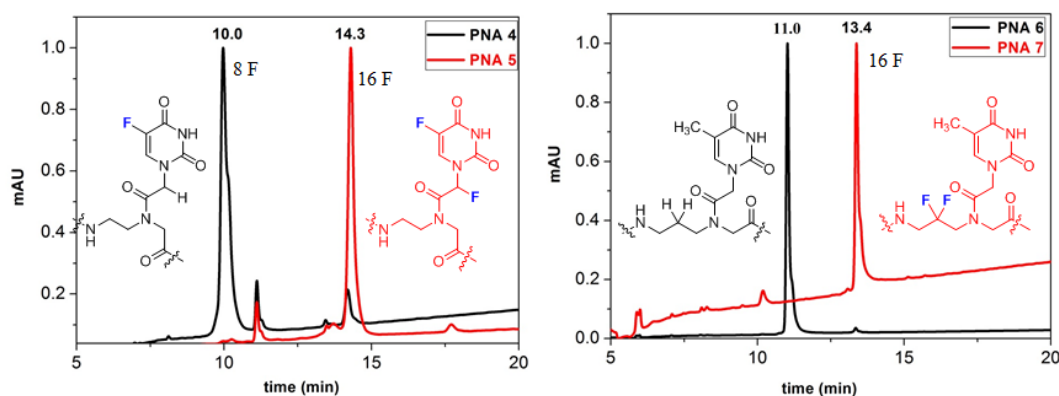


Figure 3.5 Comparison of HPLC retention times (R_t) of *5FU-aeg* and δ -*F-5FU-aeg* PNA octamers and *apg* and γ - CF_2 -*apg* PNA octamers.

Table 3.1 Comparison of octamers retention times with respect to No. of fluorines present in the PNA

PNA	PNA sequence	No. of F's	R_t	ΔR_t
PNA 1	H-TTTTTTTT-Lys	0	10.1	---
PNA 2	H-U ^{CF₃} U ^{CF₃} U ^{CF₃} U ^{CF₃} U ^{CF₃} U ^{CF₃} U ^{CF₃} U ^{CF₃} -Lys	24	17.7	7.6
PNA 3	H-T ^F T ^F T ^F T ^F T ^F T ^F T ^F T ^F -Lys	8	14.2	4.2
PNA 4	H-U ^F U ^F U ^F U ^F U ^F U ^F U ^F U ^F -Lys	8	10.0	---
PNA 5	H-U ^F _F U ^F _F U ^F _F U ^F _F U ^F _F U ^F _F U ^F _F -Lys	16	14.3	4.3
PNA 6	H-TTTTTTTT-Lys	0	11.0	---
PNA 7	H-T ^{CF₂} T ^{CF₂} T ^{CF₂} T ^{CF₂} T ^{CF₂} T ^{CF₂} T ^{CF₂} T ^{CF₂} -Lys	16	13.4	2.4

ΔR_t is difference in HPLC retention time between fluorinated and control PNA octamers

Though difluoromethylene group in the backbone of *apg* PNA **6** increased the hydrophobicity compared to methylene, the magnitude was much lower than that of side chain fluorinated PNAs (PNA **3** and PNA **5**) or nucleobase fluorinated PNA **2**.

The overall results suggest that increasing the number of fluorines in the PNA homooligos generally increases their hydrophobic character (as measured by their HPLC retention times) and the extent of enhanced hydrophobicity depends on the site of the fluorine

substitution in the PNA. Thus for the same number of 16 F atoms, fluorine in side chain (PNA 5) seems to be more hydrophobic than fluorine in backbone (PNA 7).

3.3 Biophysical studies of fluorinated PNAs with complementary DNA

This section describes the applications of UV-dependent melting (T_m) to study the thermal stabilities and specificity of hybrid formation of the fluorinated PNAs towards their complementary antiparallel DNA and circular dichroism (CD) studies to investigate the secondary structure formation of the fluorinated-PNA:DNA hybrids. The structures of various fluorinated PNA units incorporated into a PNA decamer sequence at different sites are shown in the below Figure 3.6. The hybridization studies of fluorinated PNA oligomers were done with their complementation with DNA **1** (5'ACTGAGGTAA3').

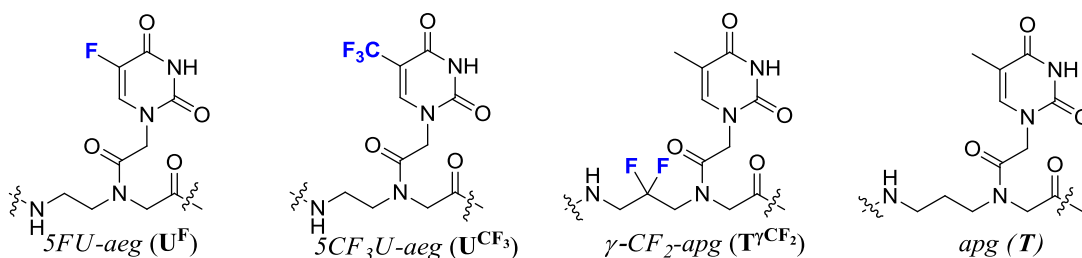


Figure 3.6 Fluorinated and control non-fluorinated PNAs

3.3.1 UV- T_m of nucleobase fluorinated PNAs

In order to study the effect of the nucleobase fluorinated PNAs on hybrid stability with their corresponding complementary DNA **1**, mixed sequence decamer PNAs incorporating units of either 5FU-aeg PNA (PNAs **9-13**), 5CF₃U-aeg PNA (PNAs **14-18**) at different positions of aeg PNA decamer were used. The thermal stability (T_m) of these PNAs with complementary DNA **1** for antiparallel binding (DNA **1**: 5'ACTGAGGTAA3') was evaluated from the temperature dependent UV absorbance plot at 260 nm. The results of binding studies of PNA:DNA duplexes are discussed as follows.

3.3.1a UV- T_m of PNAs modified with 5FU-aeg units

5FU-aeg PNA unit (U^F) was site specifically incorporated into the PNA decamers (PNAs **9-13**) and hybridized with complementary antiparallel DNA **1**. The thermal stability (T_m) of these duplexes was examined by UV-melting and the T_m values of the PNA:DNA duplexes are compared with that of control aeg PNA:DNA duplex. The temperature absorbance sigmoidal curves are shown in Figure 3.7 and the T_m derived from these plots are shown in Table 3.2.

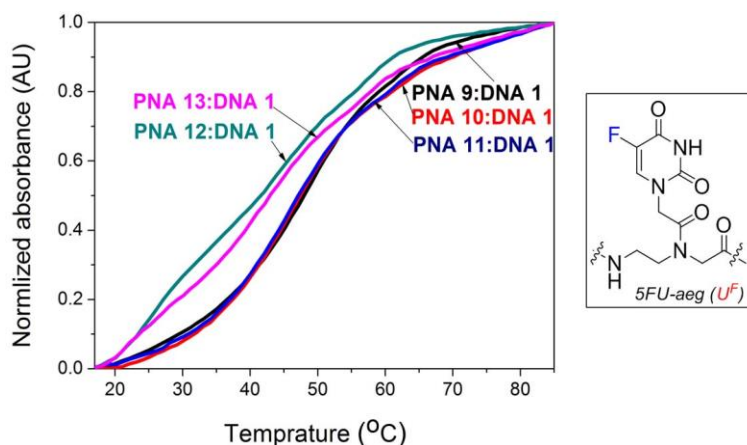


Figure 3.7 Melting curves for purine-pyrimidine mixed *5FU-aeg* PNAs (PNA **9-13**) complexed with DNA **1** (5'ACTGAGGTAA3'); (10 mM sodium phosphate buffer, pH = 7.4, 10 mM NaCl).

Single site modifications: The N-terminus modified PNA **9** mildly stabilized the derived PNA:DNA duplex by 1.1 °C (entry 2), while the centrally modified PNA **10** showed a destabilization (ΔT_m -2.7 °C) with cDNA (entry 3). PNA **11** with C-terminal modification destabilized the derived DNA duplex by 1.7 °C (entry 4) as compared to unmodified *aeg* PNA sequence.

Table 3.2 UV- T_m values of PNA:DNA duplexes with *5FU-aeg* PNA units

Entry	Seq. code	PNA sequence	DNA 1: 3'AATGGAGTCA 5'	ΔT_m
			UV- T_m (°C)	
1	PNA 8	H-TTACCTCAGT-Lys	48.6	---
2	PNA 9	H-TU ^F ACCTCAGT-Lys	49.7	1.1
3	PNA 10	H-TTACCU ^F CAGT-Lys	45.9	-2.7
4	PNA 11	H-TTACCTCAGU ^F -Lys	46.9	-1.7
5	PNA 12	H-TU ^F ACCU ^F CAGT-Lys	44.3	-4.3
6	PNA 13	H-TU ^F ACCU ^F CAGU ^F -Lys	45.0	-3.6

* ΔT_m indicates difference in T_m of *5FU-aeg* PNA:DNA duplex with control *aeg* PNA:DNA duplex; The values are accurate to ± 0.5 °C.

Double site modifications: PNA **12** carrying two U^F modifications at N-terminus and in the middle formed hybrids with DNA **1** with a T_m of 44.3 °C (entry 5) corresponding to destabilization of -4.3 °C compared to unmodified *aeg* PNA oligomer.

Triple modification: The triple modified PNA **13** (N-terminus, middle and C-terminus) formed duplex with complementary DNA **1** with a decrease in T_m by -3.6 °C compared to unmodified *aeg* PNA oligomer (entry 6).

The differences in ΔT_m of duplexes of *5FU-aeg* modified PNAs relative to unmodified *aeg* PNA **8**, varies from +1.1 °C to -4.3 °C, with increasing number of substitutions, causing

more destabilization. The N-terminus fluorinated unit slightly stabilized while the middle and C-terminus fluorinated units destabilized the PNA:DNA hybrids.

3.3.1b UV- T_m of PNA oligos modified with $5CF_3$ -*U aeg* units

To examine the effect of the nucleobase modified PNA monomer having 5- CF_3 in place of 5- CH_3 of thymine (T) on the hybridization of the corresponding duplexes with DNA, the mixed purine-pyrimidine PNA oligomers (PNA **14-18**) incorporating the modified PNA unit (U^{CF_3}) at different sites on *aeg* PNA sequence were synthesized. The temperature absorbance sigmoidal curves are shown in Figure 3.8 and the T_m values derived from these plots are shown in Table 3.3.

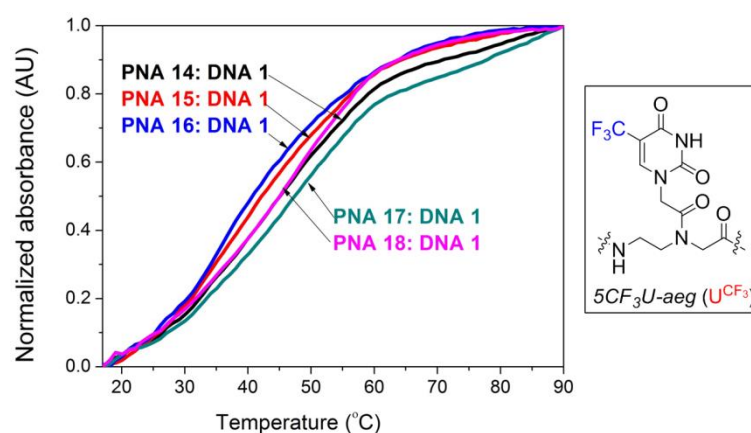


Figure 3.8 Melting curves for purine-pyrimidine mixed $5CF_3U$ -*aeg* PNAs (PNA **14-18**) complexed with DNA **1** (5'ACTGAGGTAA3'); (10 mM sodium phosphate buffer, pH = 7.4, 10 mM NaCl).

Single site modifications: The PNA **14** modified at the N-terminus destabilized the cDNA by 5.5 °C (entry 2). The PNA **15** with middle modification destabilized the DNA hybrid by 7.4 °C (entry 3) while the C-terminus modified PNA **16** destabilized the DNA by 13.3 °C (entry 4). The destabilization decreases in the order of N < M < C.

Table 3.3 UV- T_m values of complementary PNA:DNA duplexes with $5CF_3U$ -*aeg* PNA unit

Entry	Seq. code	PNA sequence	DNA 5'ACTGAGGTAA3'	ΔT_m
			UV- T_m (°C)	
1	PNA 8	H-TTACCTCAGT-Lys	48.6	---
2	PNA 14	H-TU ^{CF₃} ACCTCAGT-Lys	43.1	-5.5
3	PNA 15	H-TTACCU ^{CF₃} CAGT-Lys	41.2	-7.4
4	PNA 16	H-TTACCTCAGU ^{CF₃} -Lys	35.3	-13.3
5	PNA 17	H-TU ^{CF₃} ACCU ^{CF₃} CAGT-Lys	45.9	-2.7
6	PNA 18	H-TU ^{CF₃} ACCU ^{CF₃} CAGU ^{CF₃} -Lys	49.4	0.8

ΔT_m indicates difference in T_m of $5CF_3U$ -*aeg* PNA:DNA with control *aeg* PNA:DNA. The values are accurate to ± 0.5 °C.

Double and triple modifications: The fluorinated PNA **17** with double modifications at N-terminus and center destabilized the cDNA by 2.7 °C (entry 5) and PNA **18** triply modified at N-terminus, center and C-terminus stabilized the cDNA by 0.8 °C (entry 6) compared to the control unmodified sequence PNA **8**. Thus the trifluoromethyl-uracil modification destabilized the derived PNA:DNA duplexes significantly.

3.3.2 UV- T_m of backbone fluorinated γ -CF₂-ap γ PNAs

Comparative thermal stabilities of PNA oligomers fluorinated in backbone with γ -CF₂-ap γ PNA (T ^{γ CF₂}) unit (PNAs **19-23**) and the ap γ PNA-T unit (PNAs **24-26**) with complementary DNA **1** were examined by temperature dependent UV-absorbance (Figure 3.9) and the derived T_m values are summarized in Table 3.7.

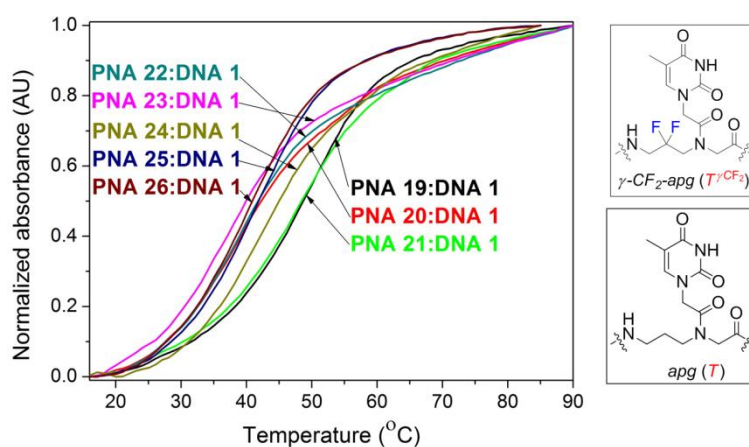


Figure 3.9 Melting curves for purine-pyrimidine mixed γ -CF₂-ap γ and ap γ PNAs (PNA **19-26**) complexed with DNA **1** (5'ACTGAGGTAA3'); (10 mM sodium phosphate buffer, pH = 7.4, 10 mM NaCl).

Single modifications: The N- and C- terminus modifications (PNA **19**, PNA **21**) did not have much effect on of duplexes with DNA **1** thermal stability and showed T_m^s of 50.6 and 48.8 °C (entry 1, 3) respectively. The centrally modified γ -CF₂-ap γ PNA **20** (entry 4) destabilized the duplex with cDNA by 4.4 °C as compared to the T_m of corresponding centrally modified control ap γ PNA **24**:DNA **1** duplex (entry 3).

Double and Triple modifications: The doubly modified γ -CF₂-ap γ PNA **22** (N-terminus and middle, entry 6) destabilized the duplexes with cDNA by 2.2 °C when compared to duplex with respective doubly modified control ap γ PNA **25** (entry 5). The triply modified γ -CF₂-ap γ PNA **23** (entry 8) showed duplex thermal stability almost same as that of the corresponding triply modified ap γ PNA **26** (entry 7). The ΔT_m values are shown in Figure 3.10.

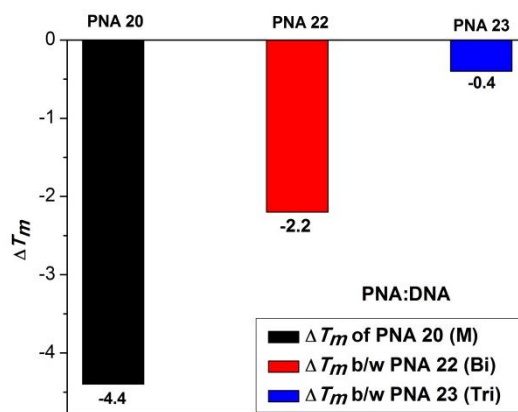


Figure 3.10 ΔT_m indicates the difference in T_m of γ -CF₂-*apg* PNA:DNA duplexes with respect to corresponding *apg* PNA:DNA duplexes.

Table 3.4 UV- T_m values of complementary PNA:DNA duplexes with γ -CF₂-*apg* PNA and *apg* PNA units

Entry	Seq. code	PNA sequence	DNA1: 5'ACTGAGGTAA3'	ΔT_m
			UV- T_m (°C)	
1	PNA 19	H-TT ^{γCF₂} ACCTCAGT-Lys	50.6	---
2	PNA 21	H-TTACCTCAGT ^{γCF₂} -Lys	48.8	---
3	PNA 24	H-TTACCTCAG T-Lys	42.6	---
4	PNA 20	H-TTACCT ^{γCF₂} CAG T-Lys	38.2	-4.4
5	PNA 25	H-T TACC TCAGT-Lys	42.1	---
6	PNA 22	H-TT ^{γCF₂} ACCT ^{γCF₂} CAGT-Lys	39.9	-2.2
7	PNA 26	H-T TACC TCAG T-Lys	38.8	---
8	PNA 23	H-TT ^{γCF₂} ACCT ^{γCF₂} CAGT ^{γCF₂} -Lys	38.4	-0.4

ΔT_m indicates difference in T_m of γ -CF₂-*apg* PNA:DNA 1 with corresponding modified control *apg* PNA:DNA 1 hybrids. The values are accurate to ± 0.5 °C. DNA 1 = 5'ACTGAGGTAA3'.

The ΔT_m values clearly indicate that the binding affinity of γ -CF₂-*apg* PNA oligomers is almost equal to that of the corresponding control *apg* PNA oligomers (from ΔT_m values, Table 3.4). This indicates that replacing methylene group with difluoromethylene group in the backbone of *apg* PNA unit destabilizing the PNA:DNA duplex stability in the range of 0- to 5°C.

3.4 UV- T_m studies of the fluorinated PNAs with complementary RNA

This section describes the hybridization properties of the fluorinated PNAs with complementary antiparallel RNA 1 (5'ACUGAGGUAA3').

3.4.1 UV- T_m of nucleobase modified PNAs

The thermal stability (T_m) of the nucleobase fluorinated PNAs (PNAs 9-18) with complementary RNA 1 for antiparallel binding mode (5'ACUGAGGUAA3') was evaluated

from temperature dependent UV absorbance. The results of binding studies of PNA:RNA duplexes are discussed below.

3.4.1a UV- T_m of 5FU-*aeg* PNA:RNA duplexes

The thermal stability T_m values of RNA duplexes with 5FU-*aeg* PNAs (PNAs **9-13**) compared with that of *aeg* PNA:RNA duplex are tabulated in Table 3.5. The T_m values were obtained from the first derivative of sigmoidal curves (Figure 3.11).

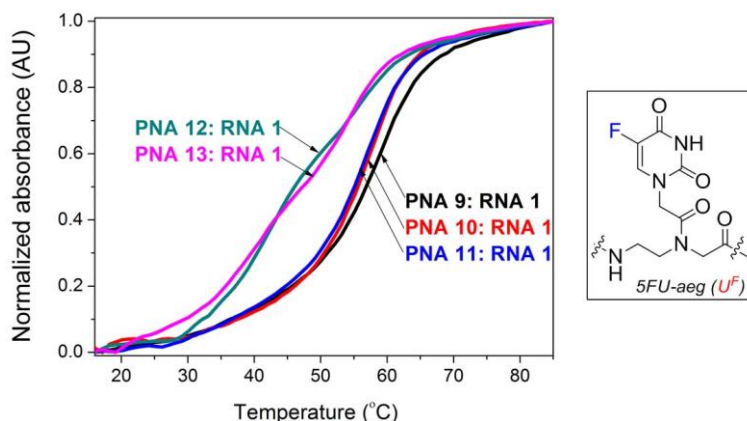


Figure 3.11 Melting curves for purine-pyrimidine mixed 5FU-*aeg* PNAs (PNA **9-13**) complexed with RNA **1** (5'ACUGAGGUA3'); (10 mM sodium phosphate buffer, pH = 7.4, 10 mM NaCl).

Single site modifications: Incorporation of 5FU-*aeg* (U^F) unit in *aeg* PNA decamer at different sites showed a slight decrease in duplex stability of PNA:RNA hybrids. N-terminus modified PNA **9** (entry 2) stabilized the derived duplex as that of unmodified control *aeg* PNA **8** (entry 1). The centrally modified PNA **10** showed a ΔT_m of -4.2 °C for duplex with complementary RNA **1** (entry 3). PNA **11** with C-terminal modification destabilized the derived RNA duplexes by 2.1 °C (entry 4) respectively as compared to unmodified *aeg* PNA sequence.

Table 3.5 UV- T_m values of complementary PNA:RNA duplexes with 5FU-*aeg* PNA units

Entry	Seq. code	PNA sequence	RNA 1: 5'ACUGAGGUA3'	ΔT_m
			UV- T_m (°C)	
1	PNA 8	H-TTACCTCAGT-Lys	60.6	--
2	PNA 9	H-TU ^F ACCTCAGT-Lys	60.2	-0.4
3	PNA 10	H-TTACCU ^F CAGT-Lys	56.4	-4.2
4	PNA 11	H-TTACCTCAGU ^F -Lys	58.5	-2.1
5	PNA 12	H-TU ^F ACCU ^F CAGT-Lys	55.8	-4.8
6	PNA 13	H-TU ^F ACCU ^F CAGU ^F -Lys	54.0	-6.6

ΔT_m indicates difference in T_m of 5FU-*aeg* PNA:RNA with control *aeg* PNA:RNA. The values are accurate to ± 0.5 °C, RNA **1** = 5'ACUGAGGUA3'.

Double and triple modifications: PNA **12** carrying two modifications at N-terminus and the middle formed hybrid with RNA **1** with destabilization of -4.8 °C (entry 5) compared to unmodified *aeg* PNA **8**, whereas the triple modified PNA **13** at N-terminus, middle and C-terminus formed duplex with complementary RNA **1** with ΔT_m of -6.6 °C (entry 6).

In case of cDNA the T_m values varied from 45.0 to 49.7 °C while in case of cRNA the T_m s varied from 54.0 to 60.2 °C. Thus the *5FU-aeg* modified PNAs showed higher affinity of their duplexes with cRNA than that with cDNA.

3.4.1b UV- T_m of PNAs modified with *5CF₃U-aeg* units

The fluorinated PNAs containing base modified *5CF₃U-aeg* unit in the mixed purine-pyrimidine PNA decamer sequence at various sites (PNA **14-18**) were studied for their hybridization properties with corresponding complementary RNA **1**. The T_m values derived from the melting profiles (Figure 3.12) are summarized in Table 3.6.

Single site modifications: The PNA **14** with modification at N-terminus destabilized the duplex with complementary RNA **1** by 2.5 °C (entry 2), while PNA **15** with middle modification destabilized the corresponding RNA hybrid by 10.4 °C (entry 3). The C-terminus modified PNA **16** destabilized the RNA duplex by 17.8 °C (entry 4). The destabilization order is in the order of $N < M < C$.

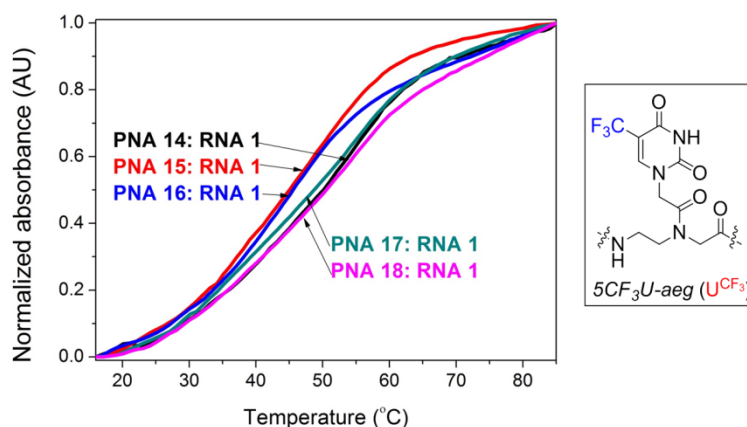


Figure 3.12 Melting curves for purine-pyrimidine mixed *5CF₃U-aeg* PNAs (PNA **14-18**) complexed with RNA **1** (5'ACUGAGGUA3'); (10 mM sodium phosphate buffer, pH = 7.4, 10 mM NaCl).

Double and triple modifications: The PNA **17** with double modifications at N-terminus and in middle (entry 5) destabilized the duplex with cRNA by 4.7 °C and the PNA **18** with triple modifications destabilized the cRNA hybrid by 0.6 °C (entry 6) as compared to

the duplex form of control unmodified PNA **8**. Thus increase in the number of modifications resulted in less destabilization.

Table 3.6 UV- T_m values of complementary PNA:RNA duplexes with $5CF_3U$ -*aeg* PNA units

Entry	Seq. code	PNA sequence	RNA 1: 5'ACUGAGGUA3'	ΔT_m
			UV- T_m ($^{\circ}C$)	
1	PNA 8	H-TTACCTCAGT-Lys	60.6	--
2	PNA 14	H-TU ^{CF₃} ACCTCAGT-Lys	58.1	-2.5
3	PNA 15	H-TTACCU ^{CF₃} CAGT-Lys	50.2	-10.4
4	PNA 16	H-TTACCTCAGU ^{CF₃} -Lys	42.8	-17.8
5	PNA 17	H-TU ^{CF₃} ACCU ^{CF₃} CAGT-Lys	55.9	-4.7
6	PNA 18	H-TU ^{CF₃} ACCU ^{CF₃} CAGU ^{CF₃} -Lys	60.0	-0.6

ΔT_m indicates difference in T_m of $5CF_3U$ -*aeg* PNA:RNA with control *aeg* PNA:RNA. The values are accurate to ± 0.5 $^{\circ}C$.

The fluorinated PNAs (PNAs **14-18**) having $5CF_3U$ -*aeg* showed higher T_m for duplexes with cRNA compared to that with cDNA. In case of PAN:cRNA duplexes the T_m values varied from 42.8 to 60.0 $^{\circ}C$ and in case of duplexes with cDNA, the T_m values were in the range of 35.3 to 49.4 $^{\circ}C$.

3.4.2 UV- T_m of PNAs modified with γ - CF_2 -*apg*-PNA and *apg* PNA units

The thermal stability of PNA oligomers modified with γ - CF_2 -*apg* PNA ($T^{\gamma CF_2}$) unit and *apg* PNA (*T*) unit with duplexed with complementary RNA **1** were monitored by temperature dependent UV-absorbance and UV- T_m profiles are shown in Figure 3.13 and the T_m values are shown in Table 3.7

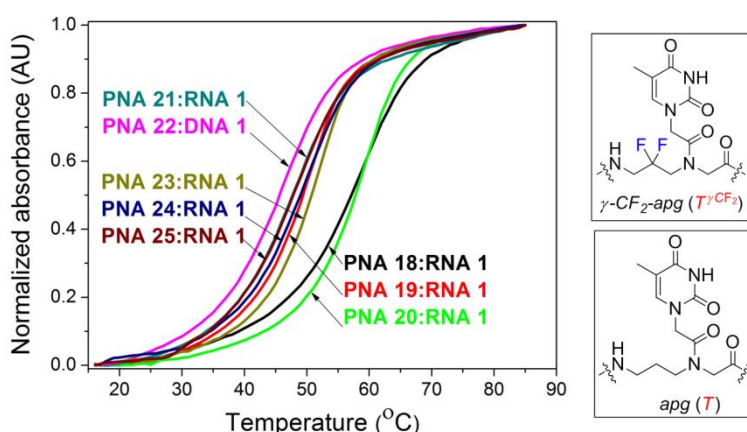


Figure 3.13 Melting curves for purine-pyrimidine mixed γ - CF_2 -*apg* and *apg* PNAs (PNA **19-26**) complexed with RNA **1** (5'ACUGAGGUA3'); (10 mM sodium phosphate buffer, pH = 7.4, 10 mM NaCl).

Single modifications: The duplexes from the N- and C-terminus modified PNAs (PNA **19**, **21**) with γ -CF₂-ap_g showed T_m s of 60.0 °C and 59.7 °C respectively (entry 1, 2) and the modifications did not have much effect on thermal stability. The centrally modified PNA **20** (entry 3) destabilized the cRNA duplex by 2.0 °C when compared to that from the corresponding centrally modified ap_g PNA **24** (entry 4).

Table 3.7 UV- T_m values of complementary PNA:RNA duplexes with γ -CF₂-ap_g PNA and ap_g PNA units

Entry	Seq. code	PNA sequence	RNA 1: 5'ACUGAGGUA3'	ΔT_m
			UV- T_m (°C)	^m
1	PNA 19	H-TT ^{γCF₂} ACCTCAGT-Lys	60.0	---
2	PNA 21	H-TTACCTCAGT ^{γCF₂} -Lys	59.7	---
3	PNA 24	H-TTACCTCAG T-Lys	53.1	---
4	PNA 20	H-TTACCT ^{γCF₂} CAG T-Lys	51.1	-2.0
5	PNA 25	H-TTACCTCAGT-Lys	49.1	---
6	PNA 22	H-TT ^{γCF₂} ACCT ^{γCF₂} CAGT-Lys	48.3	-0.8
7	PNA 26	H-TTACCTCAGT-Lys	48.3	---
8	PNA 23	H-TT ^{γCF₂} ACCT ^{γCF₂} CAGT ^{γCF₂} -Lys	47.9	-0.4

ΔT_m indicates difference in T_m of γ -CF₂-ap_g PNA:RNA **1** with corresponding modified control ap_g PNA:RNA **1** hybrids. The values are accurate to ± 0.5 °C. DNA **1** = 5'ACUGAGGUA3'.

Double and Triple modifications: The RNA duplex from the doubly modified PNA **22** (N-terminus and middle, entry 6) with γ -CF₂-ap_g unit had same stability as that of the corresponding control ap_g PNA **25** (entry 5). The triple modified PNA **23** (entry 8) hybridized with cRNA showed a T_m of 47.9 °C, almost equal to that of corresponding control ap_g PNA **26** (entry 7). The ΔT_m values are shown in the Figure 3.14.

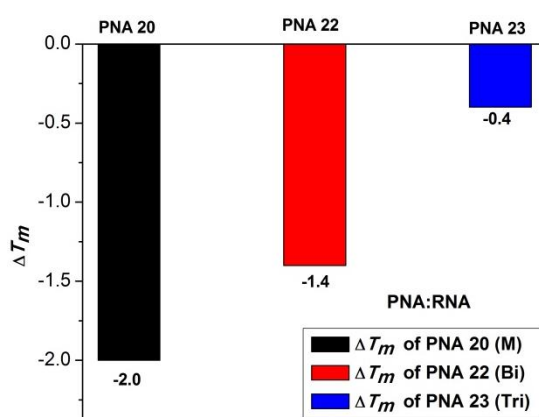


Figure 3.14 ΔT_m indicates the difference in T_m of γ -CF₂-ap_g PNA:RNA duplexes with respect to corresponding ap_g PNA:RNA duplexes.

From these results it is seen that the T_m values of RNA duplexes with fluorinated PNAs modified with γ -CF₂-ap_g units are almost unaffected compared to corresponding ap_g

PNA oligomers. This indicates that replacing methylene group in the backbone of the *apg* PNA with difluoromethylene group does not alter PNA:RNA duplex stability.

3.4.3 Comparative UV- T_m studies of γ -CF₂-*apg* and *apg* PNAs (PNA 29-31) with cDNA and cRNA

The PNA sequence complementary to telomerase sequence for the inhibition of telomerase activity was Lys-ACAGATTGGGATTG-Gly was made with incorporation of γ -CF₂-*apg*, *apg* units at four sites in the telomeric sequence. Their duplex stability with antiparallel cDNA $\mathbf{3}$ and cRNA $\mathbf{3}$ (PNA $\mathbf{30}$ and $\mathbf{31}$) were studied. These PNAs bound with their complementary DNA $\mathbf{3}$ and RNA $\mathbf{3}$ (from T_m values, Table 3.8). The duplexes from PNA $\mathbf{30}$ and PNA $\mathbf{31}$ showed T_m s of 66.6 °C, 65.4 °C with complementary DNA $\mathbf{3}$ and 74.9 °C, 76.3 °C with complementary RNA $\mathbf{3}$. The T_m profiles are shown in Figure 3.15.

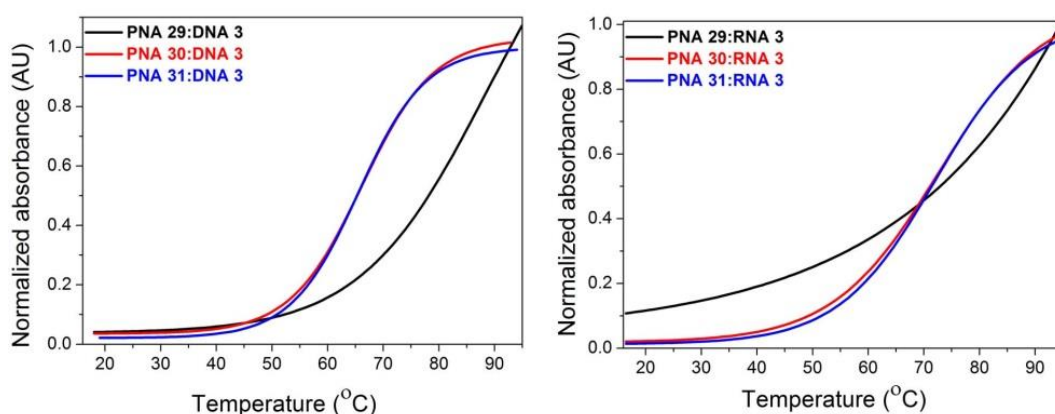


Figure 3.15 Melting curves for purine-pyrimidine mixed γ -CF₂-*apg*, *apg* and *aeg* PNAs (PNA $\mathbf{29-31}$) complexed with DNA $\mathbf{3}$ (5'TGTCTAACCCCTAAC3') and RNA $\mathbf{3}$ (5'UGUCUAACCCUAAC3'); 10 mM sodium phosphate buffer, pH = 7.4, 10 mM NaCl.

Table 3.8 UV- T_m values of PNA:DNA $\mathbf{3}$ and PNA:RNA $\mathbf{3}$ duplexes

Seq. code	PNA sequence	UV- T_m (°C)	
		PNA:DNA	PNA:RNA
PNA $\mathbf{29}$	H-Gly-GTTAGGGTTAGACA-Lys	76.1	84.2
PNA $\mathbf{30}$	H-Gly-GTTAGGGTTAGACA-Lys	66.6	74.9
PNA $\mathbf{31}$	H-Gly-GT γ CF ₂ T γ CF ₂ AGGGT γ CF ₂ T γ CF ₂ AGACA-Lys	65.4 (-1.2)	76.3 (+1.4)

T_m of PNA:DNA $\mathbf{3}$ and PNA:RNA $\mathbf{3}$ duplexes modified with γ -CF₂-*apg* and *apg* PNAs. The values are accurate to ± 0.5 °C. DNA $\mathbf{3}$ = 5'TGTCTAACCCCTAAC3'; RNA $\mathbf{3}$ = 5'UGUCUAACCCUAAC3'.

The T_m values of DNA/RNA duplexes with PNAs modified with γ -CF₂-*apg* (PNA $\mathbf{31}$) and *apg* PNA (PNA $\mathbf{30}$) units were almost equal indicating that replacing methylene group in the *apg* PNA backbone with difluoromethylene group does not alter the duplex stability. The RNA hybrids slightly more stable than the DNA hybrids.

3.5 UV- T_m mismatch studies of PNA:DNA and PNA:RNA hybrids

The retention of fidelity of PNA:DNA/RNA hybridization is an important attribute necessary for biological applications. The sequence specificity of the PNAs **8-26** were examined by studying their hybridization properties with DNA **2** and RNA **2** containing single-site mismatch. The PNA:DNA complexes comprising of control sequence PNA **8** and the fluorinated PNAs (**9-26**) were individually subjected for UV-melting with PNA hybrids of the mismatch DNA **2** and RNA **2**. The T_m data is summarised in Table 3.9 and the melting curves are shown in Figures 3.21-3.23 (Appendix-II, page no.221).

Table 3.9 UV- T_m values of mismatch PNA:DNA **2** and PNA:RNA **2** duplexes

Entry	PNA	PNA sequence	UV- T_m (°C) PNA:DNA 2	ΔT_m	UV- T_m (°C) PNA:RNA 2	ΔT_m^I
1	PNA 8	H-TTACCTCAGT-Lys	28.6	-20.0	40.5	-20.1
2	PNA 9	H-TU ^F ACCTCAGT-Lys	27.2	-22.5	39.2	-21.0
3	PNA 10	H-TTACCU ^F CAGT-Lys	27.4	-21.5	38.9	-17.5
4	PNA 11	H-TTACCTCAGU ^F -Lys	25.4	-21.5	37.3	-21.2
5	PNA 12	H-TU ^F ACCU ^F CAGT-Lys	26.2	-18.1	38.8	-17.0
6	PNA 13	H-TU ^F ACCU ^F CAGU ^F -Lys	23.3	-21.7	37.1	-16.9
7	PNA 14	H-TU ^{CF₃} ACCTCAGT-Lys	36.8	-6.3	37.6	-20.5
8	PNA 15	H-TTACC U ^{CF₃} CAGT-Lys	38.1	-3.1	33.7	-16.5
9	PNA 16	H-TTACCTCAG U ^{CF₃} -Lys	32.7	-2.6	36.8	-6.0
10	PNA 17	H-TU ^{CF₃} ACCU ^{CF₃} CAGT-Lys	36.3	-9.6	34.8	-21.1
11	PNA 18	H-TU ^{CF₃} ACCU ^{CF₃} CAGU ^{CF₃} -Lys	36.9	-12.6	38.6	-21.4
12	PNA 19	H-TT ^{γCF₂} ACCTCAGT-Lys	32.1	-18.5	38.4	-21.6
13	PNA 20	H-TTACCT ^{γCF₂} CAGT-Lys	35.2	-3.0	34.8	-16.3
14	PNA 21	H-TTACCTCAGT ^{γCF₂} -Lys	28.8	-20.0	38.3	-21.4
15	PNA 22	H-TT ^{γCF₂} ACCT ^{γCF₂} CAGT-Lys	33.4	-6.5	33.4	-14.9
16	PNA 23	H-TT ^{γCF₂} ACCT ^{γCF₂} CAGT ^{γCF₂} -Lys	33.2	-5.2	38.4	-9.5
17	PNA 24	H-TTACCTCAGT-Lys	31.1	-11.5	34.0	-19.1
18	PNA 25	H-TTACCTCAGT-Lys	27.6	-14.5	28.1	-21.0
19	PNA 26	H-TTACCTCAGT-Lys	27.8	-11.0	36.2	-12.1

ΔT_m indicates the difference in T_m of PNA with cDNA **1** and mismatch DNA **2**; ΔT_m^I indicates the difference in T_m of PNA with cRNA **1** and mismatch RNA **2**. The values are accurate to ± 0.5 °C. DNA **2** = 3'AATGGCGTCA5', RNA **2** = 3'AAUGGCGUCA5'.

The nucleobase *5FU-*aeg** fluorinated PNAs (PNAs **9-13**) have almost equal sequence specificity for both DNA and RNA as that of *aeg* PNA **8**. In case of PNAs fluorinated with *5CF₃U-*aeg** units (PNAs **14-18**), though sequence specificity is same for both DNA and RNA as that of *aeg* PNA **8**, but showed higher sequence discrimination with RNA compared to that of DNA. Backbone fluorinated *γCF₂-*apg** PNAs (**19-23**) exhibited higher sequence specificity for both DNA and RNA. Mismatch discrimination of *γCF₂-*apg** PNAs was more for RNA compared to DNA.

3.6 CD Studies of PNA:DNA and PNA:RNA Duplexes

This section describes the effect of fluorinated PNAs on the conformation of PNA:DNA/RNA duplexes. The CD-spectra for *ss*PNAs (**8-26**), *ss*DNA **1**/RNA **1** and their hybrids with *c*DNA **1**/RNA **1** were recorded. CD-pattern of unmodified *ss*PNA **8**, DNA **1**, RNA **1** and its PNA:DNA **1** and PNA:RNA **1** duplexes were shown in Figure 3.16. The CD-spectrum of PNA **8**:DNA **1** duplex showed positive bands at 222 nm, 265 nm and a negative band at 242 nm. In case of PNA **8**:RNA **1** duplex, positive bands at 224 nm, 260 nm and negative bands at 240 nm, 291 nm were observed (Figure 3.16). These are similar to those reported in literature.¹³

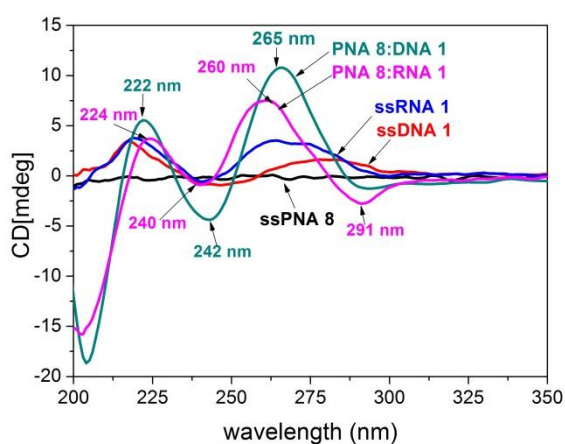


Figure 3.16 CD signatures of unmodified *ss*PNA **8**, PNA **8**:DNA **1** and PNA **8**:RNA **1** duplexes, *ss*DNA **1**, and *ss*RNA **1**.

The CD-patterns of the fluorinated *ss*PNAs (**9-26**), PNA:DNA **1** (PNA **9-26**) and PNA:RNA **1** (PNA **9-26**) duplexes are described below in detail.

3.6.1 CD of 5FU-*aeg* with complementary DNA and RNA

The CD spectra for mixed purine:pyrimidine single stranded (*ss*) PNAs **9-13**, and their hybrids formed with complementary DNA **1**/RNA **1** for antiparallel binding were recorded (Figure 3.17). All CD spectra showed two positive bands at ~ 220 nm, 264 nm and a negative band at ~ 243 nm with complementary DNA **1**; with complementary RNA **1**, two positive bands at ~ 223 nm, 262 nm and two negative bands at ~ 239, 291 nm were observed.

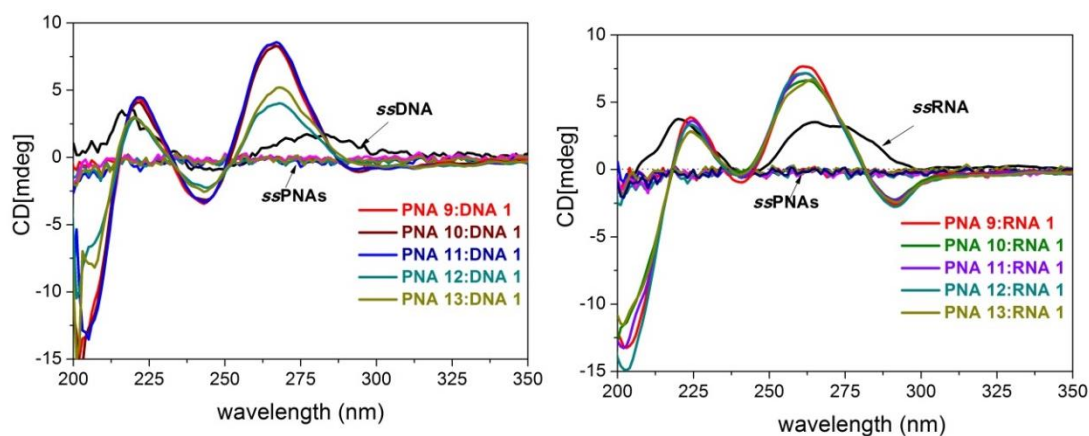


Figure 3.17 CD spectra of single strands PNAs **9-13** and their respective duplexes with cDNA **1** and cRNA **1** (Phosphate buffer: 10 mM sodium phosphate, pH=7.2, 10 mM NaCl).

3.6.2 CD of $5CF_3U$ -*aeg* PNA with complementary DNA and RNA

The CD spectra for mixed purine pyrimidine single stranded (*ss*) oligomers of $5CF_3U$ -*aeg* PNA **14-18**, and their duplexes formed with complementary DNA **1** and RNA **1** for the antiparallel binding mode was recorded (Figure 3.18).

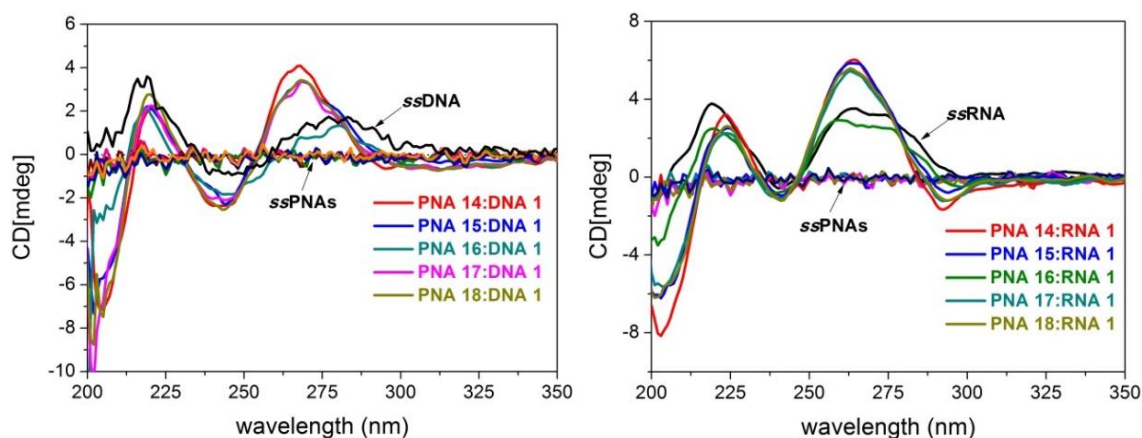


Figure 3.18 CD spectra of *ss* $5CF_3U$ -*aeg* PNAs **14-18** and their respective duplexes with cDNA and cRNA (Buffer: 10 mM sodium phosphate, pH=7.2, NaCl 10 mM).

These spectra showed two positive bands at ~ 218 nm, 268 nm and a negative band at ~ 243 nm with complementary DNA **1** and two positive bands at ~ 222 nm, 263 nm and two negative bands at ~ 240 nm, 292 nm with complementary RNA **1**.

3.6.3 CD of γ - CF_2 -*apg* PNAs with complementary DNA and RNA

The CD spectra for mixed purine pyrimidine single stranded (*ss*) oligomers of γ - CF_2 -*apg* PNAs **19-23**, *apg* PNAs **24-26** and their complexes formed with complementary DNA and RNA for the antiparallel binding mode was recorded (Figure 3.19). These spectra showed two positive bands at ~ 220 nm, 266 nm and negative band at ~ 242 nm with complementary

DNA **1**, and two positive bands at ~ 222 nm, 260 nm and two negative bands at ~ 239 nm, 290 nm with complementary RNA **1**. All these CD signatures were in agreement with the CD signature of control *aeg* PNA **8**:DNA **1** and PNA **8**:RNA **1** duplexes.

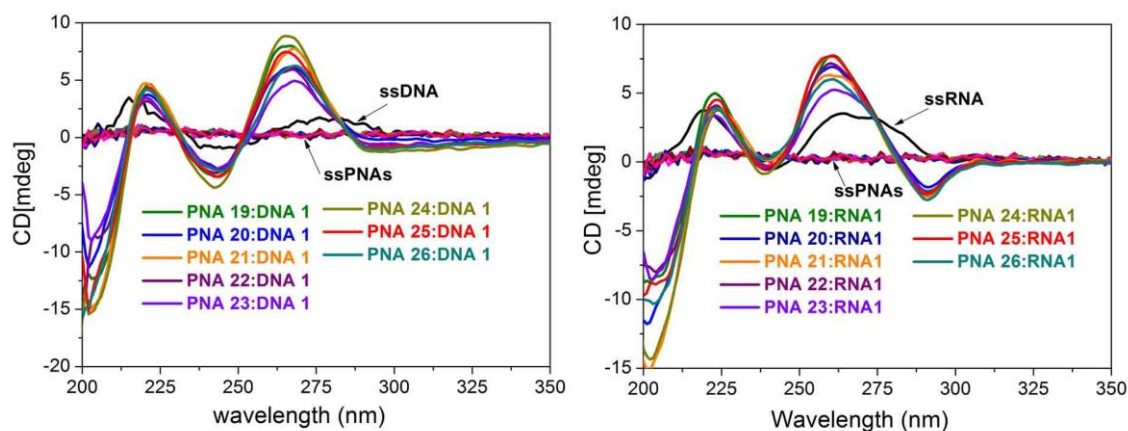


Figure 3.19 CD spectra of single stranded and duplexes of PNAs 19-26 with cDNA and cRNA respectively (Phosphate buffer: 10 mM, pH=7.2, NaCl: 0 mM).

3.6.4 CD of *aeg* PNA, *apg* PNA and γ -CF₂-*apg* PNA 14mers with cDNA and cRNA

The CD spectra for mixed purine pyrimidine oligomers of PNAs **29-31** with their complementary DNA **3** and RNA **3** for the antiparallel binding mode were recorded. These spectra showed two positive bands at ~ 221 nm, 259 nm and a negative band at ~ 235 nm with complementary DNA **3** and two positive bands at ~ 221 nm, 256 nm and a negative band at ~ 234 nm with complementary RNA **3** (Figure 3.20). These CD signatures were in agreement with the CD signature of control *aeg* PNA **29**:DNA **3** and PNA **29**:RNA **3** duplexes

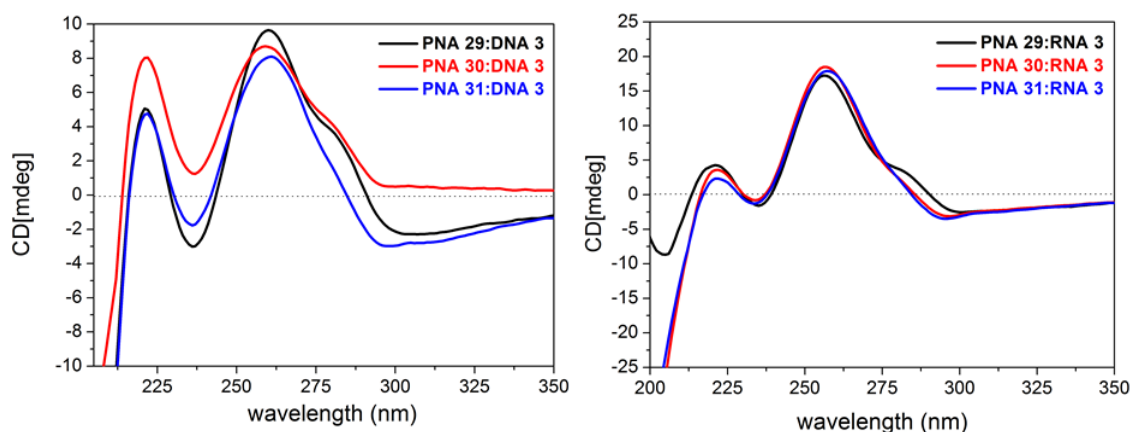
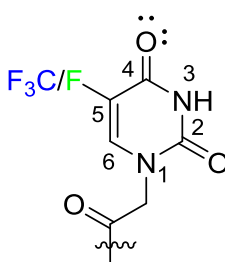


Figure 3.20 CD spectra of PNAs **29-31** with cDNA and cRNA (Buffer: 10 mM sodium phosphate, pH=7.2, NaCl 10 mM).

3.7 Discussion

The PNA oligomers fluorinated at nucleobase, side chain and backbone were studied for their binding affinity for cDNA and cRNA with sequence specificity.

- The nucleobase fluorinated PNAs showed slight reduction in T_m , which might be encountered due to the electronegative fluorine substitution at C⁵ decreasing the electron density on C⁴-carbonyl oxygen. This in turn might be resulted in decreased hydrogen bonding efficiency of the modified nucleobases (5-fluorouracil and 5-trifluoromethyl uracil) with their complementary nucleobase adenine.



Insertion of deoxy 5-(trifluoromethyl)uridine in a DNA sequence decreased binding affinity with its complementary DNA sequence by 3°C per modification.¹⁴ In comparison, the insertion of 5-*CF₃aeg* PNA monomer into PNA sequence decreased the binding affinity by ~ 2.1 °C per modification except C-modification (ΔT_m -13 °C). However, as number modifications increases its binding affinity towards its complementary sequence also increased (ΔT_m -2.7 and +0.8 °C for double and triple modifications respectively). Virta *et al.*¹⁵ reported insertion of 5-*CF₃U-aeg* PNA monomer in a PNA sequence decreased the duplex stability by ~ 1.0 °C. This comparison clearly indicates that insertion of trifluoromethyl uracil base in a sequence generally decreases their duplex stability, also depends on PNA sequence used for the duplex binding study. This might be attributed to (-) inductive effect of trifluoromethyl group present at 5th position of the nucleobase uracil.

- PNA decamers modified with γ -*CF₂-apg* PNA and *apg* PNA monomers showed almost equal T_m either with cDNA or cRNA suggesting that the methylene substitution in *apg* PNA backbone with difluoromethylene group does not significantly alter the duplex stability, although it enhances the hydrophobicity (From HPLC retention times).

- The mixed 14-mer PNA oligomers modified with γ -CF₂-apg PNA and apg PNA monomers showed no difference in T_m further proving that replacing methylene substitution with difluoromethylene group in the backbone of the apg PNA does not alter the thermal stability of the PNA:DNA/RNA duplexes. This effect seems to be independent of sequence context.
- The nucleobase 5FU-aeg fluorinated PNAs have almost equal sequence specificity for both DNA and RNA whereas in case of PNAs modified with 5CF₃U-aeg units, though sequence specificity is same for both DNA and RNA, higher sequence discrimination with RNA was seen compared to that of DNA.
- Backbone fluorinated γ -CF₂-apg PNAs (**19-23**) exhibited higher sequence specificity for both DNA and RNA. Sequence specificity of γ -CF₂-apg PNAs was more for cRNA compared to cDNA.
- All the fluorinated PNAs showed a conformational change upon binding to complementary DNA and RNA and the CD-signatures are in conformity with unmodified PNA:DNA and PNA:RNA duplexes.

Overall the backbone fluorinated PNAs seem to be optimal in terms of their biophysical properties for taking up to next steps of biological studies.

3.8 Experimental procedures

Chemicals: The PNA oligomers were synthesized by solid phase protocol manually and under microwave conditions using Boc-Strategy as described in chapter 2. The DNA and RNA oligonucleotides were obtained commercially from IDT (integrated DNA technologies). All other chemicals were of analytical grade.

UV- T_m measurements: UV-melting experiments were carried out on Varian Cary 300 UV-spectrophotometer equipped with a Peltier temperature programmer and Julabo water circulator.

1) The samples for T_m measurements were prepared at 4 μ M concentration of each PNA and DNA/RNA (500 μ L of 10 mM phosphate buffer, pH 7.2 and 10 mM NaCl).

2) The PNA and cDNA or cRNA were mixed together in stoichiometric amounts of 1:1 and annealed at 90 °C for 3 min and cooled to room temperature slowly.

- 3) The samples were transferred to quartz cell, sealed with Teflon stopper and the optical density (OD) was recorded at 260 nm with a rate of 1.0 °C/min temperature increment from 16 °C to 85 °C.
- 4) The normalized absorbance at 260 nm was plotted as a function of the temperature and the T_m was determined from the first derivative plots with respect to temperature and is accurate to ± 0.5 °C.
- 5) The data were processed using Microcal Origin 8.0. The concentration of DNA, RNA and PNA were calculated with the help of extinction coefficients of nucleobases ($A = 15.4$, $T = 8.8$, $C = 7.3$ and $G = 11.7$).

Circular Dichroism: CD spectra were recorded on JASCO J-715 spectro-polarimeter. The CD spectra of the PNA:DNA and PNA:RNA complexes and the relevant single strands were recorded using 4 μ M duplexes in 10 mM sodium phosphate buffer, 10 mM NaCl at pH 7.2. The temperature of the circulating water was kept below the melting temperature of the PNA:DNA and PNA:RNA complexes, i.e., at 20 °C. The CD spectra of PNA:DNA and PNA:RNA duplexes were recorded by addition of 5 scans from 300 to 190 nm, with a resolution of 0.1 nm, bandwidth of 1.0 nm, sensitivity of 2 mdeg, response of 2 sec and a scan speed of 50 nm/min.

3.9 References

1. Hansch, C.; Fujita, T. *J. Am. Chem. Soc.* **1964**, *86*, 1616.
2. Leahy, D. E.; Taylor, P. J.; Wait, A. R. *Quant. Struct. Act. Relat.* **1989**, *8*, 17.
3. Pawliszyn J. *Solid Phase Microextraction. Wiley-VCH, Toronto* **1997**, 37.
4. Arthur, C. L.; Pawliszyn, J. *Anal. Chem.* **1990**, *62*, 2145.
5. Saghaie, L.; Hider, R.; Mostafavi, S. A. *Daru* **2003**, *11*, 38.
6. Danielsson, L. G.; Zhang, Y. H. *Trends Anal. Chem.* **1996**, *15*, 188.
7. Sangster, J. Octanol-water Partition Coefficients: *Fundamentals and Physical Chemistry*. Wiley, New York **1997**.
8. OECD/OCDE Guidelines for the testing of chemicals. Partition coefficient (n-octanol/water): pH-metric method for ionisable substances. *117*, **2004**.
9. Jana, S.; Mandlekar, S.; Marathe, P. *Curr. Med. Chem.* **2010**, *17*, 3874.
10. Bohm, H. J.; Banner, D.; Bendels, S.; Kansy, M.; Kuhn, B.; Muller, K.; Obst-Sander, U.; Stahl, M. *Chem BioChem* **2004**, *5*, 637-643.
11. Kelly, S. M.; Price, N. C. *Current Protein and Peptide Science* **2000**, *1*, 349-384.

12. Ivanov, V. I.; Minchenkova, L. E.; Minyat, E. E.; Frank-Kamenetskii, M. D.; Schyolkina, A. K.; *J. Mol. Biol.* **1974**, *87*, 817-833.
13. Jain, R. D.; Libi, V. A.; Lahiri, M.; Ganesh, K. N. *J. Org. Chem.* **2014**, *79*, 9567-9577.
14. Markley, J. C.; Chirakul, P.; Sologub, D. and Sigurdsson, S. T. *Bioorg Med Chem Lett.* **2001**, *11*, 2453-2455.
15. Kiviniemi, A.; Murtola, M.; Ingman, P. and Virta, P. *J. Org. Chem.* **2013**, *78*, 5153-5159.

3.10 Appendix-II

UV- T_m profiles of PNAs **9-26** with mismatch DNA **2** and RNA **2**

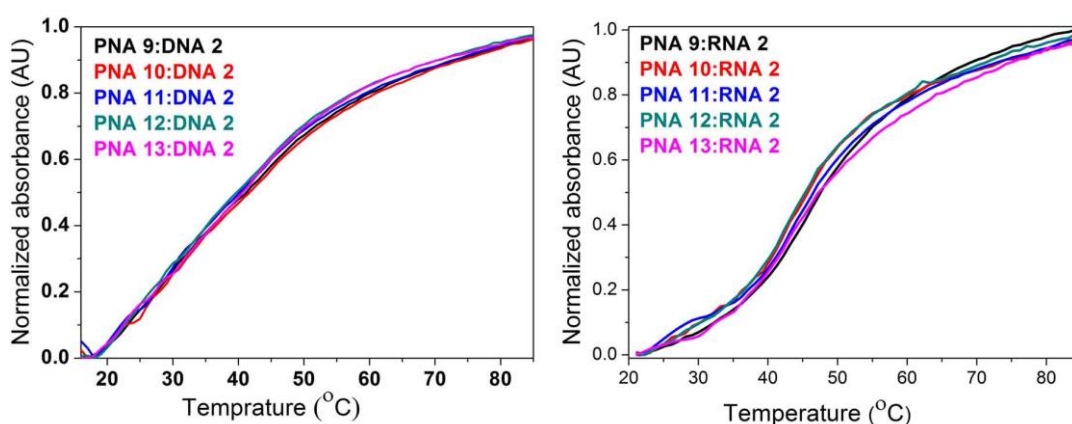


Figure 3.21 UV- T_m profiles of *5FU-aeg* PNAs (**9-13**) with mismatch DNA **2** and RNA **2**.

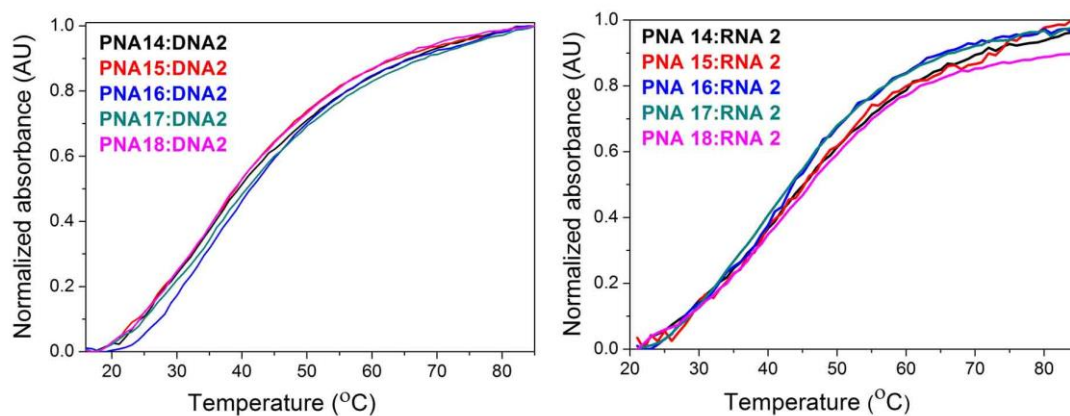


Figure 3.22 UV- T_m profiles of *5CF₃U-aeg* PNAs (**14-18**) with mismatch DNA **2** and RNA **2**.

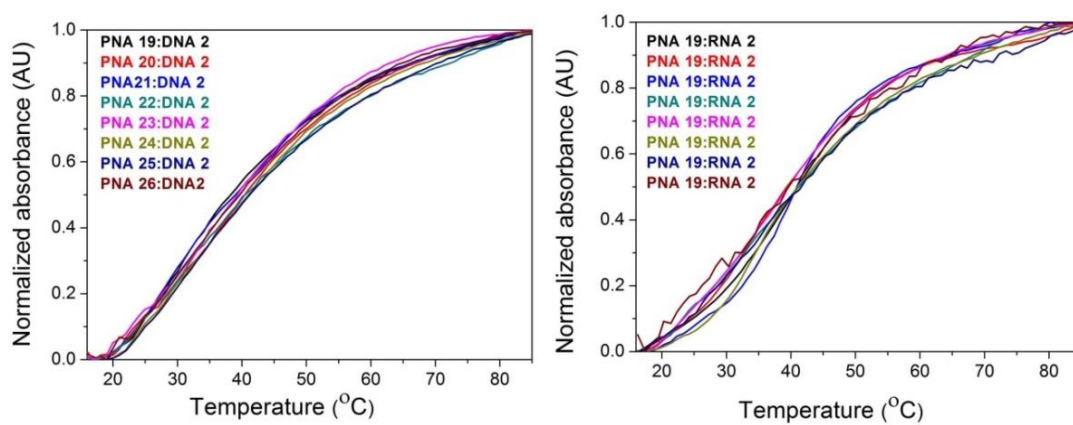


Figure 3.23 UV-T_m profiles of γ -CF₂-ap_g PNAs (**19-23**) and ap_g PNAs (**24-26**) with mismatch DNA **2** and RNA **2**.

Chapter 4: Cell Permeation Studies of Fluorinated PNAs and Nanoparticles formation of PNA:DNA/RNA duplexes

4.1 Introduction

The fluorinated PNA oligomers were designed to take advantage of fluorine to improve the cell permeability of PNAs. This chapter describes studies on the efficiency of cell uptake and localisation of fluorinated PNA oligomers monitored through their fluorescent conjugates and live cell imaging using confocal microscopy. The quantification of the cell uptake of various fluorinated PNAs has been carried out in NIH 3T3 and HeLa cell lines using fluorescence activated cell sorter (FACS) analysis. The principle behind confocal microscopy and FACS techniques are explained below.

4.1.1 Confocal microscopy

The principle of confocal imaging was patented in 1957 by Marvin Minsky.^{1,2} In a conventional fluorescence microscope (wide-field microscope) all parts of the specimen in the optical path are excited at the same time and the resulting fluorescence detected by the microscope's photodetector/ camera including a large unfocused background part. In contrast, a confocal microscope uses point illumination and a pinhole in an optically conjugate plane in front of the detector to eliminate out-of-focus signal. As only light produced by fluorescence very close to the focal plane can be detected, the image's optical resolution, particularly in the sample depth direction, is much better than that of wide-field microscopes. However, as much of the light from sample fluorescence is blocked at the pinhole, this increased resolution is at the cost of decreased signal intensity. The schematic illustration of the principle of confocal microscopy is shown in Figure 4.1.

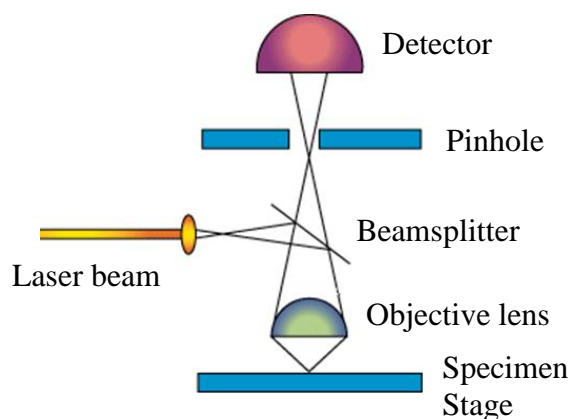


Figure 4.1 Schematic diagram of principle of confocal scanning light microscope.³

4.1.2 FACS experiment

Mack Jett Fulwyler, pioneer of flow cytometry and flow sorting which is a device capable of separating biological cells suspended in a conducting medium. The cells isolated in the form of droplets are charged according to the sensed volume. The charged droplets then pass through an electrostatic field and deflected into a collection vessel according to the charge of the droplet.^{4,5}

Fluorescence-activated cell sorting (FACS) is a specialized flow cytometry. It provides a method for sorting a heterogeneous mixture of biological cells. It is an important scientific instrument because it provides fast and quantitative recording of fluorescent signals from individual cells as well as physical separation of the cells of particular interest. The working principle of the FACS is shown in the schematic diagram (Figure 4.2).

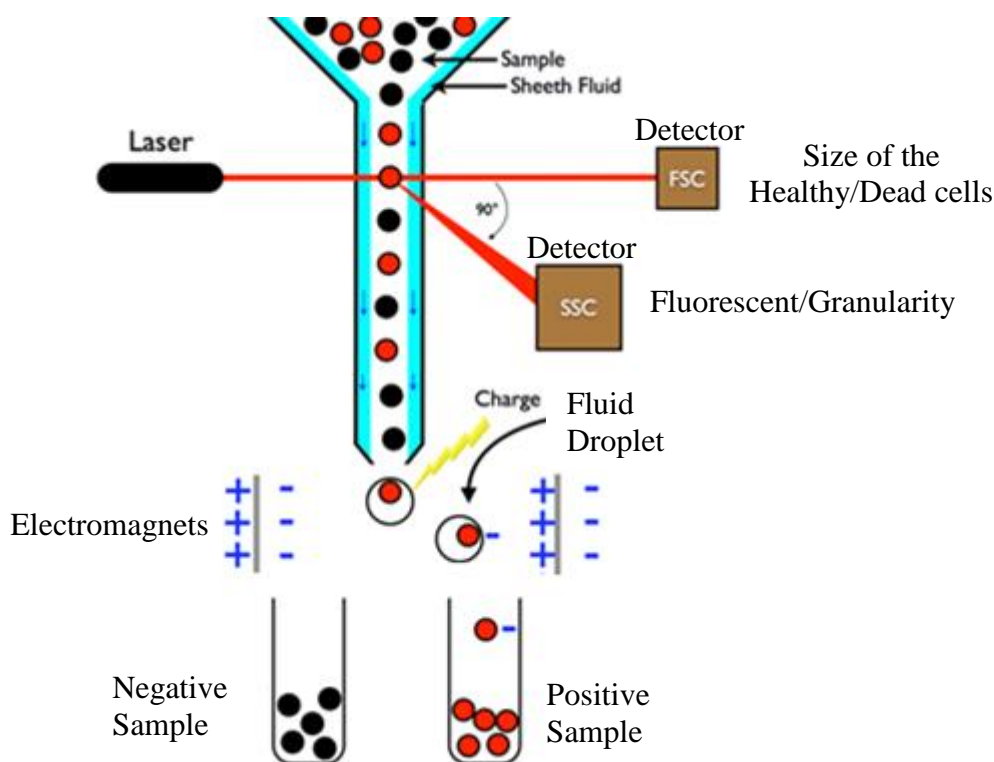


Figure 4.2 Schematic illustration of the FACS working principle.⁶

4.2 Aim of the present work

The specific objectives of this section are,

1. Synthesis of 5(6)-carboxyfluorescein labelled fluorinated PNA oligomers
2. Synthesis of per-fluorocarbon/hydrocarbon chain derivatized fluorescent PNAs

3. Studies on cell uptake of fluorinated PNA oligomers and their localization in NIH 3T3 and HeLa cell lines by confocal microscopy

4. Quantification of cell permeation abilities of the PNA oligomers by FACS studies

4.3 Results and discussion

The synthesis, purification, characterization and cellular uptake efficiency of fluorescently labelled PNA oligomers have been discussed in this section.

4.3.1 Synthesis of fluorescein conjugated PNA oligomers

In order to follow comparative cell permeation studies of standard and fluorinated PNA analogs, the different PNA oligomers were conjugated with carboxy fluorescein (CF). The solid phase peptide synthesis of each oligomer was followed by tagging with 5(6)-carboxyfluorescein (CF) through a lysine spacer unit at the final step. The conjugation was done using DIC and HOBt as coupling reagents (Scheme 1) and followed by their cleavage from the resin (Figure 4.3). The fluorescent, fluorinated PNAs synthesized are shown in Table 4.1.

Scheme 1 Synthesis of 5(6)-carboxyfluorescein attached PNA oligomers

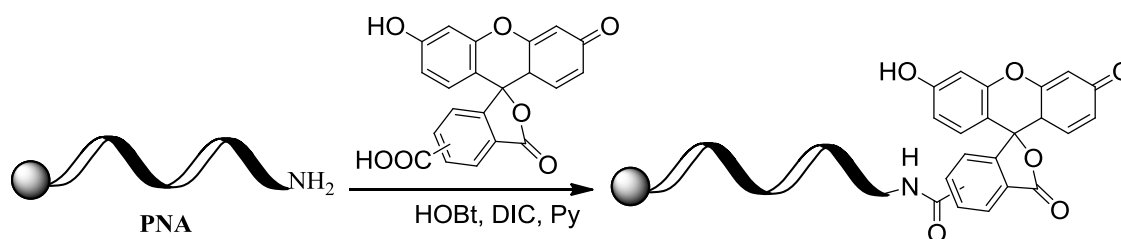


Figure 4.3 Labelling of PNA oligomers with fluorescent 5(6)-carboxyfluorescein

4.3.2 Synthesis of per fluoroalkyl chain and hydrocarbon chain attached PNA oligomers

It has been shown that attachment of per-fluoro alkyl chain to the 5' end of the DNA leads to improvement in the cellular localization of the DNA.⁷ In this context, PNAs conjugated with fluoro alkyl chain were synthesised in order to test the cell permeability compared to that of unmodified *aeg* PNAs. Carboxyfluorescein was attached to these PNAs in order to visualize their cellular localization using confocal microscopy. As a negative control, PNAs conjugated with hydrocarbon chain and carboxy fluorescein were synthesized for comparative studies.

Lysine was coupled to the unmodified PNA (TGA₂CTCCATT-NH₂) at the N-terminus after solid phase peptide synthesis protocol. The fluorocarbon/hydrocarbon acid was coupled

to the side chain of lysine using HBTU/HOBt as coupling reagent under microwave conditions (Scheme 2). The α -amine of the lysine was coupled to carboxy fluorescein using DIC/HOBt as coupling reagent. The PNA sequences are shown in the Table 4.1.

Scheme 2 Synthesis of fluoro/hydrocarbon chain attached PNAs

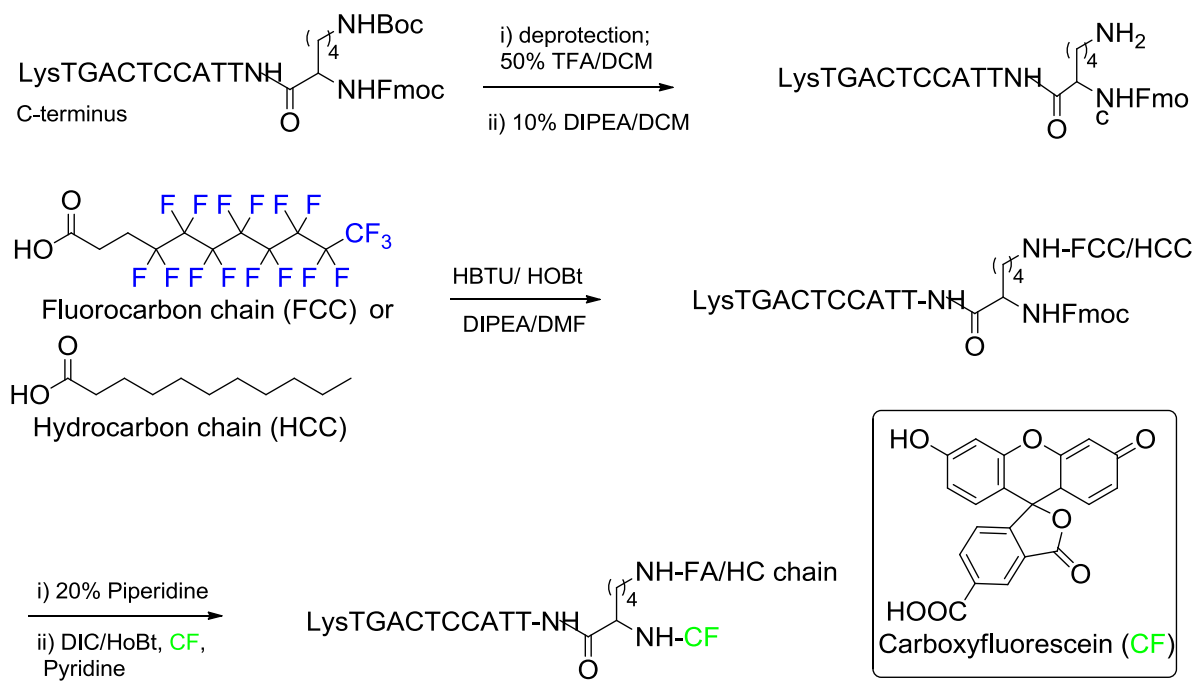


Figure 4.4 Scheme for the synthesis of fluoro/hydrocarbon chain attached PNAs

Table 4.1 Synthesis of fluorescein conjugated PNA oligomers and per-fluoro/alkyl chain attached PNA oligomers

Entry	PNA	PNA sequence
1	PNA 32-CF	CF-Lys-TTACCTCAGT-Lys
2	PNA 33-CF	CF-Lys-TT ^{γCF₂} ACT ^{γCF₂} CAGT ^{γCF₂} -Lys
3	PNA 34-CF	CF-Lys-TT ^{Ph} ACCT ^{Ph} CAGT ^{Ph} -Lys
4	PNA 35-CF	CF-Lys-TT ^{FPh} ACCT ^{FPh} CAGT ^{FPh} -Lys
5	PNA 36-CF	(CF, HCC)-Lys-LysTTACCTCAGT-Lys
6	PNA 37-CF	(CF, FCC)-Lys-LysTTACCTCAGT-Lys

PNA 35 and PNA 36 both have 15 fluorine atoms but labelled differently, PNA 35 with aromatic fluorines and PNA 36 with aliphatic fluorines. The cleavage of carboxy fluorescein tagged PNAs from solid support was performed using TFMSA/TFA solution. The PNAs were purified by HPLC and characterized using MALDI-TOF spectrometry. The HPLC retention times and MALDI-TOF values are shown in Table 4.2.

Table 4.2 MALDI-TOF spectral analysis of the synthesized PNA oligomers

Entry	PNA	Mol.formula	Calcd m/z	Obsvd m/z	Rt (min)
1	PNA 32-CF	C ₁₄₃ H ₁₈₀ N ₅₇ O ₄₀	3335.3803	3335.8125	12.9
2	PNA 33-CF	C ₁₄₃ H ₁₇₄ F ₆ N ₅₇ O ₄₀	3443.3238	3444.3088	13.2
3	PNA 34-CF	C ₁₆₁ H ₁₉₁ N ₅₇ O ₄₀	3562.4658	3564.1889	15.5
4	PNA 35-CF	C ₁₆₁ H ₁₇₇ F ₁₅ N ₅₇ O ₄₀	3833.3323	3833.3306	16.9
5	PNA 36-CF	C ₁₅₂ H ₁₉₂ N ₅₆ O ₄₁	3459.4817	3461.3769	13.4
6	PNA 37-CF	C ₁₅₂ H ₁₇₇ F ₁₅ N ₅₆ O ₄₁	3765.3084	3766.8883	15.2

The absorption spectra were recorded for the tagged PNA oligomers which showed absorbance maxima at 260 nm and 445-490 nm due to nucleobases and 5(6)-carboxyfluorescein respectively (Figure 4.5 A). The fluorescence emission spectra were also recorded for the tagged PNA oligomers which showed emission maxima at ~ 515 nm when excited at ~ 445 nm wavelength (Figure 4.5 B).

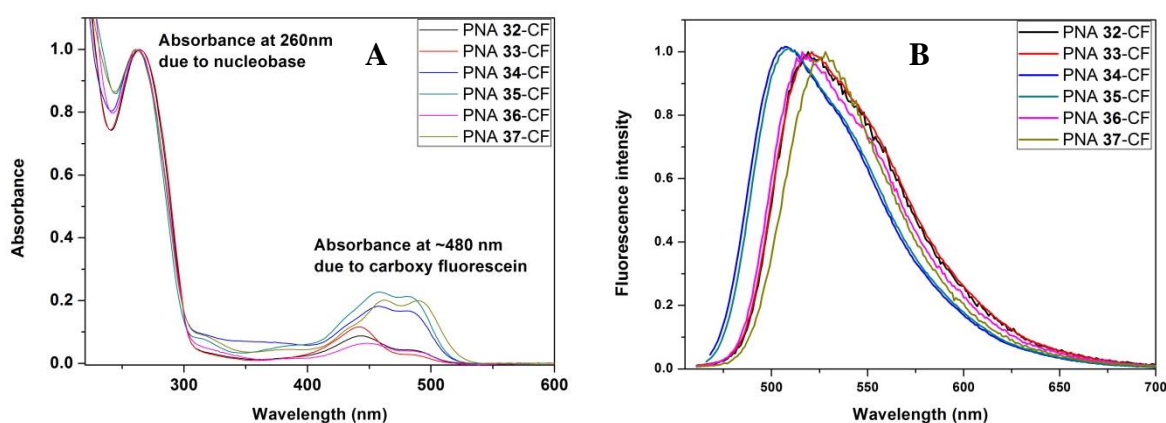


Figure 4.5 (A) UV-Visible absorption spectra and (B) Fluorescence emission spectra of the tagged PNA oligomers.

4.4 Cellular Uptake Studies

To study the comparative cell permeation abilities and intra cellular distribution of various fluorinated PNA oligomers (PNAs 32-37), the PNA oligomers were tested in two different cell lines (NIH 3T3 and HeLa). Confocal microscopic technique was used to observe the cellular uptake of carboxyfluorescein labelled PNAs.

4.4.1 Cellular uptake experiment using confocal microscopy

The immortal HeLa cells and the embryonic fibroblast cells NIH 3T3 were used for cell uptake experiments. Cell permeability of fluorophore tagged PNA oligomers was monitored by green fluorescence seen in confocal microscopy. The green fluorescence due to 5(6)-CF tagged PNA oligomers was seen to be localized in endoplasmic reticulum in cytoplasm. This

was supported from staining with endo tracker ER-red giving yellow colour upon superimposition of its red colour with green from PNA.

4.4.2a Cell Permeation in HeLa Cells

The cell permeation of PNA oligomers was confirmed by visualization of green fluorescence in the cell compartments. A more convincing evidence of the PNA uptake by cells comes from the superimposition of bright field image, green fluorescent image and nuclear stained image (blue). The cells were stained with the tracker dye ER-red in order to ascertain the localization of PNAs within the endoplasmic reticulum. Fluorinated as well as non-fluorinated PNA oligomers can penetrate into HeLa cell line used in the study. The fluorescein tagged PNA oligomers were observed to transverse into the cytoplasm and some of the PNA localized in the endoplasmic reticulum (from ER experiment). The backbone fluorinated γ -CF₂-ap_g incorporation in the aeg PNA sequence seems to be enhanced the cell penetration of the PNA in the HeLa cells as compared to the respective control ap_g PNA. The hydrophobic γ -5FBn-aeg and γ -Bn-aeg PNAs were found to enhance the cell penetration in the HeLa cells. Fluorocarbon as well as hydrocarbon chain conjugated PNAs were also seem to increase the efficiency of the cell penetration in the HeLa cells. The cell uptake images of the PNA oligomers by HeLa cell line are shown in Figures 4.6-4.11.

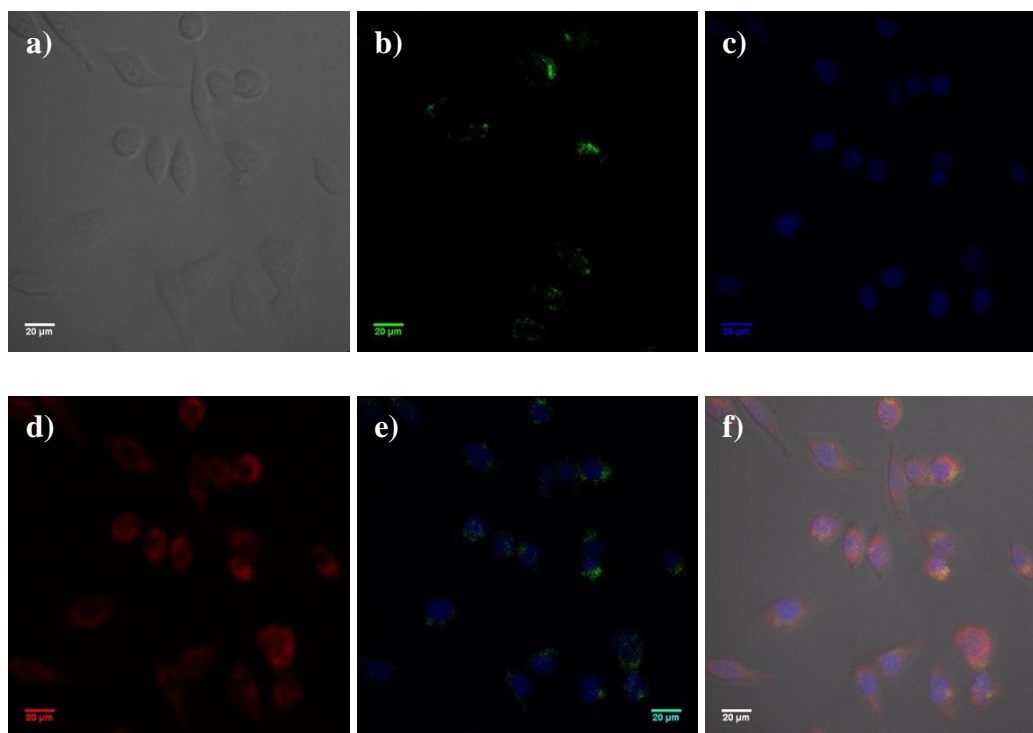


Figure 4.6 Confocal microscopy images for PNA 32-CF (a) bright field image of HeLa cells; (b) Green fluorescent image; (c) Hoechst 33342 stained image; (d) ER-red stained image and (e) Superimposed image of (b) and (c); (f) Superimposed image of (a) - (d).

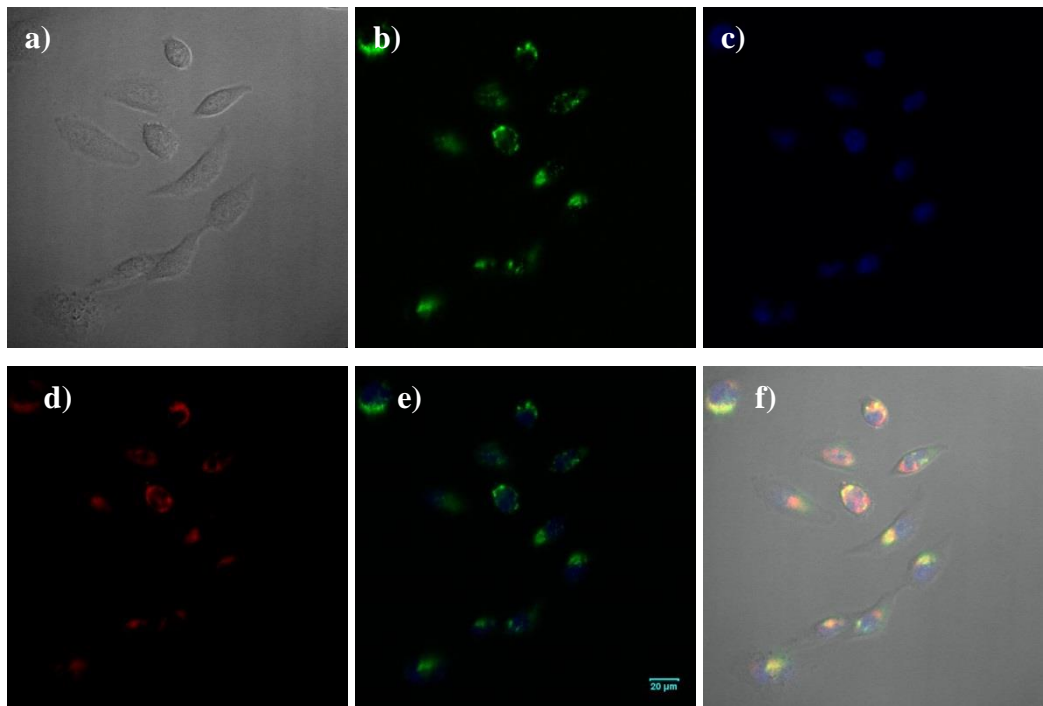


Figure 4.7 Confocal microscopy images for PNA 33-CF (a) bright field image of HeLa cells; (b) Green fluorescent image; (c) Hoechst 33342 stained image; (d) ER-red stained image and (e) Superimposed image of (b) and (c); (f) Superimposed image of (a) - (d).

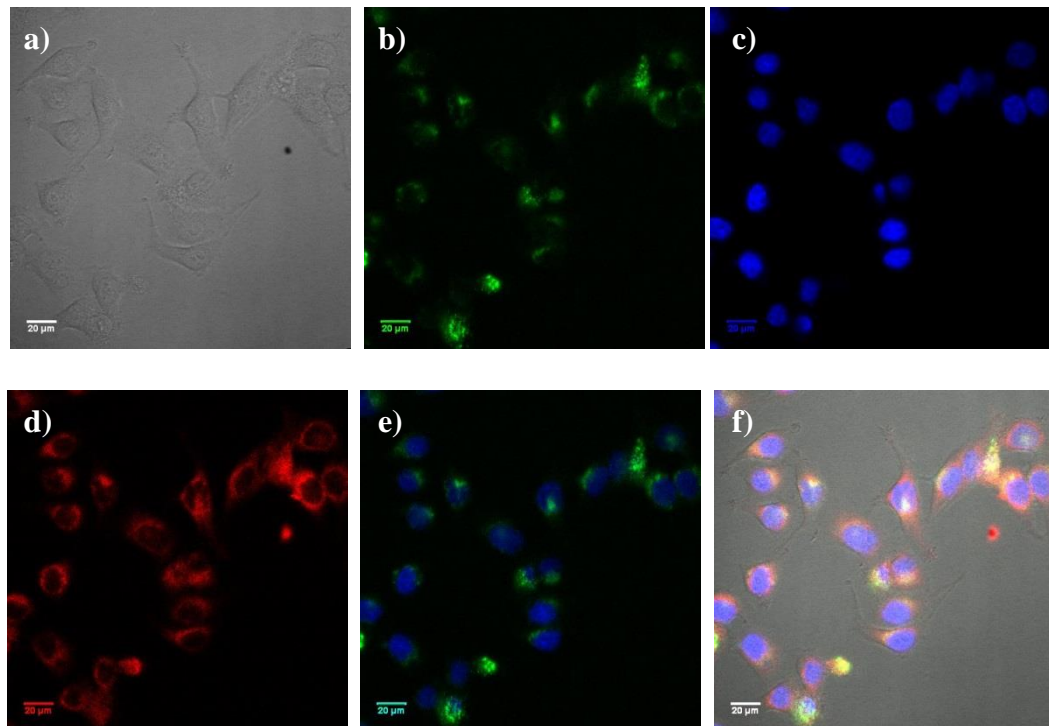


Figure 4.8 Confocal microscopy images for PNA 34-CF (a) bright field image of HeLa cells; (b) Green fluorescent image; (c) Hoechst 33342 stained image; (d) ER-red stained image and (e) Superimposed image of (b) and (c); (f) Superimposed image of (a) - (d).

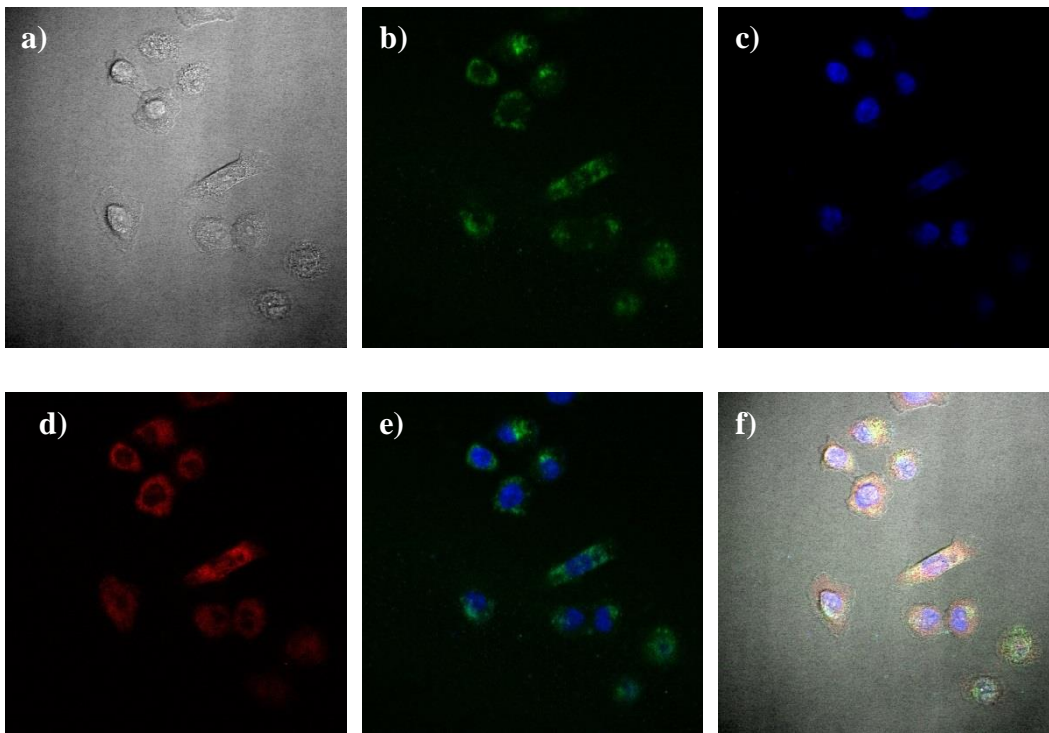


Figure 4.9 Confocal microscopy images for PNA 35-CF (a) bright field image of HeLa cells; (b) Green fluorescent image; (c) Hoechst 33342 stained image; (d) ER-red stained image and (e) Superimposed image of (b) and (c); (f) Superimposed image of (a) – (d).

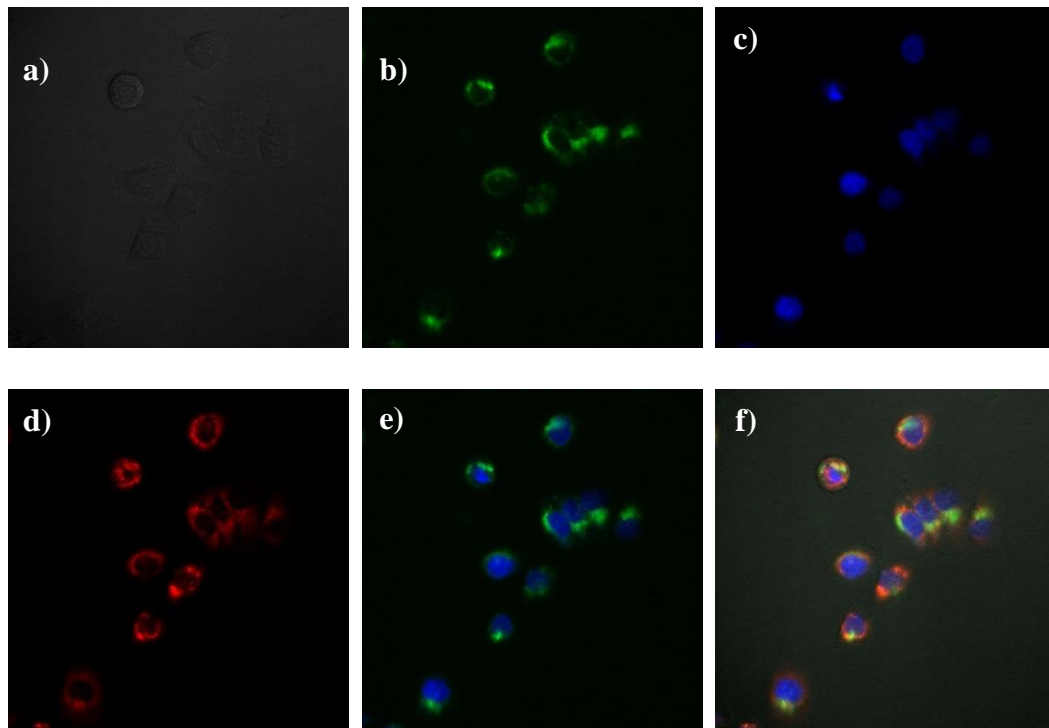


Figure 4.10 Confocal microscopy images for PNA 36-CF (a) bright field image of HeLa cells; (b) Green fluorescent image; (c) Hoechst 33342 stained image; (d) ER-red stained image and (e) Superimposed image of (b) and (c); (f) Superimposed image of (a) – (d).

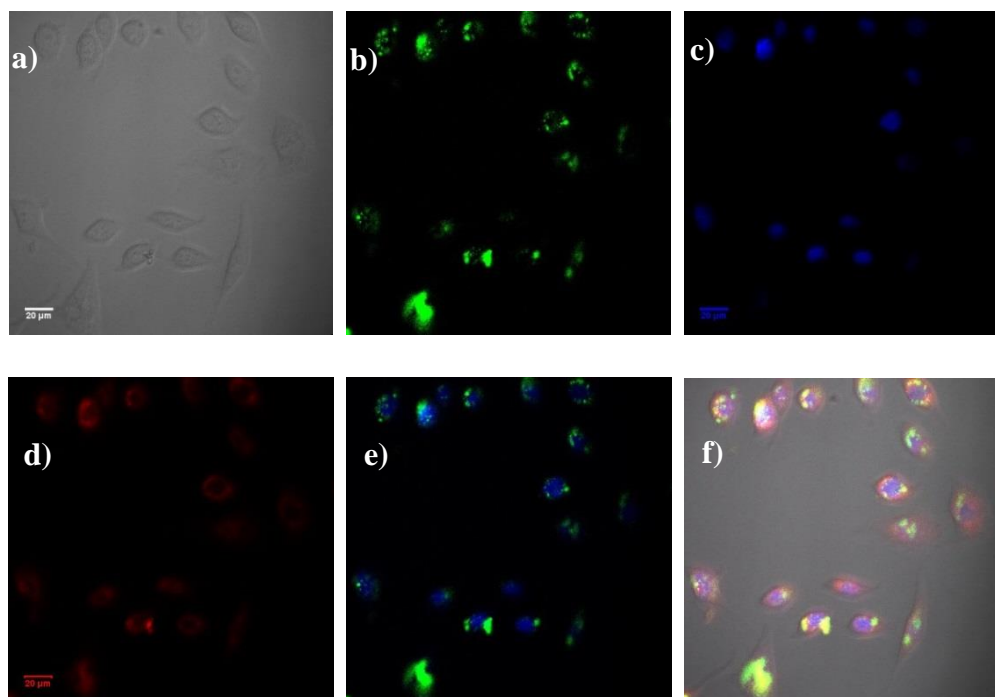
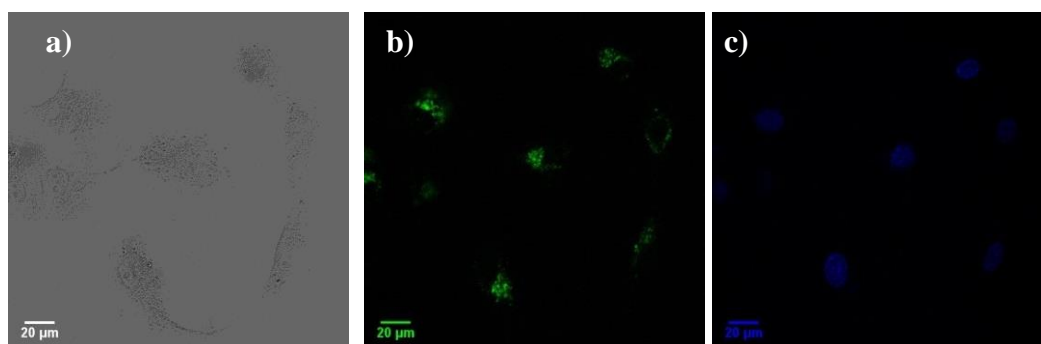


Figure 4.11 Confocal microscopy images for PNA 37-CF (a) bright field image of HeLa cells; (b) Green fluorescent image; (c) Hoechst 33342 stained image; (d) ER-red stained image and (e) Superimposed image of (b) and (c); (f) Superimposed image of (a) – (d).

4.4.2b Cell Permeation in NIH 3T3 cells

Cell permeability of the fluorinated PNA oligomers investigated in normal mouse embryonic fibroblast 3T3 cells. This was done to evaluate whether the ability of fluorinated PNA oligomers going inside the normal cell line 3T3 is different from cancerous cell line HeLa. All the backbone modified PNAs entered into the NIH 3T3 cells irrespective of modification, but the cell uptake ability of the fluorinated PNAs seem to be more than that of non-fluorinated PNAs seen from the confocal images. From ER-tracker experiment, it was observed that some of the PNA entered into the endoplasmic reticulum where generally protein synthesis happens. Thus PNAs entry into ER may help in gene suppression and thereby stop the protein synthesis. The cellular uptake results of fluorinated and non-fluorinated control PNA oligomers are shown in Figures 4.12-4.117.



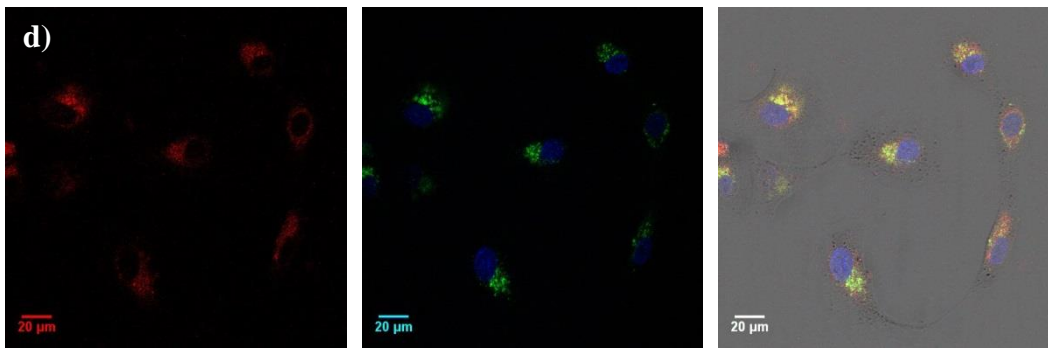


Figure 4.12 Confocal microscopy images for PNA 32-CF (a) bright field image of NIH 3T3 cells; (b) Green fluorescent image; (c) Hoechst 33342 stained image; (d) ER-red stained image and (e) Superimposed image of (b) and (c); (f) Superimposed image of (a) – (d).

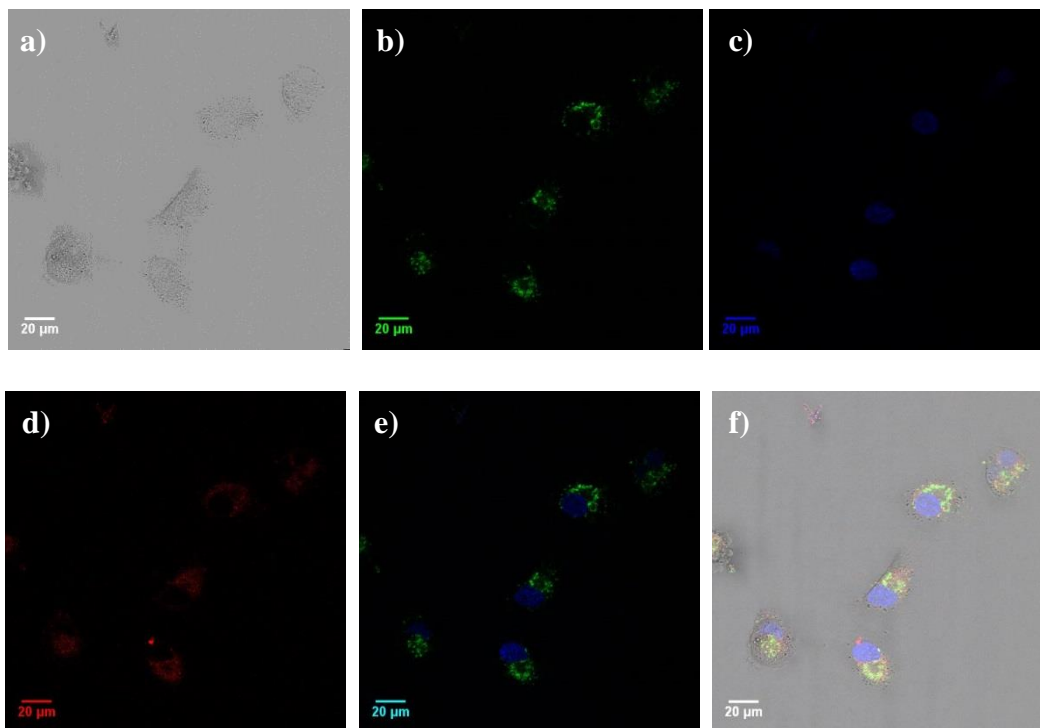
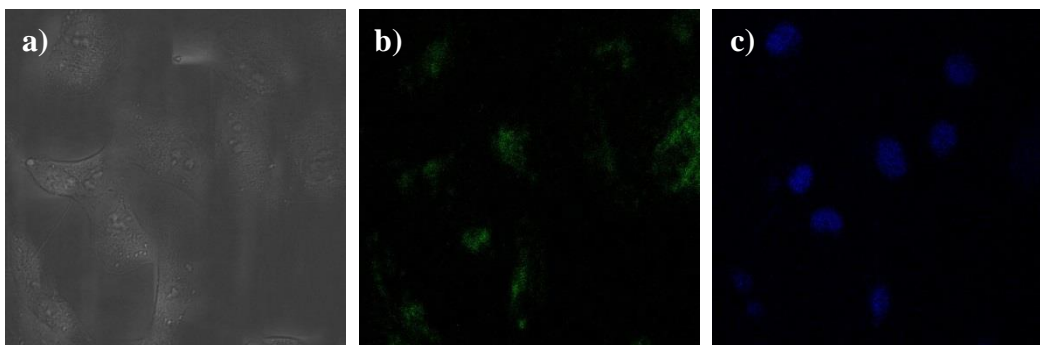


Figure 4.13 Confocal microscopy images for PNA 33-CF (a) bright field image of NIH 3T3 cells; (b) Green fluorescent image; (c) Hoechst 33342 stained image; (d) ER-red stained image and (e) Superimposed image of (b) and (c); (f) Superimposed image of (a) – (d).



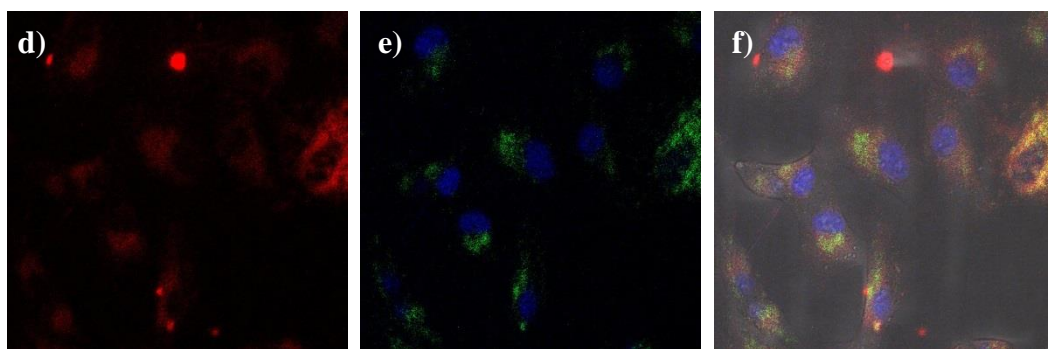


Figure 4.14 Confocal microscopy images for PNA **34-CF** (a) bright field image of NIH 3T3 cells; (b) Green fluorescent image; (c) Hoechst 33342 stained image; (d) ER-red stained image and (e) Superimposed image of (b) and (c); (f) Superimposed image of (a) – (d).

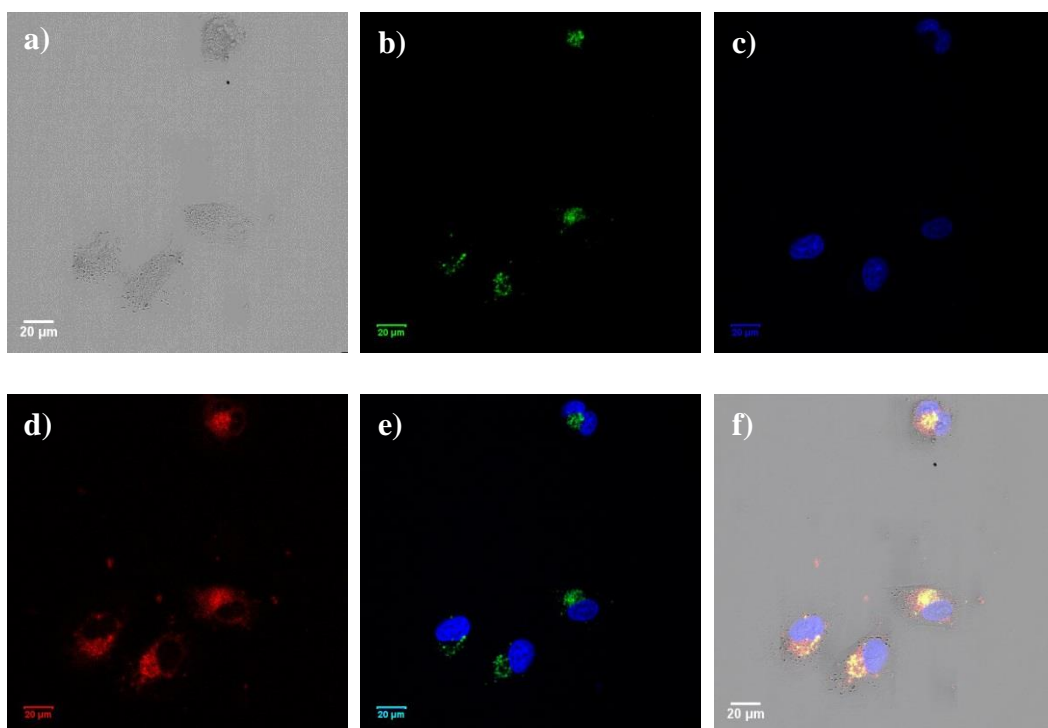
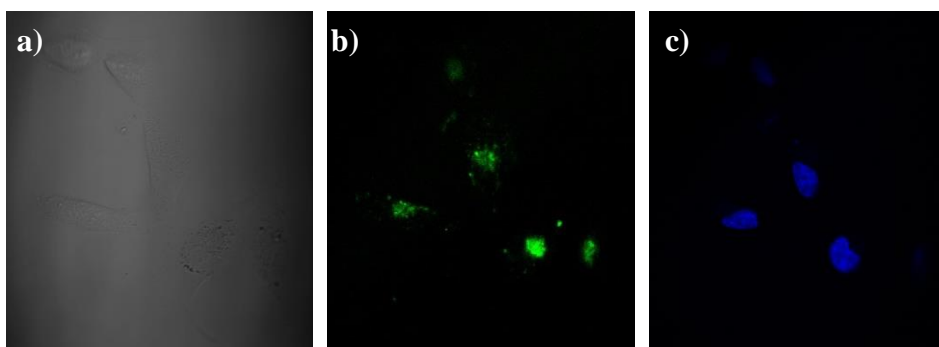


Figure 4.15 Confocal microscopy images for PNA **35-CF** (a) bright field image of NIH 3T3 cells; (b) Green fluorescent image; (c) Hoechst 33342 stained image; (d) ER-red stained image and (e) Superimposed image of (b) and (c); (f) Superimposed image of (a) – (d).



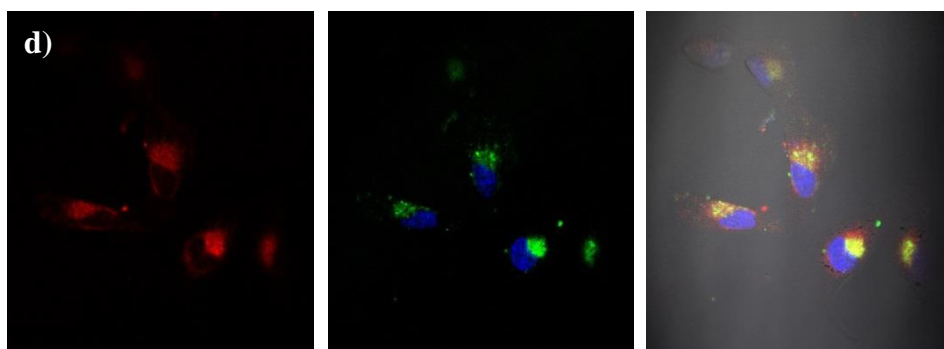


Figure 4.16 Confocal microscopy images for PNA **36-CF** (a) bright field image of NIH 3T3 cells; (b) Green fluorescent image; (c) Hoechst 33342 stained image; (d) ER-red stained image and (e) Superimposed image of (b) and (c); (f) Superimposed image of (a) – (d).

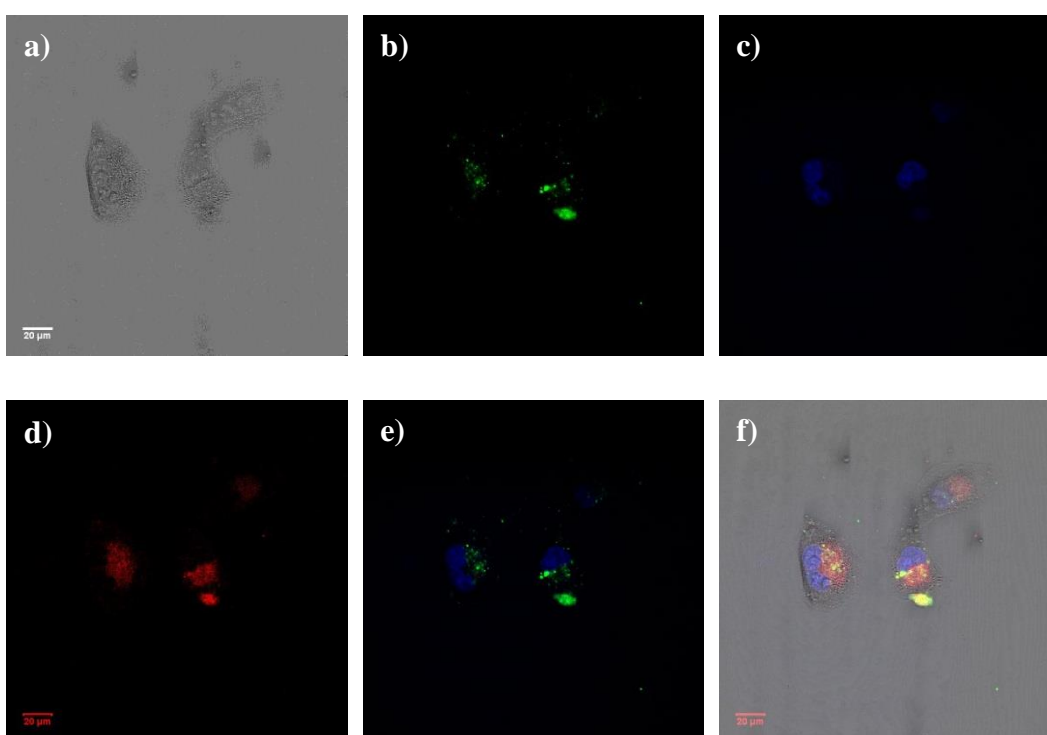


Figure 4.17 Confocal microscopy images for PNA **37-CF** (a) bright field image of NIH 3T3 cells; (b) Green fluorescent image; (c) Hoechst 33342 stained image; (d) ER-red stained image and (e) Superimposed image of (b) and (c); (f) Superimposed image of (a) – (d).

4.5 Quantitative estimation of cell permeation in HeLa and NIH 3T3 cells using FACS

Although the figures 4.6-4.17 provide qualitative evidence that both fluorinated and non-fluorinated PNAs penetrate the cells, they do not provide quantitative information on relative efficiencies of the cell uptake. This was done by fluorescence assisted cell sorter (FACS) which sorts individual cells depending on the fluorescence signal observed from the fluorophore tagged PNA. The individual cells showing green fluorescence of PNA are termed ‘positive cells’, while those not giving fluorescence signal for PNA are ‘negative

cells'. The percentage of positive cell count can be used to quantify the cellular uptake of different modified PNAs.

4.5.1 Quantitative estimation of cell permeation in HeLa cells

The control *apg* PNA (PNA **32**-CF, Table 4.1) is uptaken by ~ 8 % of HeLa cells, whereas the difluoro methylene γ -CF₂-*apg* PNA (PNA **33**-CF, Table 4.1) is taken up by ~ 14% of HeLa cells (Figure 4.21). The mean fluorescence intensities were found to be more for fluorinated γ -CF₂-*apg* PNA (PNA **33**-CF) as compared to control *apg* PNA (PNA **32**-CF) suggesting that fluorinated PNAs enter the HeLa cells better than the non-fluorinated PNAs (Figure 4.18).

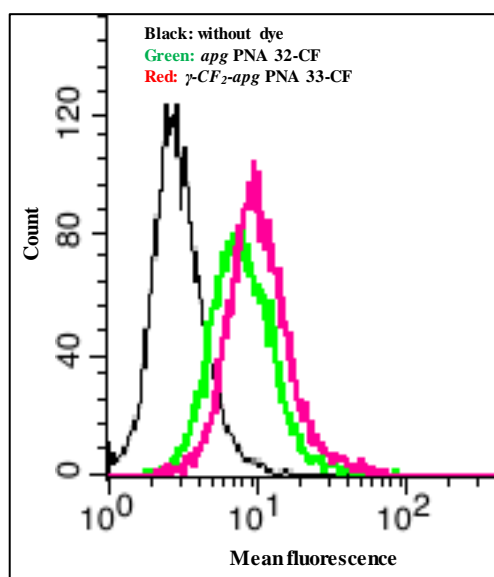


Figure 4.18 Comparative analysis showing mean fluorescence for quantification of PNA cell permeation in HeLa cells.

Incorporation of three γ -Bn-*aeg* PNA units (PNA **34**-CF, Table 4.1) into *aeg* PNA sequence increased the percentage of positive cells up to ~ 47 % while incorporation of three γ -5FBn-*aeg* units in *aeg* PNA sequence (PNA **35**-CF, Table 4.1) resulted in only ~ 29 % of positive cells (Figure 4.21). Both PNA **34**-CF and PNA **35**-CF showed almost equal mean fluorescence intensities suggesting that both the PNAs were taken by the HeLa cells almost in equal amounts but the PNA **34**-CF was taken by more number of cells compared to the PNA **35**-CF (Figure 4.19).

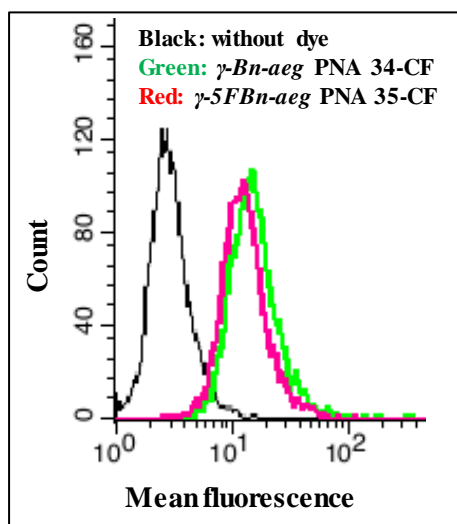


Figure 4.19 Comparative analysis showing mean fluorescence for quantification of PNA cell permeation in HeLa cells.

These results indicate that the efficiency of cell uptake depend on the site, number and pattern of fluorination of PNAs. In order to examine this point in more details, PNAs were labelled with per-fluorocarbon chain at the N-terminus for cell uptake studies.

Hydrocarbon chain attached *aeg* PNA sequence (PNA **36**-CF, Table 4.1) gave ~ 51% of positive HeLa cells whereas the per-fluorocarbon attached *aeg* PNA (PNA **37**-CF, table 4.1) penetrated into a high percentage (~ 99%) of cells (Figure 4.21). The mean fluorescence intensities was found to be significantly higher for per-fluorocarbon chain linked *aeg* PNA (PNA **37**-CF) as compared to the control non-fluorinated *aeg* PNA (PNA **36**-CF). This confirmed that fluorinated PNAs are taken up by the HeLa cells more than the non-fluorinated PNAs (Figure 4.20).

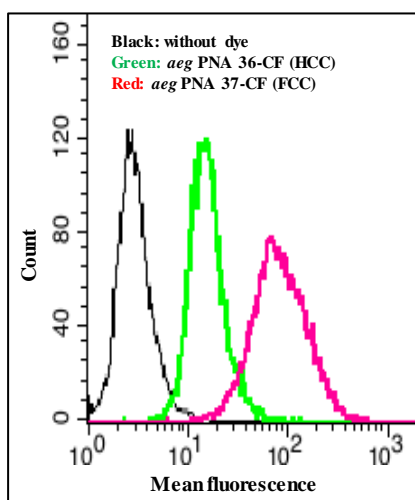


Figure 4.20 Comparative analysis showing mean fluorescence for quantification of PNA cell permeation in HeLa cells.

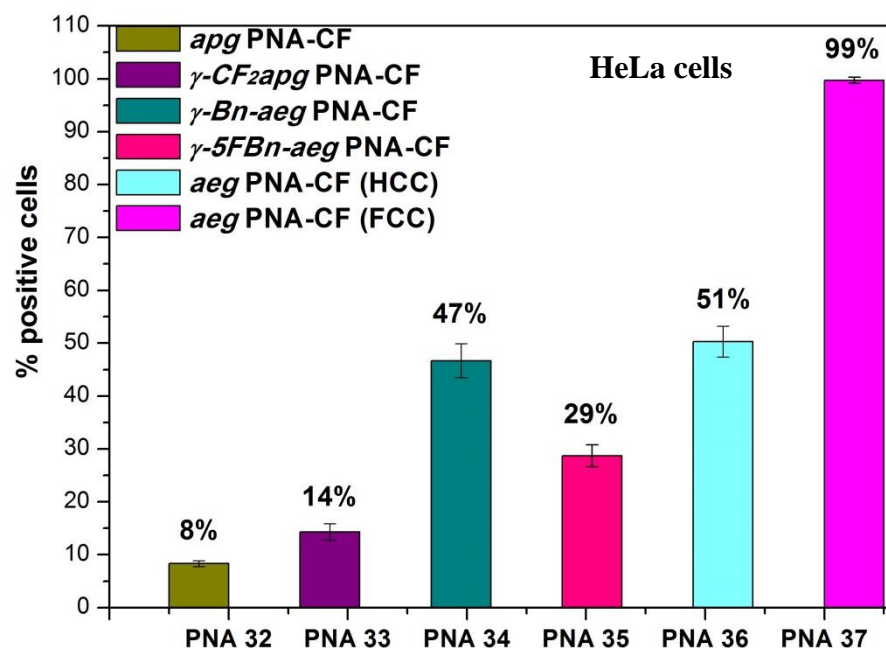


Figure 4.21 comparison of percentage positive cells between fluorinated and their control non-fluorinated PNAs in HeLa cells.

4.5.2 Quantitative estimation of cell permeation in NIH 3T3 cells

Incorporation of three γ -CF₂-apg PNA units in aeg PNA sequence gave 29 % positive cells, almost 3-fold more than corresponding control apg PNA (PNA 32-CF, Table 4.1) that exhibited only ~ 10 % of positive cells (Figure 4.25). The mean fluorescence intensity was far higher for fluorinated PNA (PNA 33-CF) taken up by NIH 3T3 cells compared to control apg PNA (PNA 32-CF, Figure 4.22).

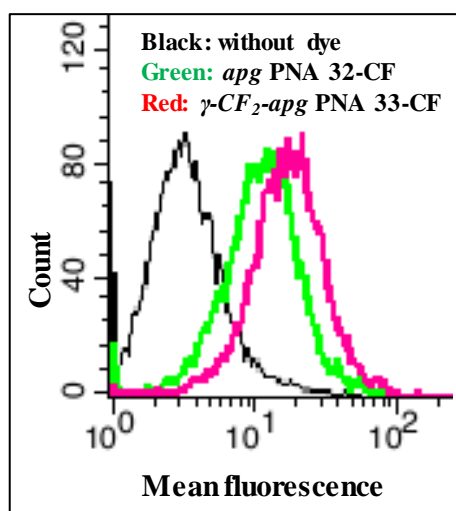


Figure 4.22 Comparative analysis showing mean fluorescence for quantification of PNA cell permeation in NIH 3T3 cells.

In case of three γ -Bn-aeg PNA units in the aeg PNA the cell uptake was by 73 % of cells, while the fluorinated γ -5FBn-aeg in the aeg PNA resulted in only 44% of positive cells (Figure 4.25). The mean fluorescence intensities also indicated that more γ -Bn-aeg PNA **34**-CF was taken by the cells than that of γ -5FBn-aeg PNA **35**-CF (Figure 4.23). Thus the cell uptake seems to be determined by the site of fluorination as well.

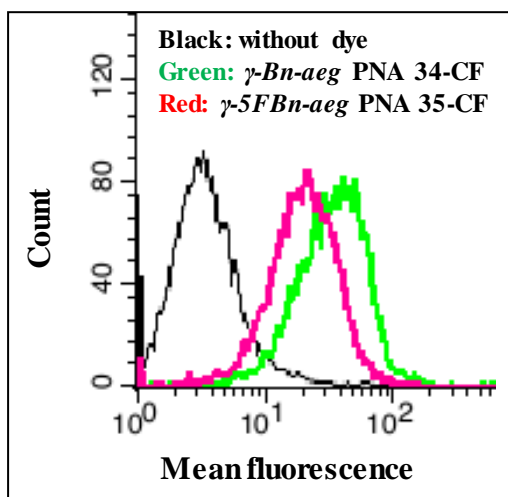


Figure 4.23 Comparative analysis showing mean fluorescence for quantification of PNA cell permeation in NIH 3T3 cells.

Attachment of hydrocarbon chain to the unmodified aeg PNA (PNA **36**-CF, Table 4.1) showed ~ 32 % of positive cells, while per-fluorocarbon attached aeg PNA (PNA **37**-CF, Table 4.1) increased the % positive cells up to ~ 95 % (Figure 4.25). The per-fluorocarbon chain linked aeg PNA was taken by the cells in larger extent than that of hydrocarbon chain attached aeg PNA (Figure 4.24), also supported by a higher mean fluorescent intensities.

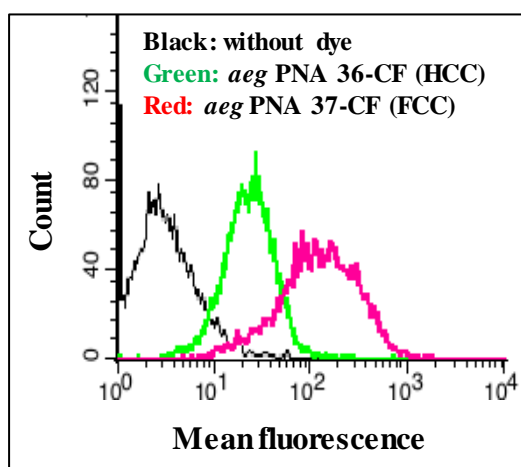


Figure 4.24 Overlay histogram of mean fluorescence: left) control cells without dye; center) PNA **36**-CF and right) PNA **37**-CF.

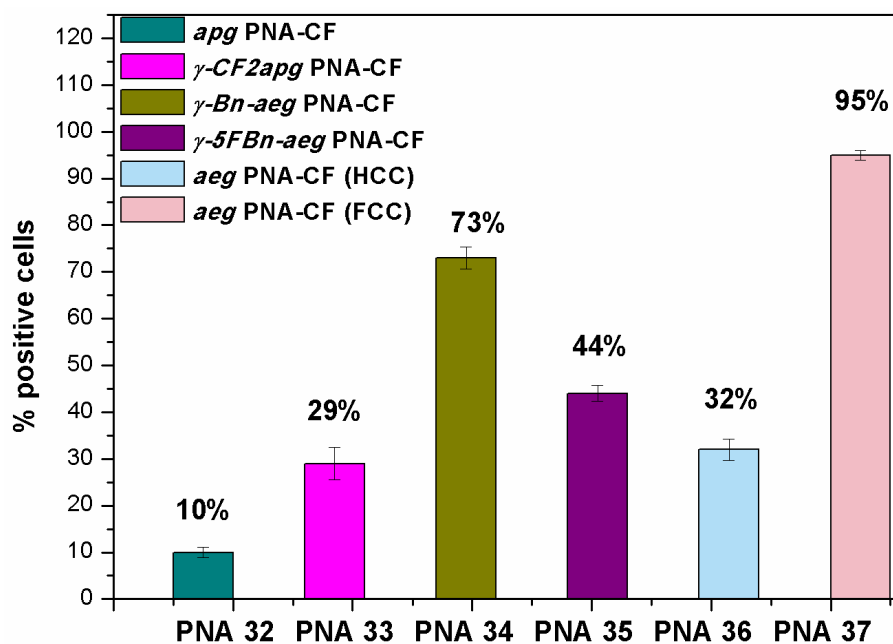


Figure 4.25 Comparison of percentage positive cells between fluorinated and their control non-fluorinated PNAs in NIH 3T3 cells.

4.6 Discussion

The triple modified γ -CF₂-*apg* PNA, *apg* PNA, γ -Bn-*aeg* PNA, γ -5FBn-*aeg* PNA and per-fluorocarbon/hydrocarbon chain conjugated *aeg* PNA oligomers were tagged with 5(6)-carboxyfluorescein to visualize the PNA inside the cells. The site of localization was determined by a combination of nuclear stain (Hoechst stain) and Endo nuclear red dye. The live cell imaging of cell permeation was studied for all modified PNA oligomers in NIH 3T3 and HeLa cell lines. The quantification of differential cellular uptake of PNA oligomers was achieved by FACS analysis.

- ❖ Fluorinated as well as non-fluorinated PNA oligomers can penetrate into both HeLa and 3T3 cell lines used in the study.
- ❖ The PNA oligomers were observed to transverse into the cytoplasm and some of the PNA localized in the endoplasmic reticulum.
- ❖ The backbone fluorinated γ -CF₂-*apg* incorporation in the *aeg* PNA sequence enhanced the cell penetration of the PNA in both NIH 3T3 and HeLa cells as compared to the respective control *apg* PNA.
- ❖ The side chain labelled γ -5FBn-*aeg* and γ -Bn-*aeg* modified PNAs were found to enhance the cell penetration in both cell lines (NIH 3T3 and HeLa cells) but the fluorinated PNA showed lower cell uptake efficiency than the corresponding non-fluorinated PNA.

- ❖ Covalent conjugation of a fluorocarbon chain at the N-terminus of PNA through a lysine unit increased the efficiency of the cell penetration, compared to the simple hydrocarbon chain attached PNA in both NIH 3T3 and HeLa cells.
- ❖ Differential cellular uptake was observed in two different cell lines: in HeLa cells, γ - CF_2 -*apg* and *apg* PNAs showed less cell penetration, while in NIH 3T3 cells, γ - CF_2 -*apg* PNA showed 3-fold increase in cell penetration as compared to control *apg* PNA. The fluorinated γ - CF_2 -*apg* PNA seems to be more selective to the NIH 3T3 cells compared to HeLa cells.
- ❖ The side chain modified γ -*Bn-aeg* and γ -*5FBn-aeg* PNAs showed good cell penetration in both the cell lines. γ -*Bn-aeg* PNA showed more cell penetration in NIH 3T3 cells (73%) as compared to that of in HeLa cells (47%). The same trend was observed with γ -*5FBn-aeg* PNA, In NIH 3T3 cells, showing higher percentage positive cells (44%) compared to that by HeLa cells (29%).
- ❖ The hydrocarbon/per-fluorocarbon chain attached *aeg* PNAs showed best results with higher cell penetration in both the cell lines but hydrocarbon chain attached *aeg* PNA is more efficient in HeLa cell line as compared to NIH 3T3 cells whereas per-fluorocarbon chain attached *aeg* PNA did not show any preference.

The next section deals with study of ability of fluorinated PNAs to form nanoparticle and cell uptake of duplex nanoparticle.

4.7 PNA based Nanoparticles Formation and their Cellular Uptake Studies

This section describes the PNA based nanoparticle formation with its complementary DNA **1** and RNA **1**.

4.7.1 Rationale behind the work

The success of antisense therapy to regulate expression of genes associated with disease depends on successful delivery of antisense oligonucleotides and their stability in biological systems. Recently nanotechnology based delivery systems are being delivered, with synthetic lipid- and polymer-based nano-carriers as nucleic acid delivery systems.⁸ It is known that self-assembling peptides organise into well-ordered nanostructures such as nano fibrils, nanotubes, nano spheres or vesicles, depending on the constituent peptide and environmental conditions during assembly.⁹⁻¹² The relatively weak non-covalent interactions act together to form intact and well-ordered supramolecular nanostructures.¹³ Gazit *et al.*,¹² demonstrated the self-assembly of homo-aromatic dipeptides substituted on phenyl ring, groups such as halogens,

nitro, phenyl, naphthyl etc that can modulate with the non-covalent interactions. It was found that these form various nanostructures such as tubular structures, nano-spherical assemblies and fibrillar structures (Figure 4.26). Many examples in literature point to peptides with hydrophobic moieties in the backbone that can form nanostructures.

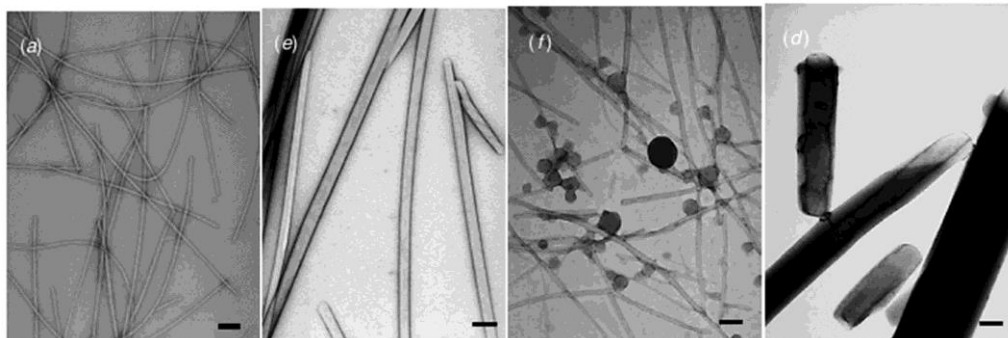


Figure 4.26 Di-aromatic peptides nanostructures

It was surmised that the self-assembling and hydrophobic properties of peptides and base pairing properties of nucleic acids, simultaneously present in PNA may lead to interesting nanostructures. The hydrophobic PNAs used for the study of nanoparticles formation with their complementary DNA **1** and RNA **1** are shown in Figure 4.27.

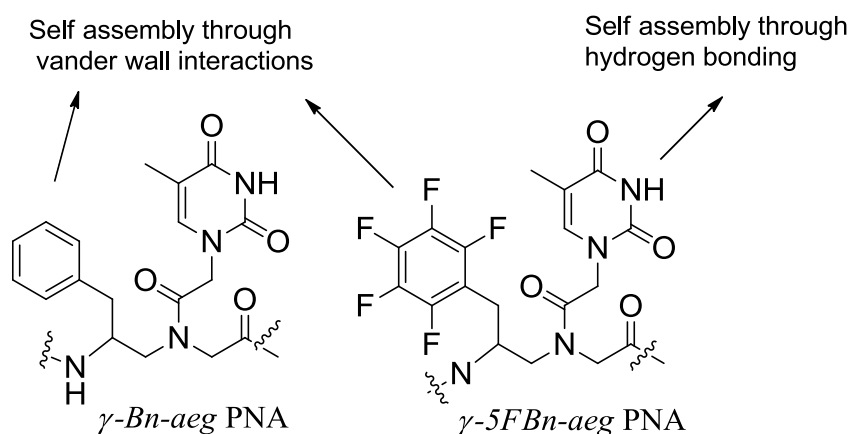


Figure 4.27 PNAs used for nanoparticles formation

4.8 Objective of the present work

1. Study of nanostructure formation of the hydrophobic PNAs **27** & **28** with their complementary DNA **1** and RNA **1** using FESEM and DLS.
2. Cell uptake studies of the derived PNA:DNA/RNA duplexes using confocal microscopy.

4.9 Results and Discussion

4.9.1 UV- T_m studies of γ -5FBn-aeg and γ -Bn-aeg PNAs

The triply modified PNA oligomers (PNA **27** & **28**) with γ -5FBn-aeg (T^{FPh}) and γ -Bn-aeg (T^{Ph}) PNA units were synthesized as described before and their duplex stabilities were studied with their complementary DNA **1** and RNA **1**.

Table 4.4 UV- T_m values of complementary PNA:DNA and PNA:RNA duplexes with γ -5FBn aeg and γ -Bn aeg PNA units

Entry	Seq.code	PNA sequence	UV- T_m	UV- T_m
			PNA:DNA	PNA:RNA
1	PNA 8	H-TTACCTCAGT-Lys	48.6	60.0
2	PNA 27	H-TT ^{FPh} ACCT ^{FPh} CAGT ^{FPh} -Lys	29.0	39.3
3	PNA 28	H-TT ^{Ph} ACCT ^{Ph} CAGT ^{Ph} -Lys	31.4	38.9

The T_m values are accurate to ± 0.5 °C. DNA **1** = 5'ACTGAGGTAA3'; RNA **1** = 5'ACUGAGGUAA3'.

These PNAs showed lower stability with their complementary DNA **1** and RNA **1**. The PNA modified with γ -Bn-aeg PNA unit showed a T_m value of 31.4 °C with cDNA **1** ($\Delta T_m = 19.6$) whereas 38.9 °C with cRNA **1** ($\Delta T_m = 20.7$) (entry 3) and the PNA modified with γ -5FBn-aeg PNA unit showed a T_m value of 29 °C with cDNA **1** ($\Delta T_m = 17.2$) whereas with cRNA **1** it was 39.3 °C ($\Delta T_m = 21.1$, entry 2). The sigmoidal profiles are shown in Figure 4.28.

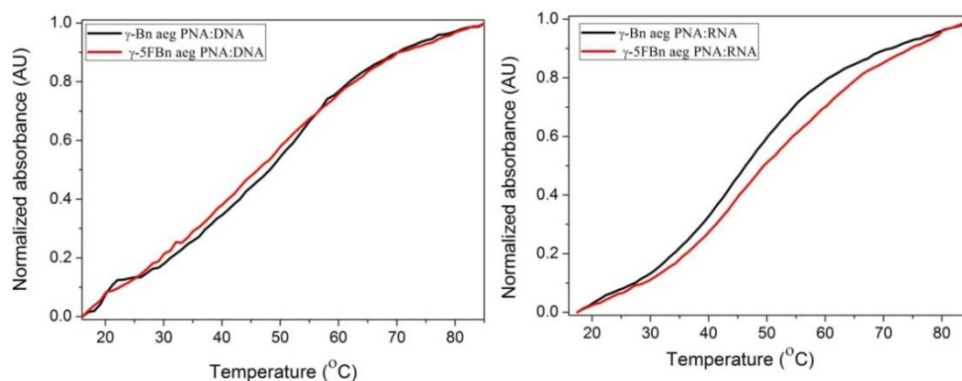


Figure 4.28 UV absorbance curves for complementary PNA:DNA and PNA:RNA duplexes; Phosphate buffer = 10 mM, pH = 7.2, NaCl = 10 mM.

The results indicated that γ -PNAs (PNAs **27** & **28**) derived from D-pentafluoro phenylalanine and D-phenylalanine decrease the stability of duplexes with their complementary DNA/RNA (entry 2 & 3) as compared to unmodified aeg PNA oligomer (entry 1) by 19.6, 17.2 °C with DNA **1** and 20.7, 21.1 °C with RNA **1** respectively.

4.9.2 Study of nanostructures formation using FESEM and DLS

The combined hydrophobicity and the lower binding affinity properties of the γ -substituted PNAs (PNA 27 & 28) were explored to generate effective nanocarriers by PNAs. The nanostructure formation from the ssPNAs (PNA 8, PNA 27 & 28) and duplexes derived from these with complementary DNA/RNA was studied using (FESEM) and (DLS) at different concentrations and the results are shown in Figures 4.29-4.41.

4.9.2a Single stranded (ss) PNAs, DNA and RNA nanostructures formation

Nanoparticle formation from the ssPNAs at 30 μM concentration showed that the unmodified *aeg* PNA forms irregular flake type structures (Figure 4.29) while the backbone modified *ss- γ -Bn-aeg* and *ss-5FBn-aeg* PNAs form nice nanospheres in the range of 50-100 nm (Figure 4.29).

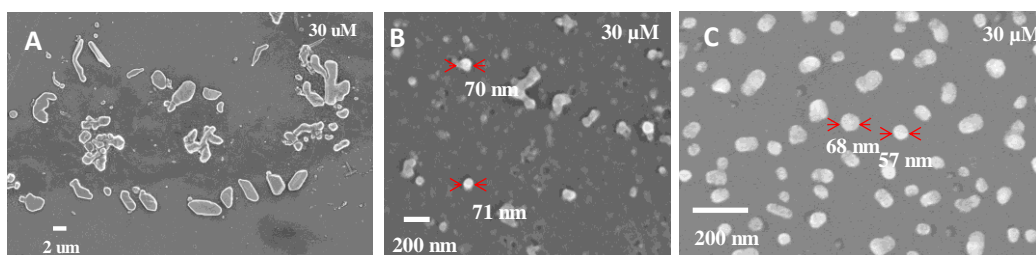


Figure 4.29 FESEM images of (A) *ssaeg* PNA; (B) *ss γ -Bn-aeg* PNA; (C) *ss-5FBn-aeg* PNA.

ssDNA and *ssRNA* alone showed the formation of nanospheres in the range of 100-150 nm at the similar concentration 30 μM (Figure 4.30).

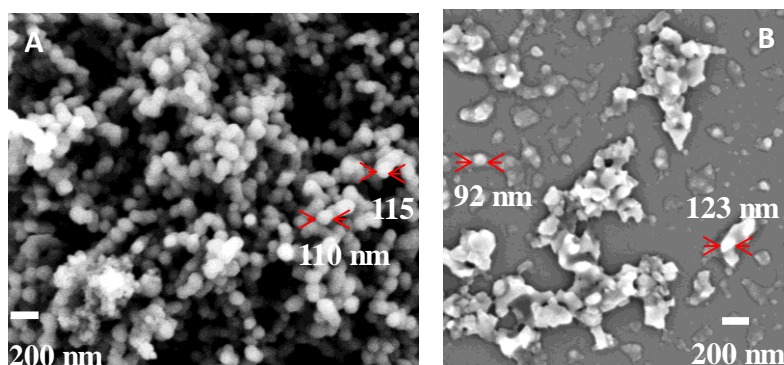


Figure 4.30 FESEM images of (A) *ssDNA* and (B) *ssRNA*.

4.9.2b PNA:DNA/RNA nanostructure formation

The fluorinated/ non-fluorinated PNA and its complementary DNA or RNA were taken in 1:1 ratio of individual concentrations of 30 μM and heated to 90 $^{\circ}\text{C}$ for 5 min and cooled to room temperature. The derived duplexes were studied for their nanostructure formation. The unmodified *aeg* PNA:DNA duplexes exhibited formation of random nanostructures whereas *aeg* PNA:RNA duplex showed the formation of nanospheres of ~ 200 nm (4.31).

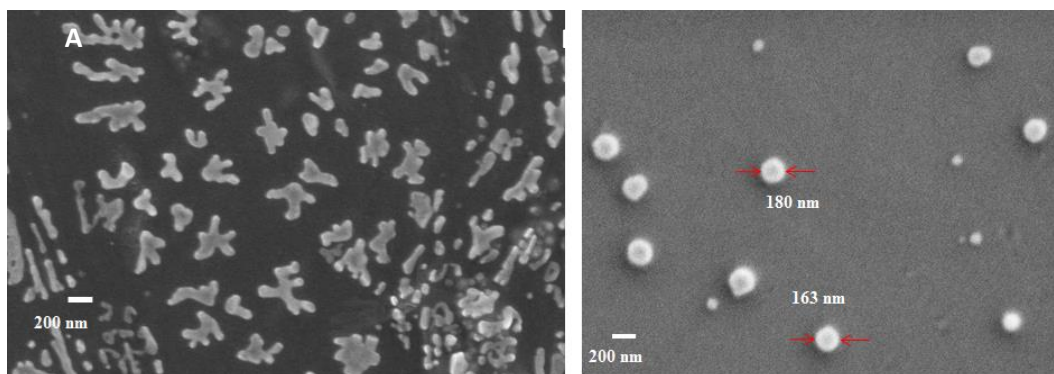


Figure 4.31 FESEM images of (A) *aeg* PNA:DNA and (B) PNA:RNA duplexes.

Duplexes derived from γ -*Bn-aeg* PNA:DNA formed microspheres in the range of 1.0 to 1.5 μm whereas the γ -*Bn-aeg* PNA:RNA duplex showed microsphere formation in the range of 1.0 to 1.3 μm (Figure 4.32).

In case of γ -5*FBn-aeg* PNA, the derived PNA:DNA duplex showed the formation of smaller size nanospheres in the size range of ~ 800 nm (Figure 4.33) whereas the γ -5*FBn-aeg* PNA:RNA duplex form microspheres in the size range of ~ 1.2 μm (Figure 4.33).

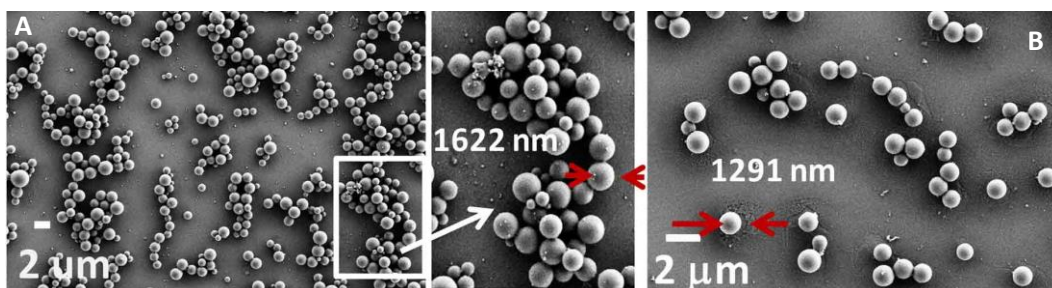


Figure 4.32 FESEM images of (A) γ -*Bn-aeg* PNA:DNA and (B) γ -*Bn-aeg* PNA:RNA.

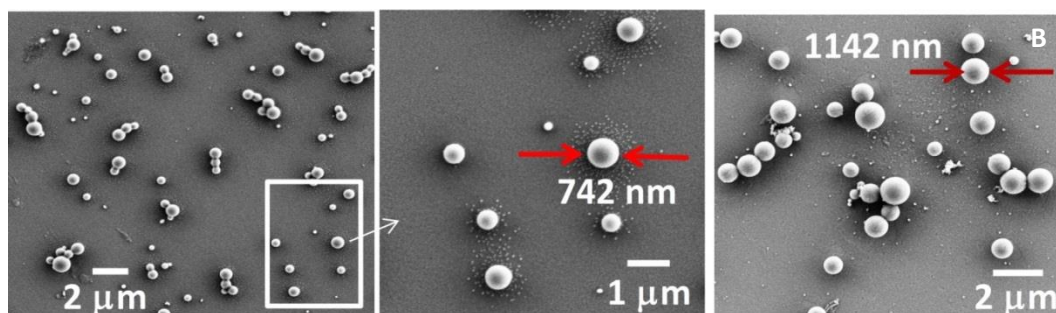


Figure 4.33 FESEM images of (A) γ -5FBn-aeg PNA:DNA and (B) γ -5FBn-aeg PNA:RNA.

The spherical formation in solution was confirmed using dynamic light scattering (DLS). The γ -Bn-aeg PNA:DNA duplex form microspheres of size in the range of 2.3 μm whereas its PNA:RNA duplex form microspheres of size 1.7 μm (Figure 4.34). γ -5FBn-aeg PNA:DNA/RNA complexes form microspheres in the range of 1.3 μm and 1.5 μm size respectively (Figure 4.35).

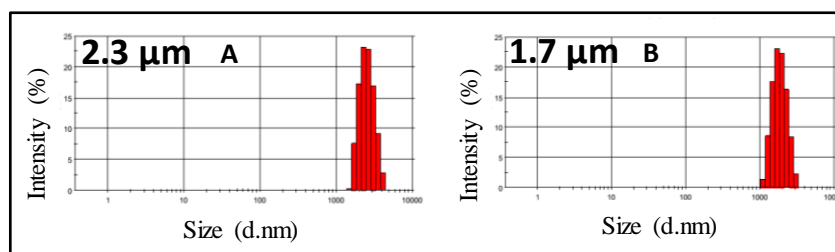


Figure 4.34 DLS of (A) γ -Bn-aeg PNA:DNA and (B) γ -Bn-aeg PNA:RNA duplexes.

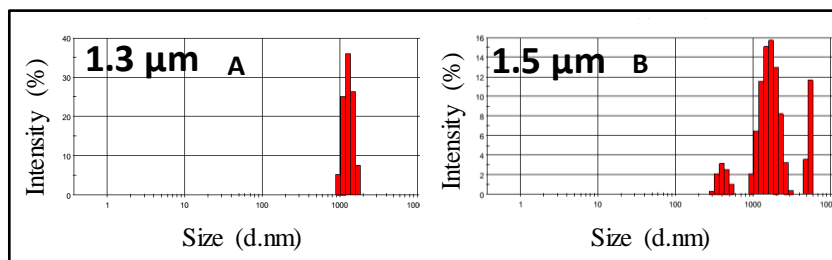


Figure 4.35 DLS of (A) γ -5FBn-aeg PNA:DNA and (B) γ -5FBn-aeg PNA:RNA duplexes.

The concentration dependent nanoparticle formation from various duplexes was studied and it was observed that the size of the spherical assemblies was altered by varying the concentration of the duplex derived from PNA:DNA/RNA in the range of size from nm to μm .

4.9.3 PNA:DNA/RNA nanostructure formation at 10 μM and 2 μM concentrations

Upon decreasing the concentration of PNA:DNA/RNA duplex from 30 μM to 10 μM , the nanoparticles size dramatically decreased to 100-350 nm and further decreased to 50-100 nm

upon lowering the PNA:DNA/RNA duplex concentration to 2.0 μM . The FESEM results and DLS results for the various concentrations were discussed below.

Nanoparticles formation at 10 μM : $\gamma\text{-Bn-aeg}$ PNA:DNA duplex formed nanospheres in the range of 50 nm - 250 nm whereas the same PNA with cRNA showed in the range of 100 nm - 350 nm (Figure 4.36). The $\gamma\text{-5FBn-aeg}$ PNA, with cDNA showed spherical structures in the range of 80 nm to 150 nm and with cRNA the nanospheres formed in the range of 200 to 300 nm (Figure 4.37). The size of nanoparticle formed was confirmed by Dynamic light scattering (DLS) measurements (Figure 4.38 & 4.39).

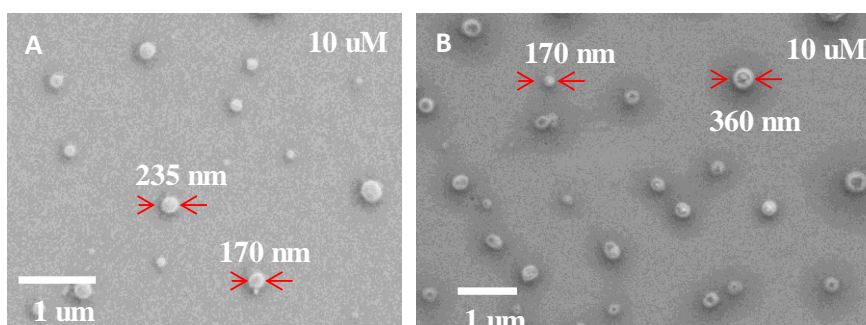


Figure 4.36 FESEM images of (A) $\gamma\text{-Bn-aeg}$ PNA:DNA and (B) $\gamma\text{-Bn-aeg}$ PNA:RNA duplexes at 10 μM concentrations.

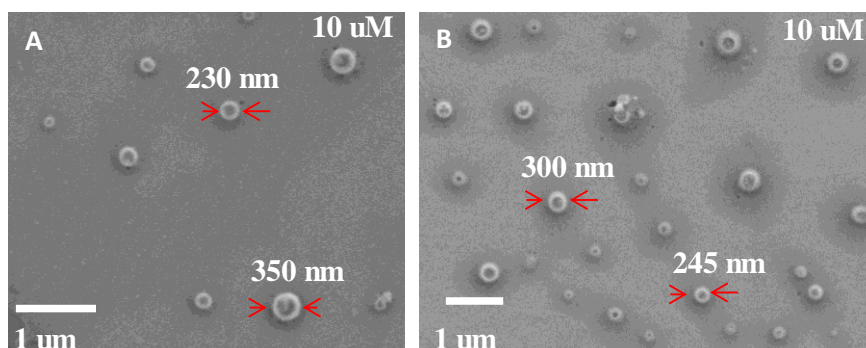


Figure 4.37 FESEM images of (A) $\gamma\text{-5FBn-aeg}$ PNA:DNA and (B) $\gamma\text{-5FBn-aeg}$ PNA:RNA duplexes 10 μM concentrations.

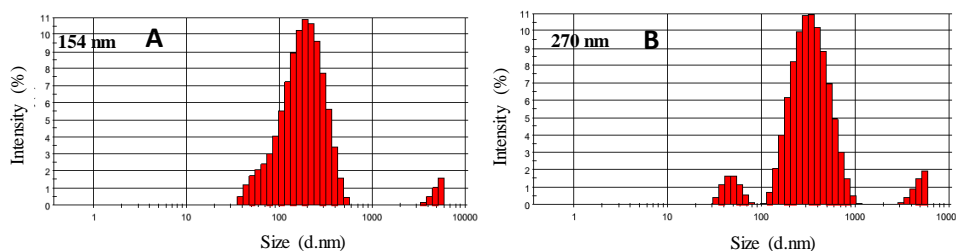


Figure 4.38 DLS of (A) $\gamma\text{-Bn-aeg}$ PNA:DNA and (B) $\gamma\text{-Bn-aeg}$ PNA:RNA duplexes.

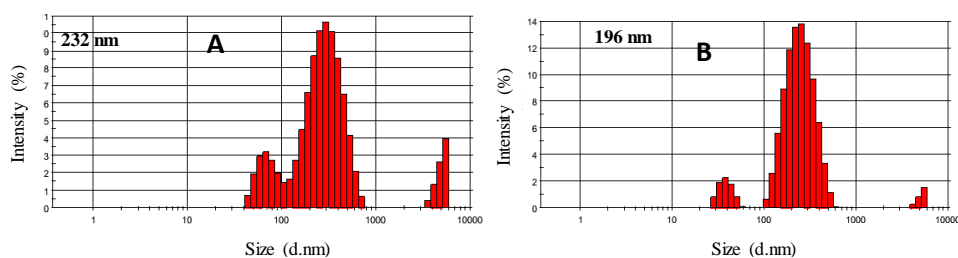


Figure 4.39 DLS of (A) γ -5FBn-aeg PNA:DNA and (B) γ -5FBn-aeg PNA:RNA duplexes.

Nanoparticle formation at 2 μ M: The DNA/RNA Duplexes derived from γ -Bn-aeg formed nanospheres in the range of \sim 100 nm (Figure 4.40). In case of γ -5FBn-aeg PNA, PNA:DNA/RNA duplexes showed nanospheres in the range of 50 to 100 nm (Figure 4.41).

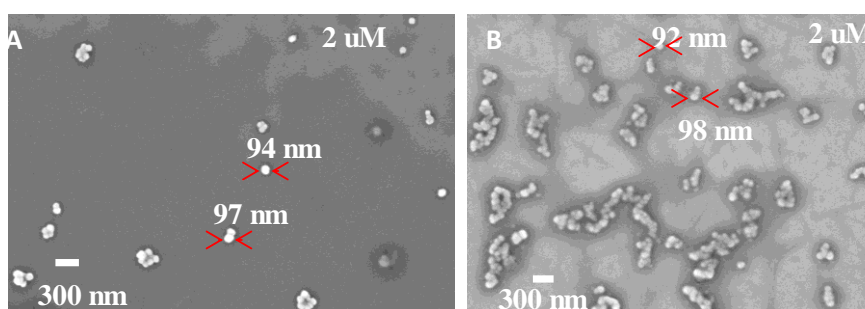


Figure 4.40 FESEM images of (A) γ -Bn-aeg PNA:DNA and (B) γ -Bn-aeg PNA:RNA duplexes.

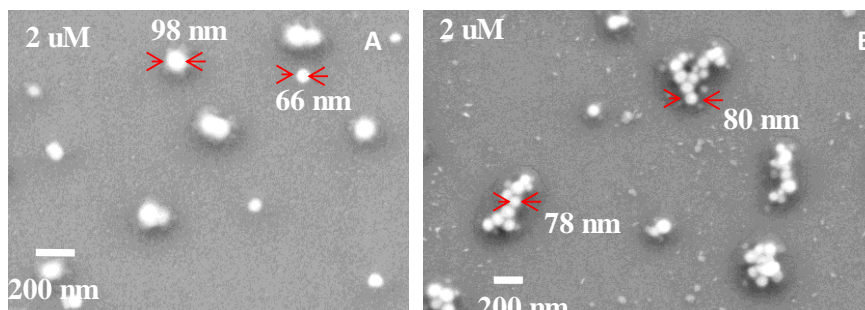


Figure 4.41 FESEM images of (A) γ -5FBn-aeg PNA:DNA and (B) γ -5FBn-aeg PNA:RNA duplexes.

Thus lowering the concentration lead to formation of nanospheres in nanometer dimensions.

4.9.4 Cellular uptake studies of the PNA:DNA/RNA nanoparticles

The duplexes derived from the PNAs **34-CF** & PNA **35-CF** were tested at lower concentration range of 2 μ M for cell uptake ability using confocal microscopy. The nanoparticle solution (2 μ M) was incubated with 3T3 cells for 24 h. It was observed from green fluorescent signals that these particles entered into the cells. (Figure 4.42-4.45). Thus the PNA:DNA/RNA combination can aid delivery of antisense oligonucleotides into the cells successfully. The low

binding affinity and the nanoparticle formation property of these γ -Bn/5FBn-aeg PNAs may assist oligonucleotides delivery in future medicinal chemistry. Further studies are needed to test the full strength of these systems.

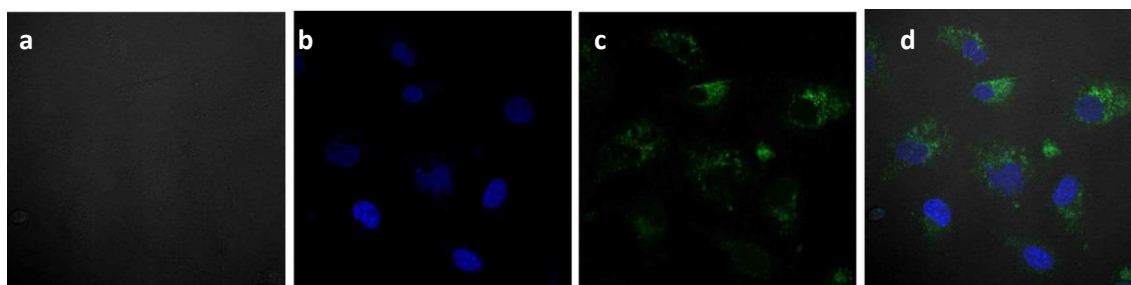


Figure 4.42 Confocal microscopy images for γ -Bn-aeg PNA:DNA (a) Bright field image (b) Hoechst 33342 stained image (c) Green fluorescence image and (d) Superimposed image of (a) - (d).

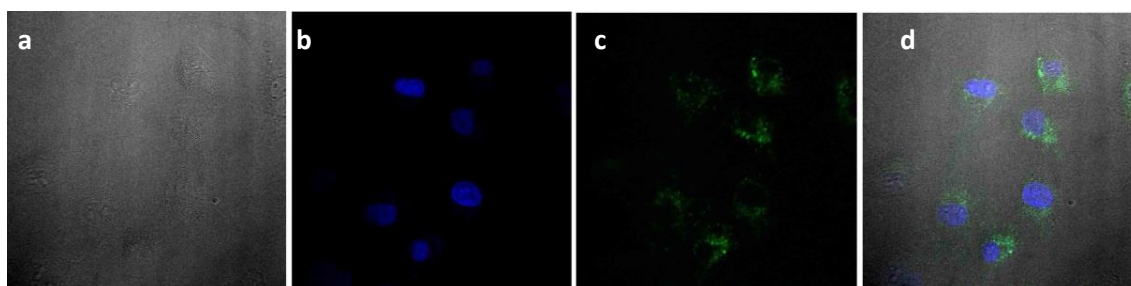


Figure 4.43 Confocal microscopy images for γ -Bn-aeg PNA:RNA (a) Bright field image (b) Hoechst 33342 stained image (c) Green fluorescence image and (d) Superimposed image of (a) - (d).

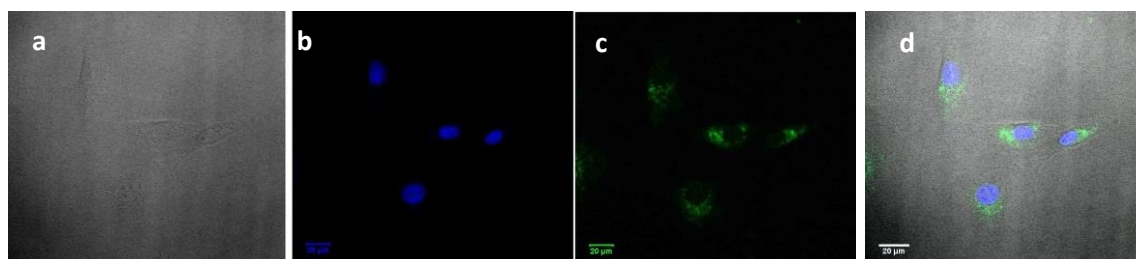


Figure 4.44 Confocal microscopy images for γ -Bn-aeg PNA:RNA (a) Bright field image (b) Hoechst 33342 stained image (c) Green fluorescence image and (d) Superimposed image of (a) - (d).

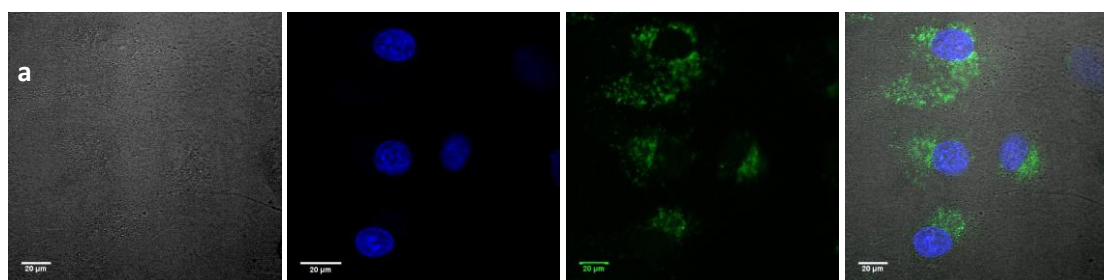


Figure 4.45 Confocal microscopy images for γ -Bn-aeg PNA:RNA (a) Bright field image (b) Hoechst 33342 stained image (c) Green fluorescence image and (d) Superimposed image of (a) - (d).

4.10 Summary

1. Nanoparticle formation by *ssPNAs*, PNA:DNA and PNA:RNA duplexes were studied using FESEM and DLS techniques. These form nanoparticle in the range from μm to nm and their size can be tuned based on control of concentration and sample processing.
2. Fluorine effect on size of particle formation was observed at higher concentration 30 μM where duplexes derived from γ -5*FBn-aeg* PNA showed lower size particles formation than that of duplexes derived from γ -*Bn-aeg* PNA but at lower concentrations (2 and 10 μM) these duplexes did not show considerable difference in size of the nanoparticles.
3. The nanoparticles were delivered to 3T3 cells successfully, PNA:DNA or PNA:RNA entry into the cells was visualized using confocal microscopy. This may contribute to DNA or RNA delivery to the cells and thereby may regulate gene function.

4.11 Experimental procedures

4.11.1 Cleavage and purification of the fluorescently labelled PNA oligomers

5(6)-carboxyfluorescein a fluorescent dye, was tagged to the N-terminal end of PNA oligomers through a lysine unit using the solid phase peptide synthesis protocol. The α -amine of the lysine unit was coupled with 5(6)-carboxyfluorescein using HOBt and DIC in pyridine. After completion of reaction the reaction mixture was washed with DMF/DCM and the carboxyfluorescein attached PNAs were cleaved from the resin using trifluoromethane sulfonic acid (TFMSA) in the presence of trifluoroacetic acid (TFA); (Low, High TFMSA-TFA method). After the cleavage reaction, the peptide was precipitated with cold diethyl ether and was isolated by centrifugation. The precipitate was dissolved in deionized water.

PNA purification was carried out on Dionex ICS 3000 HPLC system using semi-preparative BEH130 C18 (10 X 250 mm) column. Purification of PNA oligomers was performed with gradient elution method: A to 100% B in 20 min; A = $\text{CH}_3\text{CN}:\text{H}_2\text{O}$ (5:95); B = $\text{CH}_3\text{CN}:\text{H}_2\text{O}$ (50:50) having 1% TFA in each with a flow rate of 3 mL/min. All the HPLC profiles were monitored at 254 and 490 nm wavelength.

4.11.2 Sample preparation for confocal microscopy experiment

- 1) NIH 3T3 or HeLa cells were plated in 8-well chambered cover glass in 200 μL Dulbecco's Modified Eagle Medium (DMEM) containing 10 % Fetal Bovine Serum (FBS) at the concentration of 1.5×10^4 to 2×10^4 cells per well.

2) The cells were grown by maintaining at 37 °C in a humidified atmosphere containing 5 % CO₂ for 12 h. The required amounts of 5(6)-carboxyfluorescein tagged PNAs were added to the corresponding wells to achieve the desired final concentration of 2 μM. The cells incubated with tagged PNA oligomers were maintained at 37 °C in a humidified atmosphere containing 5 % CO₂ for 24 h.

3) After 24 h incubation the medium was aspirated and the cells were washed thrice with ice-cold PBS. The cells were then replenished with 200 μL of DMEM medium containing Hoechst 33342 and ER-red of 1 μM final concentration of each, and incubated for 30 minutes at 37 °C.

4) The excess nuclear stain Hoechst and ER-red were removed by washing thrice with cold PBS. Then fresh OPTIMEM medium was added to the cells and the cells were immediately visualized using 60 X objective of Zeiss LSM 710 laser scanning confocal microscope. The confocal microscopy imaging has been repeated at least twice for each PNA.

4.11.3 FACS sample preparation

1) NIH 3T3 or HeLa cells were plated in 9 X 60 mm dishes in 2.0 mL DMEM medium at a concentration of 2 x 10⁶ cells per dish.

2) The cells were maintained at 37 °C in a humidified atmosphere containing 5 % CO₂ for 48 h. The required amounts of 5(6)-carboxyfluorescein tagged PNA stock solutions were added to the corresponding wells to achieve the final concentration of 1 μM. The cells incubated with tagged PNA oligomers were maintained at 37 °C in a humidified atmosphere containing 5% CO₂ for 24 h.

3) After the incubation period was over, the medium was aspirated and cells were washed thrice with ice-cold PBS. Cells were collected by trypsinization using 0.5 mL of 0.05 % trypsin-EDTA for each dish. After trypsinization 2 mL of DMEM medium was added and the cells were transferred to 15 mL falcon tubes.

4) These tubes containing cells were centrifuged for 5 min at 4 °C, the supernatant was aspirated and the cells were washed thrice with ice-cold PBS.

5) To the cell suspension 1.0 mL of PBS containing 1.0 MM EDTA and 25 MM HEPES was added and washed for 5 min at 4 °C.

6) To the cell suspension 200 μL of 1% PFA was added and incubated on ice for 10 min for fixation of the cells.

7) The cell suspension was again washed once with ice cold PBS for 5 min at 4 $^{\circ}\text{C}$, to the cell suspension 1 mL of ice cold PBS was added and filtered through 70 μm cell strainers. The samples were transferred to FACS tubes and were analysed on BD Biosciences FACS Calibur flow cytometer.

The data obtained from FACS was processed using Cell Quest Pro acquisition software. The cell permeation of PNA oligomers has been confirmed by histograms obtained from the experiment. The Percent positive cells for each individual PNA were plotted on Microcal origin 8.

4.11.4 Sample preparation for FESEM and DLS

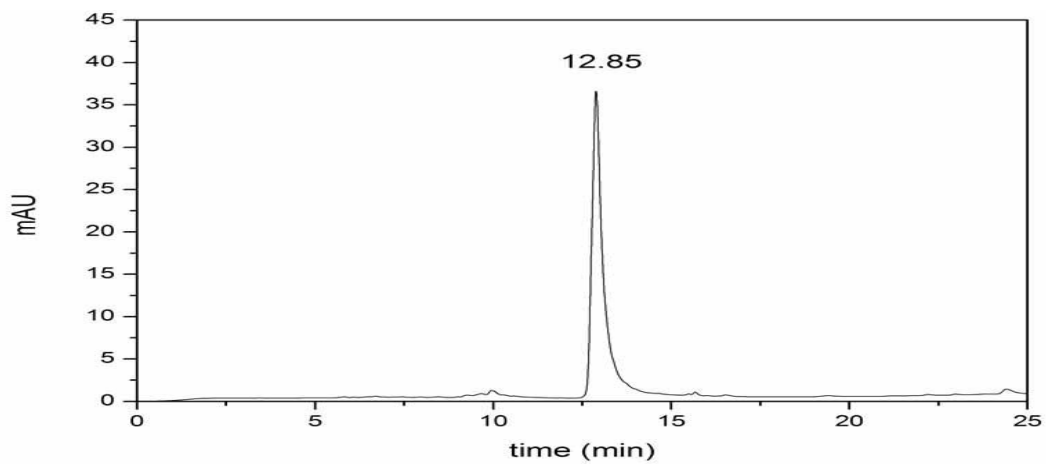
PNA and its complementary DNA or RNA were taken in 1:1 ratio of final concentration of 30 μM and heated to 90 $^{\circ}\text{C}$ for 5 min and cooled to room temperature. 10 μL of each sample was placed on a silicon wrapper and subjected for FESEM imaging. 10 or 2.0 μM solutions were prepared by diluting the 30 μM stock solutions to the respective concentrations by adding water and annealed at 90 $^{\circ}\text{C}$ for 5 min and then cooled to room temperature. The resulting PNA:DNA/RNA samples were used for the FESEM imaging. The same procedure was employed to make DLS samples.

4.12 References

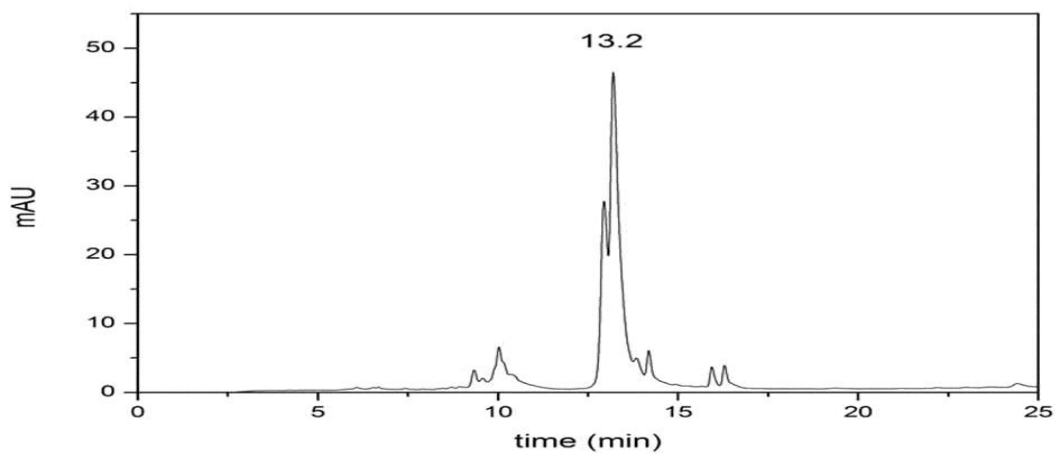
1. Minsky, M. *Scanning* 1988, *10*, 128-138.
2. Minsky, M. US patent 3013467, 12 Dec 1961.
3. <http://emu.uct.ac.za/training/intro-to-electron-microscopy-for-biologists/confocal-laser-scanning-microscopy/>
4. Fulwyler, M. J. *Science* 1965, *150*, 910-911.
5. Fulwyler, M. J. US Patent 3,380,584; 30 April 1968.
6. http://en.wikipedia.org/wiki/File:Fluorescence_Assisted_Cell_Sorting_%28FACS%29_B.jpg
7. Godeau, G.; Arnion, H.; Brun, C.; Staedel, C.; Barthelemy, P. *MedChemComm* **2010**, *1*, 76.
8. Li, J.; Wang, Y.; Zhu, Y.; Oupicky, D. *J. Control. Release* **2013**, *172*, 589-600.
9. Zhang, S. *Nat. Biotechnol.* **2003**, *21*, 1171-1178.
10. Song, Y.; Challa, S.R.; Medforth, *et al.* *Chem. Commun.* **2004**, *9*, 1044-1045.
11. Reches, M.; Gazit, E. *Nat. Nanotechnol.* **2006**, *1*, 195-200.
12. Reches, M.; Gazit, E. *Phys. Biol.* **2006**, *3*, S10-S19
13. Reches, M.; Gazit, E. *Current Nanoscience*, **2006**, *2*, 105-111.

4.13 Appendix-III

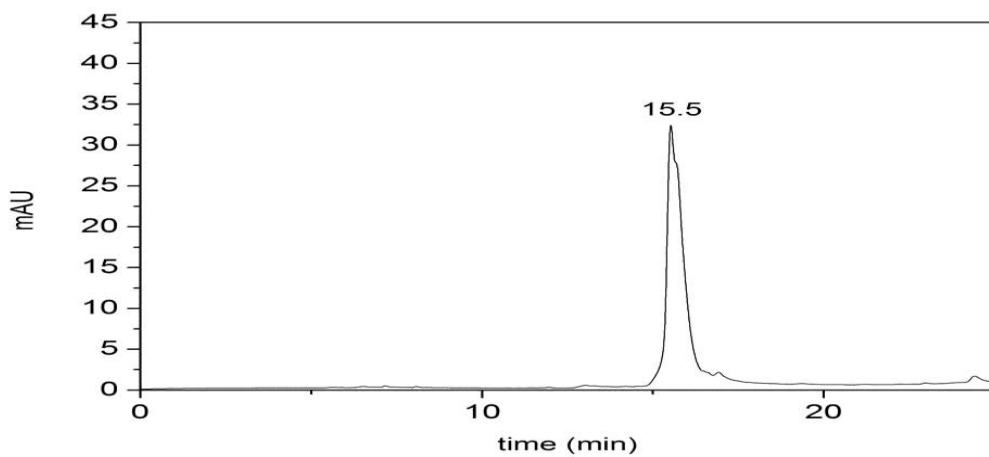
HPLC of PNA 32-CF



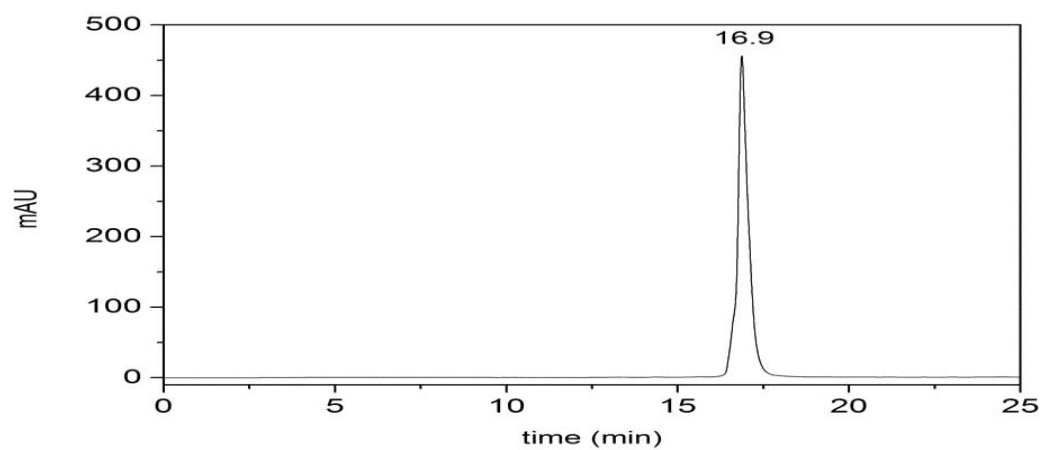
HPLC of PNA 33-CF



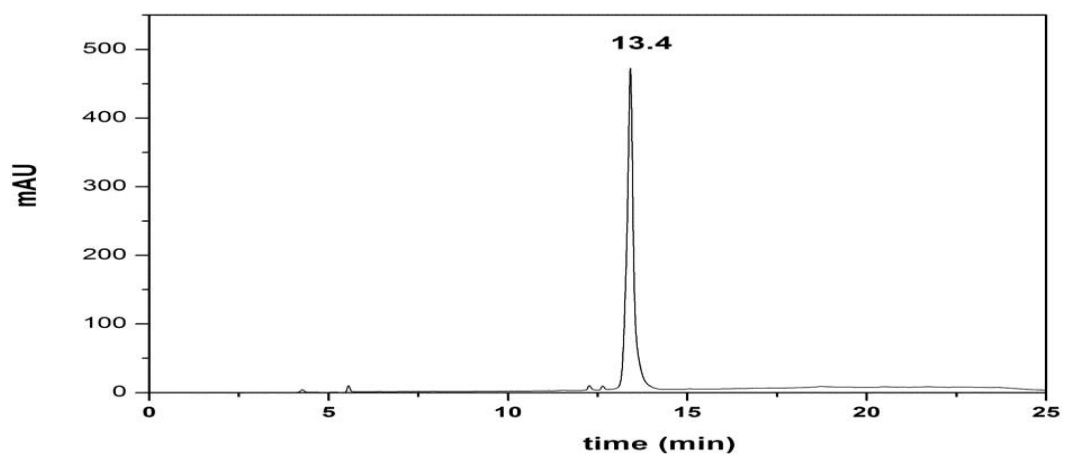
HPLC of PNA 34-CF



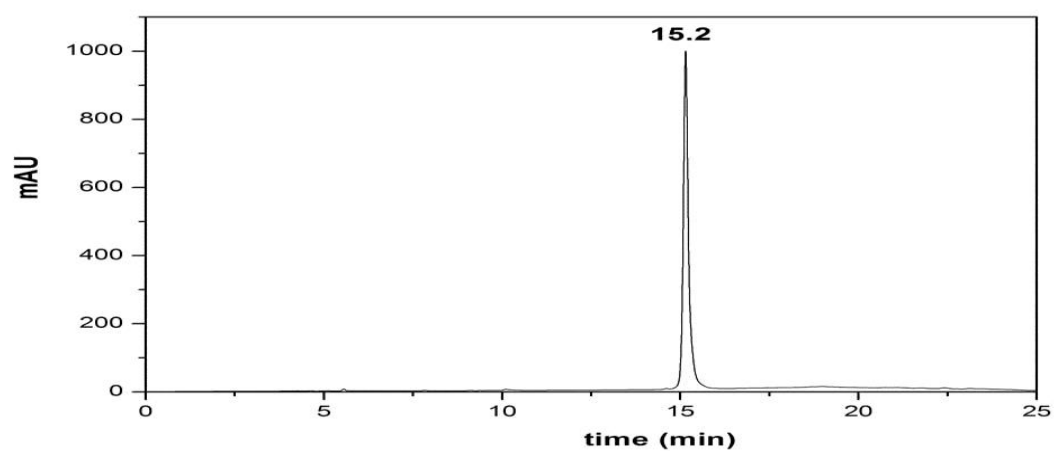
HPLC of PNA 35-CF



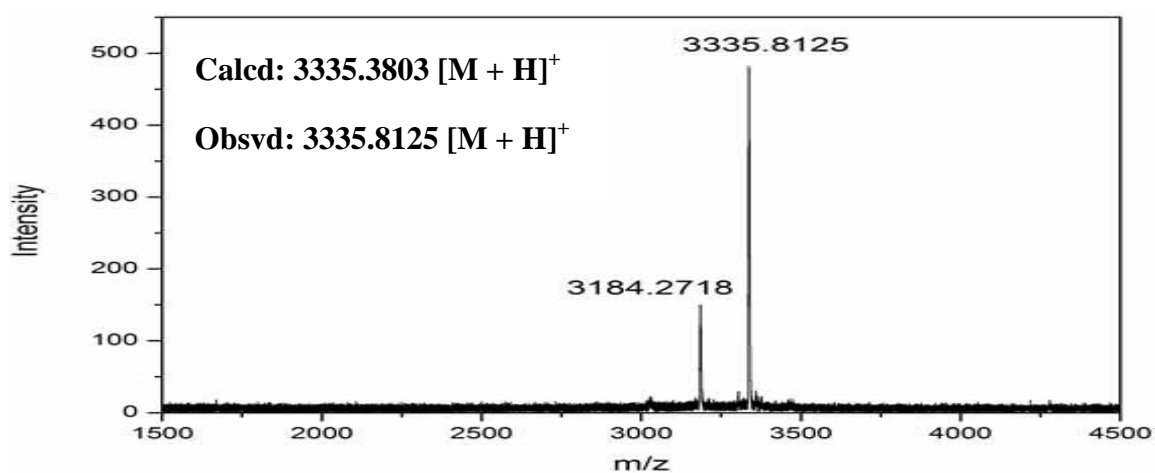
HPLC of PNA 36-CF



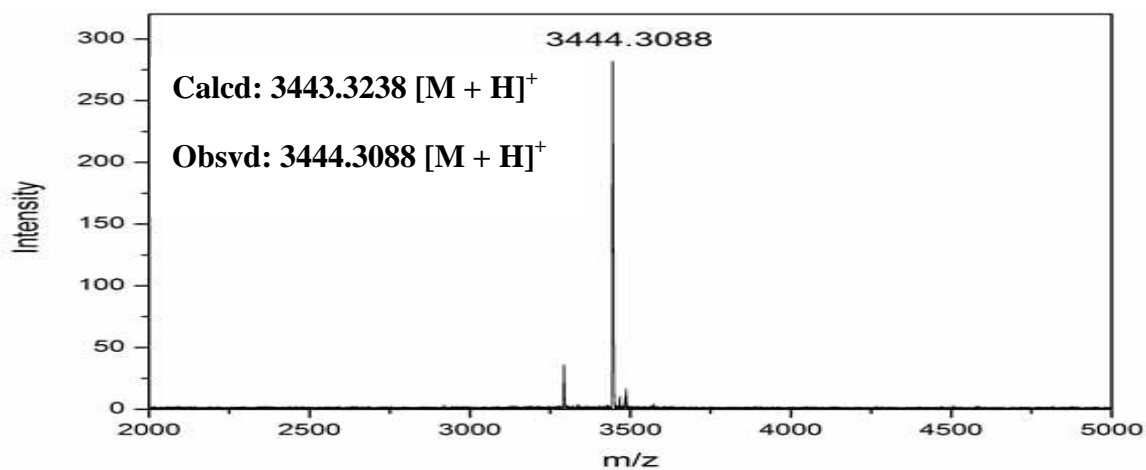
HPLC of PNA 37-CF



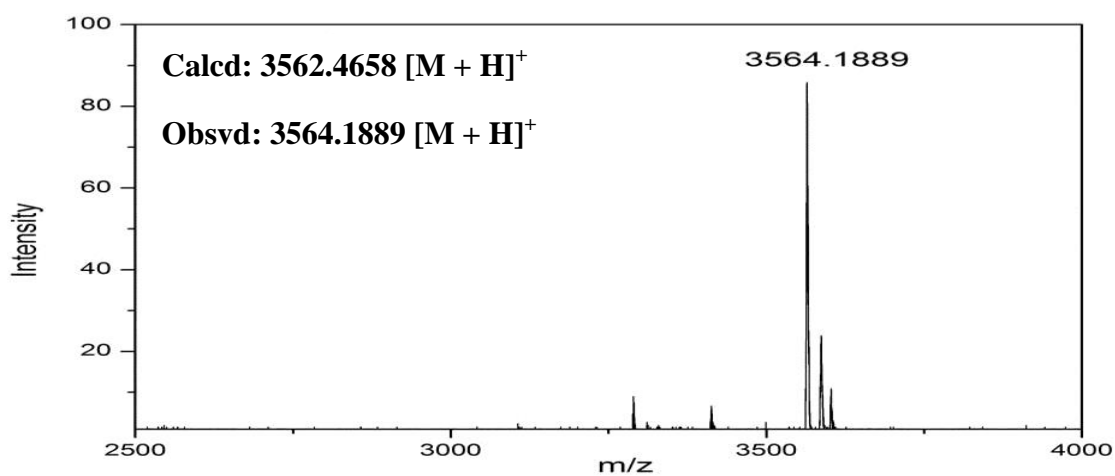
MALDI-TOF PNA 32-CF



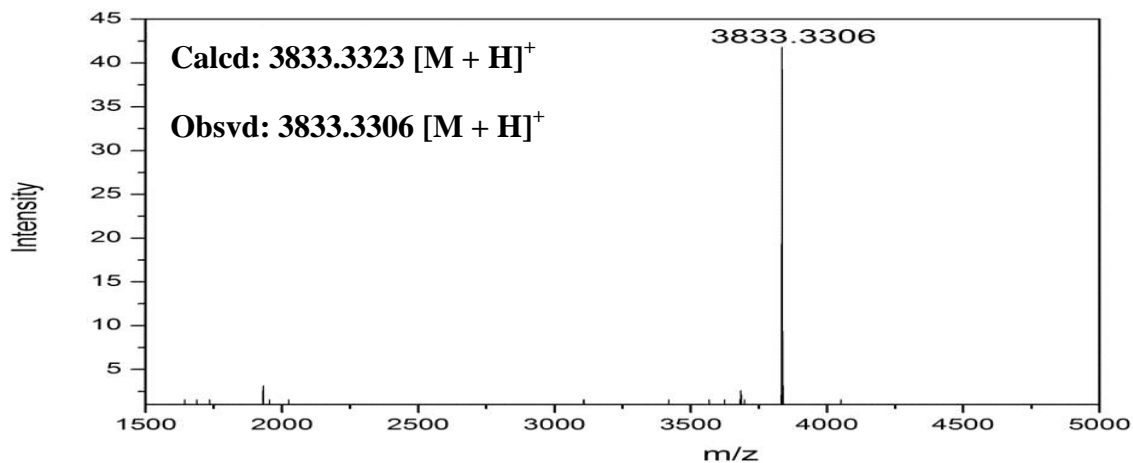
MALDI-TOF PNA 33-CF



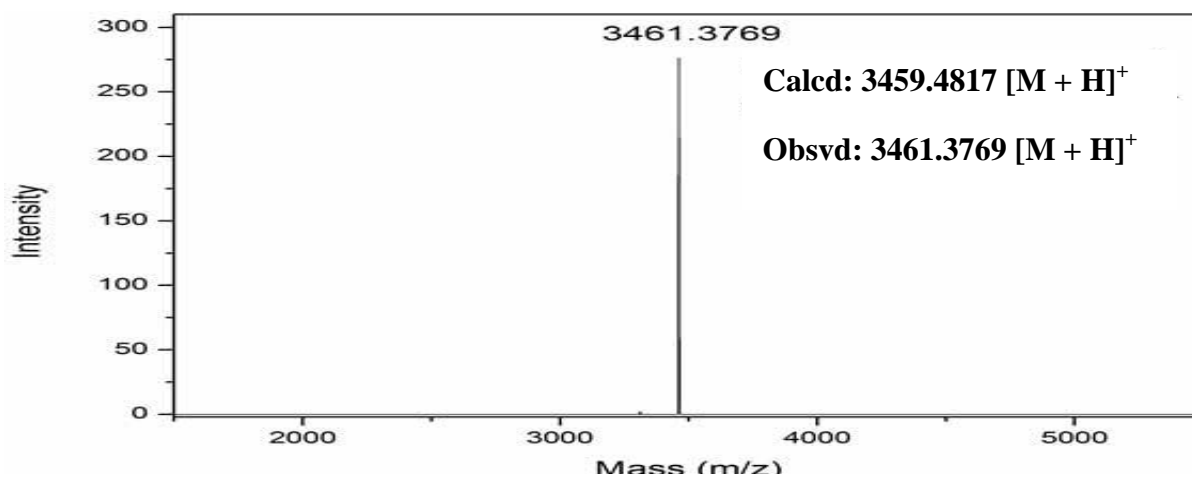
MALDI-TOF PNA 34-CF



MALDI-TOF PNA 35-CF



MALDI-TOF PNA 36-CF



MALDI-TOF PNA 37-CF

